STUDY OF TRANSPORT AND INTERMOLECULAR INTERACTIONS IN COMPRESSED SUPERCRITICAL FLUIDS

J. Jonas and D. M. Lamb

Department of Chemistry, School of Chemical Sciences
University of Illinois, Urbana, Illinois 61801

General overview of several studies of transport and intermolecular interactions in compressed supercritical fluids will be presented. The unique aspects of the instrumentation used in these studies will also be emphasized. First, the results of NMR studies of self-diffusion in supercritical ethylene and toluene will be discussed. These experiments are using the fixed field gradient NMR spin-echo technique. Second, the novel NMR technique for the determination of solubility of solids in supercritical fluids will be described. Third, the promising potential of laser scattering experiments investigating interaction induced spectra will be illustrated on several specific studies of depolarized Rayleigh scattering. The interaction induced spectra offer valuable information about intermolecular interactions in supercritical fluids.

Introduction

Research on the properties of supercritical fluids and supercritical fluid mixtures has become very important in recent years due to the great promise of supercritical fluid extraction techniques. These techniques and their applications have been reviewed by several authors (1-4). There are many advantages of using supercritical fluid extraction over conventional extraction techniques. Many low volatility molecular solids show greatly enhanced solubilities in supercritical dense fluids. Solvent recovery is easily accomplished by manipulating the density, and therefore the solvating power, of the supercritical fluid to precipitate the solid. In addition, although the densities of the supercritical fluids are comparable to liquid densities, the viscosities are generally an order of magnitude smaller, and diffusivities an order of magnitude larger than liquids. A more efficient separation can therefore be achieved.

Unfortunately, there is a lack of fundamental data on transport and relaxation in model fluids at supercritical conditions. Not surprisingly, there is a corresponding lack of theoretical models to explain the dynamics of supercritical fluids on a molecular level, particularly at the intermediate densities.

The main purpose of our work is the improvement of molecular level understanding of solute-solvent interactions under supercritical conditions. Unique nuclear magnetic resonance (5) and laser scattering techniques (6) are employed to obtain new information about dynamics of molecules in supercritical fluids at high pressures.

The main results of several of our studies will be discussed. First, the results of NMR studies of self-diffusion in supercritical ethylene (7) and toluene (8) will be discussed. These experiments are using the fixed field gradient NMR spin-echo technique. Second, the novel NMR technique (9) for the determination of solubility of solids in supercritical fluids will be described. Third, the promising potential of laser scattering experiments investigating interaction induced spectra (6) will be illustrated on several specific studies of depolarized Rayleigh scattering.

Experimental

The self-diffusion coefficients in supercritical ethylene were measured using the pulsed NMR spectrometer described elsewhere (10), automated for the measurement of diffusion coefficients by the Hahn spin echo method (11). The measurements were made at the proton resonance frequency of 60 MHz using a 14.2 kG electromagnet.

The pressure was generated using the gas compression system described previously (12). A Heise-Bourdon pressure gauge was installed between the compression system and the high pressure vessel to supplement the 30,000 psi pressure transducer. The oxygen scavenger system was bypassed as the amount of oxygen in the ethylene was below the minimum detection level (10 ppm) of the oxygen analyzer (Beckman Instruments, Inc.). In order to depress the extremely long T_1 values of pure ethylene (13) at the experimental conditions studied, small quantities (< 1000 ppm) of oxygen were mixed with the ethylene before measurement of the diffusion coefficient. The addition of oxygen brought the T_1 values down to 2-3 sec, but should not affect the value of the diffusion coefficient. The shorter T_1 values allowed a much shorter measurement time.

The self-diffusion coefficients in supercritical toluene-d_8 were measured at the deuterium resonance frequency of 9.21 MHz, using a 14.1 kG electromagnet with a wide gap (3.8") to accommodate the high pressure vessel. The pulsed NMR spectrometer and receiver system were described in detail elsewhere (10). The argon pressurized high pressure, high temperature NMR probe (14) was used previously for studies of relaxation (15) and diffusion (16) in compressed supercritical water. It consists of two high pressure vessels: the primary vessel, containing an internal furnace, two thermocouples and the RF coil and sample, and the secondary vessel, containing the stainless steel sample bellows. Quartz sample cells were used rather than ceramic cells, as corrosion is not a problem. The RF coil was constructed by winding 14 1/2 turns of 22 gauge nichrome (Chromel A) wire. The coil was silver soldered to nichrome conductor coaxial high pressure leads. The tuning circuit consisted of a six foot impedance transforming coaxial cable terminated with a tapped-parallel capacitor box with both fixed and variable capacitors totalling 70 pF in series and 10 pF in parallel. The observed signal peak to rms noise ratio in liquid toluene-d_8 (30°C) was 60:1 after one scan.

Some experimental detail (9) on the experimental NMR setup for the measurement of solubilities of organic solids in supercritical fluids will be given in the section dealing with Results and Discussion.

The description of equipment and experimental techniques for laser Rayleigh scattering experiments on supercritical fluids at high pressures were given earlier (6,17,18).

Results and Discussion

Self-Diffusion in Compressed Supercritical Ethylene

The main purpose of our work (7) was to provide transport data on dense supercritical ethylene and to analyze the data in terms of currently available theories. Ethylene was chosen for the study for a number of reasons. First, it is one of the most widely used solvents in industry due to its easily accessible critical temperature, its relatively low cost and wide availability. Highly accurate compressibility data are available (19,20,21) in the literature over a wide range of temperature and pressures. These data are necessary for a complete analysis of the transport data.

Some measurements have been made of self diffusion in pure ethylene and in ethylene-sulfur hexafluoride mixtures (22), but these measurements were made very close to the critical temperature and up to pressures of only about 100 bar. Proton spin-lattice relaxation times (T_1) of ethylene have been measured at temperatures from 0°C to 50°C and pressures up to about 2300 bar (13). The relaxation time values were 40-50 sec for much of the region studied. Several relaxation mechanisms contribute to this long relaxation time and make both the measurement and analysis of the relaxation times very difficult. For these reasons, we decided to limit our study to the measurement of the self-diffusion coefficient in supercritical ethylene.

The measurements were made as a function of density for pressures from 1 - 2000 bar and at 50°, 75°, 100° and 125°C. The temperatures chosen correspond to those for which density data (19-21) for ethylene and ethylene-CO_2 are available.

The density dependence of the ethylene self-diffusion coefficients was analyzed using the Enskog theory (23) of diffusion of hard spheres corrected for the effects of correlated motion (24). The corrected Enskog theory considers only repulsive forces between molecules, but it has proved to be in excellent agreement with experiment for the transport coefficients of supercritical dense gases such as argon, krypton, methane and carbon tetrafluoride (25). At densities less than the critical density (ρ_c), the attractive forces between the molecules become important and deviations from the theory are observed.

In previous work on supercritical fluids, Jonas et al. (26-28) measured self-diffusion, shear viscosity and angular momentum correlation times in very dense ($\rho > 2\rho_c$) supercritical fluids of simple polyatomic molecules such as SF_6, CF_4, $CFCl_3$ and C_4F_8. The goal of the experiments was to investigate the applicability of the rough hard sphere (RHS) model (29) at very high densities. At these high densities, the harsh, short ranged repulsive forces screen out the long range attractive forces. The RHS model accounts for the coupling between rotational and translational motion and was found to agree well with the experimental data for $\rho > 2\rho_c$. However, at the lower densities, deviations between the theory and experiment were observed for angular momentum relaxation in CF_4 (12) and mixtures of CF_4 with argon and neon (30). These deviations were attributed to the effects of attractive forces, causing the RHS model to break down. A theoretical model based on optimized cluster theory (31) was proposed (12) to account for the effects of attractive forces and was found to give a good explanation of the experimental data.

Another problem with applying the Enskog theory to explain the ethylene data is that ethylene is not spherical. Attempts to develop a theoretical description of the dynamics in fluids of non-spherical molecules have been made for many years. The model which most closely corresponds to the molecular shape of ethylene is the prolate spherocylinder. Curtiss and Muckenfuss (32) developed a kinetic theory for non-spherical molecules in the dilute gas region and applied it to the calculation of the diffusion coefficient of a spherocylinder in this region (33). They showed that diffusion in a spherocylinder fluid is faster than in a fluid composed of spheres of the same volume as the spherocylinder. In a limited molecular dynamics study (34) the values of the self-diffusion coefficient at two different densities in the intermediate region for a spherocylinder of length-to-breadth ratio equal to one were calculated. More extensive calculations have been made of the equations of state, compressibility ratios and virial coefficients for a variety of length-to-breadth ratios for spherocylinders (35-37). However, due to the lack of any complete theoretical description or molecular dynamics data for the density dependence of diffusion in a spherocylinder fluid with the ethylene length-to-breadth ratio, we used hard sphere theory to interpret our data.

Self-Diffusion in Compressed Supercritical Toluene-d_8

Our investigation was motivated by the interest in supercritical toluene as a solvent in the extraction of thermally generated coal liquids (38,39). Typically, coal is heated to temperatures between 350° and 450°C in the presence of a supercritical fluid at a pressure of 100-200 atm. As the large molecular weight components depolymerize thermally, the resulting hydrogen rich material dissolves in the supercritical solvent and is removed. Toluene is a convenient solvent to use for the extraction, as its critical temperature is 319°C, and critical pressure is 41 atm. Recent experimental studies of supercritical fluid extraction in the process of coal liquefication investigate the basic steps involved by varying solvents, pressure and temperatures (40). The goal of our experiment was to provide fundamental data on transport in supercritical toluene-d_8. These data should help in the design and interpretation of extraction processes using supercritical toluene.

We have measured the self-diffusion coefficient in supercritical toluene-d_8 for temperatures from 300°C to 450°C ($0.97 \leq T_r \leq 1.22$) for pressures of 100, 500 and 1000 bar.

Self diffusion coefficients of deuterated toluene were measured, rather than protonated toluene in order to minimize the experimental difficulties associated with very long proton spin lattice relaxation times (T_1). Since the value of the T_1 determines the length of time between pulse sequences, a long relaxation time leads to prohibitively long measurement times. Previous measurements (41-43) of proton and deuterium relaxation times in liquid toluene have been made as a function of temperature and pressure. The relaxation is due to dipolar interactions in protonated toluene and quadrupolar interactions in toluene-d_8. Therefore, the relaxation times can be expected to increase with increasing temperature. However, the quadrupolar relaxed deuterium T_1 values are smaller than the proton T_1 values, resulting in a comparatively shorter measurement time. The self diffusion coefficients of deuterated toluene should not be significantly different from those of protonated toluene at the temperatures of the measurement and will provide an excellent estimate.

Our previous study (16) of self diffusion in compressed supercritical water compared the experimental results to the predictions of the dilute polar gas model of Monchick and Mason (44). The model, using a Stockmayer potential for the evaluation of the collision integrals and a temperature dependent hard sphere diameters, gave a good description of the temperature and pressure dependence of the diffusion. Unfortunately, a similar detailed analysis of the self diffusion of supercritical toluene is prevented by the lack of density data at supercritical conditions. Viscosities of toluene from 320°C to 470°C at constant volumes corresponding to densities from $\rho/\rho_c = 0.5$ to 1.8 have been reported (45). However, without PVT data, we cannot calculate the corresponding values of the pressure.

The diffusion data at 100 bar are compared to values obtained using various estimation schemes for the self diffusion coefficient of protonated toluene. No attempt was made to estimate coefficients at 500 and 1000 bar, as these correspond to reduced pressures ($P_r = 11.9$ and 24.7) well beyond the range of the approximative methods.

Naphthalene Solubility NMR Measurements in Supercritical Carbon Dioxide

We have completed our study of naphthalene solubilities in supercritical carbon dioxide (9). Our unique, in situ NMR method has been used to obtain solubility data for this system at 50.0, 55.0 and 58.5°C in the pressure range of 120-500 bar. Although this system had been previously investigated (46) we have defined better the solubilities near the upper critical end point of the binary mixture. And finally, we have completed our determination of the three phase solid-liquid-vapor curve of the system.

We have developed our static NMR method for the determination of solid solubilities in supercritical fluids. Using this technique we found our 55°C solubility data to agree to within 5% of that taken by Paulaitis, et al. (46), with their technique. We have since proceeded to take data along the previously uninvestigated 50.0 and 58.5°C isotherms. A number of interesting features can be noted. First, by extending the pressure range to 500 bar we were able to observe the limiting solubilities at these isotherms, an effect not before seen for this system. Secondly, the isotherms cross at about 160 bar showing the presence of the two critical end points for the naphthalene/carbon dioxide system. And finally, the 58.5°C isotherm shows a point of inflection at about 235 bar. This behavior shows the close proximity to the upper critical end point (UCEP) temperature and pressure.

The location of the UCEP is quite important to supercritical solubilities, as this critical point gives the maximum temperature at which solid-gas equilibrium exists at all pressures. We have also developed an NMR method to determine for the first time the S_2LG phase line for this mixture. Since this phase line is terminated by the UCEP, with this data and the inflection point in the 58.5°C isotherm we can now locate the UCEP at 60.1°C and 235 bar. Our determination of the UCEP location is about 3°C lower than that reported previously by Paulaitis, et al. (46). However, the in situ nature of our NMR method allows us to precisely measure this UCEP temperature since we can determine the S_2LG phase line. These results indicate that our NMR technique can be greatly advantageous for solubility determinations near the UCEP. A more detailed analysis of our experimentally determined solubility data is now in progress.

Density and Temperature Effects on Collision Induced Scattering in Supercritical CO_2

In view of the importance of CO_2 in supercritical fluid extraction, we carried out an experimental study of the pressure and temperature effects on depolarized Rayleigh lineshapes in supercritical CO_2 (47). Collision induced scattering (6) (CIS) is of considerable interest because it is a fairly unique probe of intermolecular interactions. Depolarized Rayleigh spectra (DRS) of dense atomic fluid and the DRS of spherical molecules have been extensively studied because the entire DRS of these fluids may be attributed to collision induced effects. For linear triatomics the interpretation of the DRS is necessarily more complicated as the time dependence of the polarizability anisotropy of the molecule will contain contributions from both the permanent anisotropy of the molecule, whose time dependence arises from molecular reorientation, and the induced polarizability which arises from multi-body interactions. The part arising from the permanent anisotropy may be referred to as the allowed part and the induced component as the non-allowed part. Despite these complications, significant progress has been made in the study of collision induced effects on the DRS of linear triatomics.

The results of our study were as follows. We obtained experimental data on the density dependence of the DRS of carbon dioxide at temperatures both above and below the critical temperature. By using Madden's theories (48-51) and the analogous results from other linear triatomics [CS_2, COS] (17,18) as a guide, we showed the effects of CIS on the DRS of CO_2. Lastly, we showed how failure to adequately account for CIS in the DRS of linear triatomics can cause ambiguity in the interpretation of the information on molecular reorientation present in the DRS.

Acknowledgments

This work was partially supported by the Department of Energy under Grant DE-FG-82PC50800.

References

1. C. A. Irani and E. W. Funk, in "Recent Developments in Separation Sci ence," N. N. Li, Ed., CRC Press, Cleveland, Ohio, 1977, v. 3A, p. 171.
2. D. F. Williams, Chem. Eng. Science 36, 1769 (1981).
3. G. M. Schneider, Angew. Chem. Int. Ed. 17, 716 (1978).
4. G. Brunner and S. Peter, Ger. Chem. Eng. 5, 181 (1982).
5. J. Jonas, Science 216, 1179 (1982).
6. "Pressure - An Essential Experimental Variable in Spectroscopic Studies of Liquids," J. Jonas in "Phenomena Induced by Intermolecular Interactions," Ed. G. Birnbaum, Proceedings of NATO Advanced Workshop, Bonas, France, 1983; Elsevier, 1984.
7. E. S. Baker, D. R. Brown and J. Jonas, J. Phys. Chem. 88, 5425 (1984).
8. E. S. Baker, D. R. Brown, D. M. Lamb and J. Jonas, J. of Chem. and Eng. Data 30, 141 (1985).
9. D. M. Lamb and J. Jonas, Manuscript in preparation.

10. J. Jonas, Rev. Sci. Instrum. 43, 643 (1972).
11. D. M. Cantor and J. Jonas, J. Mag. Res. 28, 157 (1977).
12. R. J. Finney, M. Wolfe and J. Jonas, J. Chem. Phys. 67, 4004 (1977).
13. N. J. Trappeniers and K. O. Prins, Physica 33, 435 (1967).
14. W. J. Lamb and J. Jonas, J. Chem. Phys. 74, 913 (1981).
15. D. M. Cantor and J. Jonas, J. Mag. Res. 28, 157 (1977).
16. W. J. Lamb, G. A. Hoffman and J. Jonas, J. Chem. Phys. 74, 6875 (1981).
17. B. Hegemann and J. Jonas, J. Phys. Chem. 88, 5851 (1984).
18. B. Hegemann and J. Jonas, J. Chem. Phys. 82, 2845 (1985).
19. W. F. L. Dick and A. G. M. Hedley, in "Thermodynamic Functions of Gases," F. Din, Ed., Butterworths, London, 1962, v. 2, p. 88.
20. A. Michels and M. Geldermans, Physics 9, 967 (1942).
21. A. Sass, B. F. Dodge and R. H. Bretton, J. Chem. Eng. Data 12, 158 (1967).
22. H. Hamann, H. Richtering and U. Zucker, Ber. Buns. Phys. Chem. 70, 1084 (1966).
23. S. Chapman and T. G. Cowling, "Mathematical Theory of Non-Uniform Gases," Cambridge Univ. Press, Cambridge, 1970, 3rd Ed.
24. B. J. Alder, D. M. Gass and T. E. Wainwright, J. Chem. Phys. 53, 3813 (1970).
25. J. H. Dymond, Physica 75, 100 (1974).
26. J. Jonas, Ann. Rev. Phys. Chem. 26, 167 (1975).
27. J. Jonas in "NATO ASI on High Pressure Chemistry," H. Kelm, Ed., D. Reidel Publ. Co., Dordrechi, Holland, 1978, p. 65.
28. J. Jonas, Rev. Phys. Chem. Japan 50, 19 (1980).
29. D. Chandler, J. Chem. Phys. 60, 3500, 3508 (1974).
30. M. Wolfe, E. Arndt and J. Jonas, J. Chem. Phys. 67, 4012 (1977).
31. H. C. Andersen, D. Chandler and J. D. Weeks, Adv. Chem. Phys. 34, 105 (1976).
32. C. F. Curtiss and C. Muckenfuss, J. Chem. Phys. 26, 1619 (1957).
33. C. Muckenfuss and C. F. Curtiss, J. Chem. Phys. 29, 1259 (1958).
34. D. W. Rebertus and K. M. Sando, J. Chem. Phys. 67, 2585 (1977).
35. T. Boublik, Adv. Chem. Ser. 204, 173 (1983).
36. P. A. Monson and M. Rigby, Mol. Phys. 35, 1337 (1978).
37. P. A. Monson and M. Rigby, Chem. Phys. Lett. 58, 122 (1978).
38. J. C. Whitehead and D. E. Williams, J. Inst. Fuel 48, 397 (1975).
39. N. Berkowitz, "An Introduction to Coal Technology," Academic Press: New York, 1979.
40. W. Worthy, Chem. Eng. News 61, 35 (1983).
41. H. J. Parkhurst, Y. Lee and J. Jonas, J. Chem. Phys. 55, 1368 (1971).
42. D. J. Wilbur and J. Jonas, J. Chem. Phys. 55, 5840 (1971).
43. D. J. Wilbur and J. Jonas, J. Chem. Phys. 62, 2800 (1975).
44. L. Monchick and E. A. Mason, J. Chem. Phys. 35, 1676 (1961).
45. A. Knappwost, F. Ruhe, M. Raschti, H. Wochnowski and U. Ankara, Z. Phys. Chem. (Wiesbaden) 122, 143 (1980).
46. M. E. Paulaitis and M. McHugh, J. Chem. Eng. Data 25, 326 (1980).
47. K. Baker and J. Jonas, Manuscript in preparation.
48. T. I. Cox, M. R. Battaglia and P. A. Madden, Mol. Phys. 38, 1539 (1979).
49. T. I. Cox and P. A. Madden, Chem. Phys. Lett. 41, 188 (1976).
50. P. A. Madden and T. J. Cox, Mol. Phys. 43, 287 (1981).
51. P. A. Madden and D. J. Tildesley, Mol. Phys. 49, 193 (1983).

SUPERCRITICAL FLUID SOLVENT PROPERTIES AS A FUNCTION OF TEMPERATURE AND DENSITY MEASURED BY THE SOLVATOCHROMIC METHOD

S. L. Frye, C. R. Yonker, D. R. Kalkwarf, and R. D. Smith

Chemical Methods and Kinetics Section
Pacific Northwest Laboratory
(Operated by Battelle Memorial Institute)
Richland, Washington 99352

INTRODUCTION

In the past few years supercritical fluids have attracted interest as solvents for both analytical and chemical process applications. They possess interesting combinations of solvent properties, such as high diffusivity and liquid-like solvating properties which can be drastically changed with moderate changes in temperature and pressure, making them attractive for a variety of uses.

One hindrance to the further development of supercritical fluid extraction or chromatographic techniques is that relatively little is known about the dependence of solvent properties of supercritical fluids, and fluid mixtures, upon various physical parameters. This study of the interactions between solutes and supercritical fluid solvents was aimed at extending the understanding of supercritical fluids as solvents, and to help in the selection of the most appropriate fluid for a particular application.

EXPERIMENTAL

Absorption spectra were measured on a Cary model 1605 spectrophotometer used in the dual beam mode. The measurements using liquid solvents were made using 1 cm square quartz cells with a solvent blank in the reference beam. The vapor and supercritical fluid spectra were taken versus air in the reference beam.

A specially constructed high pressure cell was used in taking the spectra in the supercritical fluid solvents. This cell has a cylindrical stainless steel body approximately 1" in diameter which has a 3/16" diameter hole drilled along the axis. Two connections for 1/16" tubing are present to allow for inlet and outlet flow. Each end of the cell has a seat for a 1/4" diameter 1/4" thick quartz window and is threaded to accept a brass nut. A 1/4" o.d. Teflon o-ring is placed on each side of each window to provide cushioning and a gas tight seal. The optical path between the windows was approximately 1/4". The absorption cell was wrapped with heating tape, insulated and equipped with a thermocouple. This arrangement allowed temperature regulation to within ±0.5 C.

A Varian 8500 syringe pump was used to supply the supercritical fluid solvent at the appropriate pressure. The pump was connected to the cell via a Rheodyne valve equipped with a 10 μl sample loop. A pressure transducer was connected to the cell outlet to allow accurate pressure measurement.

The experiments were conducted as follows: the sample was loaded in to sample loop and the valve switched to allow fluid from the pump to flow to the cell through the loop. A shut-off valve at the cell outlet was opened to allow solvent flow through the cell and the absorbance at a selected wavelength was measured to detect the appearance of the sample in the cell cavity. Often it was necessary to

partially purge the cell with additional solvent to decrease the sample concentration to the point that the absorbance measurement was on scale. When a usable concentration of sample had been obtained the outlet valve was closed and the absorption spectrum was taken under isobaric and isothermal conditions. After a scan the pressure or temperature was increased to the next level and the cell allowed to equilibrate at the new conditions before the next measurement. In all cases the spectrum of the pure fluid was also recorded to insure that there was no interference with the spectrum of the solute.

RESULTS AND DISCUSSION

Since interest centers on the specific interactions between solute and solvent, and how those interactions change as the density and composition of the supercritical fluid solvent are varied, an experimental technique is needed which is sensitive to the cybotactic environment of the solute. One such technique is the solvatochromic method, which probes the effect of solvent on the optical absorption spectrum of the solute molecule (1).

Using the solvatochromic method to study solvent effects of supercritical fluids is particularly efficacious in view of the extensive work of Taft and coworkers in measuring the solvatochromic shifts of a large number of solute molecules in a wide range of liquid solvents (2). They have been successful in developing a π^* solubility scale which encompasses a wide range of solute types and which can account for variance in several solvent properties, including polarity, polarizability, hydrogen bonding ability, etc.

The π^* polarizability scale was originally developed from observations of solvent effects on $n \rightarrow \pi^*$ and $\pi \rightarrow \pi^*$ transitions in the probe molecules. By using a select group of solutes and solvents which minimized hydrogen-bonding, Taft and co-workers were able to relate solvent polarity to relative shifts in the position of the absorption maximum. These data were primarily dependent on the interaction between solute and solvent dipoles. Further refinements have since been made to account for solvent-solvent interaction, the presence of induced dipoles, and hydrogen bonding between solute and solvent (3).

Since the π^* scale is well established for the study of conventional solvents it may afford a convenient basis for the comparison of liquid and supercritical solvents. Further, by determining the various scale parameters for these fluids it should be possible to obtain some insight into the specific solvation mechanisms involved, and how those mechanisms change as the solvent composition and conditions are altered.

The compounds 2-nitroanisole (2NA) and 4-ethylnitrobenzene (4ENB) were chosen to be the initial probe molecules in our initial solvatochromic studies of supercritical fluid solvents. These compounds have been previously used by Taft et al. in the studies of conventional liquid solvents, thus making it easier to integrate supercritical fluid solvents into the π^* solvent polarity scale. It is also advantageous that these compounds are liquids and have absorption maxima at convenient wavelengths in the UV.

The maxima of the absorption spectrum of each of these compounds are shifted in wavelength when in liquid solvents of varying polarities (Table 1). The position of the absorption band of the vapor (essentially a solvent with no polarity or hydrogen bonding ability) is used as a reference. As the solvent becomes more polar the absorption maximum is shifted to longer wavelengths (lower energies). This type of shift indicates that the excited electronic state is being stabilized

TABLE 1. Wavelength of Absorption Maximum of 2NA and 4ENB in Various Solvents

Solvant[a]	2NA Observed[b]	2NA π^*[c]	4ENB Observed	4ENB π^*
Vapor	286	285	250	251
CO_2(a)	295	--	257	--
N_2O(a)	297	--	--	--
$CClF_3$(a)	299	--	--	--
NH_3(a)	303	--	260	--
Pentane(d)	306	305	263	265
Tetrahydrofuran	318	312	273	275
Acetonitrile	324	325	276	278
Methanol	322	322	272	275

(a) The supercritical fluids (CO_2, N_2O, $CClF_3$, and NH_3 had $T_r = 1.01$ and $P_r = 1.05$.
(b) Observed wavelength of absorption maxima, in nm.
(c) Predicted by π^* scale using parameters from Table 2.
(d) Predicted wavelength using parameters for heptane.

with respect to the ground electronic state, thus decreasing their energy gap. These results are in accord with the prediction of the π^* model when the proper coefficients are used for each of the solutes and solvents (Table 2) (4).

Having established the behavior of the probe molecules in conventional solvents, it is possible to compare their behavior in some common supercritical fluids. It is evident from Table 1 that supercritical fluid solvents at moderate reduced temperatures and pressures have relative solvating abilities in accordance with their polarities. The less polar fluids CO_2, N_2O, and $CClF_3$ (Freon-13) shift the absorption maxima to an intermediate position between that measured in the vapor phase and pentane. NH_3 is more polar and the wavelength of the maximum falls close to that of pentane.

The interest in using supercritical fluids as solvents for extraction processes and chromatography is in great extent due to the fact that it is possible to change the solvent properties of the fluid by changing the density and temperature. A large part of the interest in using the solvatochromic method to study these solvents is to see if it is possible to observe and quantify these changes in solvating ability via the absorption shift.

TABLE 2. π^* Solubility Scale Parameters

Solvent	π^*	Solute	ν_o (cm^{-1})	-s
Vapor (4)	-1.06	2NA (2)	32.56 kK	2.428
Heptane (4)	-0.08	4ENB (2)	37.60 kK	2.133
Tetrahydrofuran(4)	0.58			
Acetonitrile(4)	0.75			
Methanol (3)	0.60			

Figure 1 shows that the wavelength of the absorption maximum changes most rapidly at pressures just above the critical pressure. This observation can be explained by examining the relationship between pressure and density is a non-linear function of pressure, and changes most rapidly at reduced pressures near 1. The data are re-plotted in Figure 3 to illustrate the relationship between the energy of the transition (in wave numbers) and the fluid density. This plot also contains data obtained by maintaining a constant pressure and varying the temperature to change the density. It is apparent from this data that fluid density, and not temperature, is of primary importance in determining the amount of spectral shift. This correlation with fluid density is in agreement with the predictions of numerous solubility studies. Finally, Figure 4 shows how the absorption maximum varies with pressure for 2NA in NH_3.

Clearly, the solvatochromic method holds promise for comparison of supercritical fluid solvents with conventional liquid solvents, due to sensitivity to changes in solvation arising from varying the density of the fluid solvent. By using the data on pure fluid solvents as a foundation it should be possible to extend this work to the study of mixed supercritical fluid solvent systems. Since this technique probes the cybotactic environment of the solute it should be feasible to determine how the solvating power of a fluid changes as small amounts of a modifier are added.

ACKNOWLEDGMENTS

This work was supported by the U.S. Department of Energy, Office of Basic Energy Sciences, under contract DE-AC06-76-RLO-1830.

REFERENCES

1. P. Suppan, J. Chem. Soc. (A), 3125, (1968).

2. M. J. Kamlet, J. L. Abboud, and R. W. Taft, J. Am. Chem. Soc., 99, 6027, (1977).

3. M. J. Kamlet, J. L. Abboud, M. H. Abraham, and R. W. Taft, J. Org. Chem., 48, 2877, (1983).

4. J. L. M. Abboud, G. Guihenuef, M. Essfer, R. W. Taft, and M. J. Kamlet, J. Phys. Chem., 88, 4414, (1984).

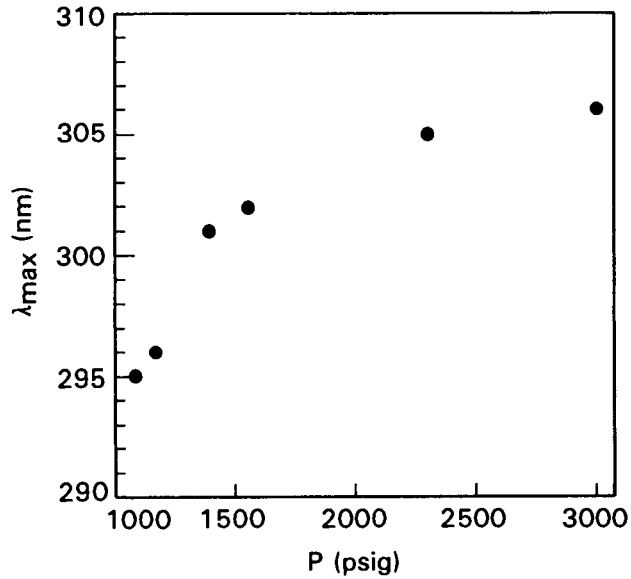

FIGURE 1. 2-Nitroanisole in CO_2. Temperature = 50°C.

TYPICAL PRESSURE-DENSITY BEHAVIOR

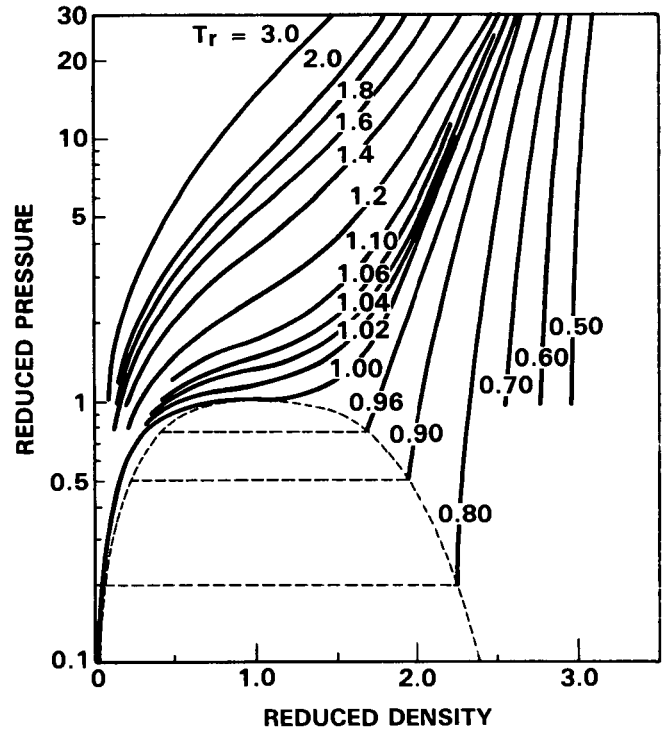

T_r = REDUCED TEMPERATURE

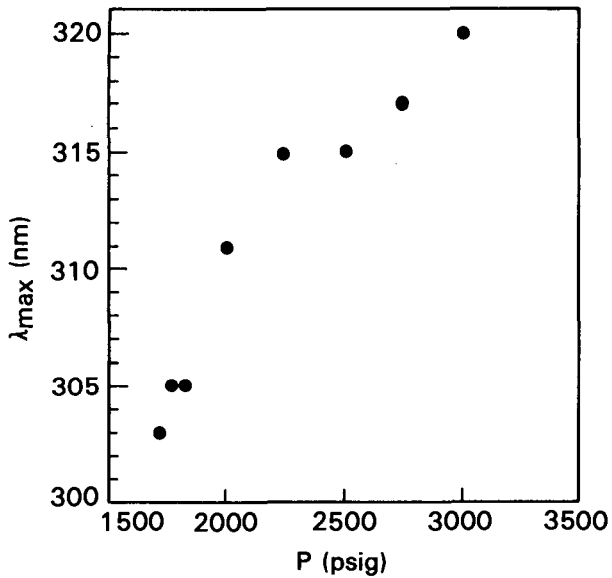

FIGURE 4. 2-Nitroanisole in NH_3. Temperature = 140°C.

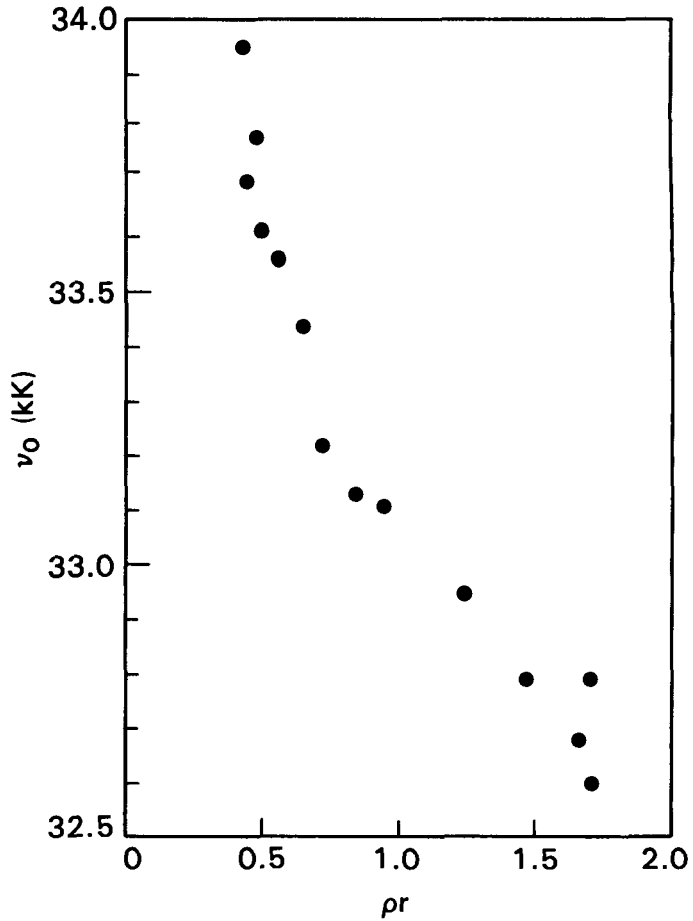

FIGURE 3. 2-Nitroanisole in CO_2.

Mixed Supercritical Solvents for Selective Solubility Enhancement

J. G. Van Alsten and C. A. Eckert

Department of Chemical Engineering
University of Illinois
Urbana, IL 61801

Supercritical fluids have generated a great deal of interest in the chemical engineering community for a variety of applications, including enhanced oil recovery, resid upgrading, and extraction (1). This being the case, we have been involved in an intensive program designed to understand both qualitatively and quantitatively the complex phase behavior inherent in mixtures of solutes dissolved in supercritical solvents.

This program involves measurements on thermodynamic modeling of selected supercritical systems. Our work first involved analysis of solutes dissolved in pure supercritical fluids to determine what differences, if any, solute nature had on the solubility behavior. Our data analysis requires two properties of the solute: first, its solubility in the selected supercritical fluid, second, the solute sublimation pressure at system temperature. Combining these two quantities yields the enhancement factor

$$E = \frac{y_2 P}{P_2 sat} \qquad 1)$$

which is simply a dimensionless solubility that scales out the saturation pressure contribution to the solubility. Comparison of enhancement factors (not solubilities!) yields the true solution behavior of the various solutes used in these studies.

We have compared enhancement facors for a variety of solid compounds of different polarities and functionalities in pure supercritical fluids and have found that the solution behavior is relatively insensitive to the chemical nature of the solute species. Thus, as Figure 1 illustrates, the solution behavior of the solutes phenanthrene and acridine is virtually identical, even though acridine has a relatively large dipole moment at 2.1 Debeyes and is a heterocyclic analogue to the base pyridine. To understand why this is so, a rough order of magnitude calculation was performed to determine the relative magnitudes of the various forces involved in this system. Table 1 shows that the contribution from polar forces, e.g. those dipole/induced dipole forces between the acridine and CO_2 molecules, is only one one hundredth that of the contribution from non-specific van der Waals forces, which should be nearly identical for the acridine/CO_2 and phenanthrene/CO_2 systems. Since the forces involved in solutions of pure fluids arise almost exclusively from these van der Waals forces, one expects the solubility behavior to be the same in the class of solutes we have studied.

It is apparent that to induce some differentiability into the solution behavior, one will need to either use some associating fluid (such as ammonia) or modify the supercritical fluid by adding chemical "entrainers" to the solution. We have begun such studies in which dilute (1-5%) concentrations of polar entrainers are added to the bulk supercritical phase (CO_2). Dilute solutions are necessary for two reasons. First and foremost is the fact that dilute solutions allow us to operate over a broad range of pressures and tempeatures without having to be concerned with separation into entrainer-rich and CO_2-rich phases; we can be assured that we always have a single, homogeneous phase. The second reason concerns the fact that while we would like to modify the fluid's solution behavior, we also wish to leave its useful phase behavior as intact as possible.

The two entrainers chosen were methanol and acetone. Both are small, relatively polar molecules which go into solution with CO_2 readily (2,3). Methanol, with its hydroxyl proton, is also a likely candidate for hydrogen bond formation with proton accepting species.

The entrainer effect can be quite large, as seen in Figure 2, where we show the solubility increase of the solute acridine in doped SCF's. This figure shows an over 500% increase in the solute's solubility over that in a pure supercritical solvent. Of even greater interest is the fact that this solubility increase is quite sensitive to the chemical nature of the solute species involved; Figure 3 illustrates this behavior. Here, the highly polar species acridine and fluorenone are seen to have solubilities greatly promoted by the presence of the entrainer methanol in supercritical CO_2. The much less polar species dibenzofuran is promoted to a much lesser extent, and the non-polar species phenanthrene and fluorene show virtually no solubility promotion in the entrained solvent. This behavior is in marked contrast to that of pure SCF's, where there is little if any solvent selectivity to these solute species.

As Table 1 illustrates, the relative magnitudes of the dipole-dipole and dipole-forces between a polar solute and polar entrainer molecule do not appear to be great enough to account for this solubility increase if the entrainer were randomly dispersed within the fluid. This suggests an aggregation or clustering of the entrainer species around the solute molecule in solution. Spectroscopic information is needed, however, to confirm this speculation.

REFERENCES:

(1) Paulaitis, M. P.; Krukonis, V.; Reid, R.; Kurnik, R.; Reviews in Chemical Engineering, 1 (2), 1983, 179.

(2) Semenova, A.; Emel yanova, E.; Tsimmerms, S.; Tsiklis, D.; Russ. J. Phys. Chem., 53 (10), 1979, 1428.

(3) Katayama, K.; Ohgaki, K.; Maekawa, G.; Goto, M.; Nagano, T.; J. ChE Japan, 8 (2), 1975, 89.

(4) Prausnitz, J. M.; "Molecular Thermodynamics of Fluid Phase Equilibria", copyright 1969 Prentice-Hall, Englewood Cliffs, NJ.

TABLE 1

RELATIVE MAGNITUDES OF INTERMOLECULAR FORCES (4)

System: acridine/CO_2/acetone

CO_2 disp	CO_2 ind dip	acetone disp	acetone ind dip	acetone dip/dip
1	.01	.89	.30	.27

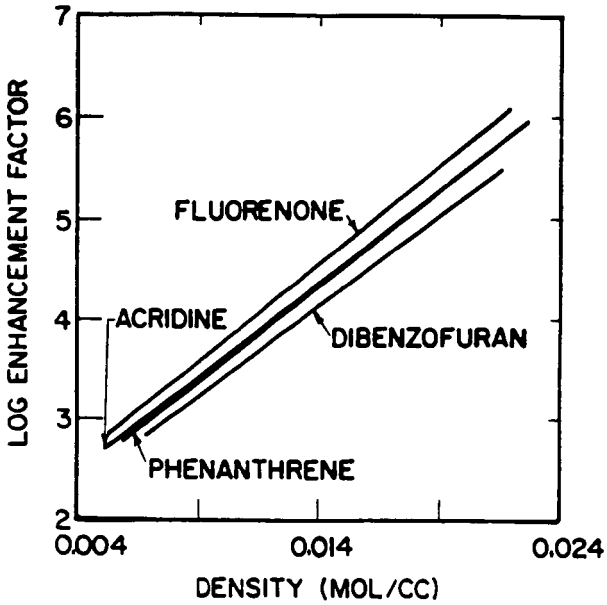

ENHANCEMENT FACTOR FOR SEVERAL SOLUTES IN CO_2 AT 323 K

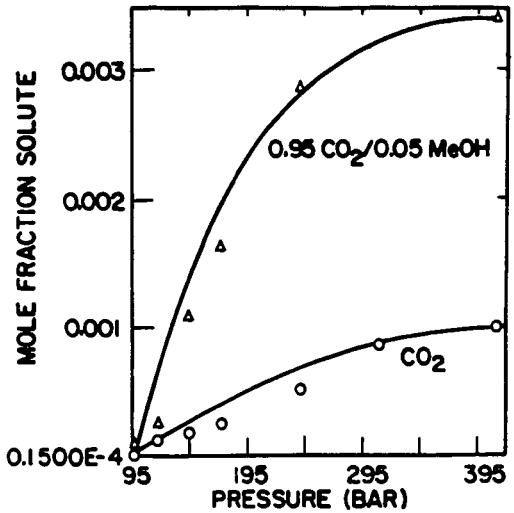

INCREASE IN SOLUBILITY WITH ENTRAINER-DOPED SOLVENT SYSTEM : ACRIDINE @ 323 K

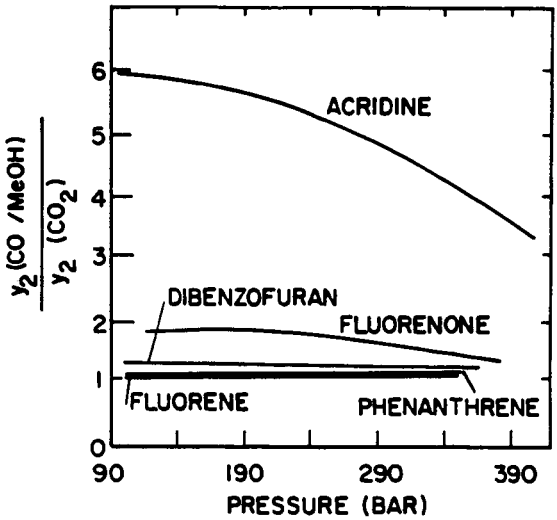

ENTRAINER EFFECT WITH VARIOUS SOLUTES
5 mole % MeOH/CO_2 @ 323 K

ELECTROCHEMISTRY IN SUBCRITICAL AND SUPERCRITICAL WATER

W. M. Flarsheim, A. C. McDonald, A. J. Bard, K. P. Johnston,
Departments of Chemical Engineering and Chemistry,
The University of Texas, Austin, TX 78712

Introduction

Supercritical fluids have received significant interest recently because of their unique solvent properties. Gases such as carbon dioxide and ethylene have been used to perform a number of difficult separations. Some of these processes, for example the decaffeination of coffee, have been commercialized (1).

Water has not been studied extensively for use as a supercritical solvent because of the high temperature and pressure of its critical point (T_c = 374°C, P_c = 221 bar). We are performing electrochemical research in supercritical water to take advantage of its unusual properties. The areas of study include the effect of temperature on the electrochemical potential of ions in water and the electrochemical reaction of organic compounds in aqueous solution.

The chemical behavior of an ion in water is of course influenced by water molecules that are oriented around it. A change in the structure of the solvation sphere around an ion will affect the electrochemical potential of the ion. Such a change in structure can be achieved by heating water to the critical region where the internal structure of hydrogen bonding is very sensitive to temperature changes. In this region, the electrochemical potential can also be a strong function of temperature. A study of these potential shifts should provide insight into the structure of solvation spheres in water and of water itself.

At high temperature, the breakdown of hydrogen bonding in water greatly reduces the dielectric constant. At the critical point, the dielectric constant of water is 3, approximately the same as that of benzene. Not surprisingly, water becomes miscible with non-polar organics at high temperatures. In the miscible region, it is possible to react organics electrochemically without using the more toxic and expensive organic solvents that are necessary for dissolution at 25°C. While many compounds will decompose in high temperature water, others, which are not active at normal conditions, will become subject to electrochemical attack at high temperature.

Though no definite predictions can be made, supercritical water appears to be a promising area for study. A cell has been designed which will operate at supercritical conditions, and preliminary data have been obtained for electrolyte solutions.

Experimental

The high temperature section of the electrochemical cell is made of an aluminum oxide ceramic. The volume of heated solution is less than 1 cm^3, so the stored energy of the system is very small. All measurements were made with the solution stationary in the cell, but a high pressure pump allows the cell to be flushed with fresh solution. This prevents reaction products from contaminating the electrolyte. The platinum working and silver reference electrodes are in close proximity in the heated zone. The working electrode area is approximately 3 x 10^{-4} cm^2. The platinum counter electrode is in a cool region downstream from the heated zone. All seals are made of teflon, and are in unheated parts of the cell.

Results

Cyclic voltammetry has been carried out in solutions of 0.05M H_3PO_4, 0.2M $NaHSO_4$, and 0.2M KCl. The pressure was held at 240 bar while the temperature was varied. The scan rate was 200 mV/sec.

In 0.05M H_3PO_4, the potential difference between the evolution of hydrogen and

oxygen declined from 1.7 V at 25°C to 1.0 V at 375°C. At high temperature, the solution resistance increased dramatically indicating the dissociation of the acid was declining.

In 0.2M $NaHSO_4$, the potential difference between the evolution of hydrogen and oxygen declined from 2.0 V at 25°C to 1.3 V at 375°C.

In 0.2M KCl, the potential difference between the evolution of hydrogen and oxygen declined from 1.8 V at 25°C to 1.6 V at 300°C. The potential difference between the chloride/chlorine couple and oxygen declined from 0.2 V to <0.1V over this same temperature range.

Summary

The data presented here represent the first steps into a new area of electrochemistry. Much more data will be necessary before any major conclusions can be drawn. Even so, these results do show that electrochemistry can be carried out under near critical and supercritical conditions, and that there are significant changes in the behavior of ions in solution.

References

1. M. E. Paulaitis, J. M. L. Penninger, P. Davidson, and R. D. Gray, Chemical Engineering at Supercritical Fluid Conditions, Ann Arbor Science (1983).

ORGANIC CHEMISTRY IN SUPERCRITICAL FLUID SOLVENTS: PHOTOISOMERIZATION OF trans-STILBENE

Tetsuo Aida and Thomas G. Squires

Applied Organic Chemistry
Energy & Minerals Resources Research Institute
Iowa State University
Ames, Iowa 50011

INTRODUCTION

The unusual solvent properties of supercritical fluids (SCF's) have been known for over a century (1). Just above the critical temperature, forces of molecular attraction are balanced by kinetic energy; and fluid properties, including solvent power, exhibit a substantial pressure dependence. Many complex organic materials are soluble at moderate pressures (80 to 100 atmospheres); and SCF solvent power increases dramatically when the pressure is increased to 300 atmospheres. The pressure responsive range of solvent properties thus attainable has provided the basis for investigating the fundamental nature of molecular interactions and, more recently, for exploitation of supercritical fluids in areas of applied research (2,3).

In the latter activity, supercritical fluids have been utilized extensively in the thermochemical solubilization of coal (4), for selective extraction of naturally occurring materials (5,6), and in various separation techniques including destraction (7) and supercritical fluid chromatography (8,9). The physicochemical principles underlying these applications have also been investigated (10). In view of the high level interest in manipulating complex organic mixtures with supercritical fluids, it is surprising that these fluids have seen little use as solvents for organic reactions (11,12). The pivotal role of solvent properties in controlling the course and rate of chemical reactions is well established (13); and, thus, the same kind of pressure responsive solvent-solute interactions which control extractions and separations in SCF's can be expected to direct chemical pathways and influence reaction rates.

Moreover, much of our understanding of the nature of chemical reactions has been derived by observing the responses of these processes to changes in solvent properties. While investigations of this type have been highly productive, interpretation of the results has often been blurred by uncertainties inherent in the experimental approach. Heretofore, liquid solvents have been used in these investigations, and solvent properties have been changed by adjusting the solvent composition. Unfortunately, no quantitative relationship between bulk solvent properties and chemical phenomena has emerged, presumably due to selective solvent-solute interactions which result in differences between bulk solvent composition and microscopic solvent composition (13).

In contrast to liquid solvents, the properties of a single SCF solvent can be altered over a wide range through modest manipulations of pressure and/or temperature. Thus, SCF's provide an opportunity to investigate the effects of solvent properties on chemical reactions without changing the solvent composition. Experimentally, in order to

induce the greatest response of solvent properties to changes in pressure, it is generally best to operate at a constant reduced temperature, T_R, between 1.0 and 1.1 and to vary the reduced pressure, P_R, between 1.0 and 3.0 (14).

For several reasons, we chose carbon dioxide for these initial investigations. In the first place, the properties of supercritical carbon dioxide are well known, and the solubility of a relatively large number of organic materials have been examined in this medium. Secondly, although carbon dioxide is interactive with solute molecules, it is generally unreactive. Finally, the supercritical working range ($1.0 < T_R < 1.1$), 31.5 to 60°C, is experimentally convenient; and many organic reactions have been extensively investigated in this temperature range.

Investigations of organic reactions in supercritical solvents are subject to several constraints, one attributable to supercritical fluid properties and others imposed for interpretive and experimental simplicity. Because supercritical fluid properties are affected by changes in temperature, a reaction should be selected which does not require heat for initiation and is not highly exothermic. Secondly, for experimental simplicity and clarity of interpretation, a clean, well understood reaction should be chosen; and one should expect an experimentally observable response to changes in pressure. Finally, a unimolecular reaction which produces a single product obviates the complication of controlling the concentrations of two reactants and simplifies product analysis. The photoisomerization of trans-stilbene meets these requirements.

The photoisomerization of stilbene is one of the most extensively studied and best understood photoreactions (15). Solvent effects have been thoroughly investigated for both the direct and photosensitized isomerizations, and a model has been developed which attributes these effects to solvent viscosity (16). Increased viscosity inhibits direct photoisomerization of the cis isomer, but facilitates that of trans-stilbene. As a result, the cis/trans ratio of the photostationary state increases with increasing solvent viscosity. The wide range of viscosities which are attainable by pressure manipulation of supercritical carbon dioxide provides an excellent opportunity to probe the effect of viscostiy on stilbene photochemistry in the same solvent.

EXPERIMENTAL

Construction of the SCF photochemical reactor and experimental techniques are described elsewhere (12). Photoisomerizations were carried out using a 450 watt Hanovia medium pressure mercury source, and each reaction was followed to the photostationary state by gas chromatographic determination of the cis/trans ratios.

RESULTS & DISCUSSION

A widely used method for assessing supercritical fluid phenomena consists of comparing physical and chemical behavior above the critical point with corresponding behavior in the subcritical liquid. Because this approach (unrealistically) seeks to observe discontinuous behavior between states, the results of such experiments are often ambiguous. In the present study, we have compared the photoisomerization of trans-stilbene in subcritical and supercritical CO_2; and, as a

model for condensed phase behavior, we have also carried out these isomerizations in cyclohexane. In all three systems, we have probed and compared the effects of temperature, concentration, and, most significantly, pressure on the photostationary state as reflected in the cis/trans ratio. The results from these experiments are shown in Tables 1 and 2 and are plotted in Figures 1 through 3.

From the results obtained in cyclohexane (Table 1), it is clear that, in the condensed phase, we can expect very little effect on the photostationary state due to changes in temperature or concentration. On the other hand, these factors cause large changes when the reaction is carried out in liquid or (especially) SCF CO_2. The contrast in behavior is even more apparent in Figures 1 and 2.

Table 1. Photoisomerization of trans-Stilbene in Cyclohexane[a]

Initial Concentration (mg/ml)[b]	Temperature (°C)	Irradiation Time (Minutes)	Photostationary State (cis/trans)
2.14	21.7	70.0	6.1
2.14	40.0	70.0	6.1
1.07	21.7	20.0	6.9
1.07	40.0	30.0	6.9
0.50	21.7	10.0	6.4
0.50	40.0	15.0	6.7
0.25	21.7	10.0	6.4
0.25	40.0	5.0	6.6

a. Direct irradiation with a Hanovia 450 watt medium pressure mercury vapor lamp.
b. Pure trans-stilbene was used.

Table 2. Photoisomerization of trans-Stilbene in Carbon Dioxide[a]

Initial Concentration (mg/NL)[b]	Reactor Concentration (mg/ml)[c]	Temperature (°C)	Photostationary State (cis/trans)
2.00	0.98	25	8.63
2.00	0.87	40	8.68
0.80	0.39	25	7.15
0.40	0.20	25	6.42
0.40	0.17	40	6.73
0.28	0.13	35	5.66
0.28	0.12	40	6.54
0.28	0.11	50	7.04
0.24	0.10	40	6.29
0.12	0.052	40	4.80

a. Irradiation in a flow reactor with a 450 watt Hanovia medium pressure mercury vapor lamp.
b. Pure trans-stilbene was used. Normal liter (NL): the quantity of CO_2 which has a volume of 1 liter at 25°C and 1 atmosphere.
c. Calculated from the reported density of pure CO_2.

In Figure 3 is shown the effect of pressure on the cis/trans ratio. While there is a noticeable effect on liquid CO_2, the dramatic response of the ratio to decreases in pressure gives us a clear signal that we can expect to manipulate chemical pathways, rates, and equilibria in the SCF state. This will be the focus of future studies.

ACKNOWLEDGEMENT

We wish to thank Professor R. S. Hansen and Dr. C. G. Venier for helpful discussions. We gratefully acknowledge the support of Iowa State University through the Energy & Minerals Resources Research Institute.

REFERENCES

1. Hannay, J.B.; Hogarth, J. J. Proc. Royal Soc. (London) Ser. A **1879**, 29, 324.

2. Paulaitis, M.E.; Krukonis, V.J.; Kurnik, R.T.; Reid, R.C. Rev. in Chem. Eng., **1983**, 1(2), 179.

3. Johnston, K.P. in "Kirk-Othmer Encyclopedia of Chemical Technology"; John Wiley & Sons: New York, 1984.

4. Maddocks, R.R.; Gibson, J.J. J. Chem. Eng. Prog. **1977**, 73(6), 59.

5. Caragay, A.B. Perfumer Flavorist, **1981**, 6(4), 43.

6. Hubert, P.; Vitzthun, O.G. Angew. Chem., Int. Ed. Engl. **1978**, 17, 710.

7. Zosel, K. Angew. Chem., Int. Ed. Engl. **1978**, 17, 702.

8. Meyers, M.N.; Giddings, J.C. Prog. Sep. Purif., **1970**, 3, 133.

9. van Wasen, U.; Swaid, I.; Schneider, G.M. Angew. Chem., Int. Ed. Engl. **1980**, 19, 575.

10. Schneider, G.M., ibid., **1978**, 17, 716.

11. Hyatt, J.A. J. Org. Chem. **1984**, 49, 5097.

12. Squires, T.G.; Venier, C.G.; Aida, T. Fluid Phase Equil. **1983**, 10, 261.

13. Reichardt, C. J. Pure & Appl. Chem. **1982**, 54, 1867.

14. Bartmann, D.; Schneider, G.M. J. Chromatogr. **1973**, 83, 135.

15. Saltiel, J.; Charlton, J.L. in "Rearrangements in Ground and Excited States, Vol. 3"; Academic Press: New York, 1980, pp. 25-89.

16. Saltiel, J.; D'Agostino, J.T. J. Am. Chem. Soc. **1972**, 94, 6445.

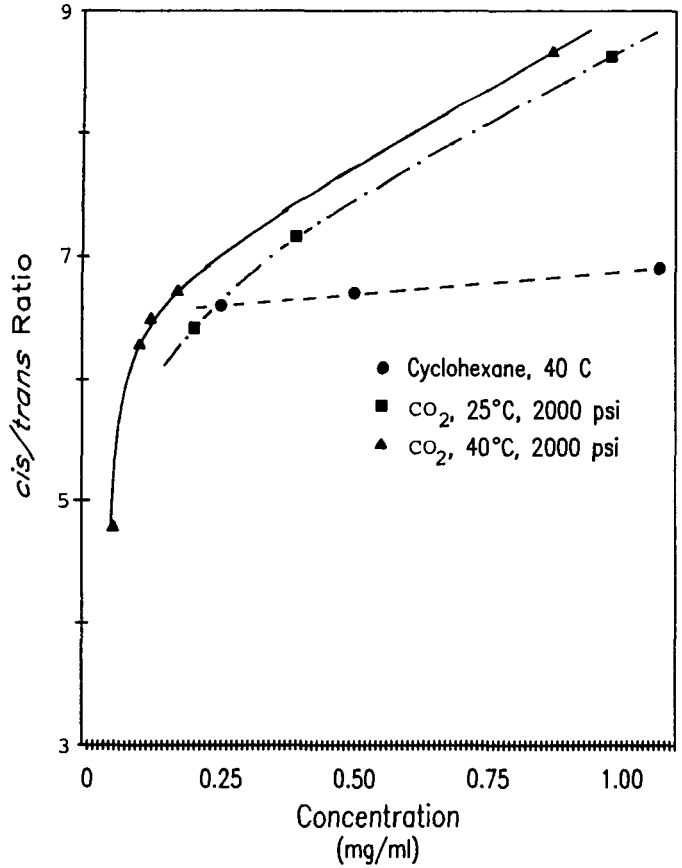

Figure 1. Concentration Effects in the Photo-isomerization of trans-Stilbene.

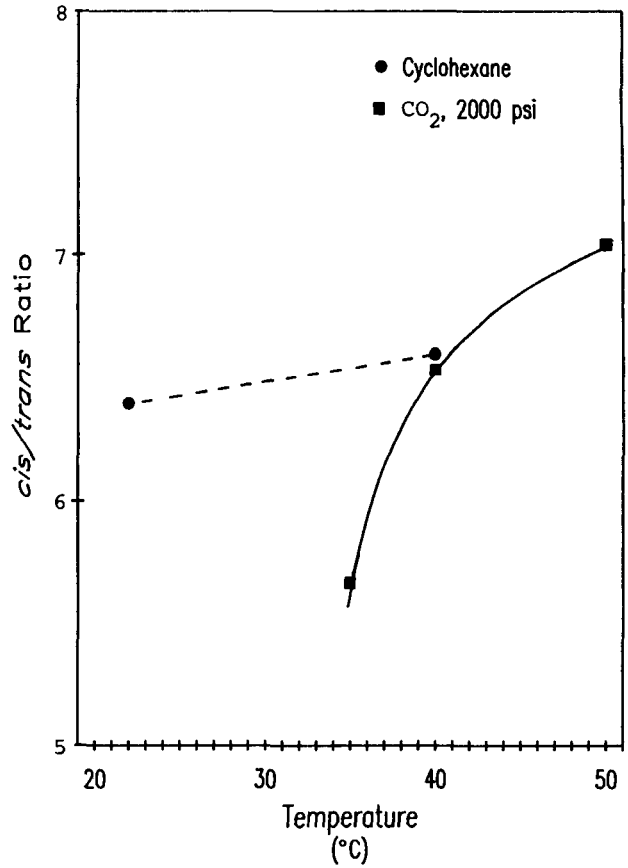

Figure 2. Temperature Effects in the Photo-isomerization of trans-Stilbene.

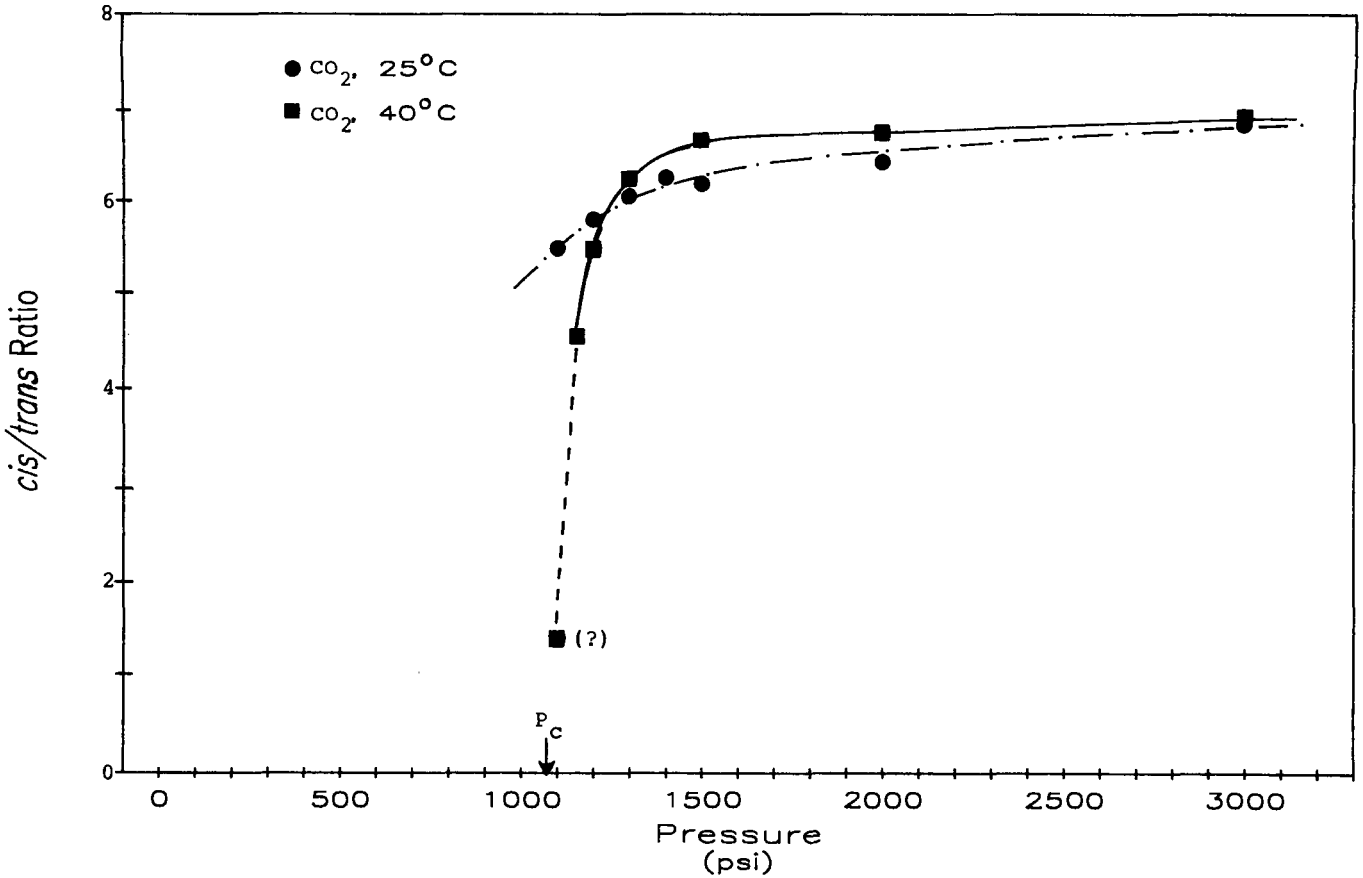

Figure 3. Pressure Effects in the Photoisomerization of trans-Stilbene.

EFFECTS OF SUPERCRITICAL SOLVENTS ON THE RATES OF HOMOGENEOUS CHEMICAL REACTIONS

K. P Johnston and S. Kim
Department of Chemical Engineering
University of Texas, Austin, TX 78712

Discussion

A number of recent reviews describe supercritical fluid extraction (1,2,3), however, the literature contains relatively few examples where supercritical fluid solvents have been used to modify or control reaction rate constants. Liquid phase reactions have been studied over wide pressure ranges, e.g. 1-10 kbar, to determine activation volumes, i.e. the pressure derivative of the rate constant. These studies essentially ignore the highly compressible near supercritical region where activation volumes can become infinite, either positively or negatively.

It is ironic that the large growth in SF extraction at the Max Planck Institute in Germany in the 1960's was the result of a serendipitous discovery of the solvent power of supercritical ethylene during the "Aufbau" reaction of triethylaluminum with ethylene (4). The literature contains few examples where supercritical fluids have been used as a medium to modify or control reaction rate constants (5,6,7).

Simmons and Mason (7) observed an abrupt decrease in $\Delta v^{\neq}$ near the critical conditions for the cyclic dimerization of C_2F_3Cl. It is due to the large negative partial molar volume of the dimer in the transition state. At 120°C, the rate constant doubled for a pressure increase from 43 to 53 bar. Paulaitis (6) measured activation volumes as low as -500 cc/mol for the Diels-Alder cycloaddition of isoprene and maleic anhydride in CO_2. The rate constant increased about 60% for a change in pressure of several bar. The pronounced solvent effect is due to the large dipole moment of the transition state, which is on the order of 3-7 Debye for other dienes with maleic anhydride (8).

The objective is to measure and to predict the effects of supercritical fluid solvents on reaction rate constants. In the near critical region, all of the density dependent variables such as the dielectric constant, refractive index, fugacity coefficient, and solubility parameter are extremely strong functions of temperature and pressure. This sensitivity, which is used advantageously in supercritical fluid extraction, could also be exploited in reaction processes. For example, rate constants could be changed orders of magnitude using modest changes in the temperature and pressure in the critical region. A UV-visible spectroscopic technique has been applied to supercritical fluids for the first time to determine the solvent polarity as a function of temperature and pressure. Solvent polarity scales based on solvatochromism, i.e., shifts in the absorption wavelength of indicator dyes caused by the solvent, are used commonly to correlate and to predict rate constants for liquid phase reactions. Novel processes could be developed using supercritical fluid solvents to achieve and control the desired selectivity in parallel reactions, the yield in reversible reactions, and to recover and purify reaction products efficiently using supercritical fluid extraction.

Conclusions

For dyes such as phenol blue, solvatochromic shift data provide a sensitive indication of the structure and polarity of supercritical fluid solvents. The polarities of supercritical ethylene and liquid hexane become equivalent for a density ratio of C_2/C_6 of 2.7 since the latter is more polarizable. At 25°C and 66 bar, the data were used to predict that the activation volume is -5000 cc/mol for the Menschutkin reaction of tripropylamine and methyl iodide. This large negative value is due to the high compressibility of SF ethylene in the critical region. These results suggest that rate constants may be altered markedly in SF solvents using small changes in

temperature and pressure.

The theory of solvent effects on electronic spectra can be extended to the SF state by including the effects of the isothermal compressibility. The local density of the SF solvent about the solute can be obtained by comparing the experimental E_T with the intrinsic value, $E_T°$, which is calculated straightforwardly for incompressible liquids. At the bulk density, the polarity of the SF solvent is equivalent to that of a hypothetical reference liquid at the local density. The specific polarity, which is due to hydrogen bonding, may be obtained by comparing this hypothetical reference fluid with the experimental data. For CF_3H, the specific polarity appears to be less sensitive to density than the intrinsic polarity. The understanding of the polarity of SF solvents at the microscopic level will benefit the development of both extraction and reaction process at SF conditions.

References

1. Paulaitis, M.E.; Krukonis, V.J.; Kurnik, R.T.; Reid, R.C., Rev. in Chem. Engr., 1(2), 179-250 (1983).

2. Johnston, K.P., "Kirk-Othmer Encyclopedia of Chemical Technology," John Wiley and Sons, Inc., New York (1984).

3. MuHugh, M.A., "Extraction with Supercritical Fluids," in "Recent Developments in Separation Science," Li, N.N.; Carlo, J.M., Ed.; CRC Press, Inc.: Boca Raton, FL, vol. IX, 1984.

4. Zosel, K., Angew. Chem. Int. Ed. Engl., 17, 702 (1978).

5. Randall, L.G., Sep. Sci. Technol., 17, 1 (1982).

6. Alexander, G.; Paulaitis, M.E., AICHE Annual Meeting, #140 d, San Francisco (1984).

7. Simmons, G.M.; Mason, D.M., Chem. Eng. Sci., 27, 89 (1972).

8. Eckert, C.A.; Hsieh, C.K.; McCabe, J.R., AICHE J., 20(1), 20-36 (1974).

Flow Adsorption Calorimetry with Supercritical Fluids on Silica Gel

Edward M. Arnett, B. Chawla[+], Elaine A. Dwyer, and Charles H. Lochmuller

Department of Chemistry
Duke University
Durham, North Carolina 27706

The supercritical state has long held a fascination for chemists as a "fourth state of matter."[1,2] Recently, it has been recognized that supercritical extractants are also of industrial value and play an important role in geochemical and extraterrestrial chemistry.[3,4] Of particular significance is the use of supercritical carbon dioxide for tertiary oil recovery, coal extraction, and chromatography in all of which supercritical fluids interact with solid phases.[5-8] In the course of a thermometric study of solid acids with basic solutions we became interested in determining heats of adsorption by flow calorimetry and extending this to elevated temperatures and pressures.

The apparatus shown in Figure 1 may be assembled, for the most part, from readily available components following recent accounts of high pressure, and high temperature flow calorimeters assembled for heats of mixing.[9-11]

After preliminary calibration of the calorimeter under various batch conditions by heats of solution of KCl and $BaCl_2$ in water[12] and heats of immersion of silica gel in water[13], and ΔH_{ads} of isopropylamine from an isopentane solution was determined on silica gel using again heats of immersion (batch mode) at ambient temperature (Table I) to establish standards of reference for the more difficult flow studies.

TABLE I

ΔH_{imm} (Batch Mode) of Silica Gel in Some Liquids at 26°C

Liquid	ΔH_{imm}/cal g^{-1}	Tc/°C[a]	P_c/psi[a]
(1) Isopentane	-4.83 +0.63	187.8	483.5
(2) 10% Isopropylamine	-21.66 +0.81	190.0[b]	527.0[b]
(3) Isopropylamine	-20.33 +0.30	209.7	700.0[c]

$$(2) - (1) = \Delta H_{ads} = -16.83 + 1.02 \text{ cal } g^{-1}$$

ΔH_{ads} (flow mode) at 30 PSI = -17.97 +PH 0.27 cal g^{-1}

a. Ref. 16
b. Ref. 17
c. Ref. 18

[+]On leave from Indian Institute of Technology, New Delhi, India

Table II presents ΔH_{ads} values of isopropylamine on the same sample of silica gel (Fisher grade 62) from an isopentane carrier stream over a range of temperatures and pressures from subcritical to supercritical. Results are given in terms of calories per gram of silica gel. Since this is a saturation experiment, the observed values at a given temperature and pressure should be (and are) independent of flow rate (7-30 ml/hr) or concentration (10-20%) of isopropylamine.

TABLE II

Heats of Adsorption, ΔH_{ads} of Isopropylamine on Silica Gel at Different Temperatures and Pressures by Flow Calorimetry

Temp. (°C)	P (PSI)	ΔH_{ads} (cal/g)
26	30	-17.97 +0.27
	1000	-17.44 +0.84
80	500	-15.79 +0.22
	1000	-15.34 +0.23
160	500	-12.52 +0.80
200	500	-9.86 +1.30
	1000	-11.52 +0.72
	1500	-13.61 +0.16
250	1000	-4.30 +0.16

The most obvious results from Table II are: a) The insignificant effect of pressure on ΔH_{ads} in the subcritical range. b) The decrease of ΔH_{ads} in response to increasing temperature at a given pressure. c) The significant increase in ΔH_{ads} with increase in pressure above the supercritical threshold at 200°C. These observations are consistent with the notion that isopropylamine, a strong base, is primarily chemisorbed on the silica gel surface by hydrogen-bonds.[14] Increasing the temperature weakens this interaction. However, close to the critical temperature, a small increase in pressure results in a substantial increase in density causing an increase in the effective concentration of the base. Thus, an increase in pressure above the critical temperature manifests itself as an increase in the ΔH_{ads}. It remains to be seen how less strongly adsorbed materials will respond to crossing into the supercritical region.

A crucial component for extending flow calorimetry into the supercritical range is the use of a Setaram-80 heat flow calorimeter which may be operated in the flow mode at temperatures up to 300°C using the sample cell (5) in Figure 1. This was designed for adsorption thermochemistry so that a bed of adsorbent in cell (5) can be placed downstream from the switching valves in the pumps so that either of the fluid streams leaving the piston pumps (A and B) may be directed through the adsorbent bed. An important problem in flow calorimetry (even at ambient conditions) is to balance mass transfer and heat transfer.[15] Unless the stream of fluid containing the adsorbate has been

brought to exactly the temperature of the adsorbent (in cell 5) the observed ΔH_{ads} will contain a contribution due to incomplete thermal equilibration of the streams. Figure 2 shows how this problem was solved by forcing the stream through a coil of 1/8" (OD) x 0.60" (ID) 316 stainless steel tubing positioned in the preheating chamber of the calorimeter.

In each experiment, about 100-150 mg. of silica gel was used. After initial cleaning with methanol followed by hexane, the system was then purged with N_2 for about 10-15 min. before the assembled cell was put in line. The system was brought to the appropriate pressure by pumping an inert solvent (isopentane) at 75 ml/hr and adjusting the back pressure regulators. Once the appropriate pressure was obtained, the solvent flow rate was reduced to either 7 or 15 ml/hr and then the system was thermally equilibrated as demonstrated by a steady baseline on the recorder. Once a steady baseline was achieved, the reactive liquid in pump B was pressurized while still closed to the system to avoid a pressure drop and backflow when switching pumps. Simultaneously, pump A was turned off and pump B was opened to the system at the same flow rate as that of pump A. Heat evolved during the process of interaction of the isopropylamine with the silica gel was monitored by both digital and analog outputs, and was presented as an exothermic release of heat up to the point of surface saturation after which the system returned to its original baseline temperature in about 30 min.

ACKNOWLEDGEMENTS

This work was made possible through grants from the Exxon Educational Foundation and the Department of Energy (Contract No. FG22-82PC50807) to E.M.A. and the National Science Foundation (Grant CHE-8119600 to C.H.L.). We are glad to acknowledge the expertise of Mr. Milton L. Whitfield in the Duke Physics Shop.

REFERENCES

1. a. Hannay, J. B. Proc. Roy. Soc. (London) 1880, 30, 484
   b. D. I. Mendelejeff has also been credited with arriving at the notion of the critical state as early as 1861; Glasstone, S., "Textbook of Physical Chemistry" Van Nostrand, N.Y. 1940, 421.
2. van der Waals, J. D. Zittingsv. V. Akad. Wet. (Amsterdam) 1894, 133.
3. Street, W. B. Astrophys. J. 1973, 186, 1107.
4. Street, W. B. Icarus 1976, 29, 173.
5. Orr, F. M. Jr.; Taber, J. J. Science 1984, 224 (no. 4649), 563 and the references cited therein.
6. Worthy, W. C. & EN 1983, Aug. 29, 18.
7. Peader, P. A.; Lee, M. L. J. Liquid Chrom. 1982, 5, 179.
8. Maddocks, R. R. Chem. Eng. Prog. 1977, 73(6), 59.
9. Christensen, J. J.; Izatt, R. M. Thermochim. Acta 1984, 73 117 and the references cited therein.
10. Siddiqi, M. A.; Lucas, K. J. Chem. Thermodyn. 1982, 14, 1183.
11. Wormald, C. J.; Lewis, K. L.; Mosedale, S. J. Chem. Thermodyn. 1977, 9, 27.

12. Our ΔH_{soln} values for KCl and $BaCl_2$ of 4.25 +0.0.4 at 25°C and -6.65 ±0.30 kcal $mole^{-1}$ at 75°C agree well with the literature values of 4.20 and -6.76 kcal $mole^{-1}$ respectively (Gunn, S. J. Phys. Chem. 1965, 69, 2902 and Criss, C. M.; Cobble, J. W. J. Amer. Chem. Soc. 1961, 83, 3223).
13. Our ΔH_{imm} value of - 12.55 cal g^{-1}. for Silica gel in water agree with the range of values -11.95 to -13.14 cal g^{-1} obtained at Bartlesville Laboratory (Noll, L. A. private communication) using different samples of silica gel (Fisher, grade 62).
14. Iler, R. K. "The Chemistry of Silica" 1979, John Wiley & Sons, New York.
15. It is also important to reduce dead space in cell 5 by the use of a machined metal insert so that mixing of the flow stream is minimized following switching from pure solvent to the solution of base.
16. Handboook of Chemistry and Physics, 57th Edition, 1976-1977, CRC Press Inc., Cleveland.
17. Kay's approximation has been used to calculate pseudocritical constants for a mixture (Kay, W. B. Ind. Eng. Chem. 1936, 28, 1014 and Reid R. C.; Sherwood, T. K. "The properties of gases and liquids, their estimation and correlation" 1958. McGraw-Hill Book Co. Inc., New York).
18. Pc (isopropylamine) is an average value from estimates using Riedel's and Lydersen's methods reported in ref. 17.

Figure 1. Schematic of Adsorption Flow Calorimeter

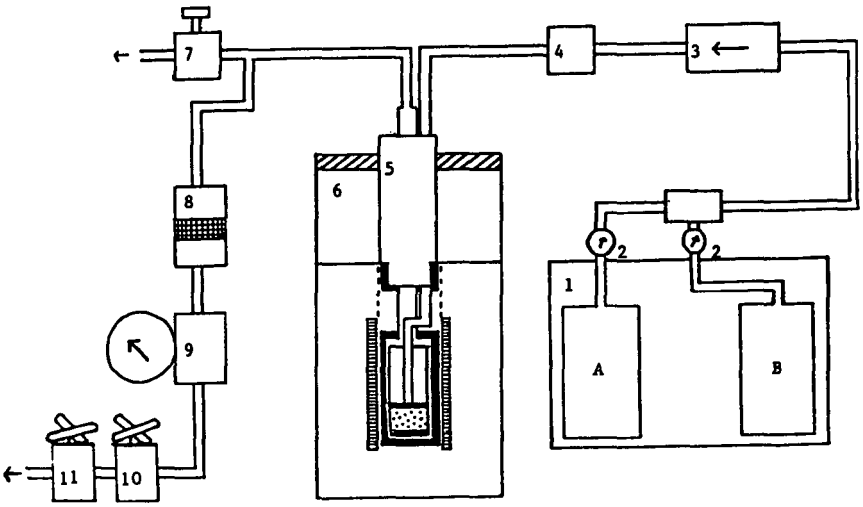

1. Perkin Elmer Model 601 Dual Piston Pumps
2. Perkin Elmer Bourden Pressure Gauges
3. High Pressure Equipment Co. Check Valve
4. High Pressure Equipment Co. Safety Valve
5. High Pressure Cell
6. C-80 Setaram Calorimeter
7. Butech Pressure Systems High Temperature Valve
8. Valco Filter
9. Pilgrim Instruments Bourden Pressure Gauge
10,11. Tescom Back Pressure Regulators, Model 26-1724-24

Figure 2. Detail of Adsorption Cell (5 in Figure 1) Showing Preheater Coil

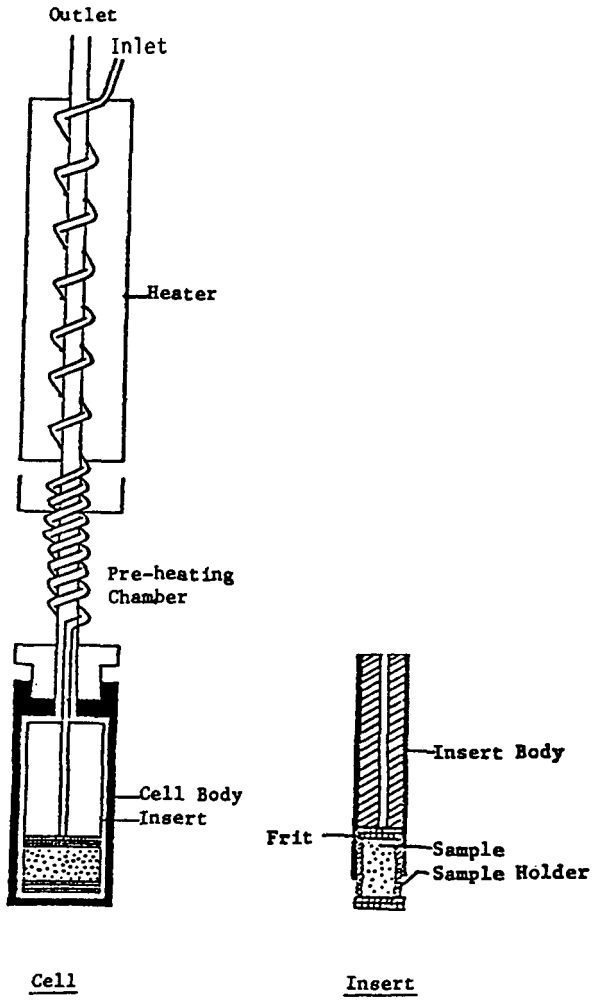

SUPERCRITICAL FLUID ADSORPTION AT THE GAS-SOLID INTERFACE

Jerry W. King

CPC International, Moffett Technical Center, Argo, Illinois 60501

INTRODUCTION

Supercritical fluids (SCF) in tandem with adsorbent media are currently being used in a number of chemical processes. Such applications as the regeneration of adsorbents, catalysis under supercritical conditions, analytical and preparative chromatography, and the proposed storage of radioactive gases in their supercritical state (1-4) require an understanding of the role of SCF at the sorbent/gas interface. Adsorbate equilibrium between a dense gas and adsorbent is not totally controlled by the "volatility enhancement" of the sorbate by the supercritical fluid, but can include such additional mechanisms as displacement of the sorbate from the interface by the SCF as well as thermally-induced desorption (5). Unfortunately, many investigators do not appreciate the competitive adsorption effect of the SCF at the gas-solid interface and employ extraction conditions which are solely based on the solubility of the adsorbate in the supercritical fluid. In this presentation, we shall discuss the adsorption of supercritical fluids on active adsorbents and show the relevance of this information for the design of adsorbent regeneration processes.

The physical conditions for regenerating adsorbents vary widely as shown by the reduced state correlation in Figure 1. The choice of these regeneration conditions is partially empirical or based on solute solubilities in the SCF. Whereas, high reduced temperatures (T_r) and pressures (p_r) maybe required to displace polar species or higher molecular weight components from the carbon surface, these conditions can have an adverse effect on the cycle lifetime of the adsorbent. The displacement capability of supercritical fluids on previously adsorbed solutes can be maximized by studying the adsorption isotherm of the SCF on the adsorbent of interest. The results presented in this paper are relevant to the latter phenomena and can be of significant importance in regenerating weak to moderately adsorbed species from the solid surface using minimal gas compression.

EXPERIMENTAL AND DATA SOURCES

Data for the adsorption of supercritical gases on activated carbon were taken from the studies of Ozawa and Ogino (6-8). Correlation of the adsorption maxima for supercritical fluids on various adsorbents as a function of pressure were derived from the work of Menon (9). Tracer pulse chromatographic experiments were performed by the author at the University of Utah. The basic apparatus required for performing these experiments has been previously described (10). Desorption breakthrough volumes were determined at 40°C using supercritical CO_2 and He as carrier gases. Two sorbent columns packed with alumina and crosslinked styrene/divinylbenzene resin were utilized in these studies. Retention volume data were determined for a a homologous series of n-alkanes (n-propane through n-heptane) as well as benzene and naphthalene on the above adsorbents.

RESULTS AND DISCUSSION

A typical adsorption isotherm for a supercritical gas adsorbing on activated carbon is shown in Figure 2. Such isotherms show a linear increase in the amount of gas adsorbed with increasing pressure and eventually exhibit a maxima in the pressure range corresponding to p_r = 0.5-1.0. The shape of such isotherms is partially influenced by the adsorption and pressure scales that are utilized (11), the maxima being more pronounced when the surface excess is used as a measure of the quantity

of gas adsorbed. Further compression of the SCF results results in a decrease of the surface excess as the density of the bulk fluid becomes equal to or exceeds the density of the adsorbed gas. The occurence of a pressure maximium in the adsorption isotherm for the supercritical gas on a given adsorbent is important, since it represents a condition favorable for the displacement of the adsorbed specie from the adsorbent surface. Typical conditions associated with the occurence of the pressure maximium (p_{max}) are presented in Figure 3 for microporous carbons. Note that the pressure requirements for attaining p_{max} are lower when the adsorption is conducted close to the critical temperature of the gas. This is consistent with the larger uptake of supercritical fluid by the porous medium.

Menon (11) has correlated p_{max} for various gases in terms of their respective critical properties and has proposed the following equation which is applicable for adsorption on macroporous adsorbents:

$$p_{max} = p_c T_r^2 \qquad 1)$$

The predicted p_{max} from this relationship have been plotted in Figure 4 from 20 to 100°C for carbon dioxide, ethylene, and chlorotrifluoromethane. The values for p_{max} obtained from Equation 1 occur at reduced temperatures which are greater then unity, a result which is quite different from the cases cited in Figure 3 for the microporous sorbents.

Studies by several investigators (6-8) utilizing different adsorbent/gas combinations indicate that the pore structure of the adsorbent has a pronounced effect on the value for p_{max}. As shown in Figure 5, a decrease in the mean pore diameter of the activated carbon decreases the pressure to attain maximium adsorption of the gas. This suggests that there maybe some advantage to utilizing a microporous adsorbent in a supercritical fluid regeneration process, provided there is no inhibition to desorption due to restricted diffusion of the displaced adsorbate from the sorbent bed. For activated carbons, the p_{max} occurs between 25-72 atmospheres depending on the pore size distribution of the adsorbent. Prediction of the adsorption isotherm for the supercritical gas on activated carbons of varying pore size distribution can be accomplished by application of the Pickett equation (6).

The temperature dependence for p_{max} on carbons exhibiting microporosity is similar to that predicted by Equation 1, however the absolute values for p_{max} are correspondingly lower due to the pore size dependence. Figure 6 suggests that lower values for p_{max} can be obtained by reducing both the temperature and pore size of the adsorbent. However, a corresponding reduction in adsorbent surface area occurs upon decreasing the pore size and this is usually undesirable in terms of providing a large adsorbent capacity.

A knowledge of the dependence of adsorbate breakthrough volume on pressure can greatly aid in the design of a supercritical fluid regeneration process. There is a paucity of information in the literature concerning this phenomena, hence, we have measured the desorption breakthrough volumes for reversibly adsorbed species on beds of alumina and crosslinked styrene/divinylbenzene resin using the elution pulse analog of frontal analysis. The desorption breakthrough volume, V_r, can be readily obtained from the capacity factor, k', for the various injected sorbates and is given by Equation 2 as:

$$V_r = V_o(k' + 1) \qquad 2)$$

where V_o is the void volume of the column.

Figure 7 illustrates the dependence of the desorption breakthrough volume on gas pressure for benzene desorbing from crosslinked resin matrix. Close examination of the plot reveals that there is a linear decrease in the breakthrough volume for benzene up to a pressure of approximately 70 atmospheres. Beyond this pressure, there is a rather dramatic decrease in breakthrough volume which continues up to a pressure of 100 atmospheres. Benzene breakthrough volumes at pressures beyond 100

atmospheres tend to asymptotically appraoch a constant volume largely determined by the dimensions associated with the bed voidage. This general trend in desorption breakthrough behavior has been confirmed by running additional solutes on both alumina as well as the crosslinked resin. Interestingly, the transition to a constant breakthrough volume occurs in approximately the same pressure range for all of the adsorbates we have studied suggesting the maximium adsorption of the carrier fluid occurs in this pressure interval. This result suggests that carbon dioxide is displacing the adsorbate from the surface of the adsorbent. It should be noted, that selective fractionation of the adsorbed solutes can be achieved by operating in the lower pressure regime, but this segregation capability is rapidly lost when pressures exceed 80 atmospheres

The above behavior has been verified with similar adsorbates on alumina columns. Figure 8 shows the dependence of the capacity factor for n-butane adsorbing on alumina as a function of gas pressure. The recorded decrease in the capacity factor parallels the reduction in adsorbate breakthrough volume as a function of pressure and it becomes constant as the breakthrough volume approaches the void volume of the adsorbent bed. Additional experiments performed using helium as a carrier gas also showed a decrease in the k' for n-butane as a function of increasing gas pressure. As shown in Figure 8, the magnitude of this change was not as dramatic as that exhibited for the alumina-CO_2-n-butane system, however the recorded reduction in k' suggest that a displacement mechanism is responsible for the capacity factor changes when using this relative inert gas.

The above results strongly support the hypothesis that displacement of bound adsorbates by a supercritical fluid can be a major factor in regenerating adsorbent beds. Additional support for this concept can be found from the regeneration studies of Eppig and coworkers (3) who recovered ethanol, methyl ethyl ketone, and toluene from activated carbon beds using modest CO_2 pressures (100 atm.). Competitive adsorption studies of CO_2/light hydrocarbon mixtures desorbing from molecular sieves (12) also indicate that CO_2 is preferentially adsorbed over the alkane moieties. Clearly, this mode of adsorbent regeneration can be used for desorbing selected solutes without the need for excessive gas compression.

REFERENCES

1. M. Modell, R. deFilippi, and V. Krukonis in "Activated Carbon Adsorption of Organics from the Aqueous Phase-Vol. 1", I.H. Suffet and M.J. McQuire, eds., Ann Arbor Science Publishers, Inc., Ann Arbor, Michigan, (1983), pgs. 447-461.

2. R. deFilippi, V. Krukonis, R. Robey, and M. Modell, "Supercritical Fluid Regeneration of Activated Carbon for Adsorption of Pesticides", EPA Report 600/2-80-054, USEPA, (1980).

3. C. Eppig, R. deFilippi, and R. Murphy, "Supercritical Fluid Regeneration of Activated Carbon Used for Volatile-Organic-Compound Vapor Adsorption", EPA Report 600/2-82-067, USEPA, (1982).

4. G.H. Findenegg, B. Korner, J. Fischer, and M. Bohn, Ger. Chem. Eng., 6, 80 (1983).

5. R. Kander and M. Paulaitus in "Chemical Engineering at Supercritical Fluid Conditions", M. Paulaitus, J. Penninger, R. Gray, Jr., and P. Davidson, eds., Ann Arbor Science Publishers, Inc., Ann Arbor, Michigan, (1983), pgs. 461-476

6. S. Ozawa, S. Kusumi, and Y. Ogino in "Proceedings of the 4th International Conference on High Pressure-Kyoto-1974", The Physico-Chemical Society of Japan, Kyoto, Japan (1975), pgs. 580-587.

7.)S. Ozawa and Y. Ogino, Nippon Kagaku Kaishi, (1972), 1.

8. S Ozawa and Y. Ogino, Nippon Kagaku Kaishi, (1972), 8.

9. P.G. Menon, J. Phys. Chem., 72, 2695 (1968).

10. J.C. Giddings, M. Myers, and J.W. King, J. Chrom. Sci., 7, 276 (1969).

11. P.G. Menon, Chem. Rev., 68, 277 (1968).

12. D. Basmadian and D. Wright, Chem. Eng. Sci., 36, 937 (1981).

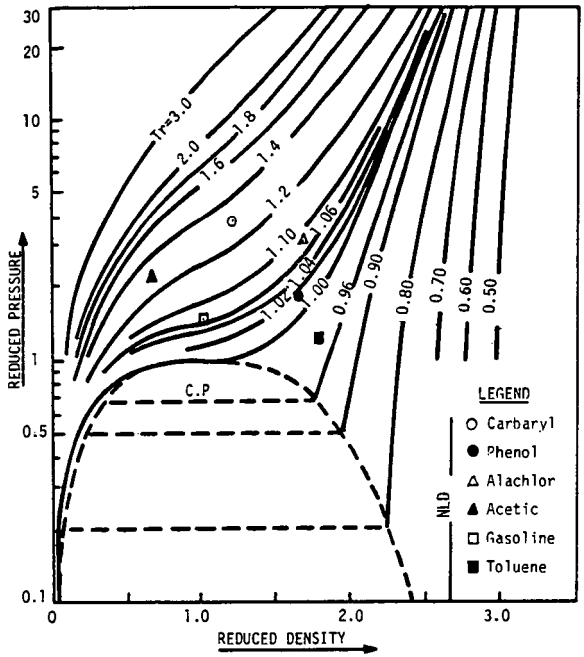

FIGURE 1. Reported Conditions for SCF Desorption of Selected Adsorbates from Activated Carbon

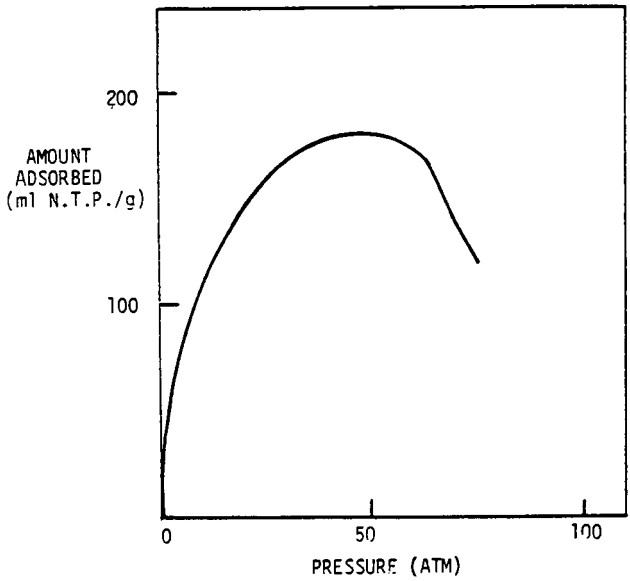

FIGURE 2. Adsorption Isotherm for the CO_2/ Activated Carbon System

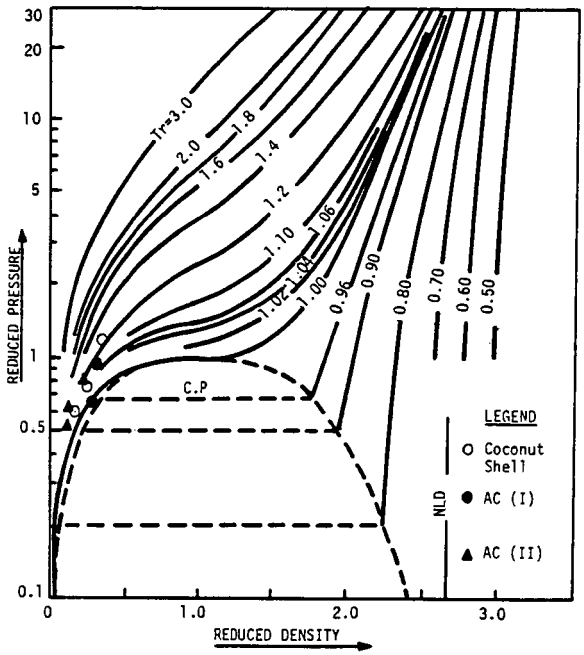

FIGURE 3. Conditions for Occurence of Adsorption Maximium (P_{max}) in CO_2/Activated Carbon Systems

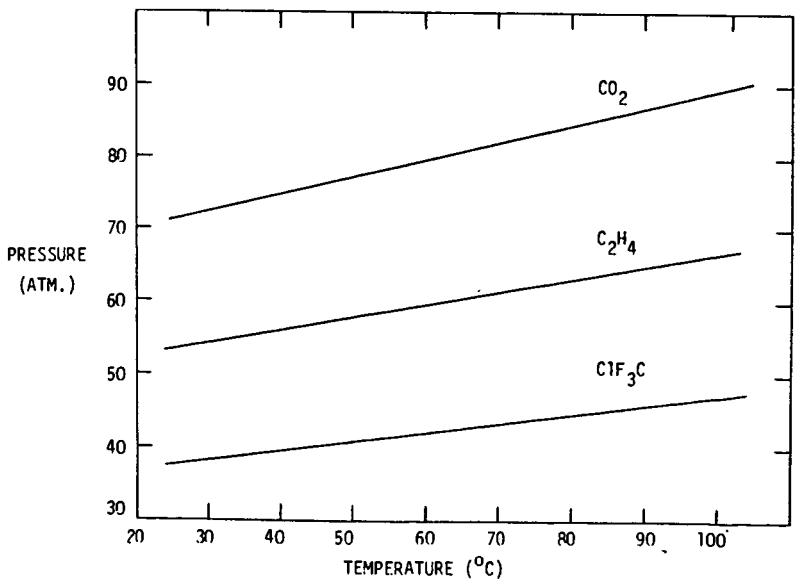

FIGURE 4. Dependence of P_{max} on Temperature According to Menon for Various Gases

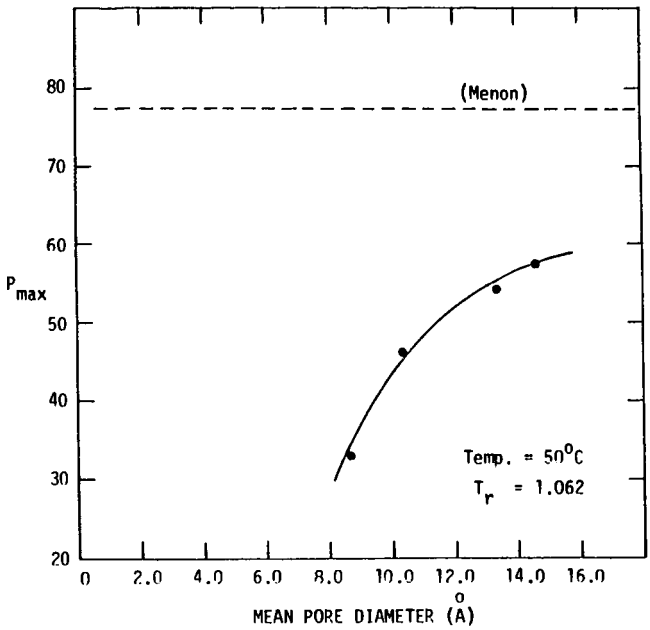

FIGURE 5. Pressure For Maximium Gas Adsorption vs. Mean Pore Diameter of Activated Carbons

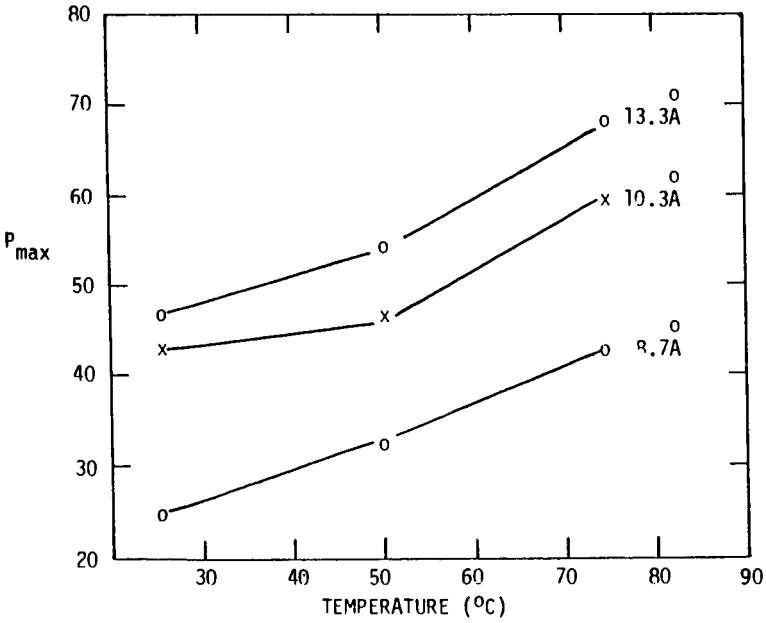

FIGURE 6. P_{max} vs. Temperature for CO_2 Adsorption on Activated Carbons of Various Pore Sizes

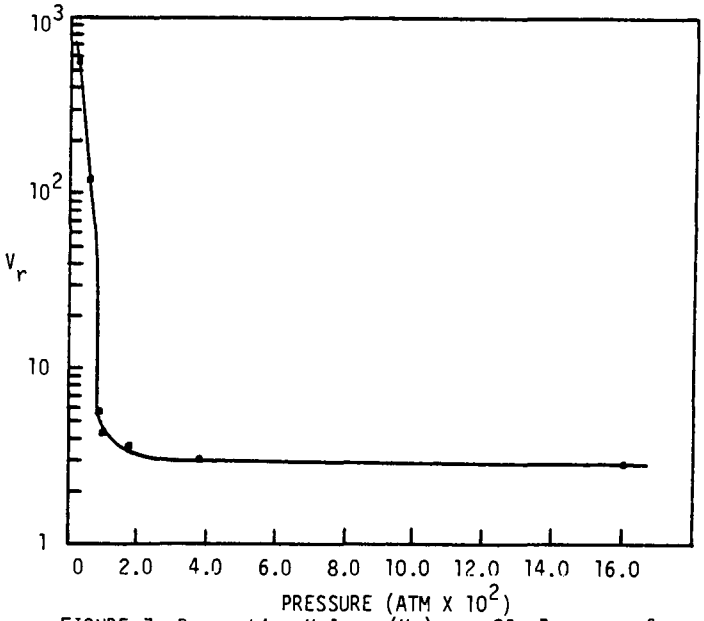

FIGURE 7. Desorption Volume (V_r) vs. CO_2 Pressure for Benzene/Styrene-Divinylbenzene Resin System

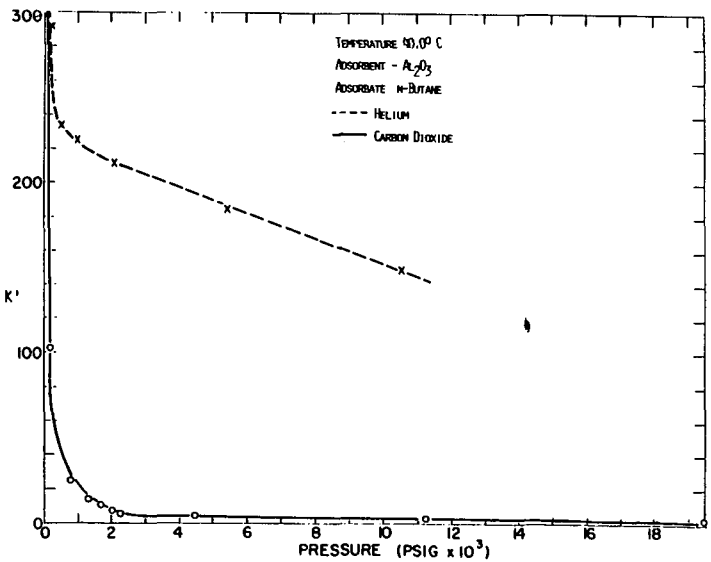

FIGURE 8. Capacity Factor (k') for n-Butane on Al_2O_3 vs. Carbon Dioxide or Helium Pressure

SOLUBILITIES OF SOLID n-ALKANES IN SUPERCRITICAL ETHANE

Iraj Moradinia and Amyn S. Teja
School of Chemical Engineering
Georgia Institute of Technology
Atlanta, Georgia 30332-0100

ABSTRACT

The solubilities of solid n-triacontane (n-$C_{30}H_{62}$) and n-Dotriacontane (n-$C_{32}H_{66}$) in supercritical ethane at temperatures between 308K and 319K and pressures upto 20 MPa are reported in this work. The results have been correlated using an equation of state, using sublimation pressures which are extrapolated from data available for the lower even-numbered members of the alkane series.

INTRODUCTION

Then n-alkanes are an interesting series because they display great regularity in their behavior. Many of their fluid phase properties, for example, can be correlated with the number of carbon atoms in the molecules. In order to develop general relations for supercritical extraction, therefore we have studied the solubilities of solid n-alkanes in supercritical ethane. The solubilities of n-triacontane (n-$C_{30}H_{62}$) and n-dotriacontane (n-$C_{32}H_{66}$) in ethane are reported in this paper. Results for n-tetracosane (n-$C_{24}H_{50}$) , n-hexacosane (n-$C_{26}H_{54}$) and n-octacosane (n-$C_{28}H_{58}$) will also be presented at the symposium. One reason for studying only the even-numbered members of the n-alkane series is that they exhibit different packing properties than the odd-numbered members of the series [1,2,3]. Thus their solid phase properties such as heats of sublimation and vapor pressures follow different trends from those of the odd-numbered members. This is shown in Fig. 1 for the heats of sublimation. Any generalizations for supercritical extraction of solids must therefore take account of this difference in behavior.

EXPERIMENTAL

The apparatus used in this study was a single-pass flow system shown

schematically in Fig. 2. The apparatus is similar in principle to those used by Kurnik et al [4] and others [5,6,7]. Solvent gas is first liquefied and then compressed past its critical pressure by means of a Milton Roy minipump A. Its temperature is increased to supercritical conditions in the heat exchange coil B immersed in a constant-temperature water bath C. The bath temperature was maintained constant to ± 0.1K and the temperature monitored by means of a copper-constantan thermocouple D calibrated against an NBS-certified platinum resistance thermometer. The pressure of the system was measured by a Heise gauge E calibrated against a dead-weight gauge. The pressure was maintained constant by a back pressure regulator F. The supercritical solvent was then brought into contact with the solute in a modified Jerguson equlilbrium cell G. The equilibrium temperature was measured by a second copper-constantan thermocouple K calibrated against an NBS-certified platinum resistance thermometer. This thermocouple was inserted inside the cell by means of a fitting. For better solid contact, layers of glass beads were packed with the solute in the equilibrium cell. The loaded supercritical fluid was then depressurized at the micrometering valve H and the diposited solute was collected in a separation vessel J. The micrometering valve was heated to compensate for the Joule-Thompson effect upon depressurization and all the lines outside the constant temperture bath were heat traced. In spite of these precautions, however, some of the long-chain n-alkanes still precipitated inside the micrometering valve. This deposited solid was flushed out with liquid hexane at the end of each run. The solute collected was weighted to ± 0.10 mg using a Mettler electronic balance. Solvent volume was recorded using a wet test meter L. We estimate the precision of our temperature, pressure and volume measurements to be 0.5 K, 0.5 mmHg and ± 1/2% respectively; the accuracies were typically twice the magnitude of the precision.

RESULTS

For comparison purposes, the solubilities of 2,3-dimethylnapthalene in CO_2 along three isotherms were first measured and the results compared with those of Kurnik et al [4]. These results are presented in table 1 for the 308.15K isotherm. In no case did our solubilities differ from those of Kurnik et al by more than 3.6% for any of the isotherms.

Our results for the C_2H_6 + n $C_{30}H_{62}$ and C_2H_6 + n $C_{32}H_{66}$ systems are shown in Tables 2 and 3. Since the sublimation pressures of the higher n-alkanes were not available in the literature, we have treated these as adjustable parameters in our equation of state correlations of the solubility data. The sublimation pressures were not freely adjustable, however, but were bounded by the values obtained by extrapolating propane and n-octadecane sublimation pressures 25%. Our results are shown in Fig 3 and 4. Additional results will be discussed at the symposium. The equation of state used was that of Patel and Teja [8].

REFERENCES

1. Morawetz, E., "Ethalpies Of Vaporization from C_{12} to C_{20}", J. Chem. Thermo. 4, 139 (1972).

2. Bondi, A., "Heat of Sublimation of Molecular Crystals A Catalog of Molecular Structure Increments", J. Chem. Eng. Data 8, 371 (1963).

3. Broadhurst, M. G., J. Res. Nat. Bur. Stand. A 66, 241, (1962).

4. Kurnik, R. T., Holla, S. J. and Reid, R. C., "Solubility of Solids in Supercritical Carbon Dioxide and Ethylene", J. Chem. Data, 26, 47 (1981).

5. Adachi, Y., Benjamin, C. and Lu, Y., "Supercritical Fluid Extraction with Carbon Dioxide and Ethylene", Fluid Phase Equil., 14, 147 (1983).

6. Mchugh, M. A. and Paulaitis, M. E., "Solid Solubilities of Naphthalene and Biphenyl in Supercritical Carbon dioxide", J. Chem. Eng. Data, 25, 326 (1980).

7. Johnston, K. P. and Eckert, C. A., "Analytical Carnahan-Starling-van der Waals Model for Solubility of Hydrocarbon Solids in Supercritical Fluids", AIChE J., 27, 773-779 (1981).

8. Patel, N. C. and Teja, A. S., "A New Cubic Equation of State for Fluids and Fluid Mixtures", Chem. Eng. Sci., 37. 463 (1982).

TABLE I

Comparison of CO_2 + 2,3 Dimethylnaphthalene
Data at 308.15K

System Pressure MPa	$Y_{2,3\text{-DMN}} \times 10^3$ This Work	Kurnik et al
9.87	2.28	2.2
14.25	4.36	4.41
19.60	5.45	5.42
24.12	5.76	5.82
27.92	6.45	6.43

TABLE II

Results for Ethane-n-Triacontane ($C_{30}H_{62}$)

System Pressure MPa	$Y_{C30H62} \times 10^3$ 308.15K	313.15K
6.57	0.549	0.486
10.10	1.24	1.95
13.64	1.71	3.50
16.67	2.24	
20.20	3.20	

TABLE III

Results for Ethane-n-Dotriacontane ($C_{32}H_{66}$)

System Pressure MPa	$Y_{C32H66} \times 10^3$ 308.15K	313.15K	319.15K
6.57	0.216	0.177	0.149
10.10	0.713	0.953	1.28
13.64	0.958	1.44	2.14
16.67	1.26	1.73	
20.20	1.81	2.18	

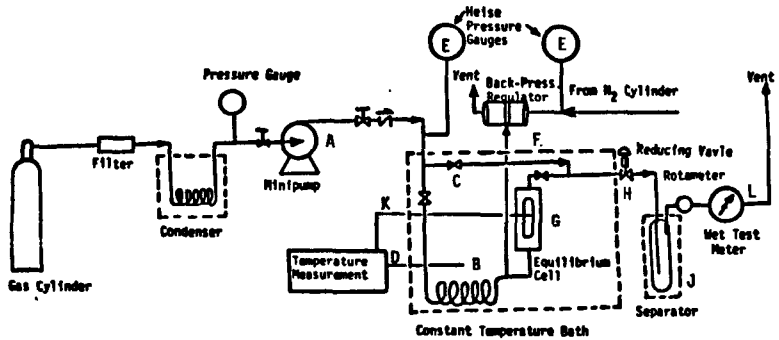

Figure 2. Supercritical Flow Apparatus

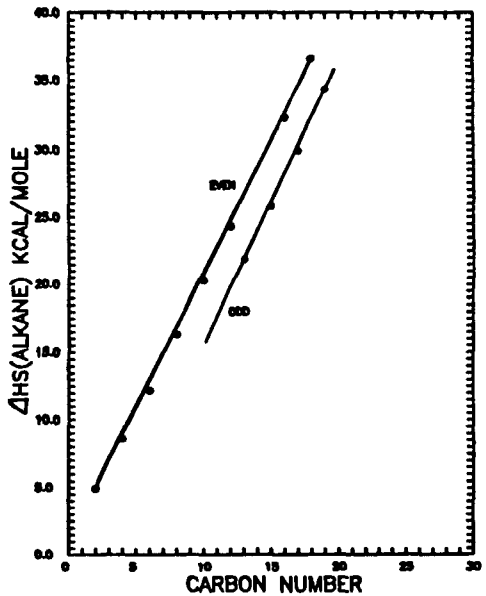

Figure 1. Heat of Sublimation vs. Carbon Number

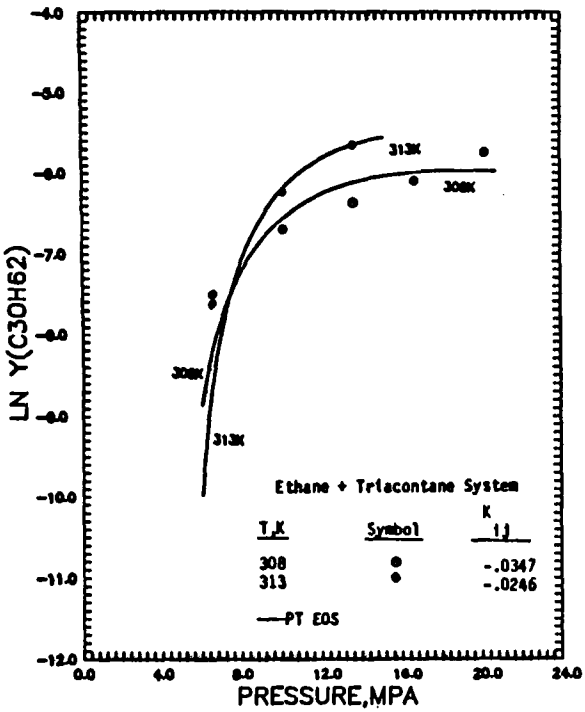

Figure 3. Solubility of Triacontane in Supercritical Ethane

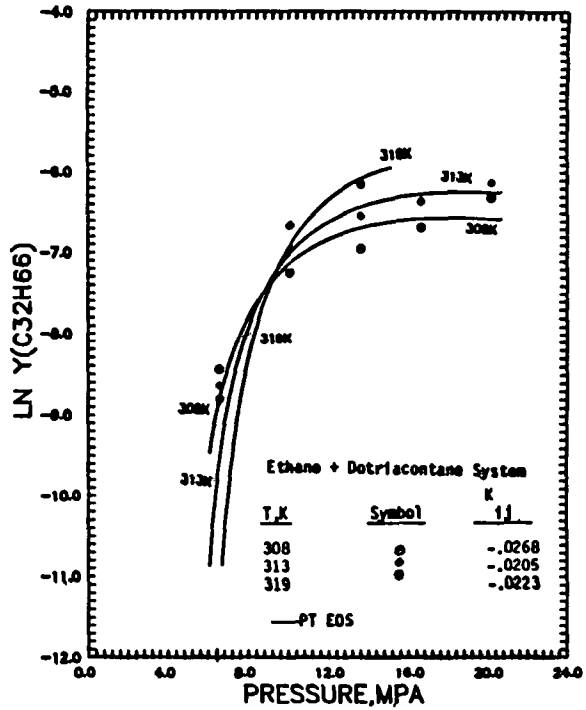

Figure 4. Solubility of Dotriacontane in Supercritical Ethane

High-Pressure Phase Equilibria in Ternary Fluid Mixtures with a Supercritical Component

A.Z. Panagiotopoulos and R.C. Reid

Department of Chemical Engineering
Massachusetts Institute of Technology
Cambridge, MA 02139

The potential of supercritical extraction (SCE), a separation process in which a gas above its critical temperature is used as a solvent, has been widely recognized in the recent years. The first proposed applications have involved mainly compounds of low volatility, and processes that utilize supercritical fluids for the separation of solids from natural matrices (such as caffeine from coffee beans) are already in industrial operation. The use of supercritical fluids for the separation of liquid mixtures, although of wider applicability, has been less well studied, as the minimum number of components for any such separation is three (the solvent, and a binary mixture of components to be separated). The experimental study of phase equilibrium in ternary mixtures at high pressures is rather complicated, and theoretical methods to correlate the observed phase behavior are lacking.

One important potential application of supercritical extraction is in the recovery of polar organic compounds from aqueous solutions. Such mixtures arise very frequently as products of biochemical syntheses. In many cases, the costs of the energy-intensive separations are quite high. It is the objective of an ongoing research project at MIT to investigate the applicability of SCE for such separations.

Previous work in the area of high-pressure phase equilibrium of aqueous solutions of organic compounds with supercritical fluids includes the pioneering work of Elgin and Weinstock (1) carried out in the 1950's. Francis (9) presented a large number of qualitative results for ternary systems of liquid CO_2 at 25 °C. In the more recent years, Paulaitis et al. (2,3), Kuk and Montagna (4), McHugh et al. (5) and Radosz (6) have reported measurements in systems with some of the first alcohols, water and supercritical fluids.

Experimental

The experimental setup that is being used is shown in Figure 1. The main element of the equipment is a visual high pressure cell (Jerguson gage model 19-TCH-40) with an internal volume of about 50 cm^3 , that serves as a mixing and separating vessel, as well as for the visual observation of the number and quality of the coexisting phases. Connections at the bottom, top and side of the vessel permit withdrawal of the lower, upper and middle phases, any two of which can be recirculated externally with a dual high pressure Milton-Roy Mini Pump. An on-line Mettler-Paar vibrating tube density meter (DMA 60 with a DMA 512 cell) is used to measure the density of one of the recirculating phases at a time, and can be switched between any of them.

The Jerguson gage is immersed in a constant temperature bath with silicon fluid as the heat-transfer medium, that also thermostats the density meter. The bath temperature is controlled to ± .01 K with a Thermomix 1460 temperature regulator, and the temperature is measured with a calibrated mercury-in-glass thermometer to within .01 K. The lines external to the bath are maintained at the bath temperature with the help of heating tapes, and the temperature at several points is monitored with thermocouples. Pressure is measured with two calibrated Heise pressure indicators to within ±.16 bar for pressures up to 160 bar, and to within ±.4 bar for pressures up to 350 bar.

Sampling is done with two high pressure-switching valves of internal volume .5 µl (for the upper phase) and .2 µl (for the lower or middle phases). The samples are directly depressurized into a He carrier gas stream and analyzed with a Perkin Elmer Sigma 2 Gas Chromatograph, using a Porapak Q column supplied by Supelco . The response factors for the materials used were found to be close to those reported by Dietz (7). Typical reproducibility of the analysis is ±.003 in mole fraction, with somewhat larger deviations for the gas-phase composition at low pressures.

After purging and evacuation of the equipment the cell is charged with a liquid mixture of known composition and with the supercritical component up to the desired pressure. The recirculation pumps are started, and the approach to equilibrium monitored by the stability of the pressure, density, and composition measurements with time. For the mixtures studied, a typical equilibration time is 15 min., but at least 30 min are allowed before the final sampling. At least two samples are taken from each phase at equilibrium. A new pressure point can then be established immediately by introducing or removing supercritical fluid and/or liquid, so that the level of the interfaces in the cell at the new desired pressure is appropriate for sampling through the available ports .

Results

Binary Systems

As a test of the validity of the equipment design and the experimental procedures, we first investigated a binary system for which results have been previously published. Knowledge of the behavior of the binary systems is in itself important, since the data provide the appropriate limits for the corresponding ternary systems.

In Figure 2 we present the experimental results and literature data for the system CO_2 - acetone at 313 and 333 K (literature results are available only at the lower temperature). As can be seen, the agreement between the two sets of results is excellent. Also shown on the same figure as continuous lines are the results of the fitting of the experimental data using a modified Peng-Robinson equation of state that is described in the Appendix. The agreement between experimental and predicted phase compositions is within the experimental uncertainty of the data, except in the critical region.

Several of the features of the phase behavior shown on Figure 2 are quite general. In particular, it can be seen that the solubility of CO_2 in the liquid phase is quite high, even at moderate pressures. The system critical pressure is, in general, comparable to the critical pressure of CO_2, and increases with temperature at the temperature range studied. Although the solubility of acetone in the gas phase is low in the two-phase region, there is complete miscibility between CO_2 and acetone at pressures that are not very high. CO_2 at liquid-like densities is an excellent solvent for a wide range of organic compounds, as was first observed by Francis (9) for near critical liquid CO_2 .

One additional example of the same general type of behavior is demonstrated by the CO_2 - ethanol system. Three measured isotherms for this system are presented in Figure 3. No comparable set of experimental results appears to be available in the open literature. Again, the agreement between experimental results and model predictions is very good.

Ternary Systems

As one of a series of model systems, we studied the CO_2 - acetone - water system at 313 and 333 K. The most striking feature of the system behavior, is a very extensive three-phase region at both temperatures. The three-phase region is first observed at a pressure of only 25 bar at 313 K, and extends to approximately the critical pressure of the binary CO_2 - acetone system. Table 1 provides the experimental results for the composition of the three phases at equilibrium as a function of pressure and temperature.

The physical picture that underlies this behavior, as pointed out first by Elgin and Weinstock (1), is the 'salting out' effect by a supercritical fluid on an aqueous solution of an organic compound. As pressure is increased the tendency of the supercritical fluid to solubilize in the organic liquid results in a phase split in the aqueous phase, at what can be named a lower critical solution pressure (which varies with temperature). As pressure

is further decreased, the second liquid phase and the supercritical phase become more and more similar to each other, and merge at an upper critical solution pressure, above which only two phases can coexist.

This pattern of behavior was also observed by Elgin and Weinstock for the system ethylene - acetone - water at 15 °C. In addition, the same type of behavior, but at quite different pressures relative to the pure solvent critical pressure was reported by Paulaitis et al.(3) for the system CO_2 - isopropanol - water, by McHugh et al.(5) for the system ethane - ethanol - water and again by Paulaitis et al.(2) for the CO_2 - ethanol - water system, and therefore appears to be quite general.

A more complete picture of the phase equilibrium behavior is given in Figure 4 for the system under study at 333 K. The darker lines and squares on this figure are experimentally measured tie-lines and phase compositions. The light lines are model predictions, using values of interaction parameters determined solely from regression of binary data (see Appendix). The two sets of results are in good agreement with each other.

An interesting feature of the phase equilibrium behavior is the relative insensitivity of the phase envelope and positions of the tie-lines to variations in pressure in the two-phase region, as evidenced by comparison of the diagrams at 100 and 150 bar in Figure 4. This would seem to imply that similar separations can be achieved by operation at pressures just above the upper critical solution pressure of ~95 bar as compared to operation at higher pressures.

The phase equilibrium behavior at 313 K is quite similar to that at 333 K, with the three-phase region shifted to lower pressures, as presented in Table 1.

From an engineering point of view, the most important quantities in the evaluation of a separation scheme based on a phase behavior pattern such as the one shown, are the selectivity of the separation with respect to the desired component, as well as the loading of the desired component in the extractant phase. It is well known that those two factors usually increase in different directions. Figures 5 and 6 present experimental data and model predictions for the distribution coefficient of acetone, and for the selectivity ratio α of acetone over water (defined as the ratio of distribution coefficients of acetone and water in the liquid and fluid phases), as a function of the water concentration in the liquid phase. The distribution factor shows a sharp maximum at both temperatures, with a higher value at the higher temperature, whereas the selectivity decreases smoothly from the limiting value of ~300 at low acetone concentrations to 1 as the plait point is approached. The experimental data show the same trends, although there is some scatter that is due to the fact that small absolute errors in the low supercritical phase concentrations of acetone and water result in large relative errors for the distribution coefficient and selectivity factors. Selectivities are generally higher for the lower temperature, but loadings are lower. Based on the observed behavior for the system, the maximum CO_2-free acetone concentrations in the upper phase is 85% mole (~95% w/w) acetone for operation at 150 bar and 333 K.

Conclusions

An apparatus for the determination of high pressure phase equilibrium data for mixtures of water, polar organic liquids and supercritical fluids was constructed and successfully operated for binary and ternary systems with supercritical carbon dioxide.

The system CO_2 - acetone - water was extensively investigated at 313 and 333 K. The system demonstrates several of the general characteristics of phase equilibrium behavior observed earlier for similar systems, including an extensive LLV region that appears at relatively low pressures.

A model based on a modified form of the Peng-Robinson equation of state was able to reproduce quantitatively all features of the observed phase equilibrium behavior, with model parameters determined from only binary data. The use of such models may facilitate substantially the task of process design and optimization for separations that utilize supercritical fluids.

A substantial sensitivity of the separation efficiency, as determined by the ability of the solvent to selectively extract the organic compound with high loadings was observed when the operating conditions were varied.

Acknowledgement

Financial support for this research was provided by a grant from the National Science Foundation. One of the authors (AZP) was also supported by a Halcon Inc. Fellowship. We gratefully acknowledge both sponsors.

References

1. Elgin, J.C. and Weinstock, J.J., J. Chem. Eng. Data (1959), 4(1) 3-12.
2. Paulaitis, M.E., Gilbert, M.L. and Nash, C.A., 'Separation of Ethanol - Water Mixtures with Supercritical Fluids', paper presented at the 2nd World Congress of Chemical Engineering, Montreal, Canada, Oct. 5, 1981.
3. Paulaitis, M.E., Kander, R.G. and DiAndreth, J.R., Ber. Bunsenges. Phys. Chem.(1984), 88, 869-875.
4. Kuk, M.S. and Montagna, J.C., 'Solubility of Oxygenated Hydrocarbons in Supercritical Carbon Dioxide', Ch. 4 in Paulaitis. M.E. et al.(ed), 'Chemical Engineering at Supercritical Fluid Conditions', Ann Arbor Science Publishers, Ann Arbor, Mich., 1983 p. 101-111.
5. McHugh, M.A., Mallett, M.W. and Kohn, J.P., 'High Pressure Fluid Phase Equilibria of Alcohol - Water - Supercritical Solvent Mixtures, paper presented at the 1981 annual AIChE meeting, New Orleans, Louisiana, Nov. 9, 1981.
6. Radosz, M., Ber. Bunsenges. Phys. Chem. (1984), 88, 859-862.
7. Dietz, W.A., J. Gas Chrom. (1967), 5(2) 68-71.
8. Panagiotopoulos, A.Z. and Reid, R.C., 'A New Mixing Rule for Cubic Equations of State for Highly Polar, Asymmetric Systems', paper presented at the national American Chemical Society meeting in Miami,

Florida, May 1, 1985
9. Francis, A.W., J. Phys. Chem. (1954), 58, 1099-1114
10. Katayama, T., Oghaki, K., Maekawa, G., Goto, M. and Nagano, T., J. Chem. Eng. Jpn. (1975), 8(2) , 89-92.
11. Panagiotopoulos, A.Z. and Kumar, S. 'A generalized technique to obtain pure component parameters for two-parameter equations of state', Fluid Phase Equil. (1985), in print.

APPENDIX

Equation of State used

For the correlation of the experimental results, we used a modification of the Peng-Robinson equation of state developed by the authors. The essence of the method, which is presented in detail in (8), is the use of a non - quadratic mixing rule for the attractive parameter a , that involves two binary interaction parameters. The equations for the pressure, the mixing rule used and the resulting expression for the chemical potential of a component in a mixture are shown below.

$$P = \frac{RT}{V - b_m} - \frac{a_m}{V^2 + uVb_m + wb_m^2} \qquad 1)$$

$$a_m = \sum_i \sum_j x_i \, x_j \, a_{ij} \qquad 2)$$

$$b_m = \sum_i x_i \, b_i \qquad 3)$$

$$a_{ij} = \sqrt{a_i \, a_j} \, [1 - k_{ij} + (k_{ij} - k_{ji}) x_i] \qquad 4)$$

$$\ln\phi_k = \ln \frac{\hat{f}_k}{x_k P} = \frac{b_k}{b_m} \left(\frac{PV}{RT} - 1 \right) - \ln \frac{P(V-b)}{RT} +$$

$$+ \left[\frac{\sum_i x_i (a_{ik} + a_{ki}) - \sum_i \sum_j x_i^2 x_j (k_{ij} - k_{ji}) \sqrt{a_i a_j} + x_k \sum_i x_i (k_{ki} - k_{ik}) \sqrt{a_k a_i}}{a_m} - \frac{b_k}{b_m} \right] \times$$

$$\times \frac{a_m}{\sqrt{u^2 - 4w} \; bRT} \ln \frac{2V + b_m (u - \sqrt{u^2 - 4w})}{2V + b_m (u + \sqrt{u^2 - 4w})} \qquad 5)$$

For the estimation of the subcritical pure component parameters, we used the technique of Panagiotopoulos and Kumar (11), that provides results that exactly reproduce the vapor pressure and liquid density of a subcritical component. Table 2 presents the pure component parameters that were used. For the supercritical components, the usual acentric factor correlation was utilized.

It is important to note, that the interaction parameters between the components (two per binary) were estimated solely from binary phase equilibrium data (including low-pressure VLE data for the binary acetone - water); no ternary data were used in the fitting. The values of the interaction parameters obtained are shown in Table 3.

TABLE 1 : Three phase equilibrium compositions for the system Water (1) - Acetone (2) - CO_2 (3)

P (bar)	lower phase		upper phase		middle phase	
	x_1	x_2	y_1	y_2	z_1	z_2
			T = 313 K			
29.3	0.810	0.153	0.005	0.025	0.294	0.454
35.9	0.864	0.106	0.006	0.019	0.197	0.427
43.2	0.904	0.075	0.003	0.017	0.153	0.360
55.9	0.920	0.052	0.002	0.015	0.119	0.230
61.1	0.942	0.037	0.004	0.015	0.114	0.191
65.8	0.944	0.032	0.002	0.015	0.130	0.148
75.2	0.959	0.017	0.002	0.014	0.020	0.069
79.6	0.966	0.011	0.002	0.015	0.049	0.035
			T = 333 K			
39.4	0.795	0.163	[1]	[1]	0.400	0.398
51.1	0.880	0.091	[1]	[1]	0.182	0.418
59.4	0.906	0.068	0.006	0.030	0.173	0.359
70.3	0.925	0.049	0.008	0.035	0.117	0.300
79.2	0.939	0.039	0.006	0.032	0.089	0.234
92.6	0.946	0.029	0.010	0.046	0.084	0.127

[1] not available

TABLE 2 : Pure component parameters

Component	T(K)	a ($J \times m^3/mol$)	10^6 b (m^3/mol)
Acetone	313.15	2.1772	62.35
	333.15	2.1165	62.65
Ethanol	308.15	2.0292	48.23
	323.15	1.9679	48.44
	338.15	1.9069	48.61
Water	313.15	.81614	16.07
	333.15	.79123	15.99

TABLE 3 : Interaction parameters

System	T (K)	k_{12}	k_{21}
CO_2(1) - acetone(2)	313.15	-0.02	0.00
	333.15	-0.02	0.00
CO_2(1) - ethanol(2)	308.15	0.072	0.069
	323.15	0.093	0.077
	338.15	0.089	0.061
CO_2(1) - water(2)	313.15	-0.205	0.162
	333.15	-0.185	0.160
acetone(1) - water(2)	313.15	-0.310	-0.150
	333.15	-0.293	-0.132

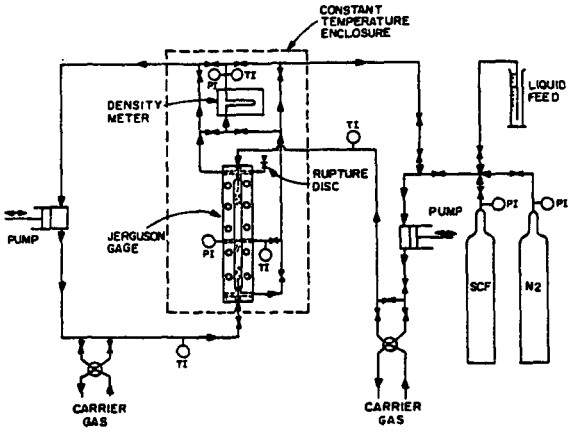

Figure 1 Schematic drawing of the equipment

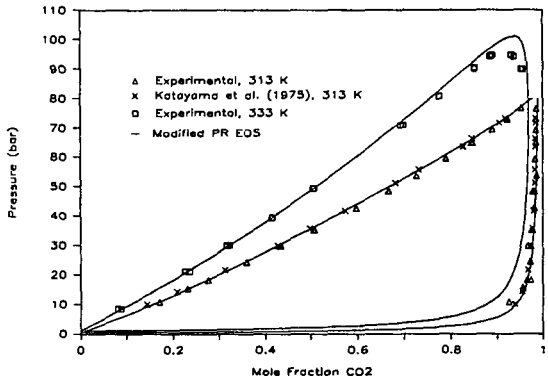

Figure 2 Experimental (crosses), literature (squares) and predicted (lines) phase equilibrium behavior for the system CO_2(1) - Acetone(2) at 313 and 333 K. Experimental data are from reference (10).

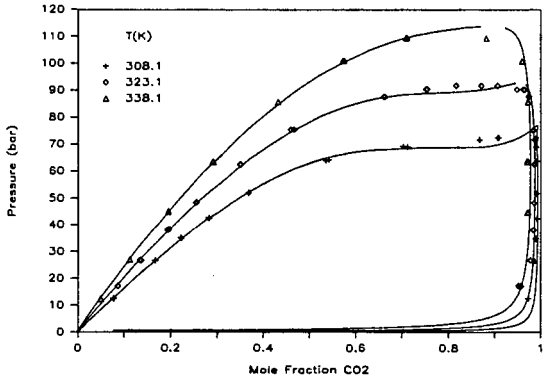

Figure 3 Experimental (symbols) and predicted (lines) phase equilibrium behavior for the system $CO_2(1)$ - water(2) at 308, 323 and 338 K

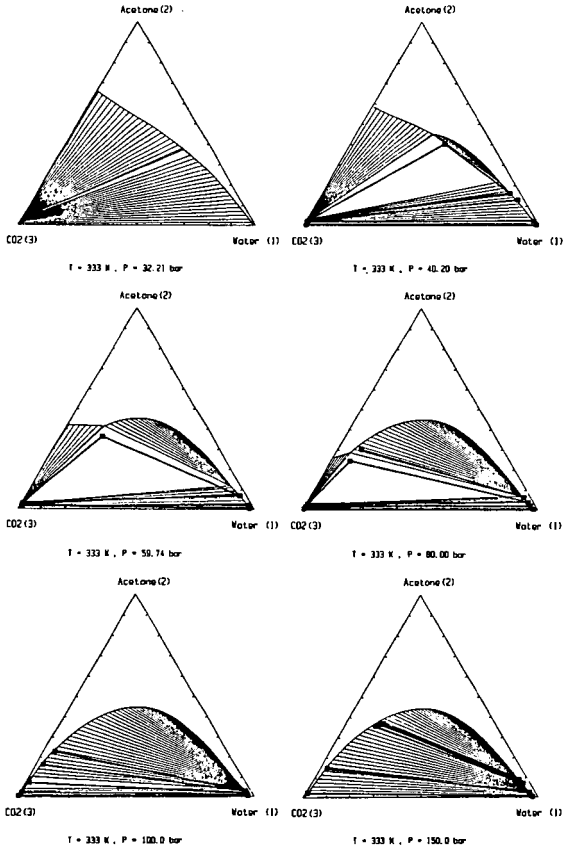

Figure 4 Experimental (dark lines and squares) and predicted (light lines) phase equilibrium behavior for the water(1) - acetone(2) - $CO_2(3)$ system at 333 K.

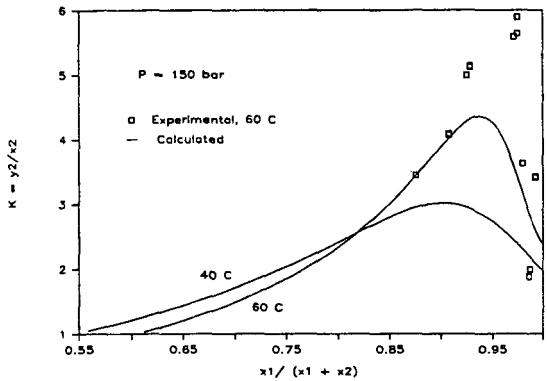

Figure 5 Distribution coefficient for acetone from experimental data (points) and model predictions (lines) for the water(1) - acetone(2) - CO_2(3) system at 150 bar, as a function of the water concentration in the lower phase (on a CO_2-free basis).

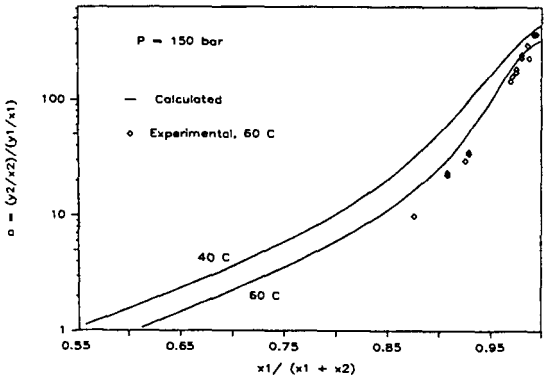

Figure 6 Selectivity factor for acetone over water for the water(1) - acetone(2) - CO_2(3) system at 150 bar, as a function of the water concentration in the lower phase (on a CO_2-free basis).

Multiphase Behavior in Ternary Mixtures of Elevated Pressures

J. R. DiAndreth and M. E. Paulaitis

Department of Chemical Engineering
University of Delaware
Newark, Delaware 19716

INTRODUCTION

Separations using supercritical or near-critical fluids as solvents are frequently carried out in the presence of water. Extraction of products from fermentation broths, tertiary oil recovery by CO_2 flooding, and supercritical-fluid (SCF) chromatography are examples of separations in which water can be present. Such systems will often exhibit phase behavior in which several coexisting fluid phases are present at equilibrium. For example, extensive regions of liquid-liquid-gas equilibrium have been observed for water-alcohol-SCF mixtures (1-3), and even four coexisting phases (liquid-liquid-liquid-gas) have been observed for n-propanol-water-CO_2 mixtures[4].

There are several practical implications of three-phase, liquid-liquid-gas equilibrium. For conventional extraction processes, it is desirable to avoid such regimes, or in the case of CO_2 flooding of oil reservoirs, to accurately account for multiple phases in determining extraction efficiency. Alternatively, the formation of two liquid phases in the presence of a compressed gas can be exploited to achieve a desired separation.

In this paper, we present the results of an investigation of fluid phase equilibria at elevated pressures for the system isopropanol-water-CO_2. These results include measured equilibrium compositions for two, three, and four coexisting fluid phases over a range of temperatures and pressures in the vicinity of the critical point of CO_2. A computer simulation of the phase equilibria for this three-component system is also presented. The simulation, which is based on the Peng-Robinson equation of state[7] and the experimental results, demonstrates the complexity of phase behavior that can be obtained for aqueous solutions in the presence of SCF solvents. This phase behavior must be understood for correct interpretation of SCF extraction experiments, and for design of separation processes using supercritical or near-critical solvents at elevated pressures.

EXPERIMENTAL SECTION

Phase compositions (tie lines) for liquid-gas equilibrium were measured using a flow technique for mixing and for continuous sampling of the phases. Equilibrium compositions for three and four coexisting phases were obtained using a static technique with a variable-volume view cell. This technique

involved calculating phase compositions from component material balances and measured phase volumes at known cell loadings; no sampling of the individual phases is required. Both experimental techniques are described in detail elsewhere[5,6].

Phase compositions for liquid-gas and liquid-liquid-gas equilibria were measured as a function of pressure at several constant temperatures. Figure 1 shows these results for 60°C in the form of triangular phase diagrams corresponding to different pressures. The two-phase regions which bound the three-phase triangles at the intermediate pressures have been omitted for clarity. At lower temperatures, four equilibrium phases were observed, and Figure 2 gives the measured compositions of these phases at 40°C and 1110 psia.

EQUILIBRIUM PHASE BEHAVIOR

The phase behavior depicted in Figure 1 shows a dramatic shift in the tie lines for liquid-gas equilibrium as pressure is changed from 1500 psia to 2000 psia. At the lower pressure, the solubilities of water and isopropanol in supercritical CO_2 are low, although the selectivity for the alcohol is high. At 2000 psia, high solubilities are obtained with lower alcohol selectivities. A continuous shifting of the tie lines between these two pressures can not obtained, however, as three coexisting phases emerge at intermediate pressures. With increasing pressure, the water-rich liquid phase splits into two liquid phases at a pressure between 1500 and 1600 psia (a critical endpoint). As pressure is increased further, the composition of the liquid phase of intermediate density, L_2, approaches that of the carbon dioxide-rich gas phase, and the alcohol concentration initially increases and then decreases. Eventually the L_2 phase and the gas phase merge to form a single fluid phase (another critical endpoint) at a pressure just below 2000 psia.

One practical implication of this phase behavior is that the solvent properties of CO_2 can be changed significantly over a relatively small pressure range. Thus solvent/extract separation can be easily achieved, and an optimal ratio of solvent capacity to selectivity can potentially be selected, depending on whether three coexisting phases can be avoided in the separation process. It is also possible to use the two liquid phases to separate other components that would be present in dilute aqueous solution by distributing these components between the L_1 and L_2 phases. The advantage of such a separation would include (1) moderate operating temperatures and pressures, (2) the ability to control the composition of the intermediate phase with pressure, (3) the complete reversibility of the phase splitting, and (4) the ability to form two liquid phases with components that are similar in molecular nature.

The four-phase equilibrium illustrated in Figure 2 suggests that the phase behavior for this ternary mixture can be quite complex at conditions near the critical point of CO_2. In order to describe global phase equilibria for this system, the Peng-Robinson equation of state was fit to the

experimental results and than used to predict phase behavior over an extended region of temperatures and pressures. Details of these calculations are given elsewhere[6]. The calculated pressure-temperature projection for isopropanol-water-CO_2 is given in Figure 3. This projection depicts the four-phase (LLLG) line for the ternary mixture, the three-phase (LLG) line for the binary water-CO_2 system, the vapor pressure curve for carbon dioxide (CO_2 VP), and the liquid-gas and liquid-liquid critical lines (dashed lines) which bound the three-phase regions for the ternary mixture.

Two important aspects of the phase behavior are evident from this projection. First, the three-phase region extends to relatively high temperatures and pressures; that is, the multiphase behavior is not limited to conditions close to the critical point of CO_2. Second, at temperatures and pressures near this critical point, the phase behavior can be quite complex. Four different three-phase regions bound the four-phase line, and there are five different two-phase regions which bound these three-phase regions. Obviously, simple screening experiments on this three-component system to obtain "representative" alcohol/water solubilities in compressed CO_2 could give dramatically different results depending on the temperature, pressure, and mixture composition examined. At temperatures below 20°C, even more complex behavior is possible since a solid hydrate phase can also be obtained.

In conclusion, our experimental results and model calculations demonstrate that complex multiphase behavior can occur for mixtures containing water and supercritical or near-critical fluids at elevated pressures. The ability to predict such behavior is an important factor in interpretting solubility behavior for SCF solvent extractions and for the design of separation processes using dense fluids at elevated pressures. The ability to form two liquid phases in the presence of a compressed gas can also be exploited to achieve a desired separation of nonvolatile components in dilute aqueous solutions where it is not possible to dissolve these components in a dense fluid such as compressed CO_2.

REFERENCES

1. Elgin, J.C.; Weinstock, J.J. J. Chem. Eng. Data 1959, 4, 3.

2. Efremova, G.D.; Shvarts, A.V. Russ. J. Phys. Chem. 1970, 44, 614 and 1972, 46, 237.

3. Paulaitis, M.E.; Gilbert, M.L.; Nash, C.A. Proc. 2nd World Conference of Chemical Engineering, Montreal, 1981.

4. Fleck, R.E. Ph.D. Thesis, University of California - Berkeley, 1967.

5. Kander, R.G. Ph.D. Thesis, University of Delaware, 1985.

6. DiAndreth, J.R. Ph.D. Thesis, University of Delaware, 1985.

7. Peng, D.-Y.; Robinson, D.B. IEC Fund. 1976, 15, 59.

FIGURE 1.

Experimental Two-Phase
and Three-Phase Equilibria at 60°C

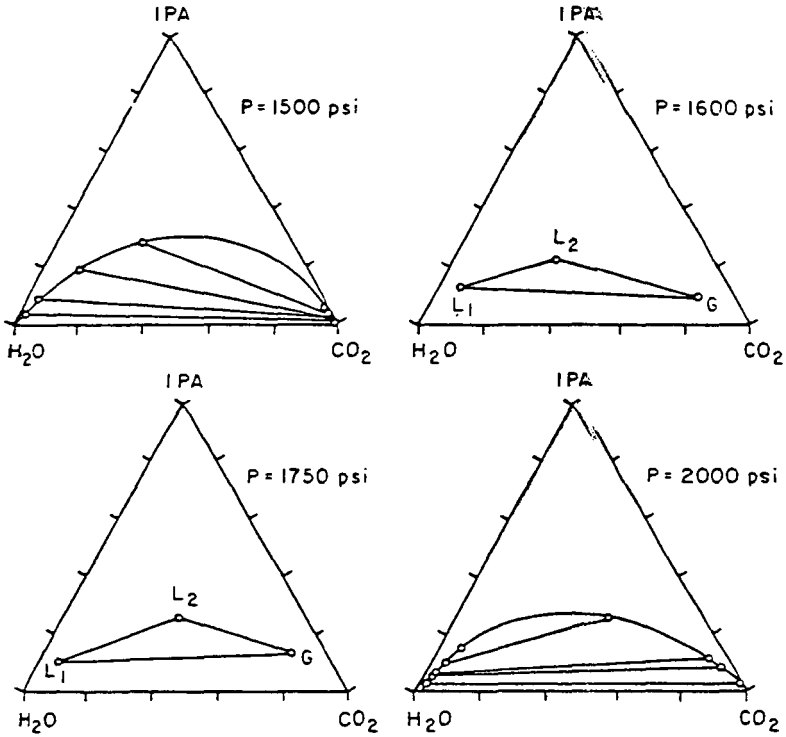

Two-Phase Data of Kander, 1984

Figure 2.

Experimental Four-Phase Compositions
at 40°C and 1110 psi

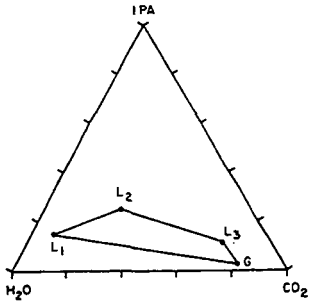

Figure 3.

Model Generated Pressure-Temperature Projection
for Isopropanol-Water-Carbon Dioxide

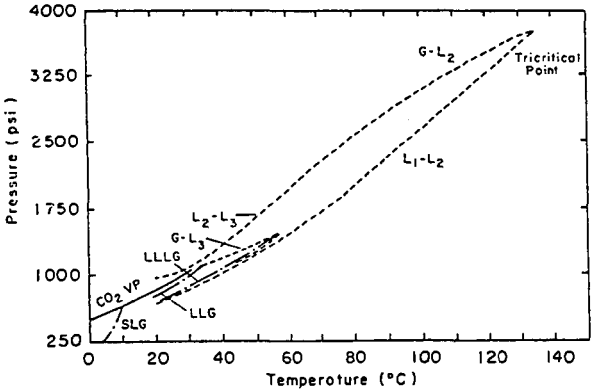

Estimation of Supercritical Fluid-Liquid Solubility Parameter Differences from Stirred Reactor Data

R.L. Eissler and J. P. Friedrich
Northern Regional Research Center, Agricultural Research Service,
U.S. Department of Agriculture, Peoria, Illinois 61604

INTRODUCTION

Solubility parameters provide a means to explain and predict solubilities of both pure and mixed materials (1). Although computation of solubility parameters involves idealized approximations, it provides a valuable tool in applications as diverse as paint and polymer formulation and chromatographic analysis. Calculation of solubility parameters has been extended to supercritical fluids (2) and we are currently investigating its utility in our research concerning the extraction of oil seeds and other materials.

Attempts to measure solubility in supercritical fluids quantitatively with a Jurgeson gage (Jurgeson Gage and Valve Co., Burington, MA) designed for pressures up to 10,000 psi were not successful because of a tendency for droplets to hang up in the apparatus. The gage however did provide an opportunity to observe when two clear phases were present. We were able to use a small, stirred reactor for mixing and for sampling from both phases after equilibration to overcome the problems of the Jurgeson gage. Solubility parameter differences between supercritical carbon dioxide and liquid solute were calculated from composition of the two phases. For the series of experiments discussed here, we selected three vegetable oils and, for contrast, four polar liquids which were expected to give relatively higher differences in solubility parameter than the oils.

EXPERIMENTAL

The soybean oil selected was a refined, bleached and deodorized commercial oil, whereas the castor oil was a cold-pressed product obtained from a local drug store. Jojoba oil had been extracted with supercritical carbon dioxide from nuts obtained from a commercial supplier. The glycerol, ethylene glycol and n-butanol were reagent grade, whereas the triethylene glycol was listed as purified. All were obtained from Fisher Chemical Co. Carbon dioxide used in these experiments was Carbon Dioxide Liquified UN2187 (Matheson Division, Searle Medical Products Inc.) furnished in tanks without dip tubes.

Our stirred reactor was a 300 cc Bench Scale Magne-Drive Packless Autoclave (Autoclave Engineers Inc., 2930 West 22nd Street, Erie, PA 16512). The autoclave had two sampling ports, one of which was used to sample from the upper phase. The other port, equipped with a dip tube, was used for sampling from the lower phase. The reactor was equipped with a gas dispersion impeller for mixing. Temperature of the system (52° or 72°) was maintained by thermostatically controlled external heating tapes placed on the head and jacket of the reactor. Both external and internal reactor temperatures were measured with thermocouples. Pressure in the system was maintained with a 30,000 psi rated, two-stage, double-ended, electric motor-driven, diaphragm compressor (Aminco Model J46-13427, American Instrument Company, Division of Travenol Laboratories, Inc., 830 Georgia Avenue, Silver Springs, MD 20190).

Fifty ml. of liquid was placed in the stirred reactor and carbon dioxide at supercritical temperature charged into the system until the desired pressure was obtained. All charges were mixed at 1,000 rpm for at least 10 min and settled for the same length of time before sampling.

Use of longer agitation times did not appear to change results. At least 3 and frequently 4 or more samples of each phase were taken. Pressure drops during sampling were recorded, but results were not affected by differing pressure drops. Normally, all samples of a phase (usually the top one) were taken before sampling the other. Where a different order was followed, results were not changed.

Samples of 3.7 ml. were taken from both upper and lower phases. The apparatus provided for isolating the samples in a section of tubing by means of valves. The isolated sample was drawn off into a weighed container which allowed the carbon dioxide to come to a standard temperature and pressure and escape into another part of the apparatus for volume measurement. After rinsing the sample tube with a suitable solvent, the liquid was recovered by solvent evaporation and weighed with an analytical balance. Molecular volumes of each of the components as well as mole fractions and volume fractions in each of the phases were computed from weight, density and molecular weight. Solubility parameter differences were computed from Equation 1, which was published by Fujishiro and Hildebrand (3) for calculation of solubility parameter differences between immiscible liquids:

$$(\delta_1-\delta_2)^2 = \frac{RT}{2}\left(\frac{1}{V_1}\ln\frac{X_{1B}}{X_{1A}} + \frac{1}{V_2}\ln\frac{X_{2A}}{X_{2B}}\right)/(\phi_{1B}-\phi_{1A}) \qquad 1)$$

where δ is the solubility parameter, x the mole fraction, ϕ the volume fraction, T temperature and V the molecular volume. In Equation 1, subscripts 1 and 2 refer to components and A and B to phases. In our experiments, phase B was arbitrarily selected as the upper phase. This upper phase was sometimes liquid rich and sometimes carbon dioxide rich. Some systems, because of a greater change in supercritical fluid density than in liquid density, inverted within the pressure range of the experimental series.

RESULTS

Absolute values for solubility parameter differences, $|\delta_{CO_2}-\delta_{liq}|$ are given in Table I. Values were computed for system pressures of 5000, 8000 and 10,000 psi for all liquids and also at 16,000 and 20,300 psi for soybean oil. When compared to the oils a greater parameter difference between polar liquids and supercritical carbon dioxide correlates with experience indicating that the latter fluid acts as a relatively non polar solvent. For the series of polar liquids solubility parameter differences were estimated at 52°C which was a convenient temperature for operation of the stirred reactor. Because we wanted to compare data for the oils with results from other experiments, measurements were taken at 71 to 72°C, although control of temperature at this level was more difficult. Standard deviation for calculated values of $|\delta_{CO_2}-\delta_{liq}|$ from the same charge was .23 cal $^{1/2}$ cm $^{-3/2}$.

DISCUSSION

Our method requires incomplete miscibility and relatively rapid attainment of equilibrium. Miscibility can be checked with the Jurgeson Gage. Equilibrium is more rapidly attained in super critical fluid-liquid than in liquid-liquid systems due to greater fluidity. Phase inversion, where it occurred, was apparently at pressures far enough removed from those where solubility was measured that any increased time required to reach equilibrium did not change computed parameter differences. For most of the liquids shown in Table I parameter differences were calculated by assuming the liquids incompressible, but

where information was available, theoretical (4) or actual (5) compressibilities were also used. Comparison of results indicated that errors arising from neglect of liquid compressibility were less than experimental ones. Trial calculations assuming reasonable errors (10% or less) in determined quantities of carbon dioxide and liquid in each phase also failed to produce large errors. The small change in parameter difference resulting from large changes in pressure is also in accord with theoretical calculations (4). Larger differences between parameters of polar liquids and supercritical carbon dioxide than between oils and the same supercritical fluid also agrees with the experience that supercritical carbon dioxide acts much like a nonpolar solvent, such as hexane, in vegetable oil extractions.

Employment of solubility parameters involves too many approximations to provide an exact method for predicting miscibility. Results, however, are valid often enough to be useful. In liquid-liquid systems composed of hydrocarbons and fluorocarbons, parameter difference estimates from Equation 1 were shown to more nearly reflect actual differences than calculated "theoretical" parameters based on the geometric mean assumption and regular solution theory (1). Since the final result of our estimate is an absolute value of the difference, we cannot tell from this calculation which parameter has the higher value. Judgment concerning actual magnitudes of the two solubility parameters can frequently be made from values for liquids under conventional conditions. For example, the solubility parameter of supercritical carbon dioxide can be computed from Equation 2 which was proposed by Giddings et al (2) for dense gases:

$$\delta_{gas} = 1.25\, P_c^{\frac{1}{2}}\, (P_r/2.66) \qquad 2)$$

where δ_{gas} is the solubility parameter of the supercritical fluid, P_c its critical pressure, P_r is the reduced density of the gas and 2.66 is a constant which is equivalent to an average reduced density for the corresponding liquid. Computed from Equation 2 the solubility parameter of carbon dioxide at 52°C and 8000 psi pressure is about 8.5 cal $^{\frac{1}{2}}$ cm $^{-3/2}$. Values taken from literature (6) are 17.7, 17.1, 14.2 and 14.0 cal $^{\frac{1}{2}}$ cm $^{-3/2}$ for solubility parameters of glycerol, ethylene glycol, triethylene glycol and n-butanol, respectively. Values for liquids are usually presented for 25°C and one atmosphere pressure, but for most liquids they exhibit only little variation with increase in pressure and increase in temperature to 52°C.

While most data in Table I appear reasonable, we have no explanation for the relatively high values for ethylene glycol at 8000 psi. Our parameter differences also do not explain the increased solubility of soy oil in supercritical carbon dioxide that occurs at 11000 to 12000 psi pressure (7).

CONCLUSION

Calculated absolute values of solubility parameter difference for the series of polar liquids used in our experiment agree well enough with values taken or computed from literature to indicate that data from a stirred autoclave can provide a useful estimate. With sufficient attention to temperature, pressure and attainment of equilibrium, results are reproducible and the calculation does not seem unduly sensitive to small environmental variations. Results appear to correlate well with extraction experience.

The mention of firm names or trade products does not imply that they are endorsed or recommended by the U.S. Department of Agriculture over other firms or similar products not mentioned.

REFERENCES

1. Hildebrand, J. H., J. M. Prausnitz, and R. L. Scott, "Regular and Related Solutions", Van Nostrand Reinhold Co., New York (1970).
2. Giddings, J. C., M. N. Myers, L. McLaren, and R. A. Keller, Science 162;67 (1968).
3. Fujishiro, R. and J. H. Hildebrand, J. Phys. Chem. 66;573 (1962).
4. Allada, S. R., Ind. Eng. Chem. Process Des. Dev. 23;344 (1984).
5. Gibson, R. E., and O. H. Loeffler, J. Am. Chem. Soc. 63;898 (1941).
6. Barton, A. F. M., Ed. "Handbook of Solubility Parameters and Other Cohesion Parameters," CRC Press, Boca Raton, Fla. (1983), p 156-157.
7. Quirin, K. W., Fette Seifen Anstrichmittel, 84;460 (1982).

TABLE I

Absolute Values† for Solubility Parameter Differences, $|\delta_{CO_2}-\delta_{liq}|$,

Between Supercritical Carbon Dioxide and Liquid

Liquid	Pressures (Psi)				
	5000	8000	10000	16000	20300
Soy Oil	1.9	1.7	1.6	1.6	1.6
Jojoba Oil[a]	2.1	1.9	1.9		
Castor Oil[a]	2.0	1.8	1.8		
Glycerol[b]	6.0	6.2	6.1		
Ethylene glycol[b]	5.7	7.9	6.7		
Triethylene glycol[b]	5.4	5.5	5.1		
n Butanol[b]	4.5	4.5	4.6		

†Solubility parameter differences in $cal^{\frac{1}{2}}\ cm^{-3/2}$

[a]Oil solubilities were measured at 71-72°C

[b]Polar liquid solubilities were measured at 52°C

A STATISTICAL-MECHANICS BASED LATTICE MODEL EQUATION OF STATE: APPLICATIONS TO MIXTURES WITH SUPERCRITICAL FLUIDS

Sanat K.Kumar, R.C.Reid and U.W.Suter

Department of Chemical Engineering,
Massachusetts Institute Of Technology, Cambridge, MA 02139

During the last decade, increasing emphasis has been placed on the use of the equation of state (EOS) approach to model and correlate high-pressure phase equilibrium behaviour. More successful applications have employed some form of cubic EOS (1-3) although others (e.g., 4) have been proposed. However, as the types of systems studied have become more complex, the inherent weaknesses of a cubic EOS have become apparent. We, in particular, are interested in studying phase behaviour of systems comprising polymer molecules in the presence of a supercritical fluid. Here the size disparity of the component molecules can be large. One approach would have been to adopt the modified perturbed hard chain theory (5,6) which has been adapted for mixtures of large and small hydrocarbon molecules. We, however, elected to study whether lattice theory models could be of value for systems of our interest. Studies based on this approach, have been attempted for different systems (7-11), and an interesting general model proposed by Panayiotou and Vera (12). Our approach is similar in many respects to the last reference although significant differences appear in treating mixtures.

Pure Components

Theory

Molecules are assumed to "sit" on a lattice of coordination number z and of cell size v_H. Each molecule (species 1) is assumed to occupy r_1 sites (where r_1 can be fractional), and the lattice has empty sites called holes. There are N_0 holes and N_1 molecules. To account for the connectivity of the segments of a molecule, an effective chain lenth q_1 is defined as,

$$zq_1 = zr_1 - 2r_1 + 2 \qquad 1)$$

wherein it has been assumed that chains are not cyclic. zq_1 now represents the effective number of external contacts per molecule. The interaction energy between segments of molecules is denoted by $-\varepsilon_{11}$, while the interaction energy of any species with a hole is zero. Only nearest neighbour interactions are considered, and pairwise additivity is assumed. The canonical partition function for this ensemble can be formally represented as:

$$\Omega = \sum_{\substack{\text{all} \\ \text{states } \{n\}}} \exp(-\beta E_{\{n\}}) \qquad 2)$$

where $\beta = 1/kT$. On the assumption of random mixing of holes and molecules, and following the approach of Panayiotou and Vera (12), we obtain an expression for Ω which is valid outside the critical region of the pure component, i.e.,

$$\Omega = \left(\frac{\delta}{\sigma}\right)^{N_1} \frac{(N_0 + r_1 N_1)!}{N_0!\ N_1!} \left(\frac{(N_0 + N_1 q_1)!}{(N_0 + N_1 r_1)!}\right)^{z/2} \exp\left(\frac{\beta}{2} z N_1 q_1\ \epsilon_{11} \frac{N_1 q_1}{N_0 + N_1 q_1}\right) \qquad 3)$$

where δ is the number of internal arrangements of a molecule and σ a symmetry factor. Using the following reducing parameters

$$(z/2)\epsilon_{11} = P^* v_H = RT^* \qquad 4)$$

and defining $\underline{V}$, the total volume of the system,

$$\underline{V} = v_H(N_0 + r_1 N_1) \qquad 5)$$

an EOS that defines the pure component is obtained, i.e.,

$$\frac{\tilde{P}}{\tilde{T}} = \ln\left(\frac{\tilde{v}}{\tilde{v} - 1}\right) + \frac{z}{2} \ln\left(\frac{\tilde{v} + (q/r) - 1}{\tilde{v}}\right) - \frac{\theta^2}{\tilde{T}} \qquad 6)$$

Here θ is the effective surface fraction of molecules and the tilde (~) denotes reduced variables. All quantities except v, in the EOS are reduced by the parameters in Eq.(4). The specific volume v, is reduced by v^*, the molecular hard-core volume,

$$v^* = N_1 r_1 v_H \qquad 7)$$

Expressions for the chemical potential of a pure component can also be derived from Eq.(3) and standard thermodynamics (13).

Determination of pure component parameters

In order to use the obtained EOS to model real substances one needs to obtain ϵ_{11} and v^*. For a pure component below its critical point, a technique suggested by Joffe et al., (14) was used. This involves the matching of chemical potentials of each component in the liquid and the vapour phases at the vapour pressure of the substance. Also the actual and predicted saturated liquid densities were matched. The set of equations so obtained were solved by the use of a standard Newtons method to yield the pure component parameters. Values of ϵ_{11} and v^* for ethanol and water at several temperatures are shown in Table 1. In this calculation v_H and z were set at 9.75×10^{-6} m^3 $mole^{-1}$ and 10, respectively (12). The capability of the lattice EOS to

fit pure component VLE was found to be quite insensitive to variations in z ($6<z<26$) and v_H (1.0×10^{-7} $m^3mole^{-1}<v_H<1.5\times 10^{-5}$ m^3mole^{-1}).

For SCF, the pure component parameters were obtained by fitting P-v data on an isotherm. Preliminary data for these substances suggest that although the computed v^* is a function of temperature, ε_{11} is a constant within regression error.

Discussion

In order to qualitatively understand the behaviour of the lattice EOS, it was examined in the limit of small molecules ($q,r \longrightarrow 1$). In this case Eq.(6) simplifies to the form,

$$\frac{\tilde{P}}{\tilde{T}} = \ln\left(\frac{\tilde{v}}{\tilde{v}-1}\right) - \frac{1}{\tilde{T}\,\tilde{v}^2} \qquad 8)$$

The first term can be identified with a "hard-sphere" repulsion term, while the second acconts for attractive forces. The second term can be rewritten as,

$$Z_a = \frac{P_a\, v}{R\, T} = -\frac{(P^* v^{*2})}{v^2} = -\frac{a}{v^2} \qquad 9)$$

Thus, the attractive term represented in Eq.(9) has the same form as the attractive term in the van der Waals EOS (15). On examining the data in Table 1, and computing the parameter a in Eq.(9), it was found that for variations of up to 150K, the variation of this parameter was always less than 3%, although the computed values of v^* and ε_{11} themselves showed a 7% variation. In the limit of small molecules, therefore, the lattice EOS has a term that approximates the van der Waals type attractive term closely.

The behaviour of the repulsive term of the lattice EOS is more complicated and will not be discussed in detail. At liquid-like densities this repulsion term is a better approximation to the hard spheres repulsion than the van der Waals repulsion term. At gas-like densities, however, the oppósite behaviour is observed.

Binary Mixtures

Theory

Consider a mixture of N_0 holes, N_1 molecules of species 1 and N_2 molecules of species 2. Following Panayiotou and Vera (12) the following mixing rules are assumed for the mixture parameters r_M, q_M and v_M^*.

$$r_M = \sum x_i\, r_i \qquad 10)$$

$$q_M = \sum x_i \, q_i \qquad 11)$$

$$v_M^* = \sum x_i \, v^*_i \qquad 12)$$

Lattice coordination numbers (z) and the cell volumes (v_H) for both the pure components and mixture lattices are assumed to have the same value. The partition function for this ensemble can be formulated following Eq.(2). It is assumed now that the partition function, far from the binary critical point can be approximated by its largest term. Since molecule segments and holes can distribute themselves nonrandomly, the partition function must incorporate terms to account for this effect. The nonrandomness correction Γ_{ij} allows for distribution of the segments of species i about the segments of species j over the random values of such contacts. It is defined through the equation

$$N_{ij} = N^0_{ij} \quad \Gamma_{ij} \qquad 13)$$

where N_{ij} is the actual number of i-j contacts and $N_{ij}{}^0$ is the number of i-j contacts in the completely random case. Expressions for the nonrandomness correction must be obtained through the solution of the "quasichemical" equations(16). These equations can be solved in a closed analytic form only in the case of a two component system. In order to ensure the mathematical tractability of the binary results, it is therefore assumed that holes distribute randomly while molecules do not.

The solution for the quasichemical expressions for the pseudo two component system yields an expression for the nonrandomness correction Γ_{ij}, which can be represented mathematically as,

$$\Gamma_{ij} = \frac{2}{1 + (1 - 4\bar{\theta}_i \, \bar{\theta}_j \, (1 - g))^{1/2}} \qquad 14)$$

where,

$$g = \exp (\theta \Delta\varepsilon / kT), \qquad 15)$$

$$\Delta\varepsilon = \varepsilon_{11} + \varepsilon_{22} - 2\varepsilon_{12} \qquad 16)$$

$\bar{\theta}_i$ is the surface fraction of i molecule segments on a hole-free basis and θ is the total surface area fraction of molecule segments. Eq.(16) immediately suggests a combining rule for ε_{12} as a measure of the departure of the mixture from randomness, i.e.,

$$\varepsilon_{ij} = \begin{cases} \varepsilon_{ii} \, , & i=j \\ 0.5 \, (\varepsilon_{ii} + \varepsilon_{jj} \,) \, (1 - k_{ij}), & i \neq j \end{cases} \qquad 17)$$

The mixing rule for ε arises naturally through the formulation of the canonical partition function, i.e.,

$$\varepsilon_M = \theta \sum_i \sum_j \bar{\theta}_i \bar{\theta}_j \Gamma_{ij} \varepsilon_{ij} \qquad 18)$$

An EOS for the mixture and chemical potentials for component i in the mixture can now be derived using standard thermodynamics.

$$\frac{\tilde{P}}{\tilde{T}} = \ln\left(\frac{\tilde{v}}{\tilde{v}-1}\right) + \frac{z}{2}\ln\left(\frac{\tilde{v}+(q/r)-1}{\tilde{v}}\right) - \frac{\theta^2}{\tilde{T}} +$$

$$+ 0.5zg\frac{\Delta\varepsilon}{kT}\frac{(\bar{\theta}_1\bar{\theta}_2\theta\,\Gamma_{12})^2}{(1-4\bar{\theta}_1\bar{\theta}_2(1-g))^{(1/2)}}\ln\left(\frac{\Gamma_{11}\,\Gamma_{22}}{4\,\Gamma_{12}^2\,g^{\theta}}\right) \qquad 19)$$

$$-\frac{\mu_i}{kT} = \lambda(T) + \ln q_i - \ln\theta\,\bar{\theta}_i + r_i(0.5z-1)\ln\left(\frac{\tilde{v}+(q/r)-1}{\tilde{v}}\right)$$

$$-\frac{q_i\theta^2}{\tilde{T}} + \frac{q\,\theta_i}{\tilde{T}\,\varepsilon^*}\Big[\,2\bar{\theta}_i\varepsilon_{ii}\Gamma_{ii} + 2\bar{\theta}_j\varepsilon_{ij}\Gamma_{ij} + \bar{\theta}_1\varepsilon_{11} + \bar{\theta}_2\varepsilon_{22} - \bar{\theta}_1\varepsilon_{11}\Gamma_{1i}$$

$$-\bar{\theta}_2\varepsilon_{22}\Gamma_{2i}\Big] - \left[\frac{\theta\,\Delta\varepsilon}{\tilde{T}\,\varepsilon^*} + \ln\frac{\Gamma_{11}\,\Gamma_{22}}{\Gamma_{12}^2}\right]\frac{\bar{\theta}_1\bar{\theta}_2\,\Gamma_{12}^2\,q_i}{(1-4\,\bar{\theta}_1\bar{\theta}_2(1-g))^{(1/2)}}$$

$$\left[\bar{\theta}_j\,(\bar{\theta}_j-\bar{\theta}_i)(1-g) - \bar{\theta}_1\bar{\theta}_2 g\frac{\Delta\varepsilon}{kT}\theta\,(1-\theta)\right] - \ln\Gamma_{12} - 0.5zq_i\left[\theta_1(1-\Gamma_{1i})\right.$$

$$\left.\ln\frac{\bar{\theta}_1\,\Gamma_{11}}{\bar{\theta}_2\,\Gamma_{12}} + \bar{\theta}_2\,(1-\Gamma_{i2})\ln\frac{\bar{\theta}_2\,\Gamma_{22}}{\bar{\theta}_1\,\Gamma_{12}}\right] + 0.5zq_i\left[\ln\frac{\bar{\theta}_1}{\bar{\theta}_2} - \Gamma_{11}\ln\frac{\bar{\theta}_1\Gamma_{11}}{\bar{\theta}_2\Gamma_{12}}\right]$$

$$\bar{\theta}_1\,(2\delta_{1i}-\bar{\theta}_1) + 0.5zq_i\left[\ln\frac{\bar{\theta}_2}{\bar{\theta}_1} - \Gamma_{22}\ln\frac{\bar{\theta}_2\,\Gamma_{22}}{\bar{\theta}_1\,\Gamma_{12}}\right]\bar{\theta}_2\,(2\delta_{2i}-\bar{\theta}_2) \qquad 20)$$

where μ_i represents the chemical potential of component i in a binary mixture, j=3-i and $\lambda(T)$ is some universal temperature function. δ_{ij} is the Dirac-delta function. Parameters used for obtaining these equations in a dimensionless form are defined in manner analogous to Eq.(4).

The mixture EOS [Eq. (19)] has the three terms that are present in the pure component EOS. Also, it has an additional term which accounts for the nonrandomness corrections that have been incorporated into the partition function expression. This last term, for all cases tested, is always at

least 4 orders of magnitude smaller than the other three terms and can effectively be neglected. However, it is retained for the sake of mathematical consistency.

Results and Discussion

The expressions derived for the EOS and the chemical potential of component i in a binary mixture were used to model the phase equilibria of binary mixtures. A set of non-linear equations was obtained and solved by the use of a Newton's method.

Mixtures of small molecules (acetone-benzene, ethanol-water) were considered first. In Figures 1 and 2, a comparison is made between the predicted and experimental low-pressure VLE data (17,18) for these systems. An excellent fit to the data is obtained in both cases, with the use of one apparently temperature independent parameter (k_{ij}) per binary.

The interesting aspect of this modelling is the temperature independence of k_{ij}. It was shown earlier that, if the pure components were small molecules, the lattice EOS has an attractive term with an essentially temperature independent a. Extending this argument to mixtures results in the prediction of the temperature independence of k_{ij} for binary mixtures of small molecules. A temperature independent interaction parameter is a property of the binary, which could, in concept, be calculated by group contribution techniques. This scheme, if implemented, would make the modelling technique a predictive one.

In examining the sensitivity of the model to the assumed value of z, it was found for the ethanol-water system that the model predictions were insensitive to the z value in the vicinity of z=10. For large values of z (z>15), however, it was found that the model was incapable of even qualitatively prediciting mixture VLE behaviour.

The applicability of the lattice EOS in the modelling of the VLE of mixtures of molecules of different sizes was examined next. The results for the H_2S-n-heptane system at 310K and 352K are shown in Figure 3 (19). For the temperatures modelled, it is seen that there is a good agreement between the prediction and the experimental data, again with the use of one temperature independent binary interaction parameter.

The lattice model thus provides the capability to obtain good, quantitative fits to experimental VLE data for binary mixtures of molecules below their critical point. Its value lies in the fact that it performs equally well regardless of the size differences between the component molecules.

The model was then extended to the phase equilibrium modelling of solid-supercritical fluid (SCF) binaries. In Figures 4 and 5, the model behaviour is compared to experimental data for the naphthalene-carbon dioxide binary at 308 and 318K respectively. Outside the critical region, the lattice EOS provides a good fit to the measured data (20). The k_{ij} values, however,

were not temperature independent.

The agreement of the model with the data in the critical region is not satisfactory. The reason for this failure is believed to be two fold. Firstly, the partition function expression for the binary is valid in a region where the largest term in the summation in Eq.(2) dominates all other terms. In the critical region this assumption breaks down. Secondly, it has been assumed (for mathematical tractability) that holes distribute randomly while molecules do not. This assumption could be another cause of the poor fits obtained in the critical region.

In order to test the applicability of the model to polymer-SCF systems, a hypothetical system of CO_2 and a monodisperse x-mer with a monomeric unit molecular weight of 100 was simulated. Reasonable values for the pure component parameters for the polymer were chosen (12). Constant values of k_{ij} were used for the polymer system, where the degree of polymerization, x, varied between 1 and 7. It was assumed that all chains had the same ε, and v^* scaled as the molecular weight of the chain. Figure 6 shows the results of the predicted mole fraction of the x-mer in the SCF phase.

The model simulates an experimentally observed trend (20) that the solubility of chains in a SCF shows a strong inverse dependence on the molecular mass of the polymer. Figure 6 shows that changing the molecular weight of the chain molecule from 100 to 700 causes a reduction in solubility of nearly 6 orders of magnitude. The model also shows that all the solubility plots tend to flatten out around 300 bar, as observed in experiments. Classically used EOS like a modified cubic EOS (22), when applied to such systems, produce solubility curves which tend to show a sharp maximum around 200 bar. For polymer-SCF systems, therefore, the lattice EOS is believed to be superior to modified cubic EOS.

Conclusions

A new attempt towards the development of a statistical-mechanics based model for mixtures of molecules of disparate sizes has been made. Results obtained to date demonstrate that the lattice EOS is superior to modified cubic EOS for polymer-SCF equilibria, while for the other systems, outside the critical region, it performs as well as classically employed techniques. The removal of the assumption regarding the random mixing of holes is expected to improve the performance of the model in the critical region.

The temperature independence of the a parameter [Eq.(9)] and the binary interaction parameter (k_{ij}) for systems of small molecules are interesting phenomena that merit closer examination.

Table 1: Pure Component parameters for ethanol and water at several temperatures (z=10, v_H=9.75 x 10^{-6} m^3mole^{-1})

	Ethanol		Water	
T (K)	ϵ_{11}/k (K)	v^* (cm^3g^{-1})	ϵ_{11}/k (K)	v^* (cm^3g^{-1})
283	1357.59	1.2018	3596.56	0.9602
293	1355.47	1.2016	3516.20	0.9685
303	1314.34	1.2193	3438.16	0.9767
313	1294.18	1.2276	3362.54	0.9588
323	1274.90	1.2358	3289.36	0.9943
333	1256.49	1.2437	3218.53	1.0030
343	1238.87	1.2515	3150.14	1.0123
353	1222.04	1.2589	3083.99	1.0216
363	1205.89	1.2661	3020.02	1.0310
373	1190.43	1.2731	2958.16	1.0406
393	1161.42	1.2864	2840.43	1.0602
413	1134.68	1.2989	2730.13	1.0804
433	1109.83	1.3109	2626.57	1.1011

REFERENCES

1. Peng D.Y., Robinson D.R., "A new two constant equation of state", Ind. Eng Chem. Fundam., **15**(1),59(1976)

2. Soave G., "Equilibrium constants from a modified Redlich-Kwong equation of state", Chem. Eng. Sci., **27**,1197(1972)

3. Carnahan N.F., Starling K.E., "Intermolecular forces and the equation of state for fluids", AIChEJ, **18**(6),1184(1972)

4. Dieters U.K., "A new semi empirical equation of state for fluids I", Chem. Eng. Sci., **36**,1139(1981)

5. Donohue M.D., Prausnitz J.M., "Perturbed hard chain theory for fluid mixtures: Thermodynamic properties for mixtures in natural gas and petroleum technology", AIChEJ, **24**(5), 850(1975)

6. Vimalchand, Donohue M.D., "Thermodynamics of quadropolar molecules: The Perturbed Anisotropic Chain Theory", submitted to Ind. Eng. Chem. Fundam

7. Vezetti D.J., "Solubilities of solids in supercritical fluids", J. Chem Phys.,**77**,1512(1980)

8. Vezetti D.J., "Solubilities of solids in supercritical gases II. Extension to molecules of differing sizes", J. Chem. Phys.,**80**(2),868-71(1984)

9. Simha R., Somcynysky T., "On the statistical thermodynamics of spherical and chain molecule fluids", Macromolecules, **2**(4),342-350(1969)

10. Jain R.K., Simha R., "On the equation of state of argon and organic liquids", J. Chem. Phys.,72(9), 4909-4912(1980)

11. Hirshfelder J.O., Curtiss C.O., Bird R.B., "Molecular theory of gases and liquids", pp275-320, John Wiley and sons., 1954

12. Panayiotou C., Vera J.H., "Statistical thermodynamics of r-mer fluids and their mixtures", Polymer Journal, 14(9),681(1982)

13. Modell M., Reid R.C., "Thermodynamics and its applications",2 ed., Prentice Hall, 1983.

14. Joffe J., Schroeder G.M., Zudkevitch D., "Vapor-liquid Equilibria with the Redlich-Kwong Equation of State", AIChEJ, 48,261-266(1970)

15. van der Waals J.D., Doctoral thesis, Leiden,1873.

16. Guggenheim E.A., "Mixtures", Clarendon Press, Oxford, 1954.

17. Weisphart J., "Thermodynamic equilibria of boiling mixtures", Springer-Verlaeg. Berlin,1975

18. Pemberton R.C., Mash C.J., "Thermodynamic properties of aqueous non-electrolyte mixtures II. Vapour pressures and excess Gibbs energies for water + ethanol at 303.15 K to 363.15 K determined by an accurate static method"., J. Chem. Therm.,10,867-888(1978)

19. Ng H-J., Kalra H., Robinson D.B., Kubota H., "Equilibrium phase properties of the toluene-hydrogen sulfide and n-heptane-hydrogen sulfide binary systems", J. Chem. Eng. Data.,25, 51-55(1980)

20. Tsekhanskaya Yu. V., Iomtev M.B., Muskina E.V., "Solubility of naphthalene in ethylene and carbon dioxide under pressure", Russ. J. Phy. Chem., 38(9), 1173(1964)

21. Schröeder E., Arndt K-F., "Löslichkeitverhalten von Makromolekülen in komprimierter Gasen", Faserforschung und Textiltechnik, 247(3), 135(1976)

22. Panagiotopoulos A.Z., Reid R.C., "A new mixing rule for cubic equations of state for highly polar, asymmetric systems", Paper presented at the ACS meeting in Miami, Florida (1985)

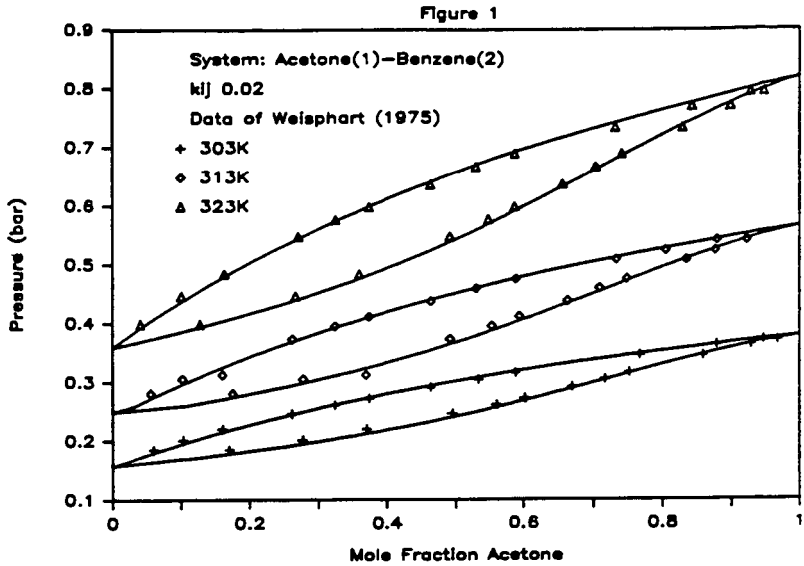

Figure 1: Comparison of lattice model prediction and experimental data of Weisphart (17) for the acetone-benzene binary at 303, 313 and 323 K (z=10, v_H=9.75 x 10^{-6} m^3mole^{-1}, k_{ij} =0.02).

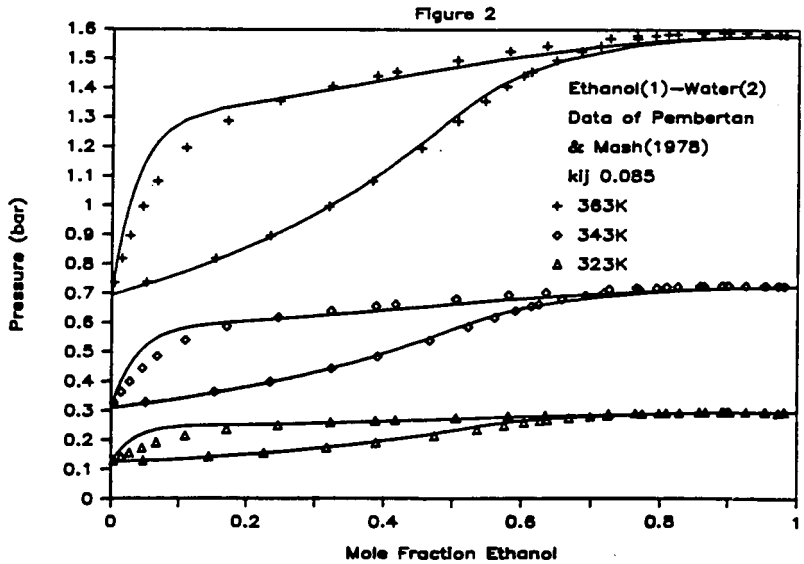

Figure 2: Comparison of the experimental data of Pemberton and Mash (18) for the ethanol-water binary at 323, 343 and 363K with the lattice model predictions with z=10, v_H=9.75 x 10^{-6} m^3mole^{-1} and k_{ij}=0.085.

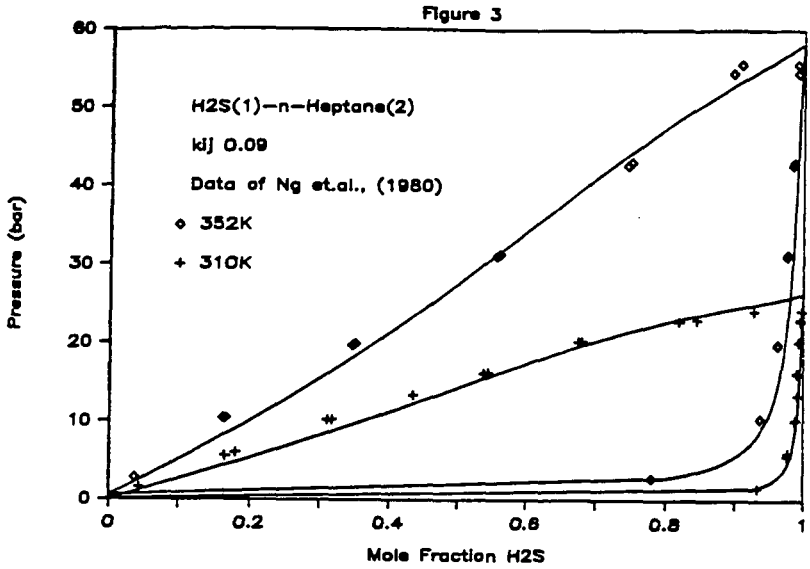

Figure 3: Comparison of the lattice model predictions and experimental data of Ng. et. al., for the H_2S- n-heptane system at 310 and 352K (z=10, v_H=9.75 x 10^{-6} m^3mole^{-1} and k_{ij}=0.09).

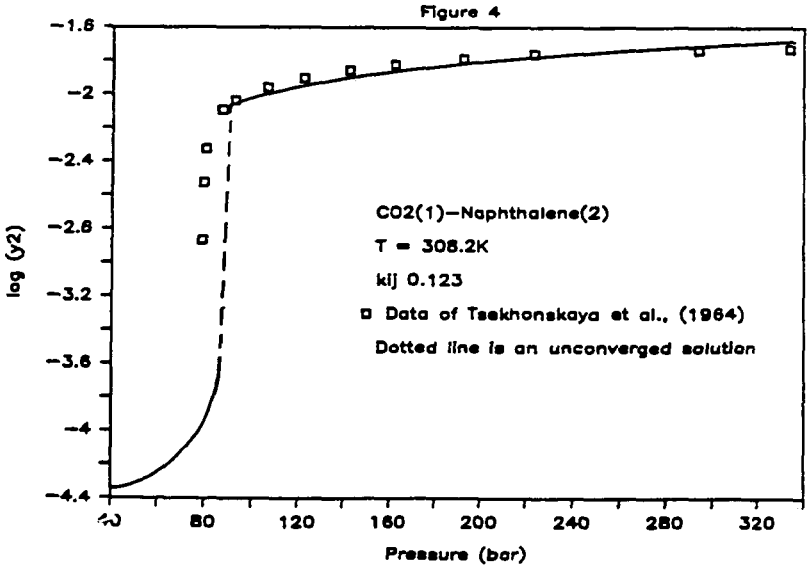

Figure 4: Comparison of the model predictions for the CO_2-napthalene binary at 308K with the experimental data of Tsekhanskaya et. al., (20).(z=10, v_H=9.75 x 10^{-6} m^3mole^{-1}, k_{ij} =0.123).

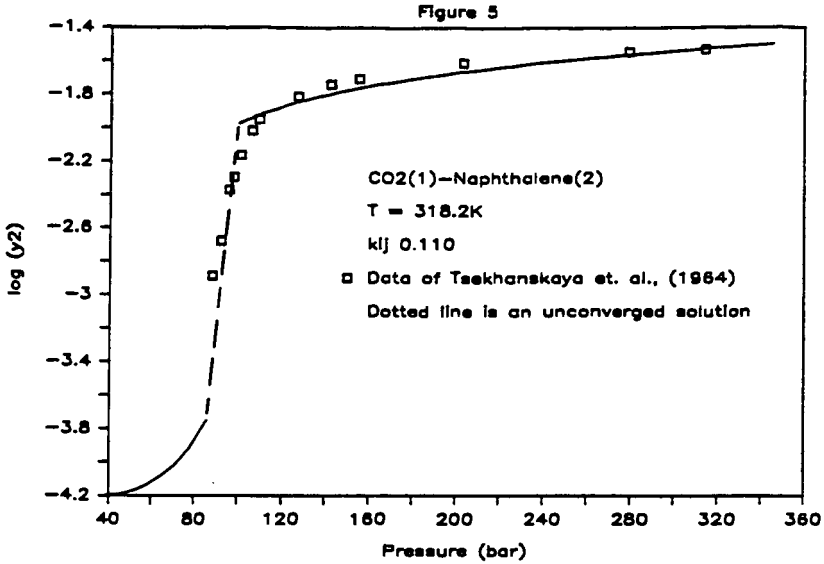

Figure 5: Comparison of the model predictions for the CO_2-napthalene binary at 318K with the experimental data of Tsekhanskaya et. al., (20). (z=10, v_H=9.75 x 10^{-6} m^3mole^{-1}, k_{ij} =0.11).

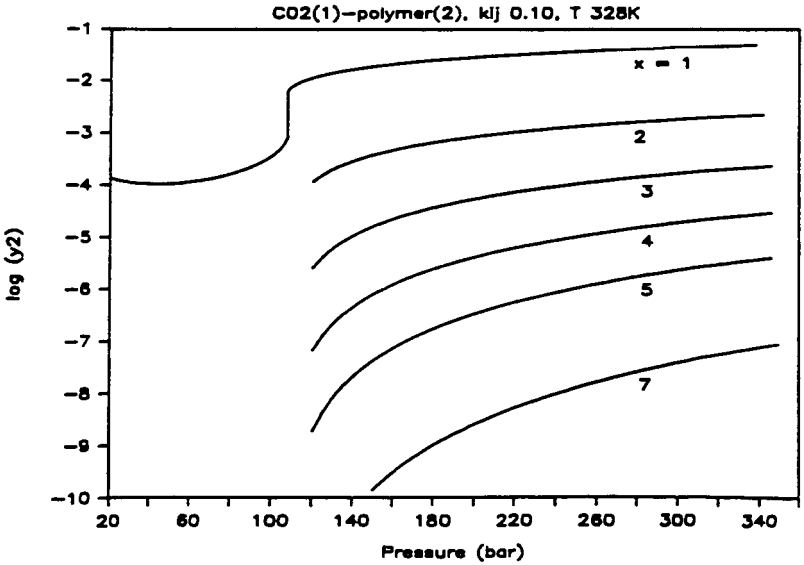

Figure 6: Lattice model predictions for the equilibrium fluid phase composition for a CO_2-polymer system at 328K. Molecular weight of a monomeric unit is 100, while the degree of polymerization, x, varies between 1 and 7. (z=10, v^H=9.75 x $10^{-6}m^3mole^{-1}$, k_{ij} =0.10).

HETEROLYSIS AND HOMOLYSIS IN SUPERCRITICAL WATER

Michael Jerry Antal, Jr., Andrew Brittain,
Carlos DeAlmeida and Sundaresh Ramayya

Department of Mechanical Engineering
University of Hawaii, Honolulu, Hawaii 96822

INTRODUCTION

Efficient thermochemical processes underlie the conversion of crude oil and natural gas liquids to higher value chemicals and fuels. Unfortunately, attempts to develop similar conversion processes for biomass feedstocks (such as wood chips and bagasse) have been frustrated by the non-specificity of high temperature pyrolysis reactions involving biopolymer substrates (1,2). For example, the pyrolysis of bagasse yields a liquid mixture of carbohydrate sirups and phenolic tars, a gas composed primarily of carbon oxides and hydrogen, and a solid charcoal. Variations of the conventional engineering parameters (temperature, heating rate, residence time and pressure) do not provide a good control over the complex set of concurrent and consecutive pyrolysis reactions. Thus it has not been possible to engineer the pyrolysis reactions to produce a few high value products from biomass materials.

Recent advances in materials technology, high pressure pumps and other high performance liquid chromatography (HPLC) equipment, have created new opportunities (3) for fundamental studies of chemical reactions in solvents at very high pressures (>30 MPa) and temperatures (>400° C). For sufficiently dilute solute-solvent mixtures at pressures $P>P_c$, no liquid-vapor phase transition occurs as the mixture is heated. Furthermore, when the temperature T is near the solvent's critical temperature T_c and $P>P_c$ many solvents manifest extraordinary properties (4,5). These unusual properties provide new parameters for the control of chemical reactions involving biopolymers and other substrates.

As discussed in the following sections, when the density of supercritical (SC) water exceeds 0.4 g/cm$_3$ the fluid retains its ionic properties (high dielectric constant and ion product) - even at high temperatures. These properties provide new opportunities to catalyze a variety of heterolytic bond cleavages with a high degree of specificity. Examples discussed in this paper include the dehydration of ethanol to ethylene, the dehydration of glycerol to acrolein, and the conversion of 1,3 dioxolane to glycol and formaldehyde. In each of these examples the specificity of the heterolytic bond cleavage is high (approaching one mole of desired product per mole of reactant); whereas the conventional, higher temperature, free radical reactions offer lower yields of the same desired products. In the case of ethanol dehydration, findings reported here have exciting implications for the production of ethylene from ethanol, which may find early application in Brazil.

PRIOR WORK

Interest in the use of SCF solvents as a reaction media is founded upon recent advances in our understanding of their unique thermophysical and chemical properties. Worthy of special note are those thermophysical properties (6) which can be manipulated as parameters to selectively direct the progress of desirable chemical reactions. These properties include the solvent's dielectric constant (7), ion product (8,9), electrolyte solvent power (10,11), transport properties (viscosity (12), diffusion coefficients (13) and ion mobilities (14)), hydrogen bonding characteristics (15), and solute-solvent "enhancement factors" (6). All these properties are strongly influenced by the solvent's density ρ in the supercritical state.

For example, SC water with $\rho = 0.47$ g/cm^3 at 400° C (P = 35. MPa) enjoys a dielectric constant of about 10 (comparable to a polar organic liquid under normal conditions), an ion product of 7×10^{-14} (vs 10^{-14} at room conditions) and a dynamic viscosity =0.57 millipoise (vs 10 at room conditions). Under these conditions SC water behaves as a water-like fluid with strong electrolytic solvent power, high diffusion coefficients and ion mobilities, and considerable hydrogen bonding. These properties favor chemical reactions involving heterolytic (ionic) bond cleavages which can be catalyzed by the presence of acids or bases.

Dramatic changes occur when the temperature of the SC water is raised to 500° C at constant pressure (ρ=0.144 g/cm^3). Decreases in the dielectric constant to a value of 2 and ion product to 2.1×10^{-20} cause the fluid to lose its water-like characteristics and behave as a high temperature gas. Under these conditions homolytic (free radical) bond cleavages are expected to dominate the reaction chemistry. Thus by using the engineering parameters of temperature and pressure one can dramatically change the chemical properties of the solvent (dielectric constant and ion product) to favor heterolytic or homolytic bond cleavages. This paper emphasizes the manipulation of these parameters as a means for engineering the reaction chemistry of biopolymer materials.

APPARATUS AND EXPERIMENTAL PROCEDURES

Figure 1 is a schematic of the SC flow reactor. Prior to the initiation of flow, the system is brought up to pressure by an air compressor. Afterwards, an HPLC pump forces a pure solvent into the reactant accumulator at a measured rate of flow. This flow displaces the solvent/solute reactant mixture out of the accumulator, through the reactor and a 10 port valve dual loop sampling system, and into the product accumulator. The flow of products into the second accumulator displaces air through a back-pressure regulator and into a water displacement apparatus, which measures the rate of air flow at ambient conditions. The

reactant flow is rapidly heated to reaction temperature by the entry heat guard, and maintained at isothermal conditions by a Transtemp Infra-red furnace and an exit heat guard. Samples captured in 5.4 ml sample loops are released into sealed, evacuated test tubes for quantitative analysis by GC, GC-MS, and HPLC instruments within the laboratory. The outer annulus of the reactor is a 4.572 mm ID Hastelloy C-276 tube, and the inner annulus is a 3.175 mm OD sintered alumina tube, giving the reactor an effective hydraulic diameter of 3.2 mm. The alumina tube accommodates a movable type K thermocouple along the reactor's axis, which provides for the measurement of axial temperature gradients along the reactor's functional length. Radial temperature gradients are measured as differences between the centerline temperature and temperatures measured at 10 fixed positions along the outer wall of the reactor using type K thermocouples. The location of the movable thermocouple within the reactor is measured electronically to within 0.01 mm by a TRAK digital position read out system. The entire reactor and sampling system is housed in a "bullet proof" enclosure which can be purged of air (oxygen) during studies involving flammable solvents (such as methanol).

The reactor can be characterized by the following representative nondimensional numbers: Re = 33, Pr = 1.3, Sc = 0.43, $Pe_{thermal\ diffusion}$ = 43, $Pe_{species\ diffusion}$ = 56 and Da = 0.15. Figure 2 displays a typical temperature profile of the reactor during operation. Because the thermal diffusivity of SC water is comparable to that of many high quality insulation materials, gross radial temperature gradients can easily exist in a flow reactor. As shown in Figure 2, radial temperature gradients within the annular flow reactor are negligible. A computer program, which accurately accounts for the effects of the various fluid (solvent, solvent and solute, air) compressibilities on flow measurements, calculates mass and elemental balances for each experiment. A typical experiment evidences mass and elemental balances of 1.00±0.05.

RESULTS AND DISCUSSION

Results of experiments probing the dehydration chemistry of ethanol in SC water (P = 34MPa) are summarized in Table 1. The low temperature (400° C), uncatalyzed dehydration is very slow, and little ethylene is formed. However, in the presence of 0.1 M H_2SO_4 the reaction is both rapid and highly specific. The effectiveness of the acid catalyst is a result of the high degree of dissociation of H_2SO_4 in SC water at 400° C and 34 MPa, as well as the high mobility of H^+ ions in SC water. These results contrast with the conventional (16) acid catalyzed dehydration, which requires heating the alcohol in 95% H_2SO_4 at 170° C. Figure 3 displays the acid catalyzed heterolytic reaction mechanism for ethanol dehydration.

Table 1 also reveals a dramatic loss in specificity at higher temperatures (500° C) due to the increasing role of homolysis in the reaction chemistry. Unwanted products of

homolysis include CH_4, H_2, and C_2H_6, which serve to decrease the yields of the desired product ethylene. Homolysis is favored under these conditions because the water has lost its ionic properties (ion product = 10^{-20}) and will not facilitate the dissociation of acid catalysts or the formation of carbonium ion intermediates.

Table 2 summarizes similar results for the dehydration of glycerol (40). As shown in Figure 4, the observed products (acetaldehyde, acrolein, and the gases CO_2, H_2, CO, CH_4, C_2H_4 and C_2H_6) can be explained by any one of several different pathways and mechanisms. However, an experiment with the posited intermediate acetol as the reactant produced only gases; hence pathway 1 cannot be the source of acrolein. The dramatic increase in the relative yield of acrolein in the presence of $NaHSO_4$ at 360° C supports the role of the heterolytic pathway 2 in forming acrolein. The significant influence of the free radical scavenger hydroquinone in reducing acrolein yields supports the role of homolytic bond cleavage (pathway 3) in the formation of acrolein at higher temperatures (500° C). These findings are in accord with earlier studies of the vapor phase pyrolysis of glycerol (17), and the results of experiments involving ethanol given in Table 1. Here again we observe the high specificity of dehydration reactions involving acid catalyzed, heterolytic bond cleavages.

In addition to the dehydration of ethanol and glycerol, we have also completed less detailed studies of the reaction chemistry of 1,3 dioxolane, glycol, acetaldehyde and acetic acid in SC water, and (in some cases) SC methanol. At 350° C and 34 MPa the facile reaction of 1,3 dioxolane with water produces glycol and formaldehyde (99.8% yield) via a carbonium ion intermediate. Here again is an example of the extraordinary specificity heterolytic reaction chemistry. The model compounds glycol, acetaldehyde and acetic acid undergo negligible decomposition in SC water at temperatures up to 500° C, pressures to 34 MPa, and residence times approaching 3 minutes.

Because of the potential commercial significance of ethanol dehydration in SC water, we are presently developing kinetic expressions for the rate of ethylene formation in the SC water environment. We are also measuring the rate of ethanol dehydration in the vicinity of the critical point of water to determine if the properties of the fluid near the critical point have any influence on the reaction rates. In the near future we plan to begin studies of the reaction chemistry of glucose and related model compounds (levulinic acid) in SC water.

CONCLUSIONS

The significance of this work is its identification of SC water as a media which supports and enhances aqueous phase chemistry ordinarily observed at much lower temperatures. Fundamental studies of the reaction chemistry of biopolymer related model compounds described in this paper offer insights

into the details of reaction mechanisms, and facilitate the choice of reaction conditions which enhance the yields of valuable products. Chemical reaction engineering in supercritical solvents, based on the ability to choose between heterolytic and homolytic reaction mechanisms with a foreknowledge of results, holds much promise as a new means to improve our utilization of the vast biopolymer resource.

ACKNOWLEDGMENTS

This research was supported by the National Science Foundation under grant CPE 8304381, the Department of Planning and Economic Development of the State of Hawaii, and the Coral Industries Endowment. The authors thank Dr. Maria Burka (NSF), Kent Keith and Dr. Tak Yoshihara (DPED), and David Chalmers (Coral Industries) for their interest in this work. The authors also thank William Mok for his continuing assistance with the flow reactor, Dr. Ali Tabatabaie-Raissi, Dr. Jiben Roy, and Professor Maitland Jones (Princeton) for many stimulating discussions.

REFERENCES

1. Antal, M.J. "Biomass Pyrolysis. A Review of the Literature - Part 1: Carbohydrate Pyrolysis" in Advances in Solar Energy, (Eds. K.W. Boer and J.A. Duffie) Vol. 2, Plenum Press, New York, 1985.

2. Antal, M.J. "Biomass Pyrolysis. A Review of the Literature - Part 2: Lignocellulose Pyrolysis" in Advances in Solar Energy, 2, American Solar Energy Society, Boulder, 1985.

3. Paulaitis, M.E., Penninger, J.M.L., Gray, R.D, Jr. and Davidson, P. "Chemical Engineering at Supercritical Fluid Conditions" Ann Arbor Science, Ann Arbor, 1983.

4. Franck, E.U. "Supercritical Water" Endeavor, 1968,**27**, 55-59.

5. Marshall, W.L. "Water at High Temperatures and Pressures" Chemistry, 1975, **48**, 6-12.

6. Franck, E.U. "Thermophysical Properties of Supercritical Fluids with Special Consideration of Aqueous Systems", Fluid Phase Equilib. 1983, 10(2-3), 211-22.

7. Franck, E.U. "Water and Aqueous Solutions at High Pressures and Temperatures".

8. Marshall, W.L and Franck, E.U., J. Phys. Chem. Ref. Data, 1981, 10, 295-304.

9. Quist, A.S., Marshall, W.L., and Jolley, H.R. J. Phys. Chem., 1965, 69, 2726-2735.

10. Marshall, W.L., Rev. Pure. Appl. Chem., 1968, **18**, 167-186.

11. Quist, A.S., J. Phys. Chem., 1970, **74**, 3396-3402.

12. Bruges, E.A. and Gibson, M.R., J. Mech. Eng. Sci., 1969, **11**, 189-205.

13. Lamb, W.J., Hoffman, G.A., Jonas, J., J. Chem. Phys., 1981, **74**(12), 6875-80.

14. Franck, E.U., Hartmann, D., and Hensel, F., J. Phys. Chem., 1968, **72**, 200-206.

15. Gorbatyi, Yu.E., Probl. Fix.-Khim. Petrol., (Eds. Zharikov, V.A., Fonarev, V.I., Korikovskii, S.P.) 1979, 2, 14-24.

16. Morrison, R.T. and Boyd, R.N. "Organic Chemistry" (3rd Edition), Allyn and Bacon, Inc., London, 1978.

17. Stein, Y.S., Antal, M.J. and Jones, M. J. Analytic and Applied Pyrolysis, 1983, **4**, 283-296.

TABLE 1

Ethanol Dehydration in Supercritical Water
at 34.5 MPa

PRODUCT	YIELD (%)*			
C_2H_4	71	93	65	56
C_2H_6	6	--	16	21
CH_4	--	--	22	22
CO	47	1	--	6
CO_2	--	14	15	19
H_2	57	--	10	560
REACTANT CONCENTRATION(M)	1.02	1.02	0.53	0.53
CATALYST	--	H_2SO_4	--	$NaHSO_4$
TEMPERATURE (° C)	400	400	500	500
RESIDENCE TIME(S)	151	151	79	76
Degree of Conversion (%)	7.2	26.0	4.2	0.7

*100 (mole product/mole reactant converted)

TABLE 2

Glycerol Dehydration in Supercritical Water
at 34.5 MPa

PRODUCT	YIELD (%)*			
	360° C		500° C	
	w/o $NaHSO_4$	w $NaHSO_4$	w/o scav.	w scav.
Acrolein (x)	24	70	34	11
Acetaldehyde (v)	38	35	74	88
Ratio (x/v)	0.6	2.0	0.5	0.1

*100 (mole product/mole reactant converted)

FIGURE 1. SUPERCRITICAL FLOW REACTOR

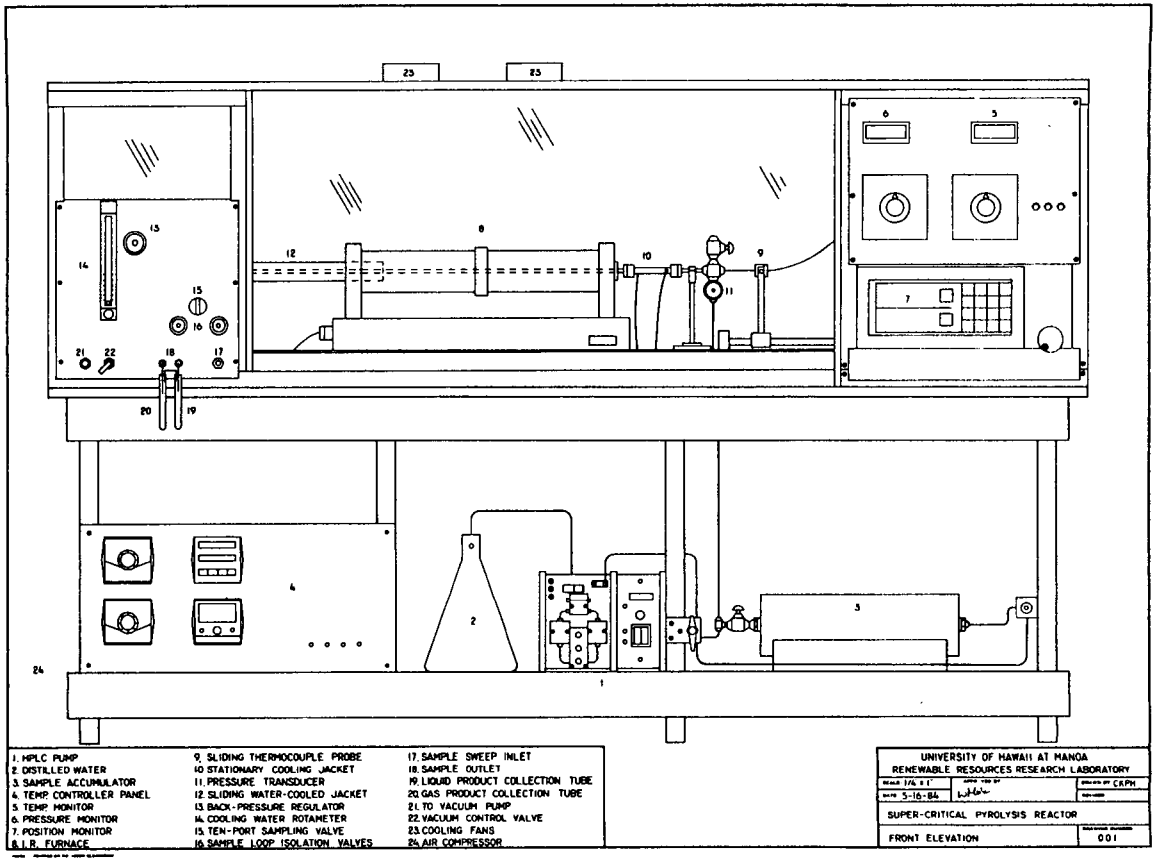

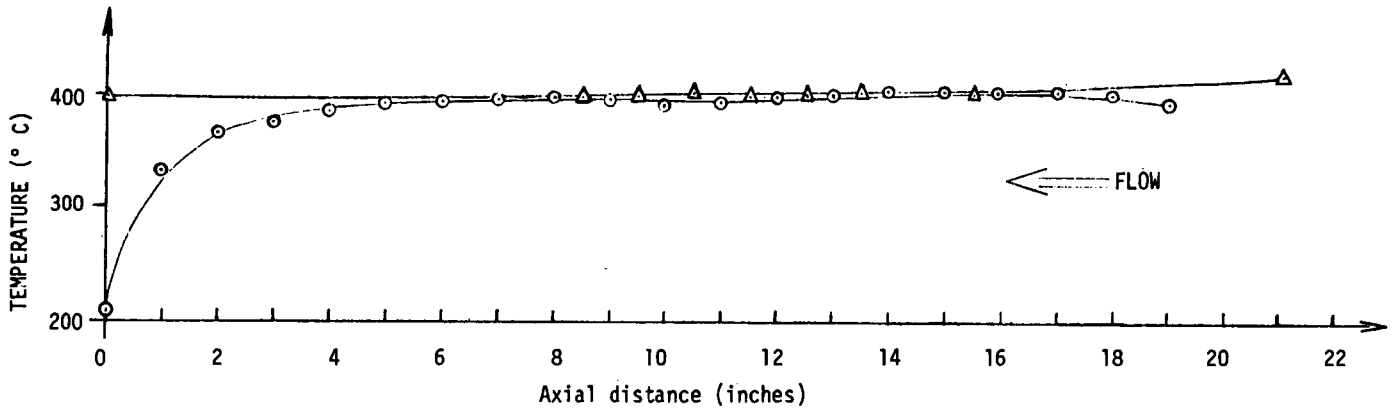

FIGURE 2. TYPICAL WALL (Δ—Δ) AND CENTERLINE (Θ—Θ) TEMPERATURE PROFILES OF THE SUPERCRITICAL FLOW REACTOR

FIGURE 3. ETHANOL DEHYDRATION

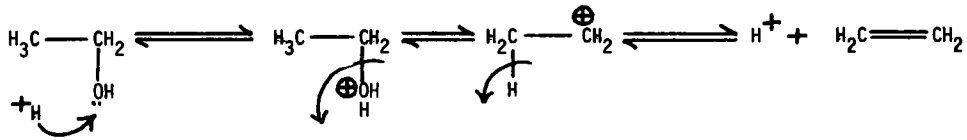

FIGURE 4. REACTION PATHWAYS FOR GLYCEROL DEHYDRATION

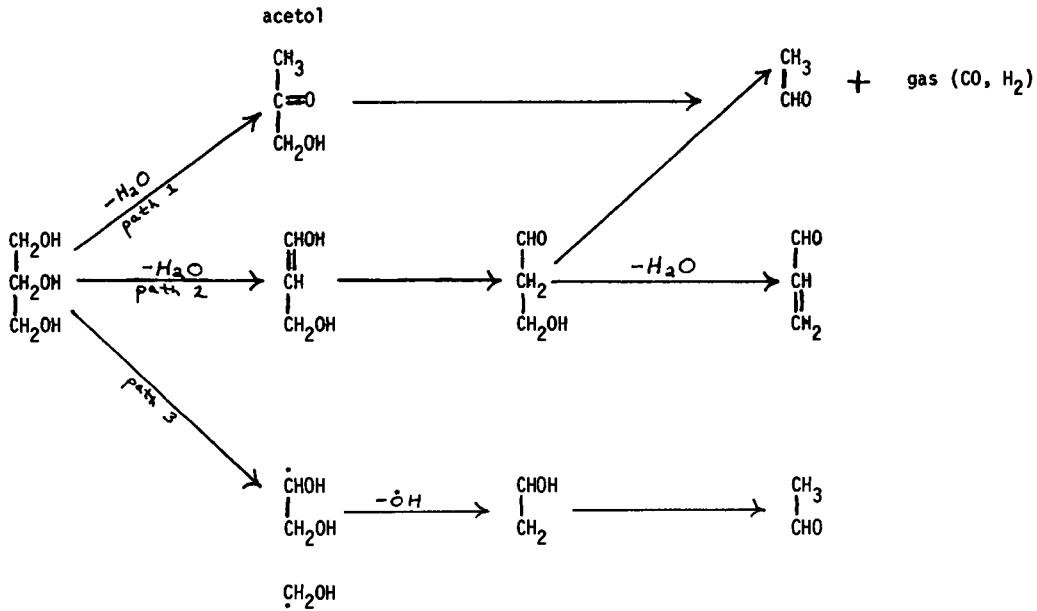

SOLVENT EFFECTS DURING THE REACTION OF COAL MODEL COMPOUNDS

M. A. Abraham and M. T. Klein
University of Delaware
Department of Chemical Engineering
Newark, DE 19716

INTRODUCTION

The chemical reactions that accompany the extraction of volatiles (1) from hydrocarbon resources with supercritical solvents are frequently obscured by the complexities of the reaction system. In contrast, the comparitive simplicity of model compound structures and product spectra permit resolution of reaction fundamentals (2) and subsequent inference of the factors that control the reactions of real reacting systems. Herein we use model compounds to probe the kinetics of pyrolysis and solvolysis reactions that likely occur during the extraction of volatiles from coals and lignins.

Previous studies of the reactions of guaiacol (orthomethoxyphenol) (3) and benzyl phenyl amine (4) in supercritical water elucidated parallel hydrolysis and pyrolysis pathways, the selectivity to the latter increasing linearly with water density. Reactant decomposition kinetics were interestingly nonlinear in water density, which was consistent with at least two possible mechanistic interpretations. The first possibility was that of unusual "cage" or solvent effects attributable to operation in dense fluids. The second possibility was a straightforward reaction scheme with pressure-dependent rate constants. Herein we present our analysis of these two mechanistic possibilities for reaction in water and reaction in methanol.

EXPERIMENTAL

Table I summarizes the experimental conditions of reactants' concentration, solvent loading, and holding time; all reactions were at 386°C. Measured amounts of the commercially available (Aldrich) substrate benzyl phenyl amine (BPA), the solvent (water or methanol) and the inert internal standard biphenyl were loaded into room temperature "tubing bombs" that have been described elsewhere (4). Sealed reactors were immersed into a fluidized sand bath held constant at the desired reaction temperature, which was attained by the reactors in about 2 min; this heat-up period was small compared to ultimate reaction times (up to 60 min) and was, in any case, identical for all runs. Products were identified by GC-MS and quantitated by GC as described elsewhere (4,6).

RESULTS

Table II summarizes the major products observed from BPA reaction neat, in tetralin, in water, and in methanol; BPA disappearance kinetics are shown in Figure 1. Neat pyrolysis of BPA led to toluene, aniline, and benzalaniline as major products and minor products including 1,2-diphenylethane, diphenylmethane, and 2-benzylaniline. Thermolysis in tetralin yielded qualitatively similar results, with the selectivity to toluene and aniline increased and selctivity to benzalaniline decreased relative to neat pyrolysis. BPA reaction in water was to benzyl alcohol and benzaldehyde as well as the neat pyrolysis products. BPA reaction in methanol produced a product spectrum similar to that found from reaction in water, with the addition of N-methylaniline as a major product.

The effect of water density on BPA conversion and product selectivity, for a constant reaction time of 10 minutes, is shown in Figure 2. BPA conversion passed through a minimum at a reduced water density of 0.2, whereas the selectivity to each individual product was essentially linear in solvent loading. The yield of aniline was relatively unaffected by solvent density but toluene and benzalaniline yields decreased and total yield of oxygenated products (benzaldehyde plus benzyl alcohol) increased with increases in solvent loading.

The reaction of BPA in methanol, at a constant reaction time of 60 minutes, was qualitatively

similar, as illustrated in Figure 3. Here the minimum conversion occurs at a reduced methanol density of 0.6 and the selectivity to each particular product was once again apparently linear in solvent loading. The yield of toluene was relatively unaffected by changes in the methanol density, whereas the yields of aniline and benzalaniline decreased and that of N-methylaniline and total oxygenated products increased as the solvent loading increased.

The foregoing results are consistent with the reaction pathways shown in Figure 4. The neat pyrolysis pathway, illustrated in Figure 4a, requires two molar equivalents of BPA for the formation of one mole each of toluene, aniline, and benzalaniline. The network for thermolysis in tetralin is a combination of the neat pyrolysis pathway (Figure 4a) and a pathway wherein tetralin and BPA react to one mole each of toluene, aniline, and 0.5 molar equivalents of naphthalene. Figure 4b depicts a direct solvolysis pathway for the "active" solvents water and methanol. Here the BPA can either (i) react by the neat pyrolysis pathway with the addition of another BPA, to give one mole each of toluene, aniline, and benzalaniline or (ii) can proceed through the solvation pathway to give oxygenated products and aniline (or N-methylaniline for reaction in methanol). The yield of oxygenated products would be expected to increase while the toluene yield would decrease as the solvent loading is increased; the yield of N-methylaniline would be expected to increase with increases in solvent loading during reaction in methanol.

The minima in BPA conversion observed for reaction of BPA in water and methanol were explained by allowing the rate constants of Figure 4b to be dependent on pressure. For each solvent loading (and thus pressure) studied the pseudo-first order rate constants for the pathways of Figure 4b are shown in Table 3. These were calculated using a sequential simplex search where the objective function was the square of the deviations between predicted and experimental values. The pressure generated by water was estimated from P\T data (7) and the methanol pressure was estimated using a Peng-Robinson equation of state.

DISCUSSION

BPA reaction in water or methanol yielded solvation products in addition to those observed from pyrolysis neat. BPA conversion passed through a minimum at a reduced solvent density of 0.6 and 0.2 for reaction in methanol and water respectively; product selectivity was essentially linear in solvent density. These results are consistent with reaction networks comprising parallel pyrolysis and solvolysis pathways with pressure-dependent rate constants; the selectivity to the latter pathway increased with increasing solvent loading. Results qualitatively similar to those observed in Figures 2 and 3 have been noted previously for reactions in solution with reaction networks containing presure-dependent rate constants (8).

The effects of pressure on the rates of chemical reactions in solution have been summarized (5,8). These effects can be interpreted in terms of transition state theory, which shows that

$$\frac{\partial \ln k}{\partial P} = \frac{\Delta V^{\ddagger}}{RT} \qquad (1)$$

where $\Delta V^{\ddagger}$ is the volume of activation, i.e. the difference between the partial molar volumes of the reactants and the activated state. $\Delta V^{\ddagger}$ is strictly a function of pressure which is often approximated by the expression

$$\ln k = a + bP + cP^2. \qquad (2)$$

Generally, volumes of activation are of the order of ± 25 cm^3 and thus rate constants for reactions in solution do not begin to show a significant pressure dependence below approximately 1000 atm (5). Also, the volume of activation is often broken into two separate values, $\Delta_1 V^{\ddagger}$ and $\Delta_2 V^{\ddagger}$, where the

former represents a structural contribution and the latter represents a change in the volume of the solvent shell.

It is important to note that, although the operating pressures in the present study were of the order of 10 - 1000 atm., the minimum in reactant conversion, from which we have inferred a likely kinetic effect of pressure, occurred at pressures of only 100 atm. Thus the apparent global volume of activation associated with the present interpretation of the non-linear kinetics of Figures 2 and 3 would be an order of magnitude larger than that observed for liquid systems. These apparent volumes of activation may consist of at least three components; first, $\Delta_1 V\ddagger$ associated with structural changes, second, $\Delta_2 V\ddagger$ associated with changes in the solvent shell, and third, a contribution due to the compressibility of the fluid. The supercritical fluid is highly compressible in the critical region and lack of an unequivocal equation of state for the reaction mixture has hindered unambiguous analysis of the compressibility term. Further analysis is being undertaken to ascertain the quantitave contributions of each of these factors to the overall global volume of activation.

REFERENCES

1. Squires, T.G.; Aida, T.; Chen, Y.; Smith, B.F., ACS Div. Fuel Chem. Preprints, 1983, 28, No. 4, 228.

2. Simmons, M.B.; Klein, M.T. "Free Radical and Concerted Pathways in Dibenzyl Ether Thermolysis"; Ind. Eng. Chem. Fundam., 1985, 24, 55.

3. Lawson, J.R.; Klein, M.T. "The Influence of Water on Guaiacol Pyrolysis"; Ind. Eng. Chem. Fundam., 1985, 24, 203.

4. Abraham, M.A.; Klein, M.T. "Pyrolysis of Benzyl Phenyl Amine Neat and with Tetralin, Methanol, and Water Solvents," I&EC Prod. Res. and Dev. (accepted for publication 1985)

5. Eckert, C.A. "High Pressure Kinetics in Solution", Ann Rev Phys Chem, 1972, 23, 239.

6. Townsend, S.H.; Klein, M.T. "Dibenzyl Ether as a Probe into the Supercritical Fluid Solvent Extraction of Volatiles from Coal with Water"; Fuel (accepted for publication 1985)

7. Keenan, J.H., Keyes, F.G. *Thermodynamic Properties of Steam*, John Wiley & Sons, New York, 1966.

8. Kohnstam, G. "The Kinetic Effects of Pressure", in Porter, G., Jennings, K.R., Suppan, P., eds., *Progress in Reaction Kinetics*, Pergamon Press, New York, 1965. Vol. 5, p. 335.

Table 1
Experimental conditions for reaction of BPA

Solvent	BPA concentration (mol/lit)	solvent loading (ml)	holding time (min)
Neat	.64	-	5 - 50
Tetralin	.59	.225	5 - 60
Water	.59	0.1 - .25	5 - 50
Methanol	.59	0.02 - .35	5 - 60

Table 2
Major products of BPA thermolysis

Solvent	Products
Neat	Toluene, Aniline, Benzalaniline
Tetralin	Toluene, Aniline
Water	Toluene, Aniline, Benzyl alcohol, Benzalaniline
Methanol	Toluene, Aniline, N-Methylaniline, Benzaldehyde, Benzalaniline

Table 3
Pseudo-first order rate constants

Reaction in water at 386°C

Reduced density	Estimated pressure [psi]	k_1 [min^{-1}]	k_2 ($\times 10^3$) [lit/(mol)(min)]
0.0	0.0	.193	-
0.1	1280	.0276	8.98
0.3	2720	.0272	3.95
0.5	3350	.0301	4.12
0.8	3660	.0255	2.85
1.2	3880	.0240	1.95

Reaction in methanol at 300°C

Reduced density	Estimated pressure [psi]	k_1 ($\times 10^3$) [min^{-1}]	k_2 ($\times 10^3$) [lit/(mol)(min)]
0.0	0.0	22.1	-
0.1	526.1	15.8	3.31
0.3	1294.9	7.86	2.62
0.5	1819.8	4.32	2.06
0.8	2413.9	1.98	1.59
1.2	3391.2	0.613	1.44

FIGURE 1

Summary of BPA yield for all solvents

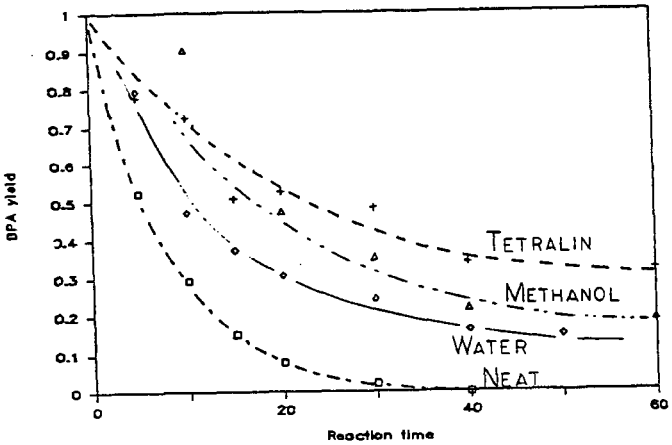

FIGURE 2

BPA conversion and product selectivity

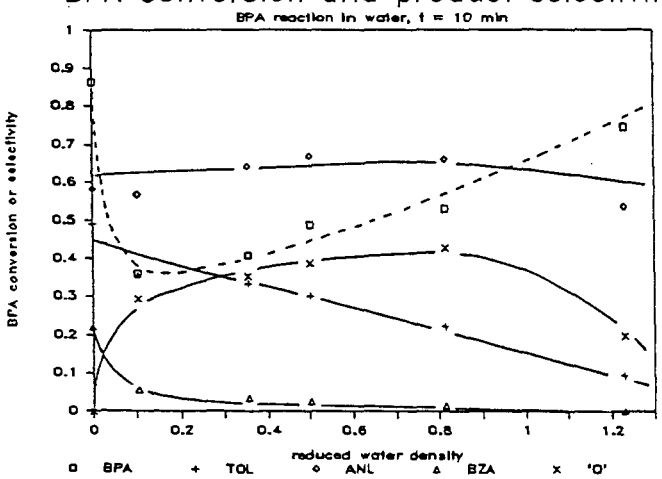

FIGURE 3
BPA conversion and product selectivity

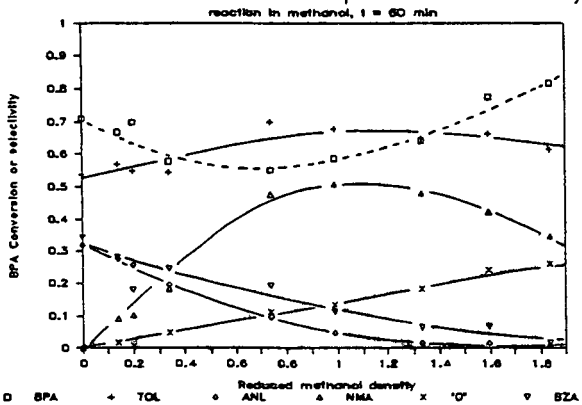

Figure 4
Proposed reaction pathways

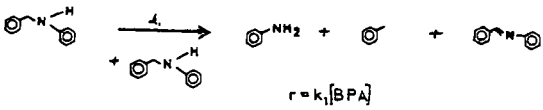

Figure 4a: Neat pyrolysis

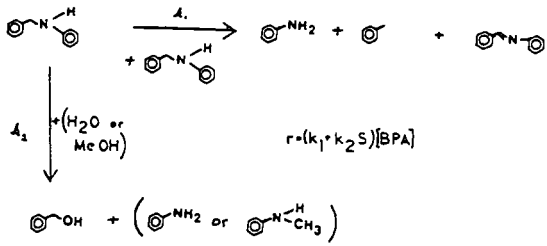

Figure 4b: Reaction in supercritical solvent

ISOTOPE EFFECTS IN SUPERCRITICAL WATER--KINETIC STUDIES OF COAL LIQUEFACTION

David S. Ross*, Georgina P. Hum, and Tiee-Chyau Miin
Fuel Chemistry Program
SRI International
Menlo Park, CA 94025, USA

Thomas K. Green
Western Kentucky University
Bowling Green, KY, USA

Riccardo Mansani
Eniricerche S.p.A
Milan, ITALY

INTRODUCTION

The chemistry of coal liquefaction is not very well understood, even after more than two decades of research into the kinetics and mechanism of the process. There have been a number of models for conversion proposed, most of them focused on the several liquefaction products, including preasphaltenes, asphaltenes, oils, and gases. A survey of some of the models has been presented (1), and a common feature among them is the multiplicity of paths connecting all of the components.

Kinetic model studies have invariably been carried out in organic donor media, and while the use of these media may be convenient in large scale conversion systems, they do not lend themselves well to laboratory study of conversion. Not the least significant of the problems to be faced in such a study is the unavoidable participation in the overall chemistry of various interrelated and interlocked free radical chain reactions, most of which having no direct bearing on, and perhaps only a secondary relationship with, the liquefaction process.

The complications presented by this network of incidental reactions, coupled with the multiple reaction paths to products, prompted the study of the kinetics of coal liquefaction using supercritical water as the medium. The action of CO/water to reduce both low rank and bituminous coals to upgraded products has been known for more than half a century, having been introduced in the work of Fischer and Schrader (2). Hydrothermal media are recognized as being excellent solvents for aromatics, with tetralin and naphthalene, for example, being fully miscible with water at all proportions at temperatures as low as 300°C (3). A review of the CO/water conversion process, including the most recent work, has recently appeared (4).

In the research described here, batch runs were performed using samples of an Illinois No. 6 coal (PSOC 1098) in a stirred, 300 ml stainless steel autoclave. All of the runs were for 20 min at 400°C. The only product considered is the toluene-soluble fraction (TS), separated from the toluene-insoluble fraction (TI) by simple filtration.

RESULTS

Working Model. Our working model evolved from consideration of the profiles typically noted in the modeling literature. Products are seen to grow with time, and then level off at some level below quantitative conversion. At the same time the quantities "unreacted coal" decline, leveling off at a value above total conversion. A picture of the coal organic matrix derived from this view of conversion would depict a collection of organic units, connected to each other through a series of links increasingly more difficult to break.

On this basis conversion is limited by coal structure. And in terms of the conventional homolytic scission/H-capping view of conversion, increased yields of coal liquids are therefore obtainable only through increases in conversion temperature or residence time. Unfortunately, increases in the thermal severity of the process result in products reflecting the rise of dealkylation and aromatization reactions at higher temperatures. Thus increased product yields are brought about at a considerable cost to product quality (5).

The fact that the profiles of both the desired soluble product and the insoluble product ("unreacted coal") level off at intermediate values suggest a simpler model for conversion. This scheme, presented in Figure 1, is our working model, and is tested in the study described here. In the scheme coal is partitioned in parallel, competitive routes between i) reaction with some reducing component in the system to yield TS, and ii) thermal loss of convertible sites to yield char. In this work we have avoided consideration of specific mechanism for decrease in molecular weight with liquefaction, including in particular the perceived need for thermal scission of C-O and C-C bonds during conversion. Thus we view conversion simply as a process requiring some kind of nonspecific reduction chemistry.

This two-reaction scheme, if truly operative, suggests a view of the potential utility of liquefaction more optimistic than that derived from the conventionally accepted scheme. The yield of TS is a function of the rates of the two reactions. Therefore an increase in the rate of the TS route, or a decrease in the rate of char formation, would bring about increased TS yields. In turn, an increase in the rate of TS formation could be brought about with an increase in the reducing capacity of the system, rather than through an increase in reaction temperature. And thus in principle, increases in TS yield to product quantities representing all of the convertible portion of the starting coal could be obtained, and at no cost to product quality.

CO/Water Conversions. In contrast to the more-or-less fixed reducing capacity available in conventional donor systems, the CO/water system offered considerable latitude. We had earlier demonstrated that changes in the initial pH of the system brought about wide variation in the TS yields for Illinois No. 6 coal (6). In accord with the findings of several other groups including Appell, et al. (7), the conversions were found to be base promoted. The present study included a range of initial pH values, and focused on a comparison of the results in H_2O with those from a substitution in parallel experiments of D_2O.

The results for several runs in the two media are presented in Figure 2. The figure presents a plot of %-toluene soluble products vs quantity of H_2 produced in the run (cold). There is a range of TS yields from values up to around 50% for the protio medium. These conversions were attained by ranging the initial pH from 7 to 13.

We have pointed out that the water gas shift reaction

$$CO + H_2O \longrightarrow H_2 + CO_2$$

parallels the conversion (6), and the results when presented as a function of product H_2 show that the hydrogen from this reaction is not the effective reducing species. Thus in the figure is a result for a run with H_2/H_2O, plotted at an abscissa value equal to the starting quantity of hydrogen (cold). This point falls well below the CO/H_2O results, and it is clear that the TS yield is below that which would be produced for a run with CO yielding that quantity of hydrogen.

Also present in the plot is a result for a conversion in tetralin for 60 min at 400°C. Again the hydrothermal CO system provides the superior results, and at a

shorter residence time.

The major finding in this work is the isotope effect. We find that the deuterio system provides higher TS yields than does the protio system. Moreover, the deuterio results level off at a substantially higher conversion level. This result, an inverse isotope effect, is not very common in isotope effect studies, and has recently been discussed by Keeffe and Jencks (8). The implication of these findings as regards conversion mechanism and structure is considerable, and is discussed below.

Products of Conversion. Conversion product analyses are presented in Figure 3. The procedure used here is that developed by Farcasiu (9), with which we have separated the toluene-soluble fractions into subfractions of increasing polarity. The TS fractions for different coals yield different profiles, and yet we find here for the Illinios No. 6 coal that the TS fractions for conversion in water of 29% and 60% are virtually the same. Further, the TS fraction from the tetralin run is also essentially identical in its profile.

This result can be considered along with the molar H/C ratios for both the TS and TI fractions from several runs, shown in Figure 4. We find that within the bounds of the scatter in the data, the ratios are unchanging with conversion. The TI results include those from a run in which N_2 replaced CO.

DISCUSSION

Taken alone, the conversion profile from the protio work is consistent with the view that the conversion of coal is limited by its structure. Thus if the organic portion of coal contained a limited network of breakable links, the scission of which would liberate about 50% of the material to TS product, then runs with increasing conversion capacity would show increased conversion, leveling off at about 50% TS yield.

The inverse isotope effect, however, requires a different picture. Thus a simple change to the heavy medium brings about not only increased conversions, but a leveling off of conversion at a significantly higher level. Whatever the reduction mechanism, it is highly unlikely that isotopic switch from ^1H to ^2H would increase the inherent bond breaking capacity of the system. And so we conclude that the starting coal must contain many more breakable links than supposed above, but that some portion of the links are lost through other reactions. The proposed model in Figure 1 is thereby confirmed.

The full scheme for conversion is presented in Figure 5. In this scheme, formate is partitioned between reaction with coal, and a hydrogen ion transfer reaction with water to yield formic acid. The acid is unstable at the conversion temperatures (10), decomposing rapidly to carbon dioxide and hydrogen. Thus with the switch from protio to deuterio, the formic acid formation experiences a normal deuterium effect, i.e. protio > deuterio, and is slowed. The result is an increase in the steady-state concentration of formate, and an accordant increase in the TS yield.

These results, including most especially the product data, contrast decidedly with those discussed by Whitehurst et al., noted above (5). In the present work, we find that with increased reducing capacity and at constant temperature, the system gives increased yields of product, and at no cost to product quality.

In summary, we find that conversion is not limited by coal structure, but rather by the kinetics of the reducing step(s). Systems with even greater reducing capacity, and where the water gas shift reaction can be suppressed, should provide even higher conversions to toluene-soluble products. The products in turn should be

no less rich in hydrogen than those from lower conversion runs.

It is still necessary to bring about an understanding of the specific reducing chemistry. From our present data we can conclude that the conventional thermal scission/H-capping sequence does not apply here. And since the TS product from tetralin conversion is no different from those from aqueous conversion, it would appear that the reduction in conventional donors breaks the same links broken by the hydrothermal system.

Thus the question of the nature of critical link scission in conventional conversions must be reconsidered. Brower has recently questioned the conventional scheme (11 a,b), and it is clear that the detailed mechanism of coal conversion is yet to be developed.

NOTE ADDED IN PROOF. The model dealt with here demands that the TI fractions be unconvertible in subsequent conversion attempts. That expectation is realized in work proceeding at present, in which the product from N_2/water runs is being studied. The product, virtually fully toluene-insoluble, yields only 5% TS yields in subsequent CO/water conversions. In fact when the times for the N_2/water runs are reduced to only around 1 min, the subsequent TS yields are still below 10%. The char-forming reaction must be very rapid at 400°C.

ACKNOWLEDGEMENT

We acknowledge the generous support of the U.S. Department of Energy. We also acknowledge the close cooperation of ASSORENI (Milan), who provided RM with support for a stay at SRI as an International Fellow.

REFERENCES

1. G. Mohan and H., Silla, Ind. Eng. Chem. Process Des. Dev., 20, 349-358 (1981).

2. F. Fischer and H. Schrader, Brennst.-Chem., 2 161-172, (1921); C.A. 15, 3193.

3. G. M. Schneider and R. Jockers, Ber. Bunsenges. Phys Chem. 82, 576-582 (1978).

4. D. S. Ross in "Coal Science," M. Gorbaty, J. Larsen and I. Wender, eds., Academic Press, Inc., New York, 1984, pp. 301-338.

5. M. Farcasiu, T. O. Mitchell and D. D. Whitehurst, Chem. Tech. 7, 680-686, (1977).

6. D. S. Ross, J. E. Blessing, Q. C. Nguyen, and G. P. Hum, Fuel 63, 1206-1210 (1984).

7. H. R. Appell, R.D. Miller and I. Wender, preseted before the Division of Fuel Chemistry of the American Chemical Society, 163rd National Meeting of the ACS, April, 1972.

8. J. R. Keeffe and W. P. Jencks, J. Am. Chem. Soc., 103, 2457-2459 (1981).

9. M. Farcasiu, Fuel 56, 9-14 (1977).

10. V. I. Stenberg, R. L. Van Buren, R. L. Baltisberger, and N. F. Woolsey, J. Org Chem. 47, 4107-4110 (1982).

11. a) K. R. Brower, J. Org. Chem. 47, 1889-1893 (1982);

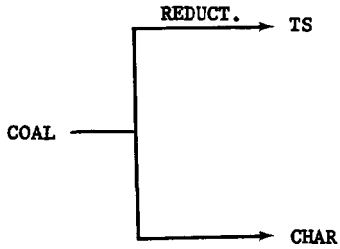

Figure 1. Working Model. TS = toluene soluble

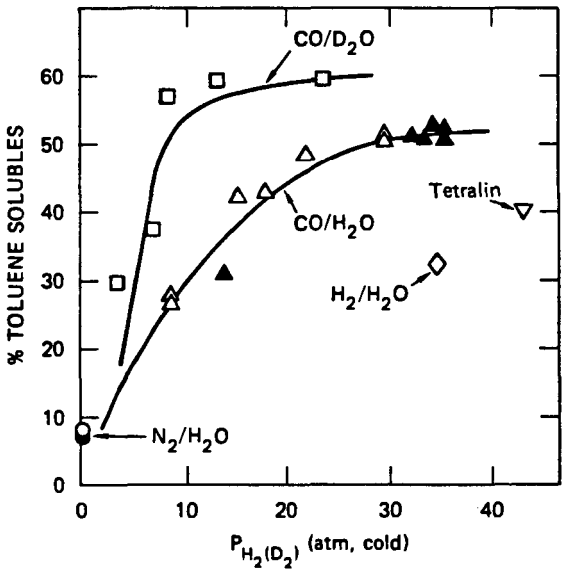

Figure 2. Plot of TS vs Final H_2. The runs were at 400°C for 20 min.

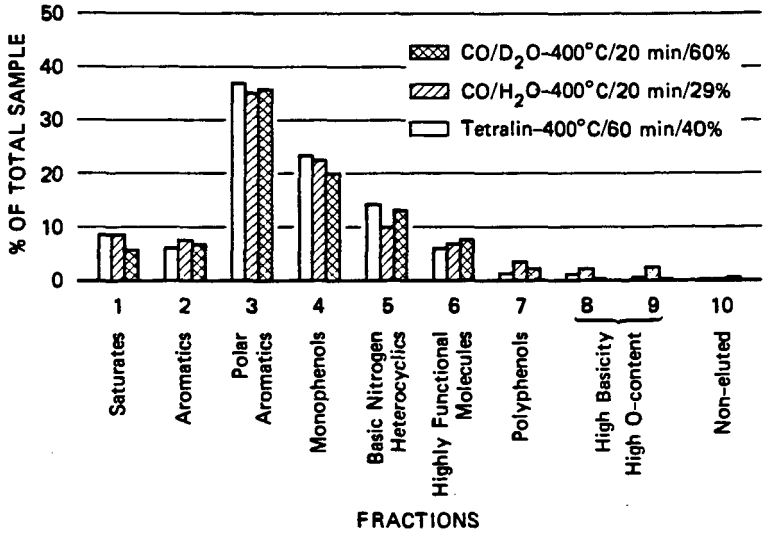

Figure 3. SESC Separations of TS Fractions.

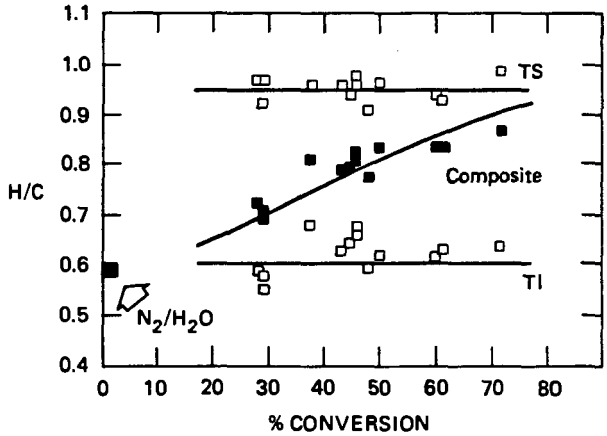

Figure 4. H/C Ratios vs %-Conversion. The N_2/H_2O point refers to a run in which CO was replaced by N_2.

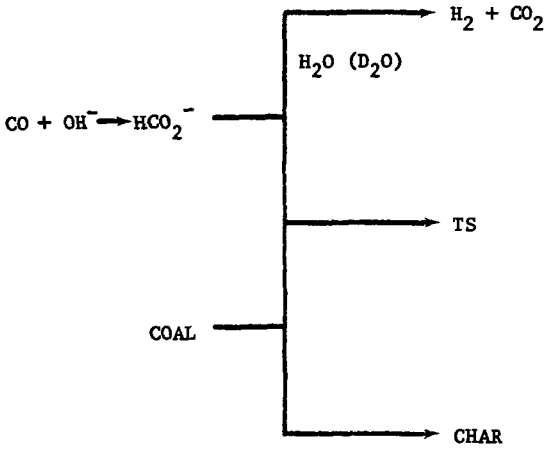

Figure 5. Overall Scheme for Conversion in Hydrothermal Systems

EXTRACTION OF AUSTRALIAN COALS WITH SUPERCRITICAL WATER

John R. Kershaw and Laurence J. Bagnell

CSIRO Division of Applied Organic Chemistry,
G.P.O. Box 4331, Melbourne, Victoria 3001, Australia.

INTRODUCTION

The extraction of coals with supercritical fluids is a promising route for the production of liquid fuels and chemical feedstocks from coal. Generally, hydrocarbon solvents, notably toluene, have been used as the supercritical fluid. Supercritical water extraction has not received the same attention and only recently the first detailed study was reported. In that work, Holder et al. (1) obtained high conversion for extraction of a German brown coal and a Bruceton bituminous coal with supercritical water at ca. 375°C and 23 MPa. They reported conversions of 70-75% for the brown coal and ca 58% for the bituminous coal, when the coal was injected into the reactor. However, the conversion was lower (ca 58% for the brown coal) when the coal was present during the heating-up period. These high yields contrast with the work of Scarrah (2), who obtained a conversion of approximately 35% and a liquid yield of only about 10% for the extracton of a North Dakota lignite at 400°C and 28 MPa, while Holder et al. also obtained very low conversion with a high sodium lignite (1). In other brief reports (3-5) on the extraction of bituminous coals with supercritical water, conversions were considerably less than produced with the Bruceton coal (1). However, the conditions used in at least one of these studies (4) were not ideal for supercritical water extraction as the solvent density was relatively low. Nevertheless, there appears to be considerable variation in the extractive power of supercritical water with different coals. None of the above reports discussed in any detail the chemical nature of the products, nor how the products compare with those obtained from more conventional solvents.

The potential use of supercritical water appears especially attractive for the extraction of brown coals with their high water content, 50-70% for Victorian brown coals, thus removing the need for a coal-drying stage. The drying and extraction of these low rank coals would occur in a single process. The purpose of the present study was to investigate the feasibility of the extraction of Australian black and brown coals with supercritical water. The chemical nature of the products is discussed together with a comparison with toluene extraction of the same coals.

EXPERIMENTAL

The analyses of the coals used are given in Table 1.

Supercritical gas extractions

Method A Extractions were carried out for 1 h at temperature in a 1 l semi-continuous reactor (6). The reactor was charged with coal (50 g dry basis) and solvent (600 ml) and heated. When the temperature reached 300°C, solvent (1 l h^{-1}) was pumped via a dip tube, which acts as a pre-heater, into the bottom of the reactor and through the coal bed. The pressure was controlled by adjusting throttling valves and the gaseous phase was condensed by a water-cooled condenser.

For the toluene extractions, the work-up procedure was as described previously (6). For the water extractions, most of the extract is insoluble in water, after cooling and lowering of the pressure, and precipitates out in the condenser and receiver. The product adhering to the sides of the condenser and receiver was collected by washing with acetone and then THF. The aqueous suspension was evaporated to dryness on a rotary evaporator and the residue extracted with acetone and THF. The solvents were removed under reduced pressure from the combined acetone and THF solutions to give the total extract (liquid product). In calculating the conversion figures, any product which was insoluble in THF was assumed to be unreacted coal, which had been carried over. The liquid product was extracted with hot toluene and the cooled solution filtered to give the pre-asphaltene fraction. After the toluene was removed under reduced pressure from the filtrate, the residue was re-dissolved in a small volume of toluene and a 20 fold excess of pentane added to precipitate the asphaltene which was filtered off. The pentane and toluene were then removed from the filtrate under reduced pressure to give the oil. For the NaOH extractions, the NaOH solutions were neutralised with HCl. The insoluble extract was washed with water and then extracted with THF.

Method B Extractions were carried out in a 500 ml rocking autoclave fitted with a stainless steel liner. The internal volume of the autoclave with liner was 420 ml. The autoclave was charged with coal and solvent, heated to 380°C and maintained at that temperature for 1 h. The residue was washed out of the cooled reactor with acetone, filtered, washed with pyridine and then acetone and dried under vacuum. In some cases, g.c. analyses of the gases in the cooled reactor were carried out.
Analytical procedures for the products were as described previously (7).

RESULTS AND DISCUSSION

Good conversions were obtained for extraction of a number of Victorian brown coals at conditions (380°C and 22 MPa) close to the critical temperature (374°C) and pressure (22 MPa) of water (see Table 2). The conversion increased as the volatile matter content of these coals increased (see Fig. 1). Similar trends were also obtained for toluene and 5% tetralin/toluene extraction. The highest conversions were obtained for the two pale lithotypes (F and G). These were slightly lower than obtained by Holder et al. (1) for extraction of a high volatile German brown coal and may be due to differences in the extraction procedure. Except for the low ash Loy Yang coal, data for the brown coals are given on a dry mineral and inorganic free (dmif) basis which is the preferred basis for recording data on these coals (8). The conversions were not as high for Millmerran (sub-bituminous) and Liddell (bituminous) coals (see Table 2). Holder et al (1) only obtained high conversions for extraction of Bruceton coal with high reactor stirrer speeds which were not possible with our reactor. The conversion and liquid yield data in Table 2 are the average of duplicate determinations. Average variation between the duplicates was 1.8%. The asphaltene and pre-asphaltene contents of the liquids are high (see Table 2), as is the case with supercritical gas extraction using hydrocarbon solvents. Two of the coals, Morwell and Yallourn were as-mined samples that had not been dried and were broken into small pieces for the extraction. The promising results obtained with these coals indicates the feasibility of extracting 'wet' brown coals with supercritical water.

Extractions of two of the coals, Loy Yang and Coolungoolun, were also

carried out in a rocking autoclave (method B) mainly to allow analysis of the gases to be carried out. The results of these extractions are shown in Table 3. The high carbon dioxide yields obtained, especially from Loy Yang coal, were indicative of the high carboxylic content of the brown coals. The hydrocarbon gas make was low as was the yield of carbon monoxide. Studies of the pyrolysis of Victorian brown coals have shown that significant quantities of water are evolved together with the carbon dioxide (9). The loss of water (and also hydrogen sulphide in the case of Coolungoolun coal) presumambly accounts for some of the difference between the conversion figures and the sum of the extract yield and the gas figures in Table 3. The carbon dioxide yield was noticeably lower on extraction of Coolungoolun coal, which has the lowest oxygen content of the seven brown coals, than for extraction of Loy Yang coal.

Chemical Nature of the Product

Analytical data for the oils, asphaltenes and pre-asphaltenes from the various extractions are summarised in Table 4. There appeared to be little difference between the liquids produced from the coals A-E under the same conditions (380°C, 22 MPa). This is not surprising considering the similarity between the coals (see Table 1). The liquids have a high oxygen and hydroxyl content, especially in the asphaltene and pre-asphaltene fractions, in keeping with the high oxygen content of these coals. The H/C atomic ratio of the oils, asphaltenes and pre-asphaltenes are higher than for most coal liquids.

^{13}C-NMR spectra showed the presence of substantial amounts of unsubstituted alkyl chains, with a chain length of more than eight carbon atoms, in both the oils and asphaltenes by strong signals at ca 14, 23, 32, 29 and 29.5 ppm, which are due to the respective α, β, γ, δ and ε carbons (10). Weak signals at ca 178 ppm indicated the presence of COOH groups in the oils and asphaltenes.

Analytical data on the residues from four extractions are given in Table 5. The high calorific value of the extraction residues indicates that they should be attractive materials for combustion.

^{13}C CP-MAS NMR spectra were recorded for Coolungoolun coal and for the residue from extraction of this coal with supercritical water. The major difference between the two spectra was a much more intense aliphatic peak centered at 30 ppm in the spectrum of the starting coal. The decrease in the intensity of the aliphatic signal on processing is in agreement with the aliphatic nature of the liquid product especially the presence of long methylene chains in the oil and asphaltene. These methylene chains contribute significantly to the peak at 30 ppm in the starting coal (11).

The extraction of Coolungoolun coal with supercritical water can be summarisied as:-

		Char, 57.6%, H/C=0.60, f_a=0.84
		+
Coal	H_2O	
H/C=0.87	$380\,^0C^{\rightarrow}$	Pre-asphaltene, 7.6%, H/C=0.96, f_a=0.79
f_a = 0.62	22 MPa	+
		Asphaltene, 5.3%, H/C=0.99, f_a=0.66
		+
		Oil, 13.2%, H/C=1.35, f_a=0.47
		+
		CO_2, 9.7%

(This shows the major products. The amount of CO_2 produced was assumed to be the same using the semi-continuous reactor (method A) as using the rocking autoclave (method B).)

The effect of pressure and temperature

The conversion and liquid yield both increase considerably as the pressure increases (see Fig. 2). The asphaltene and pre-asphaltene content of the liquids also increase with pressure (compare 5,6 and 7 in Table 2). The H/C atomic ratios of the oil and asphaltene fractions decrease, while the hydrogen and carbon (for the oil) aromaticities increase (see Table 4) with increasing pressure. This presumably indicates that the more aliphatic products are extracted preferentially.

Extractions of Gelliondale coal were carried out at 380°C, 420°C and 460°C. There were only small differences between the conversions, liquid yields and nature of the products at these various temperatures (compare 2, 3 and 4 in Tables 2 and 4). This is somewhat surprising as it was expected, especially in light of the recent work of Holder et al. (1), that the highest conversion would occur at the highest water density, namely at 380°C. However, this was not the case. Possibly, increased thermal fragmentation of the coal compensates for the decrease in the extractive powers of the supercritical water as the temperature is increased.

Generally, raising the temperature increases the aromaticity of coal liquefaction products. However, there were no significant changes in either the H/C atomic ratios or the hydrogen aromaticities (see Table 4) of the oils, asphaltenes or pre-asphaltenes with temperature. The most noticeable change in the liquid product with temperature was a slight decrease in the pre-asphaltene content. The results in Table 6 do, however, suggest that there is a trend towards decreasing H/C ratio of the extraction residue with temperature.

Comparison between toluene and water extractions

At 380°C and 22 MPa, the conversions for the brown coals were considerably higher but for black coals slightly lower for extraction with water than with toluene (see Table 2 and Fig. 2). The difference between coals of various rank is further shown by extraction with water/toluene mixtures of a brown, a sub-bituminous and a bituminous coal at a constant gas density in a rocking autoclave. The presence of water was more advantageous for the extraction of the brown coal than for the higher rank coals (see Fig. 3), though in all cases the presence of water increased conversion. The highest conversions were obtained for mixtures of the two solvents. The difference between the liquid yields from water and toluene extractions was less pronounced than between the conversions. Extraction with water is more pressure dependent than with toluene (see Fig. 2).

Although the oils are similar, there are significant differences in the composition of the toluene and water extracts of Gelliondale coal at 380°C and 22 MPa (compare 1 with 2 in Tables 2 and 4). The oxygen content of both the asphaltene and the pre-asphaltene as well as the pre-asphaltene content are significantly higher in the water extract than in the toluene extract. It is also noticeable that the asphaltene form the water extraction has a lower H/C atomic ratio and molecular weight but a higher hydroxyl content and

aromaticity than the asphaltene form the toluene extraction. This work is unable to explain whether the differences between the water and toluene extracts are due to the supercritical water extracting more polar substances from the coal, or whether reactions occur between the coal fragments and supercritical water which give rise to the high oxygen content of the extract.

Extraction with alkali and tetralin/water mixtures

A considerable increase in conversion of Morwell brown coal occurs when dilute sodium hydroxide was used in place of water (see Table 6 and Fig. 4). Dilute sodium carbonate and formate had a similar effect (see Table 6). The conversion and liquid yield increases with the molarity of the sodium hydroxide (Fig. 4). The dissolution of low rank coals by sodium (or potassium) hydroxide solutions has been previously documented (11-13) and, therefore, an increase in conversion was expected. It is noticeable that the increase in liquid yield is mainly due to an increase in the pre-asphaltene fraction (Fig. 4). The composition of the oils and ashaltenes from the sodium hydoxide extractions appear similar to those obtained form water extraction but the pre-asphaltenes from the alkali extractions have lower H/C ratios and high hydrogen aromaticities than from water extraction.

Increase in conversion is also obtained with tetralin/water mixtures (see Table 6) in an analogous manner to the increased conversion with the addition of small amounts of tetralin to toluene (6 and Fig.1).

CONCLUSIONS

This study indicates that extraction with supercritical water could be an attractive route for liquefaction of Victorian brown coals . The low cost and ready availability of the solvent (water), the relatively high H/C ratio of the extracts, and also as neither hydrogen nor a coal-drying stage are required, are positive factors.

REFERENCES

1 Deshpande, G.V., Holder, G.D., Bishop, A.A., Gopal, J. and Wender, I. Fuel, 1984, 63, 956.
2 Scarrah, W.P. in 'Chemical Engineering at Supercrtical Fluid Conditions' (M.E. Paulaitis, J.M.L. Penninger, R.D. Gray and P. Davidson Eds.). Ann Arbor Science, Ann Arbor, 1983, pp. 395-407.
3 Modell, M., Reid, R.C. and Amin, S.I. U.S. Patent 4,113,446, September 12, 1978.
4 Jezko, J., Gray, D. and Kershaw, J.R. Fuel Processing Technology, 1982, 5, 229.
5 Vasilakos, N.P., Dobbs, J.M. and Parasi, A.S. Amer. Chem. Soc., Div. Fuel Chem. Preprints, 1983, 28(4), 212.
6 Kershaw, J.R. and Overbeek, J.M. Fuel, 1984 63, 1174.
7 Kershaw, J.R. Fuel Processing Technology, 1984, 9,235.
8 Kiss, L.T. and King, T.N. Fuel, 1979 58, 547.
9 Schafer, H.N.S. Fuel, 1979, 58, 667 and 673.
10 Pugmire, R.J., Grant, D.M., Zilm, K.W., Anderson, L.L., Oblad, A.G. and Wood, R.E. Fuel, 1977, 56, 295.
11 Russell, N.J., Wilson, M.A., Pugmire, R.J. and Grant, D.M. Fuel, 1983, 62, 601.
12 Lynch, B.M. and Durie, R.A. Aust. J. Chem., 1960, 13, 567.
13 Brooks, J.D. and Sternhell, S. Fuel, 1958, 37, 124.
14 van Bodegom, B., van Veen, J.A.R., van Kessel, G.M.M., Sinnige - Nijssen, M.W.A. and Stuiver, H.C.M. Fuel, 1984, 63, 346.

Table 1 Analyses of coal used

	Loy Yang (A)	Gelliondale (B)	Coolungoolun (C)	Morwell (D)	Yallourn E	Morwell Pale (F)	Yallourn Pale (G)	Millmerran (H)	Liddell (I)
Moisture	10.8[a]	7.3[a]	11.5[a]	52.6[a]	65.0[a]	56.5[a]	57.2[a]	4.9[a]	3.3[a]
Ash	0.6[b]	4.5[b]	2.2[b]	2.7b	1.3[b]	3.7[b]	1.6[b]	18.1[b]	29.0[b]
Minerals and inorganics		1.8[b]	2.0[b]	1.6[b]	1.0[b]	2.0[b]	1.3[b]		
Volatile matter	48.3[c]	51.4[d]	48.9[d]	50.2[d]	51.7[d]	56.0[d]	61.2[d]	50.7[c]	44.6[c]
C	71.0[c]	66.5[d]	70.7[d]	69.6[d]	67.3[d]	71.5[d]	71.2[d]	79.0[c]	80.6[c]
H	4.8[c]	4.7[d]	5.1[d]	5.0[d]	4.7[d]	5.8[d]	6.2[d]	6.3[c]	6.0[c]
N	0.6[c]	0.6[d]	0.6[d]	0.6[d]	0.6[d]	0.6[d]	0.5[d]	1.2[c]	2.1[c]
S	0.3[c]	0.8[d]	4.1[d]	0.3[d]	0.2[d]	0.7[d]	0.2[d]	0.7[c]	0.4[c]
O (by difference)	23.3[c]	27.4[d]	19.5[d]	24.5[d]	27.2[d]	21.4[d]	21.9[d]	12.8[c]	10.9[c]
H/C atom. ratio	0.81	0.85	0.87	0.86	0.84	0.97	1.04	0.96[c]	0.89

[a] wt%; [b] wt% dry basis; [c] wt% dry ash free basis; [d] wt% dry mineral and inorganic free (dmif) basis.

Table 2 Conditions, conversions, liquid yields and product distribution for extraction of Australian coals using a semi-continuous reactor (method A)

Extraction No.	Coal	Solvent	Temperature (°C)	Pressure (MPa)	Conversion	Liquid Yield	Oil	Asphaltene	Pre-asphaltene
					(wt% coal dmif)				
1	Gelliondale	Toluene	380	22	33.6	17.5[b]	7.9[b]	5.8	3.8
2	Gelliondale	Water	380	22	52.7	22.6	9.0	6.5	7.1
3	Gelliondale	Water	420	22	56.7	23.1	10.7	6.4	6.0
4	Gelliondale	Water	460	22	57.2	20.5	9.4	6.3	4.8
5	Loy Yang	Water	380	7	22.8[a]	5.7[a]	3.7[a]	1.2[a]	0.8[a]
6	Loy Yang	Water	380	15	38.6[a]	13.7[a]	8.1[a]	3.0[a]	2.6[a]
7	Loy Yang	Water	380	22	51.1[a]	25.5[a]	11.3[a]	6.5[a]	7.7[a]
8	Coolungoolun	Water	380	22	42.4	26.1	13.2	5.3	7.6
9	Morwell	Water	380	22	51.7	22.7	9.8	5.7	7.1
10	Yallourn	Water	380	22	54.4	25.1	9.4	5.6	9.8
11	Morwell Pale	Water	380	22	57.6	32.0	13.5	8.8	9.7
12	Yallourn Pale	Water	380	22	67.3	44.0	16.9	11.1	16.0
13	Millmerran	Toluene	380	22	38.8[a]				
14	Millmerran	Water	380	22	34.7[a]				
15	Liddell	Toluene	380	22	30.4[a]				
16	Liddell	Water	380	22	25.5[a]				

[a] daf basis not dmif; [b] corrected for bibenzyl formed on toluene pyrolysis

Table 3 Conversions and products from extraction of Victorian brown coals (25 g) with water (137 g) in a rocking autoclave (method B) at 380°C.

Coal	Pressure	Conversion	Liquid Yield	CO_2	CO/air	$CH_4/C_2H_6/C_3H_8$
		(wt% coal)				
Loy Yang	24	45.6[a]	21.7[a]	16.9[a]	0.3[a]	0.4[a]
Coolungoolun[c]	23	39.8[b]	21.3[b]	9.7[b]	0.9[b]	0.7[b]

[a] daf; [b] dmif; [c] phenols (0.19%), acetone (0.23%), methanol (0.05%) and ethyl methyl ketone (0.05%) were also formed.

Table 5 Analytical data for extraction residues

Extraction No.	2	3	4	8
Moisture (wt%)	10.8	10.6	9.8	6.0
Ash (wt% dry basis)	8.9	9.2	9.4	3.6
Volatile Matter (wt% dry basis)	31.7	27.1	21.6	26.6
C (wt% dry basis)	71.8	73.9	76.2	76.3
H (wt% dry basis)	3.6	3.5	3.2	3.8
N (wt% dry basis)	0.7	0.7	0.7	0.7
S (wt% dry basis)	0.9	0.9	0.8	3.7
H/C atom. ratio	0.60	0.57	0.50	0.60
Specific energy (MJ/kg, dry basis)	27.5	28.1	28.9	30.4
Aromatic carbon (% C)				84

Table 6 Conversions for extraction of Morwell coal (15 g dry) in a rocking autoclave (method B) with aqueous solvents (150 g) at 380°C

Solvent	Conversion (wt% coal dmif)
Water	48.7
0.5 M NaOH	66.6
0.25 M Na_2CO_3	63.8
0.5 M $HCO\bar{O}Na$	67.0
10% Tetralin/Water	55.3
20% Tetralin/Water	59.8

Table 4 Analyses of Liquid Products

Extraction No.	1	2	3	4	5	6	7	8	9	10
Oil										
H/C	1.40[b]	1.41	1.40	1.38	1.48	1.45	1.41	1.33	1.34	1.37
O (wt%)[a]	9.2[b]	9.5	10.0	10.8	9.5	7.2	7.2	(9.3)	7.7	9.3
OH (wt%)	4.1[b]	5.1	4.4	4.8	4.2	3.4	2.6	3.7	4.4	4.7
Mol. Wt.	285[b]	271	295	287	287	263	243	314	291	287
Aromatic H (%)	16[b]	17	18	18	13	15	17	17	18	17
Aromatic C (%)	40[b]	44				41	44	47		
Asphaltene										
H/C	1.23	1.07	1.09	1.08	1.26	1.13	1.07	0.99	1.02	1.11
O (wt%)	13.5	19.4	16.4	17.9	17.4	19.4	16.9	(18.3)	14.9	18.5
OH (wt%)	7.2	10.3	10.0	11.6				9.3	9.2	10.1
Mol. Wt.	470	374	349	350	332	368	393	415	369	323
Aromatic H (%)	28	36	35	36	27	33	36	34	32	33
Aromatic C (%)	53	69						66		
Pre-asphaltene										
H/C	0.88	1.03	0.99	0.97				0.96	0.93	0.93
O (wt%)	14.8	19.6	17.1	16.9				(21.1)	17.1	19.7
OH (wt%)								8.3		
Mol. Wt.								469		
Aromatic H (%)								45	42	43
Aromatic C (%)								79		

[a] oxygen figures are by direct determination except for those in parenthesis which are by difference; [b] corrected for bibenzyl

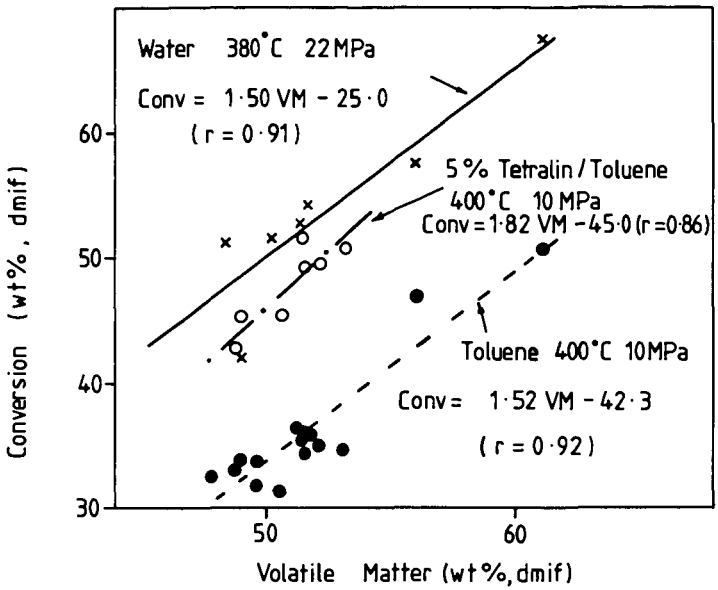

Fig.1 Variation in Conversion with Volatile Matter Content of Victorian Brown Coals

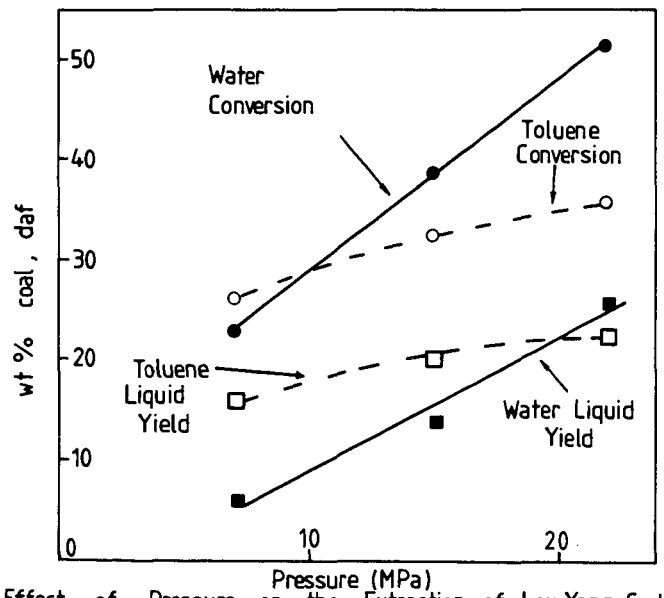

Fig. 2 Effect of Pressure on the Extraction of Loy Yang Coal at 380°C

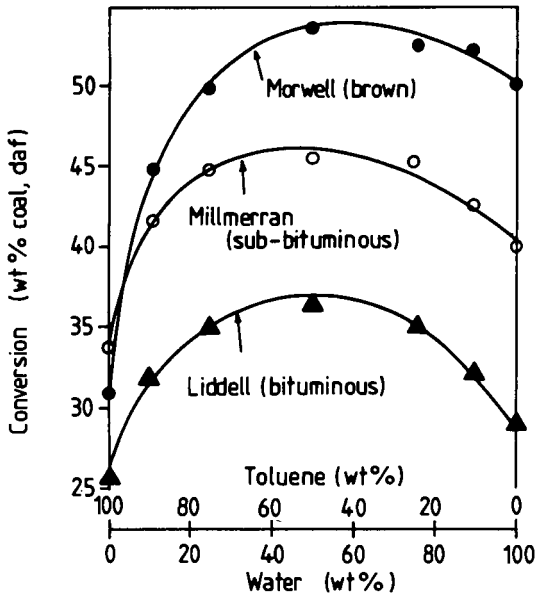

Fig. 3 Extraction with Toluene / Water Mixtures in a Rocking Autoclave at 380°C and a Gas Density of 0·44g/ml.

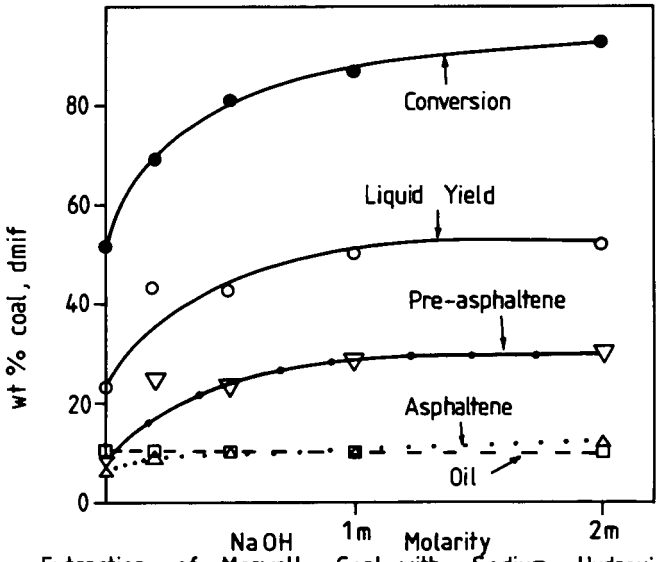

Fig. 4 Extraction of Morwell Coal with Sodium Hydroxide

Effect of Solvent Density on Coal Liquefaction Under Supercritical Conditions

G.V. Deshpande
G.D. Holder
and
Y.T.Shah

Department of Chemical and Petroleum Engineering
University of Pittsburgh
Pittsburgh, PA 15261

ABSTRACT

Supercritical fluid extraction is an attractive process primarily because the density and solvent power of a fluid changes dramatically with pressure at temperatures near the critical. In complex supercritical extractions, such as the extraction of coal, the density of the supercritical fluid should also change the extractability of the coal. In this experiment a non-reacting supercritical fluid, toluene, was studied to determine the effect of density on the coal extraction/reaction process. Extractions were carried out for two to 60 minutes at reduced densities between 0.5 and 2.0 and at temperatures between 647 and 698K. the data obtained can be explained by the hypothesis that coal dissolution is required preceding liquefaction reactions and that the degree of dissolution depends upon solvent density and temperature.

INTRODUCTION

Earlier efforts aimed at understanding supercritical extraction of coal used both flow and batch reactors.

In the flow reactors(1)-(5), coal was packed into the reactor and the supercritical fluid was passed through the bed of coal until the condensed effluent was clear. The conversion was defined as the total weight loss of the coal due to extraction by the solvent.

In batch systems(7)-(12), the coal and solvent were placed in a reactor and heated together to the reaction temperature.

More recent studies(13),(14) have employed a rapid injection autoclave, where coal is injected into a preheated supercritical solvent. After the reaction is over the products are quenched by passing water through internal cooling coils.

The general trends observed in the studies discussed above do provide some important insights; higher temperatures and higher densities result in higher conversions partially because more coal dissolves in the supercritical solvent as temperature and density are increased. Blessing and Ross(6) correlated the coal conversion to pyridine solubles with the Hildebrand Solubility Parameter, δ, which they defined as

$$\delta = 1.25\ P_c^{1/2} \rho_r / \rho_\ell \qquad 1)$$

where P_c is the critical pressure of the medium in atmospheres, ρ_r is its reduced density and ρ_ℓ is generalized reduced density of liquids, taken to be 2.66. They found the product pyridine solubility to be a linear function of δ.

EXPERIMENTAL

Bruceton bituminous, a Pittsburgh Seam coal was used in the experiment. The chemical analysis of coal is given in Table I. The coal was dried in vacuum @ 343 K prior to use and stored in glass containers under nitrogen.

Supercritical Coal Liquefaction Procedure

The experimental apparatus is shown in Figure 1 and consists of a 1-L stainless steel autoclave equipped with a Magnedrive stirrer and a coal injection system. The reactor is charged with a known quantity of toluene depending on the fluid density desired for the experiment and is heated at 3-4 K/min to the temperature desired. Once this temperature is reached, ambient coal is injected into the reactor from a coal reservoir using high-pressure Argon. The average weight of injected coal was 30g. Reaction times are measured from the time at which the coal is injected.

The liquid and solid contents were collected from the reactor and placed in an extraction thimble which was then placed in a soxhlet unit. The contents were then extracted with toluene until the extractant was clear after which the thimble was dried and weighed. The weight of the dried product is designated as toluene insolubles.

The conversion, based on the extraction results, are defined below.

Gases, Oils and Asphaltenes (GOA), % = 100 x

$$\left(\frac{\text{coal injected (g)} - \text{toluene insolubles (g)}}{\text{coal injected (g)}}\right) \qquad 2)$$

All weights are on a moisture and ash free basis.

Discussion

Experiments were carried out with Bruceton coal and toluene at supercritical toluene densities in the range of 0.157-0.601 g/cc. The temperature range studied was 647-698 K and the reaction time was varied from two minutes to 60 minutes.

The results of experiments at 647K and reduced densities of 0.5 to 2.0 (toluene densities of 0.157 g/cc and 0.601 g/cc) are given in Figures 2a and 2b. The experimental results show that toluene solubles (oils, asphaltenes, and gases) are produced during the reaction. They also show that the amount of toluene solubles formed at low reaction times increases with both temperature and density. In addition, solubility studies have shown that the amount of a solid which can dissolve in a supercritical fluid increases with density and, generally, with temperature. Hence, we concluded that the conversion of coal to oils + asphaltenes + gases is in some sense limited by the dissolution of the coal in the solvent.

We hypothesize that the only part of the coal which undergoes reaction to gas, oils and asphaltenes is the dissolved fraction, which increases with temperature and density. Increases in the dissolved fraction thus lead to higher conversions and faster reaction rates. These conversion products then participate in retrogressive reactions (Amestica and Wolf[12]) forming char, so that at longer times (15 minutes or more) the yield of gases + oils + asphaltenes decreases. At lower temperatures (647 K), the retrogressive reactions are insignificant and conversion does not decrease with time.

The above hypothesis is well explained by the results given in Figures 2a and 2b. At a lower density of 0.157 g/cc the fraction of coal dissolved in the supercritical fluid is much lower than when the density of the supercritical fluid is 0.601 g/cc. Hence, the fraction of coal, which is converted to asphaltenes, oils and gases, is also lower.

The results of experiments at 673 K and reduced density of 1.0 and 1.5 (supercritical toluene density of 0.301 g/cc and 0.444 g/cc) are given in Figure 3a. As observed at 647 K, the coal conversion to gases + oils + asphaltenes (toluene solubles) increase with reaction time and with the density of the

supercritical fluid. The retrogressive reactions are more significant now and hence, the toluene solubles show a maxima in conversion with time.

The results of experiments at 698 K and reduced density of 1.0 and 1.5 (supercritical toluene density of 0.301 g/cc and 0.444 g/cc) are given in Figure 3b. As observed at 647 K and 673 K, the coal conversion to gases + oils + asphaltenes (toluene solubles) increases with reaction time and density of the supercritical fluid. The retrogressive reactions are more pronounced than that at 673 K but we still observe a maxima in the toluene solubles as a function of reaction time. The initial rate of formation of toluene solubles (as seen from the steepness of the curves of toluene solubles versus reaction time) is higher at higher density and higher temperature. Also note that the amount of toluene solubles at the maxima is higher when the temperature and density of the supercritical fluid is higher. This is consistent with the hypothesis that the soluble fraction of the coal increases with temperature and density of the supercritical fluid.

Because coal is heterogeneous in nature, as the density is increased, heavier and heavier coal fractions (as opposed to more and more of the same fraction) are dissolved in the supercritical fluid. These would not dissolve if the density of the supercritical fluid were lower, and the supercritical fluid is, in general, unlikely to be saturated with any given fraction that is substantially dissolved (i.e. either zero or 100% of a fraction is dissolved). For example, if coal is considered to be composed of 100 fractions characterized by increasing molecular weight, more and more of these fractions dissolve as density is increased, but the solubility of a given fraction goes from (approximately) zero to 100% over a small change in density. If a given fraction, number 46 for example, is dissolved, then more of that molecular weight group would dissolve at that density if it were present, but none of the undissolved fractions would dissolve regardless of the amount of coal present. Hence, the fraction of the coal and not the amount of coal which dissolves in the supercritical fluid is a strong function of density and temperature of the supercritical fluid. In other words, if the amount of coal injected into the supercritical fluid at given temperatures and density was reduced to its half value, the absolute amount dissolved will fall by 50%.

If the amount of coal injected was increased indefinitely, then a point might be reached where the supercritical fluid is saturated with dissolved coal. If the amount of coal injected is increased beyond this value, the fraction of dissolved coal and the fractional coal conversion will start decreasing. The amount of dissolved coal in the supercritical fluid will be independent of the amount of coal injected in such a case.

Conclusions

When coal is contacted with a non-donor supercritical fluid a part of the coal instantaneously dissolves in the supercritical fluid. The dissolved coal undergoes liquefaction reactions which are thermal in nature resulting in toluene soluble products being formed from coal. These products can subsequently undergo retrogressive reactions yielding insoluble material. Hence the toluene solubles show a maxima in conversion with time.

The fraction of coal which dissolves instantaneously in the supercritical fluid increases with an increase in the density and temperature of the supercritical fluid. This effect is similar to that generally observed for the solubility of a solid in a supercritical fluid. With an increase in density and temperature higher molecular compounds present in coal go into solution, resulting in an undersatured solvent with the fraction, not the amount, of the coal which is being dissolved.

Literature Cited

1. Slomka, B. and Rutkowski, A., "A Kinetic Study of the Supercritical Toluene Extraction of Coal at 9.8 MPa," Fuel Processing Technology, 5, 247 (1982).

2. Jezko, J., Gray, David and Kershaw, J.R., Fuel Processing Technology, 15, 229 (1982).

3. Kershaw, J.R., Fuel Processing Technology, 5, 241 (1982).

4. Whitehead, J.C and Williams, D.F., "Solvent Extraction of Coal by Supercritical Gases," J. Inst. Fuel (London) 182 (1975).

5. Penninger, J.M.L., "Oil Extraction from Sub-bituminous Coal with Compressed Aqueous Gas Extractants-Stoichiometry and Mechanism of Extraction," presented at 1984 Annual AIChE Meeting, San Francisco, California, November (1984).

6. Blessing, J.E. and Ross, D.S., "Supercritical Solvents and the Dissolution of Coal and Lignite," ACS Symposium Series 71, Washington, D.C., (1978).

7. Bartle, K.D., Calimli, A., Jones, D.W., Matthews, R.S. and Olcay, A., Fuel 58, 423 (1979).

8. Tugrul, T. and Olcay, A., Fuel 57, 415 (1978).

9. Bartle, K.D., Martin, T.G. and Williams, D.F., Fuel 54, 226 (1975).

10. Kershaw, J.R., S. Afr. J. Chem., 30, 205, (1977).

11. Barton, Paul, Ind. Eng. Chem. Process Des. Dev., 22, 589 (1983).

12. Amestica, L.A. and Wolf, E.E., "Supercritical Toluene and Ethanol Extraction of an Illinois No. 6 Coal," Fuel 63, 227 (1984).

13. Deshpande, G.V., Holder, G.D., Bishop, A.A., Gopal, J. and Wender, I., "Extraction of Coal Using Supercritical Water," Fuel 63, 958 (1984).

14. Towne, S.E., "Supercritical Coal Extraction Using Aqueous-Organic Solvent Mixtures," M.S. Dissertation, University of Pittsburgh, December (1983).

TABLE 1

Analysis of Bruceton Bituminous Coal

ASH	3.93[a]
Carbon	82.69[b]
Hydrogen	5.56[b]
Sulfur	1.46[b]
Nitrogen	1.72[b]

[a] - moisture free basis
[b] - moisture and ash free basis

FIGURE 1: **EXPERIMENTAL SETUP FOR SUPERCRITICAL EXTRACTION**

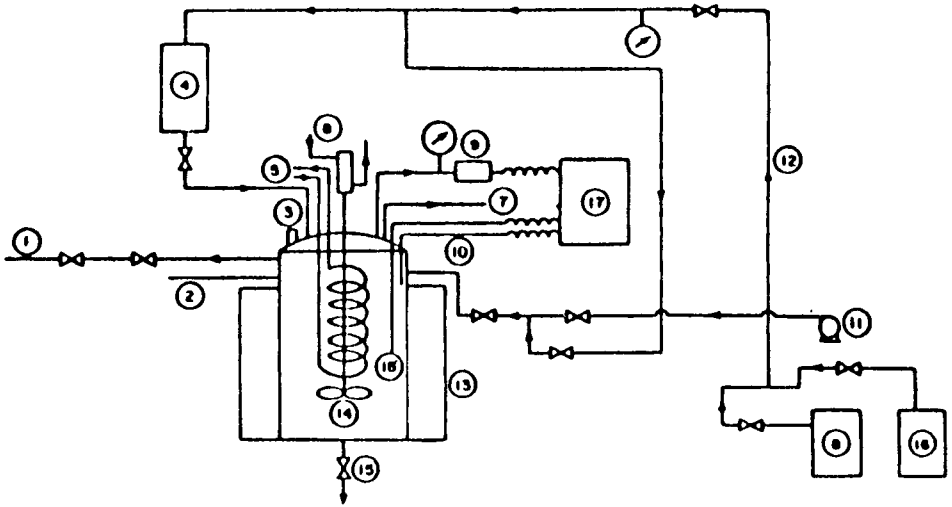

(1) GAS SAMPLE LINE
(2) RUPTURE DISC TO HOOD
(3) LIQUID SAMPLE PORT
(4) COAL BOMB
(5) COLD WATER (FOR STIRRER)
(6) COLD WATER (FOR MAGNETIC HEAD)
(7) VENT LINE TO HOOD
(8) HELIUM CYLINDER
(9) PRESSURE TRANSDUCER
(10) THERMOCOUPLE
(11) PUMP
(12) GAS LINE
(13) FURNACE
(14) AGITATOR
(15) DRAIN VALVE
(16) ARGON CYLINDER
(17) DATA LOGGER
(18) REACTOR

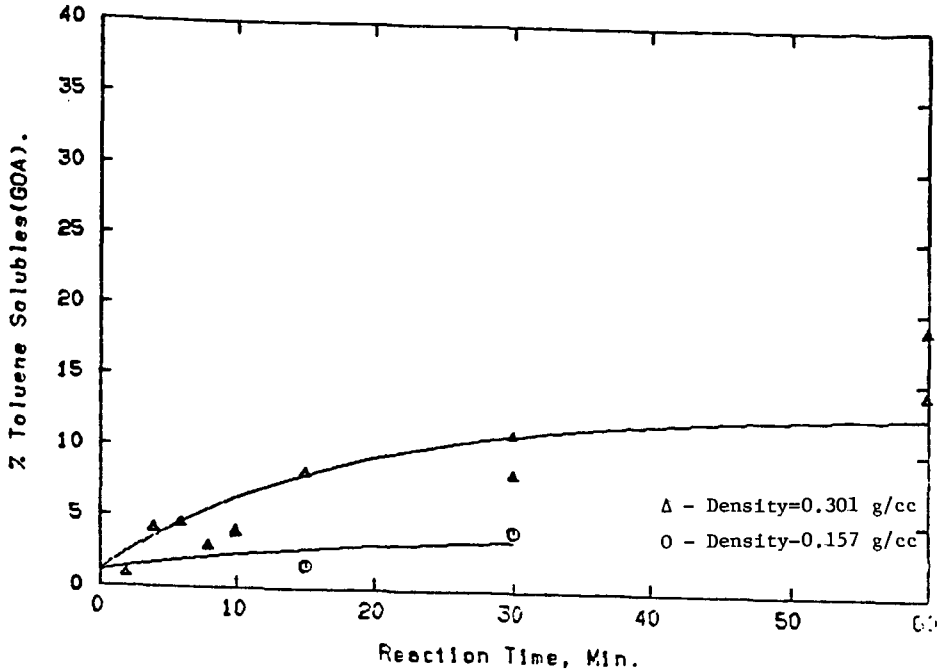

Figure 2a Effect of Reaction Time & Density on % GOA @ 647 K

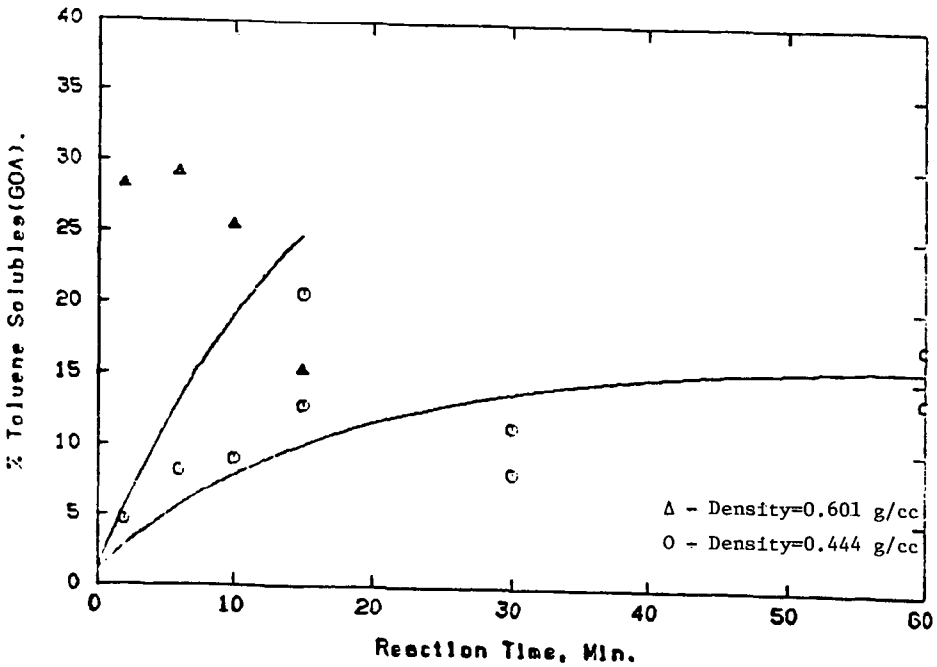

Figure 2b Effect of Reaction Time & Density on % GOA @ 647 K

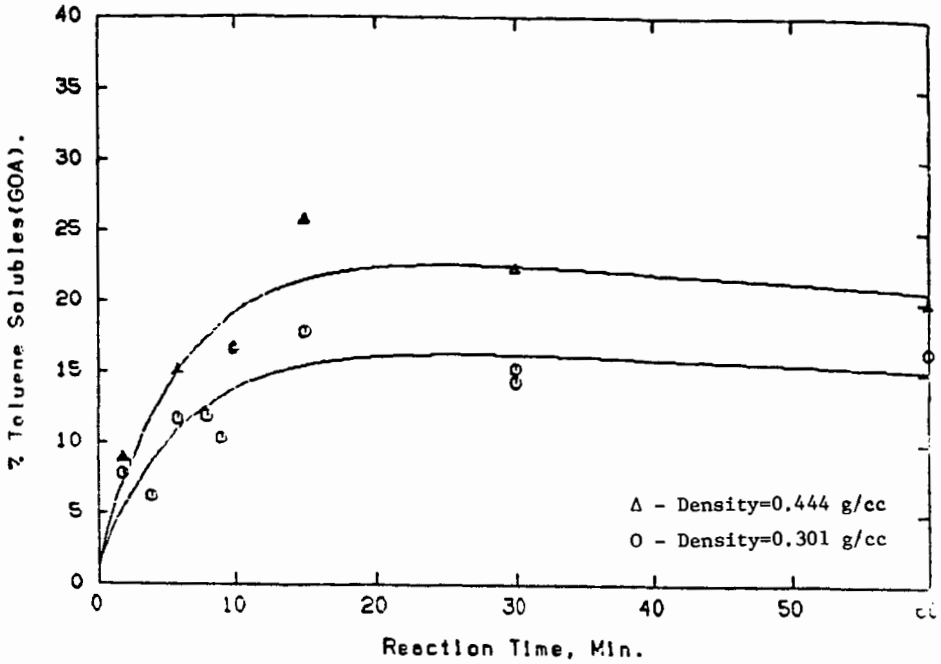

Figure 3a Effect of Reaction Time & Density on % GOA @ 673 K

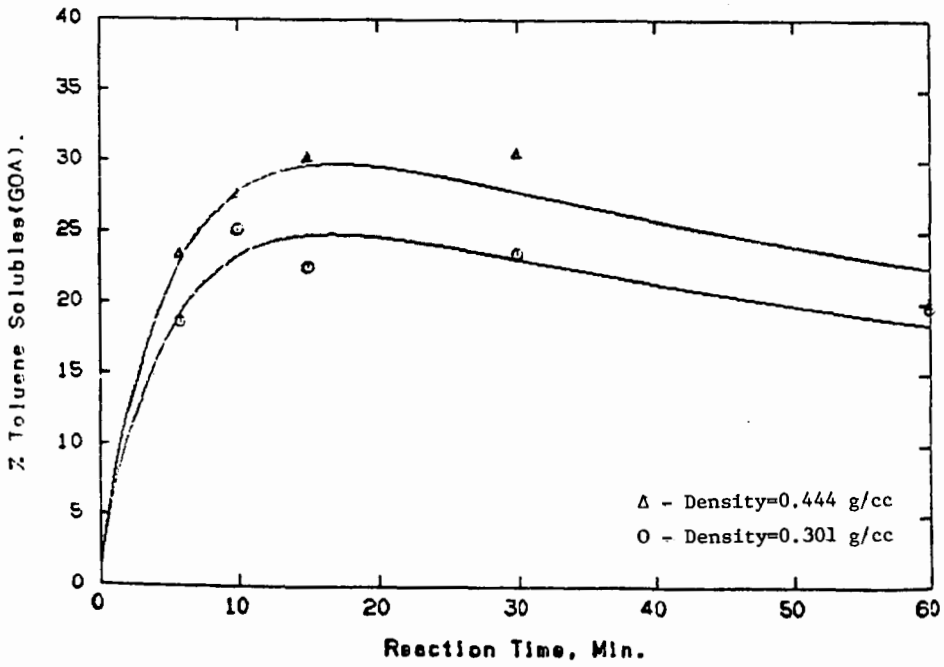

Figure 3b Effect of Reaction Time & Density on % GOA @ 698 K

VAN DER WAALS MIXING RULES FOR CUBIC EQUATIONS OF STATE
(Applications for Supercritical Fluid Extraction Modeling and Phase Equilibrium Calculations)

T. Y. Kwak, E. H. Benmekki and G. A. Mansoori

Department of Chemical Engineering
University of Illinois
BOX 4348 Chicago, Illinois 60680

Introduction

There has been extensive progress made in recent years in research towards the development of analytic statistical mechanical equations of state applicable for process design calculations (1,2). However cubic equations of state are still widely used in chemical engineering practice for calculation and prediction of properties of fluids and fluid mixtures (3). These equations of state are generally modifications of the van der Waals equation of state (4,5),

$$P = \frac{RT}{v - b} - \frac{a}{v^2} \qquad [1]$$

which was proposed by van der Waals (4) in 1873. according to van der Waals for the extension of this equation to mixtures, it is necessary to replace a and b with the following composition-dependent expressions :

$$a = \sum_i^n \sum_j^n x_i x_j a_{ij} \qquad [2]$$

$$b = \sum_i^n \sum_j^n x_i x_j b_{ij} \qquad [3]$$

Equations [2] and [3] are called the van der Waals mixing rules. In these equations a_{ij} and b_{ij}, $(i=j)$ are parameters corresponding to pure component (i) while a_{ij} and b_{ij}, $(i \neq j)$ are called the unlike-interaction parameters. It is customary to relate the unlike-interaction parameters to the pure-component parameters by the following expression :

$$a_{ij} = (1 - k_{ij}) \ (a_{ii} \ a_{jj})^{1/2} \qquad [4]$$

$$b_{ij} = (b_{ii} + b_{jj})/2 \qquad [5]$$

In Eq.[4] k_{ij} is a fitting parameter which is known as the coupling parameter. With Eq.[5] replaced in Eq.[3], the expression for b will reduce to the following one-summation form:

$$b = \sum_i^n x_i b_{ii} \qquad [3.1]$$

The Redlich-Kwong equation of state (6),

$$P = \frac{RT}{v - b} - \frac{a}{T^{1/2} v(v-b)} \qquad [6]$$

and the Peng-Robinson equation of state (7),

$$P = \frac{RT}{v-b} - \frac{a(T)}{v(v+b)+b(v-b)} \qquad [7]$$

$$a(T) = a(T_c)\ \{1 + \kappa(1 - T_r^{\frac{1}{2}})\}^2 \qquad [8]$$

$$a(T_c) = 0.45724\ R^2\ T_c^2\ /\ P_c \qquad [8.1]$$

$$\kappa = 0.37464 + 1.54226\omega - 0.26992\omega^2 \qquad [9]$$

$$b = 0.0778\ RT_c/P_c \qquad [10]$$

are widely used for thermodynamic property calculations.

The Theory of the Van Der Waals Mixing Rules

Leland and Co-workers (8-10) have been able to re-derive the van der waals mixing rules with the use of statiscal mechanical theory of radial distribution functions. According to these investigators for a fluid mixture with a pair intermolecular potential energy function ,

$$u_{ij}(r) = \epsilon_{ij} f(r/\sigma_{ij}) \qquad [11]$$

the following mixing rules will be derived :

$$\sigma^3 = \sum_i^n \sum_j^n x_{ij}\ x_{ij}\ \sigma_{ij}^3 \qquad [12]$$

$$\epsilon\sigma^3 = \sum_i^n \sum_j^n x_{ij}\ x_{ij}\ \epsilon_{ij}\sigma_{ij}^3 \qquad [13]$$

In these equations, ϵ_{ij} is the interaction energy parameter between molecule i and j while σ_{ij} is the intermolecular interaction distance between the two molecules. Knowing that coefficients (a) and (b) of the van der Waals equation of state are proportional to ϵ and σ according to the following expressions :

$$a = 1.1250\ RT_c v_c \propto N_o\ \epsilon\sigma^3 \qquad [14]$$

$$b = 0.3333\ v_c \propto N_o\ \sigma^3 \qquad [15]$$

We can see that Eq.[12] and Eq.[13] are identical with Eqs.[2] and [3] respectively. Statistical mechanical arguments which are used in deriving Eq.[12] and Eq.[13] dictate the following guidelines in using the van der Waals mixing rules :

(1) The van der Waals mixing rules are for constants of an equation of state.

(2) Equation [12] is a mixing rule for the molecular volume, and Eq.[13] is a mixing rule for (molecular volume).(molecular energy). It happens that b and a of the van der Waals equation of state are proportional to (molecular volume) and (molecular volume).(molecular energy), respectively, and as a result, these mixing rules are used in the form which was proposed by van der Waals.

(3) Knowing that σ_{ij} (for $i \neq j$), the unlike-interaction diameters, for spherical molecules is equal to

$$\sigma_{ij} = (\sigma_{ii} + \sigma_{jj})/2 \qquad [16]$$

This will make the expression for b_{ij} for spherical molecules to be

$$b_{ij} = [\ (b_{ii}^{1/3} + b_{jj}^{1/3})/2\ ]^3 \qquad [17]$$

Then for non-spherical molecules expression for b_{ij} will be

$$b_{ij} = (1-l_{ij})[\ (b_{ii}^{1/3} + b_{jj}^{1/3})\ ]^3 \qquad [18]$$

With the use of these guidlines, we now derive the van der Waals mixing rules for the two representative equations of state. Similar procedure can be used for deriving the van der waals mixing rules for other equations of state.

Mixing Rules for the Redlich-Kwong Equation of State

The Redlich-Kwong equation of state ,Eq.[6], can be written in the following form:

$$Z = \frac{PV}{RT} = \frac{v}{v-b} - \frac{a}{RT^{1.5}\ (v+b)} \qquad [19]$$

In this equation of state, b has the dimension of a molar volume,

$$b = 0.26 v_c \propto N_o \sigma$$

Then the mixing rule for b will be the same as the one for the first van der Waals mixing rules, Eq.(3), However mixing rule for a will be different from the second van der Waals mixing rule, Eq.[2]. Parameter a appearing in the Redlich-Kwong equation of state has dimension of $R^{-1/2}$. (molecular energy)$^{3/2}$ (molecular volume), that is

$$(\ a = 1.2828 R T_c^{1.5} v_c \propto N_o (\epsilon/k)^{1.5} \sigma^3)$$

As a result the second van der Waals mixing rules, Eq.[13], cannot be used directly for the a parameter of the Redilch-Kwong equation of state. However, since $(R^{1/2} a b^{1/2})$ has the dimension of (molecular energy).(molecular volume), the second van der Waals mixing rules, Eq.[13], can be written for this term. Finally the van der Waals mixing rules for the Redlich-Kwong equation of state will be in the following form:

$$a = \{\sum_i^n \sum_j^n x_i\ x_j\ a_{ij}^{2/3} b_{ij}^{1/3}\}^{1.5} / (\sum_i^n \sum_j^n x_i\ x_j\ b_{ij})^{1/2} \qquad [20]$$

$$b = \sum_i^n \sum_j^n x_i\ x_j\ b_{ij} \qquad [3]$$

These mixing rules, when joined with the Redlich-Kwong equation of state, will constitute the Redlich-Kwong equation of state for mixtures that is consistent with the statistical mechanical basis of the van der Waals mixing rules.

Mixing Rules for the Peng-Robinson Equation of State

In order to separate thermodynamic variables from constants of the Peng-Robinson equation of sate, we will insert Eq.[8] and Eq.[9] in Eq.[7] and we will write it in the following form :

$$Z = \frac{v}{v-b} - \frac{c/RT + d - 2\sqrt{(c\ d/RT)}}{(v+b) + (b/v)(v-b)} \qquad [21]$$

where $c = a(T_c)(1 + \kappa)^2$ and $d = a_c\kappa^2/RT_c$

This form of the Peng-Robinson equation of state suggests that there exist three independent constants which are b, c, and d. Now, following the prescribed guidelines for the for the van der Waals mixing rules, mixing rules for b, c, and d of the Peng-Robinson equation of state will be

$$c = \sum_i^n \sum_j^n x_i \; x_j \; c_{ij} \qquad [22]$$

$$b = \sum_i^n \sum_j^n x_i \; x_j \; b_{ij} \qquad [23]$$

$$d = \sum_i^n \sum_j^n x_i \; x_j \; d_{ij} \qquad [24]$$

with the following interaction parameters :

$$c_{ij} = (1-k_{ij}) \; (c_{ii} \; c_{jj})^{1/2} \qquad [25]$$

$$b_{ij} = (1-l_{ij}) \; \{(b_{ii}^{1/3} + b_{jj}^{1/3})/2\}^3 \qquad [26]$$

$$d_{ij} = (1-m_{ij}) \; \{(d_{ii}^{1/3} + d_{jj}^{1/3})/2\}^3 \qquad [27]$$

Applications for Supercritical Fluid Extraction Modeling

A serious test of mixture equations of state is shown to be their application for prediction of solubility of solutes in supercritical fluids (11). In the present report, we apply the van der Waals , the Redlich-Kwong and the Peng-Robinson equations of state for supercritical fluid extraction of solids and the effect of choosing different mixing rules on prediction of solubility of solids in supercritical fluids.

Thermodynamic Model

Solubility of a condensed phase, y_2 , in a vapor phase at supercritical conditions (12) can be define as :

$$y_2 = (P_2^{sat}/P) \; (1/\phi_2) \; \phi_2^{sat} \; \mathrm{Exp}\{\int_{P^{sat}}^{P} (v_2^{solid}/RT)\, dP\} \qquad [28]$$

where ϕ_2^{sat} is the fugacity coefficient at pressure P. Provided we assume v_2^{solid} is independent of pressure and for small values of of P_2^{sat} the above expression will be converted to the following form:

$$y_2 = (P_2^{sat}/P)\,(1/\phi_2) \; \mathrm{Exp}\; \{ v_2^{solid}(P-P_2^{sat})/RT\} \qquad [29]$$

In order to calculate solubility from Eq.[29] we need to choose an expression for the fugacity coefficient. Generally for calculation of fugacity coefficient an equation of state with appropriate mixing rules is used (12) in the following expression :

$$RT \ln \phi_i = \int_V^{\infty} [(\partial P/\partial n_i)_{T,V,n_j} - (RT/V)]\, dV - RT\ln Z \qquad [30]$$

Solubility Calculations

In Figure 1 solubility of 2,3 dimethyl naphtalene (DMN) in supercritical carbon dioxide is reported versus pressure at 308 kelvin along with predictions using the

van der Waals equation of state. According to this figure predictions by the van der Waals equation of state will improve when Eq.[3], along with combining rule in Eq.[17], is used as the mixing rule for b instead of Eq.[3.1] which is customarily used. This comparaison and other similar comparaisons which are reported elsewhere (11) for other solute-solvent systems establish the superiority of double-summation mixing rules, Eq.[3], for b over single summatiom expression, Eq.[3.1].

In Figure 2 the same experimental solubility data as in Figure 1 are compared with predictions using the Redlich-Kwong equation of state. According to this figure the corected van der Waals mixing rules for the Redlich-Kwong equation of state, Eqs.[3] and Eq.[20], are clearly superior to the mixing rules that are customarily used,Eq.[2] and Eq.[3.1], for this equation of state. Similar observations are made for prediction of solubilities of other solids in supercritical fluids which will not be reported here.

The Peng-Robinson equation of state with its customary mixing rules, Eqs.[2] and [3.1], is widely used for prediction of solubility of heavy solutes in supercritical gases and for petroleum reservoir fluid phase equilibrium calculations (13-15). In Figure 3 the same experimental solubility data as in Figures 1 and 2 are compared with predictions using the Peng-Robinson equation of state with its original mixing rules with the corrected mixing rules. According to Figure 3 corrected van der Waals mixing rules of the Peng-Robinson equation of state apparently do not improve solubility predictions over the original mixing rules. However, variation of solubility versus pressure for the new mixing rules is more consistent with the experimental data than the old mixing rules. Also considering the fact that new mixing rules for the Peng-Robinson equation of state contain three adustable parameters (k_{ij} , l_{ij} and m_{ij}) while the old mixing rules contain only one adjustable parameter (k_{ij}), it makes the new mixing rules more attractive. To demonstrate the superiority of the new mixing rules for the Peng-Robinson equation of state we have reported here Figures 4 to 9. According to these figures when the unlike-interaction adustable parameters of the mixing rules are fitted to the experimental data, the Peng-Robinson equation of state with the corrected van der Waals mixing rules can predict solubility of heavy solids in supercritical fluid more accurately than with the original mixing rules over different ranges of temperature and pressure and for different solutes and supercritical solvents.

Applications for Correlations of Vapor-Liquid Equilibria

When applied to both vapor and liquid phases , cubic equations of state can be used to generate thermodynamically consistent data, particularly equilibrium data. Good correlations of vapor -liquid equilibria depend on the equation of state used and, for multicomponent systems, on the mixing rules.

Thermodynamic Model

In the equilibrium state,the intensive properties - temperature, pressure and chemical potentials of each component - are constant in the overall system.Since the fugacities are function of temperature,pressure and compositions ,the equilibrium condition

$$f_i^V(T,P,\{y\}) = f_i^L(T,P,\{x\}) \qquad [31]$$

can be expressed by

$$y_i\ \phi_i^V = x_i\ \phi_i^L \qquad [32]$$

The expression for the fugacity coefficient ϕ_i depends on the equation of state that is used and is the same for the vapor and liquid phases

$$RT \ln \phi_i = \int_V^{\infty} [(\partial P/\partial n_i)_{T,V,n_j} - (RT/V)]\, dV - RT\ln Z \qquad [33]$$

In calculations of mixture properties with the Peng-Robinson equation of state we used the following combining rules:

$$c_{ij} = (1 - k_{ij})[c_{ii} \cdot c_{jj}/b_{ii} \cdot b_{jj}]^{1/2}\, b_{ij} \qquad [34]$$

$$b_{ij} = (1 - l_{ij})^3 \left[\frac{b_{ii}^{1/3} + b_{jj}^{1/3}}{2}\right]^3 \qquad [35]$$

$$d_{ij} = (1 - m_{ij})^3 \left[\frac{d_{ii}^{1/3} + d_{jj}^{1/3}}{2}\right]^3 \qquad [36]$$

A three parameter search routine using a finite difference Levenberg - Marquardt algorithm was used to evaluate the interaction parameters which minimize the objective function

$$OF = \sum_{i=1}^{M} \left[\frac{P(exp) - P(cal)}{P(exp)}\right]_i \qquad [37]$$

where M is the number of experimental points considered.
The average pressure deviation is expressed as

$$\Delta P/P = (OF/M)^{1/2} \qquad [38]$$

Phase Equilibrium Calculations

Attention will be given to complex binary systems such as water-acetone. In order to apply the Peng-Robinson equation of state to such polar compounds , some modifications must be incorporated (16). These modifications concern the values of the pure-component parameters.
The relationship α (T_r, ω) for water must be changed to

$$\alpha^{1/2} = 1.008568 + 0.8215(1 - T_r^{1/2})$$

this correlation is good for $T_r^{1/2} < 0.85$

Figures 10,11 and 12 show both the prediction by the Peng-Robinson equation of state with classical mixing rules and one parameter , $k_{1,2}$, fitted to bubble point data, and the net improvment provided by the proposed mixing rules with three fitted paramaters. Figure 13 shows the Peng-Robinson prediction with new mixing rules and binary interaction parameters set to zero. It should be noted that no prediction is observed by the Peng-Robinson equation of state with classical mixing rules and binary interaction parameter, $k_{1,2}$, equal to zero.

Nomenclature

a, b, c, d	:equation of state parameters
f	:fugacity
k, l, m	:binary interaction parameters
n	:number of components
N_o	:Avogadro number
OF	:objection function to be minimized
P	:pressure
T	:temperature
u	:intermolecular potential function
v	:molar volume
x	:mole fraction
y	:mole fraction in the vapor phase
Z	:compressibility factor
ϕ	:fugacity coefficient
σ	:intermolecular distance parameter
ϵ	:interaction energy parameter
ω	:acentric factor
κ	:a function of the acentric factor

Subscripts

c	:critical property
i, j	:component identification
2	:solute

REFERENCES

(1). Alem,A. H. and Mansoori,G. A., AICHE J.,30,468 (1984)

(2). Nauman,K. H., and Leland,T. W., Fluid Phase Equilbria, 18,1 (1984).

(3). Renon,H.,(Ed.),"Fluid Properties and Phase Equilibrium for Chemical Process Design",Procedings of the 3rd international Conference , Callaway Gardens, GA., April 10-15, Fluid Phase Equilibria,13,(1983).

(4). Van der Waals,J.D., Phd Thesis, Leiden,1873.

(5). Rowlinson,J. S. and swinton,F.L.,"Liquid and Liquid Mixtures",3rd Ed.Butterworths, Wolborn, Mass.1982

(6). Redlich,O. and Kwong,J. N. S.,Chem.Rev.,44,233 (1949)

(7). Peng,D. Y. and Robinson,D. B..Ind.Eng.Chem.Fund., 5,59,(1976)

(8). Leland,T. W. and Chapplear,P. S.,Ind.Eng.Chem., 60,15 (1968)

(9). Leland,T. W., Rowlinson,J. S., and Sather,G. A., Trans. Faraday Soc.,64,1447 (1968)

(10). Leland ,. W.,Rowlinson,J. S., Sather,G. A., and Watson,I. D.,Trans.Faraday Soc.,65,2034 (1969)

(11). Mansoorì,G. A. and Ely,J. F.,J.Chem.Phys.,82,Jan.(1985)

(12). Prausnitz,J. M.,"Molecular Thermodynamics of Fluid Phase Equilibria",Prentice-Hall,Englewood Cliffs,NJ,1969

(13). Kurnik,R. T.,Holla,S. J. and Reid,R. C.,J.Chem.Eng. Data, 26, 47 (1981)

(14). Katz,D. L. and Firoozabadi,A.,J.Petrol.Tech.,Nov, 1649(1978)

(15). Firoozabadi,A., Hekim,Y. and Katz,D. L.., Canadian J. Chem.Eng.,56, 610 (1978)

(16). Robinson,D. B.,Peng,D. Y. and Chung,S. Y. K.,"Development of the Peng-Robinson Equation of state and its Application to a System Containing Methanol".

(17). Griswold,J. and Wong,S. Y., Chem.Eng.Progr.Sympos. Series,48, No 3, 18 (1952)

(18). Ohgaki,K., Katayama, T., J.Chem.Eng.Data,21,53 (1976)

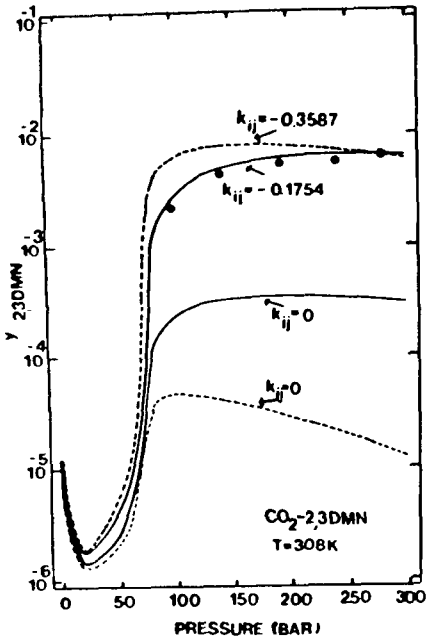

Figure 1 : Solubility of 2,3 dimethyl naphtalene (DMN) in supercritical carbon dioxide at 308 K versus pressure. The solid dots are the experimental data (13). The dashed lines are results of the van der Waals equation of state with Eqs.[2] and [3] as the mixing rules. The solids lines are results of the van der Waals equation of state with Eqs.[2] and [3] as the mixing rules and Eqs.[4] and [17] as the combining rules. The circled dot is the experimental data point used to calculate k_{ij}

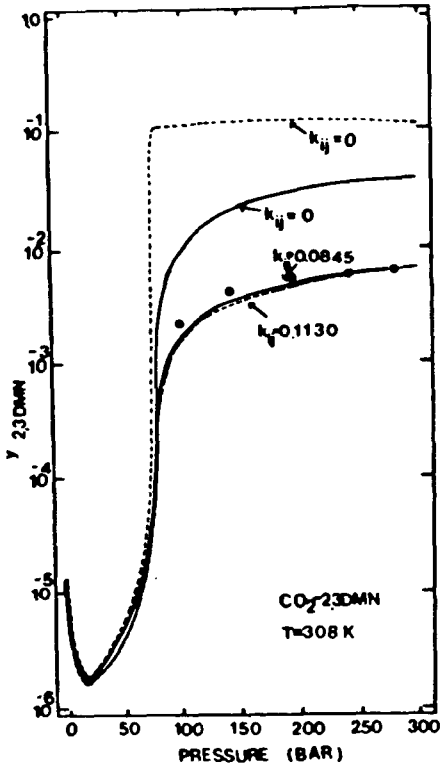

Figure 2 : Solubility of 2,3 DMN in supercritical carbon dioxide at 308 K versus pressure. The solid dots are the experimental data (13). The dashed lines are the results of the Redlich-Kwong equation of state with Eqs.[2] and [3.1] as the mixing rules. the solid lines are the results of the Redlich-Kwong equation of state with Eqs.[3] and [20] as the mixing rules and Eqs.[4] and [17] as the combining rules. The circled dot is the experimental data point used to calculate k_{ij}

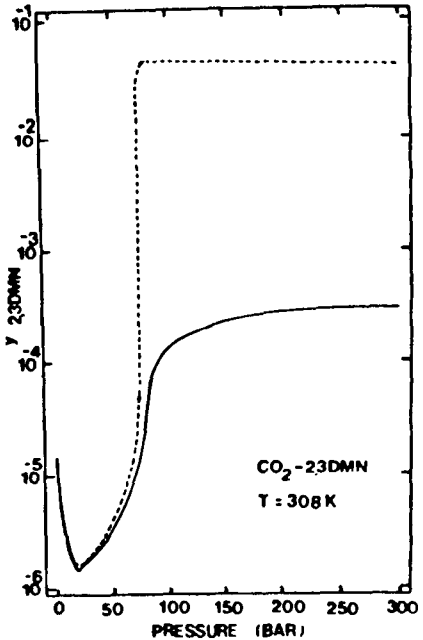

Figure 3 : Solublity of 2,3 DMN in supercritical carbon dioxide at 308 K versus pressure. The dashed lines are results of Peng-Robinson equation of state with Eqs.[2] and [3.1] as mixing rules. The solid lines are results of Peng-Robinson equation of state with Eqs. [3] and [20] as the mixing rules. Both two lines are for k_{ij} = 0

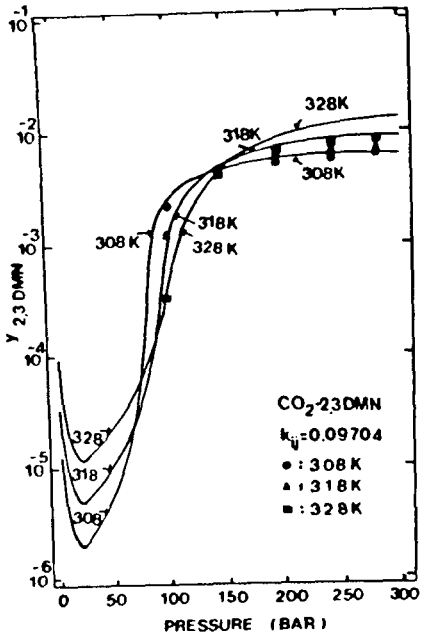

Figure 4 : Solubility of 2,3 DMN in supercritical carbone dioxide calculated by the Peng-Robinson equation of state using [eqs.[2] and [3.1] as mixing rules.

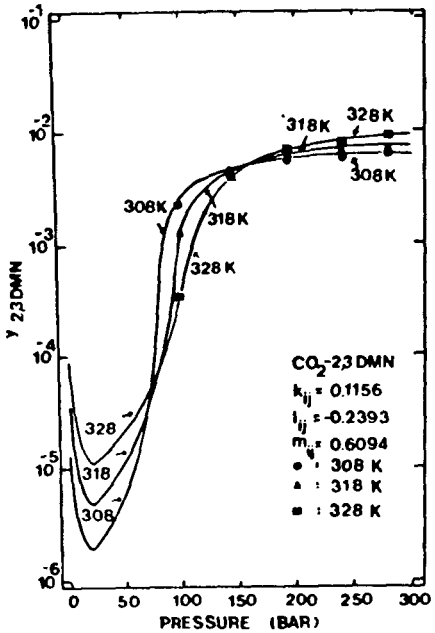

Figure 5 : Solubility of 2,3 DMN in supercritical carbon dioxide calculated by the Peng-Robinson equation of state with [eqs.[22-24] as mixing rules.

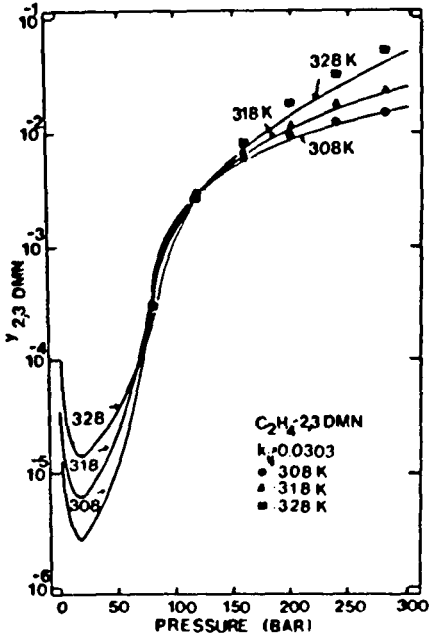

Figure 6 : solubility of 2,3 DMN in supercritical ethylene predicted by the Peng-Robinson equation of state with eqs.[2] and [3.1] as mixing rules.

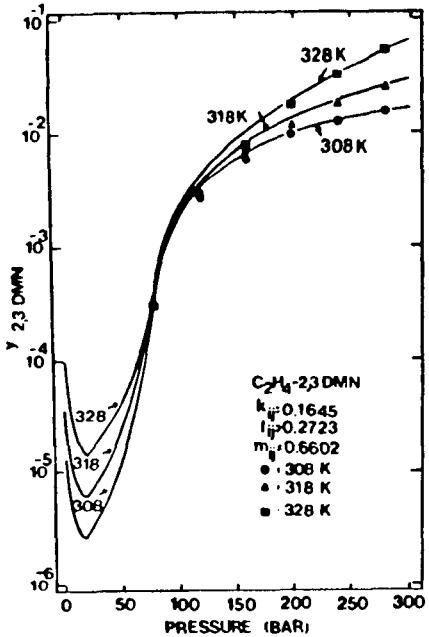

Figure 7 : solubility of 2,3 DMN in supercritical ethylene predicted by the Peng-Robinson equation of state with Eqs.[22-24] as the mixing rules.

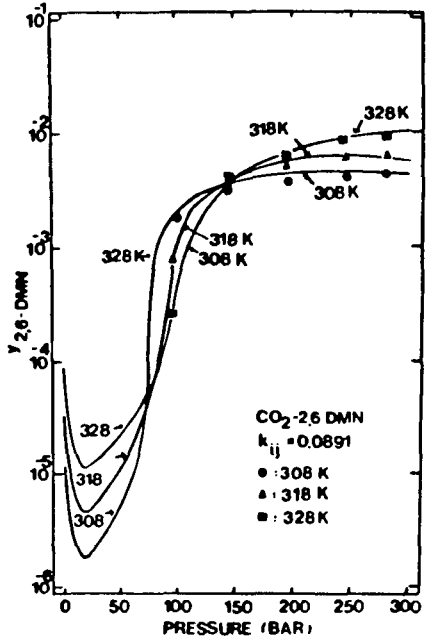

Figure 8 : solubility of 2,6 dimethyl naphtalene (DMN) in carbon dioxide calculated by the Peng-Robinson equation of state with Eqs.[2] and [3.1] as mixing rules.

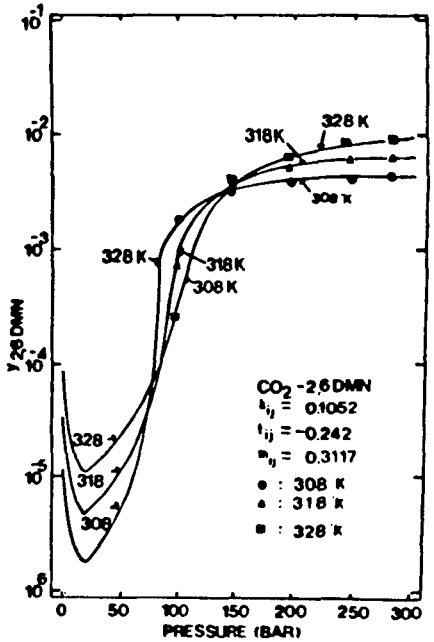

Figure 9 : Solubility of 2,6 DMN in supercritical carbon-dioxide predicted by the Peng-Robinson equation of state using Eqs.[22-24] as mixing rules.

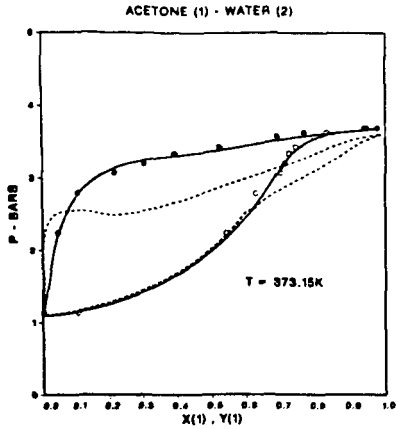

Figure 10

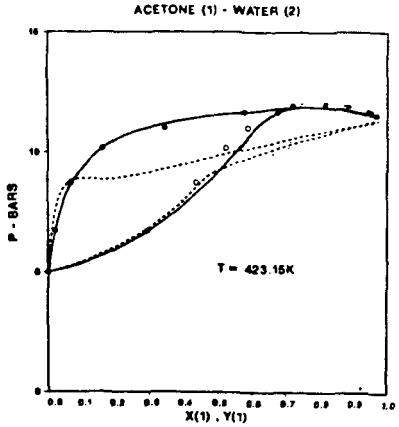

Figure 11

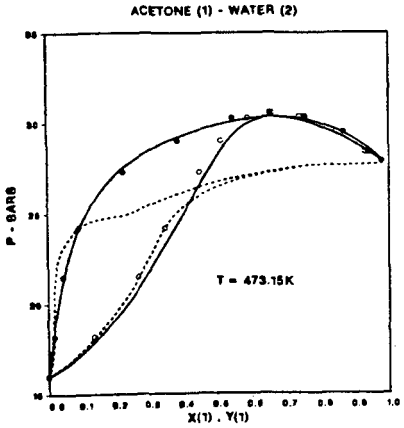

Figure 12

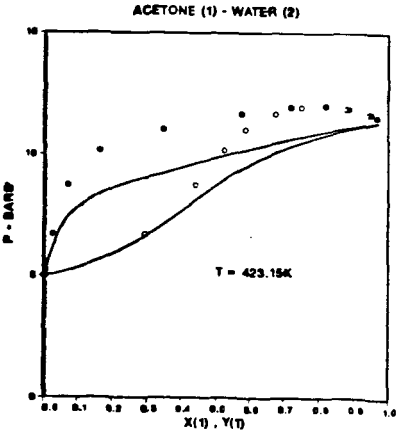

Figure 13

Figures 10, 11, 12 : Phase behavior of acetone-water systems. The solids lines are the Peng-Robinson prediction with three fitted parameters and the corrected mixing rules. The dashed lines are for Peng-Robinson prediction with one fitted parameter and the classical mixing rules.The dots and circles are experimental data (17).

Figure 13 : Acetone-water system predicted by the Peng-Robinson equation of state with the proposed mixing rules and the binary interaction parameters ($k_{1,2}$, $l_{1,2}$, $m_{1,2}$) equal to zero.

EXTRACTION OF A NORTH DAKOTA LIGNITE WITH SUPERCRITICAL ALIPHATIC SOLVENTS

M.L. Swanson, J. Dollimore, E.S. Olson, and J.W. Diehl

University of North Dakota Energy Research Center
Box 8213, University Station
Grand Forks, North Dakota 58202

Introduction

Extraction of coal with various solvents has been a commonly used method for obtaining knowledge about the structure of coal and its chemical composition. Solvent extraction of coal has been classified into four different types by Oele and others (1), and Dryden (2,3). A recent review of solvent extraction was prepared by Pullen (4).

1. Nonspecific extraction - nonspecific solvents extract only a small percentage of the coal. These solvents tend to primarily dissolve the waxy and resinous compounds which reside in the coal's physical structure in the form of resin bodies and particles.

2. Specific extraction - specific solvents extract a larger portion of the coal (up to ~40%) with the extracted material closely resembling the insoluble coal residue. The effectiveness of these solvents has been attributed to the existence of an unshared pair of electrons on nitrogen or oxygen in the solvent molecule thereby making the solvent behave as a polar fluid (3,4).

3. Extractive disintegration or degradation - this type of extraction occurs at temperatures between 200° and 400°C where the percent extraction is dependent on the production of smaller soluble fractions by the thermal decomposition of the coal. Solvents under these conditions can dissolve up to ~40% of the coal at temperatures of 400°C.

4. Extractive chemical disintegration - these extractions dissolve the coal by thermally decomposing and chemically reacting with the coal to form smaller molecular fragments (1). Most of this work involves using hydrogen-donor solvents (i.e., solvents that can either donate hydrogen to the various reactive coal species or at least act as a hydrogen transfer agent) to manufacture liquid products from the coal.

Interest in the extraction of coal (and other substrates) with supercritical solvents has been increasing rapidly over the past fifteen years. This interest is primarily due to the enhanced solubility of substrates in the fluid phase that occurs at or above the critical point. Also, the solvent power of the solvent (which depends on the solvent density) can be conveniently controlled over a large range with small changes in the solvent pressure or temperature (5,6). Most of the coal extractions using supercritical fluids have been performed at temperatures above 350°C. Squires and others (7) reported that thermal decomposition processes were becoming significant above 325°C for the extraction of an Illinois No. 6 coal with supercritical methanol. This suggests that results from supercritical fluid extractions above this temperature are a combination of physical and chemical solvent-coal interactions.

The twofold objectives of this research are to investigate, in the context of the solvent extraction model presented above, the fundamental principles of solute-solvent interactions at or above the solvent critical point and to use supercritical solvent extraction (SCSE) as a method for determining various molecular fractions present in low-rank coals. In order to minimize the thermal decomposition component in the supercritical fluid extraction of low-rank coals, solvents were selected with critical temperatures below the temperature at which volatile matter is evolved by destructive distillation (i.e., <325°C).

Experimental

Materials

The solvents used were n-pentane through n-octane and cyclohexane available commercially in HPLC grade. The coal used was Indian Head lignite (Indian Head mine, Zap, ND) vacuum dried for at least a week at 10 micron Hg and room temperature. The proximate and ultimate analyses for this lignite are shown in Table I.

Table I. Proximate and Ultimate Analyses for Indian Head Lignite (mf basis).

Proximate Analysis	
Volatile Matter	39.8
Fixed Carbon (By difference)	46.7
Ash	13.5
Ultimate Analysis	
Hydrogen	3.85
Carbon	60.79
Nitrogen	1.47
Sulfur	0.89
Oxygen (By difference)	19.51
Ash	13.5

Supercritical Fluid Processing

Extractions of Indian Head lignite samples were performed using the aliphatic solvents mentioned above. These experiments were performed using a semicontinuous supercritical solvent extraction system. A flow sheet for this system is shown in Figure 1. In this system a fixed bed of coal (~50 gm) was contained in a 25.4 cm by 1.75 cm ID section of high pressure tubing by one micron sintered metal frits. The preheating coils and fixed bed of coal were then immersed in a preheated fluidized sand bath where supercritical conditions were achieved in less than seven minutes. A Ruska positive displacement pump and high pressure accumulator were used to provide a pulseless flow of solvent through the system once supercritical conditions were reached. A solvent flow rate of 120 mℓ/hr was maintained for two hours. The pressure of the supercritical solvent was reduced to atmospheric pressure after passing a back pressure regulator. The extract and solvent were collected in a chilled sample

vessel. The noncondensable product gas was measured and collected for subsequent analysis.

Analytical

After each experiment, the extracted lignite residue and solvent-extract mixture were rotary vacuum distilled at ~30 mm Hg and 80°C and weighed. This procedure insured that a solvent and moisture-free product was obtained for material balance purposes. The collected product gases were analyzed by gas chromatography. Residues were analyzed by thermogravimetric analysis (TGA). Proximate and ultimate analyses were performed on selected samples.

Analysis of the solid extracts obtained by the supercritical hydrocarbon extractions were accomplished by column separations, infrared spectroscopy, 60 MHz proton NMR and capillary GC. Separations of the acids from the extracts was acomplished by the following procedure. The extract was dissolved in a warmed chloroform-methanol mixture (1:1). The soluble portion was added to a column containing Sephadex A25 ion exchange resin. The eluent from the column was evaporated and the acid-free fraction was weighed. The column was eluted again with a solution of formic acid (7 mℓ) in chloroform-methanol (1:1, 33 mℓ). Evaporation of this eluent gave a fraction consisting of fatty and resin acids. The acid-free wax was dissolved in carbon tetrachloride and analyzed by an infrared calibrated for the ester carbonyl peak and the alcohol OH-stretching peak.

Discussion and Results

Temperature and Pressure Effects

As mentioned above, one of the potential advantages of supercritical fluid extraction is the relatively large change in the solute solubility that can be achieved with small changes in solvent pressure or temperature. This premise was tested in the following way. A series of isobaric experiments using supercritical pentane to extract Indian Head lignite at various temperatures was carried out to investigate the effects of operating temperature on the percent conversions. The operating conditions of these runs and their resulting conversions are shown in Table II. As shown in

Table II. Operating Conditions and Results for Supercritical Pentane Extractions of Indian Head Lignite at Constant Pressure, P_r = 1.50.

Operating Temp., °C	T_r**	Operating Pressure (Psia)	% Conversion (maf)*	% Yield (maf)*
206	1.020	735	1.50	1.1
235	1.083	735	1.50	0.34
270	1.158	735	1.50	1.4
300	1.222	735	1.50	0.63 (?)

*% conversion $\frac{\text{wt maf coal - wt maf residue}}{\text{wt mf coal}}$; % yield = $\frac{\text{wt maf extract}}{\text{wt maf coal}}$

**$T_r = \frac{\text{operating temperature of solvent (°K)}}{\text{critical temperature of solvent (°K)}}$; $P_r = \frac{\text{operating pressure of solvent (psia)}}{\text{critical pressure of solvent (psia)}}$

Figure 2, the percent conversion initially decreased with an increase in operating temperature up to 235°C. This decrease was caused by the decrease in the solvent density that occurs with increasing temperature. The conversion then increased with further increases in the operating temperature up to 270° and 300°C, respectively. These increases were due to increased thermal effects in the coal which more than offset the decrease in solubility caused by the decreased solvent density.

Table III shows how temperatures affected the percent conversions and yields of three (two hexanes and one heptane) supercritical extractions. These results also indicate that percent conversions increase with increasing temperature. However, the differences observed between the isothermal hexane and heptane experiments indicate that higher conversions are obtained as the operating temperature approaches the solvent critical temperature (i.e., T_r goes to one). These results are consistent with those reported by Blessing and Ross (8).

Table III. Operating Conditions and Results for Supercritical Hexane and Heptane Extractions of Indian Head Lignite at Constant Reduced Pressure, P_r = 2.0.

Solvent	Operating Temperature (°C)	T_r	Operating Pressures (Psia)	% Conversion (maf)	% Yield (maf)
n-Hexane	244	1.020	860	3.1	1.3
n-Hexane	278	1.087	860	5.3	1.6
n-Heptane	278	1.020	795	6.5	1.7

The effect of pressure on supercritical fluid extractions was investigated by performing a series of isothermal extractions using supercritical hexane at various pressures to extract Indian Head lignite. The operating conditions and results of these experiments are shown in Table IV. The percent conversions and yields for these experiments are plotted in Figure 3. The results displayed in Figure 3 suggest that a maximum in the solubility of Indian Head lignite in supercritical hexane occurs in the vicinity of P_r = 2.0. The existence of a maximum in solute solubility occurring as a function of pressure have been reported for a South African coal in supercritical toluene (9) and for biphenyl in supercritical CO_2 (10). The reasons stated for these maxima were the differences between the pressure dependent solubility parameters of the coal and the solvent or by performing extractions at pressures above the upper critical region end point together with "free volume" effects (size asymmetry between the solute and solvent) as in the case of the biphenyl - CO_2 system. Figure 4 illustrates the improved solvent power that resulted from small increases in the solvent pressure from P_r = 1.5 to 2.0 for the extractions using supercritical heptane, octane and cyclohexane. This figure also suggests that changes in the operating pressure have a larger effect on the solvent power of the supercritical solvent at higher operating temperatures. It appears from the data presented above that the yields from the extraction of Indian Head lignite with supercritical aliphatic solvents were not affected to a large extent by either the operating temperature or pressure. This could be due to a limited amount of compounds present in the coal which are selectively extracted by aliphatic solvents under 325°C. The differences between the percent yield and conversion data were due to the production of gas (primarily CO_2) and the formation of water from the coal.

Table IV. Operating Conditions and Results for Supercritical Hexane Extraction of Indian Head Lignite at Constant Temperature, T_r = 1.02.

Operating Temp. (°C)	Operating Pressure (Psia)	P_r	% Conversion (maf)	% Yield (maf)
244	450	1.05	2.2	0.9
244	650	1.50	2.3	1.0
244	860	2.00	3.2	1.4
244	1080	2.50	2.6	1.3
244	1295	3.00	3.0	1.1

Analytical Results and Discussion

The effect of supercritical extraction on the thermal characteristics of the resulting residues was investigated using thermogravimetric analyses. Table V shows the operating conditions and conversions obtained for each of the residues analyzed by TGA. Figure 5 displays the differential weight loss for the five supercritical fluid extracted residues as functions of the sample temperature. A sample of the vacuum dried "as run" Indian Head lignite was also plotted for comparison purposes. This figure suggests that the supercritical fluid solvents used in this paper were extracting more of the compounds that would devolatilize below ~400°C with the increased operating temperature necessary with the longer solvent chain length.

Table V. Operating Conditions and Results for Supercritical Extraction of Indian Head Lignite at Constant Reduced Temperatures and Pressures, T_r = 1.02, P_r = 2.0.

Solvent	Operating Temp (°C)	Operating Pressure (Psia)	% Conversion (maf)	% Yield (maf)
n-Pentane	206	980	3.1	0.6
n-Hexane	244	860	3.2	1.3
n-Heptane	278	795	6.5	1.7
n-Octane	307	720	9.8	2.2
Cycohexane	291	1180	9.1	2.5

The analyses of the extracts revealed the presence of aliphatic esters, alcohols, acids and alkanes with little or no aromatics being extracted. Separations and quantitative infrared spectroscopy have been performed on the chloroform-methanol soluble fractions (~50 wt %) from the supercritical pentane and hexane extractions to date. The yields from this preliminary data averaged 0.19%, 0.06%, and 0.26% for the waxy esters, aliphatic alcohols and the fatty acids, respectively. Proton NMR showed that the aromatic content of the extracts tended to increase slightly with increasing operating temperature. Capillary GC analyses on whole samples and silica gel column separated samples using a 15 m SE-54 column provided data on the distribution of normal

and cyclic alkanes, waxy esters, and fatty alcohols and acids. The series of n-alkanes occurred between C_{21} and C_{33} with a maximum concentration of the C_{29} alkane. A number of triterpanes and C_{15} to C_{20} cyclic alkanes were present. The fatty alcohols were found to be mainly C_{24}. The fatty acids were converted to their methyl esters for analysis. A series of esters was observed with maximum concentration at C_{24} and C_{26}. From the composition and yield data, it appears that extraction of Indian Head lignite with supercritical aliphatic solvents with critical temperatures below 325°C still has the characteristics of nonspecific extraction.

Acknowledgment

This research was performed with the support of the U.S. Department of Energy under contract No. DE-FC21-83FE60181.

Literature Cited

1. Oele, A.P., H.I. Waterman, M.L. Goedkoop, and D.W. Van Krevelan, "Extractive Disintegration of Bituminous Coals", Fuel, 30 (7), 169-178, 1951.
2. Dryden, I.G.C., "Action of Solvents on Coals at Lower Temperatures - Mechanism of Extractions of Coals by Specific Solvents and the Significance of Quantitative Measurements", Fuel, 30, pp. 145-158, 1951.
3. Dryden, I.G.C., "Chemical Constitution and Reactions of Coal", In Chemistry of Coal Utilization, (Lowry, H.H., editor), John Wiley and Sons, New York, pp. 232-295, 1963.
4. Pullen, J.R., "Solvent Extraction of Coal", Coal Science, Vol. 2. (Goraty, M.L., J.W. Larsen, and I. Wender, editors), Academic Press, New York, pp. 173-288, 1983.
5. Rowlinson, J.S., "Critical and Supercritical Fluids", Fluid Phase Equilibria, 10, (2-3), pp. 135-139, 1983.
6. Schneider, G.M., "Physiochemical Aspects of Fluid Extraction", Fluid Phase Equilibria, 10, (2-3), pp. 141-157, 1983.
7. Squires, T.G., T. Aida, Y. Chen, and B.F. Smith, "The Role of Thermal Chemical Processes in Supercritical Gas Extraction of Coal", ACS National Meeting Fuel Chemistry Division Preprints, Vol. 28, No. 4, pp. 228-234, 1983.
8. Blessing, J.E. and D.S. Ross, "Supercritical Solvents and the Dissolution of Coal and Lignite", ACS Symposium Series, (71), pp. 172-185, 1978.
9. Jezko, J., D. Gray, and J.R. Kershaw, "The Effect of Solvent Properties on the Supercritical Gas Extraction of Coal", Fuel Processing Technology, 5, pp. 229-239, 1982.
10. Paulaitis, M.E., M.A. McHugh, and C.P. Chai, Solid Solubilities in Supercritical Fluids at Elevated Pressures", Chemical Engineering at Supercritical Fluid Conditions, (Paulaitis, M.E., J.M.L. Penninger, R.D. Gray, P. Davidson, editors), Ann Arbor Science, Ann Arbor, MI, pp. 139-158, 1983.

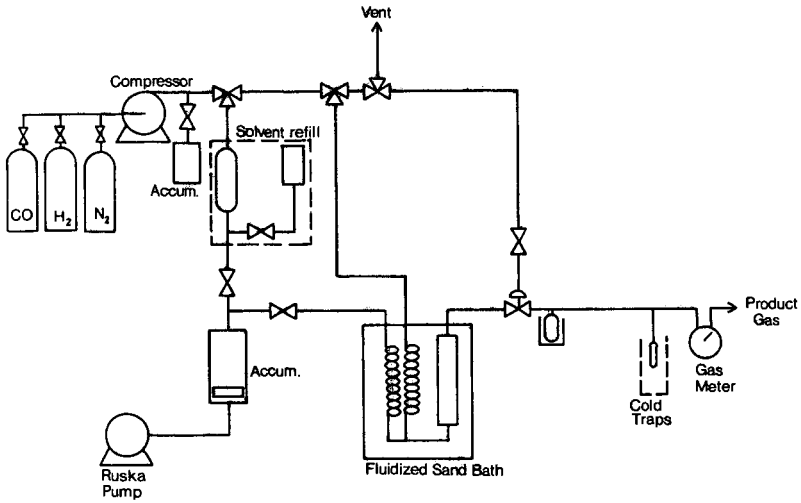

Figure 1. Equipment flowsheet for the semi-continuous supercritical solvent extraction system.

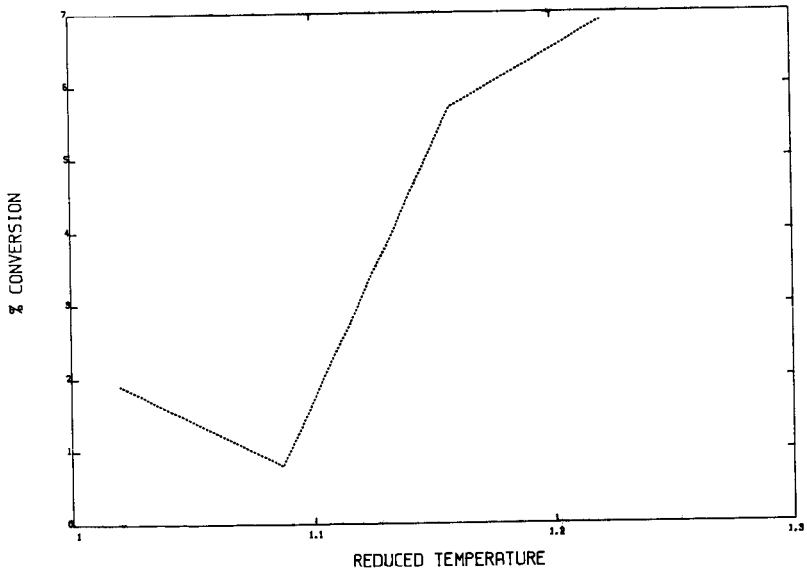

Figure 2. Temperature effects of supercritical pentane extraction on conversions.

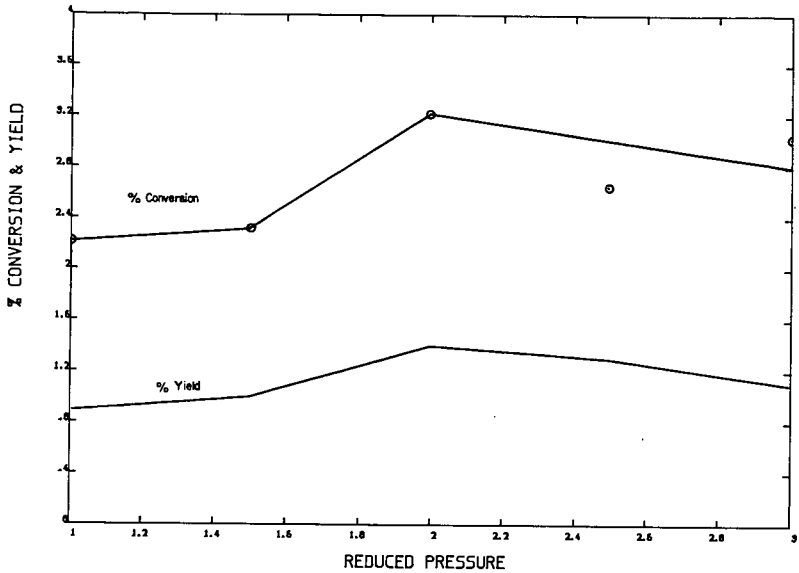

Figure 3. Pressure effects of supercritical hexane extractions on conversions and yields.

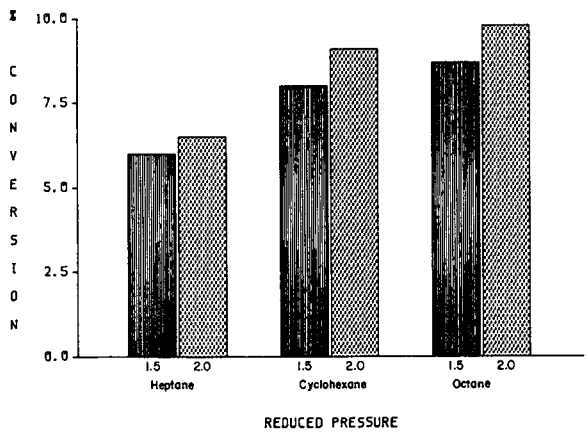

Figure 4. Pressure effects of heptane, cyclohexane and octane supercritical extractions on conversion.

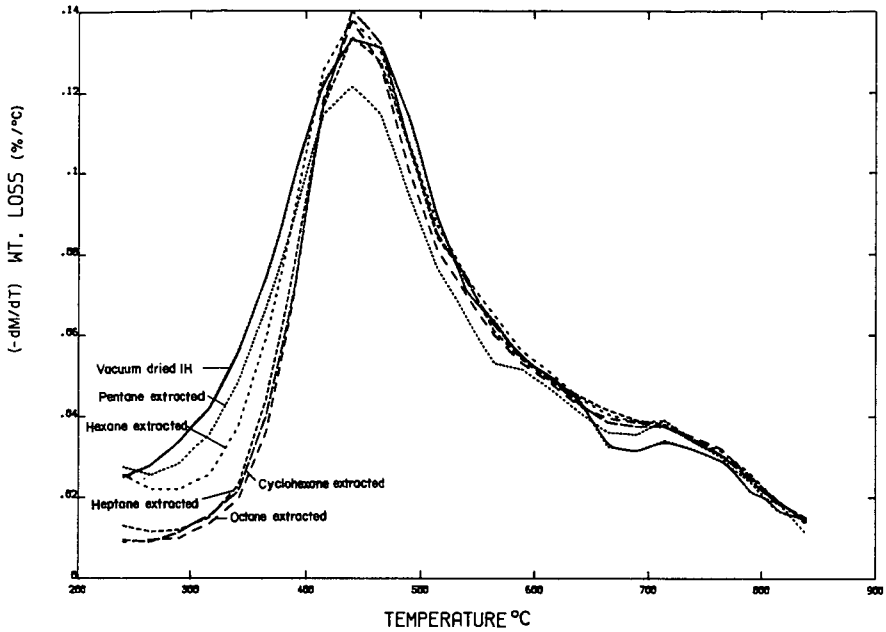

Figure 5. TGA rate of weight loss for supercritical solvent extracted residues.

FRACTIONAL DESTRACTION OF COAL-DERIVED RESIDUUM

Robert P. Warzinski

U.S. Department of Energy
Pittsburgh Energy Technology Center
P.O. Box 10940
Pittsburgh, Pennsylvania 15236

ABSTRACT

An apparatus has been developed to fractionate coal-derived residuum by exploiting the solvent power of fluids near their critical points. Termed Fractional Destraction, the method fractionates residuum according to the solubility of its constituent components in a supercritical fluid. The novel aspect of the approach is the incorporation of a system to promote reflux of less-soluble components onto a packed bed. Fractionation of residuum will facilitate the determination of previously unattainable information concerning the composition and process-related behavior of this complex material. This paper describes operation of the unit to fractionate a residuum sample produced at the Wilsonville Advanced Coal Liquefaction Test Facility.

INTRODUCTION

Describing the behavior of undefined mixtures, whether from natural or synthetic sources, often begins with the separation of these complex systems into effective pseudocomponents by distillation (1). Each pseudocomponent is then characterized as if it were a pure compound, and its characterization data are used in appropriate correlations. The presence of nonvolatile residuum poses a serious limitation to such methodology. For coal-derived liquids, heavy crude oils, tar sands, and shale oil, more than 50 percent of the fluid may not be distillable (1). Since this nonvolatile residue cannot be separated using conventional techniques, new methods of separation and characterization must be developed to provide the necessary information for design and operation of plants utilizing the fossil fuels mentioned above (2).

Apart from the need to fractionate residuum-containing fossil fuels for the measurement and prediction of thermophysical properties, other important problems could be resolved better through the study of residuum pseudocomponents. Two examples in the area of coal liquefaction are the role of residuum (a) in hydrogen utilization and hydrogen transfer and (b) in the manifestation of harmful biological effects.

Work at the Pittsburgh Energy Technology Center has been directed at the development of novel technology for the separation of fossil fuel residuum into effective pseudocomponents. In this respect, application of supercritical fluids in a manner similar to that reported by Zosel (3) is being developed. This approach is similar to conventional distillation in that an apparatus is used not only to extract the residuum but also to cause part of the residuum in the fluid phase to return as reflux onto a packed bed. This liquid reflux is caused by increasing the temperature of the supercritical fluid phase at constant pressure, thereby decreasing the density of the supercritical fluid and its carrying capacity for the residuum. Operation of a system in this region of retrograde condensation has recently been reported in the literature (4). Other recent investigations support the hypothesis that supercritical solubility is a density-driven phenomenon in the absence of strong associating forces in the solvent (5). The method is called either Supercritical Distillation or, as Zosel suggested, Fractional Destraction. This report describes the use of this technology to

fractionate a coal-derived residuum from the Wilsonville Advanced Coal Liquefaction Test Facility.

EXPERIMENTAL

The experimental unit, called the Fractional Destraction Unit (FDU), has been designed to contact a 3-4 kg charge of residuum with a continuous flow of supercritical fluid at conditions up to 673 K and 27.6 MPa. The heart of the FDU is the Fractional Destraction Vessel (FDV) shown in Figure 1. The FDV consists of a modified 3.8-L 316 stainless steel pressure vessel onto which is attached a 78-cm column fabricated of 316 stainless steel (6.03-cm o.d., 1.11-cm wall). The column contains a packed bed and a condenser section. In the experiments reported here, the 30-cm bed section was packed with 0.41-cm stainless steel Pro-Pak protruded metal distillation packing from Scientific Development Co., State College, Pa. This is the same packing used in a conventional Podbelniak distillation column. The condenser consists of a removable 38-cm finger made of 316 stainless steel (2.67-cm o.d., 0.78-cm wall) that is heated by an internal cartridge heater to promote reflux. A triple zone furnace is used to control the temperature in the extraction zone. Temperature control on the column is accomplished with independently controlled band heaters on the packed bed and condenser sections.

The desired charge of residuum is placed in the extraction section of the FDV, and the entire unit is purged with nitrogen. The FDU is then brought up to the operating temperature before beginning solvent flow. The destraction fluid is then pumped as a liquid through a preheater to raise its temperature above the critical point before it is introduced into the FDV through the sparging device at the bottom. The pressure is controlled by a high-temperature Badger-Meter control valve located near the outlet of the FDV. After traveling up the column, the fluid stream, which now contains destracted residuum, exits at the top of the FDV and is partially depressurized through the heated control valve into a separator constructed of a 2.25 L (approximately 10.2-cm o.d., 42.5-cm long) 304 stainless steel cylinder. The separator is operated slightly above the critical temperature of the solvent ($T_R \cong 1.02$) at a pressure of 0.8 MPa. Separation of the residuum from the supercritical fluid is accomplished by the reduction in pressure. The residuum is drained and collected from the bottom of the separator at periodic intervals, while the solvent is flashed to atmospheric pressure, condensed, and recovered as a liquid. The operation of the FDU will be reported in detail in a later publication.

Toluene (T_C = 591.7 K, P_C = 4.115 MPa) and cyclohexane (T_C = 553.4 K, P_C = 4.074 MPa) were used as the supercritical fluids in the work reported here. They were obtained in drum quantities at greater than 99 percent purity and used as received. Owing to inefficiency in the separator, some of the destracted residuum is collected with the solvent. This material is recovered in a rotary evaporator. The distilled solvent is then reused in the FDU. In the figures in this report that depict residuum overhead data, correction has been made for the residuum recovered in the spent solvent.

The residuum used in the work reported here was collected from the T102 vacuum distillation tower during Run 242 at the Wilsonville Advanced Coal Liquefaction Test Facility. This run was made using Illinois No. 6 coal from the Burning Star mine in what is termed a Short-Contact-Time Integrated Two-Stage Liquefaction (SCT-ITSL) mode (6). During the time this particular sample was collected, the T102 unit was operated at 594 K and 3.4 KPa. The residuum was crushed to minus 0.64 cm and mixed by riffling before use.

DISCUSSION

Operation of the FDU with coal-derived residuum was preceded by tests on pure compounds and distillable coal liquids using n-pentane as the supercritical fluid (7). The results of tests with the coal-derived distillate showed that the FDU was basically performing as expected. Liquid reflux was generated by means of the hot finger when the device was operated at a temperature slightly above the critical temperature of the transport fluid. When reflux was established, fractionation based upon volatility was observed. Poorer separation was achieved in the absence of reflux.

The first work on the T102 bottoms involved operation in the non-reflux mode to obtain base-line data on the transport of this residuum in various hydrocarbon solvents. Using n-pentane, cyclohexane, and toluene at a T_R of 1.02 and at a P_R of 2, the residuum brought overhead was 23, 54, and 67 percent of that charged, respectively. Based on this information, further studies were performed using cyclohexane as the supercritical fluid, since a large portion of the residuum could be destracted at a temperature similar to or less than that in the T102 separator.

A two-step destraction procedure was developed to maximize the amount of T102 residuum brought overhead. In the first step, toluene is used in a manner similar to conventional supercritical extraction to produce a nearly ash-free material for subsequent fractionation. This first step is called the non-reflux mode because the column of the FDV is maintained at the same temperature as the extraction section. In the second step, called the reflux mode, the column and finger are heated to a higher temperature than the extraction section, which causes the density of the fluid to decrease as it travels up the column and thus promotes reflux of the less-soluble components. These two steps are described below.

In the non-reflux mode, the FDU was used to process five 800-gram charges of the T102 bottoms. Repetitive operation of the unit was performed to produce sufficient quantities of the final fractions for subsequent characterization and experimentation. Figure 2 summarizes the operation of the FDU during these five destractions. Shown is the amount of residuum brought overhead as a function of the time on stream at a P_R of 2. As previously mentioned, the residuum overhead data include residuum recovered from both the separator and the spent solvent. The FDV was maintained at a T_R of 1.02, with overall variance in temperature for the five tests being $\pm$ 5 K. Temperature variance during any one test was $\pm$ 2 K. The differences observed, especially in the final amounts destracted, appear to be due to this small temperature variance betweeen runs. The higher yields were consistently obtained at temperatures nearer the critical point. This phenomenon appears to be particularly sensitive to the temperature of the extraction zone when the fluid is first introduced. The fact that the initial dissolution of the residuum in the fluid influences the overall yield suggests that components in the residuum may be acting as cosolvents.

Table 1 contains the elemental analysis of the T102 bottoms, the material brought overhead with toluene, the residue remaining after the toluene destraction, and the starting coal used at Wilsonville during Run 242. The toluene overhead represented 66.8 percent of the material charged to the FDU, and the residue accounted for 27.9 percent. Other material collected from the FDU includes 4.2 percent in the spent solvent and 2.7 percent recovered during cleaning of the FDV and separator with tetrahydrofuran. The total material balance is 101.6 percent. This number also includes any residual toluene or tetrahydrofuran in the various samples. The overhead collected from the five destractions was ground and combined before use in the reflux mode experiments.

As previously mentioned, cyclohexane was chosen for the fractionation solvent for the second step, since it could transport sufficient quantities of residuum at reasonable temperatures. In the reflux mode, the column of the FDV is operated at

a higher temperature than the extraction zone. As the carry-over of residuum decreases, the temperature of the column is reduced to cause the density in this region to increase and consequently more residuum is transported overhead. This is repeated until the column is at the same temperature as the extraction zone. In this work, four fractions were brought overhead by operating the column initially at 593 K and then decreasing the temperature to 578, 573, and 563 K as the residuum carry-over approached 1.0 gram per gram-mole of cyclohexane. This concentration value is calculated from the amount of residuum collected from the bottom of the separator after a 30-minute collection period and from the amount of cyclohexane pumped during that period. The column temperatures were selected both from density estimation and from actual experimentation. A more detailed discussion of the development of the operational parameters for the reflux mode will be presented in a future paper.

Figure 3 illustrates the difference between operation of the FDU in the non-reflux and the reflux modes with cyclohexane. This figure depicts the results in terms of the overhead concentration of residuum. The reflux mode data represent one of three replicate fractionations that were performed on the T102 toluene destraction overhead. Each point represents a 30-minute sample collection period. Owing to the limited quantity of toluene overhead produced, no non-reflux mode experiments were conducted using this material. From the earlier development work, however, several non-reflux mode experiments were performed on the T102 residuum sample from Run 242. The non-reflux mode data in Figure 3 were derived from one of these experiments and adjusted for comparability to the data from the reflux mode. The adjustment compensates for separator inefficiency and for residuum insoluble in supercritical toluene. All but the last three data points in the non-reflux mode data represent 15-minute sample periods. The only other difference between the two tests was the solvent delivery rate, which was 0.24 mole per minute for the non-reflux mode, and 0.43 mole per minute in the reflux mode.

As shown in Figure 3 the temperature of the column was initially 30 degrees higher than the pot, which produced the reduced carry-over rate by causing reflux to occur. An expanded view of the carry-over concentration is shown in Figure 4. This view shows more clearly how residuum carry-over is manipulated by changes in the column temperature. Figure 5 contains the same information for the three replicate cyclohexane fractionations performed on the toluene overhead. Conditions in all three experiments were similar; however, the small deviations due to inherent limitations of the process controllers produced some overlap between successive fractions. The amount of overlap is estimated at 2.6 percent between Fractions 1 and 2, 2.5 percent between Fractions 2 and 3, and 3.0 percent between Fractions 3 and 4. Also, 32 grams that should have been in the 573 K fraction were inadvertently collected in the 578 K fraction. The respective fractions and residues from the three fractional destractions were ground and combined before characterization.

Table 2 contains the analysis of the four overhead fractions and the residue. The overall material balance was 96.1 percent, with 57.2 percent of the charge being brought overhead (includes residuum recovered from spent solvent) and 31.7 percent remaining in the residue. An additional 7.2 percent was recovered upon cleaning the unit with tetrahydrofuran. The trends evident from the elemental analysis indicate that the components that have lower molecular weights, higher hydrogen-to-carbon ratios, and lower heteroatom contents are concentrated in the earlier fractions. Also note that the separator inefficiency is highest for the earlier fractions, indicating that the more volatile components are more readily carried through the separator with the solvent. The material carried through the separator with the solvent was not mixed with the respective fractions collected from the separator. Independent characterization of these samples will provide valuable insight into the operation of the separator.

The molecular weight data in Table 2 were determined by vapor pressure osmometry (VPO) and gel permeation chromatography (GPC). The molecular weight increases

regularly from Fraction 1 to the residue. In comparison, the VPO molecular weights for six fractions collected in the non-reflux mode cyclohexane destraction shown in Figure 3 range from 441 to 471, with no consistent trend. The polydispersity values ($\bar{M}_W/\bar{M}_N$) shown for the four fractions in Table 2 are less than those for the non-reflux mode fractions, which ranged from 1.47 for the first fraction to 1.88 for the sixth fraction. This number is a measure of the breadth of the molecular weight distribution and shows that operation in the reflux mode produces fractions with narrower molecular weight distributions than those prepared without reflux.

In Figure 6 the GPC traces for the four fractions and for the residue from each of the three cyclohexane fractional destractions are overlaid. The trend to higher molecular weight distributions as the fractionation proceeded is evident, as well as the reproducibility of the fractionation process. Additional characterization of similar samples produced in the FDU is the subject of another paper (9).

CONCLUSIONS

The main conclusion to be drawn from the experimental data presented here is that fractionation of residuum through the use of a supercritical fluid system incorporating internal reflux produced by retrograde condensation results in sharper fractions than those obtained by ordinary supercritical extraction. The capability of the FDU to process coal-derived residuum in the internal reflux mode has been demonstrated. The density-driven separation does appear to fractionate the residuum on the basis of volatility, with lower molecular weight species preceding larger ones.

Other methods of fractionation with supercritical fluids are conceivable. One such possiblility could involve manipulation of the pressure during the destraction or upon subsequent separation of the fluid and residuum. The relative merits of such possibilities remain to be explored. Successful development of such technology will result in the ability to fractionate and characterize material currently intractable by conventional methods.

DISCLAIMER

Reference in this report to any specific product, process, or service is to facilitate understanding and does not necessarily imply its endorsement or favoring by the United States Department of Energy.

REFERENCES

1. Brule, M.R., Kumar, K.H., and Watansiri, S. Oil & Gas Journal Feb. 11, 1985, 87.
2. Brule, M.R., Rhodes, D.E., and Starling, K.E. Fuel 1981, 60, 638.
3. Zosel, K. Angew. Chem., Int. Ed. 1978, 17(10), 702.
4. Brule, M.R., and Corbett, R.W. Hydrocarbon Processing June, 1984, 73.
5. Vasilakos, N.P., Dobbs, J.M., and Parisi, A.S. Ind. Eng. Chem., Process Des. Dev. 1985, 24(1), 121.
6. Technical Progress Report by Catalytic, Inc., DOE Report No. DOE/PC/50041-19, July, 1983.
7. Warzinski, R.P., and Ruether, J.A. Fuel 1984, 63, 1619.
8. Loffe, B.V., and Vitenberg, A.G. Head-Space Analysis and Related Methods in Gas Chromatography 1984, John Wiley & Sons, New York, 131.
9. Warzinski, R.P., Strycker, A.S., and Lett, R.G., Paper to be presented at the ACS meeting, Fuel Division Symposium, entitled Liquefaction and Characterization of Liquids, Chicago, 1985.

TABLE 1. Analysis of Feed Coal to Run 242, T102 Bottoms After Grinding and Mixing, and Materials Produced by Supercritical Extraction of T102 Bottoms With Toluene in the Non-Reflux Mode.

	ILLINOIS[a] NO. 6 COAL	RUN 242[b] T102 BOTTOMS	TOLUENE OVERHEAD	TOLUENE RESIDUE
C	68.4	79.1	87.4	60.3
H	4.4	5.9	6.7	3.5
O	11.9[c]	4.0[c]	4.0[d]	7.1[d]
N	1.4	1.3	1.3	1.4
S	3.2	1.0	0.7	0.9
Cl	0.1	---	---	---
ASH	10.6	8.7	<0.1	29.4
H/C	0.77	0.89	0.91	0.69
$\bar{M}_N$ (VPO, 353 K, PYRIDINE)	---	---	574	e

[a]Analysis from Wilsonville report, see reference 6. [b]Approximately 8 percent unconverted coal content. [c]Determination by difference. [d]Direct determination. [e]Insufficient solubility in pyridine.

TABLE 2. Characterization of Materials Produced From the Cyclohexane Fractional Destraction of the Toluene Overhead Sample in Table 1.

	FRACTION DESIGNATION[a]				
	593 K	578 K	573 K	563 K	RESIDUE
C	87.8	87.3	87.4	87.0	87.0
H	7.6	7.5	7.2	6.5	5.9
O[b]	3.5	3.7	3.3	3.7	4.9
N	0.9	0.9	1.2	1.4	1.8
S	0.5	0.6	0.6	0.7	0.9
ASH	---	---	---	---	<0.1
H/C	1.03	1.02	0.98	0.89	0.81
RESIDUAL CYCLOHEXANE, %[c]	0.5	0.5	0.8	0.6	0.5
RECOVERY, %[d]	23.9	13.0	13.8	6.4	31.7
SEPARATOR INEFFICIENCY, %[e]	27.5	17.8	8.4	11.1	---
MELTING RANGE, K	333-338	363-373	393-403	448-463	~573
$\bar{M}_N$, VPO[f]	393	479	578	645	1226
$\bar{M}_N$, GPC[g]	407	449	527	564	715
$\bar{M}_W$, GPC	504	601	851	1010	1996
$\bar{M}_W/\bar{M}_N$	1.24	1.34	1.62	1.79	2.79

[a]The temperature refers to the reflux and packed bed zone. The residue is the material remaining in the extraction zone. [b]Direct determination. [c]Determination by Headspace Chromatography, see reference 8. [d]Total recovery of material based upon weight of toluene overhead charged to the unit. Except for the residue this includes both residuum recovered from the fraction receiver and from the spent solvent. [e]Percent of total material overhead recovered in the spent solvent. [f]Determination in pyridine at 353 K. [g]Determination on PLgel 100Å column with THF eluent.

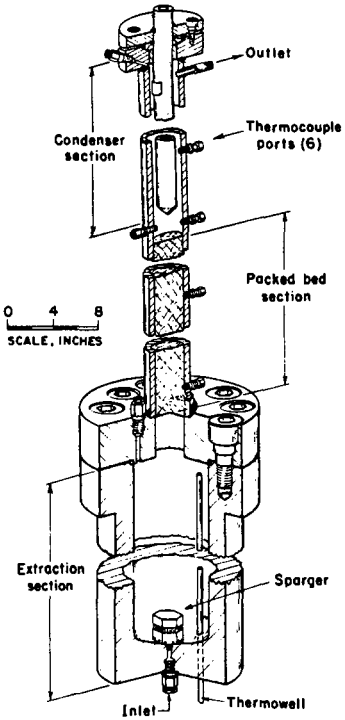

Figure 1. Sectional view of fractional destraction unit.

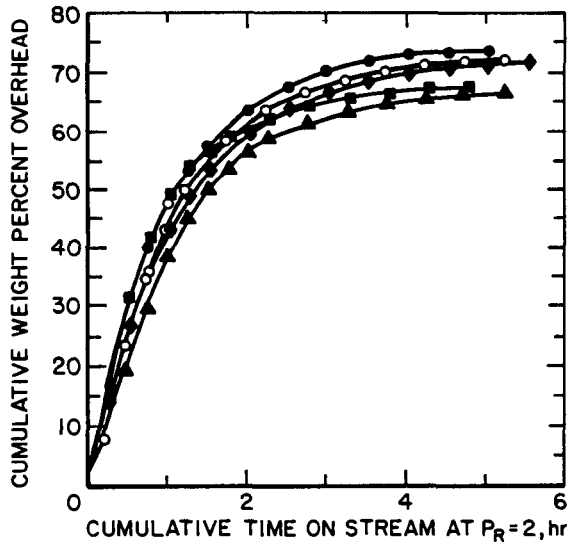

Figure 2. Comparison of five replicate destractions (non-reflux mode) of Wilsonville Run 242 T102 residuum using toluene.

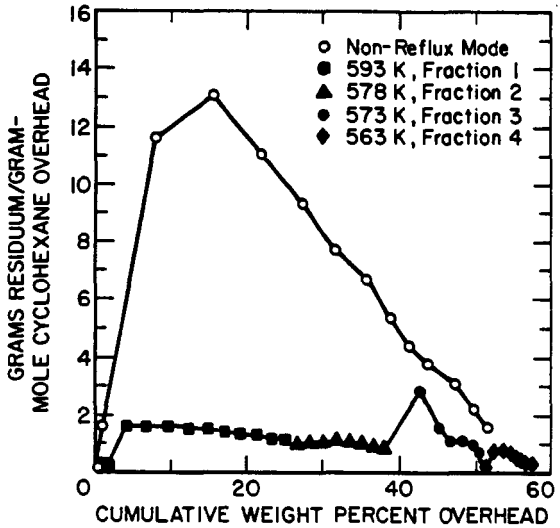

Figure 3. Comparison of non-reflux and reflux modes of operation using cyclohexane. Temperatures indicated are those of the column in the reflux mode. Pot temperture was 563 K in both modes.

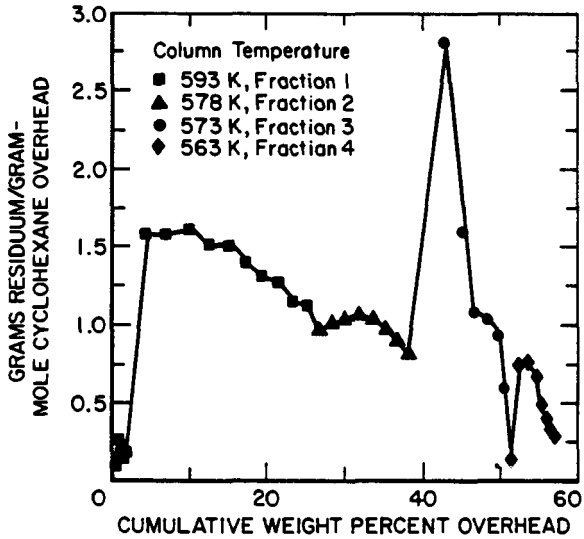

Figure 4. Fractional destraction of toluene overhead using cyclohexane.

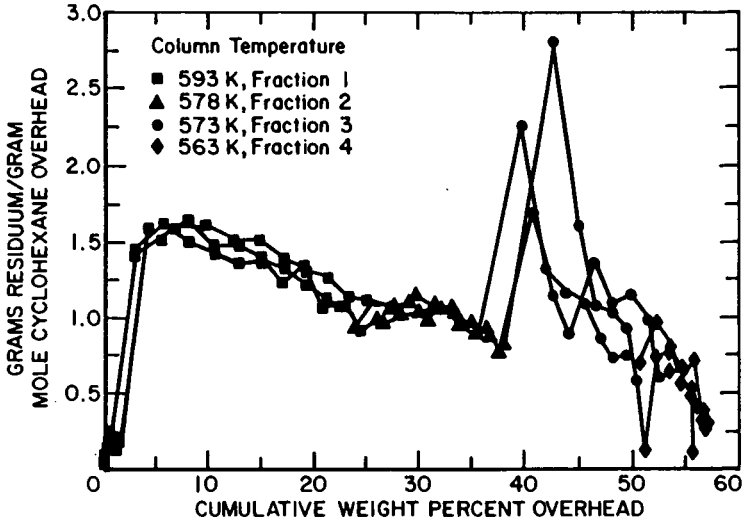

Figure 5. Comparison of three replicate fractional destractions (reflux mode) of toluene overhead using cyclohexane.

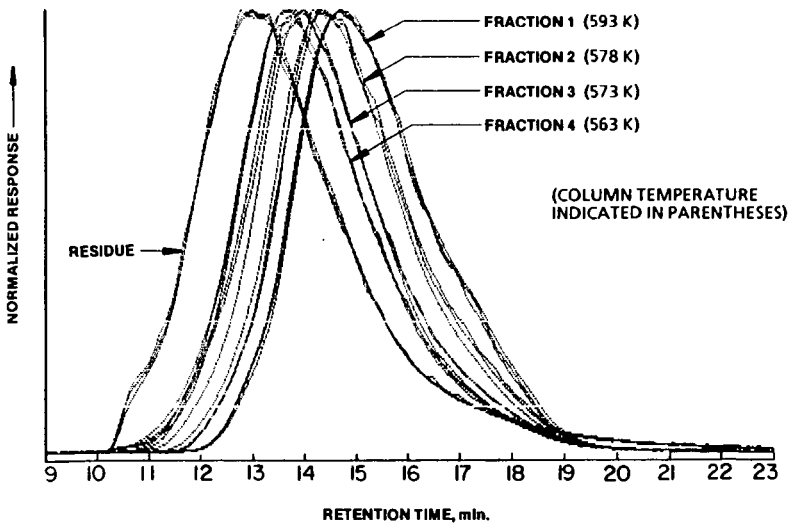

Figure 6. Comparison of the GPC results for the three replicate fractional destractions of toluene overhead using cyclohexane.

SEPARATION OF HEAVY OILS USING SUPERCRITICAL FLUIDS

Edward W. Funk

Signal Research Center, Inc.
50 UOP Plaza
Des Plaines, IL 60016

INTRODUCTION

This paper focuses on separations of heavy oils and materials from synthetic fuels which are of sufficiently high molecular weight that they cannot be separated by distillation. There is, however, the possibility of fractionating these heavy oils by solvent extraction. This is done commercially by use of low molecular weight paraffins to extract a high-quality deasphalted oil (DAO) from the low-quality asphaltene fraction.

Since 1960 consideration has been given to potential use of supercritical gases as solvents for the separation of heavy oils. A general review of this field is given by Funk and Irani (1). This paper addresses the important question of selectivity and in particular examines the selectivity differences which one can obtain with supercritical gases versus conventional liquid solvents.

New experimental data are presented for the supercritical extraction of heavy oils using carbon dioxide and CO_2/solvent mixtures and also phase-equilibrium data for extraction with liquid solvents to allow rational interpretation of differences in selectivity.

This paper also presents a non-analytical, statistically based technique for interpretation of experimental data which can complement the numerous analytical models (2,3,4) available for analysis of supercritical extraction data.

DEASPHALTING -- LIQUID SOLVENTS AND SUPERCRITICAL GASES

Table 1 presents a summary of the properties of typical heavy oils which are separated by solvent deasphalting using paraffinic solvents. This extraction aims to produce an oil which is free of the very high molecular weight asphaltenes, lower in metals content (Ni, V, Fe), and with minimal quantities of heteromolecules (N, S, O).

Figure 1 shows a schematic diagram of a typical solvent deasphalting process. It is basically a countercurrent liquid-liquid extraction. The paraffinic solvent is recovered by vaporization or advanced heat-integrated schemes which recover the solvent as a supercritical fluid (5).

Selectivity in this extraction shows very interesting behavior. It is completely predictable, and predictable over a wide variety of liquid solvents. Figure 2 shows this "universal" curve for vanadium with Athabasca bitumen as the heavy oil. One sees that the fraction of vanadium in the oil fraction is a simple function of the yield of extract. Other similar curves hold for other major properties (S, N, O) and this behavior is found with a variety of other heavy oils (Arabian Long, Tia Juana Resid, Jobo).

Figure 2 doesn't just include extraction with paraffins but a variety of other solvent types (ketones, alcohols, amines, aldehydes, etc.). It also holds for mixed solvent systems (6). These data were obtained at ambient temperature and with a solvent/oil ratio of 10.

A key question in the field of supercritical extraction is whether supercritical gases can show selectivity behavior which deviates from the type of universal curve shown in Figure 2.

A detailed study of the use of supercritical propane (1) showed that there are no differences in selectivity when the extraction is compared at the same yield (the correlating factor in Figure 2). The experimental data presented in Figure 3 illustrate this point. First, simple comparison of liquid propane at 60°C and 7.72 MPa with supercritical propane extraction at 115°C (T_c for propane = 97°C) does show very different behavior. The yield curves are shown in Figure 3 and the extraction at supercritical conditions gives metal concentrations 20-25% of those obtained with liquid propane. However, pressure is a key variable in the supercritical extraction and increasing the pressure increases the DAO solubility; at a pressure of 10.34 MPa, the yield curve matches the curve for extraction with liquid propane. For these conditions (115°C, 10.34 MPa), the extracted DAO has extremely similar properties (Ni, V, Fe, S, O, N) to the extraction at sub-critical conditions.

This study with propane suggests that for paraffins, there is no inherent selectivity to extracting with the solvent as a supercritical gas although it may appear so if results are not compared at equal yield of DAO.

EXTRACTION WITH SUPERCRITICAL CO_2 AND CO_2/SOLVENT MIXTURES

Figure 4 presents a schematic diagram of the extraction unit used for these experimental studies. The gas goes from the cylinder to a compressor which brings it to the system pressure. The extractor is stainless steel and the gas enters the bottom of the extractor and is dispersed by a stainless steel grid. The extractor contains the feedstock oil, which is distributed over glass beads to provide good contact between gaseous solvent and the oil. The extracted material and solvent leave the top of the extractor, the pressure is reduced and extracted material is collected for analysis. The basic design of the unit is similar to that proposed by Reid (7) and Eckert (8).

Figure 5 presents experimental data on the extraction of a heavy Boscan crude with supercritical CO_2 at 40°C (T_c for carbon dioxide = 31°C) from 5 to 25 MPa. Carbon dioxide was selected for this study because it is widely used in supercritical extraction and also because it may give selectivity (weakly acidic and with a quadruple moment). The results in Figure 5 show that CO_2 is a very poor solvent for heavy oils compared to propane. Even pressures of 24 MPa give only 2% oil in the extract phase (comparable results with propane (1) give 20-30% oil in the extract phase).

The selectivity results are very interesting and are summarized in Table 2. These data show a high selectivity for basic nitrogen compounds such as pyridines and quinolines. For example, the β(extract/feed) of the pyridines is 85. This is a very high selectivity and is very different for the low selectivities shown in the universal curve (Figure 2). It does seem expected that the acidic CO_2 would tend to preferentially extract the basic compounds. It is also interesting that some other classes of compounds (thiophenes and phenols) were also preferentially extracted. On the other hand, CO_2 shows no selectivity for saturated or aromatic hydrocarbons. The data in Table 2 were obtained by GC-MS analysis of the feed and extract samples.

Limited experimental studies examined the use of entrainers

(ethanol, heptane) to increase oil yield during the supercritical extraction with CO_2. For these studies the solvents were added to the oil feedstock in the extractor. For both ethanol and heptane, 10% solvent added to the oil gave a 3-5 times increase in yield, however the type of selectivity shown in Table 2 disappeared and for each compound type, selectivities were less than 5 (similar to Figure 2). Thus for CO_2 extraction, entrainers may be used to dramatically increase yield but at the price of selectivity.

DATA ANALYSIS FOR SUPERCRITICAL EXTRACTION OF HEAVY OILS

There are presently available very powerful statistical techniques to design experiments in such a way that the data can be reduced to provide quantitative measures of key variables and interactions between variables (9). These statistical techniques are used in a wide variety of other technologies which deal with complex systems but have not found application in the area of supercritical extraction. This type of statistical analysis could complement the more traditional analytical modeling of supercritical phenomena.

ACKNOWLEDGEMENTS

I would like to acknowledge the advice of C. A. Eckert (University of Illinois) on experimental design and P. Palmese of Signal Research Center, who was responsible for overall design and construction of the experimental unit.

REFERENCES

1. Funk, E.W.; Irani, C.A. Recent Developments in Separation Science **1977**, 3, 171.

2. Balder, J.R.; Prausnitz, J.M. Ind. Eng. Chem. Fund. **1966**, 5, 449.

3. Kurnik, R.T.; Reid, R.C. "Solubility of Solid Mixtures in Supercritical Fluids"; 2nd World Congress of Chemical Engineering, Montreal, Canada, 1981.

4. Paul, P.F.M.; Wise, H.S. in "The Principles of Gas Extraction"; Mills & Boon, Ltd., London, 1971.

5. Gearhar, J.A.; Garwin, L. Oil Gas Journal **1976**, 74(24), 63.

6. Funk, E.W. "Phase Equilibria in Mixtures of Athabasca Bitumen With Alcohol and Paraffin Solvents"; AIChE Meeting, Houston, Texas, 1981.

7. Kurnik, R.T.; Holla, S.J.; Reid, R.C. J. Chem. Eng. Data **1981**, 26, 47.

8. Johnston, K.P.; Eckert, C.A. AIChE Journal **1981**, 27, 773.

9. Box, G.E.P.; Hunter, W.G.; Hunter, J.S. "Statistics for Experimenters"; Wiley-Interscience, John Wiley and Sons, New York, 1978.

Table 1. Properties of Typical Heavy Oils

	Athabasca Bitumen	Cold Lake Crude	Jobo Crude
Composition, Wt.%			
Sulfur	4.9	4.29	3.87
Nitrogen	0.45	0.46	0.68
Oxygen	0.9	0.5	0.57
H/C Atomic Ratio	1.52	1.49	1.49
Metals, WPPM			
Nickel	80	61	90
Vanadium	250	180	455
Asphaltenes, Wt.%	14.2	17.9	17.7
1050°F+,Wt.%	47.3	45.2	49.4

Table 2. Analysis of Oil Extracted With Supercritical Carbon Dioxide at 40°C

Compound Type	Feed	100, atm	150, atm	200, atm
Pyridines	0.02	1.69	1.31	0.56
Quinolines	0.41	1.55	1.54	1.51
Thiophenes	0.001	0.39	0.48	0.66
Phenols	0.01	0.63	0.52	0.26
Saturated Hydrocarbons	42.94	41.35	41.21	40.37
Aromatic Hydrocarbons	23.34	26.25	26.85	27.15

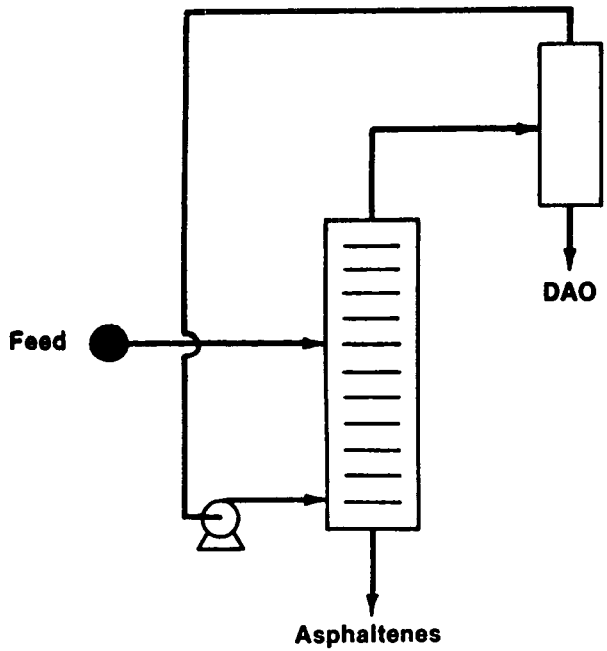

Figure 1. Schematic Diagram of a Solvent Deasphalting Process

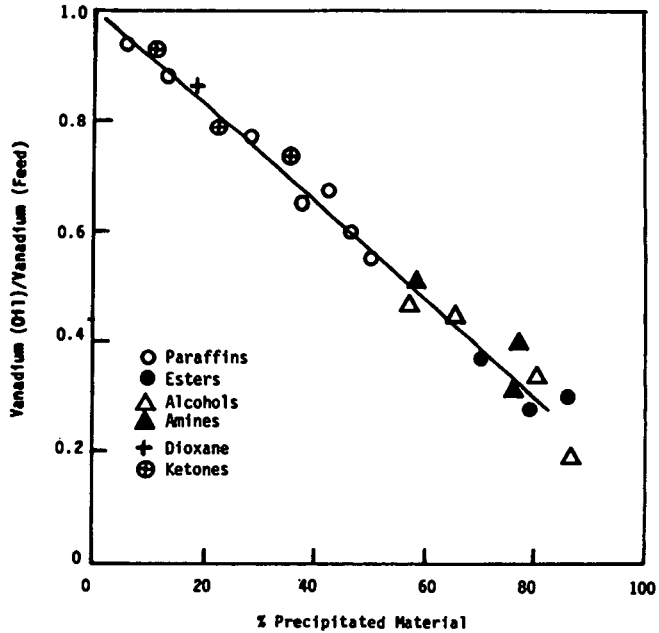

Figure 2. Correlation of Vanadium Content With Extraction Yield

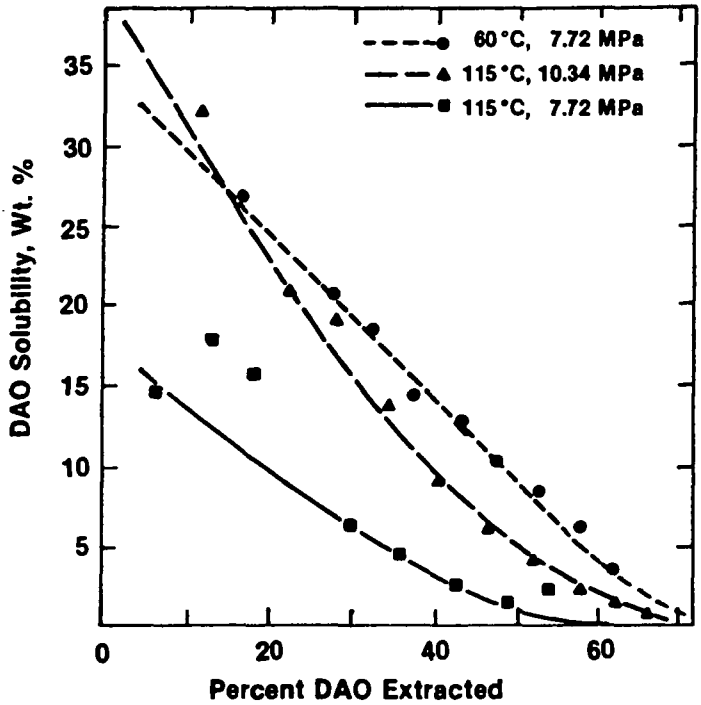

Figure 3. Extraction of Arabian Long Heavy Oil With Liquid and Supercritical Propane

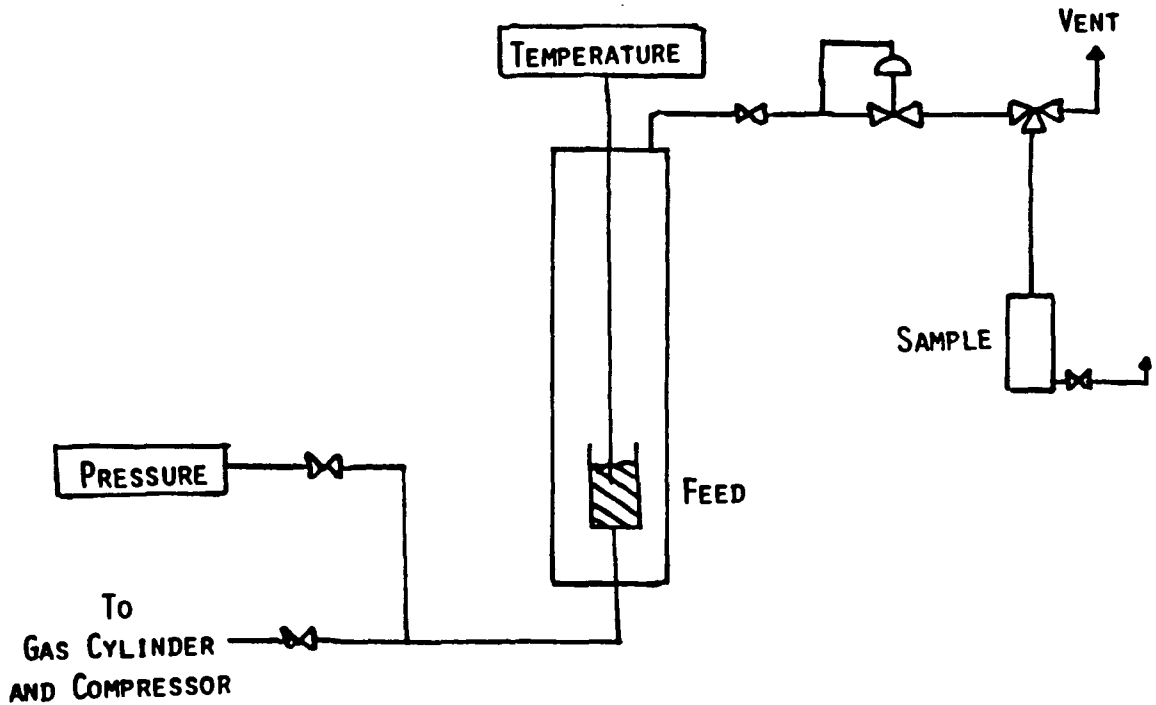

Figure 4. Experimental Unit for Supercritical Extraction With CO_2 and CO_2/Solvent Mixtures

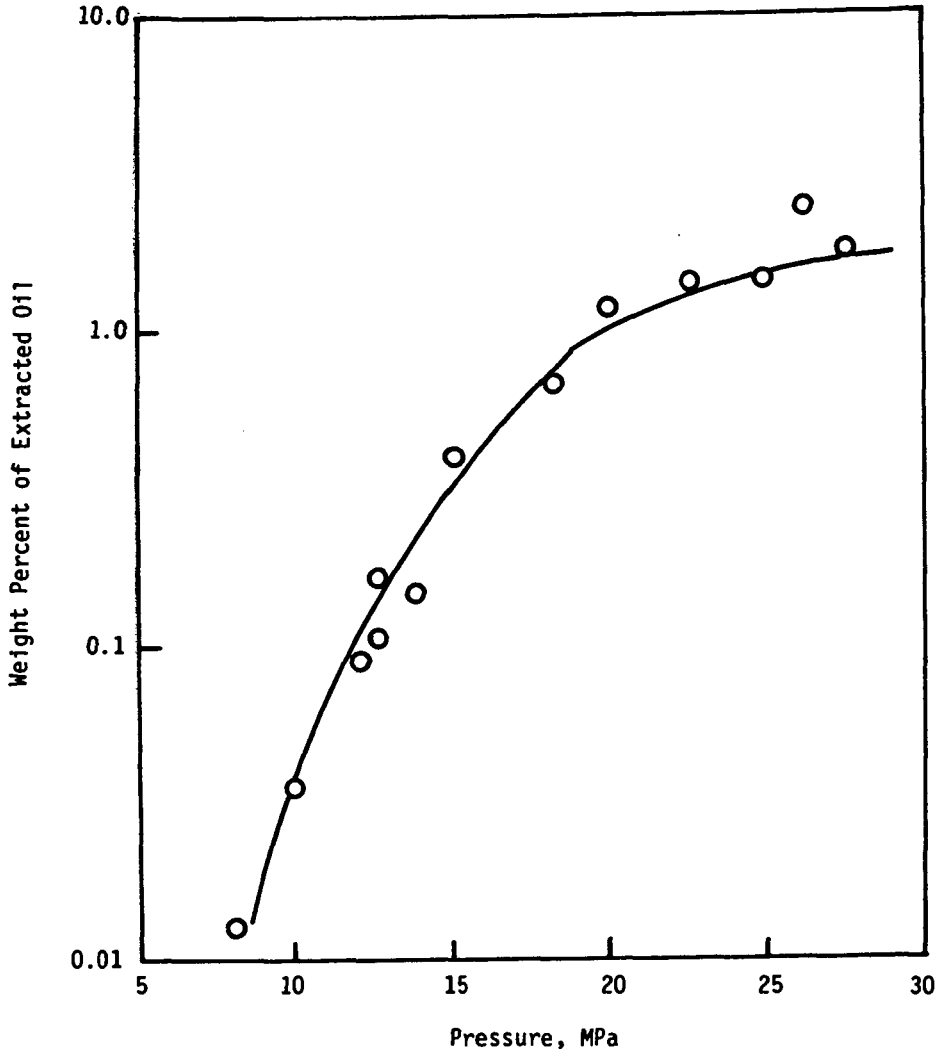

Figure 5. Supercritical Extraction of Boscan Crude With CO_2 at 40°C

IDENTIFICATION OF POLAR MATERIAL VIA SUPERCRITICAL FLUID CHROMATOGRAPHY-FOURIER TRANSFORM INFRARED SPECTROMETRY

J. W. Jordan, R. J. Skelton and L. T. Taylor
Department of Chemistry

Virginia Polytechnic Institute and State University
Blacksburg, VA 24061

INTRODUCTION

In the past several years, a great amount of interest has been generated in Supercritical Fluid Chromatography (SFC) among separation chemists. The physical properties of a supercritical fluid, namely low viscosity, high diffusivity, and good solubility, give the mobile phase characteristics intermediate to those demonstrated in high performance liquid chromatography (HPLC) and gas chromatography (GC).(1) This situation has allowed for the separation via SFC of additional compounds which are not separable by HPLC or GC. Thus, SFC offers much promise in the separation of certain complex mixtures.

Detectors that are used for HPLC and GC, ultraviolet absorption and flame ionization, are also successfully used for SFC detection. However, as in the past when dealing with more conventional chromatographic methods, the need for higher information detectors in SFC exists. The success of Fourier Transform Infrared spectrometric detection with GC(2) and HPLC(3) has led to the obvious extension of this technique to SFC. The most commonly used mobile phase in SFC is CO_2. It has relatively good solubility for many compounds, is nontoxic and inexpensive. Yet, both supercritical and subcritical CO_2 intensely absorb infrared radiation around 3600 cm^{-1} and 2400 cm^{-1}. Although these regions are opaque to any analyte which might absorb in the same region, excellent infrared spectra can be obtained in the regions of mobile phase IR transparency.

One problem in extending FTIR detection to SFC is insufficient detector sensitivity. An obvious means of improving the sensitivity in the IR is through an increase in the pathlength of the flow cell. This increase should enhance the signal-to-noise ratio of the spectra obtained. However, too great a pathlength may lead to a decrease in the width of the IR window region, a substantial drop in the IR thoughput, and/or a decrease in overall resolution and integrity of the on-line spectra. In this paper we present a comparison of two flow cells, differing in length and flow geometry and two mobile phases (CO_2, Freon 23) with UV-254 and FTIR on-line detection. In doing so, we show the eluting characteristics of basic nitrogen compounds on a packed bonded-phase silica column and compare retention characteristics of a polar model separation using two different supercritical mobile phases. A sensitivity study with a weak IR absorbing compound employing more nearly optimal chromatographic parameters than spectrometric parameters is discussed wherein the two cells are compared.

EXPERIMENTAL

A Hewlett-Packard (Avondale, PA) Model 1082B liquid chromatograph modified for supercritical fluid chromatography and equipped with a high-pressure Model 79875A variable wavelength UV detector was used in these investigations. Anaerobic grade CO_2 (Airco, Bluefield, WV) and Freon 23, CHF_3 (Dupont Co., Wilmington, DE) were used for the experiments. A Nicolet Model 6000C FTIR was used to collect time-resolved, 4 cm^{-1} resolution spectra. A Model 7010A narrow-band (5000 - 700 cm^{-1}) mercury-cadmium-telluride (MCT-A) detector was used in all experiments. Schematic diagrams of the flow cells employed in this study are shown in Figures 1 and 2. The internal surface of the 5 mm pathlength cell was a solid gold insert which had been polished longitudinally to give maximum infrared reflectivity. The internal cell dimensions were 1 mm ID x 5 mm pathlength. The cell windows were 13 mm diameter x

2 mm thick ZnSe disks, and were sealed in place with polyperfluorinated elastomer Kalrez O-rings (DuPont). The main body of the flow cell was 304 stainless steel with 0.010" ID x 1/16" OD SS inlet and outlet tubing silver-soldered in place. The second flow cell (Figure 2) was the high-pressure UV cell provided by Hewlett-Packard (1 mm ID x 10 mm). It was modified for FTIR by replacing the quartz windows used for UV detection with CaF_2 windows.

RESULTS AND DISCUSSIONS

Flow Cell Comparison

Each of the two cells has been evaluated in the same separation of a model mixture containing five basic nitrogen components. The optimum chromatographic conditions were determined via UV (254 nm) detection. The Gram-Schmidt reconstructed chromatogram arising from the optimized separation with the 5 mm cell showed only four components, while the UV trace (in-line after the FTIR) revealed all 5 components. Naturally with a UV detector, the elution order of a 5 component mixture could only be indentified by single injections of each material. Employing an FTIR, interpretation of individual file spectra afforded immediate identification. The GSR for the 10 mm cell showed the fifth component and over-all better signal-to-noise for the same amount injected than that for the shorter pathlength. In the same respect, the coadded file spectrum of each component was much sharper, and the match to the spectrum in the EPA vapor-phase library was improved.

A detection limit study was carried-out by varying the amount of N-methylaniline injected under the same chromatographic and spectrometric conditions used for the five component separation. The IR band of interest was 1608 cm^{-1}. For each cell 4 scans/file (scan time = 0.45 sec/scan) were collected, and coaddition over 1.4σ of the Gram Schmidt Reconstructed peak was performed. The injected minimum detectable quantity (IMDQ) of N-methylaniline using the 5 mm pathlength cell was found to be 156 ng ($3xN_{rms}$).

Mobile Phase Comparison

Certain fluorocarbons possess rather moderate critical pressures and temperatures. Their use as a relatively IR transparent mobile phase in HPLC is well documented.(4) Freon 23 (trifluoromethane) which has a critical temperature of 25.9°C and a critical pressure of 701.4 psi, has been suggested to exhibit similar eluting characteristics as CO_2.(5) The IR windows of CO_2 have been found to complement very well the IR windows of Freon 23. A seven component mixture of phenols, alcohols and esters has been separated on a bonded-phase phenyl derivatized silica packed column under identical chromatographic conditions using supercritical CO_2 and Freon 23. Initially the separations were optimized with UV-254 nm detection. Afterwards sequential FTIR-UV-254 nm detection was employed. Injection of approximately 30 µg/each component yielded the Gram Schmidt reconstructed chromatograms shown in Figure 3. The solvent in each case was carbon tetrachloride which consistently eluted first. With UV-254 detection this peak is a minor one, however, with FTIR detection the peak is quite intense which reflects the high infrared absorbance of CCl_4. The seven components eluted in the same order regardless of the mobile phase. The solvent strength of CO_2 appears to be slightly greater since each component has a lower retention time. This is notably the situation with benzyl benzoate, phenol, phenyl acetate and benzyl alcohol, the latter of which never eluted over a reasonable time period with Freon 23.

Examination of the on-line IR spectrum of several common components from the CO_2 and Freon 23 separations illustrates the complementary nature of IR information obtainable. For example while the O-H stretching mode of 2,6-di-tert-butyl phenol is obscured with CO_2, it is readily observable with Freon 23. Although the remainder of the Freon 23 spectra is useless, it is those regions that are

transparent with CO_2. Consequently continuous information is available through the mid-infrared region except for the triple-bonded absorbances around 2100 cm^{-1}. The on-the-fly spectra of o-nitrophenol in CO_2 and Freon 23 are shown in Figure 4. A relatively weak, broad bonded O-H stretching mode is observed in both mobile phases for o-nitrophenol. There is a loss in sensitivity at this frequency when using Freon 23 relative to CO_2 due to decreased IR throughput to the detector windows.

In summary, both lightpipe cells offer very good S/N spectra obtained on-line during a chromatographic run. Although CO_2 seems to be an adequate mobile phase for SFC-FTIR, the regions of total absorbance may hinder the identification of a component in a complex mixture. Freon 23, although relatively opaque in the IR, does have reasonable transparency from 4000 cm^{-1} to 2500 cm^{-1}. The seemingly similar elution charcteristics to CO_2 make method development with Freon 23 fairly easy and inexpensive. Thus CO_2 and Freon 23 make a good mobile phase pair for SFC-FTIR allowing for more complete identification of analyte species.

REFERENCES

1. D. R. Gere, Science, 222, 253 (1983).

2. J. R. Cooper, L. T. Taylor, Anal. Chem. 56, 1989 (1984).

3. R. S. Brown, L. T. Taylor, Anal. Chem. 55, 723 (1983).

4. C. C. Johnson, L. T. Taylor, Anal. Chem., 55, 436 (1983).

5. Private Communication, J. F. Deye, E.I. DuPont De Nemours & Co. Inc.

ACKNOWLEDGEMENTS

The authors wish to express their gratitude to Dennis R. Gere of Hewlett-Packard for enthusiastic discussions of SFC. The financial assistance of the Commonwealth of Virginia and Department of Energy Grant DE-FG22-84PC70799 is greatly appreciated.

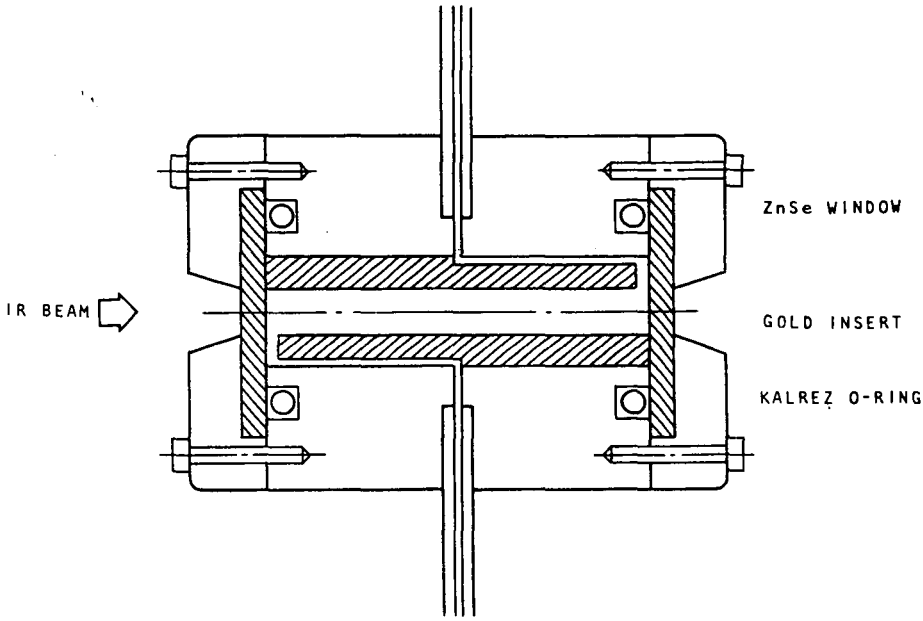

Figure 1

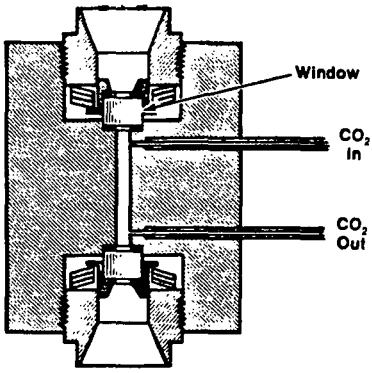

Figure 2

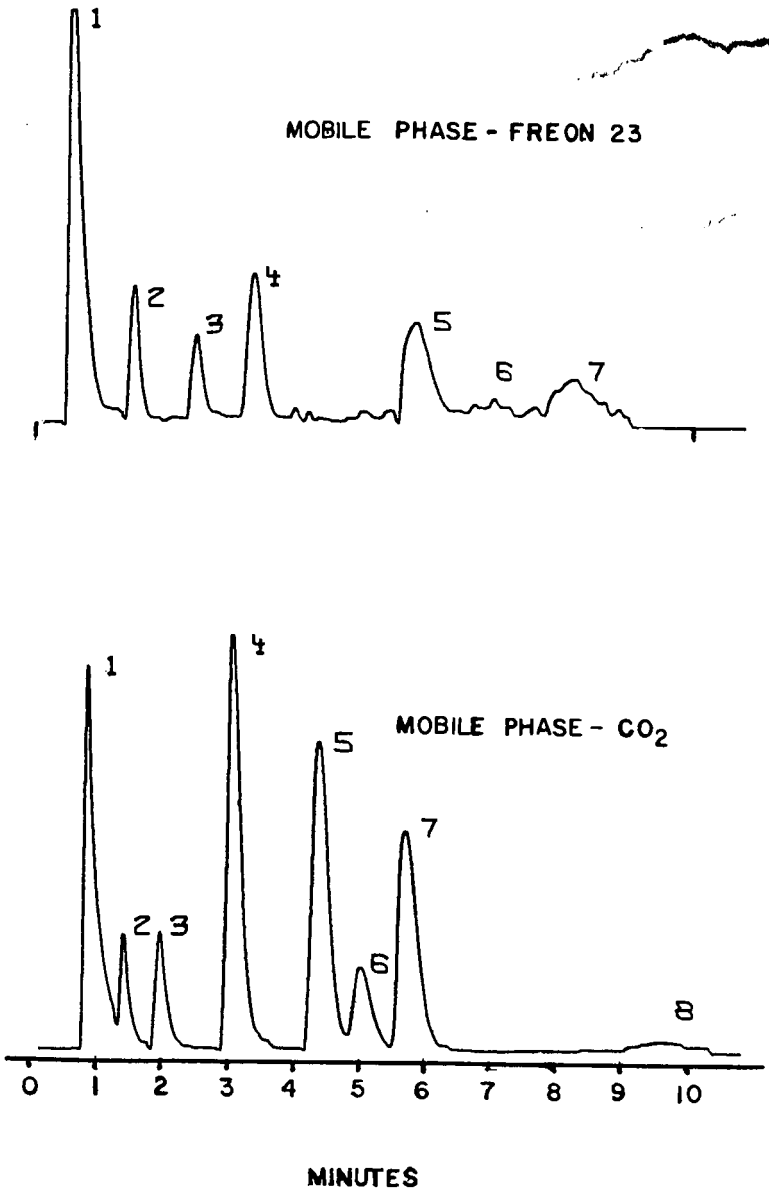
MOBILE PHASE - FREON 23
1
2
3
4
5
6
7
MOBILE PHASE - CO_2
1
2
3
4
5
6
7
8
0
1
2
3
4
5
6
7
8
9
10
MINUTES

Figure 3

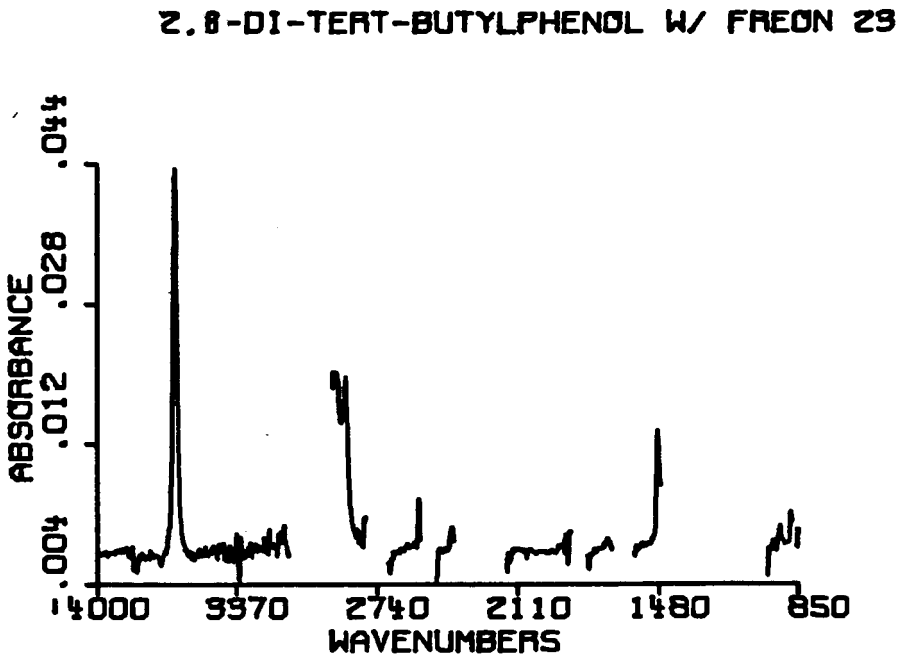
2,8-DI-TERT-BUTYLPHENOL W/ FREON 23
ABSORBANCE
.004
.012
.028
.044
14000
3370
2740
2110
1480
850
WAVENUMBERS

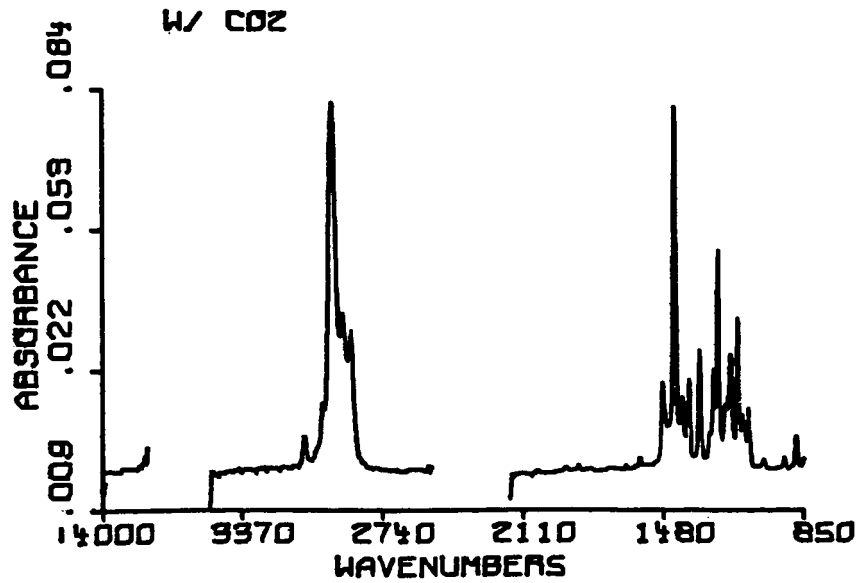
W/ CO2
ABSORBANCE
.009
.022
.059
.084
14000
3370
2740
2110
1480
850
WAVENUMBERS

Figure 4

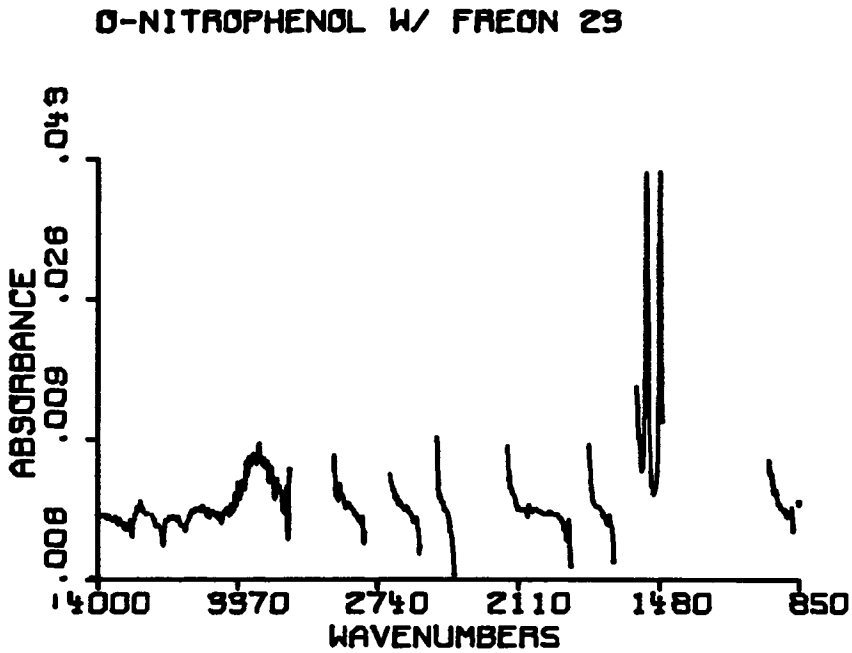
O-NITROPHENOL W/ FREON 23
ABSORBANCE
.008
.009
.026
.043
4000
3370
2740
2110
1480
850
WAVENUMBERS

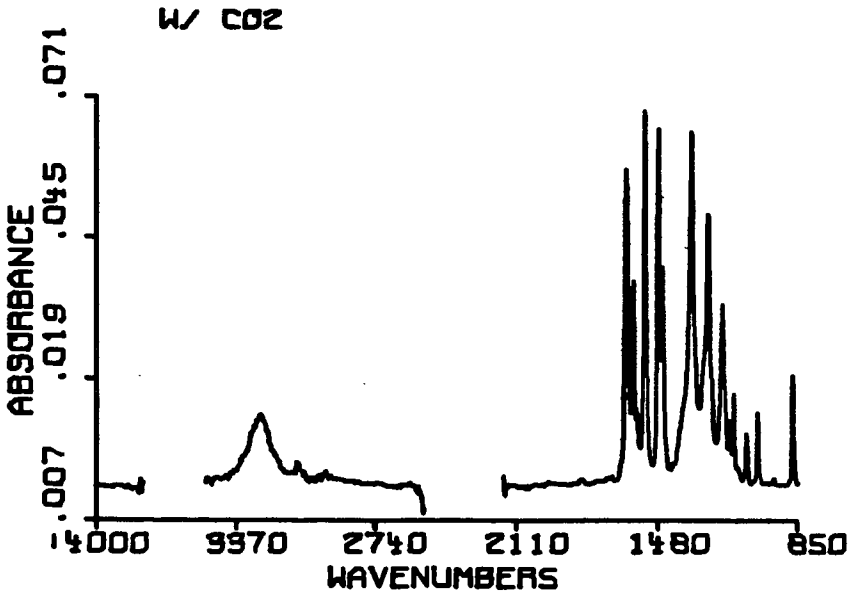
W/ CO2
ABSORBANCE
.007
.019
.045
.071
4000
3370
2740
2110
1480
850
WAVENUMBERS

Figure 5

HYDROTREATING IN SUPERCRITICAL MEDIA

by

J. Y. Low

PHILLIPS PETROLEUM COMPANY
PHILLIPS RESEARCH CENTER
BARTLESVILLE, OKLAHOMA 74004

INTRODUCTION

In recent years, supercritical fluid extraction has been a very popular technique for separations. The food and drug industries have used this technique for years on a commercial scale. Recently the energy industries have extended this application to coal liquefaction and oil shale extraction.[1-5] We, at Phillips, have also found that supercritical extraction of oil shale has improved the oil yield but produced a lower quality liquid product than those from insitu or above ground retorts. We were interested in developing an upgrading technology to upgrade the supercritically extracted (SCE) shale oil to synfuel or clean motor fuels. One of our upgrading projects was to investigate hydrotreating in the presence of the supercritical fluid which is used in the extraction step. If the hydrotreating step can be integrated with the supercritical extraction step, perhaps one can take advantage of, among other things, the pressure and heat available in the extraction step.

Our investigation consisted of essentially two parts. The first part involved the feasibility study of catalytic hydrotreating in the presence of supercritical fluid (in short, supercritical hydrotreating). If hydrotreating in the presence of supercritical media is possible, then we would like to extend the feasibility studies to other heavy feeds, such as topped crude and coal liquids. The second part of our investigation involved the parametric studies to see how reaction parameters effect supercritical hydrotreating.

CONCLUSIONS

From our extensive investigation of the potential of hydrotreating of shale oil under supercritical conditions of the solvent used and then the reaction parameter effects, we would like to make the following conclusions:

A high nitrogen, heavy oil such as shale oil can be hydrotreated under supercritical conditions to yield very low nitrogen fuels and syncrude in one step, depending on the conditions used;

The presence of a light solvent gives a better product and reduces coke formation on the catalyst surface;

- A non-aromatic solvent such as heptane improves nitrogen removal and reduces hydrogen consumption (from 2600 scf/bbl of shale oil to 1200 scf/bbl);

- With Arabian topped crude, the solvent loses its enhancement effect for nitrogen removal if the solvent is less than 50 weight percent of the feed;

- From parameter studies, for an extensive nitrogen removal, a relatively long residence time (30 minutes or longer) is required at 850°F and 1400 psig;

- And the sulfur was almost completely removed even with the mildest reaction conditions studied.

EXPERIMENTAL

A. Hydrotreating System

A bench scale hydrotreating unit was used for these experiments as shown in Figure 1. The reactor is a 316 stainless steel tube with an inner diameter of one inch and a length of 27.5 inches. The total volume is about 290 ml. The reactor was equipped with a thermocouple well (a 1/4" x 25" stainless steel tube) for temperature measurements. The reactor was first filled with about 90 ml of inert packing, 100 ml of catalyst and the rest with an inert packing again to serve as the preheating zone for the oil and hydrogen. The temperatures were measured by thermocouples placed in the middle of each of the inert beds and the catalyst bed.

B. Feeds

During the course of the investigation the following feeds were used: supercritical extracted coal liquid, supercritical extracted shale oil, Paraho shale oil, and Arabian topped crude (650°F+). Their properties are given in Table 1. To make the feed mixture, the heavy oil was usually dissolved in a solvent such as toluene or n-heptane.

C. Catalysts

The Ni-Mo catalyst was commercially available from Nalco.

D. Catalyst Presulfurization

The catalyst was generally heated to 300°F with nitrogen purging, and then the nitrogen atmosphere was replaced with a flow of 10% H_2S in hydrogen. At the same time, the temperature was slowly increased to 600°F and was kept at this temperature until the catalyst was completely sulfided. The reaction usually takes four hours at 600°F and 100 liter of 10% H_2S in H_2.

RESULTS AND DISCUSSION

In this report the results from the investigation of hydrotreatment of shale oil, Arabian topped crude, and lignite extract (under supercritical conditions) are being discussed. These experiments were carried out to investigate the potential of hydrotreatment in the presence of a light solvent under supercritical conditions for shale oil upgrading and the effect of reaction parameters in supercritical hydrotreating. In other words, these experiments are mainly exploratory in nature to find whether hydrotreatment under supercritical conditions has any advantage in the upgrading of high nitrogen heavy crudes, and if so, how do the major parameters affect the hydrotreatment under these conditions. The first few experiments were carried out with shale oil obtained from supercritical extraction. This shale oil is a very waxy grease and almost fits the definition of a solid. It has a very high nitrogen content (2.3%) and a sulfur content of 0.9%. The hydrogen content in the shale oil is relatively high with H/C atomic ratio of 1.48, equal to that of some petroleum crudes. Only a limited amount of this material was available, so only a few experiments were performed with this shale oil.

A. Supercritical Hydrotreatment of SCE Shale Oil

SCE shale oil was hydrotreated at high severity because of its high nitrogen content and extremely high viscosity (Table 1). The experimental results are shown in Table 2. Based on the shale oil fed, the product distribution is the following: 12% gases, 52% boiling less than 300°F (calculated by difference) and 36% in the heavy oil fraction (>300°F). The elemental analyses of the heavy oil fraction have indicated that better than 99% of the nitrogen was removed. The sulfur removal was equally high. The actual heteroatom removal may even be higher because part of the nitrogen and sulfur found in the heavy oil could be contributed by the presence of dissolved ammonia and hydrogen sulfide gases. No attempt was made to wash out the ammonium sulfide before the elemental analyses were carried out.

For runs 2, 3, 4, and 5 the feed entered the hydrotreater directly from the supercritical extraction unit. The extract contained about 4% shale oil in toluene. Runs 2 and 3 were carried out at 842°F, and Runs 4 and 5, at 750°F. At the lower reaction temperature (750°F), the yield of gases dropped to less than 2%, and the yield of heavy oil fraction increased by about 10%. The extent of nitrogen removal was reduced significantly at the lower temperature. However, the sulfur removal seemed to be unaffected by the lowering of reaction temperature from 842 to 750°F. Thus these experimental results suggest that the supercritically extracted shale oil can be processed to yield very low nitrogen and sulfur fuels or syncrudes.

B. Supercritical Hydrotreatment of Arabian Topped Crude

A series of experiments were performed with Arabian topped crude (650°F+) to investigate the hydrotreatment of high sulfur crudes in the presence of a light solvent under supercritical conditions. The experimental results obtained are summarized in Table 3. The overall results are comparable to those obtained from the supercritical hydrotreatment of SCE shale oil (Run 1). The sulfur removal is

very extensive (about 99% removal, reduced from 3.3% to 0.02%). The nitrogen content in the heavy oil fractions are relatively low, less than 60 ppm for runs with total liquid hourly space velocity (LHSV) of 0.5 (Runs 6 and 7) and about 770 ppm for Run 8 with an LHSV of 1.6. Thus, for extensive nitrogen removal, lower LHSV is needed.

Runs 9 and 10 were carried out to study the effect of an aliphatic solvent such as n-heptane in supercritical hydrotreating of topped crude. Comparing the results from Runs 6 and 7 in which toluene was used as the solvent, the nitrogen contents in heavy oil fractions are much lower for the heptane runs than the toluene ones. The sulfur contents are about the same. Thus, one can conclude that an aliphatic solvent is better solvent for hydrodenitrogenation than the aromatic solvent. The reason is that the aromatic solvent was competing for hydrogenation.

C. Supercritical Hydrotreatment of Lignite Extract

Lignite extract was hydrotreated in the presence of toluene under supercritical conditions (850°F, 1400 psig, 20 wt % lignite in toluene, a hydrogen GHSV of 300, and a LHSV of 1 or 1.6). The results are tabulated in Table 4. The elemental analyses of the heavy oil fraction have indicated the following changes (Runs 13 and 14): nitrogen, reduced from 0.91 to 0.14% and sulfur reduced from 4700 ppm to about 100 ppm.

Run 15 was carried out with a higher LHSV of 1.6, and the results are not too much different from Runs 13 and 14. The heteroatom removals are about the same. The heavy oil fraction, however, was increased to 43% from 30 and 36% (Runs 13 and 14). Thus the conclusion is that the lignite extract, a solid, can also be upgraded to yield a syncrude by the supercritical hydrotreatment process.

D. Supercritical Versus Conventional

A series of hydrotreating experiments were carried out under conventional conditions (without the use of a light solvent). The results are given in Table 5, along with some results obtained from a supercritical hydrotreatment experiment. The experiments performed were not under identical conditions, but they are close enough that the results obtained are valid enough for comparison.

The results from the supercritical hydrotreatment experiments are superior in almost every respect to conventional hydrotreatment experiments (without the use of solvent). Under similar conditions supercritical hydrotreating produced better products, for example: less gas yield (10% vs 25%), more of light oil fraction, <300°F, (55 vs 35%) and less coke formed on the catalyst surface (0.3 vs 3.8% based on the feed). For conventional hydrotreating we had encountered reactor plugging problems when the unit was running more than 196 hours. This problem was not found with supercritical hydrotreating.

E. Reaction Parameter Studies

Experiments were carried out with conventional shale oil (direct retorted Paraho shale oil) for the purpose of studying the

effects of reaction parameters in hydrotreating under supercritical conditions. In one group of experiments, the space velocity was varied (1.6, 3.2, and 5) while the other reaction parameters were kept constant. For temperature studies, the following reaction temperatures were investigated: 700, 750, 800, and 850°F. The pressure effect was examined at four levels -- 1000, 1400, 2000, and 2400 psig at 800°F. We have also studied the effect of solvent to feed ratio and solvent types (saturate vs aromatics).

The liquid hourly space velocities (LHSV, including the solvent) of 1.6, 3.2, and 5 were investigated at 850°F, 1400 psig, 20 wt % Paraho shale oil in toluene. The results are illustrated in Figure 2. With the LHSV of 1.6, the heavy oil fraction is only 34%, but when LHSV is increased to 3.2, the heavy oil fraction increased to 63% and did not change with further increase in LHSV. This seems to suggest that one third of the shale oil can undergo a molecular weight reduction more rapidly (a residence time of about 12 minutes) than the second third, which needs a residence time of up to an hour, while the last third survives longer than one hour.

For heteroatom removal, the results reveal that for a LHSV of 1.6 the nitrogen content in the heavy oil fraction, which is about 34 wt % of the total products, is 360 ppm (1.9% in the feed). Thus, the overall nitrogen removal is greater than 98%. For LHSV of 3.2 the nitrogen content in the heavy oil is increased to about 6,000 ppm. With a further increase in LHSV to 5, there seems to be very little change in the nitrogen removal. The sulfur removal is very rapid. Even with the LHSV of 5, there is only 53 ppm sulfur in the heavy oil.

Figure 3 illustrates the results from reaction temperature studies. The reaction temperatures used ranged from 700 to 850°F, with an increment of 50°F. The sulfur seems to be removed rather easily even at 700°F (from 7000 ppm in the feed to 200 ppm in the heavy oil fraction) or 97% removal. At higher temperatures the sulfur content in the heavy oil is much lower ($\sim$100 ppm). On the other hand, the nitrogen removal requires a much higher temperature. This, of course, is not surprising. For the purpose of obtaining relatively clean syncrude, we probably have to operate at high temperature (800°F) and low space velocity ($<$1.6).

The yield of heavy oil increases with a decrease of reaction temperature (Figure 3). For example, with the reaction temperature of 850°F, the heavy oil is only about 30% of the total products. While at the other extreme, that is, with the reaction temperature of only 700°F, the heavy oil fraction represents 90% of the whole products. Thus the higher temperature is necessary for the production of light products.

The effect of pressure on HDN and heavy oil yield in supercritical hydrotreating of shale oil is given in Figure 4. The experimental conditions used for these experiments are: 800°F, hydrogen GHSV of 600, LHSV of 1.6, 20 wt % shale oil in toluene, and reaction pressure of 1000-2400 psig. The nitrogen content in the heavy oil fractions have revealed that nitrogen removal increases with increasing reaction pressure. At the highest pressure studied (2400 psig), the nitrogen content in the heavy oil is only about 300 ppm. This is

about 98% nitrogen removal. The nitrogen removal decreased with the decrease in reaction pressure.

The effect of crude oil concentration in the feed was investigated with Arabian 650°F+ topped crude. Three concentrations (20, 50, and 80% of topped crude in toluene) were chosen, while the other experimental conditions were kept constant (see Figure 5 and Table 3). Both the nitrogen removal and heavy oil conversion are more extensive when the crude is hydrotreated at a more diluted level such as 20%. The heteroatom removal is reduced at higher crude concentrations and levels off at 50% or higher. The yield of the heavy oil fraction increases with increasing concentration of crude in the toluene.

The use of a non-aromatic solvent as the supercritical hydrotreating solvent was studied first with Arabian topped crude and then with Paraho shale oil in hope of reducing hydrogen consumption. The results are tabulated in Table 6. Run 16 used toluene as the solvent, and Runs 17 and 18 used n-heptane. The experimental results have shown that nitrogen removal is slightly higher with n-heptane than with toluene (a more significant difference was found with Arabian topped crude as the feed). The yield of heavy oil fraction is lower (37% for heptane and 47% for toluene) for the saturated solvent. This means hydrocracking was more extensive. The H/C atomic ratio of the heavy oil is also much higher for heptane than for toluene. Thus hydrogenation is deeper with heptane as the solvent. Hydrogen consumption is also significantly reduced, 1200 scf/bbl of shale oil for heptane versus 2600 scf/bbl for toluene. With everything considered, heptane is by far a better hydrotreating solvent than toluene.

To sum up, extensive research has been done to study the potential of supercritical hydrotreatment for the upgrading of shale oil and then the effects of major reaction parameters in supercritical hydrotreating. The experimental results have demonstrated that hydrotreatment in the presence of a light solvent and under supercritical conditions has some advantages over conventional hydrotreatment. Compared with conventional process, the supercritical hydrotreating process yields a better product (less gas, more distillates) and produces less coke on the catalyst. Supercritical hydrotreating appears to be a very versatile process which can be optimized for a variety of different products. This process can be applied equally well for upgrading other heavy oils, such as coal liquids and high sulfur petroleum topped crudes, to yield low nitrogen and sulfur syncrudes and transportation fuels.

Saturated solvent such as n-heptane has been examined as the process solvent. Saturated solvent seems to do better in terms of nitrogen removal and hydrogen consumption. With either solvent, sulfur removal was very extensive. From reaction parameter studies, a relatively high severity is required for extensive nitrogen removal.

TABLE I

FEED PROPERTIES

Feed	Elemental Analyses				
	C	H	N	S	H/C
SCE Shale Oil[1]	84.5	10.4	2.3	1.0	1.48
Paraho Shale Oil[2]	84.5	11.7	1.9	0.7	1.66
Arabian Topped Crude[3]	84.9	11.3	0.18	3.3	1.60
Lignite Extract[4]	82.0	9.3	0.91	0.47	1.36

1. The SCE shale oil is a waxy black semi-solid.
2. Paraho shale oil has about 70 Vol % of 650^+ F material.
3. Totally 650^+ F material.
4. Hard solid at room temperature.

TABLE II

SUPERCRITICAL HYDROTREATMENT OF SCE SHALE OIL*

Run No.[a]	Temp. °F	LHSV	Gases (C_1-C_4)Wt%	Heavy Oil (>300 F) Wt.%	N(ppm)	S(%)
1	842	0.5	12	36	52	0.03
2	842	1.6	--	46	150	0.03
3	842	1.6	--	44	150	0.02
4	750	1.6	<2	54	2300	0.08
5	750	1.6	<2	32[b]	2000	0.04

*A total operating pressure of 1400 psig and sulfided Ni-Mo/Al_2O_3 catalyst were used in these experiments. The shale oil has the following elemental analyses: C, 84.5; H, 10.4; N, 2.3; S, 1.0.

[a]The feed for Run 1 consisted of 20 wt % shale oil in 80 wt % toluene, but for Runs 2 to 5, the feed was only 4% shale oil in toluene.

[b]In this run this fraction was distilled up to 400°F instead of 300°F as usual.

TABLE III

SUPERCRITICAL HYDROTREATMENT OF ARABIAN TOPPED CRUDE (ATC)
(850°F, 1400 psig, H_2 GHSV 300, Nalco Ni-Mo Catalyst)

Run No.	Feed[A] Wt % ATC in Solvent	LHSV	Heavy Oil Wt %	Heavy Oil N (%)	Heavy Oil S (%)
6	20	0.5	34	0.006	0.02
7	20	0.5	34	0.004	0.02
8	20	1.6	59	0.068	0.04
9	20	0.5	33	2 ppm	0.02
10	20	0.5	36	3 ppm	0.03
11	50	1.6	64	0.094	0.17
12	80	1.6	72	0.094	0.13

[A]Solvent for Runs 9 and 10 was n-heptane; for others toluene was used.

TABLE IV

SUPERCRITICAL HYDROTREATMENT OF LIGNITE EXTRACT

Run No.	LHSV	Heavy Oil Fraction (>300°F) Wt %	N(ppm)	S(ppm)
13	1	30	1530	150
14	1	36	1400	90
15	1.6	43	1180	100
Lignite Extract Feed		100	9100	4700

Conditions: 850°F, 1400 psig, 300 H_2 GHSV, 20 wt % lignite extract in toluene, Nalco Ni-Mo catalyst.

TABLE V

COMPARISON OF CONVENTIONAL AND SUPERCRITICAL HYDROTREATING

(Conditions: 1400 psig, 850°F, H_2 GSHV=300, Nalco Ni-Mo)

FEED	NO SOLVENT SHALE OIL (NEAT)	WITH SOLVENT 20% SHALE OIL IN TOLUENE
LHSV	0.3	TOTAL = 1.6 SHALE OIL = 0.32
GAS YIELD (Wt %)	25	10
LIGHT (Wt %)	35	55
HEAVY OIL (Wt %)	35	35
COKE (Wt %)	3.8	0.3

TABLE VI

SUPERCRITICAL HYDROTREATMENT OF SHALE OIL IN TOLUENE OR n-HEPTANE

(850°F, 1400 psig, Nalco Ni-Mo catalyst, 1.6 LHSV, 300 H_2 GHSV)

Run No.	Feed	Heavy Oil (>300°F)				H_2 Consumption
		Wt %	N(ppm)	S(%)	H/C	Scf/Bbl
16	20% Shale Oil in Toluene	57	3149	<0.01	1.66	2600 ± 200
17	20% Shale Oil in Heptane	36	1595	<0.01	1.79	1200 ± 100
18	20% Shale Oil in Heptane	37	1890	<0.01	1.82	1200 ± 100

References

1. Blessing, J. E., and Ross, D. R., ACS Symposium Series 71, Organic Chemistry of Coal, p. 15, 1978.

2. Whitehead, J. C., "Development of a Process for the Supercritical Gas Extraction of Coal", paper presented at the 88th AIChE National Meeting, June 1980.

3. Squires, T. G.; Aida, Tetsuo; Chen, Yu-Ying; Smith, Barbara F., ACS Fuel Chemistry Preprints, Vol. 28 No. 4, p. 228, 1983.

4. Compton, L. E., ACS Fuel Chemistry Preprints, Vol. 28 No. 4, p. 205, 1983.

5. Williams, D. F., U. S. Patent 4,108,760, 1978.

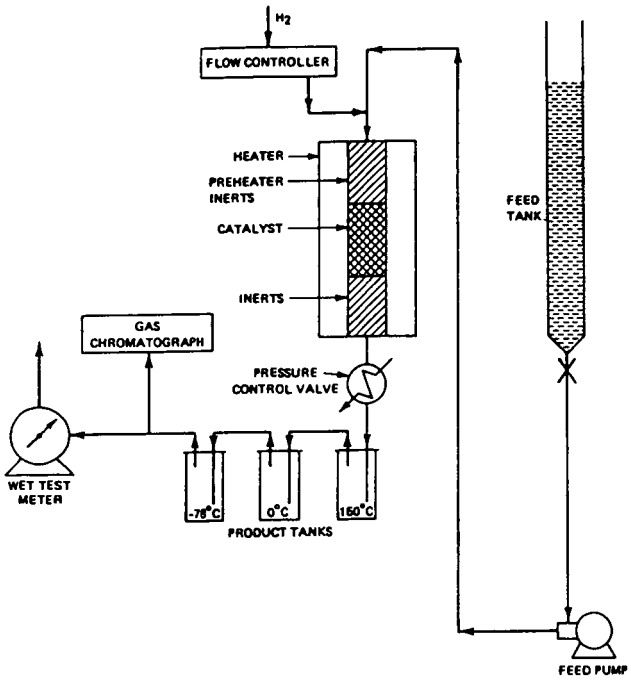

FIGURE 1
SUPERCRITIC AL HYDROTREATING SYSTEM

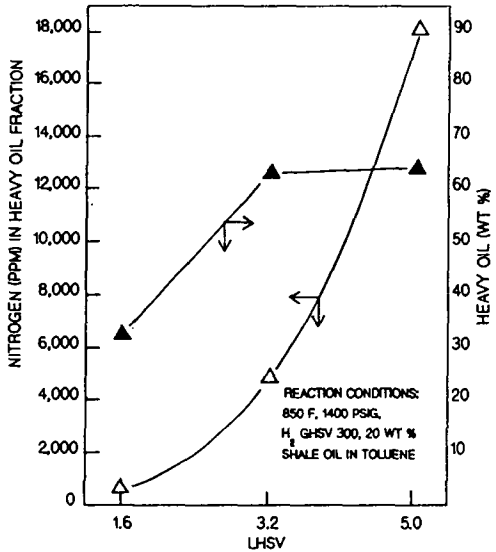

FIGURE 2
SPACE VELOCITY EFFECTS ON
SUPERCRITICAL HYDROTREATMENT OF SHALE OIL

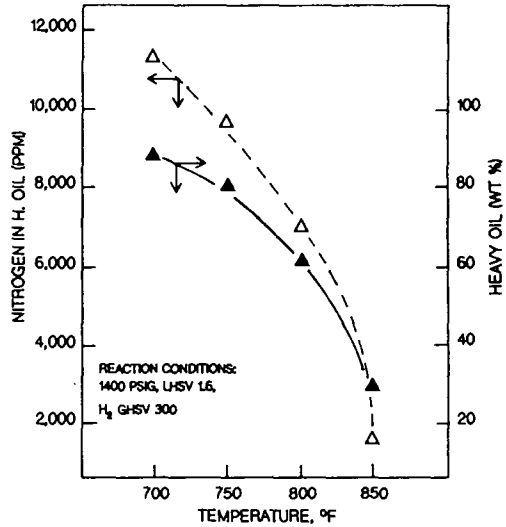

FIGURE 3
EFFECT OF TEMPERATURE ON
SUPERCRITICAL HYDROTREATMENT OF SHALE OIL

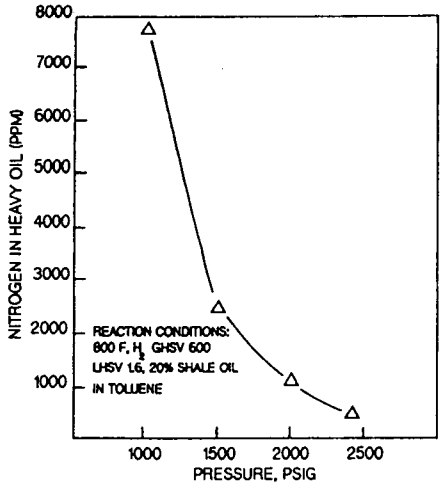

FIGURE 4
EFFECT OF PRESSURE ON
SUPERCRITICAL HYDROTREATMENT OF SHALE OIL

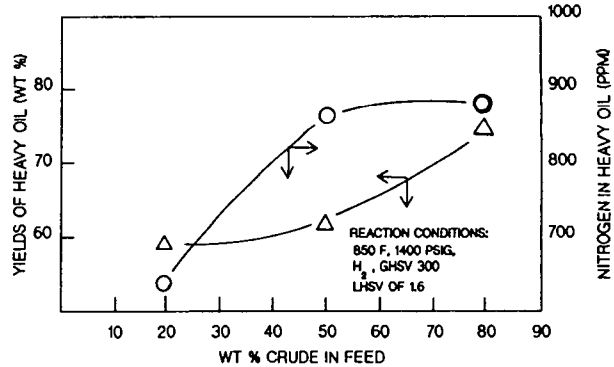

FIGURE 5
EFFECT OF OIL CONCENTRATION
IN SUPERCRITICAL HYDROTREATMENT OF
ARABIAN TOPPED CRUDE

EXTRACTION AND DESULFURIZATION OF CHEMICALLY DEGRADED COAL WITH SUPERCRITICAL FLUIDS

J. W. Chen, C. B. Muchmore, A. C. Kent and Y. C. Chang

Department of Mechanical Engineering and Energy Processes
Southern Illinois University
Carbondale, IL 62901

INTRODUCTION

In the systematic investigation of "Extraction and Desulfurization of Coal With Supercritical Fluids", it was found that sulfur materials in coal were removed selectively from the coal matrix, employing ethanol or methanol as the solvent. It is a well-known fact that a fluid under supercritical conditions exhibits an enchanced dissolution power which can increase the solubilities of various organic materials by several hundredfold. Depending upon the specific compounds and the solvent involved, solubility of each organic compound in a given solvent may vary at different temperatures and pressures. This differentiation of solubilities will allow selective removal of certain organic matter under supercritical conditions.

When ethanol or methanol is used as supercritical fluid, chemical reactions may be taking place between sulfur compounds in coal and the solvent in the presence of mineral matter. Pyritic sulfur may be reduced, and certain organic sulfur materials may be removed through chemical reactions. In this situation, the reactivity between organic sulfur in coal and supercritical alcohols is not only dependent on reaction conditions, but is also dependent on the distribution of sulfur functional groups in coal. That is to say, some forms of sulfur compounds are easier to be reacted and subsequently extracted than others. Therefore, the desulfurization potential with supercritical fluids may be affected by the coal types and sources, since various coals may have different sulfur functional groups in their respective structures.

In order to better understand the complex system of desulfurization of coal with supercritical alcohols, we have launched an extensive experimental study to achieve the following research objectives. They are: (1) to determine the selectivity of desulfurization of coal with supercritical alcohols, (2) to determine the effect of chemical pre-treatment on supercritical desulfurization potential, (3) to evaluate the gaseous and liquid product streams, and to characterize the desulfurized solid char for establishing the material and sulfur balances, and (4) to evaluate the physical and chemical transformation of coal during supercritical desulfurization.

LITERATURE REVIEW

Most work on supercritical extraction of coal reported in the literature has as a primary objective the maximum conversion of coal to liquid products. A 1975 article by Whitehead (9) [one of the first references to supercritical

coal extraction presented in the literature] presented data on supercritical extraction of coal by coal tar or petroleum naphtha fractions. Tugrul and Olcay (8) reported in 1978 extractions yields and analytical results obtained by supercritical-gas extraction of 250 mesh lignite. They found extraction nearly complete after 30 minutes; extract yields of about 24% were reported. Gas chromatography/mass spectrometry analyses of several extract fractions indicated dozens of paraffins, alkylated hydrocarbons, phenolic and oxygenated compounds; however, no sulfur compounds were reported. A kinetic study of a high-volatile bituminous coal utilizing supercritical toluene was reported by Slomka and Rutkowski (7). A close fit of their experimental data on time dependence of extraction yield was found when a second order equation was used. The use of supercritical toluene extraction of coal in pilot plant studies supported by the British Coal Board was reported by Maddocks (3). The major objective of that study was also maximum conversion of coal to liquid products; reduction of sulfur in the unconverted solid was not reported.

Some work has been reported utilizing alcohols for supercritical extraction of coal. Makabe, et al. (4) reported extraction of coal with ethanol-sodium hydroxide with the objective of maximizing extraction yield; no sulfur data was reported. Methanol reaction with a low volatile Bituminous West Virginia coal at higher temperatures (460 - 600°C) was reported by Garner, et al. (2). Promotion of coal gasification was the objective of that study; sulfur content of the resultant char was not reported.

In contrast to the previous reported work utilizing supercritical solvent extraction of coal, where major objectives have been the conversion of coal to liquid or gaseous products, the major objective of our research effort is to study supercritical desulfurization of coal with alcohols. Researchers at Purdue University have studied the supercritical desulfurization of coal by using water as a solvent. Although their data have indicated that pyritic sulfur was effectively removed, the rate of removal of organic sulfur was found to be very slow.

The recent article by Amestica and Wolf (1) does compare results obtained with toluene and ethanol when used for the supercritical extraction of an Illinois No. 6 coal. The experimental apparatus employed appears similar to ours, and temperatures utilized for the ethanol extraction (350 - 450°C) are also comparable. The ethanol/coal ratio of 7/1 is greater than the 1/1 ratio that we normally utilize in the batch reactor system, and the reaction time of 30 minutes is less than the 1 or 2 hour reaction periods we normally employ.

In the article, it is reported that the "sulfur rejected" varied from 1.7% to 11.7% in the three runs reported. However, a footnote given in the table states these values were calculated as a "sulfur percentage of daf coal feed in the gas phase". The text indicates determination of the sulfur was accomplished by scrubbing of the uncondensed gases in a zinc acetate solution. No data are givne in the article with respect ot the sulfur content of the solid product, nor is mention made of sulfur analyses on the liquid product. To interpret the sulfur captured from the uncondensed gases by a zinc acetate solution as being a measure of the "sulfur rejected" from the coal during the supercritical extraction implies that all the sulfur removed was accounted for; this seems to be a risky assumption, based on the lack of appropriate data presented in the article.

The possibility of condensation reaction of solvent degradation products occuring during supercritical extraction of coal with ethanol and alkali-ethanol is supported by data given by Makabe and Ouchi (5, 6). However, as the discussion that follows will indicate, we have not found evidence that this occurs under the conditions we employ for supercritical desulfurization of coal with alcohols.

EXPERIMENTAL

Most of the investigation was performed in two reactor systems. They are a semi-continuous reactor and a batch reactor. Their respective experimental set-ups are described in the following.

Semi-Continuous Reactor Studies

The flow chart for the semi-continuous Berty gradientless reactor, equipped with a Magnedrive impeller and internal recirculation systems, is given in Figure 1. The ground coal is held in a basket within the reactor, while solvent is pumped continuously through the system. After cooling following a run, the solid product is removed from the reactor basket for weighing and analysis. It is possible to maintain a constant pressure in this system, in contrast to the batch system where pressure increases during the course of a run, final pressure being determined by the temperature and charge size of the reactor.

Batch Reactor Studies

Figure 2 shows the flow diagram of the 300 cc batch reactor system that has been utilized in our experiments. The coal and solvent are charged to the reactor, heated to reaction temperature, and maintained at reaction temperature for a designated period; generally one or two hours. After reaction, the separation of products is accomplished by venting the fluid phase slowly from the reactor through the product collection system.

As shown in Figure 1, the product collection system consists of a water cooled condenser and primary liquid collection vessel, followed by a dry ice-acetone cooled cold trap coil and a series of three absorption vessels. The non-condensable gases are then discharged through a sample vessel and to a wet test meter for volume measurement. The first two absorbers contain ethyl alcohol; the third absorber contains an aqueous zinc acetate solution.

The total sulfur measurements were performed on a Fisher Total Sulfur Analyzer. The starting coal, the solid product resulting from the supercritical desulfurization reaction, the primary liquid product collected, additional liquid recovered from the cold trap (if any), and samples from each of the absorbers were analyzed.

RESULTS AND DISCUSSIONS

Semi-Continuous Reactor Results

Figures 3 and 4 show the data of sulfur removal and coal extraction for four different coal samples with supercritical ethanol at 325°C and 1750 psi. It can be seen that the percent of sulfur removed is much higher than the

percent coal extracted (weight loss of coal). A term called desulfurization selectivity ratio which is defined as the ratio of percent of sulfur removed to percent of coal extracted, varied between 2.96 to 4.38 under these conditions as shown in Table 1.

TABLE 1

SUPERCRITICAL ETHANOL DESULFURIZATION OF COAL

AT 325°C; 1750 psi

Desulfurization Selectivity Ratio

Extraction Time, Hours	Desulfurization Selectivity Ratio			
	Coal "A"	Coal "B"	Coal "C"	Coal "D"
0	2.81	3.40	4.09	12.0
1	3.29	2.98	3.40	7.36
2	3.81	2.88	3.10	5.49
4	3.39	2.96	3.49	4.38

A series of experiments were performed to evaluate whether or not a pre-treatment of coal with KOH solution will enhance the desulfurization efficiency. In the pre-treatment, 60 grams of coal particles were soaked in 180 grams of KOH in ethanol solution with a given concentration for five minutes, filtered, washed twice with 180 grams of ethanol and filtered again before its use. The results are presented in the following.

TABLE 2

THE EFFECT OF KOH PRE-TREATMENT

(275°C and 1800 psia)

	% of Sulfur Concentration Removed
No pretreatment	21.3
2% KOH	28.5
3% KOH	28.9
4% KOH	29.8
5% KOH	34.0

The data indicates that an improvement of desulfurization potential was realized with KOH pre-treatment.

In order to evaluate the degree of potassium ion incorporation into the coal sturcture during the pre-treatment, several experiments were conducted at 325°C and 1750 psia employing ethanol or methanol as solvent. In these experi-

ments, the soaking and washing solutions were collected, and were analyzed for potassium ion on a Perkin Elmer Atomic Adsorption Spectrometer. It can be seen in Table 3 that most of the potassium ion was found in the solution.

TABLE 3

POTASSIUM ION BALANCE

	Ethanol		Methanol	
KOH Pre-treatment	% S Removed	% K^+ Recovered	% S Removed	% K^+ Recovered
None	27.0	--	30.2	--
5% KOH, soaking, rinsing	32.16*	102	39.1	99

*Average of three experiments

Batch Reactor Results

Table 4 shows a summary of experimental data (elemental analysis) of the desulfurized coal samples for the batch reactor system under different operating conditions. The original coal has a total sulfur content of 4.27 percent, and 72.6 percent of the total sulfur is organic sulfur. Since the concentration of total sulfur in the solid product from the supercritical desulfurization is reduced nearly 50 percent or more for five out of nine cases, and the sulfur removals resulting from the supercritical desulfurization exceeds the pyritic sulfur content of the original coal, it is concluded that organic sulfur in this coal is being removed. The possibility that the selective removal of sulfur may be due to condensation reactions of the solvent, with subsequent incorporation in the coal matrix, may also be rejected by consideration of H/C ratio data in Table 4. If significant incorporation of $-CH_2-$ groups from the solvent were to occur, an increase in H/C ratio would be expected. As the data indicated, the H/C ratio actually decreases during the supercritical desulfurization.

Table 5 summarizes the sulfur balance information obtained on a series of batch reactor runs under a variety of conditions. Note that the sulfur determined in the liquid products and in the absorber total from 67.1% to 94.7% of the total sulfur removed from the coal during the supercritical desulfurization. When the sulfur content of the solid product is included, the overall sulfur balance ranges from 82.4% to 97.1% of the sulfur contained in the original coal.

The total materials balance of these experiments ranges between 92.4% to 100.6%.

CONCLUSIONS

It is concluded from experimental information obtained that sulfur, including organic sulfur in coal, is selectively recovered from coal matrix with supercritical alcohol. The effect of chemical pre-treatment with KOH soaking

and/or acid leaching is found to be significant. The pre-treatment step may help the depolymerization of coal structure which makes it easier for supercritical alcohol to reach the sites of sulfur compounds for extraction and conversion.

ACKNOWLEDGEMENTS

The authors wish to express their appreciation for the support received from the Illinois Coal Research Board and the U.S. Department of Energy.

TABLE 4

ELEMENTAL ANALYSES OF SOLID PRODUCT FOR BATCH REACTOR SYSTEM

Solvent and Conditions[a]	C	H	N	S	H/C Ratio	% S Removed (Conc. Based)
Original raw coal	66.04	4.85	1.17	4.27	0.881	
MeOH	72.63	4.04	1.31	2.99	0.667	30.0
MeOH + 5% KOH	70.37	3.72	1.25	1.96	0.634	54.1
HCl refluxed; MeOH	77.17	3.05	1.32	2.16	0.474	49.4
MeOH + 5% KOH + CO 400 psi	69.60	4.15	1.18	2.58	0.716	39.6
Acid leached[b]; MeOH + 5% KOH	71.91	3.96	1.23	1.53	0.661	64.2
Acid leached[c]; MeOH + 5% KOH	73.32	3.07	1.30	1.88	0.502	56.0
MeOH + 5% KOH; Two stage	69.16	3.18	1.12	1.47	0.552	65.6
EtOH	75.82	3.95	1.39	2.75	0.625	35.6
EtOH + 5% KOH	73.90	3.32	1.24	2.60	0.539	39.1

[a]All run at 350°C

[b]Soaked for 48 hours

[c]Soaked for 4 hours

TABLE 5

SULFUR BALANCE

Solvent	Rxn T C	% Reductn of Sulfur in Coal	% of Sulfur Removed as Found in			Overall Sulfur Balance
			Liq.	Absorber	Total	
EtOH	350	31.4	43.3	43.7	87.0	93.9
EtOH	375	36.8	13.2	81.5	94.7	97.1
MeOH + 5% KOH	350	53.9	12.4	64.3	76.7	85.7
MeOH + 5% KOH	350	56.1	7.2	74.0	81.2	88.2
MeOH	350	48.8	6.9	60.2	67.1	82.4

REFERENCES

1. Amestica, L. A. and Wolf, E. E., Supercritical Toluene and Ethanol Extraction of an Illinois No. 6 Coal, Fuel, 1984, 63, 227.

2. Garner, D.N., W.J. Huffman, and H.W. Parker, Coal Processing Using Methanol as a Reactant. Presented at 79th National Meeting, AIChE, 8th Petrochemical and Refining Exposition, Houston, TX (1975).

3. Maddocks, R.R., J. Gibson and D.F. Williams. Supercritical Extraction of Coal. Chem. Engr. Progress. (June 1979).

4. Makabe, M., Y. Hirano and K. Ouchi. Extraction Increase of Coals Treated with Alcohol-Sodium Hydroxide at Elevated Temperatures. Fuel, vol. 57 (May 1978).

5. Makabe, M. and Ouchi, K., Reaction Mechanism of Alkali-Alcohol Treatment of Coal; Fuel Processing Technology, 1979, 2, 131.

6. Makabe, M. and Ouchi, K., Solubility Increase of Coals by Treatment with Ethanol; Fuel Processing Technology, 1981, 5, 129.

7. Slomka, B. and A. Rutkowski. A Kinetic Study of the Supercritical Toluene Extraction of Coal at 9.8 MPa. Fuel Processing Technology, vol. 5 (1982).

8. Tugrul, T. and A. Olcay. Supercritical-Gas Extraction of Two Lignites. Fuel, vol. 57 (July 1978).

9. Whitehead, J.L. and D.F. Williams. Solvent Extraction of Coal by Supercritical Gases. Journal of the Institute of Fuel, (December 1975).

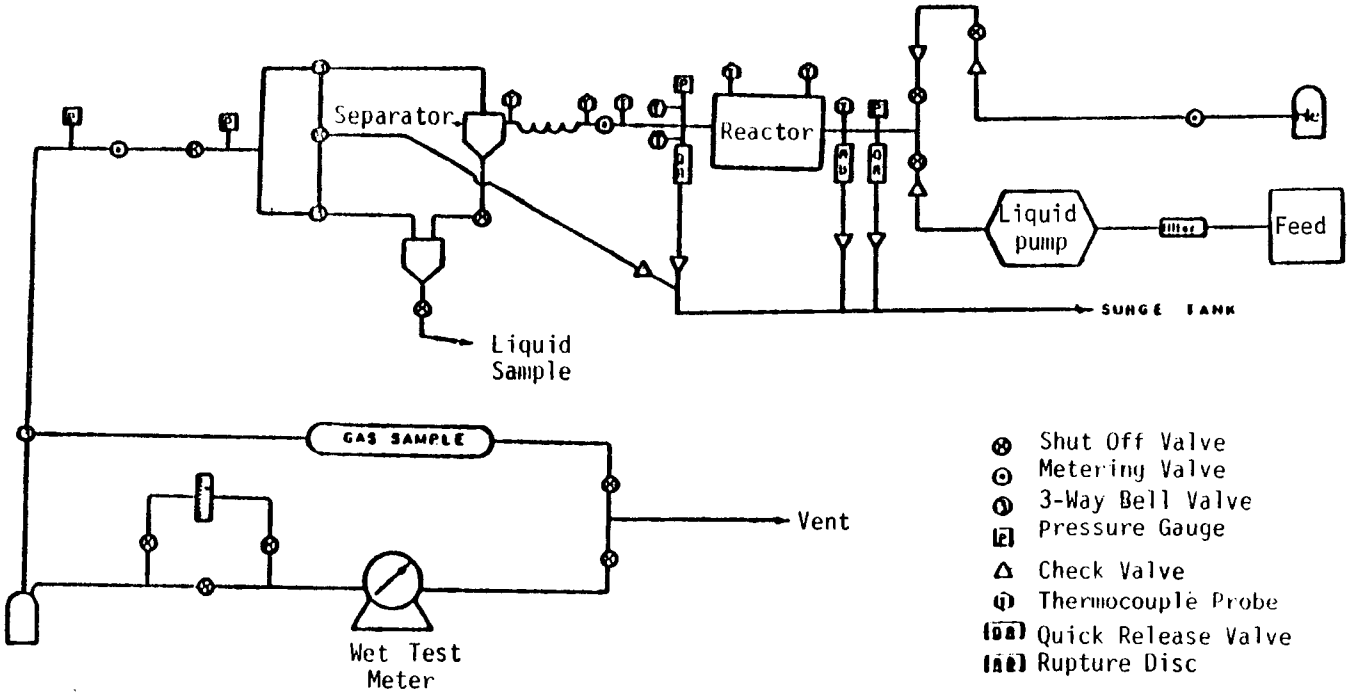

Figure 1. Flow Diagram of the Experimental Setup
Semi-Continuous Reactor

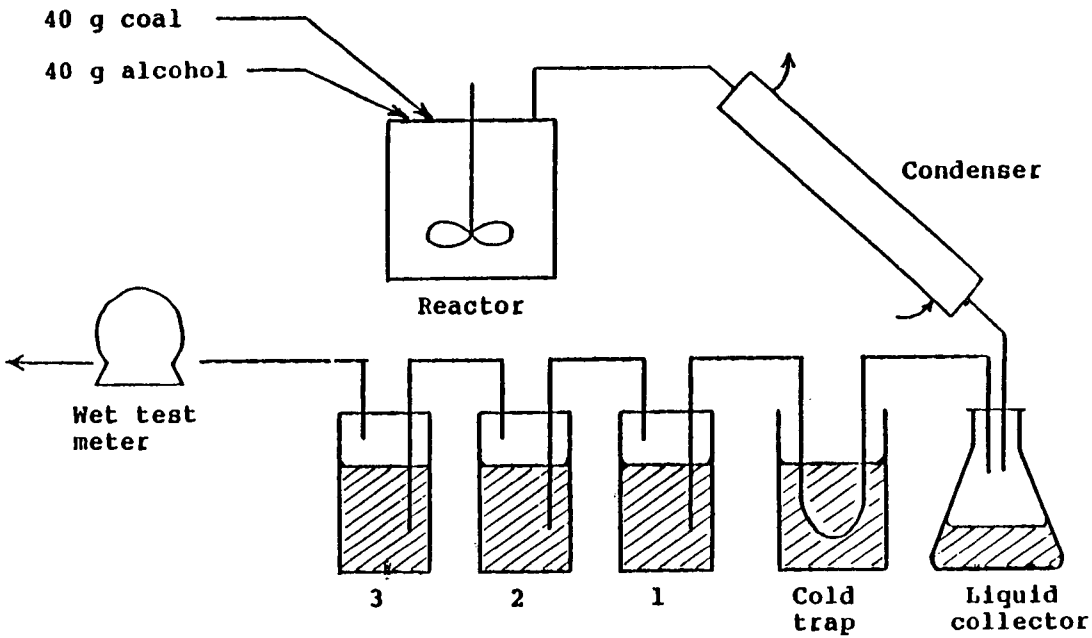

Figure 2. Batch Reactor Flow Diagram
Absorbers 1 and 2 contain ethanol, 3 contains aqueous zinc acetate solution.

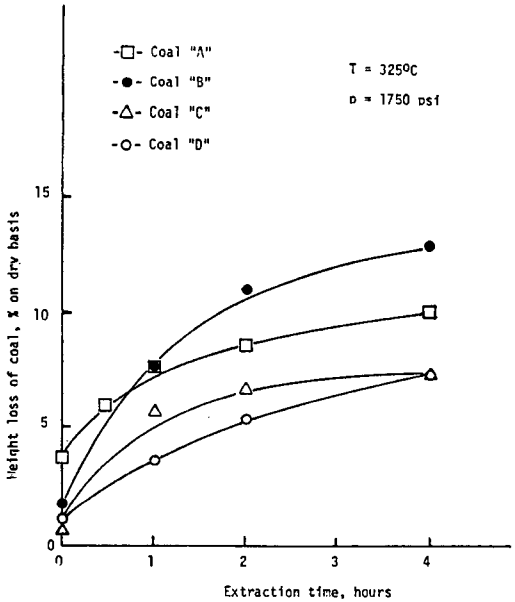

Figure 3. Percent of Coal Extracted in Semi-Continuous Reactor

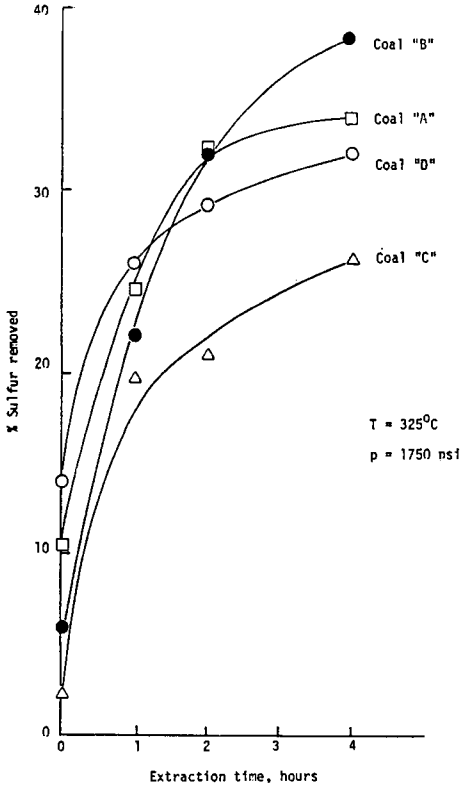

Figure 4. Percent of Sulfur Removed in Semi-Continuous Reactor

MECHANISM OF SOLUTE RETENTION IN SUPERCRITICAL FLUID CHROMATOGRAPHY

C. R. Yonker, S. L. Frye, H. R. Udseth, R. W. Wright, and R. D. Smith

Chemical Methods and Kinetics Section, Pacific Northwest Laboratory,
(Operated by Battelle Memorial Institute), Richland, Washington 99352

Introduction

Retention in supercritical fluid chromatography (SFC) is determined by solute solubility in the fluid and solute interaction with the stationary phase. The functional relationship between retention and pressure at constant temperature has been described by Van Wasen and Schneider (1). The trend in retention is shown to depend on the partial molar volume of the solute in the mobile and stationary phase coupled with the isothermal compressibility of the fluid mobile phase.

The solubility of the solute in a fluid has been discussed by Gitterman and Procaccia (2) and solute solubility has been described over the entire region of pressures of interest. The combination of solute solubility in a fluid with the equation for retention as a function of pressure derived by Van Wasen and Schneider allows one to determine the effect of solubility on solute retention.

The purpose of this work was to determine the relationship between solubility and retention. A thermodynamic model was developed which predicts the trend in retention as a function of pressure, given the solubility of the solute in the fluid mobile phase. From this model, solute retention behavior can be examined by theory and experiment in order to gain some insight into the complicated dependence of retention on the thermodynamic and physical properties of the solute and the fluid, providing a basis for consideration of more subtle effects unique to SFC.

Theory

In SFC, the basic assumption of infinitely dilute solutions of the solute in the mobile and stationary phases is valid. The concentration of the solute in these phases respectively is $C_i = X_i/V_m$, where X_i is the mole fraction of solute (i) and V_m is the molar volume of the pure mobile or stationary phase (1). Solute retention is calculated from a dimensionless retention factor, k, where,

$$k = (C_i^{stat}/C_i^{mob}) \cdot (V^{stat}/V^{mob}) \qquad 1)$$

C_i^{stat} and C_i^{mob} are the concentration of solute (i) in the stationary and mobile phases respectively, V^{stat} and V^{mob} are the volumes of the stationary and mobile phase. Substituting for concentration into equation 1,

$$k = (X_i^{stat}/X_i^{mob}) \cdot (V_m^{mob}/V_m^{stat}) \cdot (V^{stat}/V^{mob}) \qquad 2)$$

Taking the natural logarithm of both sides of equation 2 one obtains,

$$\ln k = \ln (X_i^{stat}/X_i^{mob}) + \ln (V_m^{mob}\ V^{stat}/V_m^{stat}\ V^{mob}) \qquad 3)$$

At equilibrium, the solute chemical potential in the respective phases are equal $\mu_i^{stat} = \mu_i^{mob}$ (3). Therefore,

$$\mu_i^{stat} = \mu_i^{mob} = \mu_i^{stat\,\infty} + RT\ \ell n X_i^{stat} = \mu_i^{mob\,\infty} + RT\ \ell n\ X_i^{mob} \qquad 4)$$

where μ_i^{∞} is the chosen standard state of infinite dilution of solute (i) in the two phases. Rearranging equation 4,

$$\ell n\ (X_i^{stat}/X_i^{mob}) = (\mu_i^{mob\,\infty} - \mu_i^{stat\,\infty})/RT \qquad 5)$$

Substituting equation 5 into 3,

$$\ell nk = (\mu_i^{mob\,\infty} - \mu_i^{stat\,\infty})\ /\ RT + \ell n\ (V_m^{mob}\ V^{stat}/V_m^{stat}\ V^{mob}) \qquad 6)$$

An assumption can be made that the second term on the right-hand side (RHS) of equation 6 is independent of pressure except for V_m^{mob}, the molar volume of the fluid mobile phase. Therefore differentiation of equation 6 with respect to pressure at constant temperature yields,

$$(\partial \ell nk/\partial P)_T = 1/RT\ [(\partial \mu_i^{mob\,\infty}/\partial P)_T - (\partial \mu_i^{stat\,\infty}/\partial P)_T] + (\partial \ell n\ V_m^{mob}/\partial P)_T \qquad 7)$$

The partial molar volume of a solute is defined as $(\partial \mu_i/\partial P)_T$ (3) and on rearranging the second term on the RHS of equation 7 one obtains the isothermal compressibility of the fluid mobile phase (4). Thus on substitution equation 7 reduces to,

$$(\partial \ell nk/\partial P)_T = 1/RT\ [\bar{V}_i^{mob\,\infty} - \bar{V}_i^{stat\,\infty}] - K \qquad 8)$$

where $\bar{V}_i^{mob\,\infty}$ and $\bar{V}_i^{stat\,\infty}$ are the partial molar volume of the solute (i) in the mobile and stationary phases at infinite dilution respectively and K is the isothermal compressibility of the fluid mobile phase. Equation 8 is the same as obtained by Van Wasen and Schneider (1) in their derivation of the trend in retention as a function of pressure for SFC.

The solubility of a solid in a supercritical fluid has been described by Gitterman and Procaccia (2). The region of interest chromatographically will be for infinitely dilute solutions whose concentration is far removed from the lower critical end point (LCEP) of the solution. Therefore the solubility of the solute in a supercritical fluid at infinite dilution can be approximated as,

$$(\partial \ell n X_i^{mob}/\partial P)_T = 1/RT\ [V^S - \bar{V}_i^{mob\,\infty}] \qquad 9)$$

where V^s is the molar volume of the pure solid solute. This is the same as equation 2.5 in Gitterman and Procaccia (2), describing solute solubility for dilute solutions far from criticality. Solving equation 9 for $\bar{V}_i^{mob}$.

$$\bar{V}_i^{mob} = -RT\ (\partial \ln X_i^{mob}/\partial P)_T + V^s \qquad 10)$$

Equation 10 can be substituted into equation 8 and upon rearrangement,

$$(\partial \ln k/\partial P)_T = (V^s - \bar{V}_i^{stat})/RT - (\partial \ln X_i^{mob}/\partial P)_T - K \qquad 11)$$

Equation 11 should be the relationship between retention-solubility and pressure at constant temperature for infinitely dilute solutions. The RHS of equation 11 consists of three terms, the first term will be a constant whose value depends on the partial molar volume of the solute in the stationary phase. The second term can be determined experimentally from bulk solubility measurements of the solute in the supercritical fluid mobile phase. The last term, the solvent isothermal compressibility, can be reasonably predicted from a two-parameter, cubic equation of state (EOS) such as the Redlich-Kwong EOS or the Peng-Robinson EOS (5,6).

The fluid mobile phases isothermal compressibility was determined using the Redlich-Kwong EOS to evaluate the derivative $(\partial\ V_m^{mob}/\partial P)_T$ in equation 12,

$$(\partial \ln V_m^{mob}/\partial P)_T = (1/V_m^{mob}) \cdot (\partial\ V_m^{mob}/\partial P)_T = -K \qquad 12)$$

From the Redlich-Kwong EOS,

$$(\partial V_m^{mob}/\partial P)_T = \frac{V_m^{mob}\ T^{0.5}\ (b^2 - (V_m^{mob})^2)}{P\ T^{0.5}(3\ (V_m^{mob})^2 - b^2) - RT^{3/2}\ (2V_m^{mob} + b) + a} \qquad 13)$$

where R is the gas constant, P is pressure, and T is temperature in K. The constants a and b of the Redlich-Kwong EOS are,

$$a = 0.4278\ R^2\ T_c^{2.5}/P_c \qquad 14a)$$

$$b = 0.0867\ RT_c/P_c \qquad 14b)$$

where P_c and T_c are the critical pressure and temperature of the fluid. The molar volume of the fluid was determined by the Peng-Robinson EOS, thus allowing one to solve for the isothermal compressibility of the fluid.

Therefore from equation 11, the trend in retention as a function of pressure at constant temperature can be determined and it is related to the solubility of the solute in the supercritical fluid, the isothermal compressibility of the solvent and the partial molar volume of the solute in the stationary phase at infinite dilution.

Experimental

The experimental apparatus and technique has been described in detail elsewhere (7,8). The retention factors of selected solutes under isothermal conditions at various pressures were obtained using capillary columns coated with a cross-linked phenyl polymethylphenylsiloxane stationary phase with carbon dioxide as the fluid mobile phase. A Varian 8500 syringe pump was operated under computer control providing accurate, pulsefree control of the fluid pressure. The retention times of the solute as a function of pressure were determined by a reporting integrator with an accuracy of a tenth of a second. Solubility data for the solutes in CO_2 was obtained from the literature ((9) and references therein).

Results and Discussion

Solute retention as a function of pressure has been determined experimentally for a wide number of solutes over a range of temperatures and pressures (1,10-12). The trend in retention of a solute with pressure can be predicted from the simple thermodynamic model upon which equation 11 is predicted. Experimental data for the retention of naphthalene in CO_2 at 35°C over a pressure range was reported by Van Wasen and Schneider (12). The solubility of naphthalene in CO_2 is given by McHugh and Paulaitis at 35°C, 55.0°C, 60.4°C, and 64.9°C (13). This data allows the trend in retention to be predicted from the calculation of the slope of $(\partial \ln k/\partial P)_T$ for naphthalene at 35°C in CO_2.

A plot of $\ln X_i^{mob}$ versus pressure in shown in Figure 1 based on the data from McHugh and Paulaitis (13). The slope $(\partial \ln X_i^{mob}/\partial P)_T$ at 35°C was obtained by interpolation between the data points, also the data range was extended to lower pressures than given in reference (13) by fitting the data using the method outlined by Reid et al. (14). This allowed the modeling of the trend in retention for a wider range of pressure. The fluids isothermal compressibility can be easily calculated for any temperature and pressure range of interest. The solute partial molar volume in the stationary phase was assumed constant and independent of pressure (15). Available data suggests that for a highly cross-linked stationary phase coated in a capillary column solvation is very small or negligible (16), therefore V^{stat} and V_i^{stat} would be independent of pressure. The above simplifying assumptions allow one to calculate the trend in solute retention based on the solubility of the solute in the mobile phase. Figure 2 shows the fit of equation 11 to the experimental data of Van Wasen and Schneider (12). The partial molar volume of the solute naphthalene in the stationary phase was determined to be ~180 cm^3/mole, this gave the best fit to the experimental data (naphthalene's molar volume is ~130.8 cm^3/mole). The simple thermodynamic model fits the retention data very satisfactorily. More experimental data for CO_2 in coated capillary columns is being undertaken in our laboratory at the present time but preliminary results with the model are promising.

On closer examination of equation 11, one can deduce that as the isothermal compressibility of the solvent becomes less important (temperature and pressure further removed from the critical temperature and pressure), $(\partial \ln k/\partial P)_T$ is proportional to the solubility of the solute in the fluid phase. Therefore, if solubility is found to be a linear function of density than retention will mirror this behavior and also be a linear function of density. Further, the farther one is from the critical pressure and temperature of the solvent the more likely one obtains a constant slope ($(\partial \ln k/\partial P)_T$ = constant).

Conclusion

The simple thermodyanamic relationship developed in this work has been shown to adequately describe the features of solute retention as a function of pressure at constant temperature for supercritical fluid chromatography. The importance of this model is the relationship drawn between solute solubility in the fluid mobile phase to the trend in solute retention. The trend in solute retention is demonstrated to be dependent on isothermal compressibility, solubility in the fluid and the partial molar volume of the solute in the stationary phase. The dependence of $\bar{V}_i^{stat\infty}$ on pressure is being examined and will be discussed in a future work. This change and further experimental investigations over the relevant ranges of temperature and pressure are in progress and will serve to guide future experimental and theoretical developments.

Acknowledgments

The authors acknowledge the financial support of the U.S. Department of Energy, Office of Basic Energy Science, under Contract DE-AC06-76RLO 1830.

References

(1) Van Wasen, U.; Schneider, G. M., Chromatographia, (1975), 8, 274.

(2) Gitterman, M.; Procaccia, I., J. Chem. Phys., (1983), 78, 2648.

(3) Klote, I. M.; Rosenberg, R. M., "Chemical Thermodynamics," 3rd Ed. W. A. Benjamin, Inc. (1972).

(4) Van Ness, H. C.; Abbott, M. M., "Classical Thermodynamics of Mon Electrolyte Solutions with Applications to Phase Equilibria," McGraw-Hill Book Company (1982).

(5) Redlich, O.; Kwong, J. N. S., Chem Rev., (1949), 44, 233.

(6) Peng, D. Y.; Robinson, D. B., Ind. Eng. Chem. Fundam., (1976), 15,59.

(7) Wright, B. W.; Smith, R. D., Chromatographia, (1984), 18, 542.

(8) Smith, R. D., Kalinoski, H. T., Udseth, H. R.; Wright, B. W., Anal. Chem., (1984), 56, 2476.

(9) Paulaitis, M. E., Krukonis, V. J., Kurnik, R. T.; Reid, R. C., Rev. Chem. Eng., (1983), 1, 179.

(10) Sie, S. T.; Rijnders, G. W. A., Sep. Sci., (1967), 2, 729.

(11) Semonian, B. P.; Rogers, L. B., J. Chromatogr. Sci., (1978), 16, 49.

(12) Van Wäsen, U.; Schneider, G. M., J. Phys. Chem., (1980), 84, 229.

(13) McHugh, M.; Paulaitis, M. E., J. Chem. Eng. Data,, (1980), 25, 326.

(14) Reid, R. C., Kurnik, R. T.; Holla, S. J., J. Chem. Eng. Data, (1981), 26, 47.

(15) Wicar, S.; Novak, J., J. Chromatogr., (1974), 95, 1.

(16) McHugh, M.; Private communication.

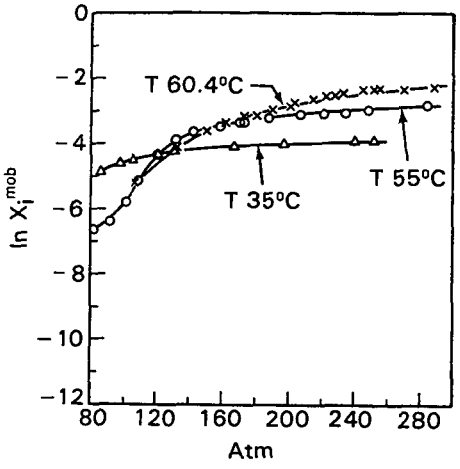

Figure 1. Plot of ln X_i^{mob} against pressure in atmospheres at 35°C, 55°C, and 60.4°C. Data from McHugh and Paulaitis (13).

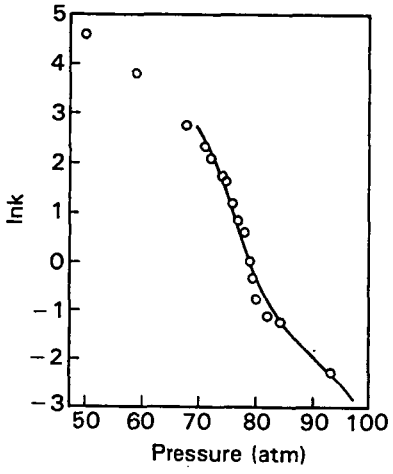

Figure 2. Experimental data for naphthalene with CO_2 (ref. 12) at 35°C and theoretical model (solid line).

SEMI-PREPARATIVE SUPERCRITICAL FLUID EXTRACTION/FRACTIONATION

R.M. Campbell and M.L. Lee

Department of Chemistry, Brigham Young University, Provo, Utah 84602 USA

Supercritical fluids have been used with considerable success both as mobile phases in chromatography and as solvents in extraction processes. While packed columns have been used in chromatography with greatly reduced analysis times (1), ease of solvent removal has been one of the major benefits of extractions with supercritical CO_2 (2). The supercritical fluid extraction of caffeine from coffee and of nicotine from tobacco are only a few of the many uses of supercritical fluids for separations which have been reported. These have been reviewed previously (2). In several studies, packed columns were used to improve the separation of closely related compounds. For example, supercritical fluid fractionation (SFF) methods were used to isolate several polycyclic aromatic hydrocarbons (PAH) in an automobile exhaust extract (3). These studies have shown that the ability to instantaneously vary the solvating power of a supercritical fluid by changing its pressure (or density) can be used to great advantage. Using the selectivity of the mobile phase, compounds were resolved in SFC which would have required many more theoretical plates to resolve in gas chromatographic systems (4). This mobile phase selectivity can only be preserved by avoiding large pressure drops across the column which can occur in columns packed with very small particles or in systems operated at very high flow rates (5). In the present study, columns packed with silica materials of intermediate particle sizes (30 to 70 µm) were used to prevent large pressure drops and allow dynamic pressure programming to achieve semi-preparative scale separations.

EXPERIMENTAL

A supercritical fluid extraction/fractionation system was constructed to provide separations and fraction collection on a semi-preparative scale. A schematic diagram of this system is shown in Figure 1. The system included a 375-mL syringe pump (Isco, Lincoln, NE) modified for pressure control at flow rates of up to 8 mL/min (liquid), a chromatographic oven (Varian, Walnut Creek, CA), and four 125-mL fraction collection vessels which were fitted with cooling jackets. During fraction collection, the vessels were cooled to 3 ± 2°C *via* a circulating cooling bath (Grant Science/Electronics, Dayton, OH). A six-port switching valve (Valco Instrument Co., Houston, TX) was used to collect successive fractions in different collection vessels. The collection vessels were pressurized with N_2 from a high pressure tank in conjunction with appropriate valving. A micrometering valve (Autoclave Engineering, Erie, PA) was used to control the flow when the effluent was vented directly to atmosphere. An extraction column (10 cm x 4.6 mm i.d.) and a separation column (25 cm x 4.6 mm i.d.) were placed in the oven, and effluents were monitored with a UV-absorbance detector (Hitachi, Model 100-10, Tokyo, Japan) equipped with a high pressure cell (Hewlett-Packard, Avondale, PA). All parts of the extraction/fractionation apparatus were constructed of stainless steel.

A coal tar was fractionated by adding 1 mg of the tar in 50 µL of methylene chloride to the top of the extraction column which had been dry-

packed with 40-63 µm silica (Sigma, No. S-0507, St. Louis, MO). The column end fittings (equipped with 2 µm frits) were tightened and the column was installed in the oven by tightening the appropriate fittings. The separation column was dry-packed with NH_2-Adsorbosil (Applied Science, Deerfield, IL, 30 - 70 µm). The oven temperature was raised to 40°C and held there for the duration of the fractionation. The pressure was brought to 72 atm, then immediately raised to 95 atm at 8 atm/min. The pressure was held at 95 atm until phenanthrene began to elute (Fraction 3), whereupon it was raised at 1.5 atm/min to 98 atm. As soon as the fluoranthene/pyrene peak (Fraction 4) started eluting, the pressure was again programmed at 1.5 atm/min to 130 atm. At this point, as the chrysene peak (Fraction 5) was finishing, the pressure was programmed at 5 atm/min to 198 atm and held for about 10 min. Fractions were collected as marked on the chromatogram in Figure 3. Fractions were analyzed by capillary gas chromatography with an HP 5880 gas chromatograph equipped with a 20 m x 0.2 mm i.d. fused silica capillary column coated with SE-54 stationary phase which was crosslinked with azo-t-butane.

RESULTS AND DISCUSSION

In 1977, Wise et al. (6) reported the separation of PAH according to number of aromatic rings using an HPLC system with a chemically bonded aminosilane stationary phase. This was very important because each of the ring-number cuts could then be analyzed by reversed phase HPLC, which provides resolution of closely related isomers. More recently, ring-number fractions of complex mixtures of PAH have been sought for analysis by GC with a liquid crystalline stationary phase, which exhibits excellent selectivity for the separation of geometric isomers (7,8).

Figure 2 shows the UV chromatogram of the fractionation of a number of standard PAH using the SFF system. A similar pressure program was used to fractionate a coal tar sample as shown in Figure 3. Figure 4 shows the capillary gas chromatograms of typical fractions of the coal tar extract obtained on the SFF system. The polar amino bonded phase provided good selectivity for separations by ring number. Alkylated species tended to elute at or near the same time as their parent compounds, while compounds of different ring structure were widely separated.

Samples were best introduced into the SFE system by applying the solutes in a small amount of solvent to the head of the column with a syringe. This method resulted in narrower bands than are obtained when the sample is distributed over the entire extraction column. An external sample loop injection valve was not used in the system because at the lower pressures used at the beginning of a fractionation run, all sample components were not dissolved, resulting in plugging of the frits at the head of the separation column.

Adsorbents of intermediate particle size (30-70 µm) were found to give the best separations. The trade-off between column efficiency and pressure drop was at or near optimum with this particle size. Smaller particles resulted in large pressure drops, while larger particles resulted in poor efficiency and large column dead volumes.

In addition, standard compounds were used to study the effect of mobile phase density on resolution of closely related compounds. The resolution of biphenyl and acenaphthalene was measured at a number of different mobile phase densities. Results of this study are listed in Table I. It was found that, in general, the resolution of a pair of closely related isomers could be improved by as much as 100% by decreasing the mobile phase pressure at

constant temperature on a given column. However, it was also concluded that the particle size of the packing in the column has a large effect on resolution as well. Column efficiency, which is solely dependent on the particle size of the column packing material, may have a greater effect on resolution than the selectivity of the mobile phase. Also, by going to smaller particle diameter of the column packing, analysis times can be shortened. However,

Table 1. Resolution of Acenaphthalene and Biphenyl at Various Pressures of CO_2 at 40 °C and using a 35-70 µm NH_2-silica column.

Pressure	Resolution
85	1.1
90	1.1
100	0.8
120	0.9
140	0.9
160	0.9
180	0.7
198	0.5

large pressure drops across columns packed with very small particles cause significant selectivity losses. For some solutes, the gain in efficiency is greater than the loss in selectivity on going to a smaller diameter packing. It was concluded that particles in the 35-80 µm range were best for the separations we have attempted thus far.

UV monitoring of the column effluents was essential to enable precise cuts during fractionation on a routine basis as well as during development. Solutes in the fractions were best collected by cooling the collection vessels to 2 to 5 °C. This created a two-phase (gas/liquid) region in the collection vessels, causing the solutes to precipitate out of the gas phase. In this way, the solutes were removed from the CO_2 before it decompressed through the fused silica restrictors. The cooling was not enough to cause precipitation of very volatile solutes such as naphthalene. Therefore, fractions containing very volatile components were collected by bubbling the effluents through methylene chloride or n-pentane.

With our current pumping system, the maximum sample capacity appears to be about 10 to 20 mg per run. Figure 5 shows the UV SFF chromatogram of 8 mg of coal tar extract obtained on a 25 cm x 6.2 mm i.d. column with a 10 cm x 6.2 mm i.d sample introduction column. The NH_2-Adsorbosil stationary phase was used in this case as well. Fractions were again collected as marked on the chromatogram. Typical analysis times for separations of components ranging from 2 to 5 rings was between 1 and 1.5 h.

Overall, it was found during this study that semi-preparative supercritical fluid fractionation shows great potential for high quality separations with easy solvent removal.

REFERENCES

1. Gere, D.R.; Board, R.; McManigill, D. Anal. Chem. **1982**, 54, 736-740.
2. Randall, L.G. Sep. Sci. Tech. **1982**, 17, 1-118.
3. Jentoft, R.E.; Gouw, T.H. Anal. Chem. **1976**, 48, 2195-2200.
4. Sie, S.T.; Rijnders, W.A. Sepn. Sci. **1967**, 2, 755.
5. Peaden, P.A.; Lee, M.L. J. Lig. Chromatogr. **1982**, 5 (Suppl. 2), 179-221.
6. Wise, S.A.; Chesler, S.N.; Hertz, H.S.; Hilpert, L.R.; May, W.E. Anal. Chem. **1977**, 49, 2306.
7. Kong, R.C.; Lee, M.L.; Tominaga, R.; Pratap, M.; Iwao, M.; Castle, R.N. Anal. Chem. **1982**, 54, 1802.
8. Markides, K.E.; Nishioka, M.; Tarbet, B.J.; Bradshaw, J.S.; Lee, M.L. Anal. Chem., in press.

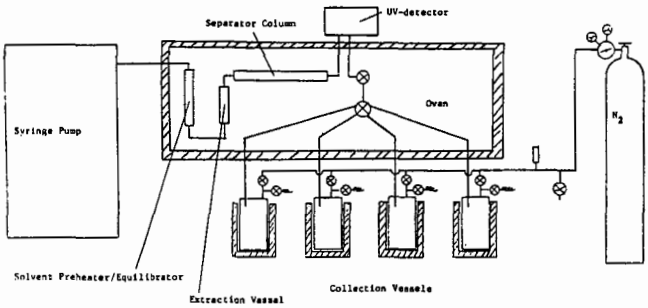

Figure 1. Schematic diagram of the supercritical fluid extraction/fractionation system.

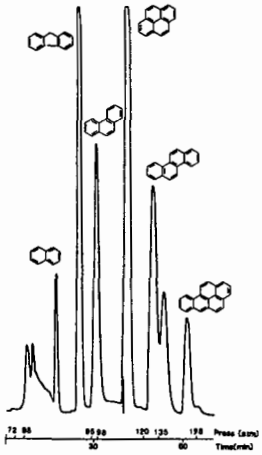

Figure 2. UV chromatogram of the supercritical fluid fractionation of a number of standard compounds with CO_2 at 40°C.

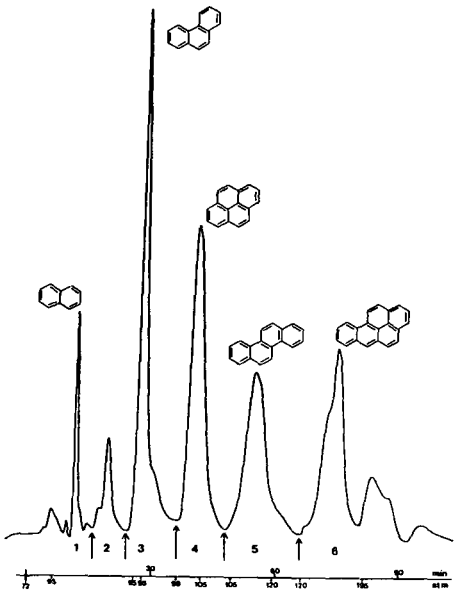

Figure 3. UV chromatogram of the supercritical fluid fractionation of 1 mg of a coal tar extract with CO_2 at 40°C. The numbers 1-6 indicate the fractions that were collected.

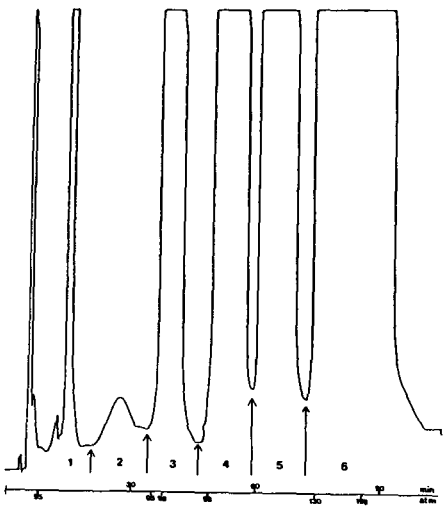

Figure 5. UV chromatogram of the supercritical fluid fractionation of 8 mg of the coal tar extract with CO_2 at 40°C.

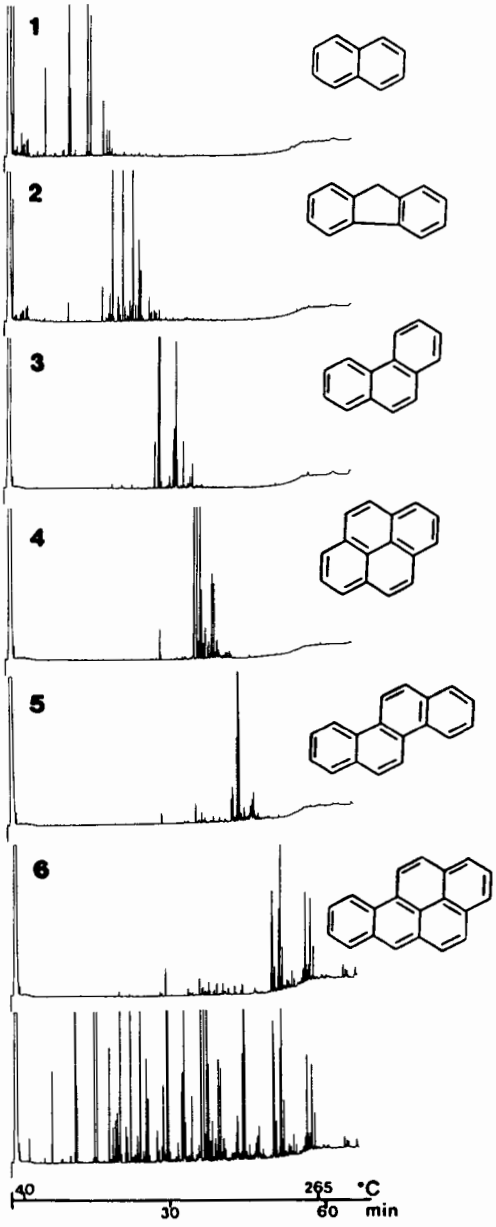

Figure 4. Capillary gas chromatograms of the six fractions collected during the supercritical fluid fractionation of the coal tar extract. The numbers refer to the fractions shown in Figures 3 and 5. The bottom chromatogram shows the total unfractionated coal tar for comparison.

Supercritical Carbon Dioxide Extraction of Lemon Oil

Steven J. Coppella and Paul Barton*

Department of Chemical Engineering
The Pennsylvania State University
University Park, PA 16802

In 1983-1984, Arizona and California produced annually over 10^6 kg of cold-pressed lemon oil. After being concentrated by distillation or liquid extraction, lemon oil is used as flavoring and/or fragrance agent in beverages and cosmetics. Distillation thermally degrades lemon oil. Extraction with organic solvents only partially reduces thermal degradation (since the solvents must be recovered by distillation) and introduces solvent contamination. Extraction with nonfermentative supercritical carbon dioxide near its critical point (304.3 K, 7.38 MPa, 0.467 g/cm^3) offers a cheap, nontoxic solvent that does not impart flavors nor thermally degrade the product. It can handle feedstocks with high wax content because these constituents can be solubilized in supercritical carbon dioxide. Supercritical extraction is a hybrid unit operation in the domain between extractive distillation and liquid extraction. Solvent recovery is accomplished by depressurization at ambient temperature.

Processes for supercritical extraction of oils have been described in numerous literature references. Several recent ones are Paulaitis et al. (1983), Ely and Baker (1983), Gerard (1984), Stahl et al. (1984), and Robey and Sunder (1984). The literature lacks detailed data on multicomponent essential oils with supercritical solvents in the proximity of the solvent critical temperature. Accurate prediction of data in this region by equations of state is limited to binary and ternary systems.

The purpose of our research is threefold: evaluate the feasibility of supercritical carbon dioxide extraction of lemon oil near ambient temperature, generate equilibrium data with carbon dioxide and multicomponent essential oil constituents, and evaluate the ability of the Peng-Robinson equation of state to model a reduced multicomponent supercritical system.

CONCENTRATING LEMON OIL

Staroscik and Wilson (1982) have quantitated various lemon oils and identified 38 compounds. These compounds can be subdivided into three major classifications: terpenes (C_{10} hydrocarbons), oxy's (oxygenated C_8-C_{12} hydrocarbons), and sesquiterpenes (C_{15} hydrocarbons). A usual goal in concentrating lemon oil is to remove the terpenes and sesquiterpenes from the desired oxy fraction.

When concentrating the lemon oil by multistage fractional distillation under vacuum, column operability coupled with condenser pressure, column pressure drop, reboiler design, and mode of operation (batch or continuous) dictate the degree of thermal exposure. Overhead temperatures increase in the range of 320 to 340 K, reboiler temperatures increase in the range of 330 to 370 K, and exposure times of 15 to 20 hours may be expected during batch distillation. In continuous distillation, exposure times are lower but reboiler temperature may be higher.

In extractive distillation with supercritical solvent, volatility amplification by the solvent rather than vacuum is used to get the components into the extract or vapor phase. Operating temperature can be made lower than in conventional distillation, and the heart-cut product will have been subjected to less thermal degradation. Carbon dioxide has a critical temperature that meets this goal.

In order to make data correlation tractable in supercritical carbon dioxide extraction, it is convenient to represent each major chemical classification by a single compound. Each select compound should have available good vapor pressure data and should be a predominant constituent in its group with regard to structure and concentration. For correlation purposes, we selected limonene, geranial, and β-caryophyllene. Their structures are shown in Figure 1.

Stahl et al. (1984) presented solubility data for limonene and caryophyllene with carbon dioxide; Gerard (1984) included carvone. Temperatures in the range of 279 to 377 K, and pressures in the range of 1.5 to 11 MPa were covered. Robey and Sunder (1984) provided solubility and relative volatility data for carbon dioxide with folded lemon oil and with limonene and citral (geranial/neral) at 323 to 353 K and 9.4 to 10.6 MPa.

Gerard (1984) describes a continuous multistage column process for carbon dioxide extraction (distillation) of essential oils at ambient temperature and 8 MPa, with solvent recovery at 273 K and 3 MPa. Robey and Sunder (1984) propose a lemon oil fractionator operated at 333 K and 10 MPa with an efficiency equivalent to 12 stages, with solvent recovery at 293 K and 5.5 MPa.

EXPERIMENTAL SECTION

Cold-pressed oil from Arizona early desert lemons was supplied by A. M. Todd Company, Kalamazoo, MI. Degassed lemon oil and dry carbon dioxide were charged into the one-liter isothermal constant volume cell shown in Figure 2. After the operating temperature was reached, the system was stirred for one hour, then allowed to settle for 15 minutes before sampling. Experiments were performed at 303 to 313 K and 4 to 9 MPa. Parallel phase visualization experiments were conducted in a sight gauge to insure operation in the two-phase region.

A sample of the equilibrated liquid phase was removed (after purging) by depressurization through a valve and hypodermic tubing into a two-stage trap cooled by dry ice - acetone. A wet test meter measured the carbon dioxide off-gas. A sample of the vapor phase was then similarly removed. Purge and sample sizes were kept small to minimize disturbance of equilibrium. Pressure changes in the cell were 0-0.1 MPa during sampling of liquid phase and 0-1.2 MPa during sampling of vapor phase. Special high-pressure sample valves with microliter-sized traps were tried in an effort to reduce pressure disturbance, but reliability was inadequate.

Estimated relative errors are 0.2% for temperature, 5% for pressure, 4% for carbon dioxide mole fraction in the liquid phase, and 10% for lemon oil mole fraction in the vapor phase.

The recovered lemon oil samples were analyzed by gas chromatography. A 0.5 mm i.d. x 30 m thin film (0.1 μm) SE-30 glass capillary column (Supelco, Inc., Bellefonte, PA) was used with a flame ionization detector in a F&M 810 chromatograph. The unit was fitted with a temperature programmer (F&M Scientific Model 240), glass-lined inlet splitter (J&W Scientic, Inc.), and integrator (Hewlett-Packard Model 3370B). No reference column was used. The following conditions were employed: 27 cm/s He carrier gas; 250 cm^3/min air, 40 cm^3/min N_2, and 55 cm^3/min H_2 to detector; 0.4 μl sample size, 27/1 split ratio; temperature program 348 K hold 8 minutes, 4 K/min, 473 K hold 15 minutes; injection port temperature 523 K; detector temperature 523 K; attenuation X1, range 10^2; slope sensitivity 0.01 mV/min; manual baseline reset; chart speed 1.3 cm/min. Baseline drift was 0.02 mV/125 K. Peak areas from the integrator were within 5% of those determined by cutting and weighing the peaks.

Peak identification was based on information of Supelco, Inc., A. M. Todd Company, and Staroscik and Wilson (1982). Staroscik (1984) provided us with the response values used in his work and we assumed that our detector would give proportionate response. Staroscik found in his work that relative standard deviations were generally less than 3%.

RESULTS

Lemon oil-carbon dioxide equilibrium was measured at 303, 308, and 313 K and in the pressure range of 4 to 9 MPa. Below 6 MPa, there was insufficient lemon oil in the vapor phase to attain good samples for analysis. Above 9.0 MPa at 313 K, above 7.8 MPa at 308 K, and above 7.4 MPa at 303 K, the system reverted to a single phase. Nine experiments provided two-phase, vapor-liquid equilibrium data suitable for correlations and generating coefficients for the Peng-Robinson equation. Detailed experimental data can be found in Coppella (1985).

The results of an experiment at 308 K and 6.98 MPa are detailed here. The liquid phase contained 48 wt% (74 mole %) carbon dioxide and the vapor phase contained 99.5 wt% (99.8 mole %) carbon dioxide. A gas chromatogram for the lemon oil from the liquid phase sample is shown in Figure 3. A chromatogram for the lemon oil in the vapor phase is shown in Figure 4. Peak identification, retention, response value, and concentration for these traces are given in Table I. Average molecular weight of lemon oil is 137.9 in liquid and 136.4 in vapor.

The relative volatility in the presence of carbon dioxide, or selectivity factor, for each component with respect to limonene is also given in Table I. Relative volatility is defined as the ratio of equilibrium vaporization K for component i to equilibrium vaporization K for limonene. Equilibrium vaporization K_i is defined as mole fraction i in the vapor (extract) phase to mole fraction i in the liquid (raffinate) phase.

By comparing the relative volatilities of various components, the ease of separation between these components can be determined. The chromatographic column employed separates components in the order of volatility; thus, the first cut point in the separation should be between terpinolene and adjacent oxygenated compounds. The chromatograph doesn't separate terpinolene from linalool or nonanal, so the separability of these compounds couldn't be determined. The next adjacent separation involves terpinolene with a relative volatility with respect to limonene of 0.7 and citronellal with a relative volatility with respect to limonene of 0.4. The relative volatility of terpinolene to citronellal is then 0.7/0.4 or 2. For the limonene/geranial pair, the relative volatility is 1.0/0.2 or 5. These separation factors for the terpene-oxy split are adequate.

The second cut point in the separation is between geranylacetate and β-caryophyllene. This separation factor is 0.06/0.07, or 0.9. This is opposite that of 0.2/0.07 or 3 for geranial to β-caryophyllene.

There is some overlap in the volatilities of C_{12} oxys and sesquiterpenes, which means that for extractions of lemon oil with supercritical carbon dioxide, some β-caryophyllene will be extracted into the heart-cut oxy product. This is the result of the nonpolar carbon dioxide preferentially extracting the less polar of the lemon oil constituents.

SOLUBILITY AND SELECTIVITY

Solubility diagrams were prepared for the phases that separated in the lemon oil extractions performed in this study with carbon dioxide. Such diagrams can serve

only as guides, since solubility is composition-dependent and is a function of extraction severity. The data are shown in Figures 5, 6, and 7 at 303, 308, and 313 K, respectively.

Extractions or extractive distillations with supercritical solvent need to be performed at as high as possible a solubility of oil in the extract or vapor phase in order to reduce the solvent or carrier gas requirement. From our lemon oil-carbon dioxide phase diagrams, it appears that the highest practical solubility level is 0.9 mole % (2.8 wt.%) essential oil. This is attainable at 313 K. At lower temperature, sensitivity of solubility to pressure requires that solubility be lower (e.g., 0.3 mole % at 308 K).

At 313 K and 8.4 MPa, slope of extract phase solubility versus pressure is 0.06 weight fraction oil/MPa. For a 15 m tall extraction tower operated at a density of 0.5 g/cm³, the pressure at the bottom is higher than that at the top by 0.025 MPa. The solubility at the bottom will then be 0.15 wt.% higher at the bottom (ignoring composition effects). At 308 K and 7.69 MPa, an increase in pressure of 0.14 MPa causes the two-phase system to revert to a one-phase system. It is imperative that temperature and pressure profiles in the supercritical extraction tower be maintained accurately. Windows are recommended to confirm that operation remains in the two-phase domain.

The selectivities in supercritical carbon dioxide extraction of terpenes from oxys, and oxys from sesquiterpenes, for lemon oil are shown in Figures 8 and 9, respectively. Figure 8 shows the relative volatility, or selectivity factor, of limonene to geranial as a function of oil solubility in the vapor phase. Operation of the extractor at 308 K and 1 wt.% solubility provides a relative volatility of 2. Operation at 313 K provides a relative volatility of 1.4. The selectivity factors, though adequate, are an order of magnitude lower than the vapor pressure ratio.

Figure 9 shows the relative volatility of geranial to β-caryophyllene as a function of oil solubility in the vapor phase. At 313 K and 1 wt.% volatility, relative volatility is 1.4. At 308 K and 1 wt.% solubility, these constituents are inseparable by supercritical carbon dioxide extraction. The ratio of vapor pressures for this pair is in the vicinity of 2.

MODELING OF EQUILIBRIA

The carbon dioxide:lemon oil P-x behavior shown in Figures 5, 6, and 7 is typical of binary carbon dioxide:hydrocarbon systems, such as those containing heptane (Im and Kurata, 1971), decane (Kulkarni et al., 1972), or benzene (Gupta et al., 1982). Our lemon oil samples contained in excess of 64 mole % limonene; so we modeled our data as a reduced binary of limonene and carbon dioxide. The Peng-Robinson (1976) equation was used, with critical temperatures, critical pressures, and acentric factors obtained from Daubert and Danner (1983), and Reid et al. (1977). For carbon dioxide, ω = 0.225; for limonene ω = 0.327, T_c = 656.4 K, P_c = 2.75 MPa. It was necessary to vary interaction parameter with temperature in order to correlate the data satisfactorily. The values of d_{12} are reasonable (0.1135 at 303 K, 0.1129 at 308 K, 0.1013 at 313 K). Comparisons of calculated and experimental results are given in Figures 5, 6, and 7.

Attempts to model the relative volatilities of the minor organic constituents to limonene using the Peng-Robinson equation proved unfruitful.

PROPOSED PROCESS

Lemon oil can be concentrated by supercritical carbon dioxide extraction in the temperature range of 308 to 313 K. Pressure in the extractor will be in the range of 7.7 to 8.5 MPa. Solubilities of oil in the extract, or vapor, phase will range from 1 to 3 wt.%. Selectivity factors near 1.4 will be attained for the terpene-oxy split and oxy-sesquiterpene split. The operation is performed in a multistage extractor with reflux. Operation can be either in the batch or continuous mode. Solvent recovery is performed at conditions slightly below the critical point of carbon dioxide.

Solubility limitations require that the solvent treat be high; an economic analysis is needed to establish process feasibility.

REFERENCES

Coppella, S. J.; M.S. Thesis, The Pennsylvania State University, University Park, PA, 1985.

Daubert, T. E.; Danner, R. P.; eds. "Technical Data Book - Petroleum Refining," 4th ed., American Petroleum Institute, Washington, DC (1983).

Ely, J. F., Baker, J. K., NBS Technical Note 1070, 1983.

Gerard, D., Chem., Ing. Tech., 1984, 56, 794.

Gupta, M. K.; Li, Y. H.; Hulsey, B. J.; Robinson Jr., R. L., J. Chem. Eng. Data, 1982, 27, 55.

Im, U. K.; Kurata, F., J. Chem. Eng. Data, 1971, 16, 412.

Kulkarni,, A.A.; Zarah, B. Y.; Luks, K. D.; Kohn, J. P., J. Chem. Eng. Data, 1972, 19, 92.

Paulaitis, M. E.; Krukonis, V. J.; Kurnik, R. T.; Reid, R. C., Reviews in Chemical Engineering, 1983, 1, 179.

Peng, P. Y.; Robinson, D. B., I.E.C. Fund., 1976, 15, 59.

Reid, R. C.; Prausnitz, J. M.; Sherwood, T. K., "The Properties of Gases and Liquids," 3rd ed., McGraw-Hill Book Co., New York (1977).

Robey, R. J.; Sunder, S., 1984 Annual Meeting American Institute of Chemical Engineers, San Francisco, CA, 1984.

Stahl, E.; Quirin, K. W.; Glatz, A.; Gerard, D.; Rau, G., BBPCAX, 1984, 88, 900.

Staroscik, J. A., Sunkist Growers, Inc., Ontario, CA, personal communication, 1984.

Staroscik, J. A.; Wilson, A. A., J. Agric. Food Chem., 1982, 30, 507, 835.

TABLE I

LEMON OIL VAPOR-LIQUID ANALYSES AT EQUILIBRIUM IN CO_2

PEAK NO.	COMPOUND	RETENTION[a] RELATIVE TO LIMONENE	WEIGHT[b] RELATIVE RESPONSE	MOLE % VAPOR	MOLE % LIQUID	VOLATILITY RELATIVE TO LIMONENE
ref	acetone	0.00	-	-	-	-
1	α-thujene	0.55	0.75	0.61	0.35	1.8
2	α-pinene	0.58	0.75	2.80	1.68	1.7
3	camphene	0.63	0.70	0.09	0.06	1.6
4	sabinene β-pinene	0.76	0.74	17.27	13.06	1.34
5	myrcene	0.79	0.73	1.87	1.59	1.2
6	octanal phellandrene	0.86	1.17	0.09	0.07	1.3
7	α-terpinene	0.92	1.19	1.21	1.10	1.1
8	limonene	1.00	0.75	67.14	68.22	1.0
9	γ-terpinene	1.09	0.78	7.59	8.45	0.91
10	terpinolene linalool nonanal	1.19	0.78	0.47	0.67	0.7
11	citronellal	1.40	1.06	0.02	0.04	0.4
12	terpinenen-4-01	1.51	0.92	0.02	0.04	0.4
13	α-terpineol	1.55	0.92	0.06	0.20	0.3
14	decanal	1.60	0.97	0.01	0.08	0.1
15	neral	1.70	0.96	0.24	0.92	0.3
16	geranial	1.80	0.96	0.29	1.45	0.2
17	nonylacetate	1.95	0.24	0.00	0.03	-
18	nerylacetate	2.12	1.02	0.03	0.25	0.1
19	geranylacetate	2.18	1.02	0.009	0.15	0.06
20	β-caryophyllene	2.36	0.78	0.013	0.18	0.07
21	trans-α-bergamotene	2.40	0.78	0.016	0.26	0.06
22	α-humalene	2.53	0.71	0.00	0.05	-
23	β-bisabolene	2.60	0.77	0.013	0.38	0.03

[a] Retention time for limonene averaged 8.7 minutes

[b] Peak area multiplier

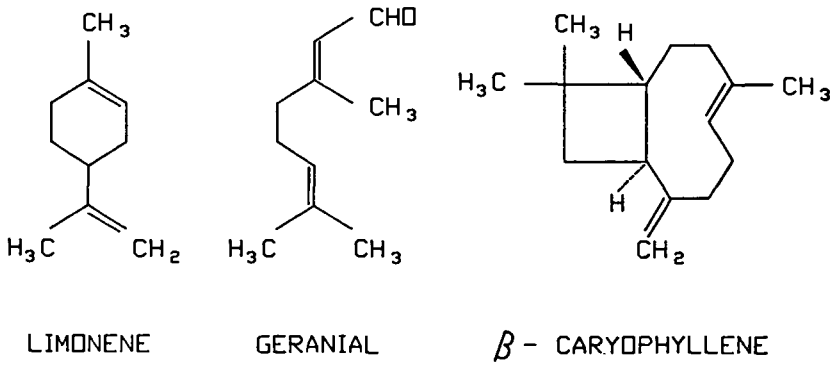

Fig. 1. Key constituents in lemon oil.

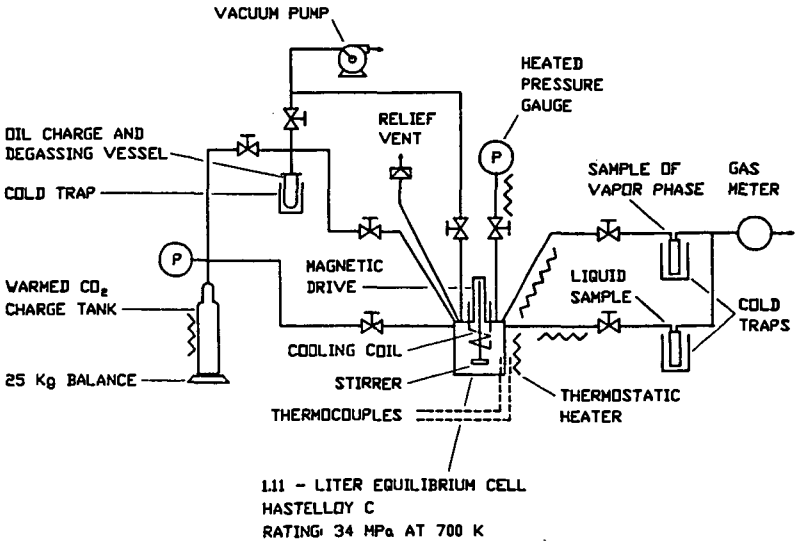

Fig. 2. Vapor-liquid equilibrium apparatus

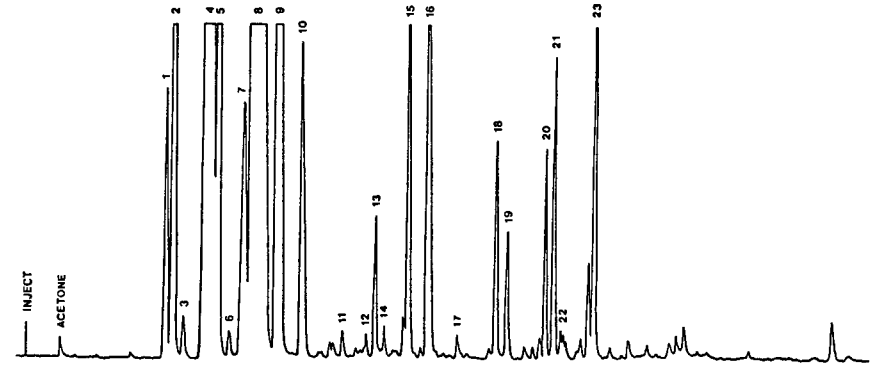

Fig. 3. Gas chromatogram of lemon oil in liquid phase sample

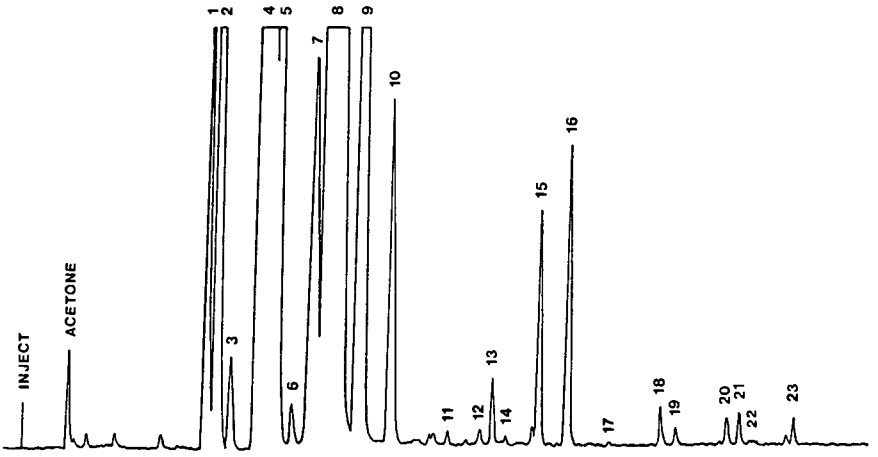

Fig. 4. Gas chromatogram of lemon oil in vapor phase sample

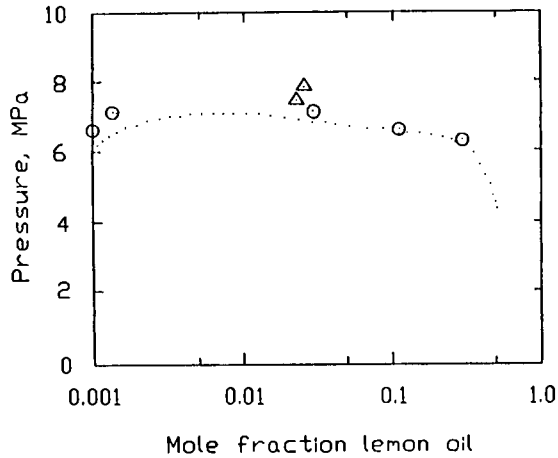

Fig. 5. Phase equilibrium for carbon dioxide : lemon oil at 303 K.
o - experimental two-phase
Δ - experimental one-phase
. . . Peng-Robinson eq.

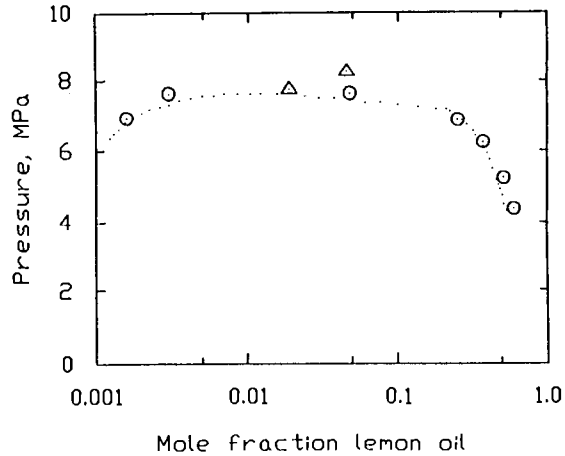

Fig. 6. Phase equilibrium for carbon dioxide : lemon oil at 308 K.
o - experimental two-phase
Δ - experimental one-phase
. . . Peng-Robinson eq.

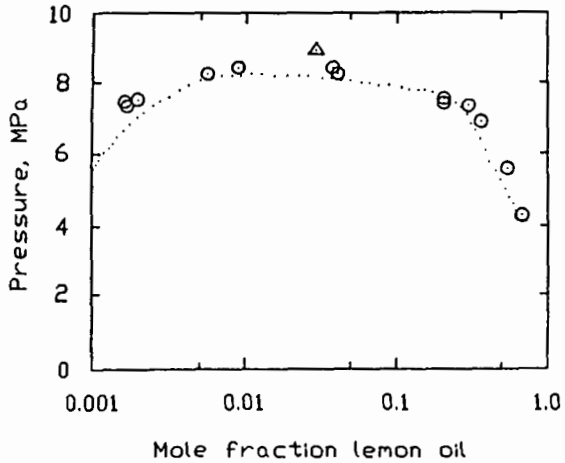

Fig. 7. Phase equilibrium for carbon dioxide : lemon oil at 313 K.
o - experimental two-phase
Δ - experimental one-phase
. . . Peng-Robinson eq.

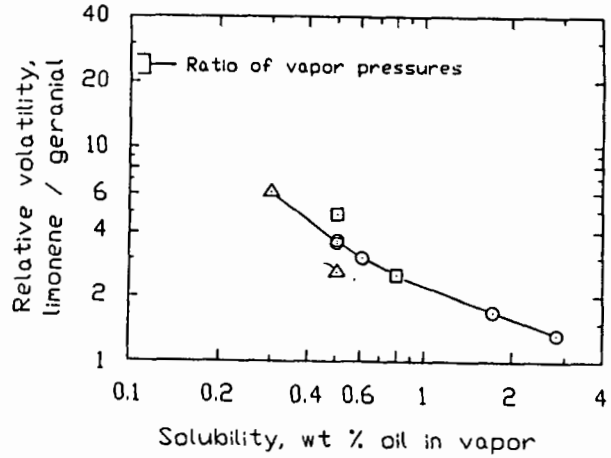

Fig. 8. Lemon oil : carbon dioxide vapor-liquid equilibria. Δ - 303 K. □ - 308 K. o - 313 K.

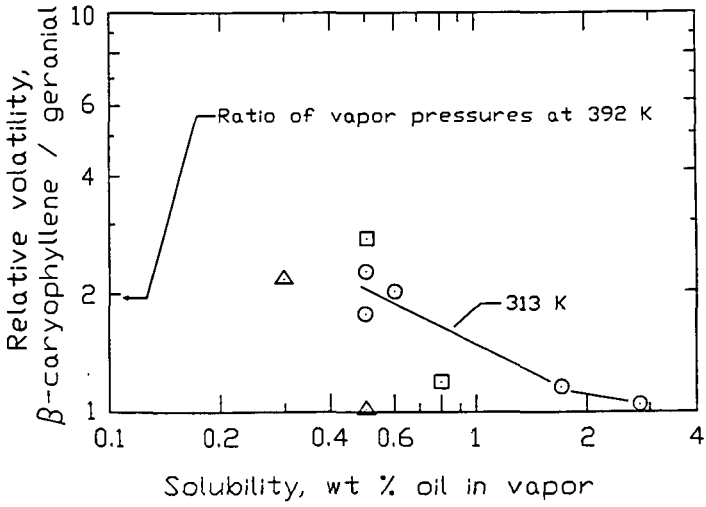

Fig. 9. Lemon oil : carbon dioxide vapor-liquid equilibria. △ - 303 K. □ - 308 K. o - 313 K.

FRACTIONATION OF ETHYL ESTERS FROM FISH OIL

by Dr. Wilhelm O. Eisenbach

Max-Planck-Institut für Kohlenforschung 4330 Mülheim-Ruhr West Germany

1. Introduction

In this paper the efficiency of supercritical fluid extraction as a separation procedure will be presented, as an example the fractionation of a mixture of high boiling substances is described. Generally the product dissolved in a supercritical fluid can be separated either by increasing the temperature at constant pressure (isobaric method) or by lowering the pressure at constant temperature (isothermal method). Both phenomena can be used in fractionation procedures.

1.1 Variation of Pressure

Discontinuous variation of the pressure in either the extraction vessel or in the separator can lead to fractionation. In the first case the pressure and hence the density of the extraction agent is increased in a stepwise manner with the result that material is taken up into the supercritical phase in order of increasing boiling point or molecular weight. The dissolved material can be isolated then in either an isobaric or isothermal manner. In practice the pressure is generally raised after extraction at the lower pressure is completed.

Alternatively the extraction can be carried out at a constant pressure in the extraction vessel and the loaded supercritical phase will be expanded in a step-wise manner whereby the least volatile components are deposited first, while the better volatile components remain dissolved in the supercritical phase.

1.2 The Hot Finger

The other application of fractionation by increasing the temperature is shown in Figure 1. The extraction vessel has been combined with a rectification column consisting of a pressure tube packed with stainless steel packings. A heated head of column, the so-called Hot Finger, is fitted onto the top of the column and is held at a higher temperature than the rest of the apparatus. On contact with the Hot Finger the density of the supercritical loaded phase decreases and the less volatile components condense and drop back into the column and are subjected to rectification in the same manner as in a conventional distillation. The product still dissolved in the supercritical phase after passing the Hot Finger is isolated by decreasing the pressure as already described.

2. Fractionation of Fatty Acid Ethyl Esters

As an example of various applications which are investigated at the Max-Planck-Institut für Kohlenforschung in Mülheim-Ruhr in this paper the fractionation of a mixture of ethyl esters of fatty acids is

described. This investigation was concerned with the separation of eicospentaenoic acid (EPA) out of a mixture of fatty acid ethyl esters from codfish oil. The starting material consisted of ethyl esters of saturated and unsaturated fatty acids from C(14) to C(22) partly containing up to 6 double bonds. In order of the high boiling points of these esters a conventional vacuum distillation needs relatively high temperatures so that, first, decomposition cannot be excluded and, second, a separation into single components is hardly possible.

In co-operation with the NIPPON SUISAN KAISHA,LTD - TOKYO (Japan) it was tried to fractionate such a mixture, the composition is shown in table 1, by using supercritical carbon dioxide to isolate a C(20-5)-rich fraction. (x-y) means the ethyl ester of a fatty acid with x carbon atoms and y double bonds.

Table 1 Composition of the Codfish Oil

Acid	%	Acid	%
14-0	5.80	20-1	11.43
15-0	0.19	20-4	0.50
16-0	12.88	20-5	14.46
16-1	9.79	22-1	8.64
18-0	2.66	22-4	0.43
18-1	23.25	22-5	0.49
18-2	0.16	22-6	5.74
18-4	2.19		

In a series of experiments carried out in an equipment similar to that shown in figure 1 various conditions were investigated to optimize this procedure, mainly the following:

1. The increase of the temperature of the Hot Finger in order to increase the the reflux ratio.
2. The increase of the pressure to get a higher loading of the supercritical phase.
3. Variation of the length of the column and of the packings

In all these experiments the temperature of the extraction vessel, column and separator was kept constant at 50°C, the supercritical loaded phase was expanded to 25 bar in the separator and the flow rate of the supercritical carbon dioxide amounted to about 25 l/h. Samples of the loaded supercritical phase after passing the Hot Finger were analyzed each hour by gaschromatography.

2.1 Variation of the Temperature of the Hot Finger

2.11 Without the Hot Finger

The first experiment was carried out without the influence of the Hot Finger that means, the temperature of the Hot Finger was kept also at 50°C. The starting material was divided into 10 fractions by SCF extraction with supercritical carbon dioxide. It shows that no separation comes off, only an enrichment of the lower boiling esters C(14) and C(16) in the first fractions and of C(20) and C(22) in the later fractions according to their boiling points.

2.12 With the Hot Finger

The variation of the temperature of the Hot Finger really led to an increase of the reflux ratio but the selectivity decreased by exceeding the temperature of 90°C.

The curves in figure 2 show the difference in selectivity at the two temperatures 90 and 100°C. Here out of the whole mixture only the content of two components in the supercritical loaded phase, that are the sum of C(16)- and C(20)-esters analyzed by GC, are plotted versus the extraction time. To get a high purity combined with a yield as high as possible at 90°C one is able to collect a fraction amounting to 13.5 % of the starting material containing 50 % of the C(20)-esters of the feed-stock with a purity of 96.2 %. At 100°C it is only possible to collect 25.7 % of the C(20)-esters with a maximum concentration of 85.5 %.

2.2 Variation of Pressure

The loading of the supercritical carbon dioxide depends on the pressure of the system. Under constant conditions of temperature and flow rate of the supercritical carbon dioxide the increase of the loading with raising the pressure can be demonstrated by the extraction rate: at 150 bar 15 g/h extract could be isolated, at 170 bar the amount was 55 g/h and at 200 bar 140 g/h. But the higher extraction rate was accompanied by a decrease in selectivity, at 200 bar no fractionation could be realized.

2.3 Results of Optimization

The results of these optimization experiments suitable only for the equipment we used are listed in table 2.

Table 2 Conditions and Results of Optimization

Nr	Temperature Hot Finger (°C)	Pressure (bar)	Rate of Extraction (g/h)	Max. Content (%) *)	50 % Yield C(20)-esters Extract (%) **)	Purity (%)
01	80	120	8.2	84.2	17.2	75.0
02 ***)	80	120	13.1	92.2	14.4	86.8
03 ****)	80	120	12.8	55.6	25.1	50.3
04	90	200	138.5	no fractionation		
05	90	170	55.3	no fractionation		
06	**90**	**150**	**14.7**	**98.9**	**13.5**	**96.2**
07	120	200	38.2	45.3	42.8	33.0
08	120	170	12.4	89.3	15.7	80.7
09	120	150	7.8			
10	100	150	15.8	92.7	14.7	84.5

*) of C(20)-esters in the loaded supercritical phase (without CO_2)
**) related to the starting material
***) with smaller packings
****) without packings

In all these experiments the extraction temperature, the length of the column and the flow rate of the supercritical carbon dioxide were kept constant. Besides the reaction conditions in this table the results of the fractionation are listed in relation to the isolation of the sum of C(20)-ester.s In this table the maximum content means the maximum concentration of C(20)-esters in the supercritical loaded phase during the extraction, analyzed by GC. Next to the last column of the table shows the amount of extract including 50 % of the C(20)-esters,s related to the starting material. The last column shows purity of this fraction.

The best result was obtained in the experiment 06 with a temperature of the Hot Finger of 90°C and a pressure of 150 bar. Both at higher temperatures and higher pressures the selectivity of the fractionation decreases.

2.4 Two-step Extraction

The last experiments have shown that it is impossible to get a higher yield than 50 % with a purity of more than 90 %. Under the best conditions described above it should be tried to raise the yield of C(20)-esters by a two-step extraction procedure.

2.41 First Fractionation Step

In this experiment the codfish oil was extracted with supercritical carbon dioxide and by means of the hourly GC-analyses of the loaded supercritical phase several fractions were collected. In the first fraction all extracts were joined in which no C(20)-esters could be detected. In the second fraction the extracts up to 10 % C(20)-esters were collected and in the third fraction the extracts which contain the last traces of C(16)-esters. The next fraction contained only C(18)- and C(20)-esters of different composition. After the content of C(20)-esters of more than 90 % in the supercritical phase was reached the main fraction was collected until the content again reached 90 % after passing a maximum content of about 99 %. The next fraction consisted only of C(20)- and C(22)-esters in various combinations. When the value of the C(20)-esters was lower than 2 %, then the rest of the inserted material was extracted without using the Hot Finger. This last fraction besides C(22)-esters contained some not identified higher molecular components. Figure 3 shows the fractionation curves where the composition of the mixture dissolved in the supercritical phase is plotted versus the extraction time respectively versus the amount of extract in percent of the starting material.

The main fraction contains 48.2 % of the C(20)-esters which have been containing in the original starting material with a purity of 95.8 %, this is the first part of the desired product.

2.42 Second Fractionation Step

The fractions got in the first fractionation step containing only C(18)- and C(20)-esters respectively C(20)- and C(22)-esters were combined to give the new starting material for the second fractionation step. The first and the last fraction which contained only C(14)- to C(18)-esters respectively C(22)-esters were rejected.

Fraction 2 with the highest concentration of C(18)-esters was stored separate. This new starting material amounted of 24.5 % of inserted material of the first fractionation step. The composition, analyzed by gaschromatography, was as followed:

C(16)-esters	traces
C(18)-esters	23.56 %
C(20)-esters	45.28 %
C(22)-esters	28.74 %

This mixture was fractionated into 5 fractions under the same conditions as used in the first step. In table 3 the results of the GC-analyses are listed.

Table 3 Composition of the Fractions of the Second Step

Nr	% Extract	% C14	% C16	% C18	% C20	% C22
01	25.5	----	1.3	76.1	20.8	----
02	17.3	----	----	25.3	73.3	----
03	**21.2**	**----**	**----**	**1.6**	**97.5**	**0.6**
04	10.8	----	----	----	48.6	51.3
05	24.3	----	----	----	0.6	98.0

In this fractionation step it was impossible to get a fraction without C(20)-esters. Therefore the first fraction was collected until the content in the supercritical phase reached about 50 %, in this fraction the main portion of C(18)-esters was found. Fraction 3 was collected in the same manner as the main fraction in the first step, herein all extracts were combined in which the content of C(20)-esters was higher than 90 %. The last fraction, a very clean C(22)-ester mixture, was extracted without the Hot Finger.

Fraction 3 consists of 45.7 % of the C(20)-esters in the starting material of the second step, respectively about 20 % related to the original Codfish oil with a purity of 97.5 %. If fraction 2 and 3 are mixed the yield of C(20)-esters raises up to 73.8 % in course of which the purity decreases to 86.6 %.

2.43 Results of the Two-step Fractionation

If the main fraction from the first step and fraction 3 from the second are mixed one gets a portion of extract which contains 67.7 % of the C(20)-esters in the original ester mixture with a very high purity of 96.3 %. Including fraction 2 from the second step, the yield increases to 80 % with the sufficient purity of 92 %. This mixture contains 77 % of the C(20-5)-ester of the inserted codfish oil.

3. Conclusions

It could be demonstrated that it is possible to separate a mixture of high boiling fatty acid ethyl esters into single components by fractionation using supercritical carbon dioxide at an extraction temperature of 50°C. Regarding the areas of the single C-numbers a rather sharp separation could be achieved. In the case of the C(20)-esters the best results were obtained but also the C(18)-esters and the C(22)-esters could be isolated with a high purity.

In the experiments described the fractions containing only C(18)- and C(22)-esters besides the desired C(20)-esters were fractionated separately in a second extraction step. The better procedure would be to recycle this portion to the starting material to enrich the concentration of the desired esters in order to increase the yield of these esters in one extraction step. Such a procedure could be carried out in the following manner: In a dicontinuous process the fractions containing only C(14)- and C(16)-esters respectively C(22)-esters were rejected, the fraction with the highest concentration of the desired esters would be the final product and all other fractions would be recycled to the process.

The main assignment of these investigations was to separate most of the C(20)-esters in high yield and high purity. It seems that it is possible to enrich the C(20-5)-ester by a suitable fractionation. But these experiments have also shown that it will be rather difficult to achieve a clean separation of C(18-1)-, C(20-5)- and C(20-1)-esters because of their similarity, the C(20-5)- and the C(20-1)-esters differ only in 8 H-atoms, i.e. 2.4 % in molecular weight related to the molecular weigth of 332.6 for eicosapentaenoic acid ethyl ester.

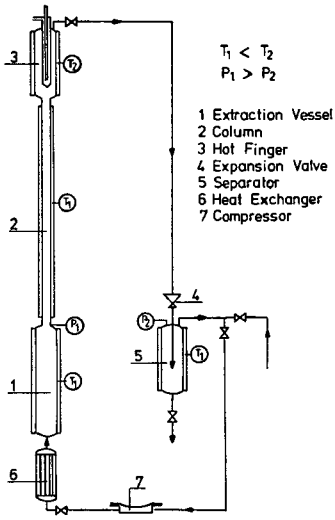

Figure 1 Fractionation Apparatus with Hot Finger

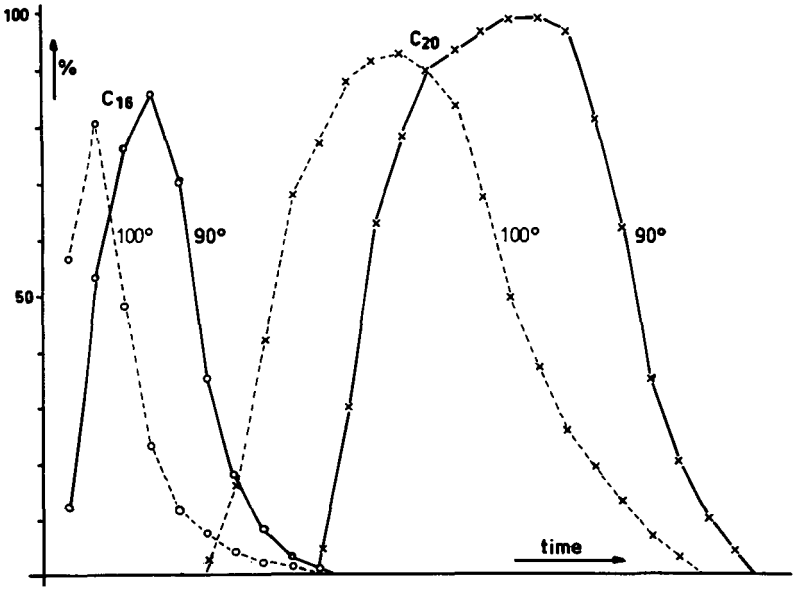

Figure 2 Separation Curves at 90 and 100°C

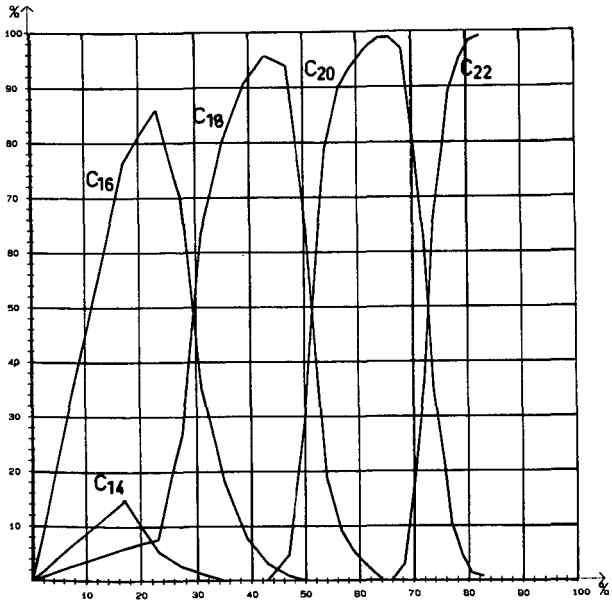

Figure 3 Separation Curves (Composition in Supercritical CO_2)

SEPARATION OF BUTADIENE BUTENE MIXTURE WITH MIXTURES OF AMMONIA AND ETHYLENE IN NEAR CRITICAL CONDITIONS

D.S. Hacker, Amoco Chemicals, Naperville,Il.,60566

Abstract

We describe the results of an investigation into the separation of mixtures of 1,3-butadiene and 1-butene conducted at near critical conditions. Selected solvents and solvents containing ammonia as an entrainer are compared with respect to their selectivity in removing 1-butene from this close boiling mixture. Separation factors of 1.4 to 1.8 at a pressure of 600 psig and a temperature of 20 C are observed for mixtures containing 5%-8% ammonia in ethylene . Pure solvent gases, on the other hand,such as ethane,ethylene, and carbon dioxide show no selectivity. This is also true for ethane /ammonia mixtures which also appear poor as separating agents for this mixture. Experimental results are compared with values predicted by a modified two parameter corresponding states equation with reasonably good agreement. A case is made for the choice of an entraining component to be made on the basis that it contributes a chemical property to the system enabling the same selection criteria described by Elgin to be used in SC processes as are in liquid-liquid extraction or extractive or azeotropic distillation processes.

Introduction:

An alternative separation process is much to be desired to replace the more conventional azeotropic or extractive distillation used in the separation of closely boiling mixtures. There is a need to reduce both the energy costs associated with solvent recovery and costs due to loss of the expensive solvent . Ideally suited to the task would be a separating agent that could be readily flashed off, leaving a relatively pure product behind, assuring almost complete recovery of the solvent with a minimum expenditure of energy. Supercritical and near critical extraction where retrograde condensation and vaporization occur may be candidates for this task.

The separation of liquid mixtures by near critical solvents is still a relatively new technology. The lack of experimental phase equilibria data for many liquid systems and the dearth of solubility data for either critical gaseous solvents in liquid mixtures or for solutes dissolved in critical solvents makes any realistic design difficult. Some estimate can be obtained from an understanding of the general physical chemical principles involved,but ultimately each system must be addressed individually and its characteristics determined experimentally. In the discussion that follows, an experimental investigation was undertaken to determine the applicability of mixed solvents, near their critical conditions to the separation of butadiene from mixtures with 1-butene.These results are compared with predictions obtained from a representative equation of state in the region of the solvent-solute critical solution envelope.

Theoretical Discussion:

The recovery of butadiene from a mixed C4 olefin stream has all of the characteristics of an energetically difficult separation resulting from the almost pinched VLE conditions existing in this mixture. As is shown in Table I, the physical properties of these components are almost identical with the exception of the large dipole moment of the 1-butene. Conventional distillation is impractical since the relative volatility of many of the C4 compounds are reasonably close to unity. A separation,nevertheless, can be effected provided a suitably polar solvent is used to selectively remove the butene. The influence of polarity can be exploited in this separation by "salting out" the more nonpolar compound(1).

As a result,virtually all industrial practice for the recovery of butadiene currently makes use of extractive distillation with an entrainer such as acetonitrile or some other strong organic base to enhance the relative volatility of the components. The potential of achieving an equally effective separation through the introduction of a mixture of a solvent and an entrainer exhibiting polar properties close to its critical solution conditions is intriguing. Ammonia, a polar gas, has already been shown to act as an effective solvent(2) for this separation although at pressures much below its critical. Its use as a supercritical solvent for this separation would be also feasible were it not for its very high critical temperature (405.45 K) which favors the polymerization of the butadiene. A method developed in this work and described in a recent publication (3) makes use of a supercritical mixture of solvents which in combination provides the chemical as well as the physical conditions for the most efficient extraction of the 1-butene solute in the mixture within the limitations imposed by the thermal stability of the system.

The ability to effect the separation of various liquid solutions in the presence of a supercritical or near critical component has been adequately demonstrated(4). In general, these solvents tend to be either inorganic gases or light hydrocarbons such as carbon dioxide, ammonia,ethane, ethylene, or propane. For example, Weinstock and Elgin (5) used pressurized ethylene to promote the separation a number of miscible aqueous-organic liquid mixtures. Through the introduction of a solvent at or near critical conditions one can effect separation by forming multiple phases. The distributed component may concentrate in either one of the newly created phases. More recently several practical processes have been developed that use carbon dioxide to efficiently dehydrate ethanol(6).Deashing and the physical separation of asphaltines by supercritical propane have been commercially developed(7). Starling et al recently applied this concept to the separation of light hydrocarbons such as n-butane and n-decane(8). The theory of separation of multicomponent mixtures by SC solvents is now of current research interest with several papers devoted to the application of concepts of continuous thermodynamics(9,10) to handle multicomponent mixtures as well.

Reid and others(11,12) have shown that supercritical solvents show varying degrees of selectivity towards a particular solute. This is not surprising since the same principle that applies in liquid solvent selection should apply in the case of SC solvents. Because of the limited number of SC solvents available, the application of SC extraction to a broad range of systems is very limited. One way of increasing the applicability of the technique is either to find ways of expanding the solvent category, which does not seem likely at this time, or to develop methods of modifying existing solvents. Since the maximum selectivity of the solvent occurs when its critical temperature matches the extraction temperature, a match between the solute and the SC solvent is not always possible with a single solvent.

To circumvent this difficulty, Brunner(13) introduced an entrainer whose function is to modify the chemical activity of the solute mixture sufficiently to enhance the separation. This was put to use in the extraction of triglycerides from a mixture of polyglycerides using carbon dioxide with acetone as an entrainer. The entrainer served as a source of hydrogen bonding to augment the separation of the desired component. The principle of the entrainer in improving separation has been widely known in liquid extraction processes and described by Treybal(14).

A ternary nonideal solution, for example, will generally exhibit a minimum in one of the pairs of activity coefficients. The addition of a second solvent, if properly selected, may further lower the activity coefficient of the solute and increase its concentration in a given phase(15). The addition of a second component to an SC solvent will result in configurational effects that enhance the extraction of a pure solid. It can be shown theoretically that a binary SC solvent at pressures close to the critical envelope will also have a strong influence on the solubility of the solid solute(16). How well this principle can be extrapolated to multicomponent solids or liquid systems is still to be determined.

In this study, we have measured the degree of extraction of butene from a binary mixture of butadiene/ butene with various solvents eg. ethane, carbon dioxide,ethylene, ammonia and ethylene and ammonia and ethane solvent mixtures in the region of critical solution pressure of the solvent mixture. The experimental results are then compared with the VLE calculations for this system using a newly developed corresponding states equation devised by Ely and Mansoori(17).

The primary features of the equation are a new generalization for the shape factors and the use of propane as its reference component. The equation allows for the inclusion of multicomponent mixtures. The model has been successfully used with non-polar compounds and for a small number of selected polar compounds. It correctly represents liquid-vapor phase relations in the region of the critical, but does not specify the formation of a second liquid phase. The mixing rules, defined as aij = (aiixajj)1/2 (1-kij) and bij = {(biil/3 +bjjl/3)/2]3, are then adjusted to account for the enhanced polar contribution of ammonia-butene through the interaction parameters,kij,and bij. All other interaction coefficients were set to kij = 0 and bij = 1. It is recognized that such a simplified model is in serious error since the polar and hydrogen bonding contributions are ignored. Nevertheless, it does permit one to obtain a "ball park" estimate of the separation likelihood. The results of these VLE flash calculations are then compared with our experimental results.

Experimental

Near-critical extraction experiments were carried out in a one-liter,stirred, stainless steel Autoclave(MR #7331), rated at 5000 psig at 600 F. Phase separations were monitored through an attached 50 cc Jerguson sight gauge (rated at 5000 psig at 72 F) which also served as a level indicator. A complete schematic of the assembly is shown in Fig.1. The autoclave was maintained at constant temperature by means of an external heating tape and an internal cooling coil. Cooling was furnished by a circulating water Freon refrigeration unit. An Autoclave magnetic stirring unit powered by an air motor was used to ensure adequate mixing of the sample volume. All lines were heat traced with electrothermal heating tapes. The reactor was depressurized before each experiment by venting the system and then evacuating the chamber under reduced pressure to ensure the complete removal of residual mixture and air from the system. Filling of the vessel was accomplished through a feed port at the base of the reactor. The samples of the upper and lower phases was removed through small bore (1/8 ") tubing through the head of the reactor and at the bottom of the reactor. No provision was made to sample any second liquid phase that may appear during an experiment.

Volumetric measurements obtained from observations through the sight glass of the Jerguson guage and were used to determine the the molar volume of all liquid components used to make up the charge. A calibrated platinum thermocouple was used to measure the temperature of the contents of the autoclave reactor. The pressure of the system and of each of the receiver vessels were measured with calibrated high pressure precision Bourdon tube guages of appropriate range. The guage glass window was calibrated to give a direct reading of the volumes of the liquids added. When ammonia was used in the solvent makeup, it was added to the contents before the addition of the pressurizing solvent gas.

Ammonia was fed through a second Whitey pump into a storage cylinder that could be independently cooled to ensure minimum vaporization of the ammonia before admitting it to the reactor. The ammonia was added under a slight helium pressure to minimize liquid vaporization at the surface and to allow for a measurement of a quiescent interface.

The solvent gases, ethylene, carbon dioxide, or ethane, were fed by a Haskel gas compressor, Model AG-62, a 25-1 air driven compression pump with a maximum outlet pressure of 9000 psig. The quantity of these gases introduced into the autoclave was determined by measuring the weight change of the gas cylinder and separately by a measurement of the change of the liquid level resulting from gas dissolving in the liquid during pressurization. The difference between the liquid level and the total volume of the vessel was measured and the second phase volume determined.

Chemically pure grade butene and butadiene were supplied in cylinders by Matheson Co. and used as received without further purification. The hydrocarbons were fed to the reactor through an LP10 Whitey laboratory positive displacement pump. A 30-pound nitrogen head was added to each hydrocarbon cylinder to maintain adequate pumping efficiency.

Heating controls were manually adjusted and the temperatures were indicated on a 10- point Acromag. The heating zones of the reactor were controlled by three Eurotherm 103 with voltage controlled manually by Variacs. The remaining sections were heat traced with self-limiting autotrace heating tapes to prevent condensation in the lines.

Sample Analysis:

The contents of the reactor were sampled before and after the introduction of the solvent gas and entrainer by trapping approximately 1 cc of the mixture from the reactor volume in a precalibrated volume of sample line located between two high pressure valves, adjacent to the vessel. The volume of the sample withdrawn was suffiently small to minimize any changes in the pressure of the main contents of the vessel. Once trapped,the high pressure sample was further expanded into a pre-evacuated 300 cc Hoke cylinder to about 5 atm. This volume of sample was again expanded into a final 70-cc Hoke cylinder to about 1 atm. Portions of this volume were introduced into the Valco valve located at the Varian 920 Gas Chromatograph. All sample loops were heat traced as well to prevent condensation in the lines. This procedure was followed in sampling the lower portion of the liquid phase as well. An additional sample port was installed in the low pressure cylinder for syringe sampling to provide an additional check on the accuracy of sampling procedures.

The pressure of the gas was slowly increased until the liquid interface disappeared, indicating the attainment of the critical region. The gas pressure was then reduced by slightly depressurizing the chamber until the interface just reappeared. It was established that this procedure permitted the contents to be within 2 to 3 psi below the region of the critical. After stirring for about five minutes, the system was allowed to equilibrate before vapor and liquid phases were sampled.

Samples withdrawn from the upper and lower sections of the reactor autoclave were analyzed in the G.C. using a thermoconductivity detector with a 20', 1/8" VZ-7 packed column with helium used as the carrier gas. The G.C. was run with the injector set at 115 C, the column oven temperature at 60 C, and the detector set at 115 C. Filament current to the detector was set at 150 ma.

Samples were injected into the column by an air-operated Valco valve, which was controlled by a timer- controlled solenoid. The detector output was integrated and a concentration analysis was performed by an Autolab System. A Leeds and Northrup recorder was used to monitor the condition changes, and peak shapes, and composition analysis. The larger volume of solvent to solute required a change in sensitivity to adequately monitor the butadiene and butene peaks. A typical record of the GC output is shown in Fig.2 and indicates the integrated values of the represented peaks of the solvent gas, and butene and butadiene. The equilibrium compositions for each run are obtained in this manner and with the initial mixture composition tie lines of the system can be generated. The entrainer-solvent gas are considered as a pseudosolvent of fixed composition. The results of the measurements obtained for the 8% ammonia/ethylene are represented in the ternary diagram in Fig.3. Butene is represented as the distributed component with the butadiene as the heavy component.

Results:

The ratio of the integrated peaks for butene(i) and butadiene(j) was used to determine the separation factor, B, where the separation factor is defined as

$$B = \frac{\{yi/xi\}\text{solvent phase}}{\{yj/xj\}\text{heavy phase}} \qquad (1)$$

The results shown in Table II and III are representative of the data collected for the studies conducted with ethylene and ethylene/ammonia and ethane and ethane/ammonia solvent mixtures. Table IV shows some selected data for other solvents and solvent mixtures as well. The results of extraction conducted with pure ethylene, carbon dioxide, and ethane in all cases showed no evidence of appreciable separation. In each set of experiments with single solvents, the same ratio of butadiene to butene was obtained in both phases. The butadiene/butene mixture is distributed in each phase in amounts that are primarily a function of the extracting gas and the temperature and pressure of the system.

Runs were made with several mixtures of ammonia/ethylene and ammonia/ethane with varying concentrations of ammonia. For both of these mixtures a separation of the butadiene was achieved, but the effect of the ethylene as a preferred solvent is most pronounced. The butene appears to concentrated in the vapor phase in agreement with the findings of the earlier pure ammonia study(2). A series of experiments were also conducted to determine the temperature and pressure conditions in which maximum separation could be attained. For the ethylene/ hydrocarbon/ 8 % ammonia mixtures, this was found to be at 20 C and 600 psia. The maximum occurs at a pressure below the critical solution temperature determined by Lentz(18) for the ethylene/ammonia binary (Fig.4). The experimental selectivity was observed to decrease with an increase in pressure with an accompanying increase in the loading in the solvent phase. The selectivity is also reduced as the temperature rises all other things being equal(Fig.5).

Discussion

The results obtained in this study are by no means comprehensive and cover only a narrow range of variables. However, they indicate the maximum effect of entrainer enhancement on the relative volatility of an otherwise close-boiling mixture through the addition of 8% ammonia/ethylene solvent mixture close to its critical solution conditions. The relatively large selectivity achieved of 1.4 to 1.8 is to be considered in light of the value obtained for pure liquid ammonia of 1.63 reported by Poffenberger(2). Moreover, it is shown that the use of a solvent and an entrainer solvent permits the separation to be effected at temperatures and pressures lower than would have been otherwise predicted had pure critical ammonia been used,a result also observed by Fong et al(19) in studies of mixed solvent extraction of coal. An explanation for the lower than expected pressure for the separation is the likely formation of a Class IV mixture according to Van Konynenburg(20). It has been observed in

several systems containing ammonia and aromatics that a second liquid phase is formed under lower pressures than expected if the mixture behaved as an ideal Class I system. The P-T projection for these classes of mixtures is shown in Fig.6. A lower critical solution temperature (LCST) and an upper critical solution temperature (UCST) are the boundaries for the VLL phases observed to be present in these experiments. The critical points are the values for the two pseudo-components. Despite the fact that these phase relations are similar to those observed for a number of binary mixtures, one can consider the present mixture as a pseudo-binary system in which the solvent mixture, comprising ammonia and excess ethylene/ or ethane and a hydrocarbon phase of butadiene and butene exhibiting very similar vapor pressures.

The enhanced solubility of the solvent in the solution phase is evidenced in Table II by the large concentration of the ethylene present in both phases. An estimate of the volume of solvent added to the hydrocarbon mixture was obtained by calculating the difference in the liquid level before and after gas solvent addition. This is approximately the volume of gas dissolved in the liquid phase. This value is added to the volume above the liquid interface to obtain the total solvent added to the system. The volume of ethylene/ammonia solvent mixture added to the volume of butadiene/butene solution was approximately 5:1.

A comparison of the calculated selectivities obtained for the ethylene mixtures given in Table II can be made with the results in Table III obtained for the ethane system. These differences cannot be explained solely in terms of the critical properties of the respective gases. Usually the efficiency of extraction of a given solvent towards a particular solute is related to the proximity of the extraction temperature to the critical temperature of the solvent. The ratio of the two temperatures, Text/Tc, or the effective reduced temperature should be unity or somewhat greater to maximize separation. For a gas of given critical temperature, the reduced temperature is inversely proportional to the solubility of the solute in the solvent.Since ethane has a reduced temperature more nearly equal to unity at the extraction conditions at 20 C (Tr = .98) as compared with ethylene (Tr = 1.47), one would expect the ethane mixtures to be a better solvent for the butene. That this is not the case suggests an alternative explanation would be that the ethylenic double bond structure has a greater chemical affinity for the olefins in the solution phase which may account for the enhanced solubilty of the butene in the ethylene phase. This is in addition to the chemical synergistic effect exerted by the ammonia which further increases the solubility of the butene in the vapor phase.

These results are also compared with calculated values obtained from the equation of state using kij = 0.8. Solvent to feed ratios as well as the effect of ammonia concentration in the solvent were independently varied to match the experimental data. The effect increasing ammonia concentration at constant pressure and temperature in both ethylene/ammonia and ethane/ammonia solvent mixtures are shown in Table V. The separation factor increases proportionally to an increase in entrainer concentration and appears to have a more important influence than either temperature or pressure. This is in contrast to the experimental observations in which the selectivity achieves a maximum at an ammonia composition of 8%. A comparison of these experimental findings with both the predictions of the present model and the Prausnitz model for the solubility of solute in mixed SC solvents suggests that chemical factors such as synergistic effects cannot be ignored and are likely to have a greater effect than anticipated. The vapor liquid equilibrium predictions are, in general, in fair agreement with the results of these experiments.

Conclusions:

1. The information presented in this study indicates the degree of mixing critical solvents with an appropriate component whose hydrogen bonding or polarity will enhance the separation of a close boiling mixture of butene-butadiene.

2. A maximum value in the selectivity of 1.4 - 1.8 can be achieved with a 5 - 8% ammonia concentration in ethylene for the butadiene - butene separation. This is in agreement with the predictions of the Ely-Mansoori equation of state. However, the presence of a maximum in the selectivity is not predicted by the model, suggesting the synergistic effect of the ammonia in the solvent rather than a concentration effect which is proportional to the added entrainer.

3. Ethylene/ammonia mixtures are more effective solvents for the separation of this mixture than is ethane/ammonia mixture with the same concentration of ammonia. It is suggested that ethylene because of its greater chemical similarity in the butene/butadiene solution exerts a greater influence on the binary activity coefficients of the system.

TABLE I

PROPERTIES OF C4 COMPONENTS

PROPERTY	1-BUTENE	1,3-BUTADIENE
Molecular Wt.	56.11	54.09
Critical Temp, C	146.4	152.20
Critical Press.MPa	4.019	4.329
Critical Vol. cc/mole	4.276	4.083
Normal BP.C	-6.25	-4.411
Solubility Param.	4.7504xE04	4.8694xE04
Dipole Mom. Debye	0.34	0.0
Acentric Factor	0.1867	0.1932

PROPERTIES OF SOLVENTS

PROPERTY	ETHANE	ETHYLENE	CARBON DIOXIDE	AMMONIA
Molecular Wt.	30.07	28.05	44.01	17.03
Critical Temp,C	32.27	9.21	31.04	132.50
Critical Press. MPa	4.88	5.03	7.38	11.27
Critical Vol. cc	4.919	4.601	2.136	4.255
Normal BP,C	-88.60	-103.7	-	-33.43
Solubility Coeff.	3.9134xE04	3.932xE04	4.605xE04	9.239xE04
Dipole Mom.Debye	0.0	0.0	0.0	1.47
Acentric Factor	0.09896	0.085	0.2276	0.2520

TABLE II

BUTADIENE-BUTENE-ETHYLENE-AMMONIA EQUILIBRIUM COMPOSITION

NH_3 (%)	--- Solvent Phase (%) --- C_2H_4	Butene	Butadiene	---Butadiene Phase (%) -- C_2H_4	Butene	Butadiene	Beta
			At T = 20° and P = 600 psia				
0	88.351	3.768	7.881	45.940	17.470	36.584	1.00
0	88.425	3.763	7.839	38.338	19.765	41.901	0.99
0	69.694	14.932	15.374	71.997	13.092	14.911	1.10
2.3	82.199	8.828	8.973	58.461	17.483	20.879	1.17
5.0	89.063	6.936	4.001	52.675	23.890	23.435	1.70
5.0	88.879	6.903	4.218	40.109	30.149	29.742	1.61
5.0	76.970	15.069	7.961	58.039	22.047	19.914	1.71
5.0	75.469	15.505	8.448	55.886	23.201	20.913	1.61
5.0	89.132	8.805	2.064	38.799	47.751	13.450	1.20
8.0	91.066	2.629	6.305	46.473	12.884	39.303	1.27
8.0	85.908	3.288	8.151	44.928	13.157	40.645	1.24
8.0	86.668	11.710	1.622	47.847	41.382	10.771	1.88
8.0	86.775	11.737	1.488	49.963	39.604	10.433	2.08
8.0	69.579	19.803	10.618	49.100	27.951	22.949	1.53
10.0	59.583	27.028	13.389	39.981	36.671	23.348	1.29
10.0	60.217	26.028	13.389	41.815	35.692	22.493	1.32
10.0	74.642	19.423	5.984	66.140	25.400	8.451	1.10
			At T = 20°C and P = 800 psia				
2.3	70.166	13.873	15.960	34.716	28.791	36.493	1.10
2.3	69.498	14.112	16.389	43.984	24.539	31.477	1.10
5.0	76.947	12.740	10.312	74.065	14.520	11.415	1.05
5.0	77.599	12.566	9.835	74.093	14.494	11.413	1.00
10.0	81.026	7.044	11.930	67.741	11.236	21.021	1.10
10.0	80.266	3.354	12.183	67.009	11.767	21.224	1.12
			At T = 20°C and P = 1100 psia				
0	69.694	14.932	15.374	71.997	13.092	14.911	0.90
0	81.759	8.583	8.713	73.607	12.124	14.270	0.86
5.0	84.760	8.380	6.860	77.316	11.457	11.227	0.84
5.0	84.074	8.457	7.451	74.816	12.849	12.335	0.92
			At T = 40°C and P = 600 psia				
5.0	85.128	8.416	6.456	34.556	34.501	30.943	1.17
5.0	86.617	7.812	5.571	29.325	37.302	33.372	1.25
			At T = 60°C and P = 600 psia				
5.0	75.099	11.814	8.756	19.215	42.621	38.163	1.21
5.0	74.163	12.412	9.471	20.693	41.856	37.451	1.17

TABLE III

BUTADIENE-BUTENE-ETHANE-AMMONIA COMPOSITION

EXPERIMENTAL VALUES

TEMP C	PRESSURE PSIA	NH3 %	SOLVENT PHASE C2H6 yi	SOLVENT PHASE BUTENE yj	SOLVENT PHASE BUTADIENE yk	BUTADIENE PHASE C2H6 xi	BUTADIENE PHASE BUTENE xj	BUTADIENE PHASE BUTADIENE xk	SELECTIVITY B
20	900	4.18	76.258	10.925	12.817	74.367	11.568	14.065	1.0
		4.18	76.505	10.834	12.661	74.993	12.079	12.929	1.09
		4.18	74.654	11.232	14.113	75.137	12.667	12.169	1.31
	620	6.97	90.406	3.998	5.596	85.647	5.830	8.523	1.04
	640	6.97	90.107	4.123	5.770	83.324	6.804	9.871	1.03
17	725	6.97	87.224	5.220	7.556	88.497	4.817	6.686	1.00
	725	6.97	87.387	5.181	7.432	88.766	4.497	6.737	1.05
	1060	6.97	88.840	4.489	6.689	93.178	2.751	4.071	1.00
	1060	6.97	88.90	4.443	6.657	93.086	2.801	4.113	1.00
19	675	6.97	85.525	7.426	7.229	88.073	6.047	5.879	1.00
	675	6.97	86.137	7.105	6.758	87.789	6.295	5.914	1.00
18	600	6.97	88.024	6.135	5.841	85.503	7.379	7.117	1.01
	600	6.97	87.722	6.201	6.077	85.812	7.185	7.002	1.00
16	550	6.97	95.867	2.252	1.977	76.208	11.624	12.168	1.19
18	600	6.97	83.134	10.507	6.358	80.277	11.959	7.577	1.05
	600	6.97	82.572	10.834	6.594	80.176	12.228	6.044	1.02
20	700	6.97	87.532	7.907	4.561	84.122	9.834	6.044	1.06
	700	6.97	87.295	8.009	4.696	83.794	10.026	6.180	1.05
22	525	1.85	89.169	5.166	5.664	69.808	15.252	14.939	1.0
	525	1.85	93.286	3.828	2.886	67.462	16.489	16.049	1.28
	525	1.85	92.362	3.900	3.737	78.235	11.064	10.701	1.01
	1100	1.85	88.100	6.345	5.555	78.508	11.205	10.288	1.04
	1100	1.85	87.700	6.328	5.973	78.581	11.078	10.341	1.00
23	550	0	82.754	8.164	3.668	53.113	22.449	24.438	1.00
	550	0	92.243	9.091	4.089	55.308	21.121	23.570	1.00
	1075	0	77.928	10.633	11.438	72.545	13.088	14.367	1.00
	1075	0	77.279	11.078	11.693	75.175	12.095	12.730	1.01

TABLE IV

SEPARATION OF EQUIMOLAR MIXTURES OF BUTENE-BUTADIENE WITH VARIOUS SOLVENTS

EXPERIMENTAL VALUES

TEMP. C	PRESSURE psia	SOLVENT	SELECTIVITY
6.0	750	C2H4	1.23
40.0	1100	CO2	1.0
22.0	1000	"	1.0
22.0	700	"	1.0
20.0	500	"	1.0
23.0	1100	C2H6/5% NH3	1.0
18.0	700	C2H6/7% NH3	1.06
20.0	900	C2H6/4% NH3	1.09
23.0	550	C2H6/	1.0

TABLE V

EFFECT OF TEMPERATURE AND PRESSURE ON THE SEPARATION OF EQUIMOLAR BUTENE BUTADIENE SOLUTIONS USING NEAR CRITICAL AMMONIA-ETHYLENE MIXTURES AS SOLVENTS

CALCULATED VALUES BY ELY-MANSOORI MODEL

kij=0.8 , all others kij=0

MIXTURE	COMPOSITION MOLE FRACTION	S/F	T K	P atm	y butene	K butene	B
NH3/C2H4							
	0.25	20	300	50	0.011	0.405	1.54
			310	50	0.0208	0.460	1.87
		10	300	50	0.0175	0.385	1.29
			305	50	0.024	0.393	1.37
			310	50	0.0317	0.407	1.40
	0.50	10	320	50	0.0332	0.641	2.86
			330	50	0.426	0.786	3.10
			310	40	0.339	0.635	3.94
			320	40	0.433	0.834	4.29
NH3/C2H6							
	0.50	10	320	40	0.0250	0.544	1.96
			330	50	0.0252	0.606	1.65
			350	58	0.0348	0.931	1.10
		20	315	40	0.0129	0.579	2.26
			320	40	0.0173	0.679	2.48
	1.0	10	390	81	0.0331	0.900	0.91
			370	65	0.3636	0.512	1.13
	0.0	2	295	20	0.5501	0.228	1.04

References:

1. Prausnitz, J.M.,"Molecular Thermodynamics of Fluid Phase Equilibria", Chap. 10,Prentice Hall, N.Y.(1969)
2. Poffenberger,N,Horsley,L.H.Nutting,H.S.,Trans. AIChE,42,815,(1946)
3. Joshi,D.K,Prausnitz,J.M.,AIChE Jour.30,522,(1984)
4. Todd, D.B.,Elgin,AIChE Jour.1,20,(1955)
5. Weinstock,J.J.,Elgin,J.C.,Jour Chem Engr.Data,4,3,(1959)
6. Fogel,W.Arlie,J.P.,Revue Franc. Petrole,39,617,(1984)
7. Brule,M.R.,Corbett,J.C.,Hydrocarbon Process. 73,(1984)June
8. Starling,K.E.,Khan,M.A.,Watanasiri,S.,Fundamental Thermodynamics of Supercritical Extraction, Presented Annual Mtg AIChE, San Francisco,Ca. (1984)
9. Prausnitz, J.M.,Fluid Phase Equil.,14,1,(1983)
10. Cotterman,R.L.,Dimitrelis, D.,Prausnitz,J.M.,Ber. Bunsen Gelsch. Phy und Chem,9,796,(1984)
11. Reid,R.C.,Schmitt,N.J.,The Influence of Solvent Gas on the Solubility and Selectivity in SC Extraction, Presented Annual Mtg AIChE., San Francisco (1984)
12. Vasilakos,N.P.,Dobbs,J.M., Parisi,A.S., IEC Process Design,24,121,(1985)
13. Brunner, G. Fluid Phase Equil, Part II,10,289,(1983)
14. Treybal,R.E.,"Liquid Extraction" 2nd Ed.McGraw-Hill,N.Y.(1963)
15. Prigogine,I.,Bull Soc. Chim,Belg.,52,115,(1943)
16. Eckert,C.A., Greiger, R.A.,IEC Process Design,6,250,(1967)
17. Mansoori.G.A.,Ely,J.F.,Density Expansion Mixing Rules,Unpublished (1984)
18. Lentz,H, Franck,E.U.,Extraction by SC Gases, Ed.Schneider,G.M. Verlag Chemie, (1980)
19. Fong,W.s.,et al,Experimental Observations on Systemmatic Approach to SC Extraction of Coal,Presented at National Mtg AIChE, New Orleans,La.(1981)
20. Van Konynenburg, P.H.,Scott,R.L.,Phil. Trans.,Royal Soc.,298,495,(1980)

Acknowledgement:

We are grateful to the AMOCO Chemical Corp. for their support for this work. In particular we express our appreciation for the interest shown in this work by D.E.Hannemann and P.Thornley and to Frank Brooks for his industry and care in carrying out these experiments.

FIGURE 1

EXPERIMENTAL APPARATUS FOR THE MEASUREMENT OF BUTENE - BUTADIENE

SUPERCRITICAL EXTRACTION WITH SOLVENT GASES.

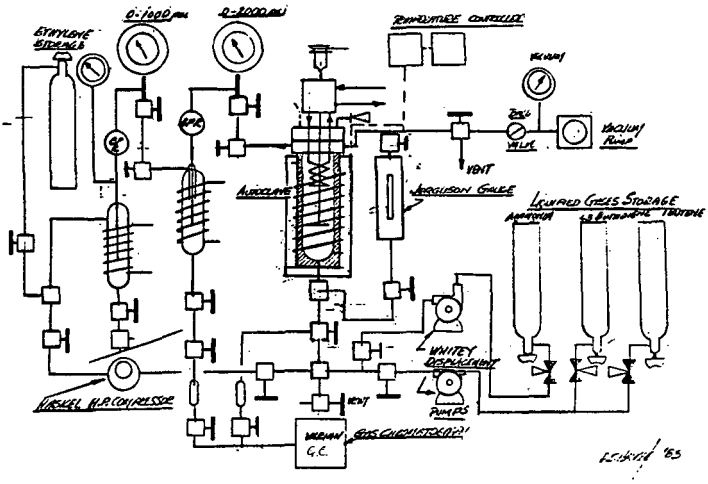

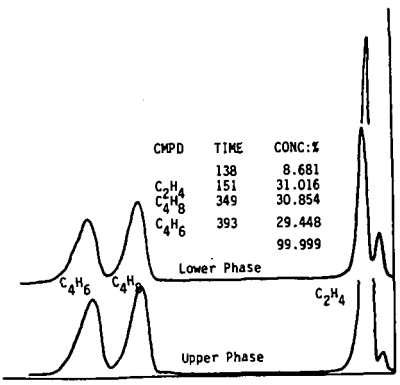

Figure 2. Typical Recorder Output Trace from a VZ-7 Column. Column Temp: 98°C. Time Runs to the Left. Ammonia is not Detected; Air Peak at Extreme Right.

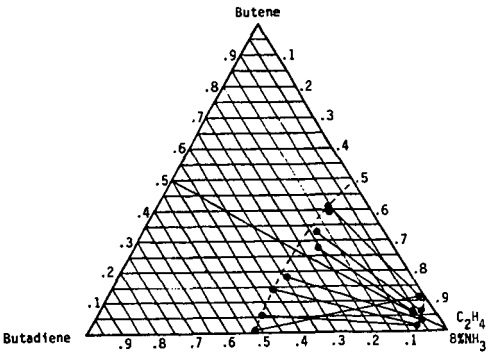

Figure 3. Ternary Phase Equilibrium for the System Butadiene - Butene with a Supercritical Solvent Mixture Ethylene - 8% Ammonia at 600 psi and 20°C. Experimental Points (●).

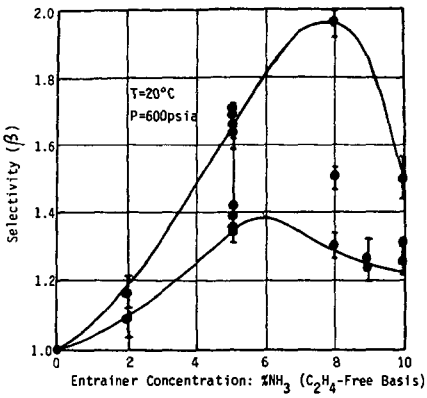

Figure 4. Influence of Entrainer Concentration on the Effectiveness of Solvent Ethylene.

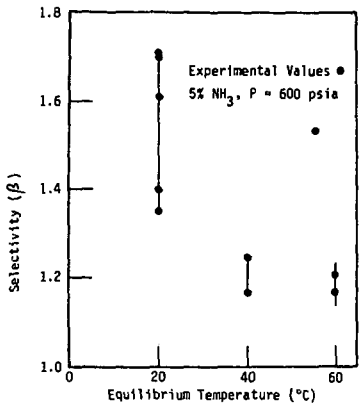

Figure 5. The Influence of Temperature on the Selectivity of Ethylene/Ammonia Solvent Mixtures on the Separation of C_4 Hydrocarbons.

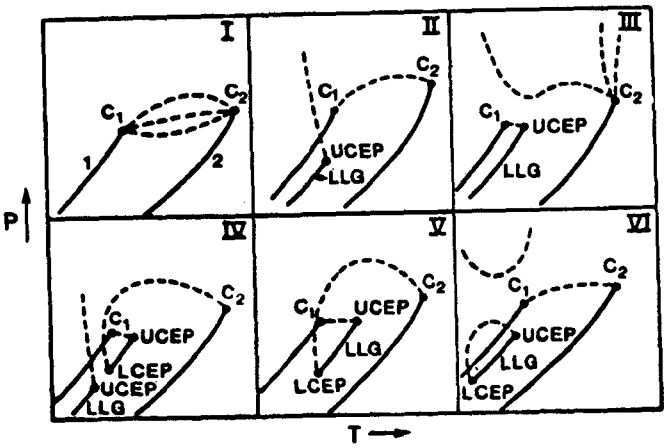

Figure 6. Classes of Different Binary Mixture Fluid Phase Behavior.

BENEFICIATION OF WATER-SENSITIVE EASTERN OIL SHALES

C. A. Audeh

Mobil Research and Development Corporation
Central Research Laboratory
P. O. Box 1025
Princeton, New Jersey, 08540

INTRODUCTION

Development of the eastern oil shale deposits of the US has been considered of secondary importance when compared with the development of the western shale. The usual reason given for this assessment is the low oil yield of the eastern shales. For example, a typical eastern shale containing 12% organic carbon yields about 12-14 gallons per ton (G/T); in comparison a western shale with the same organic carbon percent yields about 28 G/T. Thus for eastern shales to be considered as an attractive alternative source of liquid fuels a higher yield of oil has to be achieved.

Techniques are known by which an oil shale may be beneficiated so as to increase the amount of oil that is generated by retorting. One such technique described for eastern shales is froth flotation.

Beneficiation by grinding and froth flotation is a well established procedure in the mineral dressing industry. Large scale ore beneficiation facilities have been developed and are commercially applied.

In froth flotation advantage is taken of the difference between the specific gravity of the organic and inorganic components in the shale. Thus if the organic-rich portion of the shale which has a lower density than the inorganic portion could be disengaged from the organic-poor portion, the two portions will exhibit a specific gravity difference that may allow for their separation by flotation.

Unlike western shale which has essentially a layered structure of magnesium and calcium marlstones interspaced with organic-rich kerogen, eastern shale has essentially a matrix structure. This matrix is typically composed of particles of quartzite, clay, organic-rich kerogen and pyrite. To achieve the separation of the organic-rich from the organic-poor components of an eastern shale, it is thus necessary to reduce the shale matrix to its components which could then be separated by flotation.

For eastern shales, size reduction by grinding (1) can bring about the separation of the desirable organic from the inorganic components of the shale. This has also been achieved by persistent milling in a rod mill (1), ball mill, or a rod and ball mill (2,3). It has also been reported (1-6) that the finer the particles, the more successful is the beneficiation. The grinding or milling process is a major contributor to the

cost of beneficiation. It has been estimated (7) that 45% of the cost of beneficiation accrues to the grinding step with energy the major component.

Although water has been used for dust control and lubrication during grinding, it has not been used as the main medium for size reduction. Earlier work at Mobil (8) has shown that when a water slurry of an eastern shale is stirred, the shale particles crumble and lose their shape and size. This suggested the use of agitated water slurries of the shale as a means of size reduction and flotation.

EXPERIMENTAL

Apparatus

The beneficiation apparatus consisted of two components, a flotation cell and a circulating pump. Figure 1 depicts the flotation cell used. A TEEL pump manufactured by Dayton Electric Co., Model IP 810, equipped with 2 1/4 inch diameter flexible impeller driven by a 1/4 HP electric motor was used to circulate the shale and reduce its size. The outlet of the flotation cell was attached to the inlet of the impeller pump and the pump outlet was attached to the inlet of the flotation cell. A 1/2 inch 25 micron frit was used to support the shale slurry and to supply the frothing gas.

A DuPont thermogravimetric analyzer (TGA) was used to determine the weight loss; heat up rate was 10°C/min. Air or argon was used to sweep the volatiles during thermal decomposition of the kerogen.

Procedure

In a typical experiment about 750ml of water was placed in the flotation cell and the pump started. About 50g of 8-mesh shale was then added to the circulating water and the slurry was allowed to circulate for 30-60 minutes.

About 0.1g of sodium dodecylbenzenesulfonate was then added to the slurry and the mixture circulated for 10 minutes. Flotation gas was then turned on to generate a foam with small bubbles and the flow adjusted so as to achieve a steady flow of foam at the foam outlet of the flotation cell.

Samples of the foam were collected at predetermined intervals. Each sample was filtered, Büchner, and the collected solid washed well, and dried to constant weight at room temperature at a pressure of about 0.05 mm Hg, weighed and analyzed.

In TG analyses care was taken to use an amount of shale that gave a uniform layer of shale on the TGA balance. Usually a 20-25 mg sample was satisfactory.

RESULTS AND DISCUSSION

Shale Particle Size Reduction

Earlier work on eastern shale at Mobil (8) has shown that some shales are friable when wet. It was observed, for example,

that when a slurry of 8-mesh New Albany shale was stirred gently, most of the shale became smaller than the original 8-mesh size. It was clear that wet New Albany shales yield and crumble under the impact of the Teflon blade of a glass stirrer. This observation suggested to us the use of an impeller slurry pump as a means of size reduction. It was reasoned that when the impeller struck the wet shale particles, they would break down and crumble.

After several experiments with different impellers it was concluded that the impact of the impeller on the wet shale reduced the particle size of the shale but the particle size was not small enough to bring about flotation. However, when a slurry pump equipped with a flexible impeller was used, the shale size was sufficiently reduced for its flotation. This size reduction was brought about by the scraping action of the flexible impeller over the wet shale. As the impeller moved in its housing, the shale particles were trapped by the flexible vanes and scraped over the metal surface of the impeller housing; this scraping action brought about the size reduction.

Shale Flotation

Several attempts were made to apply the sink/float procedure (9) for beneficiating the shale particles generated by the action of the impeller pump. The fine shale was mixed with brines of various densities and allowed to segregate into lighter and heavier portions. Brines containing calcium chloride or calcium bromide with densities in the range of 1.05-1.64 g/cc were used. In all sink/float attempts little or no beneficiation took place.

The same brines were also used as the liquid medium of the shale slurry and circulated by the impeller pump followed by flotation. Although size reduction was affected, little or no beneficiation took place. In one example a brine with a density of 1.105 g/cc produced a small fraction containing 41% more carbon than the raw shale; organic carbon was increased from 12.83% to 18.10% by weight.

After the unsuccessful experiments with the various brines a slurry composed of 50g, 8-mesh shale and 750 ml water containing 0.013% by weight (0.1g) sodium dodecylbenzenesulfonate was circulated and was successfully beneficiated. The shale used in all these studies was a well characterized New Albany shale containing little or no carbonate carbon. Table 1 presents the elemental analyses of the raw shale and shows the yields of products obtained in the Fischer assay and selected properties and elemental composition of the oil and spent shale. The carbon content of the oil represents a 33% conversion of the carbon of the raw shale to oil. This level of carbon conversion is typical of eastern shales (10) and serves to illustrate the need for beneficiation.

Table 2 shows the elemental analyses and amounts of the beneficiated fractions of the New Albany shale studied. About 17% by wt of the shale has over 32% by weight carbon, a 2.5 fold carbon beneficiation. This 17% fraction contains 45% of the total carbon contained in the 50g sample. About 5% of the

sample remained unground and essentially had the same composition as that of the raw shale. About 95% of the fractions collected by flotation passed a 200 mesh screen, however the fractions with the high carbon content had a "waxy" feel and were difficult to sieve. These particles stuck to the sieve opening and an accurate measure of their mesh size distribution could not be made. It is estimated that over 25% would pass a 325 mesh sieve.

The leanest fraction was a finely ground portion of the shale that remained in the flotation cell upon termination of the experiment and was separated from the 8-mesh residue by sieving. This finely ground residue passed a 200 mesh sieve and had a 3% by wt. carbon content.

Estimate of Oil Yield by TGA

Since these experiments were carried out on 50g samples of shale, Fischer assay (FA) yields could not be determined on any of the beneficiated shale fractions. Although all beneficiated fractions were analysed for carbon and hydrogen content, Table 2, it was considered necessary to estimate their oil yield potential.

It has been shown (11) that small samples, 1 or 2 mg, could be used in thermal decomposition studies for comparing the oil generating potential of shales. Also, thermogravimetric (TG) analysis techniques have been used to compare shales by determining relative weight loss profiles (12,13). Weight loss from three shales of known FA yield, including the shale used in this study, was determined by TGA, Table 3. The New Albany shales have similar weight loss in TGA and have FA yields consistent with such weight loss. Also the western shale which is known to produce more oil per percent organic carbon than the eastern shales shows the same trend in the TGA.

By combining elemental analyses of the beneficiated shale fractions with their TGA weight loss and using the data for shales with known FA yields an estimate of the FA yields of the fractions could be made, Table 4. The two fractions with the highest carbon contents also have the highest weight loss in argon. Weight loss in air was also determined, Table 5, and shows that the raw shale and the unground residue have the same weight loss. Considering the elemental composition and the TGA weight loss in argon of both samples, it was concluded that the unground residue is unbeneficiated shale. The recovered unground material was similar in appearance to the raw shale and crumbled when wet. It was reasoned that this material must have been trapped at the bottom of the flotation cell and was not carried into the pump housing where size reduction takes place.

TGA weight loss in air when compared to weight loss in argon is one measure of how well carbon conversion to oil takes place during thermal decomposition of a kerogen. A spent shale with a high char content will loose that char by oxidation when air is the sweep gas. A high char content is an indication of poor organic carbon conversion to oil. The beneficiated fractons do not generate char to the same extent as the raw shale. Whereas

the weight loss in argon of the raw shale is 36% of that in air, that of the beneficiated fractions is 65%. It is possible that the inorganic matrix, in the raw shale, especially the pyrite, contributes to the inefficient conversion of the kerogen to oil.

Although the sulfur content of the beneficiated shale increases relative to that of the raw shale, the ratio of carbon to sulfur is higher, 5.22 vs. 2.69, and that of sulfur to hydrogen is lower 2.30 vs 3.38. Pyrite in shales is a hydrogen consumer (14) and competes with carbon for the available hydrogen during thermal conversion of kerogen to product oil. Shales containing pyrite are known to produce significant amounts of hydrogen sulfide (15).

CONCLUSIONS

A new approach to size reduction followed by froth flotation to beneficiate water-sensitive eastern shales coupled with thermogravimetric analysis has been investigated. Organic-rich fractions with 3.5 times the oil generating capacity of the raw shale were prepared by this procedure. It is suggested that this procedure be used as a screening test for the applicability of flotation to the beneficiation of shales.

REFERENCES

1. H. S. Hanna and W. E. Lamont, AIChE 1982 Summer National Meeting, August 1982, Cleveland, Paper No. 35A.

2. U.S. D.O.E. Contract ET 78 Col 2628, December 31, 1982.

3. P. H. Fahstrom, 12th Oil Shale Symposium, Golden, Colorado, April 1979.

4. News Feature, Chemical Engineering, February 22, 1982, p. 37.

5. Synthetic Fuels Report, September 1982, p. 2-10.

6. Synthetic Fuels Report, June 1983, p. 2-28.

7. J. D. Miller, U.S. Patent No. 4,279,743, July 21, 1981.

8. C. A. Audeh, J. J. Dickert and P. E. Fowles, U.S. Patent 4,466,882, August 24, 1984.

9. C. J. Vadovic ACS Symposium Series #230, 1983, p. 385.

10. A. M Rubel and T. T. Coburn, 1981 Eastern Oil Shale Symposium Proceedings, Lexington, Kentucky, November, 1984, p. 21.

11. J. W. Reasoner, L. Sturgeon, K. Naples and M. Margolis, 1981 Eastern Oil Shale Symposium Proceedings, Lexington, Kentucky, November, 1981, p. 11.

12. R. A. Addington , J. P. Humphrey, and E. M. Piper, 1983, IGT Symposium Synthetic Fuels from Oil Shale and Tar Sands, Louisville, Kentucky, May 17-19, 1983, P. 497.

13. M. Nakamura, R. Matsumotu, M. Saski, N. Yamagucki and N. Hirai, ibid, p. 167.

14. M. R. Abadi and R. W. Mickelson, AIChE 91st National Meeting, August, 1981, Detroit, Paper No. 16B.

15. C. A. Audeh, ACS, Division of Petroleum Chemistry, Inc. Preprints, Vol. 29, No. 1, p. 19.

Table I

Properties and Yields of Products Obtained by Fischer Assay Retorting a New Albany Raw Shale

Yields	
Oil, G/T	13.0
Oil, %wt	5.0
Spent Shale, %wt	90.2
Gas, liters/100 g	1.67
H_2S, liters/100 g (%wt)	0.53(0.81)
Total Gas, liters/100 g	2.20
Water, %wt	1.9
Oil Properties	
Gravity, °API	22.6
Specific Gravity, 60/60°F	0.9182
Viscosity at 40°C, cS	8.94
Viscosity at 40°C, SUS	51.0
Carbon, %wt	85.26
Hydrogen, %wt	10.87
Nitrogen, %wt	1.13
Sulfur, %wt	1.62
Raw Shale Analysis, %wt	
Carbon	12.83
Hydrogen	1.41
Nitrogen	0.40
Sulfur	4.77
Ash	77.4
Spent Shale Analysis, %	
Carbon	8.05
Hydrogen	0.47
Nitrogen	0.34
Sulfur	3.78
Ash	86.6

Table II

Yields and Elemental Analyses of Beneficiated New Albany Oil Shale Fractions

Fraction No	Weight	% Wt	C	H	N	S
Raw Shale	50	100	12.83	1.41	0.40	4.77
1	2.8	5.6	32.20	2.74	0.83	6.30
2	6.0	12.0	33.01	2.70	0.78	6.19
3	16.0	32.0	9.69	0.56	0.26	2.82
4	20.0	40.0	7.19	0.37	0.18	2.58
Residue (ground)	2.7	5.4	3.04	0.33	0.06	1.27
Unground Residue	2.6	5.2	11.85	0.83	0.34	5.48

Table III

Fischer Assay Yield and Thermogravimetric Weight Loss in Argon in the 210-510°C Temperature Range of 3 Shales

Shale Sample	Carbon %wt	TGA Wt Loss % wt		Fischer Assay Oil Yield G/T
		Oil	Water	
Colorado	12.1	10.5	1.0	27.8
New Albany 1	11.8	4.3	2.5	11.1
New Albany 2	12.8	5.0	2.1	13.0

Table IV

Thermogravimetric Weight Loss in Argon in the 210-510°C Temperature Range of Beneficiated New Albany Oil Shale Fractions

Fraction No	Loss, % Weight	G/T
Raw Shale	6.5	13.0
1	22.0	45.0
2	22.0	45.0
3	4.0	8.0
4	3.0	6.0
Residue (ground)	1.0	-
Unground Residue	5.0	11.0

Table V

Thermogravimetric Weight Loss in Air of Beneficiated New Albany Oil Shale Fractions

Fraction No	Loss, % Weight
Raw Shale	18.3
1	34.0
2	34.0
3	5.0
4	5.0
Unground Residue	18.0

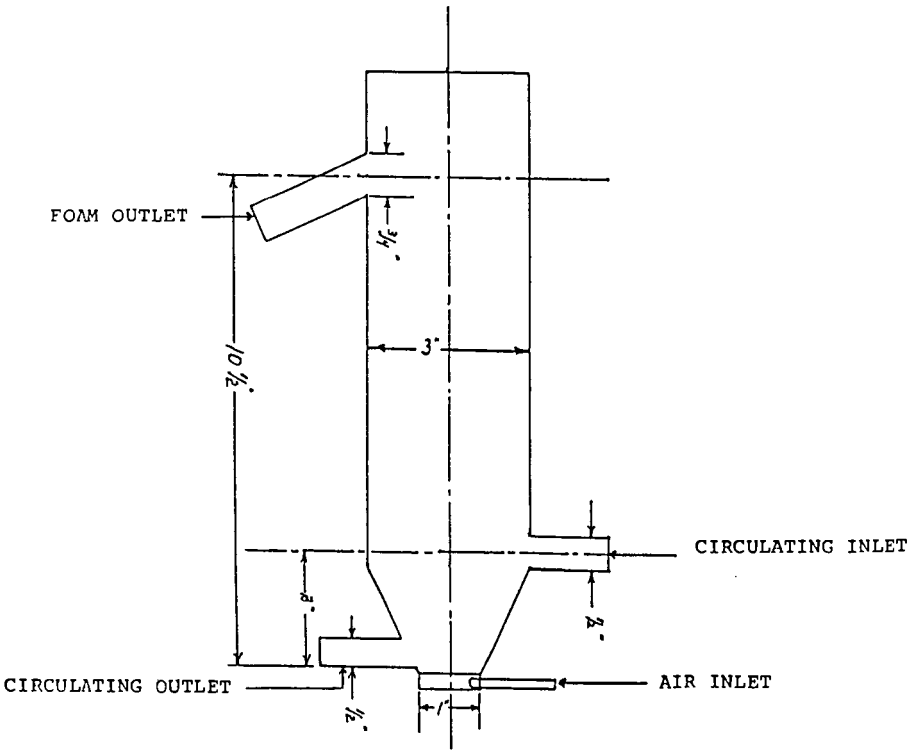

FIGURE 1

FLOTATION CELL

COMBINED BENEFICIATION AND HYDRORETORTING OF OIL SHALE

R. Bruce Tippin, University of Alabama
P. O. Box AY, University, AL 35486

and

Raymond C. Rex, HYCRUDE Corporation
10 West 35th Street
Chicago, Illinois 60616

ABSTRACT

The Mineral Resources Institute (MRI) of The University of Alabama and Institute of Gas Technology subsidiary, HYCRUDE Corporation, are evaluating the potential benefits of combining pre-concentration of oil shale by froth flotation followed by hydroretorting to recover the oil. Exploratory laboratory testing of several oil shales has been completed in a continuing research program. To date the testing includes a sample of Upper Devonian New Albany shale from Indiana, an upper Chattanooga shale from Alabama and a Permian Irati shale from Brazil.

Results of flotation tests of the three samples showed that the oil content in the beneficiation concentrates was increased by a factor of 2 to 3 with recoveries up to 90 percent. After briquetting the products, the MRI beneficiated oil shales were submitted to HYCRUDE and subjected to bench scale HYTORT processing. The yield was improved further through hydroretorting by a factor between 3 and 5.5.

INTRODUCTION

Until recent years most of the research and development work directed toward establishing a domestic oil shale industry has focused on the shales of the Green River Formation of Eocene age occurring in Colorado, Utah, and Wyoming. This is largely because the Western shales are relatively rich (in the range of 25-30 gal/ton) and respond favorably to oil production by simple thermal treatment, yielding 75-85% of their organic content (kerogen) as oil when pyrolyzed.

Recent developments in innovative retorting and fine particle technologies have altered this situation significantly. The HYTORT process, developed by HYCRUDE Corporation utilizes hydrogen rich gas during retorting to enhance oil yields from certain types of oil shales. It has provided a key to processing the Devonian-Mississippian shales of the Eastern United States to achieve oil yields comparable to those from Colorado shales. This technique permits the fullest possible recovery of oil from the kerogen present in the shale.

The range of potential oil shale resources available to HYTORT processing can be expanded by combining hydroretorting with The University of Alabama Mineral Resources Institute's (MRI) physical beneficiation process. The MRI process involves fine grinding the oil shale matrix followed by selective froth flotation of the kerogen. During flotation up to three quarters of relatively kerogen-free inorganic matter is rejected as waste.

By combining the HYTORT and MRI processes, the economics of treating oil shales can be improved, and the range of oil shales which can be processed is extended. Descriptions of the MRI and HYTORT processes, and typical results obtained on oil shales of low and moderate kerogen content are presented in this paper.

BACKGROUND

The HYTORT Process

Oil shales vary significantly in their ability to produce oil. For example, the Green River oil shales of the Western U.S. contain a high hydrogen content in

proportion to organic carbon, and exhibit relatively complete conversion of kerogen to oil. When retorted by conventional thermal processes. However, many other oil shales including the Eastern U.S. Devonian shales, contain lesser amounts of hydrogen relative to organic carbon as shown in Table 1. This deficiency in hydrogen reduces the fraction of the kerogen which can be converted to hydrocarbon products by conventional retorting (1,2). Oil yields from these shales can be substantially improved by supplying hydrogen during retorting. Thus a significant larger fraction of the kerogen is converted to hydrocarbon products rather than remaining in the spent shale in the form of coke. The degree of oil yield enhancement for each particular oil shale depends upon the partial pressure of hydrogen used.

In 1980 HYCRUDE Corporation was formed to commercialize the HYTORT process. HYTORT is a process which utilizes a hydrogen-rich gas for the hydroretorting of oil shale kerogen to produce a synthetic crude oil. The hydroretorting is carried out in a hydrogen-rich atmosphere at elevated pressure, and enables attainment of the maximum possible oil yields from most oil shales. As a result of a Development Agreement with Phillips Petroleum Company, a feasibility study was conducted by HYCRUDE Corporation, Phillips Petroleum Company, Bechtel Group, Inc., and the Institute of Gas Technology. The HYTORT process development work during the feasibility study was divided into three basic areas:

- Chemistry of hydroretorting
- Experimental development work to support mechanical design of HYTORT reactors
- Process design, reactor mechanical design, and cost estimation work.

The HYTORT experimental work and process economics were completed in May 1983 and details are available in other publications (3,4).

Throughout the course of the feasibility study, the HYCRUDE Corporation and Bechtel Group, Inc. continually reviewed the experimental efforts to assure that the experimental programs addressed areas important to the design of commercial reactions (5). This study resulted in a conceptual commercial plant design for Eastern U.S. Devonian shale processing based on the results of the experimental program. The conceptual HYTORT plant flow diagram is shown in Figure 1. The plant contains all the process areas necessary to produce upgraded shale oil including by-product recovery of sulfur and ammonia. As designed, the HYTORT reactors can be constructed using currently available equipment. All other processes are within the sizing and operating constraints of commercial facilities. Implementation of the plant design can be achieved with current process technology.

Natural gas is utilized in the production of hydrogen and as an indirect heat source for hydroretorting. This is an economic optimum for areas such as the Eastern United States where inexpensive sources of natural gas area available. For plants located in areas lacking an inexpensive natural gas source, the HYTORT process conditions would be selected to provide sufficient by-product gas as a substitute.

Although most of the HYTORT process development effort has concentrated on Eocene oil shales of the Western U.S. and on Eastern U.S. Devonian oil shales (1,2), HYCRUDE Corporation in cooperation with the U.S. Geological Survey is conducting work on other oil shales from various locations worldwide. The primary goal of this on-going work is to determine the extent of oil yield enhancement which can be obtained using HYTORT processing. Test work is conducted in a Hydroretorting Assay unit (6), which is designed to serve the same function for HYTORT processing that the ASTM D3904-80 Fischer Assay test serves for conventional thermal retorting processes. Table 2 gives results

of Hydroretorting Assay tests on some of the samples. The data show that HYTORT processing had a wide range of effects on the shales tested, with oil yield enhancements varying from no improvement to oil yields over four times those obtained in Fischer Assay tests. No trend of behavior with geological age is evident. Further details of these test results are available in a previous publication (4).

The MRI Oil Shale Beneficiation Process

Physical beneficiation techniques have long been used in the mineral and coal industries to obtain a product more enriched in the economical mineral than the run-of-mine ore. A prerequisite for physical separation is to free the valuable constituent from the associated impurities. This is normally achieved by comminution of the raw material to sizes finer than their natural particle size consist. The degree of grinding may dictate certain separation approaches. This is particularly important in the case of oil shales, which are fine grained sedimentary rocks composed of 10 micron particles (7). Thus ultrafine grinding of the shale is required to achieve reasonable liberation of oil-bearing kerogen from the intimately associated inorganic mineral matter.

Ultrafine grinding and physical beneficiation of finely disseminated ores were once considered impractical. This is because of the general belief that the grinding costs are prohibitive and that most separation techniques at sizes finer than 74 microns (200 mesh) are ineffective (8). However, this belief has been dispelled with the continuing engineering advancement in beneficiation equipment and recent advances in fine particle technology. This is evidenced by the non-magnetic taconite flotation plant of the Cleveland-Cliffs Iron Company in the Lake Superior Region (9). In this large tonnage plant the hard taconite ore is ground to a particle size finer than 30 microns (500 mesh) prior to flotation to recover high grade iron oxide products. The technical practicality and economic feasibility of extremely fine grinding of the hard, tough taconite suggests that fine grinding and flotation of the oil shale should be equally effective.

During the past six years of continuing research, MRI has developed a beneficiation process which successfully concentrates the Devonian oil shales of the Eastern U.S. The MRI process involves wet grinding the raw shale to minus 20 microns followed by froth flotation to recover a kerogen rich concentrate. Details of the development of this process are available in previous publications (10-12).

MRI test results have been used to formulate a process flowsheet for an oil shale beneficiation plant (Figure 2). The plant is designed to recover concentrates yielding 2 to 3 times as much recoverable oil per ton as can be obtained from the raw untreated shale. Unit operations of this plant are within the limits of current commercial practice. In the process, at least 50% to as much as 70% of the raw shale will be rejected as a substantially barren waste which need not be retorted.

The beneficiation plant includes the following standard mineral processing unit operations:

- Fine grinding of shale to mineral particle liberation size
- Classification
- Kerogen flotation
- Thickening and filtration
- Agglomeration or briquetting of the flotation concentrate
- Disposal of the flotation tailing

Most of the beneficiation research investigations has been directed to the Eastern oil shale deposits, particularly the Devonian shales outcropping in Northern Alabama, but several samples from the Western United States and foreign countries also have been tested in a cursory way. Typical results are shown in Table 3. Plans are to evaluate additional types of oil shales as they become available.

EXPERIMENTAL

The combined beneficiation and hydroretorting studies were conducted on two Eastern oil shale samples (Alabama and Indiana) and one foreign sample (Brazil). The Indiana sample was collected by HYCRUDE Corporation from the Upper Devonian New Albany shale formation near Henryville, Indiana. The Alabama shale sample was part of a 5-ton lot of Upper Chattanooga shale collected by MRI from the Hester Creek area in Madison County, Alabama. The Brazilian oil shale represents a typical shale from the Irati formation in the south of Brazil. Analyses and Fischer Assay oil yields from the three samples and a Western shale are shown in Table 1.

Procedures and Techniques

The beneficiation tests were conducted at the Mineral Resources Institute at the University of Alabama. In these tests the raw shale samples were stage crushed dry to minus 2 mm (10 mesh) and wet ground in a 20 x 30 cm stainless steel rod mill operated at 78% of critical speed using 26 stainless steel rods of 1.7 cm diameter as the grinding medium. A 500-gram charge of each flotation test sample was ground at 50% solids in Tuscaloosa tap water for two hours to reduce the particles to 90% minus 10 microns. Bench scale flotation tests were conducted using a Denver Model D-12 laboratory flotation machine for the conditioning, roughing and cleaning steps. The flotation products were filtered, dried at 50°C, weighed and assayed for oil yield using the modified Fischer Assay method. Samples for hydroretorting were produced from the flotation concentrate using a uniaxial compression briquetting unit to make 1.25 cm diamter by 1 cm high specimens.

Hydroretorting tests were conducted at the Institute of Gas Technology at Chicago, Illinois under the sponsorship of HYCRUDE Corporation using a Hydroretorting Assay unit designed to evaluate the hydroretorting characteristics of oil shale samples. Details of the apparatus and the test procedure have been previously published (6). In this unit a 100-gram sample of material is reacted with hydrogen gas under the following conditions.

- 1000 psig pressure
- 1000°F temperature
- 4 SCF/hr gas flow
- 25 degree/minute heat-up rate
- 30 minutes reaction time

RESULTS AND DISCUSSION

Beneficiation of Raw Oil Shale

Response of the oil shale samples to beneficiation by ultrafine grinding and flotation are given in Table 4. All three samples responded favorably to beneficiation. Good flotation of the kerogen-enriched fractions was obtained from the ground shale which indicated that reasonable liberation of the kerogen and the mineral components was achieved. As compared to the flotation feed, the concentrates recovered from the Alabama and Indiana samples were upgraded in kerogen by factors of 2.4 and 2.8,

respectively. Flotation of the Brazilian shale yielded a concentrate assaying 33.5 gallons per ton, but the ratio of concentration (1.7) was less than that of the American oil shale samples. The variations in the response of the samples to flotaton are attributed to differences in their origin, mineral substrate, and composition. The oil recoveries in all cases were comparable. Only the Alabama oil shale has been investigated extensively at MRI and improvements in the flotation results of the other shales would be expected by further research. Even with the limited number of samples evaluated, it appears reasonable to assume that beneficiation of oil shales can be accomplished with good results.

Experimental testwork is continuing on this research program at The University of Alabama to further define the beneficiation variables in an effort to optimize the process. The goal of the research is to establish the technical parameters of the process in a continuous pilot plant operation to define the process economics. The pilot testing will also produce a reasonably large quantity of kerogen enriched concentrate which will be used in more extensive hydroretorting tests.

Hydroretorting of Raw Oil Shale

Results of Hydroretorting Assay tests on the three raw shale samples are given in Table 5. Results of the tests of the U.S. samples indicate that the HYTORT process can produce oil yields of 222 to 226% of those obtained by conventional thermal retorting. The oil yeild from the Brazilian sample was less, only 156%. The hydroretorting data shows that oil yields of 27 to 29 gallons per ton can be produced from oil shale resources which would be considered too lean for commercialization by conventional retorting.

Combined Beneficiation and Hydroretorting of Oil Shale

Combined MRI beneficiation-HYTORT processing was tested on a laboratory scale by hydroretorting the flotation concentrates of three oil shale samples. Test results are shown in Table 6. The concept proved to be technically successful in substantially increasing the extraction of oil. The data indicate that the combined technique can improve the overall level of oil yield from the raw shale by a factor of 2.9 to 5.6.

CONCLUSIONS

Based on the above results, the potential of the combined beneficiation-hydroretorting approach is evident in the following areas:

-- Reduction in the capital and operating costs for oil shale production should be possible by substituting atmospheric pressure, ambient temperature, grinding and froth flotation equipment for some of the elevated pressure and temperature HYTORT reactor units. Further, because of the enhanced shale oil yields, energy savings should result in a lower cost per barrel of shale oil.

-- Pre-retorting concentration of kerogen from lean shales should extend the range of oil shales which can be considered for commercial processing.

-- Rejection of inorganic sulfur (i.e., pyrite) may be possible either by flotation or high-intensity magnetic separation. By removing the pyrite, not only will the kerogen content increase but the overall quality of the concentrate will be enhanced.

-- During grinding, trace elements are solubilized into the process water. As a result, the tailings rejected during beneficiation and the spent shale produced by HYTORT processing should be less prone to the natural leaching of harmful metals and elements. Thus, surface and groundwater contamination after disposal should be substantialy reduced.

ACKNOWLEDGEMENTS

HYCRUDE Corporation would like to acknowledge the interest and support of the Institute of Gas Technology, particularly Dr. F. S. Lou, and Mr. M. J. Roberts, in conducting the hydroretorting assay testwork. The Brazilian oil shale sample was graciously provided by Mr. Lauro Carta of Petrobras, Petroleo Brasilero, S.A.

REFERENCES

1. Janka, J. C. and J. M. Dennison, "Devonian Oil Shale: A Major American Energy Resource," Presented at the IGT Symposium on Synthetic Fuels from Oil Shale, Atlanta, Georgia, December 3-6, 1979. Published in Proceedings, April 1980, pp. 22-116.

2. Matthews, R. D., J. C. Janka, and J. M. Dennison, "New Insights into Devonian Oil Shale Resources of the Eastern United States," AAPG Bulletin, Vol. 65, No. 5 (May 1981), pg. 53. Paper presented at the following meetings: AAPG Eastern Section Meeting, October 1-3, 1980, Evansville, Indiana (AAPG Bulletin), Vol. 64, No. 8, August 1980, pg. 1285). AAPG Annual Convention, San Francisco, May 31 - June 3, 1981.

3. Rex, R. C., P. A. Lynch, M. J. Roberts, and H. L. Feldkirchner, "Experimental Test Program of the HYTORT Feasibility Study." Presented at the 1983 Eastern Oil Shale Symposium, Lexington, Kentucky, November 13-16, 1983. Published in Proceedings, February 1984, pp. 391-229.

4. Janka, J. C., and R. C. Rex, "Application of the HYTORT Process to Oil Shales Throughout the World," Paper presented at the Summer National Meeting of the American Institute of Chemical Engineers, Philadelphia, Pennsylvania, August 19-22, 1984.

5. Rex, R. C., et al, "Selection of a Commercial Plant Design for the HYTORT Process." Presented at the 3rd IGT Symposium on Synthetic Fuels from Oil Shale and Tar Sands, Louisville, Kentucky, May 17-19, 1983. Published in Proceedings, July 1983, pp. 531-544.

6. Lynch, P. A., et al., "The Hydroretorting Assay - A New Technique for Oil Shale Assessment," Paper presented at the Joint Fuel/Petroleum Division Meeting of the American Chemical Society, St. Louis, Missouri, April 8-13, 1984.

7. Nowack, P., Oil Shale Technical Data Handbook, Noyes Data Corporation, Park Ridge, New Jersey (1981).

8. Somasundaran, P., Ed. Fine Particles Processing, Pub. AIME, New York, 1, 2 (1980).

9. Villar, J. W. and G. A. Dawe, "The Tilden Mine - A New Processing Technology for Iron Ore," Mining Congress. 40-48 (1975).

10. Hanna, H. S., and W. E. Lamont, "Physical Beneficiation Studies of Eastern Oil Shales," Proceedings of the Symposium on Synthetic Fuels from Oil Shale and Tar Sands, Louisville, Kentucky, May 17-19, 1983. Published IGT, pp. 295-321, July 1983.

11. Lamont,. W. E., "Beneficiation of the Kerogen Content of Eastern Devonian Oil Shales by Flotation," Paper No. 83-621, presented at the SME-AIME Annual Meeting, Atlanta, Georgia 6-10, 1983.

12. Hanna, H. S. and C. Rampacek, "Eastern Oil Shale Investigations at The University of Alabama." Presented at the 1981 Shale Symposium, Lexington, Kentucky, November 15-17, 1981. Published in Proceedings, dated November 1981, pp. 24-25.

Table 1. Analysis and Fischer Assay Oil Yield of Selected Oil Shales				
Oil Shale Sample	Alabama	Indiana	Brazil	Colorado
ULTIMATE ANALYSIS (wt. %)				
Organic Carbon	14.20	12.53	13.70	13.60
Organic Hydrogen	1.03	0.93	1.37	2.10
Sulfur	8.02	4.41	4.98	0.50
Carbon Dioxide	2.90	2.30	N.A.	15.90
Nitrogen	0.48	0.48	0.44	0.50
Ash	79.70	77.83	80.00	66.80
Atomic H/C Ratio	0.87	0.94	1.2	1.85
FISCHER ASSAY				
Yield (wt. %)	4.9	4.6	7.1	11.4
Yield (gal/ton)	11.6	12.0	18.6	29.8
Carbon Conversion (%)	31.2	32.9	50.0	84.0

Table 2. Selected Hydroretorting Assay Test Results			
	Oil Yield (gal/ton)		
Oil Shale Sample	Fischer Assay	Hydroretorting Assay	Percent of Fischer Assay
Sweden - Billingen	3.8	17.5	440
Sweden - Naerke	10.9	32.3	300
Sicily	4.4	12.2	280
Indiana - New Albany	12.5	28.2	230
Montana - Heath Formation	16.2	33.6	210
Canada - Kittle	10.0	21.1	210
Jordan - El Lajjun	32.8	57.0	170
Brazil - Lower Irati	19.4	32.7	170

Table 3. Selected Beneficiation Test Results

Oil Shale Sample	Fischer Assay (gal/ton)		Percent Oil Recovered	Ratio of Concentration
	Flotation Feed	Flotation Concentrate		
Eastern U.S.				
Alabama	12	37	87	3.1
Kentucky	17	31	81	1.8
Indiana	12	35	81	2.9
Western U.S.				
(Lo-grade)	14	34	90	2.4
(Hi-grade)	46	88	80	1.9
Canadian	8	16	52	2.0
Brazil	20	34	89	1.7

Table 4. Flotation Response of Raw Oil Shales

Oil Shale Sample	Flotation Products	Weight Percent	Fischer Assay Yield (gal/ton)	Distribution of Oil (%)
Alabama Chattanooga Shale	Concentrate	27.0	34.3	80.0
	Reject	73.0	3.2	20.0
	Feed	100.0	11.6	100.0
Indiana New Albany Shale	Concentrate	35.5	27.2	79.0
	Reject	64.5	4.4	21.0
	Feed	100.0	12.5	100.0
Brazil Irati Shale	Concentrate	48.9	33.5	88.2
	Reject	51.1	4.3	11.8
	Feed	100.0	18.6	100.0

Table 5. Hydroretorting Assay Test Results of Raw Oil Shales			
Oil Shale Sample	Original Sample Fischer Assay (gal/ton)	Hydroretorted Sample Assay (gal/ton)	Oil Yield Percent of Fischer Assay
Alabama - Chattanooga	11.6	27.8	220
Indiana - New Albany	12.5	27.2	230
Brazil - Irati	18.6	29.0	160

Table 6. Combined Beneficiation - Hydroretorting of Oil Shales				
Oil Shale Sample	Oil Yield (gal/ton)			Overall Percent of Fischer Assay
	Original* Sample	Flotation* Concentrate	Hydroretorted Concentrate**	
Alabama - Chattanooga	11.6	34.3	65.0	560
Indiana - New Albany	12.5	27.2	54.4	430
Brazil - Irati	18.6	33.5	53.3	290

* Fischer Assay
** Hydroretorting Assay

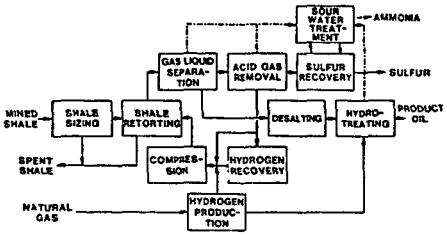

Figure 1. CONCEPTUAL COMMERCIAL HYTORT PLANT BLOCK FLOW DIAGRAM

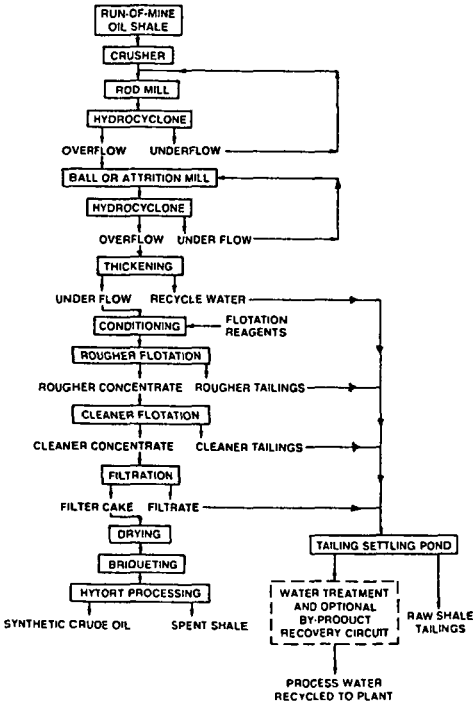

FIGURE 2. SCHEMATIC FLOWSHEET FOR MRI OIL SHALE BENEFICIATION PLANT

INVESTIGATION OF THE REACTION MECHANISMS FOR PYROLYSIS OF RUNDLE OIL SHALES BY DYNAMIC ^{1}H NMR TECHNIQUES

T. Parks, L.J. Lynch and D.S. Webster

CSIRO Division of Fossil Fuels, P.O. Box 136, North Ryde, NSW, 2113, Australia

ABSTRACT

Dynamic proton nuclear magnetic resonance (^{1}H NMR) techniques were used to study the pyrolysis behaviour of a suite of Rundle oil shale ore types. Experimental results were obtained by monitoring the ^{1}H NMR transverse relaxation signal for both the shales and their kerogen concentrates during their pyrolysis by heating at a uniform rate in open glass tubes in an inert atmosphere provided by flowing nitrogen gas.

These results indicate that while the Rundle ore types have variable pyrolysis behaviour, all of the demineralized shales pyrolyse similarly. The differences observed in the behaviour of the shales are thought to be a consequence of variations in the permeability of the inorganic matrices to evolving volatile species. Enhancement of molecular mobility marks two transitions of the specimen during pyrolysis. The first, which occurs between room temperature and ~ 500 K and involves most of the structure, is probably a "glass to rubber" type transition and the second, which occurs near 600 K indicates the presence of a relatively thermally stable component in the kerogen. The results show that the pyrolysis residue formed above 750 K is contributed to by material that passes through a transient mobile state.

INTRODUCTION

Studies over many years of the pyrolytic decomposition of oil shales have led to a variety of kinetic models which invoke intermediate species referred to as pyrobitumens (1-3) and sometimes also as rubberoid (4) and polyoil (5) species. These intermediate species are at best only loosely defined and while it is expected that such intermediate states do occur during pyrolysis their delineation in composition and occurrence are still matters for investigation. In these models the original kerogen is usually treated as being homogeneous but recently kerogen pyrolysis has been analysed in terms of the chemically distinct aromatic and aliphatic fractions (6-8).

Dynamic measurement techniques have an advantage over equilibrium measurement techniques in such investigations because of their potential to monitor transient states of the reacting system. The adaptation of proton nuclear magnetic resonance (^{1}H NMR) as a dynamic measurement technique has been described previously (9-11). The hydrogen specificity of the ^{1}H NMR experiment aids in the distinction of thermal processes associated with the organic kerogen from those of the inorganic matrix of the shale. For organic solids the most important factors governing their ^{1}H NMR behaviour are the concentration and distribution of protons and unpaired electrons in the structure and the molecular dynamics. To this extent undecoupled or "broadline" NMR can provide information on the complex interactions which determine the molecular properties and form of the bulk material. These NMR measurements will detect molecular mobility changes associated with melting and other "softening" transitions and likewise transitions of the molecular lattice back to the rigid lattice state, the loss of hydrogen from the specimen during decomposition and changes in free radical concentrations related to bond rupture and condensation reactions. The results reported here are all derived from dynamic measurements of the ^{1}H NMR transverse relaxation signal I(t). Parameters are derived from these measured signals which (a) represent the residual specimen as consisting of two

components, one containing rigid hydrogen and the other mobile hydrogen, (b) characterize the molecular mobility of the structure containing the mobile hydrogen, (c) estimate the residual hydrogen content and (d) characterize the ^1H NMR transverse relaxation signal I(t) and therefore the total residue in terms of its average molecular mobility. The temperature dependences of these parameters form a set of pyrograms reflecting changes in the specimen during the pyrolysis.

EXPERIMENTAL

The shales studied were a suite of the ore types distinguished and characterized in the Rundle deposit by Coshell (12). Specimens in the form of -100 mesh powders were supplied by ESSO Australia together with chemical analysis and Fischer assay oil yield data (Table I). A composite Rundle shale has been reported as having a ^{13}C CP-MAS aromaticity value of about 0.22 (13). Kerogen concentrates were prepared by HCl/HF digestion of the mineral matter and subsequent analysis showed them to contain large quantities of fluorine and to have total ash contents in the range 17 to 38% (13).

Predried shale and kerogen concentrate specimens of ~ 400 mg contained in 8 mm O.D. open glass tubes were used for the ^1H NMR thermal analysis experiments which were conducted under nitrogen gas flowing at 5 ml min^{-1}. Comparative studies of the shale ore types and their kerogen concentrates were made in a series of pyrolysis experiments at a uniform heating rate of 4 K min^{-1}. The ^1H NMR measurements were made using the two pulse (90_0-τ-90_{90}) sequence to generate the solid-echo form of the ^1H NMR transverse relaxation signal I(t). A sequence repetition time of 1 s avoided saturation effects which indicates that the shales are free of inorganic hydrogen with much longer ^1H NMR spin-lattice relaxation times that have been found to occur in Green River oil shales (14).

RESULTS AND ANALYSIS

The peak signal amplitude I(2τ) normalized per gram of sample at room temperature (which is a measure of the hydrogen concentration contributing to the NMR signal of the specimens) shows a linear correlation with elemental percent hydrogen (w/w) as shown in figure 1 for both the whole and the demineralized shales used in the study. The fact that both the whole and demineralized shales gave the same linearity of I(2τ) with elemental hydrogen further indicates that the ^1H NMR signals are representative of all the hydrogen in the shales. It is important therefore to know the relative contributions to the ^1H NMR signals of the organic kerogen and the inorganic matrix. Figure 2 compares the temperature variation of the relative ^1H NMR signal amplitudes (normalized per gram of shale) for three shales of different grade with that for a predried montmorillonite sample pyrolysed at 6 K min^{-1}. Analyses of these shales (15) have shown that clays which account for ~ 35% of the inorganic matter are the only significant source of inorganic hydrogen with montmorillonite being the most abundant clay variety. The data in Figure 2 therefore show that the inorganic hydrogen signal is a minor fraction of the total shale signal except for the relatively kerogen-poor ore types such as claystone (ore type III in figure 2). The mineral matter analysis data of Loughnan (15) identified montmorillonite, kaolinite and illite clays in Rundle shales. From the experimentally determined ^1H NMR signal contributions of montmorillonite and kaolinite and an estimated signal contribution of illite, the calculated signal contributions of the clays in the ore types studied range from ~ 13% for the type III claystone to ~ 6% for the most kerogen-rich type I ore.

A selection of ^1H NMR relaxation signals I(t), recorded at various stages of pyrolysis of a predried shale and its kerogen concentrate are shown in figures 3(a) and 3(b) respectively. These data are typical for all the shales studied. At room temperature the signals for both materials are dominated by a rapidly decaying component, which comprises about 90% of the total signal intensity in the case of

the raw shale. This rapidly decaying component is characteristic of a rigid lattice or "glassy" structure devoid of molecular mobility on a time scale less than $\sim 10^{-5}$ s. The more slowly relaxing minor component of each signal indicates that parts of the structure have a degree of molecular mobility on this time scale, consistent either with extended structural domains being above their glass transition temperature or with a distribution of isolated mobile molecular segments in the structure. As the temperature is raised above room temperature the slower relaxing component increases in intensity at the expense of the rapidly decaying "rigid" signal, suggesting a gradual transition of the structure from the glassy to the mobile state. This occurs earlier and to a greater extent for the demineralized shale. However, even for the shale above ~ 600 K the mobile component accounts for almost all of the signal intensity of the residual specimen. At higher temperatures the total signal intensity falls rapidly as a result of pyrolytic loss of volatile material from the specimen and there is a regrowth of a rapidly decaying signal intensity consistent with the formation of the rigid char residue.

These data were reduced to provide a number of largely independent parameters: (i) The percentage of the total initial signal intensity that is contributed by the rapidly decaying or rigid component (% rigid) is estimated. This estimate is made by fitting an exponential function to the slowly relaxing tail of the signal and extrapolating to the echo peak time of the signal to obtain the mobile signal intensity. The time constant T_2^*, of the exponential function is a second parameter which is a measure of the average molecular mobility of the mobile component. These two parameters - % rigid and T_2^* - are plotted together against temperature in figures 4a and 4b for a shale and its kerogen concentrate respectively.

(ii) The apparent hydrogen content of the specimen (%H), obtained by calibration of the total ^{1}H NMR signal intensity $I(2\tau)$ for its sensitivity to temperature, is a semi-quantitative parameter useful for monitoring the pyrolytic decomposition and loss of volatile products from the sample. Its temperature dependence for the shale and kerogen concentrate are plotted in figures 5(a) and 5(b) respectively. Also shown in these figures are the differential hydrogen contents computed from these data.

(iii) The analytical second moment M_2^* of the frequency power spectrum representation of the ^{1}H NMR signal (11) which is characteristic of the total signal and enables a qualitative measure of the average molecular mobility of the total specimen to be monitored during the pyrolysis. The temperature variations of M_2^* for the whole and demineralized specimens are also recorded in figures 5(a) and 5(b) respectively.

The apparent hydrogen loss pyrolysis profiles at 4 K min^{-1} for all of the shales were found to be similar. Two outlying profiles of this set are compared in figure 6, and in figure 7 the corresponding M_2^* pyrograms are compared. The temperature of maximum rate of loss of hydrogen as defined by the minimum in the differential percent hydrogen content curve, and the total percentage loss of hydrogen from room temperature to 875 K did not vary significantly (see Table I) between the ore types. This small variation in the total percentage loss for the shale ore types and the linear correlation between this loss when expressed as ^{1}H NMR signal loss normalized per gram of shale and Fischer assay oil yield (figure 8) show that the hydrogen loss during the pyrolysis is predominantly organic.

Previous (16) ^{1}H NMR second moment profiles presented by us on the pyrolysis of Rundle oil shale identified two regions of enhanced molecular mobility of the kerogen during pyrolysis. The first event occurred on heating from room temperature to ~ 500 K and was attributed to a possible glass to rubber transition. This observation is similar to Haddadin and Tawarah's (17) interpretation of an endotherm they detected for a Jordanian oil shale, peaking in the region 433-443 K, as a physical softening and molecular rearrangement of the kerogen, and is also

consistent with Rogers and Cane's (4) description of a "rubberoid" material present after heating to 523 K for a Permian Torbanite. The second less obvious event commenced just prior to onset of the main pyrolysis at ~ 600 K and was attributed to the mobilization of a relatively thermally stable component of the kerogen. These events occurred for all but one of the shales of the present study and in the case of this exception no second softening event was noticeable. Further as illustrated in figure 7 there are considerable variations apparent in details of the ^{1}H NMR second moment profiles for these ore types which occur above 450 K and which cannot simply be accounted for by differences in the kerogen concentration of the ores. Differences are most apparent above ~ 600 K where there is a wide range of behaviours in the total data for the ore suite as represented in figures 6 and 7 by the extreme examples. These differences certainly do not correlate with kerogen concentration. The temperature at which M_2^* reaches its maximum high temperature value is however very similar, at ~ 780 K for all ores. For those where the onset of increase in M_2^* is delayed (e.g. ore type I) the rate of increase is greater compared to that of ore types (e.g. ore type XI) where the increase commences earlier.

It can be concluded from these experiments on whole shales that although the behaviour of the different Rundle ore types is similar during heating at the lower temperatures, at higher temperatures and in the zone of main pyrolytic decomposition there are significant differences in the nature of the reacting residues that are particularly evident when the second moment pyrograms are compared. This would suggest the likelihood of corresponding differences in the pyrolysis products of these ore types.

In figures 9 and 10 respectively the sets of ^{1}H NMR hydrogen loss and M_2^* pyrograms for the demineralized ore types are superimposed for comparison. Clearly there is a close similarity in the pyrolysis behaviour of the kerogens of the various ore types. One conspicuous dissimilarity is at low temperatures where in contrast the raw shales are similar. These low temperature differences are possibly the result of variations in the effect of the demineralization treatment on the different ore types in which some degree of structural degradation occurs however it has not been possible to establish any correlation with the analytical data. The more rapid fall in M_2^* immediately above room temperature for the demineralized as compared to the shale specimens shows lesser inhibition to thermal activation of molecular mobility for the demineralized specimens. This could be contributed to both by covalent bond rupture in the kerogen structure and by reduction of binding interactions at the molecular level between the organic kerogen and the mineral matter. Most of the kerogen structure is transformed from an immobile or rigid lattice state to one of considerable molecular mobility by this low temperature transition during which there is little loss of hydrogen. This low value of M_2^* attained is sustained on further heating until about 650 K while there is only gradual loss of volatile matter to a total loss represented by 15-20% of the hydrogen at 650 K.

The M_2^* pyrograms of all the kerogen concentrates are strikingly similar above 500 K. They all show evidence of the secondary softening event and all the residues undergo a rapid transition from their highly mobile state to a rigid state between 750 K and 770 K. This rapid transition in M_2^* is not reflected in the hydrogen loss programs as a sharp increase but as a sharp decrease in the rate of hydrogen loss at ~ 760 K (figure 10). This is clear evidence of the transition of parts of the mobile material existing in the residue below 750 K by condensation reactions to a rigid coke above 770 K. This present evidence for the existence of a transient fluidity in the intermediate kerogen residue complements the microscopic evidence for mesophase formation during the pyrolysis of similar materials by Villey et al (18, 19).

CONCLUSIONS

Notwithstanding the differences in the M_2^* pyrograms at low temperatures these ^1H NMR thermal analysis experiments on the demineralized ore types clearly demonstrate the close similarity of all the Rundle oil shale kerogens tested. These Rundle kerogens all exhibit two "softening" events. The first occurs on heating above room temperature and involves the bulk of the structure. The second occurs above 650 K and involves a minor component. There is slow evolution of volatiles between 450 K and 650 K and rapid evolution between 650 K and 750 K. A rapid solidification of the residue occurs between 750 K and 770 K which identifies the secondary softening as a thermoplastic transient event akin to that of bituminous coals.

Given the similarity of the kerogens of all the ore types and the similar mineralogy of the inorganic matrices (15), the differences detected in the pyrolysis behaviour of the ore types must be related to either the concentration differences, or possible variations in the degree of dispersion and/or the nature of the interactions that occur between the organic and inorganic structures. Any of these factors could for example affect the permeability of the shale matrix to evolving molecular species. Thus it can be concluded that the differences observed in shale pyrolysis above 600 K result from differences in the rates of molecular diffusion and losses of mobile pyrolysis products.

ACKNOWLEDGEMENTS

This work was carried out in collaboration with and financially supported by Esso Australia and Southern Pacific Petroleum.

REFERENCES

1. Allred, V.D. Chem. Eng. Progress 62, 55 (1966).
2. Finucane, D., George, J.H. and Harris, H.G. Fuel 56, 65 (1977).
3. Rajeshwar, K. Thermochimica Acta 45, 253 (1981).
4. Rogers, L.J. and Cane, R.F. Aust. Chem. Inst. J. & Proc. 12, 159 (1945).
5. Wen, C.S. and Kobylinski, T.P. Fuel 62, 1269 (1983).
6. Miknis, F.P., Szeverenyi, N.M. and Maciel, G.E. Fuel 61, 341 (1982).
7. Hershkowitz, F., Olmstead, W.N., Rhodes, R.P. and Rose, K.D. In "Geochemistry and Chemistry of Oil Shales", ACS Symposium Series 230 (Eds. F.P. Miknis and J.F. McKay) 301 (1983).
8. Burnham, A.K. and Happe, J.A. Fuel 63, 1353 (1984).
9. Webster, D.S., Cross, L.F. and Lynch, L.J. Rev. Sci. Instrum. 50, 390 (1979).
10. Lynch, L.J. and Webster, D.S. In "Geochemistry and Chemistry of Oil Shales", ACS Symposium Series 230 (Eds. F.P. Miknis and J.F. McKay) 353 (1983).
11. Lynch, L.J., Webster, D.S., Bacon, N.A. and Barton, W.A. In "Magnetic Resonance Introduction, Advanced Topics and Applications to Fossil Energy". (Eds. L. Petrakis and J.P. Fraissard) NATO ASI Series, C 124, 617, Reidel, Dordrecht (1984).
12. Coshell, L. Proc. First Australian Workshop on Oil Shales, Lucas Heights, 25 (1983).
13. Wilson, M.A., Lambert, D.E. and Collin, P.J. Fuel (in press) (1985).
14. Miknis, F.P., Decora, A.W. and Cook, G.L. In "Science and Technology of Oil Shales" (Ed. T.F. Yen) Ann Arbor Science, Ann Arbor, 35 (1976).
15. Loughnan, F.C. "Rundle Oil Shale Mineralogical Analysis of Ore Types", Esso Australia Ltd. Report (1983).
16. Lynch, L.J., Webster, D.S. and Parks, T. Proc. First Australian Workshop on Oil Shales, Lucas Heights, 139 (1983).
17. Haddadin, R.A. and Tawarah, K.M. Fuel 59, 539 (1980).
18. Villey, M., Oberlin, A. and Combaz, A. Carbon 17, 77 (1979).
19. Oberlin, A., Villey, M. and Combaz, A. Carbon 18, 347 (1980).

TABLE I

Analyses and Pyrolysis Data of Rundle Ore Types

Shale Ore Type[1]	F.A. Oil Yield (L/t)	C (%w/w)	Ash (%w/w)		Temperature at Max. Rate of H Loss (K)		Hydrogen Volatile % (298-875K)	
	Shale	Shale	Shale	Demin.	Shale	Demin.	Shale	Demin.
LRC[2] I	137	17.50	72.2	16.9	725	725	90	95
LRC II	134	17.18	71.2	19.5	725	725	93	95
LRC III	29	6.71	84.0	37.9	725	725	88	91
LRC IV	63	9.38	83.5	26.7	730	720	87	91
LRC V	112	15.74	75.2	19.2	725	725	88	92
LRC VI	56	8.94	82.8	29.8	720	720	91	95
BK[3] IX	95	14.09	77.1	-	725	725	90	92
BK XI	56	8.81	82.7	-	720	725	86	92

1 Coshell (12)
2 Lower Ramsay Crossing seam
3 Brick Kiln seam

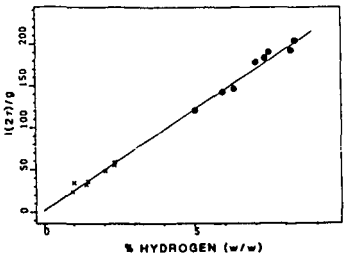

Figure 1. ^1H NMR signal peak intensity (I(2τ)) per gram of specimen versus % elemental hydrogen for Rundle shales (x) and kerogen concentrates (●).

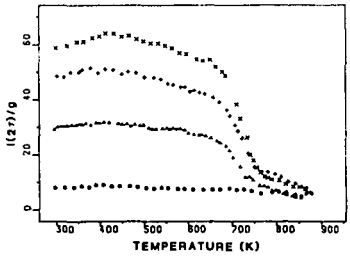

Figure 2. The apparent residual hydrogen per gram of specimen from ^1H NMR measurements versus temperature for Rundle ore types I(x), IX(+), III(▲) and montmorillonite (●).

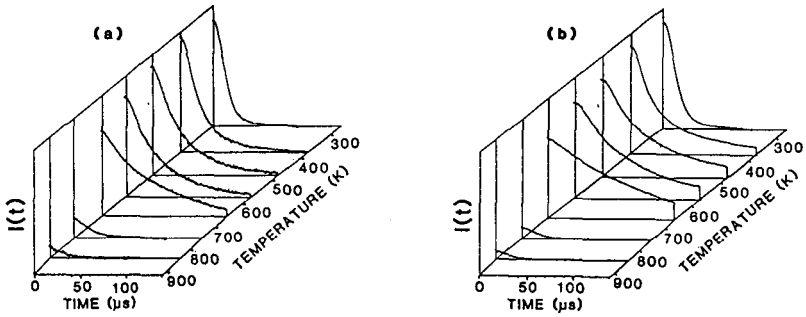

Figure 3. ^1H NMR transverse relaxation signals, I(t), recorded at various temperatures during pyrolysis of (a) the whole shale and (b) the kerogen concentrate of Rundle ore type II.

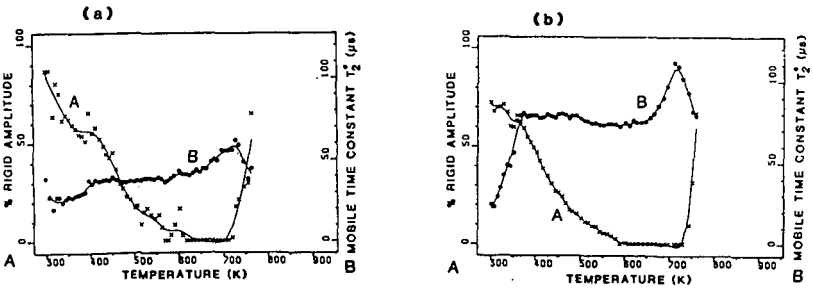

Figure 4. Pyrograms showing the temperature dependences of percentage rigid hydrogen (% Rigid) and the relaxation time constant (T_2^*) of mobile hydrogen during pyrolysis of (a) the whole shale and (b) the kerogen concentrate for Rundle ore type II.

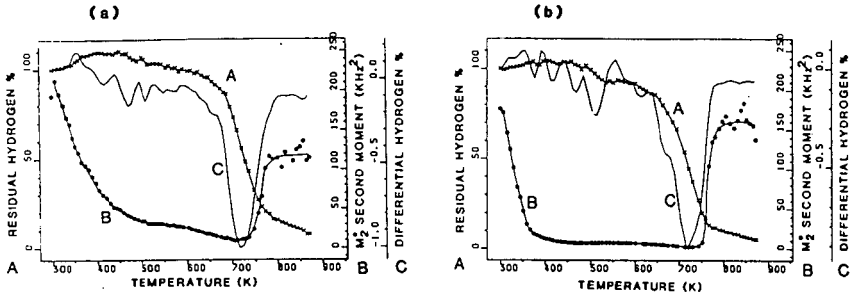

Figure 5. Pyrograms showing the temperature dependences of the apparent residual hydrogen (A), the differential hydrogen content (C) and the ^1H NMR power spectrum second moment, M_2^*, (B) during pyrolysis of (a) the whole shale and (b) the kerogen concentrate of Rundle ore type II.

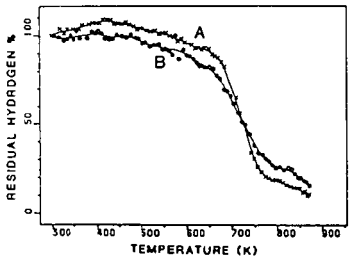

Figure 6. A comparison of pyrograms of the percent apparent hydrogen content for Rundle shale ore types (A) I and (B) XI.

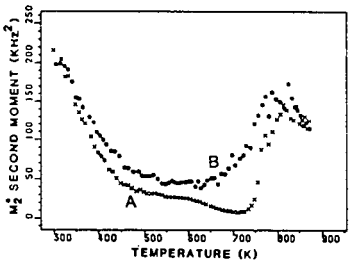

Figure 7. A comparison of the ^1H NMR power spectrum second moment (M_2^*) pyrograms for Rundle shale ore types (A) I and (B) XI.

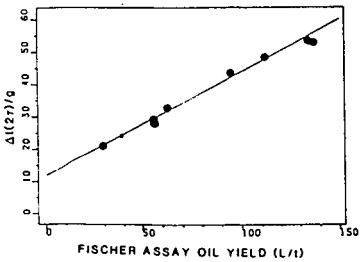

Figure 8. Loss of ^1H NMR signal intensity ($\Delta I(2\tau)$) on heating at 4 K min^{-1} from 298 to 875 K normalized per gram of shale versus Fischer Assay oil yield.

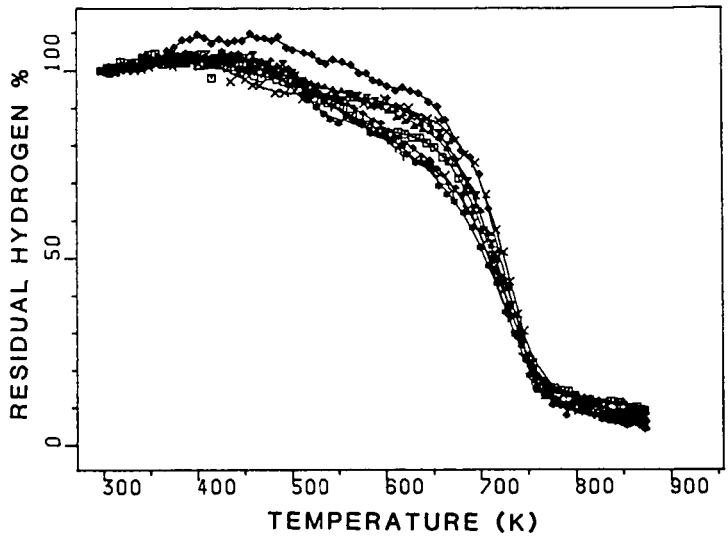

Figure 9. A comparison of pyrograms of the percent apparent residual hydrogen for demineralized specimens of eight Rundle oil shale ore types listed in Table I.

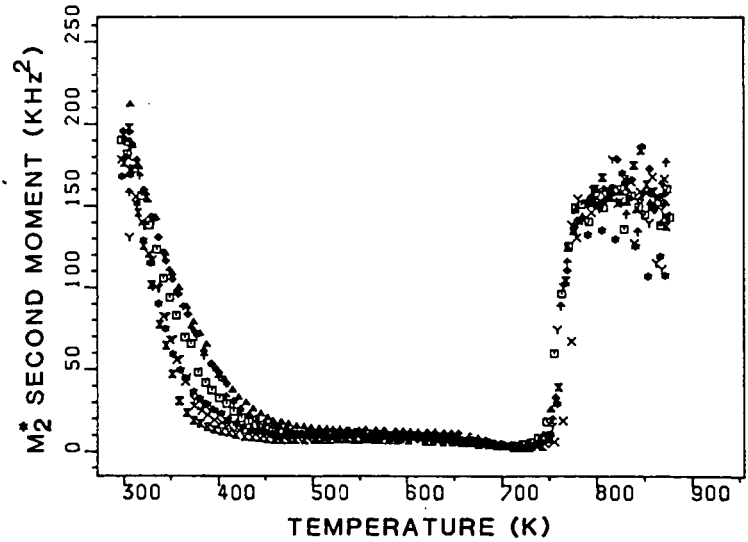

Figure 10. A comparison of the ^1H NMR power spectrum second moment (M_2^*) pyrograms for kerogen concentrates of eight Rundle oil shale ore types listed in Table I.

^{13}C N.M.R. DIPOLAR DEPHASING AS A PROBE INTO THE STRUCTURE OF AUSTRALIAN OIL SHALE KEROGENS AND PYROLYSIS RESIDUES

D.E. Lambert and M.A. Wilson

CSIRO Division of Fossil Fuels, PO Box 136, North Ryde, NSW 2113, Australia

ABSTRACT

The solid state nuclear magnetic resonance (n.m.r.) technique of dipolar dephasing was applied to a range of Australian oil shale kerogens and pyrolysis residues of an aliphatic shale (Rundle, Queensland), in order to gain more information on chemical structure than can be obtained from a conventional cross polarization spectrum. From these measurements the proportion of aliphatic carbon that is methyl or non-protonated in an aromatic shale and the pyrolysis residues was estimated. Non-protonated carbon was found to be unimportant and thus it was shown that the methyl content varied according to shale type and/or thermal history. The proportion of aliphatic methyl carbon in residues, generated at a range of temperatures from 400-500°C, was found to increase with increasing reaction temperature. This trend indicates that the β-bond in alkyl chains attached to aromatic ring structures is cleaved in preference to the α-bond during shale pyrolysis.

INTRODUCTION

Dipolar dephasing ^{13}C n.m.r has been extensively employed in determining the fraction of aromatic carbon that is protonated in a range of solid samples including model compounds, coals and other geochemical materials (1-17). In many heterogeneous samples the decay of aromatic signal intensity with increasing carbon magnetization holding time (t_1) can be expressed, in terms of the decay constants T'_{2A} and T'_{2B}, as the sum of two exponential decays from protonated and non-protonated aromatic carbon, respectively. A separation of the aromatic signal intensity into two components is possible as the minimum T'_{2B} values for model aromatic ring compounds are five times the T'_{2A} values obtained for methine carbon (1). However, this was not found to be the case for oil shales (18). We have attributed this difference in relaxation behaviour to the intrinsic nature of the oil shale kerogen. Either the non-protonated carbons are in close proximity to protonated structures and thus have reduced T'_2 values, which approach those of the protonated carbons, and/or there are significantly more protonated carbons present, which still dominate the total signal intensity at $t_1 > 45$ μs, when only signal from non-protonated carbon is normally observed.

Little work has been undertaken to investigate the chemical structure of the aliphatic components of fossil fuels by n.m.r. Some studies have been reported on coals (1), but data on oil shales are not currently available. Thus, in this work we have examined the potential of dipolar dephasing as a probe of the chemical structure of the aliphatic components in Australian shales and shale pyrolysis residues. The fraction of aliphatic carbon that is methyl in the most aromatic shale and the pyrolysis residues has been estimated. This is related to kerogen structure and the mechanism of shale pyrolysis.

THEORY

The technique of dipolar dephasing is based on the rapid loss of signal intensity from protonated carbons, when a time period (t_1), in which the proton decoupler is turned off, is inserted before data acquisition in a conventional cross polarization program. The rate at which signal intensity is lost is dependent on the magnitude of the carbon-hydrogen dipolar interaction. Hence carbons bonded to protons experience stronger dipolar interactions than non-protonated carbons, unless the dipolar interaction is modulated by molecular motion, e.g. rapid rotation of

methyl groups. It has been shown for some compounds (19) that at a dipolar dephasing time of 50 μs the signal intensity from methine and methylene carbons is almost completely eliminated from the conventional cross polarization spectrum. Resonances from quaternary carbons remain, although attenuated in intensity due to long range, weak interactions with protons. Methyl carbon resonances also remain if the methyl groups present are free to rotate at speeds sufficient to severely weaken the carbon-proton interaction. This is possible in almost all solids including coals (1).

For carbons that are weakly coupled to protons, model compound studies have shown that the decay of signal intensity is simply exponential with increasing dipolar dephasing time (t_1) (5,7,20). However, for strongly coupled methylene and methine carbons, signal intensity decays as a function of time squared, i.e. a Gaussian decay pattern (5,7,20). In more complex systems such as coals the decay of aliphatic signal intensity is closer to exponential than Gaussian, however similar T_2' values are normally obtained from either Gaussian or exponential calculations (1).

For kerogen residues and highly aromatic shales (aromaticity (f_a) > 0.60), which contain methine, methylene, quaternary and methyl carbons, our results (Figure 1) show that the decay of aliphatic signal intensity can be described as the sum of two decays given by Equation 1.

$$I_T = I_s^o \exp-[t_1^2/2T_2'(S)^2] + I_w^o \exp-[t_1/T_2'(W)] \qquad 1)$$

where I_T is the total aliphatic signal intensity; I_s^o is the initial signal intensity of the strongly coupled aliphatic carbons (CH_2,CH); I_w^o is the initial signal intensity of the weakly coupled aliphatic carbons (C,CH_3); t_1 is the delay period where the decoupler is gated off; and $T_2'(S)$ and $T_2'(W)$ are respectively the decay constants for the decay processes of strongly and weakly coupled carbon types.

If one approximates that the signal intensity of the strongly coupled carbons has decayed to a negligible amount after a delay period of 50 μs, then Equation 1 simplifies to

$$I_T = I_w^o \exp-[t_1/T_2'(W)] \qquad 2)$$

I_w^o can therefore be determined from the zero time extrapolated intercept of the graphed data for t_1 > 50 μs (see Figure 1). $T_2'(W)$ is obtained from the reciprocal slope of the least-squares fit to the data. These parameters can then be used to obtain data on the decay of the strongly coupled carbons. The plot of $\ln [I_T - I_w^o \exp-t_1/T_2'(W)]$ versus the square of t_1 (1) yields a linear relationship and $T_2'(S)$ is obtained from the slope.

The parameter, $f_w(Ali) = I_w^o/(I_w^o + I_s^o) = I_w^o/I_T^o$, gives the fraction of aliphatic carbon that is methyl or non-protonated. $F_w(Ali)$ is related to the fraction of total carbon that is methyl or non-protonated (f_w), by ($1-f_a$), where f_a is the fraction of total carbon that is aromatic,i.e.

$$f_w = f_w(Ali) \times (1-f_a) \qquad 3)$$

Alternatively, when only a single exponential decay is observed (Figure 2), an estimate of $f_w(Ali)$ can be made indirectly from the signal intensity of the aliphatic resonance at t_1 = 0 μs and a delay time at which all methylene and methine carbon has decayed completely (1). A delay of 50 μs would be appropriate for the oil shale samples examined. However, as the T_2' values of the aliphatic kerogens are > 25 μs, indicating that the methine and methylene groups in the kerogens are highly mobile, this approach is not applicable to oil shales.

EXPERIMENTAL

Sample Preparation

All samples were demineralized by hydrochloric/hydrofluoric acid treatment (18) prior to analysis by n.m.r.

Pyrolysis residues of Rundle shale (Queensland, Australia) were generated from pyrolysis experiments using a modification of the Fischer Assay method (ASTM D3904-80). Shale, crushed to -100 mesh, was heated to various temperatures between 400-500°C at a rate of 12.5°C/min, and held isothermally at temperature for the time specified between 10-40 min. The raw shale used in these experiments contained 13.35% organic C, 2.3% H, 1.3% S, 0.4 % N and 1.25% inorganic C on a dry weight basis. The major inorganic components were clay minerals (illite, kaolinite and montmorillonite), quartz, siderite, calcite and pyrite.

N.M.R.

Solid-state ^{13}C n.m.r. spectroscopic measurements were made on a Bruker CXP 100 instrument at 22.6 MHz. Kerogen was packed in a boron nitride rotor with a Kel-F base. The dipolar dephasing program chosen for this study used alternate phase inversion of the 90° r.f pulse to minimize baseline artifacts, and a refocusing 180° pulse along the spin locking co-ordinate was inserted in the middle of the t_1 period to avoid linear phase distortions. The 90° pulse width was 4.5-8 µs, with a recycle time of 0.8-1 s. Data were collected in 1 K of memory, zero filled to 4 K and Fourier transformed using line broadening factors of 30-100 Hz. Dipolar dephasing delays (t_1) between 2-200 µs were used and each experiment continued until 4,000-6,000 scans were acquired. Results were calculated from integrated signal intensities divided at the point of inflection between 80-100 ppm.

RESULTS AND DISCUSSION

Results obtained from dipolar dephasing experiments of a selection of Australian kerogens, with a range of aromatic carbon contents (f_a) are presented in Table 1. Figure 2 shows a typical plot of the logarithm of aliphatic signal intensity versus t_1 for a kerogen of low aromaticity (f_a = 0.21). Only an average T_2' value (T_{2C}') can be determined for the decay process. A slowly decaying component with a $T_2' > 30$ µs is not apparent in the plot; this indicates a very low concentration of methyl carbon in the kerogen. Figure 1 shows a similar plot for a highly aromatic kerogen (f_a = 0.60). The decay process is clearly not exponential and two rate constants governing the decay, $T_2'(S)$ and $T_2'(W)$, can be determined respectively from Gaussian (Figure 3) and exponential data calculations using Equations 1 or 2. Since two decay processes can be observed for the Condor carbonaceous shale and only one for the aliphatic shales then the aliphatic structures of the Condor carbonaceous kerogen contain large concentrations of methyl and/or non-protonated carbon whereas kerogens of lower aromatic content have relatively much lower concentrations of these species. The aliphatic moieties of the Glen Davis, Rundle, Condor brown and Nagoorin kerogens must consist mainly of chain methylene and methine carbons and an insignificant amount of quaternary carbon, whereas the highly aromatic kerogen must contain aromatic ring structures associated with relatively short alkyl chains and aliphatic cross-linking structures.

The T_{2C}' data calculated from dipolar dephasing experiments of shale pyrolysis residues from the Rundle deposit (Queensland) are listed in Table 2. The T_{2C}' values for the residues are greater than those of the aliphatic kerogens. However, the loss of aliphatic signal intensity is more appropriately described as a sum of two decays. The decay constants for strongly coupled carbon, $T_2'(S)$, lie near the lower limit for the time constants quoted for methylene and methine carbons (12-29 µs)

TABLE 1
DIPOLAR DEPHASING DATA FOR THE ALIPHATIC COMPONENTS OF AUSTRALIAN OIL SHALES[a]

Kerogen	f_a	Atomic H/C	T'_{2C} (μs)	$T'_2(S)$ (μs)	$T'_2(W)$ (μs)	$f_w(Ali)$	f_w
Glen Davis	0.19	1.52	29	-	-	-	-
Rundle	0.21	1.55	26	-	-	-	-
Condor brown	0.25	1.41	26	-	-	-	-
Nagoorin	0.49	0.83	28	-	-	-	-
Condor carbonaceous	0.60	0.93	55[b]	16[c]	88[c]	0.45	0.18

[a] T'_{2C} values are the average T'_2 values determined from exponential fit to all t_1 data points.

[b] Values obtained when data fitted to single exponential decay.
[c] Values obtained using Equation 1.

TABLE 2
DIPOLAR DEPHASING DECAY DATA FOR THE ALIPHATIC COMPONENTS OF SHALE PYROLYSIS RESIDUES FROM THE RUNDLE DEPOSIT (QUEENSLAND)[a]

Pyrolysis conditions Temperature (°C)	Time (min)	f_a	Atomic H/C	T'_{2C} (μs)	$T'_2(S)$ (μs)	$T'_2(W)$ (μs)	$f_w(Ali)$	f_w
425	10	0.33	1.26	46	19	67	0.69	0.46
425	20	0.52	1.17	52	20	82	0.64	0.31
400	40	0.38	1.18	48	16	69	0.58	0.36
425	40	0.64	1.01	57	-[b]	76	0.78	0.28
450	40	0.81	0.74	52	-	-	-	
475	40	0.85	0.64	65	-	-	-	

[a] T'_{2C} values determined from exponential fit to all t_1 data points.
[b] Insufficient points for accurate determination.

(20). The decay constants for weakly coupled carbons, $T_2'(W)$, are all less than 100 μs suggesting a predominantly methyl contribution to the signal intensity. Hence the f_w(Ali) estimates obtained for the residues reflect an increase in the proportion of aliphatic carbon that is methyl with increasing pyrolysis temperature.

The decay of aliphatic signal intensity from the highly aromatic residues could not be resolved into two components for a number of reasons. The aliphatic content of these residues is low, and there is a small contribution from spinning side bands to the total aliphatic signal intensity, owing to the greater chemical shift anisotropy of these samples. At t_1 > 45 μs these contribute most of the signal intensity in the aliphatic region and the small 'real' aliphatic signal becomes buried. Nevertheless chemical shift data (Figure 4) show that there is an upfield shift of the centre of the aliphatic resonance with increasing pyrolysis temperature of the shale residues. This resonance, centred at 31 ppm in the raw kerogen, approaches a value of 16 ppm, similar to the chemical shift expected for methyl carbon, in the high temperature residues. This progressive increase in methyl carbon content of the shale residues is more clearly illustrated by dipolar dephasing experiments. Figure 5 shows the spectra obtained after a dipolar dephasing delay of 2, 30 and 60 μs from Rundle shale and a low (425°C) and high (475°C) temperature pyrolysis residue. The aliphatic peak of the raw shale is narrow, sharp and unsplit after a delay time of 60 μs. In the 425°C residue set, a shoulder emerges from the central aliphatic resonance after a 30 μs delay and a distinct separation of a methyl resonance is obvious after a 60 μs delay. A marked upfield shift of the whole aliphatic resonance occurs after a 30 μs delay in the high temperature residue. Thus our results indicate that the proportion of aliphatic carbon that is methyl increases significantly with increasing pyrolysis temperature.

These results allow some conclusions to be drawn about the mechanism of shale pyrolysis. Although the fraction of total carbon that is methyl or non-protonated in the residues (f_w) appears to decrease with increasing pyrolysis temperature (Table 2), the aliphatic carbon of the pyrolysis residues contains a larger proportion of methyl groups than the parent shale (Rundle). Thus alkyl chains in the kerogen must be preferentially cleaved β to aromatic rings rather than α to aromatic rings during pyrolysis. It is noteworthy that similar behaviour has been observed in residues from the flash pyrolysis of coals (21).

CONCLUSIONS

Dipolar dephasing studies on shales and shale residues can yield useful information about the structure of the aliphatic components present in these solids. It has been demonstrated that in an Australian shale (Condor carbonaceous) with a high aromatic carbon content (f_a = 0.60) the aliphatic carbon consists of a high proportion of methyl groups whereas shales of lower aromaticity (Glen Davis, f_a = 0.19; Rundle, f_a = 0.21; Condor brown, f_a = 0.25 and Nagoorin, f_a = 0.49) all have very low methyl contents.

The dipolar dephasing behaviour of the aliphatic signal of the Condor carbonaceous shale can be resolved into a rapidly decaying component, with a signal intensity dependent on the square of the dipolar dephasing time and a slower exponentially decaying component. Similar behaviour has also been observed for pyrolysis residues from a highly aliphatic shale (Rundle). These results together with chemical shift data show that when shale is pyrolysed the proportion of aliphatic carbon that is methyl increases with increasing pyrolysis temperature up to 500°C. Hence during pyrolysis the β-carbon-carbon bond of alkyl chains attached to aromatic rings is cleaved in preference to the α-bond, i.e. methyl groups are more stable.

ACKNOWLEDGEMENTS

Esso Australia Ltd and Southern Pacific Petroleum are thanked for financial support.

REFERENCES

1. M.A. Wilson, R.J. Pugmire, J. Karas, L.B. Alemany, W.R. Woolfenden, D.M. Grant and P.H. Given. Anal. Chem. 1984, 56, 933.
2. M.A. Wilson, R.J. Pugmire and D.M. Grant. Org. Geochem. 1983, 5, 121.
3. F.P. Miknis, M. Sullivan, V.J. Bartuska and G.E. Maciel. Org. Geochem. 1981, 3, 19.
4. V.L. Weinberg, T.F. Yen, B.C. Gerstein and P. Dubois-Murphy. Am. Chem. Soc. Div. Pet. Chem. Prepr. 1981, 26(4), 816.
5. P. Dubois-Murphy, B.C. Gerstein, V.L. Weinberg and T.F. Yen. Anal. Chem. 1982, 54, 522.
6. B.C. Gerstein, P. Dubois-Murphy and L.M. Ryan. In "Coal Structure" Meyers, R.A., Ed: Academic Press, New York, 1982 pp. 87-129.
7. P. Dubois-Murphy, T.J. Cassady and B.C. Gerstein. Fuel 1982, 61, 1233.
8. V.A. Weinberg, T.F. Yen, P.Dubois-Murphy and B.C. Gerstein. Carbon 1983, 21, 149.
9. E.W. Hagaman and M.C. Woody. Proceedings of the International Conference on Coal Science, Dusseldorf, W. Germany, Sept 7-9, 1981, pp. 807.
10. D.W. Kuehn, A. Davis, R.W. Snyder, M. Starsinic, P.C. Painter, J. Havens and J.L. Koenig. Am. Chem. Soc. Div. Fuel Chem. Prepr. 1982, 27(2), 55.
11. J.R. Havens, J.L. Koenig and P.C. Painter. Fuel 1982, 61, 393.
12. M.J. Sullivan and G.E. Maciel. Anal Chem. 1982, 54, 1606.
13. R.L. Dudley and C.A. Fyfe. Fuel 1982, 61, 651.
14. M.A. Wilson, P.J. Collin, R.J. Pugmire and D.M. Grant. Fuel 1982, 61, 959.
15. A.R. Palmer, and G.E. Maciel. Anal. Chem. 1982, 54, 2194.
16. R.J. Pugmire, W.R. Woolfenden, C.L. Mayne, J. Karas and D.M. Grant. Am. Chem. Soc. Div. Fuel Chem. Prepr. 1983, 28(1), 103.
17. M.A. Wilson, A.M. Vassallo and N.J. Russell. Org. Geochem. 1983, 5, 35.
18. M.A. Wilson, D.E. Lambert and P.J. Collin. Fuel 1985 (in press).
19. S.J. Opella and M.H. Frey. J. Am. Chem. Soc. 1979, 101, 5854.
20. M.A. Wilson and R.J. Pugmire. Trends Anal. Chem. 1984, 3, 144.
21. P.J. Collin, R.J. Tyler and M.A. Wilson. Fuel 1980, 59, 479.

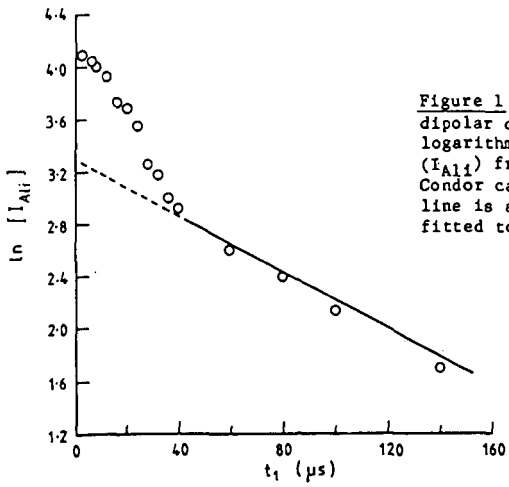

Figure 1 Effect of varying the dipolar dephasing time (t_1) on the logarithm of the signal intensity, (I_{Ali}) from aliphatic carbon in Condor carbonaceous kerogen. The line is an exponential function fitted to the data at $t_1 > 40$ μs.

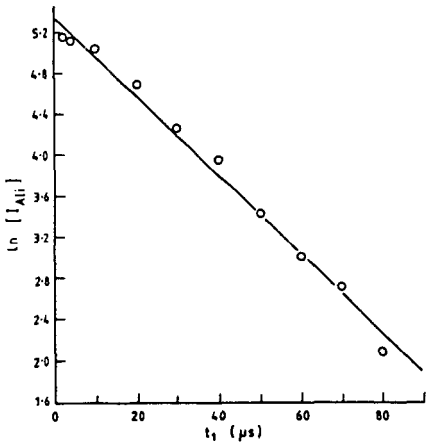

Figure 2 Effect of varying the dipolar dephasing time (t_1) on the logarithm of the signal intensity (I_{Ali}) from aliphatic carbon in Rundle kerogen.

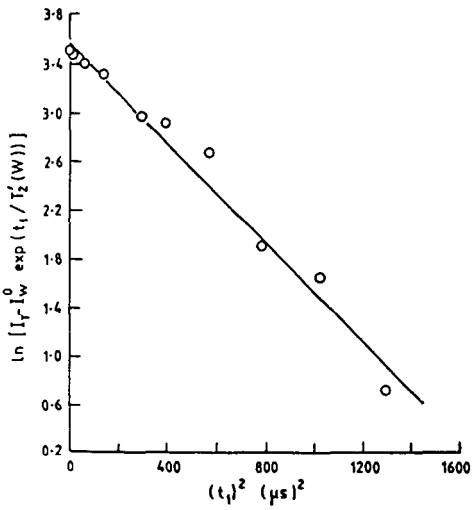

Figure 3 Plot of the square of the dipolar dephasing time (for t_1 < 40 μs) against the logarithm of signal intensity from strongly coupled aliphatic carbon (CH_2,CH) in Condor carbonaceous kerogen.

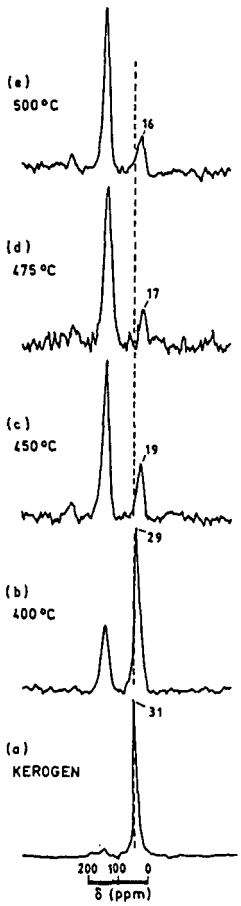

Figure 4 CP/MAS ^{13}C n.m.r. spectra of Rundle kerogen and residues. a) kerogen; residue prepared at: b) 400°C, c) 450°C, d) 475°C, e) 500°C. Note that there is a decrease in chemical shift of the aliphatic resonance with increase in pyrolysis temperature.

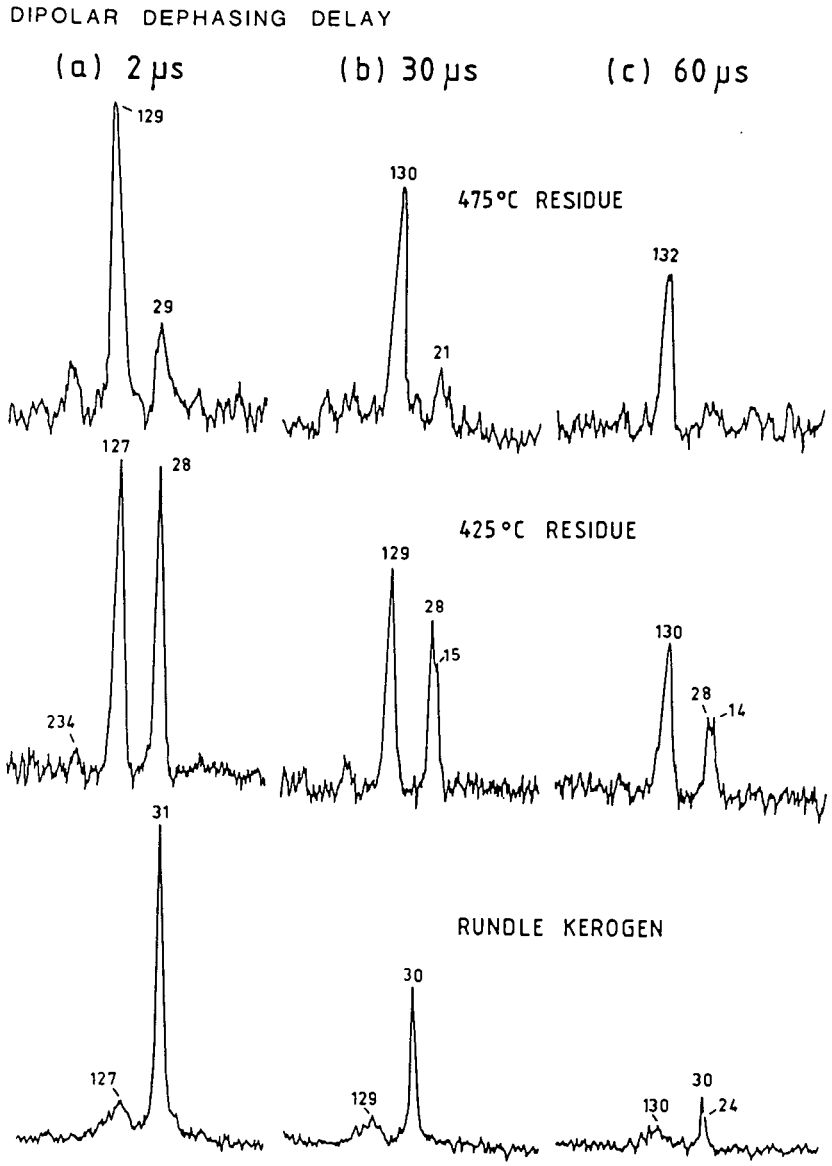

Figure 5 Dipolar dephased spectra of Rundle shale and residues prepared by pyrolysis at 425 and 475°C respectively. The dipolar dephasing times were a) 2 μs, b) 30 μs, c) 60 μs.

SYMPOSIUM ON OIL SHALE REACTIVITY AND PROCESSING
PRESENTED BEFORE THE DIVISIONS OF FUEL CHEMISTRY
AND PETROLEUM CHEMISTRY, INC.
AMERICAN CHEMICAL SOCIETY NATIONAL MEETING
CHICAGO, ILLINOIS, SEPTEMBER 8-13, 1985

THE INFLUENCE OF TEMPERATURE UPON THE PYROLYSIS OF AUSTRALIAN OIL SHALES

By

N.V. DUNG and G.C. WALL

CSIRO Division of Energy Chemistry, Lucas Heights Research Laboratories,
Private Mail Bag 7, Sutherland, NSW. 2232. Australia.

INTRODUCTION

Oil shale is one of the most prospective sources for the production of synthetic liquid fuels. Most of the Australian oil shale deposits are located in Queensland with the total in-situ resources in excess of 4×10^{12} L (25 billion barrels) of shale oil. This is more than 12 times the current Australian recoverable petroleum resources. The CSIRO Division of Energy Chemistry is undertaking a comparative study of the processing characteristics of seven oil shales from Condor, Duaringa, Lowmead, Nagoorin, Nagoorin South, Rundle and Stuart deposits which represent more than 80% of the current Australian shale oil resource.

A "fines" retorting process - arbitrarily defined as a process which accepts a feed particle size of minus 12 mm - is being investigated. The process consists of the fluidized bed pyrolysis of raw shale, fluidized bed combustion of spent shale, and recirculation of solids (spent shale and shale ash) between the combuster and the pyrolyser to supply heat to the retorting step. This process utilizes all the mined shale and is self-sufficient in process heat.

A fluidized bed pyrolyser provides, first, good mixing of the solids (raw shale and hot recycled shale ash) and good heat transfer, and hence rapid heating of oil shale and a uniform pyrolysis temperature; second, short residence time of oil vapor in the hot zones to give low oil cracking; and third, an environment of low partial pressure of oil vapor to enhance oil evaporation. These conditions give improved oil yields. Fluidized bed pyrolysis (FBP) gave oil yields in excess of the Fischer Assay (FA) for US oil shales (1,2) and Australian oil shales (3,4). The latter studies, using steam as the fluidizing gas, indicated that the yield enhancement was due to the effect of gas sweeping and that heating faster than 12°C min^{-1} had no additional effects on the oil yields from Rundle and Condor shales.

This paper presents results for the pyrolysis of Condor and Nagoorin oil shales in the temperature range 430 to 600°C using a laboratory-scale nitrogen fluidized bed pyrolyser. The Condor deposit (an in-situ shale oil resource of

1.3×10^{12} L) is the largest Tertiary oil shale deposit in Australia and a potential candidate for the first new Australian shale oil production plant. TheNagoorin deposit is a carbonaceous oil shale which gives a high yield of oil of high aromatic content.

Small-scale fluidized beds severely dilute the product oil vapours with non-condensable fluidizing gases. Quantitative recovery of the diluted oil vapours presents problems with condensing the naphtha fractions and the formation of oil mists (1,3). A dichloromethane scrubber fitted with a series of shrouded turbine mixers was used to overcome these difficulties.

APPARATUS AND PROCEDURE

The pyrolyser, which had long solids and short (<0.5 s) vapour residence times was designed to complete the kerogen decomposition and to minimize the oil loss due to the thermal cracking of oil vapor, and hence provided the ultimate yields and characteristics of the pyrolysis products. The final data will be used together with the data from pyrolysis kinetics (5) and oil cracking kinetics experiments to evaluate the performance of a large-scale continuous retort (6).

The FBP apparatus is shown in Figure 1. Metered high purity nitrogen was preheated to and controlled at the pyrolysis temperature in a coil of 9.5 mm o.d. tubing by an electric furnace before entering below a conical section at the base of the reactor vessel. The reactor was a stainless steel vessel (48 mm i.d. by 300 mm long) which was initially charged with 100 g of 0.5-1.0 mm roasted, acid-washed silica sand. The temperature of the fluidized bed was controlled to within ± 1°C by an electric heater wound around the bed section. The reactor axial temperature had a uniform profile from the bottom of the bed to a height of 220 mm. Temperature at the top of the reactor was about 30°C lower than the bed temperature. Reactor wall temperatures were recorded at three heights to monitor for hot spots. A superficial velocity of 1.35 times the minimum fluidizing velocity was used.

Samples of dried oil shale (100 g, particle size 0.6-1.4 mm) were added to the bed at the rate of 0.22 g every five seconds via an air-operated feed valve which was actuated by a cycle timer. Spent shale was accumulated in the reactor and a further retorting period of two to ten minutes after the completion of shale feeding was used to simulate an infinite solid residence time. The pyrolysis gases were passed through an internal 10 mm o.d. cyclone to remove fines from the product. The fines were then recovered, weighed and combined with the spent shale for each run. The hot gases and vapors entered a turbine scrubber (80 mm i.d. by 400 mm long), containing 1.2 L of rectified dichloromethane, via a sparger. Oil vapors condensed and dissolved in the dichloromethane which was kept at between 2 and 5°C by evaporation. The dichloromethane was refluxed through a condenser (-60°C) into the scrubber. Oil mists formed within gas bubbles were scrubbed by three shrouded turbines connected in series; big bubbles were sheared into smaller ones and then recirculated through one turbine many times before being released to the next. Before being metered, the off-gas passed through a bed packed with glass wool which trapped about 1 to 2% of the oil yield.

The oil/dichloromethane solution was pressure-filtered to remove traces of spent shale which were then weighed and included in the material balance. Dichloromethane was separated from the oil by atmospheric and vacuum distillation. The atmospheric fractionation column concentrated the solution to about 40 wt % of dichloromethane in the oil to keep the temperature of the solution below 60°C. The vacuum distillation was performed in a closed-system rotary evaporator. The equilibrium vacuum of the system was determined by the condenser temperature (0°C). The oil yield was corrected for the

dichloromethane content in the oil (1 to 3%) and the naphtha content in the vacuum distillate (1 to 4% of whole oil) which were determined using gas chromatography.

The Condor brown shale was supplied by Southern Pacific Petroleum N.L. and Central Pacific Minerals N.L. from 152 mm diamond drill No. 43 cores (from 60.65 to 68.25 m depth). The Nagoorin shale was the bulk sample from Unit Cc. The samples used in this study were split from the 0.6-1.4 mm fractions freshly crushed of 200 kg batches. Before each experiment, the shale was dried in nitrogen at 105°C for at least seven hours to a moisture content below 2 wt%.

Fischer Assays were done in accordance with ASTM standard D-3904-80 except that the particle size was 0.6 to 1.4 mm and the pyrolysis gases were collected and analysed. Raw and spent shales were analysed for total carbon, hydrogen and carbonate carbon (Australian Standard, AS 1038 part 6), and for moisture (Australian Standard AS 1038 part 3). Total sulphur in the raw and spent shales was determined by the high temperature combustion method (7) and sulphur in the oils by the reduction method (7). Simulated distillation of the oils was done on a Varian 3400 gas chromatograph according to the ASTM D-2887 method.

RESULTS AND DISCUSSION

Raw shale.

Table 1 shows the analyses and Fischer Assay yields of the Condor and Nagoorin oil shales. Compared to the Condor shale the Nagoorin shale is much richer in organic carbon, but lower in the H/C atomic ratio of the kerogen and carbonate carbon; also it produces double the oil, five times the pyrolysis water, eight times carbon monoxide, and much more hydrocarbon gas and carbon dioxide. The balances of the inorganic carbon for the shales indicated that the Condor carbon dioxide was from carbonate carbon (siderite) whereas the Nagoorin carbon dioxide was from the decomposition of kerogen (carboxyl group).

Oil yields.

The results (ultimate yields, analyses of oil and spent shale, and recovery of organic carbon) for the FBP runs at various temperatures are given and compared with the FA data in Table 2 (Condor) and 3 (Nagoorin).

For Condor shale, the ultimate yield of the whole oil was constant in the range 450 to 525°C but decreased markedly from 525 to 600°C. The loss of the oil yield in the higher temperature range was caused mainly by thermal cracking in the oil vapor which correlated with the lower atomic H/C ratio, which for the 600°C oil was 1.49 compared to 1.60 for the 500°C oil. The cracking of oil vapor with a mean residence time of 0.5s at 600°C, estimated by the Burnham and Taylor equation (8), accounted for 71% of the oil yield loss.

Figure 2 shows the effect of pyrolysis temperature on the yields of oil fractions. The yields of naphtha (C_5 to 175°C) and kerosene (175 to 240°C) increased slightly with temperature. The yields of diesel (240 to 340°C) and gas oil (340 to 450°C) had maxima at about 550 and about 525°C, respectively. The yield of heavy gas oil (+450°C) decreased markedly with increase in temperature from 450 to 600°C. However, the reduction of temperature from 450 to 430°C reduced the yields of naphtha, kerosene, diesel and gas oil slightly, and the yield of heavy gas oil significantly. More than 50% of the oil yield loss at 430°C was accounted for by the loss of the heavy gas oil fraction which was believed to remain in the spent shale. This could be caused by the combination of the increased production and the decreased evaporation of the high boiling point oils at the lower temperature.

Figure 3 shows the influence of temperature upon the ultimate yields of the oils from the Nagoorin shale. The yield of the whole oil was constant (about 16.4 wt% dry basis) for temperatures from 450 to 550°C, except for 500°C where the yield reached the maximum of 17.1 wt%. Similar to the pyrolysis of the Condor shale, the yield of the whole Nagoorin oil decreased with temperatures from 550 to 600°C where the thermal cracking of oil vapor became significant. The general trend for the production of the oil fractions was also similar to that for the Condor shale, i.e. the yields of the low boiling point oil fractions (naphtha, kerosene and diesel) increased with temperature at the expense of the high boiling point gas oils.

The averages of the FBP oil yields at temperatures from 450 to 525°C for both the shales were about 10% greater than FAs. Table 4 compares the yields of naphtha, kerosene, diesel, gas oil and heavy gas oil from the FBPs and FAs. For both the shales, about 70% of the excess oils was heavy gas oil. This substantiates the claim that the increase in oil yield can be attributed mainly to enhanced evaporation of oil in a retort of low partial pressure of oil vapor (3).

Organic Carbon Conversion.

The organic carbon conversions to oils for both the shales were consistent with the oil yields (Tables 2 and 3). Compared to the FA results, the organic carbon conversions to oils increased at the expense of the conversions to spent shales. For the Condor shale, the organic carbon conversion to spent shale was independent of temperature (450 to 550°C), but for the Nagoorin shale, the conversion decreased with increase in temperature (450 to 600°C). This implied the continuing production of CO, CO_2 and hydrocarbon gases from the Nagoorin kerogen with temperature. When the shales were heated linearly at 3°C min^{-1} to 850°C considerable amounts of carbon monoxide, carbon dioxide and methane from Nagoorin but not from Condor evolved at temperatures above 500°C, at which the production of oil ceased (9).

The Nagoorin spent shale had very high organic carbon content (about 50 wt%) which was more than ten times that of the Condor spent shale. Combustion of the Nagoorin spent shale will provide more than enough process heat for the retorting step; however, transferring the heat by recycling the hot shale ash would lead to a problem of balancing the recycled solids of suitable particle sizes.

Oil characteristics.

For both shales, the pyrolysis at the higher temperature gave oils of lower H/C atomic ratio. Figure 4 compares the short column gas chromatographs of the Nagoorin oils at 450 and 600°C. The 600°C oils had considerable more alkenes (peaks marked with 0 in Figure 4) and more light hydrocarbons (lower C_{16}/C_{27} height ratios) than the 450°C oil. This was evident from the thermal cracking of the 600°C oil vapor.

Compared to the FA whole oils, the FBP whole oils from both the shales were more aromatic (lower H/C atomic ratio). The increase in the aromaticity of the FBP whole oils was attributed entirely to the presence of the additional gas oils and heavy gas oils (see Table 4). These heavy oils were highly aromatic (10).

As was expected, the Condor oil shale produced oils (from FA and FBP) of better quality (higher H/C atomic ratio, and lower contents of heteroatoms and density) than the Nagoorin carbonaceous shale. However, the Condor oil contained more heavy gas oil (especially the fraction boiling above 550°C), as is shown in Figure 5.

Carbonate Carbon.

By contrast with the shales from Green River formation, both shales contain small amounts of mineral carbonates (siderite). However, as is shown in Figure 6, the residual carbonate carbon in the Condor spent shale reduced sharply with increase in pyrolysis temperature, to 3% of the Condor shale carbonate carbon at 500°C. This implies that the heat of the decomposition of siderite has to be provided to the retorting step, hence the content of this mineral in the feed shale is vital to the retort heat balance.

SUMMARY

The pyrolysis of Condor and Nagoorin shales was studied in the temperature range 430 to 600°C in a nitrogen fluidized bed retort with long solid and short vapour residence times.

The oil yields were constant from 450 to 525°C (Condor) and from 450 to 550°C (Nagoorin), and both were about 10% in excess of Fischer Assay. The additional oils were mainly high boiling point fractions. The distribution of oil fractions, namely naphtha, kerosene, diesel, gas oil and heavy gas oil were significantly influenced by temperature. Generally, increase in temperature reduced the high boiling point fractions (gas oil and heavy gas oil) and increased the low boiling point fractions (naphtha, kerosene and diesel).

The yields and quality of the oils decreased with temperature from 525 to 600°C where the thermal cracking of the oil vapors (having 0.5 s residence time) became significant.

ACKNOWLEDGEMENTS

This work is partly funded through a collaborative research agreement with Southern Pacific Petroleum NL and Central Pacific Minerals NL (SPP/CPM) supported by a National Energy Research Development and Demonstration Program (NERDDP) grant. The Condor and Nagoorin oil shale samples were provided by SPP/CPM. The authors gratefully acknowledge the contributions of M. Chensee who conducted the Nagoorin experiments, P. Udaja and T.A. Noble who analysed the feed and product samples, G. Kastl who designed and operated the distillation units, S.J. Smith who conducted the simulated distillation analysis on the Nagoorin oils, and R.D. Pearse who did the Fischer Assays.

LITERATURE CITED

1. M.J. Margolis, Proceedings of the 1981 Eastern Oil Shale Symposium, Lexington KY, 151 (1982).
2. A.M. Rubel and S.D. Carter, Preprints of Symposium on Characterization and Chemistry of Oil Shales, American Chemical Society, St. Louis, 202 (1984).
3. G.C. Wall, Proceedings of the First Australian Workshop on Oil Shale, Lucas Heights, 105 (1983).
4. G.C. Wall, Seventeenth Oil Shale Symposium Proceedings, Colorado School of Mines Press, 300 (1984).
5. G.C. Wall and N.V. Dung, Proceedings of the Second Australian Workshop on Oil Shale, Brisbane, 129 (1984).
6. N.V. Dung and G.C. Wall, ibid, 199.
7. P. Udaja, M.D. Chensee and T.A. Noble, ibid, 114, (1984).
8. A.K. Burnham and J.R. Taylor, Lawrence Livermore National Laboratory, Livermore, CA, UCID-18284 (1979).
9. A. Ekstrom, H.J. Hurst and C.H. Randall. American Chemical Society Symposium Series 230, 161 (1983).
10. J.A. Gray, C.J. Brady, J.R. Cunningham, J.R. Freeman and G.M. Wilson. Ind. Eng. Chem. Process Des. Dev., 22, 410 (1983).

TABLE 1

PROPERTIES OF RAW SHALES

SHALE	CONDOR		NAGOORIN	
	Mean	s.d.	Mean	s.d.
Moisture, % as received	6.61		22.20	
ANALYSIS, wt% dry basis (4 observations)				
Organic carbon	10.84	0.03	50.70	0.13
Inorganic carbon	0.82	0.01	0.09	0.01
Hydrogen (total)	1.82	0.02	4.77	0.03
Sulphur	0.65	0.01	1.34	0.02
Kerogen atomic H/C [a]	1.41		1.02	
Inorganic hydrogen [b]	0.55		0.46	
FISCHER ASSAY, wt% dry basis (4 observations)				
Oil (C_5+)	7.47	0.19	15.02	0.50
Water	0.97	0.05	6.28	0.33
Hydrogen	0.057	0.003	0.075	
Carbon monoxide	0.130	0.008	1.113	
Carbon dioxide	1.361	0.089	6.491	
Hydrogen sulphide	0.0	0.0	0.064	
Methane	0.163	0.009	0.900	
Ethane	0.132	0.007	0.442	
Propane	0.088	0.003	0.289	
n-Butane	0.063	0.003	0.126	
i-Butane	0.004	0.0	0.015	
Ethylene	0.042	0.003	0.131	
Propylene	0.080	0.006	0.213	
Butenes	0.058	0.004	0.123	
Spent shale	89.06	0.09	68.78	0.48
TOTAL	99.68	0.14	100.06	0.43

(a) Data supplied by Southern Pacific Petroleum N.L. and Central Pacific Minerals N.L.

(b) Determined by the difference between the total hydrogen and the organic hydrogen which is calculated using the kerogen atomic H/C and the organic carbon of the shale.

TABLE 4

OIL YIELDS : FBP v.s. FISCHER ASSAY

OILS	CONDOR			NAGOORIN		
	FBP [a] (500°C)	FA [a]	Distribution of additional oil [b]	FBP [a] (500°C)	FA [a]	Distribution of additional oil [b]
Naphtha (C_5 to 175°C)	9.9	9.6	3	6.2	7.5	-9
Kerosene (175 to 240°C)	10.7	10.6	1	12.8	13.9	-8
Diesel (240 to 340°C)	27.4	25.7	19	33.6	32.6	7
Gas oil (340 to 450°C)	33.4	32.8	7	39.2	33.8	39
Heavy gas oil (>450°C)	27.7	21.3	70	22.2	12.2	71
TOTAL	109.1	100.0	100	114.0	100.0	100

(a) % of the yield of FA whole oil

(b) 100 x (yield of FBP oil - yield of FA oil)/(yield of FBP whole oil - yield of FA whole oil)

TABLE 2

RESULTS FROM CONDOR OIL SHALE

Temperature, °C	FA	FLUIDIZED BED PYROLYSIS						
	500	430	450	475	500	525	550	600
YIELDS, wt% dry basis								
Oil (C_5 +) mean	7.0	7.2	8.2	8.1	8.0	8.0	7.7	7.0
s.d.	0.2	-	0.0	0.1	0.1	-	0.1	-
number of tests	4	1	2	3	3	1	2	1
Spent shale mean	89.1	88.9	87.2	85.5	84.9	84.6	84.3	84.6
s.d.	0.1	-	0.1	0.5	0.2	0.0	0.2	-
number of tests	4	1	4	3	11	2	2	1
ANALYSIS OF OIL								
Carbon, wt%	84.1	83.87	82.20	82.57	84.08	84.11	83.85	83.39
Hydrogen, wt%	11.8	11.02	10.78	11.06	11.19	11.10	10.96	10.33
Sulphur, wt%	0.44	0.44	0.44	0.43	0.45	0.44	0.45	0.45
H/C atomic ratio	1.68	1.58	1.58	1.61	1.60	1.58	1.57	1.49
Density, 60°C g/cm^3	0.84	0.89	0.89	0.88	0.88	0.91	0.87	0.90
ANALYSIS OF SPENT SHALE wt% dry basis								
Organic carbon	4.62	4.60	4.26	4.37	4.35	4.24	4.29	4.57
Inorganic carbon	0.45	0.63	0.48	0.13	0.02	0.01	0.00	0.00
Hydrogen	0.69	0.79	0.46	0.53	0.41	0.09	0.23	0.13
Sulphur	0.69	0.69	0.64	0.68	0.68	0.70	0.65	0.67
RECOVERY OF ORGANIC CARBON, %								
Oil, mean	58.0	55.8	62.5	61.2	62.1	61.7	59.1	54.3
s.d.	1.0	-	0.2	1.7	1.0	-	0.5	-
Spent shale, mean	38.0	37.1	34.2	34.1	34.0	33.1	33.3	35.7
s.d.	1.5	-	1.4	1.7	1.1	0.1	0.3	-
Gas, mean	5.2	-	-	-	-	-	-	-
s.d.	0.3	-	-	-	-	-	-	-
Not accounted for	-1.2	7.1	3.3	4.7	3.9	5.2	7.6	10.0

TABLE 3

RESULTS FROM NAGOORIN OIL SHALE

Temperature, °C	FA	FLUIDIZED BED PYROLYSIS						
	500	450	475	500	525	550	575	600
YIELDS, wt% dry basis								
Oil (C_5+), mean	15.0	16.5	16.4	17.1	16.3	16.5	16.2	15.3
s.d.	0.5	-	0.0	0.1	-	-	0.2	-
number of tests	4	1	2	2	1	1	2	1
Spent shale, mean	68.8	66.7	65.2	63.5	62.3	61.5	61.0	60.8
s.d.	0.5	0.1	0.8	1.3	-	-	0.5	-
number of tests	4	2	2	2	1	1	2	1
ANALYSIS OF OIL								
Carbon, wt%	82.60	81.94	81.79	81.00	81.51	81.78	81.70	81.28
Hydrogen, wt%	10.52	9.83	9.77	9.50	9.85	9.50	9.61	9.34
H/C atomic ratio	1.53	1.44	1.43	1.41	1.45	1.39	1.41	1.38
Density, 60°C, g/cm^3	0.914	0.959	0.951	0.946	0.940	0.960	0.946	0.924
ANALYSIS OF SPENT SHALE wt% dry basis								
Organic carbon	50.05	47.92	49.10	49.19	50.58	50.25	50.16	48.71
Inorganic carbon	0.04	0.06	0.06	0.07	0.05	0.07	0.08	0.07
Hydrogen	2.49	2.82	2.03	2.07	1.39	1.51	1.44	1.36
Sulphur				1.48	1.50	1.30	1.20	1.42
RECOVERY OF ORGANIC CARBON, %								
Oil, mean	24.4	26.7	26.5	27.3	26.2	26.6	26.1	24.5
s.d.	0.7	-	0.1	0.1	-	-	-	-
Spent shale, mean	67.9	63.1	63.1	61.6	62.1	60.9	60.4	58.4
s.d.	0.6	-	0.1	0.1	-	-	-	-
Gas, mean	7.9	-	-	-	-	-	-	-
s.d.	0.1	-	-	-	-	-	-	-
Not accounted for	-0.2	10.2	10.4	11.1	11.7	12.5	13.5	17.1

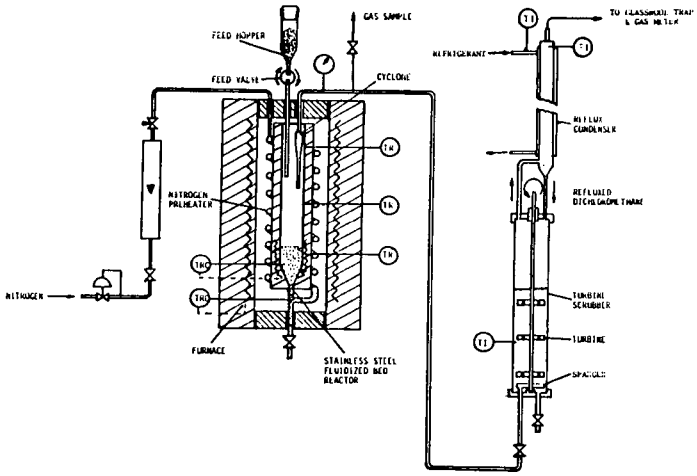

FIGURE 1. APPARATUS

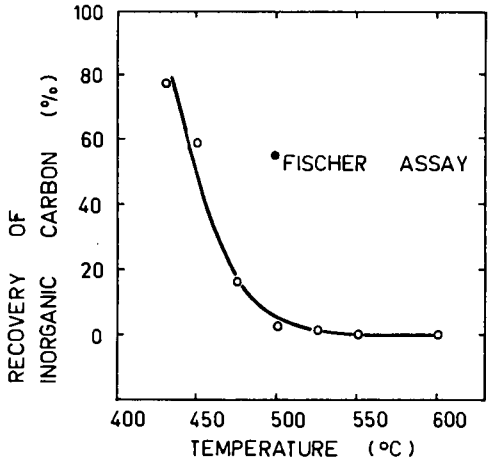

FIGURE 6. EFFECT OF TEMPERATURE ON RECOVERY OF INORGANIC CARBON IN CONDOR SPENT SHALE

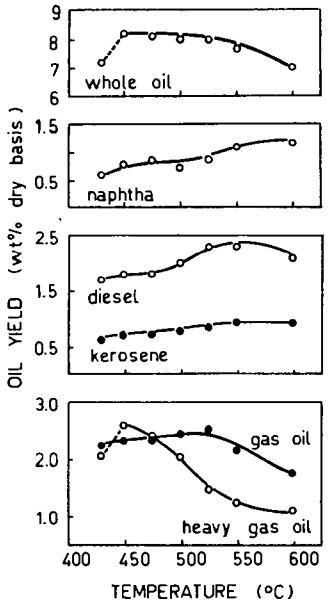

FIGURE 2. EFFECT OF TEMPERATURE ON YIELDS OF OILS FROM CONDOR SHALE

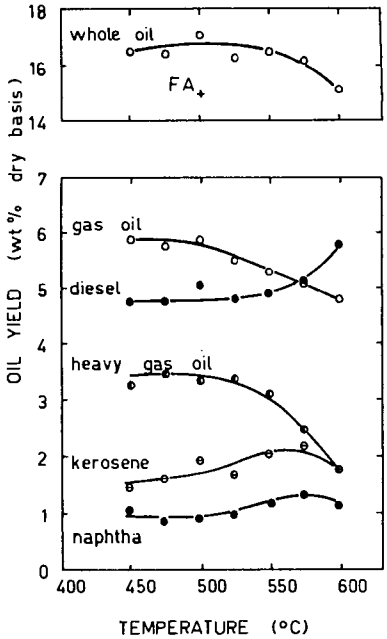

FIGURE 3. EFFECT OF TEMPERATURE ON YIELDS OF OILS FROM NAGOORIN SHALE

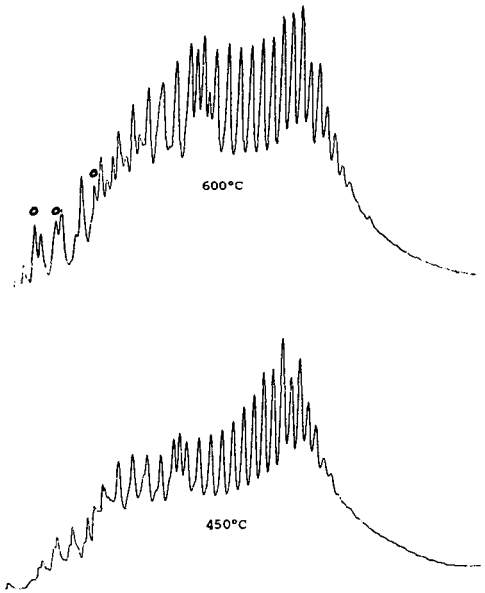

FIGURE 4. GAS CHROMATOGRAPHS OF NAGOORIN SHALE OILS AT 450 AND 600°C

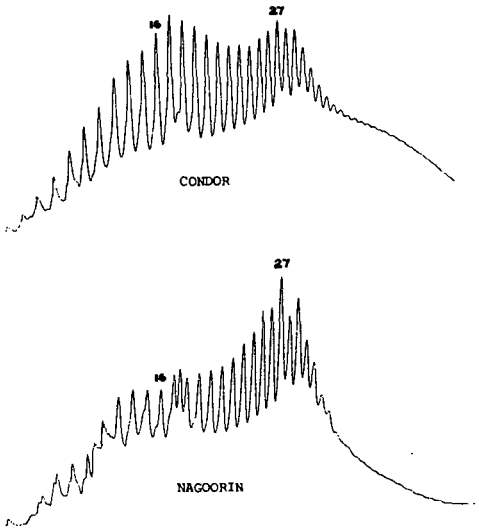

FIGURE 5. GAS CHROMATOGRAPHS OF CONDOR AND NAGOORIN SHALE OILS AT 450°C

CO-PYROLYSIS OF COAL AND OIL SHALE I: THERMODYNAMICS AND KINETICS OF HYDROGEN SULFIDE CAPTURE BY OIL SHALE

L. Johnson, M. Rostam-Abadi, I. Mirza, M. Stephenson, and C. Kruse

Illinois State Geological Survey
Champaign, Illinois 61820

Introduction

The potential for producing crude oil and a compliance char (less than 1.2 lb SO_2/ MMBtu) by pyrolysis of Illinois Basin high volatile bituminous coals has been recognized for years but it has not been realized mainly because these coals agglomerate when pyrolyzed and because the chars have a relatively high sulfur content. The feasibility of using oil shale during pyrolysis of high sulfur coals and hydrodesulfurization of the resultant coal char is currently being investigated at the Illinois State Geological Survey (ISGS). Although still in the early stages of process development, three processes have been conceived which use oil shale with coal. In the first process, coal and oil shale, or coal and retorted shale are pyrolyzed in a fluidized bed reactor(FBR). In the second process, spent oil shale and coal are processed in a FBR. In the third process, coal and oil shale are pyrolyzed in a multistaged FBR with coal and oil shale occupying separate, alternating stages. The coal char product from these processes must be hydrodesulfurized to produce a compliance char.

Pyrolyzing coal and oil shale together could have many advantages over the pyrolysis of either material separately. First, preliminary ISGS data indicates that the inert minerals in oil shale dilute the coal-shale mixture, reducing the agglomeration of caking coals. Secondly, liquid and gaseous hydrocarbons are produced from both coal and oil shale. Thirdly, the carbonate minerals found in oil shale (calcite, dolomite) and their corresponding oxides formed during pyrolysis can act as scavengers of hydrogen sulfide during pyrolysis and hydrodesulfurization. Research efforts have recently been initiated at ISGS to obtain engineering data in the above areas. The results presented are the first phase of a larger thermodynamics and kinetics study of the reactions between oil shale and H_2S. The findings of this initial literature review provide the basis for the second phase of our research which will be presented in future publications.

Decomposition Reactions

The most significant reactions of carbonate minerals which occur during the co-pyrolysis of coal and oil shale are shown in table 1. The extent and pathway of carbonate decomposition are significant because they determine which sorbent(s) are present during hydrodesulfurization or pyrolysis. The overall thermal efficiency of the process and the physical properties of the product oxide are also affected by the extent of carbonate decomposition.

Calcium carbonate in oil shale is found as calcite and dolomite. Dolomite ($CaCO_3MgCO_3$) is a single phase of calcium and magnesium carbonate with its own unique crystal structure. During decarbonation of the magnesium component to form half-calcined dolomite, $CaCO_3MgO$, (hc-dolomite) small crystallites of MgO appear indicating a separation of the calcium and magnesium phases. This separation continues through the second decarbonation to form fully-calcined dolomite, CaOMgO, (fc-dolomite). Based on this observation, one would predict that the behavior of the solid more closely resembles an intimate mixture of its calcium and magnesium components as the calcination proceeds from dolomite to fc-dolomite.

Table 1. Shale Mineral Reactions Occurring During Pyrolysis and Hydrodesulfurization

Equation	H_{298} (Kcal/mole)	Equation No
Decomposition Reactions		
$CaCO_3 \rightarrow CaO + CO_2$	43	1)
$MgCO_3 \rightarrow MgO + CO_2$	28	2)
$CaCO_3MgCO_3 \rightarrow (CaCO_3 + MgO) + CO_2$	30	3)
$CaCO_3MgCO_3 \rightarrow (CaO + MgO) + 2CO_2$	73	4)
Desulfurization Reactions		
$CaCO_3 + H_2S \rightarrow CaS + CO_2 + H_2O$	28	5)
$CaO + H_2S \rightarrow CaS + H_2O$	-15	6)
$CaCO_3MgO + H_2S \rightarrow (CaS + MgO) + H_2O + CO_2$	28	7)
$CaOMgO + H_2S \rightarrow (CaS + MgO) + H_2O$	-15	8)
$CaCO_3MgCO_3 + H_2S \rightarrow (CaS + MgO) + 2CO_2 + H_2O$	62	9)

Both the extent and mechanism of dolomite decomposition are affected by the partial pressure of CO_2. Haul and Markus (1952) followed the decomposition of dolomite by thermogravimetric analysis of powdered dolomite at 500-900°C under various partial pressures of CO_2. Their results, shown in figure 1, indicate that the decomposition occurs by two different pathways:

$$CaCO_3MgCO_3 \rightarrow [CaCO_3 + MgO] + CO_2 \rightarrow [CaO + MgO] + 2CO_2 \qquad \text{Path A}$$

$$CaCO_3MgCO_3 \rightarrow [CaO + MgO] + 2CO_2 \qquad \text{Path B}$$

The decomposition followed Path A when the partial pressure of CO_2 was 12-24 mmHg while Path B prevails at higher CO_2 pressures. Since the equilibrium constant for the decomposition reaction is simply the partial pressure of CO_2, the concentration of CO_2 affects both the mechanism and extent of decomposition. For processes in which a carbonaceous material (retorted shale or coal char) is oxidized to supply energy for the pyrolysis stage, the presence of CO_2 in the recycled combustion gases will inhibit the carbonate decomposition.

The onset of decomposition is affected by the presence of steam. MacIntire and Stansell (1953) report that calcium and magnesium components of dolomite decompose about 200°C lower than when air is used alone. The same effect was observed by Burnham et al. (1980) except dolomite was affected to a much greater extent than calcite.

Decomposition reactions are highly endothermic, thus they adversely affect the thermal efficiency of the process. Boynton (1980) described the heat balance for the calcination of limestone in a rotary kiln. Between 1.7 and 4.8 MMBtu/ton of $CaCO_3$ are expended depending on the heat recovery systems employed. The minimum heat for calcination at the dissociation temperature is 2.5 MMBtu/ton of calcite or 0.61 MMBtu/ton of shale to calcine an average western shale containing 33% carbonates. Chen et al. (1982) used the ASPEN computer simulation system to study the effect of calcite decomposition on the overall thermal efficiency of an oil shale retort.

Finally, the rate and the temperature of decomposition affect the pore structure of the carbonate mineral particles as well as the shale. Steen et al. (1980) reported an increase in porosity from 12 to 29% accompanied by an increase in surface area from 0.3 to 8.9 m^2/g after half calcination of a dolomite sample. Surface area and porosity have a strong influence on the rate of sulfidation and absorbance capacity of the minerals.

Campbell (1978) and McCarthy et al. (1984) have shown that the under typical retorting conditions $CaCO_3$ also reacts with SiO_2. The competing reactions are:

$$xCaCO_3 + ySiO_2 \rightarrow Ca_xSi_yO_{x+2y} + xCO_2$$

$$CaCO_3 \rightleftharpoons CaO + CO_2$$

When a high CO_2 partial pressure and a slow heating rate were used, the carbonate reaction to form silicates increased because of the greater length of time required to reach the decarbonation temperature. Decomposition to CaO is very rapid once this temperature is reached. Oxide formation occurs at 600 to 750°C depending on the CO_2 partial pressure whereas silicate formation occurs at about 700-800°C. Therefore, this undesirable depletion of available carbonates would not be significant during pyrolysis (600°C) but may become a problem during hydrodesulfurization (750-850°C) or if the shale is retorted prior to mixing with the coal to be pyrolyzed.

Thermodynamics of Desulfurization Reactions

The ISGS application of the minerals in oil shale differs markedly from fuel gas desulfurization by carbonates. During pyrolysis and hydrodesulfurization, H_2O, H_2, CO, CO_2 and H_2S influence the H_2S adsorption equilibria, i.e. equations 5-9, table 1. Optimal temperatures, pressures, flowrates, etc. have been specified for pyrolysis and hydrodesulfurization processes, but these conditions may not be the most favorable for H_2S adsorption. In the following discussion the thermodynamics of H_2S adsorption by oil shale minerals are reviewed while taking into consideration the limited range of operating conditions typical of pyrolysis and hydrodesulfurization processes.

The reaction between calcium oxide and hydrogen sulfide (eqs. 6 and 8) has been studied by many researchers (Uno, 1951; Rosenquist, 1951; Curran et al., 1967). Pell (1971) summarized these experimental studies with the following least squares fit of their data:

$$\log K = \log \frac{P_{H_2O}}{P_{H_2S}} = 3519.2/T - 0.268 \qquad 10)$$

Pell combined this expression with the data given by Hill and Winter (1956) for the decomposition of calcium carbonate to find the following equilibrium expression for the reaction between hc-dolomite and hydrogen sulfide (eq. 7):

$$\log K = \log \frac{P_{H_2O} \cdot P_{CO_2}}{P_{H_2S}} = 7.253 - 5280.5/T \qquad 11)$$

Combining equation 11 with the data given by Stern and Weise (1969) on the decomposition of magnesium carbonate, the following expression for the equilibrium between dolomite and H_2S (eq. 9) is obtained:

$$\log K = \log \frac{(P_{CO_2})^2 \cdot P_{H_2O}}{P_{H_2S}} = 16.19 - 10{,}553/T \qquad 12)$$

Plots of log K vs 1/T derived from equations 10-12 are shown in figures 2 and 3. Plots from thermodynamic calculations based on the data of Barin et al. (1977) and Mills (1974) are also shown. A number of interesting observations can be made from these figures.

1. The efficiency of calcium oxide as an H_2S absorbent decreases at higher temperatures whereas the efficiency of calcium carbonate increases.

2. The thermodynamic calculations of the equilibrium constant for the reaction of H_2S and lime agree well with the experimental data. Since only thermodynamic data for dolomite exists, the calculations for the sulfidation of the full and half calcines were made as shown above, i.e., starting with dolomite calculations and combining them with decomposition data. Therefore, the good match between the thermodynamic and experimental values shown in figure 3 reflect accurate predictions of the extent of carbonate decomposition, not sulfidation.

3. As was mentioned earlier, the behavior of fc-dolomite is nearly the same as that of calcium oxide, and the reaction of hc-dolomite with hydrogen sulfide is similar to that of calcite. On the other hand, dolomite behaves completely different than calcite.

When coal is pyrolyzed, pyrite (FeS_2) is converted to pyrrhotite (FeS) and hydrogen sulfide. The hydrogen sulfide may then be removed with the off-gas or be captured in the carbon matrix of the coal or char (Huang and Pulsifer, 1977). Many studies of the reaction of H_2S with char, commonly referred to as the back-reaction, have been carried out (Robinson, 1976; Zielke et al., 1954; Jones et al., 1966). Depending on the temperature and nature of the char, the back reaction can occur at H_2S concentrations as low as 300 ppm. An acceptable scavanger should limit the H_2S concentration to this level to inhibit the back-reaction. Figure 4 shows that under typical pyrolysis conditions, calcium minerals are capable of maintaining this level if equilibrium is reached. The desired equilibrium partial pressure, i.e., below 300 ppm, is predicted at all temperatures of interest when CaO is present, at temperatures above 400°C when dolomite is present, and at temperatures above 750°C when $CaCO_3$ is present. Data from the Lurgi-Rhurgas oil shale distillation process which recycles oxidized shale to the pyrolysis bed demonstrates the reactivity of CaO toward H_2S. At a recycle ratio of about 7/1 and at 650°C, hydrogen sulfide concentrations of ~1300 ppm and ~4000 ppm in the off gas have been reported by Schmalfeld (1975) and Weiss (1982), respectively. Sitrai (1984) has also shown that retorting a 1:1 mixture of oil shale and shale ash reduces the concentration of H_2S in the off-gas to less than 100 ppm.

The decomposition and desulfurization reactions of carbonates occur in parallel. Therefore, the competition between the two reactions should be considered. The FACT thermodynamics computing system (Bale et al., 1979) was used to develop the phase stability diagrams for Mg-C-H-O-S and the Ca-C-H-O-S systems shown in figures 5-7. Magnesium carbonate is unstable with respect to the oxide at 327°C and .10 atm. CO_2. As shown in figure 5, at hydrogen sulfide concentrations of 0.6% or higher, sulfidation is inhibited until about 1227°C. This result agrees with Westmoreland and Harrison (1980) who concluded that MgO is too stable to be used as an H_2S acceptor.

Phase diagrams for the Ca-O-H-S-C system at about 500°C, the maximum pyrolysis temperature, and 750°C, a typical hydrodesulfurization temperature for coal char, are shown in figures 6 and 7. At 600°C calcium oxide exists only at carbon dioxide

pressures lower than about 0.01 atm. Calcium oxide will react with H_2S at gas concentrations as low as 10 ppm whereas, depending on the CO_2 concentration, H_2S concentrations from 100 to 1000 ppm are required before the carbonate will undergo sulfidation. At 750°C the reactivity of the oxide is nearly unchanged. However, at this temperature $CaCO_3$ decomposes at CO_2 pressures as high as 0.2 atm and will undergo sulfidation at H_2S concentrations as low as 100 ppm. Nonetheless, CaO still appears to be the most reactive. These results are in agreement with the observations of Harrison and Westmoreland (1980) who reported that the most efficient desulfurization occurred at the lowest temperature (about 880°C) at which CaO was first formed from $CaCO_3$.

An increase in the total pressure, with a corresponding increase in the CO_2 and H_2O partial pressures, would inhibit desulfurization by the carbonates (eqs. 5, 7 and 9) but would not affect the equilibria between H_2S and calcium oxide (eqs. 6 and 8). However, at a higher CO_2 partial pressure recarbonation of the oxide competes with sulfidation reaction. Under a 0.4 atmosphere pressure of CO_2, CaO will recarbonate at temperatures below 827°C (Stern and Wiese, 1969). Thus H_2S adsorption by any of the sorbents considered is less efficient at higher pressure. However, most pyrolysis and hydrodesulfurization processes operate at or near atmospheric pressure.

Desulfurization Kinetics

Before any engineering decisions on the effectiveness of oil shale as hydrogen sulfide acceptor are made, detailed information on the thermodynamics and kinetics of reactions involved is required. However, thermodynamics only determine whether a given desulfurization reaction could occur, while the kinetics determine the degree of conversion of a thermodynamically allowable reaction. In particular, kinetic data are essential since in most engineering modeling calculations they are combined with transport equations to predict the performance of a given system.

The intrinsic rate constants for the reactions of calcium carbonate or calcium roxide with H_2S have been reported by a number of investigators. A summary of published work is presented in table 2. The experiments were conducted under conditions where transport effects were minimized. The reported activation energies for the reaction calcium oxide and H_2S range from 3.6 to 38 kcal/mole and those for the carbonate range from 17.3 to 60 kcal/mole. The low values of Westmoreland (1976) and Kamath and Petrie (1981) may be due to diffusion resistances. The activation energy values for the sulfidation of lime as reported by Attar (1978) and Borgwardt et al. (1984) are 37 and 31 kcal/mole. However, the former author believes that the reaction is controlled kinetically while the latter believes that diffusion through the CaS layer is the controlling step. The pre-exponential factors, shown in table 2, also vary by many orders of magnitude. It appears that the data available in the literature are inconclusive. The wide range of reactivities reported in the literature can be attributed either to differences in experimental methodology or in the physical characteristics of minerals employed.

The pore size distribution, porosity, and surface area of the sample as well as the presence of magnesium oxide have been shown to affect the reactivity of calcium minerals with H_2S. The work of Borgwardt et al. (1984) showed that the rate of reaction of lime with H_2S at 700°C is proportional to the 2.3 power of the B.E.T. surface area indicating product layer diffusion control at these conditions. Other authors, however, have observed that the reaction "stops dead" after 5 to 25% conversion due to the solid product layer (Attar, 1979; Squires, 1972). Harvey et al. (1976) concluded that the crystallites of MgO found in hc-dolomite increased the reactivity of the calcium carbonate by maintaining the porosity of the material and hindering the consolidation of the carbonate into larger crystals. Pell (1971) also found that the sulfidation of fc-dolomite particles occurred homogeneously throughout the solid. The inert minerals in oil shale could perform the same function as MgO in dolomite, thereby enhancing the reactivity of the CaO or $CaCO_3$ in oil shale.

The rate of sulfation (reaction with SO_2) of carbonates has also been shown to be highly sample dependent. Borgwardt and Harvey (1972) found the physical properties of the carbonate stones were much more important rate determinants than the composition of the carbonate. Similarly, Fee et al. (1982) found that the chemical composition, pore size distribution, and surface area of each individual limestone or dolomite must be considered before the performance of a solid as an SO_2 acceptor could be predicted. The superior sulfation characteristics of oil shale carbonates over pure dolomite was demonstrated by Fuchs et al. (1978). They observed that the initial rate of sulfation for the hc-dolomite in shale is nearly six times that of pure hc-dolomite under identical experimental conditions. This was attributed to the fine-grained nature of carbonates in oil shale and the high surface area of the devolatilized shale amoung other factors. In the case of sulfidation, as in sulfation, we believe that the reaction kinetics will more likely depend on the physical properties of the solid than on the mineral itself. Therefore only rate measurements made with the oil shale sample will be useful for process design. Published work on the reactivity of the pure minerals is not a reliable substitute.

Since H_2, CO_2, and H_2O are present during hydrotreatment and pyrolysis, their effect on the rate of sulfidation is important. Hydrogen concentrations as low as 3% have lowered the rate of sulfidation of the limestone (Borgwardt and Roache, 1984). The effect increases as the concentration of hydrogen is increased but levels off near 15%. Oddly enough, dolomite is unaffected. The effect of carbon dioxide is important because it is a common component of pyrolysis gas and a product of the sulfidation of carbonates. Ruth (1972) reported that not only the rate of reaction but also the extent of sulfidation of calcium carbonate were greatly increased when raising the CO_2 level of the reactant gas from 3% to 60%. The reaction essentially stopped after 15% conversion when using 3% CO_2 at 600°C whereas complete conversion was achieved at the 60% CO_2 level. At 700°C the effect of the CO_2 level was not particularly significant. The catalytic effect of steam on the rate of sulfidation has also been observed (Pell, 1971; Squires, 1972). Most authors theorize that the gas composition effects the growth and final crystalline structure of the calcium sulfide layer. This in turn enhances or inhibits the rate of hydrogen sulfide, H_2O, or CO_2 diffusion through the solid layer, and changes the overall rate of reaction.

Concluding Remarks

A thorough understanding of the reactions between H_2S and carbonate minerals in oil shale is essential if this material is to be used effectively as an H_2S scavenger. Thermodynamics show that under typical conditions for coal-oil shale pyrolysis, dolomite and calcium oxide are capable of maintaining the desired H_2S concentration in the reactor. Additionally, under typical conditions of char desulfurization, calcium oxide will be an effective sorbent. However, because the gas residence time in an FBR is often on the order of a few seconds, the reaction rates must be high enough for the thermodynamically allowed reactions to reach equilibrium. Therefore, the kinetics of these reactions must be experimentally determined. In addition, a thorough understanding of the influence of the gas environment and the effects of the structural properties of the oil shale particles (raw, retorted, or spent) is essential. We have begun to obtain experimental data for the reactions between H_2S and carbonate minerals in oil shale under typical conditions for pyrolysis and hydrodesulfurization. In the near future, we intend to study the structural changes of oil shale particles during H_2S capture. This information will provide a basis for employing a gas-solid reaction model such as the changing grain size model to predict the behavior of a single oil shale particle during H_2S capture.

References

Attar, A., 1978, Reactions of sulfur in coal-gas reactions, Fuel, Vol. 57, p 209.

Attar, A., and F. Dupius, 1979, The rate and fundamental mechanism of the reaction of hydrogen sulfide with basic minerals in coal, Ind. Eng. Chem. Process Development and Design, Vol. 18, No. 4, p. 607.

Bale, C. W., A. D. Pelton, and W. T. Thompson, 1979, FACT User's Guide, McGill University.

Barin, I., O. Knacke, and O. Kubaschewski, 1977, Thermo-chemical properties of inorganic substances, Springer-Verlag, Berlin.

Borgwardt, R. H. and R. D. Harvey, 1972, Properties of carbonate rocks related to SO_2 reactivity, Environmental Science and Technology, Vol. 6, p. 350-360.

Borgwardt, R. H., N. F. Roache, and K. Bruce, 1984a, Surface area of calcium oxide and kinetics of sulfide formation, Enviromental Progress, Vol. 3, No. 2, p. 129.

Borgwardt, R. H. and N. F. Roache, 1984b, Reaction of H2S and sulfur with limestone particles, Ind. Eng. Chem Process Design Development, Vol. 23, p. 742-748.

Boynton, R. S., 1980, Chemistry and Technology of Lime and Limestone, 2nd ed., John Wiley, Inc.

Burnham, A. K., C. T. Stubblefield, and J. H. Campbell, 1980, Effects of gas environment on mineral reactions in Colorado oil shale, Fuel, Vol. 59, p. 871-877.

Campbell, J. H., 1979, The kinetics of the decomposition of Colorado oil shale II: carbonate minerals, UCRL - 52089.

Chen, C. C., J. K. Floess, L. Fong, J. P. Longwell, and L. B. Evans, 1982, Modeling of an oil shale fluidized bed retorting process using ASPEN, Energy Progress, Vol. 2, No. 3, p. 147-150.

Curran, G. P., C. E. Fink, and E. Gorin, 1967, CO2 Acceptor Gasification Process - studies of acceptor properties, Advances in Chemistry Series, No. 69, American Chemical Society, p. 141-165.

Davidson, M. L., and D. P. Harrison, 1984, Evaluation of the changing grain size model, Eng. Communication, Vol. 25, p. 213-228.

Fee, D. C., K. M. Myles, W. I. Wilson, L. S. Fan, G. W. Smith, S. H. Wong, J. A. Shearer, J. F. Lenc, and I. Johnson, 1980, Sulfur control in fluidized bed combustors; methodology for predicting the performance of limestone and dolomite sorbents, Report to DOE, ANL/FE-80-10.

Harvey, R. D., G. Kan, R. A. Graff, and A. M. Squires, 1976, Behavior of dolomite in absorption of H2S from fuel gas, ISGS Reprint Series, 1977C.

Haul and Markus, 1952, J. Appl. Chemistry, Vol. 2, p. 298.

Hill, K. J., and E. K. Winters, 1956, Thermal dissociation pressure of calcium carbonate, J. Phys. Chem., Vol. 60, p. 1361-1362.

Huang, E. T. and A. H. Pulsifer, 1979, Coal desulfurization during gaseous treatment, ACS Symposium Series, No. 64, American Chemical Society, p. 290-304.

Jones, J. F., M. R. Schmid, M. E. Sacks, Y. C. Chen, C. A. Gray, R. T. Eddinger, 1966, COED final report, Jan.-Oct. 1966, OCR, Department of Interior.

Kamath, V. S. and T. W. Petrie, 1981, Rate of reaction of hydrogen sulfide - carbonyl sulfide mixtures with fully calcined dolomite, SIU Carbondale, Environmental Science and Technology, Vol. 15, No. 8, p. 966.

MacIntire, W., and T. Stansell, 1953, Ind. and Eng. Chemistry, Vol. 45, p. 1548.

McCarthy, D. J. and H. J. Poynton, 1984, Formation of calcium silicates during processing of Julia Creek oil shale, Fuel, Vol. 63, p. 769.

Mills, K. C., 1974, Thermodynamic data for inorganic sulfides, selenides and tellurides, Butterworths Inc., London.

Pell, M., 1971, Reaction of hydrogen sulfide with fully calcined dolomite, PhD thesis, City University of New York.

Robinson, L., 1976, Hydrodesulfurization of char, Fuel, Vol. 55, p. 193-201.

Rosenqvist, T., 1951, A thermodynamic study of the reaction CaS + H_2 H_2S + CaO and the desulfurization of liquid metals with lime, J. Metals Trans., Vol. 3, p. 535-40.

Ruth, L. A., A. M. Squires, R. A. Graff, Desulfurization of fuels with half-calcined dolomite: first kinetic data, Environmental Science and Technology, Vol. 6, No. 12, p. 1009.

Schmalfeld, P., 1975, The use of the Lurgi-Rhurgas process for the distillation of oil shale, Quart Colorado School of Mines, Vol. 670, No. 3, p. 129-145.

Sitnai, O., 1984, Process concept for retorting of Julia Creek oil shale, Energy Progress, Vol. 4, No. 2, p. 100-104.

Steen, C. L., K. Li, and F. Rogan, 1980, Half-calcination of dolomite at high pressures. Kinetics and structural changes, Environmental Science and Technology, Vol. 14, No. 5, p. 588.

Stern, K. H. and E. L. Wiese, 1969, High temperature properties and decomposition of inorganic salts, part 2: carbonates, NSRDS - NBS30, p. 19.

Squires, A. M., 1972, New systems for clean power, Int. J. Sulfur Chemistry, Pt B, Vol. 7, No. 1, p. 85.

Uno, T., 1951, Tetsu To Hagana (Iron and Steel) Vol. 37, p. 14-17.

Weiss, H., 1982, Retorting of oil shale - background, status, and potential of the Lurgi-Ruhrgas process, ACS symposium, Oil shale retorting - Latest developments, March 28 - April 12, Las Vegas, Nevada.

Westmoreland, P. R., J. B. Gibson, D. P. Harrison, Comparative kinetics of high-temperature reaction between H_2S and selected metal oxides, Environmental Science and Technology, Vol. 11, No. 5, p. 488.

Westmoreland, P. R. and D. P. Harrison, 1976, Evaluation of candidate solids for high-temperature desulfurization of low-Btu gases, Environimental Science and Technology, Vol. 10, No. 7, p. 659.

Zielke, C. W., G. P. Curran and G. E. Gorning, 1954, Desulfurization of low temperature char by partial gasification, Ind. Eng. Chem., Vol. 46, No. 1, p. 53-56.

Table 2. Experimental Techniques and Results of Kinetic Studies, Part I

Reference	Kinetic Expression (Temperature range)	Reactor	K_o	E_a(kcal/mole)
Attar (1978)	Rate = K[Solid][H_2S] (400-800°C)	Pulsed Differential Reactor, Packed bed design	-	$CaCO_3$ 17.3 CaO 37.0 $CaCO_3MgCO_3$ 18.9
Borgwardt (1984a)	Rate = K[CaO][H_2S] (600-900°C)	Differential Reactor, Packed bed design	1.2×10^8 L·cm/mole H_2S·min [a]	37
Borgwardt (1984b)	Rate = $\frac{K}{Dp}$ [$CaCO_3$][H_2S] (550-850°C)	Differential Reactor, Packed bed design	8×10^8 L·cm/mole H_2S·min [a] at Dp = 2.8um	42.6
Davidson (1984)	Rate = AK[H_2S]; where A = Wt% CaO (625-950°C)	Thermobalance	8.25×10^4 L·cm/mole H_2S·min [b]	27
Kamath (1981)	Rate = K[CaO] (600-800°C)	Thermobalance	$K_{600} = 1.1 \times 10^{-4}[H2S]^{0.76}$ sec^{-1} $K_{700} = 1.43 \times 10^{-4}[H2S]^{1.01}$ sec^{-1} $K_{800} = 1.61 \times 10^{-4}[H2S]^{1.22}$ sec^{-1}	
Pell (1971)	Rate = AK[H_2S]; where A = Wt% CaO (700-900°C)	Thermobalance	4.96×10^5 L/mole H_2S·min	22.9
Ruth (1972)	Rate = K'[$CaCO_3$] (550-800°C)	Modified Dupont TGA	-	60
Westmoreland (1977)	Rate = K'[CaO][H_2S]^N (300-800°C)	Thermobalance	0.038 L·cm/min·mgmole	N = 1 5.16

[a] Estimate from data given

[b] A recalculation of Pell's data

Table 2. Experimental Techniques and Results of Kinetic Studies, Part II

Reference	Material	Material Properties	Gas Composition & Flow Properties
Attar (1973)	Calcite, Lime, and Dolomite	-200 mesh, 0.1-0.5g sample	H_2S pulse = 1 x 10^{-6} mole/pulse in steady stream of He, flow rate not given but assumed to be low because gas diffusion was controlling at times
Borgwardt (1984a)	CaO from Calcined Limestone	2um limestone calcined at 700°C for 90 sec, 15 mg sample, surface area = 5.8 m^2/g, BCR 2061	5000 ppm H_2S, 70% CO_2, balance N_2
Borgwardt (1984b)	Limestone	Fredonia Valley White, Fredonia, KY, ratio Ca/Mg = 73/1, BC 2061 1-10 um limestone particles dispersed in quartz wool	5000 ppm H_2S, 70% CO_2, balance N_2, 5 L/min at 25°C, 490 cm^2/s at 750°C, gas diffusion was not a problem at this rate, exposure time = 30-55 min
Davidson (1984)	Fully-calcined Dolomite	surface area = 14 m^2/g, 124-380 mg samples, sphere diameter = 0.277 to 0.406 cm	5% H_2S, 7.5% H_2
Kamath (1981)	Fully-calcined Dolomite	-30+50 mesh, Dp = 400um, Pfizer Corp., Gibsonville, Ohio, ratio Ca/Mg = 0.84	0.5-5% H_2S, 20% H_2, 30% CO, balance N_2, 500 SCCM used, no difference at 1000 SCCM
Pell (1971)	Fully-calcined Dolomite	-80+325 mesh, ratio Ca/Mg = 1.09	0.5-20% H_2S, 7.5% H_2, balance N_2, H_2O used at times, flowrate = 0.5 L/min (STP), Reynolds number = 1
Ruth (1972)	Half-calcined Dolomite	Greenfield formation, 25mg sample, -250+270 mesh, dolomite calcined immediately before reaction in TGA, BCR 1337 and 1930	0.5-20% H_2S, various levels of CO_2, H_2, and N_2, flow rate = 100-300 mL/min
Westmoreland (1977)	Pure CaO	100 mesh heated to 500°C in an inert gas, surface area = 17.3 m^2/g	1.9-7% H_2S, ratio H_2/H_2S = 5:1, balance N_2, volumetric flowrate set to eliminate external mass transfer resistance

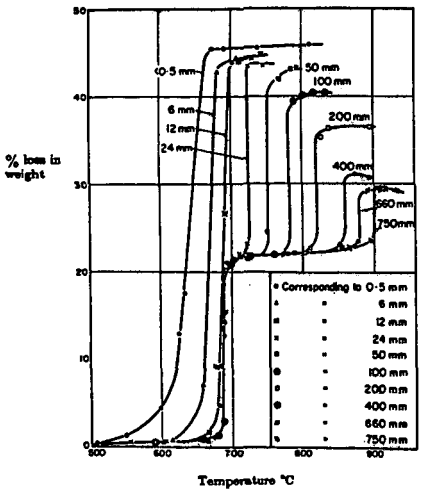

Figure 1. The thermogravimetric analysis of dolomite at various temperatures and CO_2 pressures.

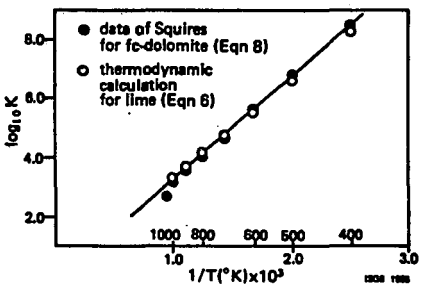

Figure 2. Log K_{eq} vs 1/T for the adsorption of H_2S by CaO.

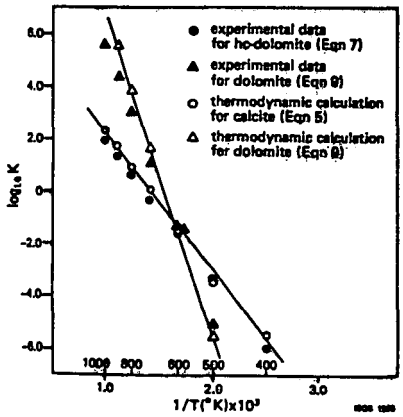

Figure 3. LogK_{eq} vs 1/T for the adsorption of H_2S by various forms of $CaCO_3$.

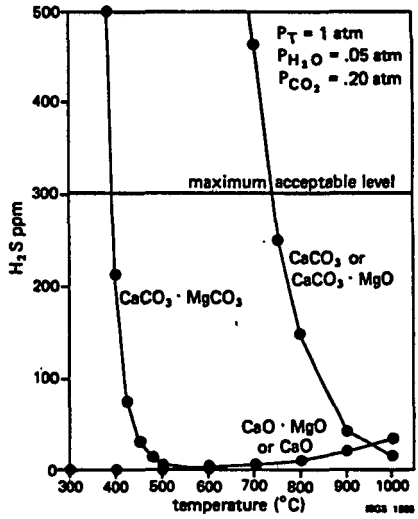

Figure 4. Equilibrium partial pressure of H_2S in the presence of oil shale minerals.

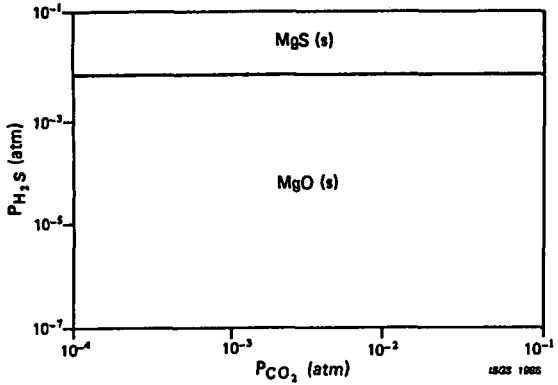

Figure 5. Phase stability diagram for the Mg-H-O-S-C system, T=1227°C, P_{H_2O} = 0.05 atm.

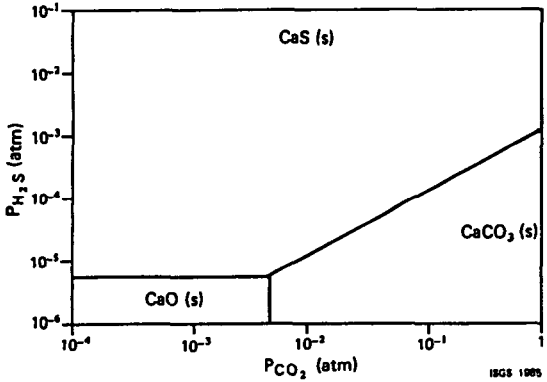

Figure 6. Phase stability diagram for the Ca-H-O-S-C system, T=600°C, P_{H_2O} = 0.05 atm.

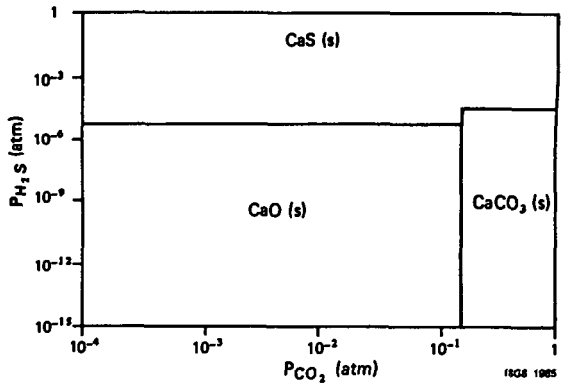

Figure 7. Phase stability diagram for the Ca-H-O-S-C system, T=750°C, P_{H_2O} = 0.05 atm.

ENHANCED OIL RECOVERY FROM PYROLYSIS OF VARIOUS AUSTRALIAN SHALES

Vetkav Parameswaran, Mark Polasky and Sunggyu Lee

Department of Chemical Engineering
The University of Akron.
Akron. Ohio 44325.

ABSTRACT

The oil yields from retorting Stuart, Rundle and Condor shales have been optimized with respect to their process operating conditions using a statistical experimental design technique. A three factor, two level factorial design of experiments was adopted to determine the main and interaction effects of variables on the yield of oil from these shales. The three variables are the particle size, the type of sweep gas and the sweep gas flow rate.

It was found that retorting with carbon dioxide as the sweep gas enhances the oil yield from Stuart shale by up to 24 percent. The strongest effect was observed from the sweep gas flow rate and the optimal condition for this variable was found through out-layer experiments. For each of the significant effects, transport processes such as the combined heat and mass transfer were explained and design criteria for a retorting system were found for scale up purposes.

INTRODUCTION

Extensive deposits of oil shale, bearing enormous amounts of equivalent synthetic fuel exist in the U.S.A., Australia, Canada, China and various other parts of the world. However, these deposits are far from uniform and there are wide variations in the physical and chemical structure of the rocks even within the same general location. As a result, engineering and fundamental data are required even for preliminary design and economic feasibility analysis. The need for data is even more vital during the detailed industrial process development. In order to maximize the yield, the kinetics as well as the physical and chemical properties of the shale and shale oil must be known. An extensive review of oil shale technology covering the historical development and the kinetics of oil shale retorting as well as the properties of oil shale has been presented by Branch (1). This paper aims at finding the optimum operating conditions for the retorting of Australian Tertiary shales. The shale samples studied were taken from the Kerosene Creek member of the Stuart deposit, the Ramsey crossing member of the Rundle deposit, and the Brown oil shale unit of the Condor deposit, all of which are located along the coastline of Queensland, Australia.

APPROACHES

Optimization studies generally involve either the solution of differential equations or the discrete techniques of linear algebra. In either case, it is necessary to have a mathematical description of the system. The physical and chemical complexity of oil shale renders such a rigorous mathematical treatment extremely difficult.

For engineering purposes however, an experimental exploration of the range of interesting process conditions can be coupled with the methods of statistical experimental design to arrive at optimum operating parameters with the minimum of experimental cost and effort. Therefore a three factor, two level design of experiments for each type of oil shale was adopted for this study.

IDENTIFYING THE CRITICAL VARIABLES

In order to ensure the reproducibility of experimental results, standard retorting procedures must be adopted without stifling the degree of freedom necessary to optimize the operating conditions. Twenty grams of oil shale were charged into the retort which was then heated at the rate of 10 C/min from 25 C to 700 C at atmospheric pressure. The details of the retorting apparatus have been published elsewhere (2). The apparatus consists essentially of a 15.75 inch long x 1 inch diameter stainless steel tube which is placed inside an electric furnace. The shale sample is loaded into the retort through a ball valve at the top of the tube. The sweep gas (which is preheated in a gas preheater following the reactor preheating schedule) flows down through the sample bed into an oil collection tube which is kept cool in a water bath.

The variables studied were the particle size (-8 +10 mesh and -20 +40 mesh (Tyler)), sweep gas type (carbon dioxide and nitrogen) and sweep gas flow rate (2 ml/sec and 5 ml/sec (STP)). The levels of these variables have been chosen based on preliminary experiments as well as prior experience (2).

The mechanism by which the oil is released from the pores of the shale is not very clear. The influence of the particle size on the retorter yield seems to depend on the type of oil shale being retorted. As the oil shales are fairly non-porous (very often below 5 % porosity), it is to be expected that crushing the oil shale would improve the process of oil evolution. However, there seems to be a minimum particle size below which the influence on the yield tends to be negative. This is due to the loss of kerogen entrapped in macropores while crushing. Therefore, two different sizes were tested, viz, -8 +10 mesh and -20 +40 mesh (Tyler).

It has been found by Lee (3), that carbon dioxide sweep gas conditions enhance the oil recovery from Colorado oil shales. Therefore tests were conducted with two types of sweep gas, i.e., nitrogen and carbon dioxide.

The flow rate of sweep gas is very important from an engineering point of view. This influences the heat and mass transfer conditions within the reactor and scale up and scale down of commercial reactors would be disastrous if the mass transfer conditions were not kept uniform in the scaled models. Therefore experiments were made with two different sweep gas flow rates, viz, 2 ml(STP)/sec and 5 ml(STP)/sec. This corresponds to vapor space velocities (calculated at STP) of 720 and 1800 per hour (superficial linear velocities of 0.4 and 1.0 cm/sec) respectively in the retort.

The influences of these three variables were studied on three different Australian Tertiary oil shales identified as Rundle, Stuart and Condor oil shales and the results were critically compared with those obtained with the Eastern and Western U.S. oil shales in terms of their yield, effects and optimal process conditions.

RESULTS AND DISCUSSION

The results of the various experiments conducted on Stuart, Rundle and Condor oil shales are presented in Table 1. The yields obtained were analyzed using Yates' algorithm (4) to determine the effects of the various treatment combinations on the yield. These effects are also summarized in Table 1. For the purpose of comparison, similar data are also included in Table 1 for the Colorado (5) and Ohio #2 (6) oil shales.

For the purpose of determining the significant effects, three replications were carried out and the effects that were larger than twice the standard deviation in these runs were identified as the significant effects. Accordingly, the minimum effects for the determination of significance were 4.80, 6.38, 2.34, 4.10, and 1.90 for the Stuart, Rundle, Condor, Colorado and Ohio # 2 shales respectively.

Stuart Shale

Of the three Australian shales tested, the Stuart shale gave the largest oil yield (Fischer Assay of 101 ml/kg) comparable to the yields obtained from most Colorado shales.

The sweep gas flow rate had the largest influence on the oil yield. This predominant effect was observed with all the oil shales so far tested. The influence in all cases was negative in the range of the variable studied indicating thereby that an increase in the flow rate from 2 ml(STP)/sec to 5 ml(STP)/sec reduces the yield. This strongly suggests that mass transfer

TABLE 1. Summary of Yields and Effects

Shale Type	Tertiary		Tertiary		Tertiary		Eocene		Devonian	
Treatment Combination	STUART Yield	Effect	RUNDLE Yield	Effect	CONDOR Yield	Effect	* COLORADO Yield	Effect	* OHIO # 2 Yield	Effect
(1)	105	110.94	80	63.13	65	51.72	94.2	92.94	32	25.75
a	125	- 4.38	82.5	1.25	67.5	- 0.31	95.8	0.57	31	2.50
b	130	5.63	65	- 5.00	60	- 2.81	105.9	8.72	29	2.00
ab	120	- 8.13	72.5	0	61.3	- 1.56	98.0	- 1.37	30	2.00
c	107.5	-18.13	50	-23.75	40	-23.44	81.0	-11.07	17	- 9.50
ac	95	- 9.38	50	- 3.75	40	- 2.19	83.3	3.72	19	2.50
bc	110	- 4.38	55	7.50	42.5	2.81	89.5	1.77	20	4.00
abc	95	6.88	50	- 2.50	37.5	- 0.94	95.8	3.37	28	1.00

Units of Yield are ml/kg
The significant effects are underlined

The Factors and the Levels are as follows:

Factor	+ Level	- Level
(a) Particle size	-8 +10 mesh -4 + 8 mesh(*)	-20 +40 mesh
(b) Sweep Gas Type	Carbon Dioxide	Nitrogen
(c) Sweep Gas Flow	5 cc/sec	2 cc/sec
Heating Rate	--------- 10 C/min ----------	

Note:(*) Particle size of -4 + 8 mesh was used for the + Level for the Colorado (5) and Ohio # 2 (6) shales.

plays an important role in shale oil extraction. Based on similar situations in gas-solid reaction systems, this implies that beyond a certain limit in the sweep gas flow rate, an increase in the flow rate adversely affects the total yield. Therefore, either a corner test or outlayer experiments have to be conducted to determine the optimal flow rate. In the corner test, the sweep gas flow rate was varied while keeping the other variables at their optimal values. The results show that the best yield is obtained with a sweep gas flow rate of 2 ml(STP)/sec.

On the other hand, the type of sweep gas used also has a significant effect on the yield. As the effect is positive, it can be concluded that carbon dioxide retorting enhances the yield. This was also the case with the Colorado and some Eastern U.S. Devonian shales (2,5). The role of carbon dioxide in enhancing the yield from such shales while having negative effects on the yield from other shales is not completely understood. However, the trend indicates that carbon dioxide enhances the retorting yield from shales with a large kerogen content. This influence is much less or even negative when the kerogen content is low (Fischer Assay below 30) or medium (Fischer Assay of the order of 60 to 70). It has been known among various investigators that kerogen swells better in a carbon dioxide medium than in a nitrogen medium. This should normally result in an improved yield; however, it also enhances the probability of caking or agglomeration inside and outside the shale particles. Therefore highly caking shales, such as the North Carolina lacustrine shale do not exhibit an increase in oil yield and this caking phenomenon is also observed.

The influence of the particle size on the oil yield was insignificant. However, the interaction effect of the gas flow rate and the particle size was negative and significant. This also shows that mass transfer plays an important role in the process. Even though improved mass transfer conditions around the shale particle should directly result in a smoother transport of oil and vapor products out of the sample bed, complex, semi-macroscopic phenomena such as the blockage of pore mouths, gel or liquid entrapment within the pores, formation of new pores, agglomeration of particles, etc., are not easily accounted for. Therefore, it can be said that the total yield of oil from oil shale is not only directly related to the heat and mass transfer conditions, but also to the morphological changes and the swelling of kerogen.

The largest yield was indeed obtained with small size particles and low sweep gas flow rates coupled with the use of carbon dioxide. The significance of carbon dioxide is also indicated by the large positive abc interaction effect.

It can therefore be concluded that the optimal operating conditions for retorting Stuart shale are:

1. Use carbon dioxide as the sweep gas.
2. Operate at low sweep gas flow rates, i.e., 2 ml(STP)/sec.
3. Use smaller particles, i.e., -20 +40 mesh.

Rundle Shale

The oil yield from Rundle shale was in the moderate range. The only significant main effect was from the sweep gas flow rate.

The influence of sweep gas flow rate in depressing the oil yield was most pronounced with the Rundle shale. Hence a corner test was performed by varying only the sweep gas flow rate while holding the particle size, type of sweep gas and the heating rate constant. The results show (Figure 1) that the optimal sweep gas flow rate is between 1 and 2 ml(STP)/sec.

It is interesting to note that even though carbon dioxide depresses the oil yield to a relatively insignificant extent, the interaction effect of the sweep gas type and flow rate is positive. This result also supports the prior conclusion that the oil yield is influenced not only by the mass transfer conditions, but also by the process of kerogen swelling and other morphological changes that occur during pyrolysis. The large interaction effect is shown schematically in a three-dimensional plot in Figure 2.

The optimal retorting conditions for the Rundle shale are therefore:

1. Use a sweep gas flow rate of 1.5 ml(STP)/sec.
2. Use nitrogen as the sweep gas, and
3. Use the larger size particles, i.e., -8 +10 mesh.

Condor Shale

The Condor shale yielded the smallest amount of oil per kilogram of sample. It was observed in this case also that the sweep gas flow rate had a large negative influence on the oil yield. Moreover, the use of carbon dioxide also depresses the yield. The standard experimental error calculated by conducting replicate experiments was smaller in this case than in the other two cases. Such an influence was also observed in the case of Ohio shale. The accuracy of experimentation is improved with smaller yields. It should be noted here that in the case of Ohio shale, the quantity of sample used was larger in order to improve the resolution of the experiments (6).

As in the case of Rundle shale, the optimal retorting conditions are:

1. Use lower sweep gas flow rate, i.e., 2 ml(STP)/sec.
2. Use smaller size particles, i.e., -20 +40 mesh.
3. Use nitrogen as the sweep gas.

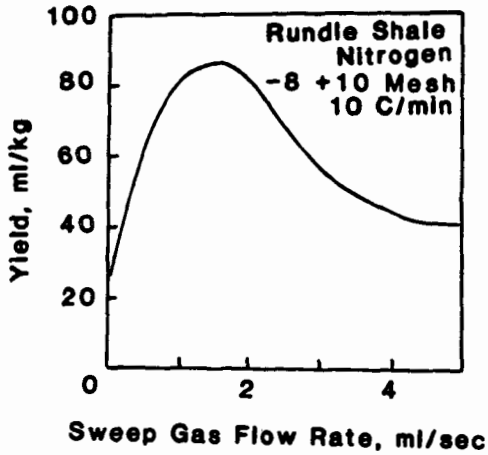

Figure 1. Optimization of Sweep Gas Flow Rate (ml (STP) of N_2 / Second).

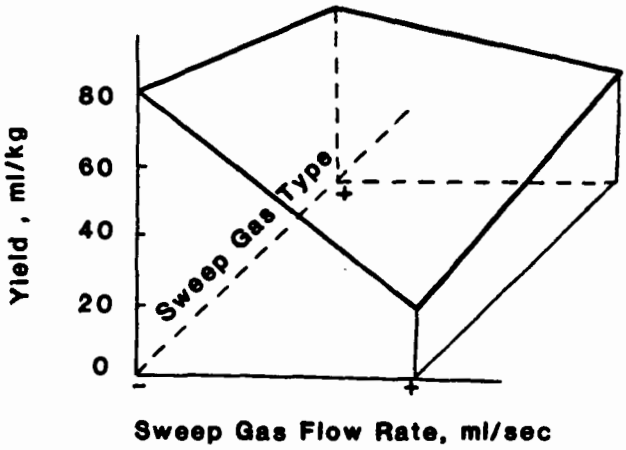

Figure 2. Schematic Representation of the Interactive Influence of Sweep Gas Type and Flow Rate on the Yield from Rundle Shale.

CONCLUSION

A statistical experimental approach was used to determine the optimal retorting conditions for three Australian oil shales. The optimal conditions are summarized below:

	Stuart	Rundle	Condor
Particle size:	-20 +40 mesh	-8 +10 mesh	-20 +40 mesh
Sweep Gas Type:	Carbon dioxide	Nitrogen	Nitrogen
Gas Flow Rate:	2 ml(STP)/sec	1.5 ml(STP)/sec	2 ml(STP)/sec

It is also concluded that the yield from oil shale pyrolysis is influenced by many mechanistic factors such as the heat and mass transfer conditions, the swelling of kerogen in the rock matrix, morphological changes during pyrolysis, agglomerating properties etc. Therefore, the factors investigated in this statistical optimization study represent a set of process variables that are most important for the successful design and operation of retorting equipment. The vapor hourly space velocity of the sweep gas was also calculated for scale up purposes.

REFERENCES

1. Branch M.C., Prog. Energy Combust. Sci., 5, pp 193 (1979).

2. Joshi R. and S. Lee, Liquid Fuels Technology, 1, pp 17 (1983).

3. Lee S., U.S. Patent No: 4,502,942. (1985).

4. Box G.E.P., W.G. Hunter, J.S. Hunter, Statistics for Experimenters, John Wiley and Sons, New York (1978).

5. Joshi R., Kinetic Study of Eastern Oil Shale Pyrolysis, Masters Thesis, The University of Akron (1983).

6. Lee S., M. Polasky, R. Joshi, Proceedings of 1983 Eastern Oil Shale Symposium, pp 225-233, University of Kentucky, Institute for Mining and Minerals Research (1984).

PYROLYSIS KINETICS OF VARIOUS AUSTRALIAN OIL SHALES IN NITROGEN AND CARBON DIOXIDE ATMOSPHERES

Mark E. Polasky and Sunggyu Lee

Department of Chemical Engineering
The University of Akron
Akron, Ohio 44325

ABSTRACT

The kinetics of oil generation from retorting of various Australian shales have been investigated under both nitrogen and carbon dioxide sweep gas conditions. Experiments were conducted both isothermally and nonisothermally with linear temperature control, in a unique fixed bed retorting system. The kinetics of these shales were directly compared with those of eastern and western U.S. shales, previously studied on the same experimental system.

The pyrolysis of the investigated Australian shales was found to comply with first-order global kinetics witin the limits of experimental error. The activation energies calculated were: 217.2 kJ/gmole (CO_2) and 114.8 kJ/gmole (N_2) for Condor shale; 252.2 kJ/gmole (CO_2) and 190.1 kJ/gmole (N_2) for Rundle shale; 154.0 kJ/gmole (CO_2) and 127.4 kJ/gmole (N_2) for Stuart shale. The average Fisher assay of these shales are 62 cc/kg for Rundle, 63 cc/kg for Condor, and 100 cc/kg for Stuart shale.

INTRODUCTION

An experimental study has been performed in order to obtain the retorting kinetics of oil generation from various Australian Tertiary oil shales under both nitrogen and carbon dioxide sweep gas conditions. The carbon dioxide retorting has been investigated first by Lee et al. and proven efficent for the western U.S. type oil shale (1). Therefore, the rather nonconventional carbon dioxide retorting as well as the conventional nitrogen retorting has been applied to Australian shales.

The shale samples studied were taken from the Kerosene Creek member of the Stuart deposit, the Ramsey Crossing member of the Rundle deposit, and the Brown oil shale unit of the Condor deposit, all of which are located along the coastline of Queensland, Australia.

In order to obtain an unbiased comparison and to eliminate unaccountable systemic errors, a unique fixed bed retorting system was used to determine the kinetic parameters of each shale (2). Both the isothermal and nonisothermal retorting techniques were employed for the kinetic measurements, and the results compared favorably with each other. The pyrolysis of the Australian shales under investigation were found to comply with global first-order kinetics within the limits of experimental errors.

THEORY

Three experiments for each shale under different isothermal conditions were carried out and the global power-law type rate expression was applied to analyze the data:

$$\frac{dx}{dt} = A[\exp(-E/RT)](1-x)^n \tag{1}$$

where x is the kerogen conversion based on the Fisher assay oil yield, E is the activation energy, kJ/gmol, A is the Arrhenius frequency factor, 1/sec, and n is the reaction order.

The nonisothermal technique eliminated the uncertainty of the initial heat-up period which had been an inherent problem with a fixed bed type retorter for an isothermal measurement. The kinetic parameters were obtained for the condition that a linear heating rate be maintained. The choice of a linear heating rate is to facilitate an easier mathematical analysis. For an overall first-order reaction, one obtains the following equation by integration (1):

$$-\ln(1-x) = \frac{AE}{CE}[e^{-u}u^{-2} - 2e^{-u}u^{-3}] \tag{2}$$

where C is the heating rate (dT/dt) in C/min and u=E/RT. Rearranging equation (2) yields

$$\frac{-\ln(1-x)}{T^2} = \frac{AR}{CE}[(1 - 2RT/E)\exp(-E/RT)] \tag{3}$$

Taking natural logarithms on both sides of equation (3) gives

$$\ln \frac{-\ln(1-x)}{T^2} = \ln\left(\frac{AR}{CE}(1 - 2RT/E)\right) - E/RT \tag{4}$$

A plot of $\ln[-\ln(1-x)/T^2]$ vs. 1/T, which turns out to be a linear plot for $RT/E \ll 1$, gives the activation energy and the kinetic frequency factor for a first-order kinetics from the slope and intercept, respectively. The goodness of fit was a good indication of the validity of the assumed reaction order. A similar analysis can be done for an n-th order kinetics using successive approximation of exponential integrals and the best fitting order can be found by a regression technique (3).

EXPERIMENTAL SYSTEM AND PROCEDURE

A schematic diagram of the apparatus used for this study and a detailed design of retorter internals are published elsewhere (2). Some of the features of this retorting system are considered to be special or unique. These features include the use of a stainless steel wire mesh distibutor plate, so that a well-defined fluid dynamic condition is achieved with a minimal pressure drop, the use of a quick opening and closing ball valve which permits the instantaneous loading of a sample in addition to permitting the application of both isothermal and nonisothermal techniques to the same retorter, introducing a chromel-alumel thermocouple directly into the shale bed to obtain good temperature control and measurements, and by connecting two specially designed graduated U-tubes in series which allows the condensable product to settle in the bottom of the tubes while the noncondensable product to pass through a bridge across the tube arms.

A 20 gram sample of -35+40 mesh Australian oil shale was used for each experiment. For an isothermal measurement the retorter was preheated to a temperature about 100 C higher than the reaction temperature to facilitate an easy and fast control of the temperature. For a nonisothermal measurement the retorter was heated up at a linear heating rate of 10 C/min, which was found to be ideal for kinetic measurement. The sweep gas was sent into the retorter at the nominally same temperature as the shale sampls for both isothermal and nonisothermal measurement. The flow rate used was 2 cc(STP)/sec and is equivalent to the vapor hourly space velocities of 720 $hour^{-1}$. Since the length of the connecting line between the retorter and the collection tube was kept short and the temperature was kept high enough to keep the product as a vapor and the liquid holdup in the retort was negligible.

DATA AND ANALYSIS

Nitrogen Retorting Kinetic parameters for the pyrolysis of Australian and eastern and western U.S. oil shales, under nitrogen sweep gas conditions are summarized in Table 1. As shown in the table, the relative rates obtained from isothermal and nonisothermal methods are nearly the same at 450 C. However, the kinetic parameters obtained from nonisothermal retorting may give a more realistic set of engineering information of the overall kinetic parameters for the design of efficent and economical retorting processes, since it comes closer to actual retorter conditions. It should be noted that the lower relative reaction rate for North Carolina shale was due to the fact that the retorting of this shale required a much higher initial retorting temperature than those for the other shales studied. Therefore, the practical retorting temperatures under nitrogen sweep gas conditions ranges from 400 to 500 degrees Celcius for all three types of Australian shales which matches the practical retorting conditions of most of the western U.S. shales.

Table 1. Kinetic Parameters for Nitrogen Retorting of Australian and Eastern United States Shales

Shale Type		Activation Energy, KJ/mol	Arrhenius Frequency Factor, $(sec)^{-1}$	Relative Rates at 450°C
Rundle	N	190.09	4.17×10^{12}	1.000
	I	180.89	9.10×10^{11}	1.008
Stuart	N	127.36	9.05×10^{7}	0.739
	I	116.79	1.74×10^{7}	0.825
Condor	N	114.83	9.92×10^{6}	0.652
	I	104.08	1.94×10^{6}	0.762
Ohio	N	170.62	3.54×10^{10}	0.217
	I	185.32	3.53×10^{11}	0.187
West Virginia	N	203.11	5.74×10^{12}	0.158
	I	201.37	5.74×10^{12}	0.173
North Carolina	N	193.40	6.92×10^{8}	1.50×10^{-5}
	I	204.62	4.74×10^{9}	1.01×10^{-4}
Colorado	N	182.58	5.62×10^{11}	0.471

N denotes nonisothermal run

I denotes isothermal run

Table 2. Kinetic Parameters for Carbon Dioxide Retorting of Australian and Eastern United States Shales

Shale Type		Activation Energy, KJ/mol	Arrhenius Frequency Factor, $(sec)^{-1}$	Relative Rates at 450°C
Rundle	N	252.17	1.39×10^{17}	1.000
	I	243.33	3.48×10^{16}	1.090
Stuart	N	154.01	1.21×10^{10}	1.076
	I	141.02	1.61×10^{9}	1.243
Condor	N	217.24	5.92×10^{14}	1.422
	I	209.17	1.65×10^{14}	1.518
Ohio	N	141.23	4.45×10^{8}	0.332
	I	136.07	2.33×10^{8}	0.410
West Virginia	N	183.56	2.27×10^{11}	0.148
	I	178.32	1.11×10^{11}	0.173
North Carolina	N	211.37	8.43×10^{9}	5.38×10^{-5}
	I	202.91	2.13×10^{9}	5.55×10^{-5}
Colorado	N	189.96	6.89×10^{12}	1.548

N denotes nonisothermal run

I denotes isothermal run

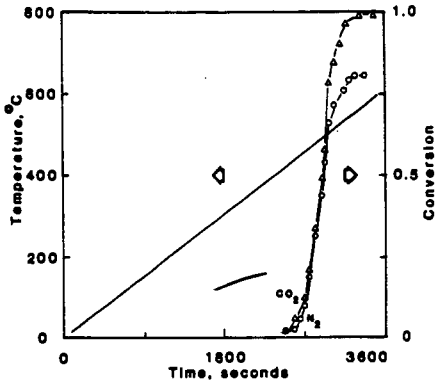

Figure 1.

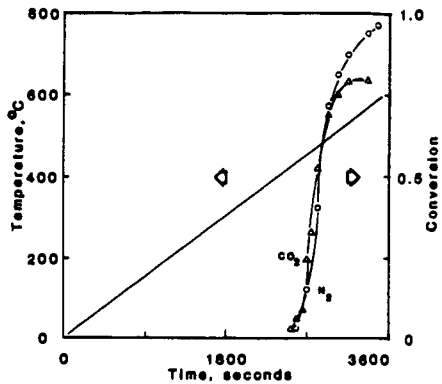

Figure 2.

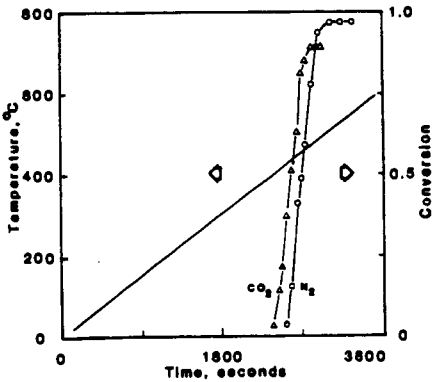

Figure 3.

Figure 1. Nonisothermal Kinetic Measurement of Stuart Shale under N_2 and CO_2.-35+40 mesh; 10 C/min; 2 cc(STP)/sec.

Figure 2. Nonisothermal Kinetic Measurement of Rundle Shale under N_2 and CO_2. (same conditions as Figure 1.)

Figure 3. Nonisothermal Kinetic Measurement of Condor Shale under N_2 and CO_2. (same conditions as Figure 1.)

Carbon Dioxide Retorting Kinetic parameters for the pyrolysis of Australian and eastern and western oil shales under carbon dioxide sweep gas conditions are summarized in Table 2. Figures 1, 2, and 3 show the experimental data for nonisothermal kinetic measurement of pyrolysis of Stuart, Condor, and Rundle shales under nitrogen and carbon dioxide sweep gas conditions. It is interesting to note the difference in kinetic parameters between nitrogen and carbon dioxide retorting conditions. This is believed to be due to the difference in kerogen swelling in both gases and/or the differences in molecular penetration into pores between nitrogen and carbon dioxide. It has been known among the researchers that the kerogen in oil shale swells better in the carbon dioxide medium than the nitrogen medium. This is why carbon dioxide retorting is always kinetically faster than nitrogen retorting at nominally identical process conditions.

SUMMARY

The pyrolysis kinetics of various Australian oil shales were experimentally obtained using both isothermal and nonisothermal retorting techniques. The results from the two methods compared favorably with each other over a practical range of retorting temperatures. The pyrolysis reaction of the investigated Australian oil shales followed a global first-order kinetics very closely and the activation energies range from 110 to 250 kJ/gmole, depending on the type of shale. These values closely followed those for eastern and western U.S. oil shales retorted using the same experimental system. Every possible effort has been made to eliminate the internal and external mass transfer influence on the kinetics obtained, viz., using finely ground shales as well as providing optimal heat and mass transfer conditions.

In addition, the pyrolysis kinetics of various Australian shales were investigated both under nitrogen sweep gas conditions and under carbon dioxide sweep gas conditions and the results were directly compared. It was found that the carbon dioxide retorting process exhibits a kinetically faster rate of oil evolution from all the Australian shales. This result was true regardless of its impact on the overall yield from the shale and was equally valid for other types of oil shales including the Eastern and Western U.S. oil shales.

REFERENCES

1. Lee S. and Joshi R., U.S. Patent, No. 4,502,942 , (1985).

2. Joshi R. and Lee S., Liquid Fuels Technology, 1, 17, (1983).

3. Polasky M. E., ` Pyrolysis Kinetics and Process Optimization of Eastern United States and Australian Oil Shales ', Master's Thesis, The University of Akron, (1985).

THE RETORTING OF SELECTED AUSTRALIAN OIL SHALES UNDER HIGH PRESSURE HYDROGEN AND NITROGEN

By

A. EKSTROM*, C.J.R. FOOKES, K. WONG

CSIRO Division of Energy Chemistry, Lucas Heights Research Laboratories, Private Mail Bag 7, Sutherland, NSW 2232, Australia.

INTRODUCTION

There is increasing interest in the effects of gas pressure on the retorting properties of oil shales, both as a means of increasing the oil yield and as an aid to developing a better understanding of the chemical processes involved in oil shale retorting. In the presence of hydrogen at pressures up to 7 MPa, significant increases in oil yield have been reported for some shales(1-5), and the technique forms the basis of the HYTORT process under development in the USA(6,7). Although the small increase in oil yield observed(8) when Green River shale was retorted under 2.7 MPa hydrogen was accompanied by a slight increase in the aromaticity(8-10), the changes in the composition of the oils produced from shales, which under higher hydrogen pressures gave very much greater oil yields (up to 500%), have not been reported.

The present work was undertaken to investigate the effects of hydrogen and nitrogen pressure at 6 MPa on the yields and composition of the oils produced from three Australian oil shales. These included Rundle as representative of the Tertiary shales of lacustrine origin found in Queensland, and Nagoorin as typical of the highly aromatic and organic rich shales of mixed lamosite/lignite origin(11). The extent of the Mt Coolon deposit, located approximately 200 km west of the city of Mackay in Queensland is at present unknown. The shale was formed in the early Miocene, is unusually rich in parts, and is probably best regarded as an immature torbanite(12).

EXPERIMENTAL

Samples of the shales were crushed and sieved to -2.8 +1.4 mm. Retorting was carried out at various pressures in a fixed bed reactor using a heating rate of 6°C/minute to 550°C followed by a 30 minute soak period. The gas flow rates were adjusted to give a constant residence time of 30 seconds at all pressures. This required very high gas flow rates at the higher operating pressures. The oils (condensed at ~10°C) were analysed by gas chromatography/mass spectrometry (GC/MS: JEOL DX300) and nuclear magnetic resonance (NMR: JEOL GX400) techniques. Solution ^{13}C spectra were determined in the presence of chromium relaxation reagents with an inverse gated decoupling and a recycle time of five seconds. Proton spectra were recorded with a recycle time of 20 seconds.

RESULTS AND DISCUSSION

(a) Properties of Shales

Table 1 illustrates the diversity of the shales used in this study with respect to their organic carbon content, atomic H/C ratio, aromaticity and retorting properties. Of particular interest are the very poor conversions of organic carbon in the shale to oil obtained under normal (Fischer Assay) retorting for the Mt Coolon and Nagoorin shales, indicating that for these shales conventional retorting procedures are not particularly effective.

(b) Effect of Pressure on Oil Yields

For all three shales, increasing nitrogen pressure resulted in only minor decreases in oil yields (Figure 1) and organic carbon conversions (Figure 2). Increasing hydrogen pressure had no effect on the oil yield from the aliphatic Rundle shale, although a reduction in the organic carbon remaining in the char was observed, presumably reflecting the conversion of the carbonaceous residue to methane, as has been previously observed for Green River shale(8).

However, increases of 150 and 350% of Fischer Assay oil yields were observed for the Mt Coolon and Nagoorin shales, equivalent to oil yields of 390 and 290 L t^{-1} respectively, assuming an oil density of 0.9 g cm^{-3}. These large increases are matched by corresponding decreases in the organic carbon remaining in the char (Figure 2) which, in the case of Nagoorin decreased from 58 to 24% at 6 MPa hydrogen. Increased hydrogen pressure resulted in only small changes in the conversion of organic carbon to gaseous products.

As shown in Figure 3, the oil yields determined for three Australian(13) aromatic shales retorted in 6 MPa hydrogen compared favourably with similar results(3) for a variety of other shales. Data on the importance of the total oil yield on the economics of HYTORT type processes do not appear to have been published, but it appears that the three Australian shales are particularly suited to retorting in high pressure hydrogen.

(c) Effect of Pressure on Oil Composition

Although increased oil yields are obviously important, the composition of the oil is equally significant from the viewpoint of the subsequent hydrotreatment and refining of the crude product.

Increasing nitrogen pressure had no effect on the ^{1}H and ^{13}C aromaticities of the whole shale oils (Figure 4), but large changes were observed with increasing hydrogen pressure, particularly for the Mt Coolon and Nagoorin shales. For example, the Nagoorin oil formed in 6 MPa hydrogen had carbon and proton aromaticities of 68 and 29% respectively. The data indicate that for the Mt Coolon and Nagoorin shales a substantial part of the additional oil formed in the presence of hydrogen is aromatic.

Examination of the whole oils by gas chromatography (GC) and gas chromatography/mass spectrometry (GC/MS) showed (Figure 5) that phenol, the cresols and dimethyl/ethyl phenols were prominent components of the oils retorted under high pressure hydrogen from the Mt Coolon and Nagoorin shales. These compounds also completely dominate the ^{13}C NMR spectra of these oils in the aromatic region but were absent in the oils retorted from the Rundle shale in both nitrogen and hydrogen.

Nitrogen had virtually no effect on the yield of any of the various molecular groups determined by proton NMR spectroscopy (Figure 6), as was expected from the absence of any corresponding effect on the total oil yield However, large increases in the proportions of particularly polycyclic aromatics were observed for the Mt Coolon and Nagoorin shales retorted in the presence of hydrogen. Very much smaller increases in the relative proportions of these compounds were observed in oils retorted from the aliphatic Rundle shale.

Taken together, the results obtained for the Nagoorin and Mt Coolon oils retorted under hydrogen suggest that these are not normal shale oils, but more closely resemble coal-derived liquids, no doubt reflecting the partial lignitic origin of these shales. The results also indicate that for these shales in the

absence of hydrogen, a major coke forming process involves the decomposition of aromatic compounds, particularly phenols.

An unusual aspect of these results is the lack of any effects of shale composition and retorting conditions on the alkene yields. Proton NMR measurements showed that 3.2% of the protons in the Rundle oil were present as alkenes, 2.8% in Nagoorin oil and 2.4% in Mt Coolon oil. Similarly, the alkene content of Green River shale oil has been reported as 3.1%(8). Furthermore, the total alkene yield and the ratio of internal/terminal alkenes were not significantly affected by the presence of high pressure hydrogen or nitrogen. Similar results have been reported for Green River shale(8).

A possible source of alkenes is the disproportionation of alkane-free radicals produced in turn from the primary decomposition of the kerogen(14). However, it is not at all clear why quite different kerogens should give almost identical yields of alkenes. Further, it is difficult to accept that a hydrogen pressure of 6 MPa does not reduce the above disproportionation reaction, and even hydrogenate the newly formed alkenes.

(d) Model for Kerogen Decomposition

Published models for the decomposition of kerogen(8-10) are based on work with Green River shale which is highly aliphatic, produces an oil of low aromaticity with a yield and composition which are only marginally affected by hydrogen pressure, and which thus generally resembles the shale from the Rundle deposit. Our work has shown that the aromatic Mt Coolon and Nagoorin shales can be retorted under conditions which give oils containing large amounts of phenols and polycyclic aromatics and thus resemble coal pyrolysis liquids. For these shales, the reactions of the dominant aromatic components of the kerogen are at least equally as, and possibly even more important than those of the aliphatic components, whose behaviour dominates the retorting chemistry of shales from Rundle or Green River. For these aromatic shales, the following retorting model is proposed:

(i) The organic matter in these shales is composed of material of algal (predominantly aliphatic) and lignitic (predominantly aromatic) origin. Varying amounts of wax and material derived from leaf cuticles may also be present and, for the Mt Coolon shale, these may be major components(12).

(ii) The aliphatic components of the organic matter decompose to give largely aliphatic products. As shown by the work of Regtop et al.,(15) some of the aliphatic oil may be converted to aromatics by reactions catalysed by the spent shale surfaces. The contribution of such reactions to the total aromatic yield must however be small because of the very short residence times.

(iii) The aromatic components of the shale organic matter decompose to aromatic and reactive products which, under normal retorting conditions, rapidly decompose to give coke and gas. Under certain circumstances, e.g. high pressure hydrogen or very short residence times, these compounds survive and appear in the oil as phenols and other aromatic compounds. The decomposition of these compounds during normal retorting serves as a preliminary clean-up of the oil, at the expense of the organic carbon conversion.

(iv) The coke formed during pyrolysis of the aromatic shales can undergo further aromatisation reactions, as is shown by the loss of hydrogen

and methane at temperatures significantly higher than those normally required for retorting(16).

ACKNOWLEDGEMENTS

The authors thank Southern Pacific Petroleum NL/Central Pacific Minerals NL (Mr. J. Gannon) and the International Mining Corp. (Mr. D. Hawley) for the samples of shale used in this work. The assistance of Mr. C.H. Randall, Miss C. Walters and Mr. I. Liepa with the experiments, Mr. G.C. Wall who arranged the Fischer Assays and Ms. P. Udaja who carried out some of the analytical work is also gratefully acknowledged.

LITERATURE CITED

1. Janka, J.C. and Rex, R.C., The HYTORT Process, presented at the Oil Shale Symposium, Rabat, Morocco, April 1984.

2. Roberts, M.J., Feldkirchner, H.L., Punwani, D.V. and Rex, R.C., American Chemical Society Fuel Division Preprints, 29, 194 (1984).

3. Lynch, P.A., Janka, J.C., Lace, F.S., Feldkirchner, H.L., and Dirksen, H.A., American Chemical Society Fuel Division Preprints, 29, 71 (1984).

4. Rex, R.C. and Roberts, M.J., Paper presented at the 1983 Eastern Oil Shale Symposium, Lexington, Kentucky, 13-16 November, 1983.

5. Furimsky, E., Synnott, J., Boormen, R.S. and Salter, R.S., Fuel Process. Technol., 8, 293 (1984).

6. Anon. Synthetic Fuels from US Oil Shales, A Technical and Economic Verification of The HYTORT Process. DOE/ET/14102 (1981).

7. Falk, A.F., Garey, M.P. and Rosemary, J.K., Final Technical Report Application of Hydropyrolysis to the Hydroconversion of Eastern Oil Shale. ESG-DOE-13406 (1983).

8. Hershkowitz, F., Olmstead, W.N., Rhodes, R.P. and Rose, K.D., American Chemical Society Symposium Series 230, 301 (1983).

9. Burnham, A.K. and Singleton, M.F., ibid., 335.

10. Burnham, A.K. and Happe, J.A., Fuel (in press)

11. Hutton, A.C., - Organic Petrology of Oil Shales. Ph.D. Dissertation, University of Wollongong, NSW, Australia (1983).

12. Chaffee, A., Ekstrom, A., Fookes, C.J.R., Glickson, M. and Loeh, H., Proceedings of the Second Australian Workshop on Oil Shale, Brisbane, 6-7 December, 1984, p.56.

13. Data for the Yaamba shale are taken from unpublished work by Ekstrom and Wong (1985).

14. Fookes, C.J.R. and Johnson, D.A., This symposium.

15. Regtop, R., Ellis, J., Crisp, P.T., Ekstrom, A. and Fookes, C.J.R., Proceedings of the Second Australian Workshop on Oil Shale, Brisbane, 6-7 December, 1984, p. 170.

16. Ekstrom, A., Hurst, H.J. and Randall, C.H., American Chemical Society Symposium Series 230, 317, (1983).

TABLE 1
PROPERTIES OF OIL SHALE

PROPERTY[a]	RUNDLE	MT COOLON	NAGOORIN
ANALYSIS			
Weight loss on drying (%)	10	50	25
Inorganic carbon (%)	0.89	-	0.14
Organic carbon (%)	13.9	45.9	44.8
Hydrogen (%)	2.1	4.3	3.1
Nitrogen (%)	0.4	0.4	2.1
Sulphur (%)	0.6	3.1	1.5
H/C ratio	1.84	1.12	0.81
^{13}C Aromaticity	0.20	0.33	0.48
RETORTING			
Fischer Assay (wt % dry shale)	11.0	24.6	7.6
Organic carbon in char (%)	14.8	45.2	41.6
Conversion of organic carbon to oil (%)	50	35	10

[a] Based on dry shale.

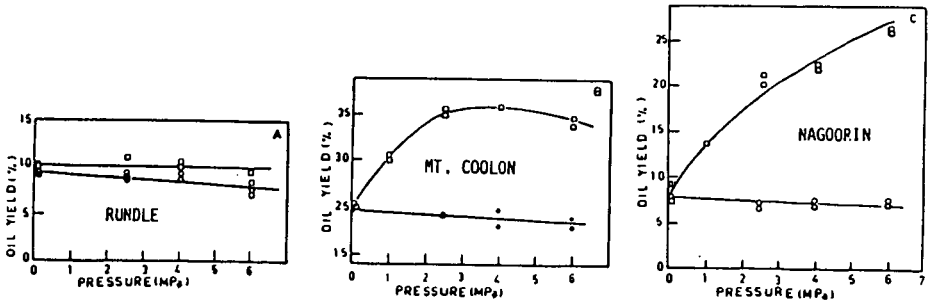

FIGURE 1. Effect of pressure on oil yields
o nitrogen, □ hydrogen

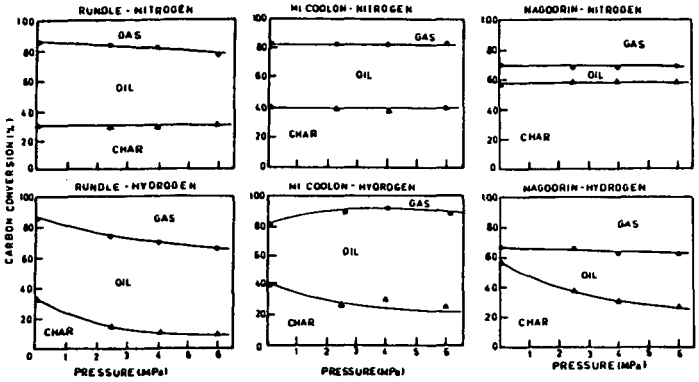

FIGURE 2. Effect of pressure on organic carbon distributions

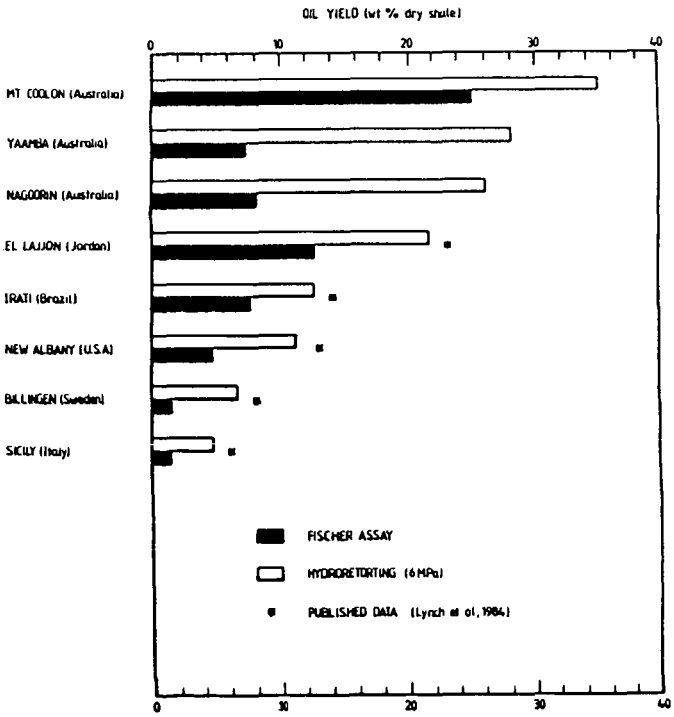

FIGURE 3. Comparison of the effects of hydrogen pressure on oil yields.

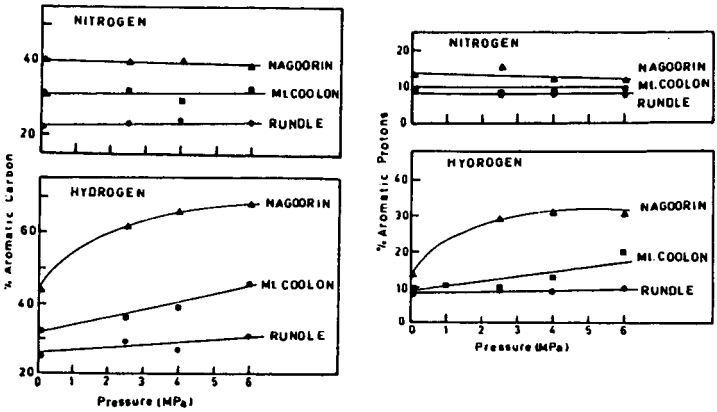

FIGURE 4 Effect of retorting pressure on carbon and proton aromaticities.

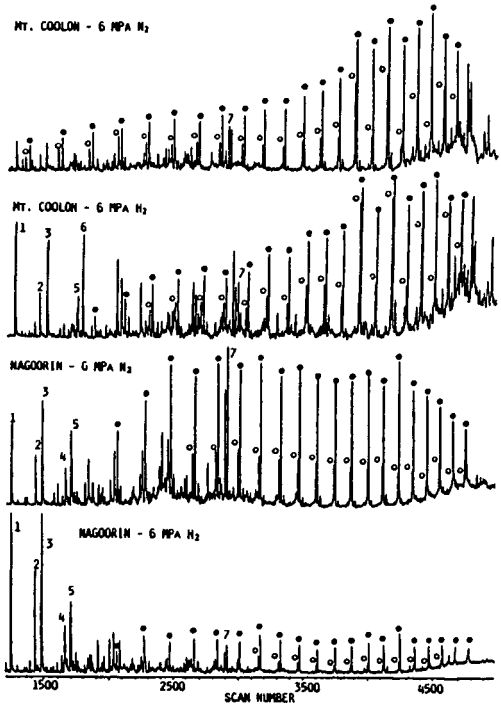

FIGURE 5. Total ion chromatograms of whole oils retorted in hydrogen and nitrogen.

1 phenol
2 o-cresol
3 m&p cresol
4 & 5 dimethyl and ethyl phenols
6 napthalene
7 pristenes

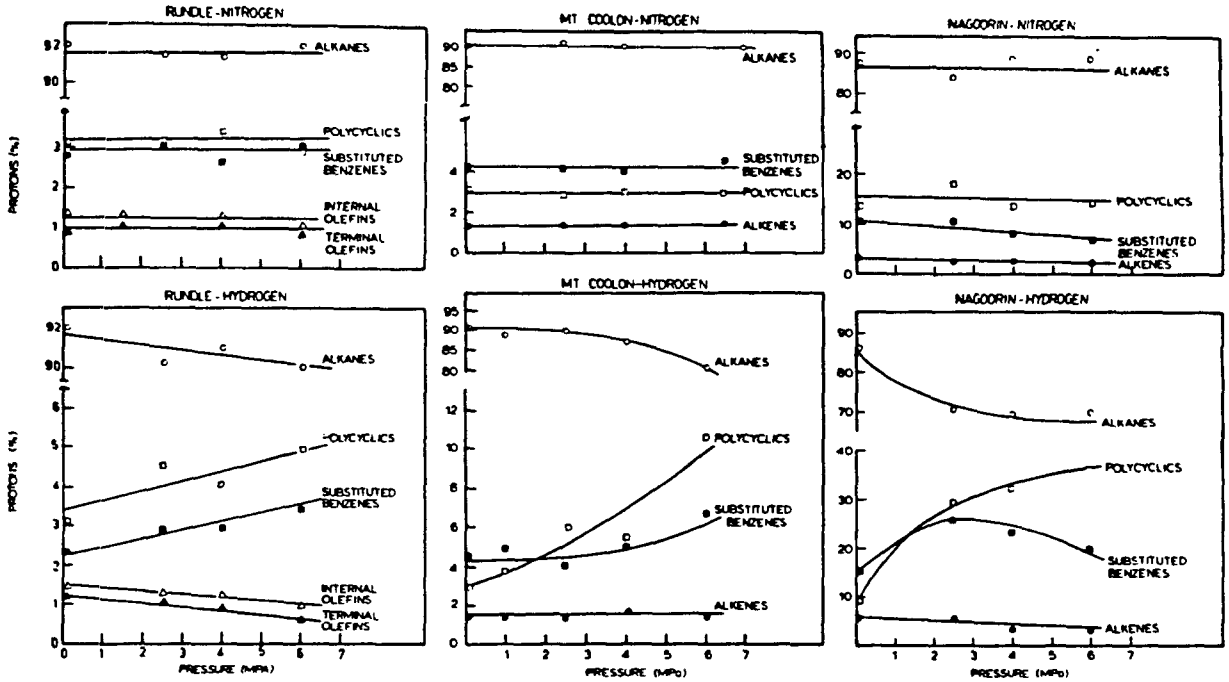

FIGURE 6. Effects of retorting pressure on the proton distributions in the shale oils.

PYROLYSIS AND HYDROPYROLYSIS OF KENTUCKY OIL SHALE IN SUPERCRITICAL TOLUENE UNDER RAPID HEATING CONDITIONS

R.M. Baldwin and J.A. Manley
Chemical Engineering Department
Colorado School of Mines, Golden, CO 80401

ABSTRACT

Oil shale from the Cleveland member of the Ohio shale, Montgomery County, Kentucky has been pyrolysed in supercritical toluene in the presence and absence of gas-phase molecular hydrogen. Data have been collected in a 300-cc stirred tank autoclave at residence times of 0^+, 5, and 30 minutes, temperatures from 653 to 733 K, and total pressures (at temperature) ranging from 15.1 to 20.6 MPa. The reactor was equipped with a gas-driven sample injector so that shale could be injected into the pre-heated dense gas at reaction conditions. Heating rates of approximately 500 C/min were obtained with this configuration. Results for conversion of organic carbon to oil have been computed based on a carbon balance on the reaction system.

The objectives of the experimental program were:
1: investigate the use of toluene as a dense gas medium;
2: elucidate the reaction kinetics and the effect of hydrogen and heating rate on the rate and extent of oil formation. The data have shown toluene to be an excellent dense-gas media for facilitating supercritical pyrolysis and hydropyrolysis. Carbon conversions and oil yields of in excess of 185% of Fischer Assay were achieved in the presence of gas-phase molecular hydrogen at very short (<2 minute) residence times . Carbon conversion to oil was found to be a function of final temperature, hydrogen partial pressure, and heating rate.

INTRODUCTION

Oil shale represents one of the largest hydrocarbon reserves in the world (1). Of the various techniques available for recovery of oil from oil shale, processes based on thermal decomposition of the organic matter in shale have received, by far, the most attention (2). Thermal decomposition or retorting technologies have been developed to a high degree of sophistication as evidenced by the TOSCO II, Union B, and Chevron. Unfortunately, retorting processes are plagued by inefficiencies in oil recovery which are inherent to the pyrolytic chemical reactions taking place. Principally, these inefficiencies result in low carbon conversion to oil due to free radical reactions such as cracking and condensation. In the case of cracking, a high gas make is promoted at the expense of oil while the oil product remaining is correspondingly high in olefin content. Regressive reactions due to condensation promote formation of coke. Both cracking and coking may be reduced to some extent by operation at low temperature and/or short residence times, or by processing in the presence of hydrogen and/or hydrogen transfer agents that act as free radical scavengers. It is the latter phenomenon that gives rise to interest in alternate oil shale processing schemes based on

reactions in dense gas media.

Kerogen in oil shale is known to be relatively insoluble in most organic solvents at or below their normal boiling points, but when oil shale is heated to temperatures above 600 K, the organic matter may be extracted in high yield (3,4). Several early patents describe solvent processing of torbanite and other shale-like materials at elevated temperatures both with and without hydrogen gas atmospheres (5,6,7,8). Jensen et al. (9) have reported on hydrogenation of Green River oil shale in vehicle oils, while Gregoli (10), Patzer (11), and Greene (12) have all recently been issued patents for hydrogenation of oil shale in hydrogen donor and non-donor solvents in the presence and absence of gas phase molecular hydrogen. Recently, McKay et al. (13) and Baldwin et al. (14) have reported on investigations using dense (supercritical) gases and subcritical fluids for extraction of shale oil from oil shale under a wide variety of processing conditions.

This paper presents the results of pyrolysis and hydropyrolysis of oil shale from the Cleveland Member of the Ohio shale group from Montgomery County, Kentucky. The objective of the research described was to investigate the effect of temperature, hydrogen partial pressure, time, and heating rate on carbon conversion and oil yield using toluene as the dense gas vehicle.

EXPERIMENTAL APPARATUS AND METHODS

All experiments were carried out in a 300-cc autoclave reactor, manufactured by Autoclave Engineers. The reactor was interfaced to an Apple II+ microcomputer for data acquisition and control of heating rate. A schematic of the system is shown in Figure 1. The as-received shale was processed by crushing (to 100% -200 mesh) and vacuum drying at 40 C. Dried shale was stored in a vacuum dessicator until used. A Fischer Assay of the feed shale is shown in Table 1. Also shown in this table are data on organic carbon conversion to oil for the Fischer Assay analysis, computed from quantitative analysis of the spent shale and retort gases for carbon, and a forced ash balance on the feed and spent shale. For the supercritical gas extraction experiments, helium and hydrogen were used as the reaction process gases, with a 1% krypton tracer employed so that gas make could be readily quantified. Spent shale recovered from the reactor was extracted with acetone and methylene chloride to remove adsorbed shale oil. Samples of the feed and spent shale were analyzed for total and inorganic carbon on a Coulometrics system.

DISCUSSION OF RESULTS

Experimental runs were made at temperatures between 653 and 733 K (380 and 460 C) in 20 degree increments, and at reaction times of 0^+, 5, and 30 minutes. Prior to initiating heating of the reactor, 2.06 MPa (300 psi) of either helium or hydrogen was added to the reactor. This initial pressure plus the autogeneous pressure of the solvent (toluene) resulted in a total presssure at reaction temperature of between 15.1 and 20.6 MPa(2200 to 3300 psi). At these conditions, toluene (critical temperature 593.9

K, critical pressure 4.07 MPa) was present in the reactor as a dense gas. After heating to reaction conditions with only gas and toluene present in the reactor, the shale was injected into the vessel with an overpressure of helium. The reaction temperature rapidly rebounded to the desired temperature (generally within one minute). Following the desired reaction time, the reactor was quenched by forced convection. Samples of the spent shale were analyzed for total and inorganic carbon, and ashed in a muffle furnace. Carbon conversion to oil plus gas was then calculated based on a forced ash balance, while carbon conversion to gas was calculated from an analysis of the reaction product gases. Carbon conversion to oil, and thus oil selectivity, was then finally computed by difference. In the following discussion, oil selectivity refers to the fraction of carbon converted that is converted to oil.

Two baseline runs in helium and hydrogen atmospheres were performed at 698 K in order to establish the thermal reactivity of the shale in supercritical toluene. These runs were, however, done with the reactor used in the true batch mode of operation where the entire reaction mass was heated slowly (approximately 8 C per minute) to the final temperature, and then held at this level for one hour. Results of this run are shown in Table 2. As may be seen, an organic carbon conversion of 44.0% and oil selectivity of 91.6%, resulting in an overall conversion of carbon to oil of only 40.3% was achieved in the absence of hydrogen. This conversion level is consistent with the results obtained in standard Fischer Assay pyrolysis (viz. Table 1). Pyrolysis under these conditions in the presence of hydrogen however raises the carbon conversion to oil to 68.9%, thus demonstrating the well-recognized benefits attendant to hydropyrolysis of aromatic oil shales. Clearly, hydrogen in the reaction gas atmosphere greatly enhances carbon conversion. This is primarily accomplished by inhibiting condensation reactions which lead to formation of coke, as the oil selectivities differ by only about 10%. This observation is consistent with a radical quenching mechanism, promoted by the presence of gas phase molecular hydrogen.

Results for pyrolysis and hydropyrolysis in supercritical toluene under rapid heating conditions (c.a. 500 C/min) are shown in Figures 2, and 3. Figure 2 presents the kinetic data for organic carbon conversion obtained with hydropyrolysis under rapid heating conditions at an initial (cold) hydrogen pressure of 300 psi. As may be seen, the low temperature isotherms (653, 673, and 693 K) exhibit the expected time/temperature behavior. Hydropyrolysis at 713 and 733 K however shows an entirely different behavior, with the organic carbon conversion reaction becoming essentially instantaneous at the highest temperature studied (733 K). Oil selectivity (the fraction of carbon reacted that is converted to oil) at the highest temperature and shortest residence time is 95.6%. This, coupled with the 61.3% organic carbon conversion achieved at this combination of reaction conditions gives rise to an overall oil yield in excess of 185% of Fischer Assay. Perhaps more interesting however, is the effect of hydrogen on the reaction that is indicated in Figure 3. As illustrated, under conditions of rapid heating and low final

temperature (673 K), the organic conversion is insensitive to the presence of hydrogen in the reaction gas atmosphere over a wide range of residence times as shown by the essentially identical results for pyrolysis (helium atmosphere) and hydropyrolysis. This is in direct contrast to the slow heating data shown in Table 2, where hydrogen has a marked effect on the ultimate yield of oil. At 713 K, the presence of hydrogen has a small beneficial effect at the short residence time (5 minutes), and a substantial beneficial effect at the extended residence time of 30 minutes. At 733 K, the effect of hydrogen is pronounced over the entire range of reaction times studied, and is especially pronounced at 30 minutes. Considering these data in light of the previous data from the slow heating rate experiments serves to indicate that a complex mechanism involving both radical quenching and oil evolution rate processes is operative in this reaction system. Under conditions of rapid heating but at low final temperatures (673 K or less) the secondary condensation reactions leading to decreased oil yield are apparently sufficiently slow such that the carbon conversion reactions are not sensitive to the presence of added hydrogen. Reaction at high heating rates but higher final temperatures (713 K and above) however shows a significant sensitivity to the presence of gas-phase molecular hydrogen, especially at extended residence times. Apparently, under these conditions, regressive (coke-forming) reactions are sufficiently rapid that inhibition of condensation by radical quenching becomes significant, thus leading to enhanced organic carbon conversions. At high heating rates, significantly higher organic carbon conversions can be obtained with inert atmosphere pyrolysis when compared to the Fischer Assay as shown by a comparison of the high temperature helium atmosphere data in Figure 3 and the data in Table 1. This enhanced yield is, however, only present at short residence times (<5 minutes). This is undoubtedly due to the well documented effect of "flash pyrolysis", where the rapid rate of volatiles evolution is successful in preventing secondary reactions which decrease carbon conversion (15). At higher reaction severity (time/temperature combinations), some form of hydrogen activity is required to prevent the onset of regressive reactions with the resultant loss of carbon conversion.

ACKNOWLEDGEMENTS

The authors wish to acknowledge the financial support of Southern Pacific Petroleum, N.L. of Sydney, Australia. Conversations with Carl S. Minden and John Gannon were also helpful in execution and interpretation of the research.

LITERATURE CITED

1. Dickson, P.F., Oil Shale, Kirk-Othmer Encyclopedia of Chemical Technology, Vol. 16, Third Edition, 1981.
2. Baughman, G.L., Synthetic Fuels Data Handbook, second edition, Cameron Engineers, Inc., 1978.
3. Gavin, M.J., and Aydelotte, J.T., "Solubilities of Oil Shales in Solvents for Petroleum", Bureau of Mines R.I. 2313, 1922.
4. Dulhunty, J.A., "Solvent Extraction of Torbanite", Proc.

Linnean Soc., New South Wales, vol. 67, 1942.
5. Ryan, H.D., "Bituminous Material from Oil Shale", U.S. Patent 1,327,572, Jan. 6, 1920.
6. Hampton, H., "Hydrocarbons from Bituminous Shale-Like Material", U.S. Patent 1,668,898, May 8, 1928.
7. Fisher, A., "Pyrolytic Conversion and Coking of Finely Divided Bituminous Material and Hydrocarbon Oil", U.S. Patent 2,073,367, March 9, 1937.
8. Buchan, F.E., "Processing Oil Shale", U.S. Patent 2,487,788, November 15, 1949.
9. Jensen, H.B., Barnet, W.I., and Murphy, W.I.R., "Thermal Solution and Hydrogenation of Green River Oil Shale", U.S. Bureau of Mines Bulletin 533, 1953.
10. Gregoli, A.A., "Fluidized Bed Hydroretorting of Oil Shale", U.S. Patent 4,075,081, February 21, 1978.
11. Patzer, J.F., "Recovery of Oil from Oil Shale", U.S. Patent 4,238,315, December 9, 1980.
12. Greene, M.I., "Process for Hydrogenation/Extraction of Organics Contained in Rock", U.S. Patent 4,325,803, April 20, 1982.
13. McKay, J.F., "Characterization of Organic Matter from Supercritically Treated Green River Oil Shale", CONFAB '84, Saratoga, Wyoming, July, 1984.
14. Baldwin, R.M., Frank, W.L., Baughman, G.L., and Minden, C.S., "Hydroprocessing of Stuart A (Australian) Oil Shale", Fuel Processing Technology, 9, 1984.
15. Anthony, D.B. and Howard, J.B., "Coal Devolitalization and Hydrogasification", AIChE Journal, vol. 22, no. 4, July, 1976.

FIGURE 1

Batch Reactor Schematic

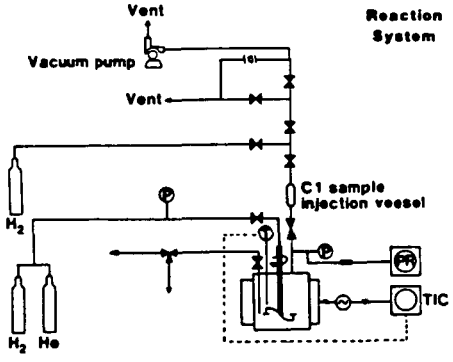

FIGURE 2

Organic Carbon Conversion Isotherms

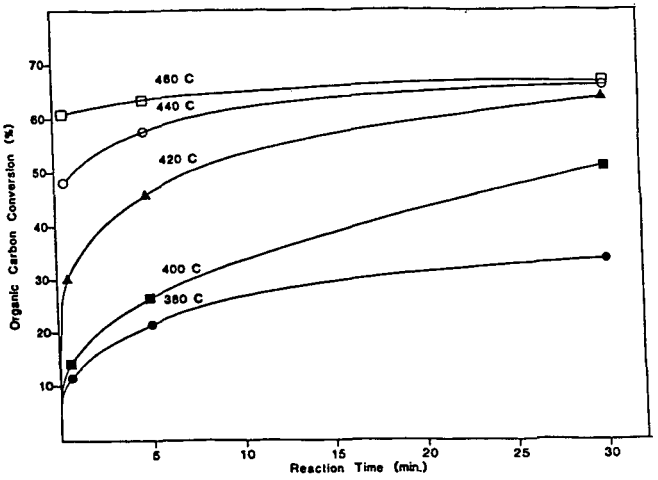

FIGURE 3

Inert Gas and Hydrogen Atmosphere Comparisons

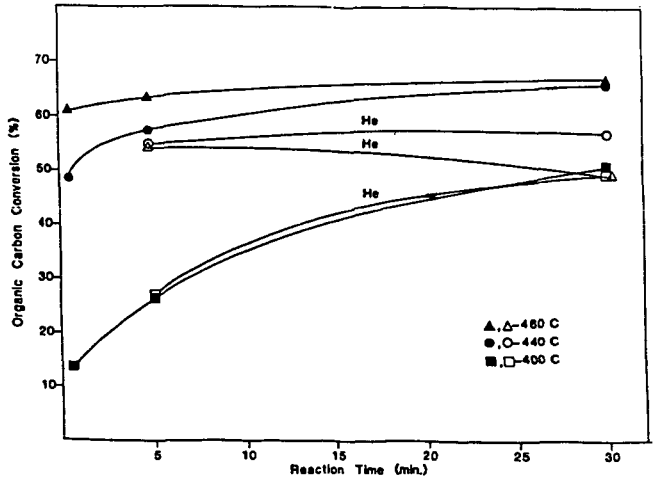

TABLE 1
Analysis of Feed Shale

	Fischer Assay[1]				
%spent shale	%oil	%water	%gas+loss	oil, GPT	OCC[2]
91.6	4.6	1.5	2.3	11.6	42.9

1. Analysis by Commercial Testing and Engineering Co., Golden, CO
2. % organic carbon conversion to oil

TABLE 2
Results under Slow Heating Rate Conditions[1]

	H_2	He
OCC[2]	72.6	44.0
OY[3]	95.9	91.6

1. Reactions carried out in true batch mode, heating rate of approximately 8 C/min, 425 C final temperature, 300 psi initial hydrogen charge, 60 minutes residence time.

2. Organic carbon conversion to oil+gas, wt%.

3. Percent of organic carbon converted that is converted to oil.

CHARACTERIZATION AND STABILITY PROPERTIES OF POLAR EXTRACTS DERIVED FROM A RECENT SHALE LIQUID

John V. Cooney*, George W. Mushrush and Erna J. Beal

Naval Research Laboratory, Code 6180, Washington, D.C. 20375-5000

INTRODUCTION

Recent studies into the mechanisms of storage instability with middle distillate fuels have indicated that the presence of polar compounds, particularly nitrogen heterocycles, is frequently related to the deterioration of aged fuel samples [1-5]. In certain instances, direct autoxidation of nitrogen containing species is indicated, which may be subject to catalytic effects made possible by trace fuel components [6,7]. At other times, the organic nitrogen compounds themselves assume the role of catalyst in the oxidation of other fuel molecules. One approach to the problem of nitrogen compound induced storage instability has involved model compound dopant studies [8,9]. A second approach involves the study of the stability properties of actual high-nitrogen middle distillate fuels [10,11]. In this paper we discuss the second approach which was applied to a recently refined high-nitrogen shale liquid. Thus, polar extract components were isolated, characterized and studied in the context of accelerated storage stability tests.

EXPERIMENTAL

The high-nitrogen shale liquid which was examined in this study was refined from Geokinetics crude shale oil refined at the Caribou-Four Corners Refinery (Utah). The sample which was studied had been distilled and partially hydrotreated, and was designated at NRL as "fuel 83-65". Fuel 83-65 is identical to processing intermediate 1-HTR-3 recently studied by Thompson and Holmes [12]. Fuel 83-65 was separated into three polar extracts using a reported procedure involving extraction with acid (1.0 N HCl) followed by batch adsorption onto silica gel, which was subsequently back-washed with methylene chloride and methanol [10,11]. The three extracts thus provided were: (a) BNC ("basic nitrogen compound" extract, the acid-extractable material, in methylene chloride), (b) NBNC(CH_2Cl_2)("non-basic" extract in methylene chloride), and (c) NBNC(CH_3OH)(methanolic wash of the silica gel). The polar extracts were examined by capillary GC/MS using reported conditions [10].

The accelerated storage stability test method used has been described in detail [4]. In summary, 300 ml samples of filtered fuel were thermally stressed in the dark in 500 ml screw-cap borosilicate Erlenmeyer flasks (Teflon-lined caps). Replicate samples were run, with both filterable sediment and adherent gum values determined after storage. Peroxide numbers (ASTM D1583-60) were also determined in samples of filtered fuel before and after stress. Extract-doping experiments employed a very stable Navy Shale-II process shale diesel fuel, fuel D-11, as diluent. Fuel

D-11 has been well-characterized and contains AO-30 (2,4-dimethyl-6-t-butylphenol) as the sole additive [4]. All extracts were stripped of their solvent (verified by GC) by gentle rotary evaporation prior to being added to fuel D-11. Nitrogen concentration levels in fuel samples were determined by a chemiluminescent technique with an Antek Model 720 instrument [4,10].

RESULTS AND DISCUSSION

Preliminary accelerated storage stability tests at 43°C and 80°C indicated that shale fuel 83-65 possessed marginal stability (Table I). The fuel was found to be relatively high in nitrogen content, containing 2290 ppm N (w/v). It was consequently of interest to us to examine the polar components of this shale liquid as part of an effort to relate fuel composition to stability behavior [10]. The high nitrogen content of fuel 83-65 permitted the convenient extraction of a significant amount of polar material for use in the subsequent doping experiments. In addition to these preliminary tests, the shale liquid was subjected to a simulated distillation analysis. Fuel 83-65 was found to be a broad-cut fraction. By ASTM D2887, IBP was 120°C, 50% was 299°C, 95% was 421°C and FBP was 485°C. Correlation to ASTM D86 gave IBP of 190°C, a 50% value of 306°C and a 95% value of 423°C. No hydroperoxide was detected in fuel 83-65 prior to or following storage stability testing (i.e., peroxide numbers were 0.0 by ASTM D1583-60).

Table I

Accelerated Storage Stability Results for Fuel 83-65
(unvented - mg/100 ml)

Storage Conditions	Filtered Sediment	Adherent Gum	Total Insolubles Duplicate	Mean	Std.Dev.
80°C-7 days	2.3	0.6	2.9		
	1.7	1.1	2.8		
	1.8	1.0	2.8	2.8	±0.1
80°C-14 days	4.5	2.6	7.1		
	3.7	4.9	8.6		
	3.5	2.9	6.4	7.4	±1.1
43°C-49 days	1.6	0.6	2.2		
	1.8	1.1	2.9		
	0.8	1.6	2.4	2.5	±0.4
43°C-91 days	2.5	2.2	4.7		
	2.4	2.2	4.6		
	2.1	3.2	5.3	4.9	±0.4

Extraction of Nitrogen Compounds

The separation scheme which was used for the removal of polar extracts was patterned after an earlier procedure [10]. A single, mild acid extraction (using 3.67 equiv. of 1.0 N HCl) was selected to minimize the opportunity for chemical changes in the fuel. The BNC extract was obtained in methylene chloride following neutralization of the acid wash. Subsequent treatment of the acid extracted fuel with active silica gel afforded two NBNC extracts (in methylene chloride and methanol). The fuel and extracts were analyzed for soluble nitrogen content in order to assess a nitrogen balance (Table II). It was possible (within analytical error) to account for nearly all of the nitrogen originally present in fuel 83-65. The accelerated storage stability of fuel 83-65 was improved by the acid/silica treatment, with only ca. 2.4 mg/100 ml of total insolubles resulting after 14 day - 80° stress (cf. 7.4 mg/100 ml before extraction).

Table II

Nitrogen Analyses for Extracted Fuel 83-65

	Sample	N Concentration (ppm w/v)
1.	Original	2290
2.	After acid extraction	700
3.	Isolated in CH_2Cl_2 wash of silica	490
4.	Isolated in CH_3OH wash of silica	75
5.	After acid and silica treatment	130

Examination of Polar Fuel Extracts

Components of the BNC, NBNC(CH_2Cl_2) and NBNC(CH_3OH) extracts were examined by GC/MS by a procedure which has been reported [10]. The results for the acid extractable material (BNC) and the NBNC(CH_3OH) extract are given together in Table III. Table III indicates that both of these extracts were rich in nitrogen heterocycles, principally alkylpyridines. The pyridines which were in the BNC extract were characterized by long alkyl chains (unbranched) while the NBNC(CH_3OH) extract pyridines were highly branched and generally of a higher molecular weight. Table IV compares the identifications of the ten largest peaks found in these two extracts. The presence of a substantial amount of tetrahydroquinolines (ca. 29%) in the BNC extract is a reflection of the hydrotreatment used during processing. For all three polar fuel extracts, over 95% of the total sample peak area was identified, so that the peaks which were examined were representative of the samples.

Table III

Examination of BNC and NBNC(CH_3OH) Extracts from Fuel 83-65

Compound Class*	BNC Extract n	BNC Extract Area %	NBNC(CH_3OH) Extract n	NBNC(CH_3OH) Extract Area %
A. Pyridines	(175)	(60.2)	(213)	(88.6)
<C_4	12	0.7	6	0.6
C_4	5	0.6	7	1.5
C_5	19	0.6	15	0.6
C_6	10	0.2	1	<0.1
C_7	14	9.8	3	0.1
C_8	20	16.4	6	0.1
C_9	24	14.6	6	0.1
C_{10}	22	9.9	10	0.8
C_{11}	43	6.3	15	1.9
C_{12}	6	1.2	28	5.5
C_{13}	-	-	34	27.9
C_{14}	-	-	39	26.4
C_{15}	-	-	34	12.7
C_{16}	-	-	9	10.3
B. Tetrahydroquinolines	(134)	(29.0)	(114)	(5.7)
<C_3	6	0.6	2	0.2
C_3	13	2.9	9	0.5
C_4	19	12.8	2	0.1
C_5	23	6.6	3	0.1
C_6	29	3.2	5	0.1
C_7	35	2.2	32	1.7
C_8	8	0.6	17	1.0
C_9	1	0.2	25	0.8
C_{10}	-	-	12	0.5
C_{11}	-	-	7	0.7
C. Quinolines	(54)	(7.9)	(12)	(0.2)
<C_3	2	0.4	-	-
C_3	7	2.1	-	-
C_4	12	1.6	-	-
C_5	18	3.2	-	-
C_6	13	0.7	-	-
C_7	2	<0.1	-	-
D. Indoles	(40)	(2.2)	(20)	(1.3)
<C_7	10	0.7	-	-
C_7	9	0.5	-	-
C_8	18	0.8	-	-
C_9	3	0.1	-	-
E. Carbazoles	(-)	(-)	(98)	(3.2)
<C_4	-	-	8	0.1
C_4	-	-	22	0.5
C_5	-	-	38	1.1
C_6	-	-	22	1.3
C_7	-	-	5	0.1
C_8	-	-	3	0.1
F. Other N Compounds	(16)	(0.8)	(16)	(0.4)
G. Other Compounds	(-)	(-)	(19)	(0.6)

*"C_x" denotes the no. of carbon atoms in substituents on the heterocyclic ring, "n" is the number of isomers observed, "Area %" is based on the total ion count from mass of 45 through 450.

Table IV

A. Ten Largest Peaks - BNC Extract From Fuel 83-65

Rank	Rel. Area	Main Component	Retention Time (min)
1	1000	Dimethylhexylpyridine	27:16
2	913	Methylpropyltetrahydroquinoline	26:26
3	870	Trimethylpentylpyridine	26:15
4	854	Dimethylheptylpyridine	30:32
5	825	Dimethylhexylpyridine	28:10
6	775	Dimethylpentylpyridine	23:51
7	676	Trimethylhexylpyridine	29:30
8	660	a C_4 Tetrahydroquinoline	25:59
9	472	Trimethylhexylpyridine	28:58
10	413	a C_8 Pyrindine	27:07

B. Ten Largest Peaks - NBNC(CH_3OH) Extract From Fuel 83-65

Rank	Rel. Area	Main Component	Retention Time (min)
1	1000	a C_{13} Pyridine	37:48
2	549	Trimethyltridecylpyridine	47:12
3	544	a C_{13} Pyridine	38:09
4	495	a C_{16} Pyridine	47:15
5	375	Trimethylundecylpyridine	42:26
6	317	Trimethyldecylpyridine	39:53
7	281	Dimethyltridecylpyridine	45:19
8	260	Trimethylundecylpyridine	40:49
9	251	Dimethylundecylpyridine	40:14
10	238	Trimethylundecylpyridine	43:29

The methylene chloride NBNC extract was found to be very complex, consisting primarily of hydrocarbons. Most of the nitrogen in this extract appeared in the form of substituted indoles. The compound classes present are summarized in Table V.

Table V

Examination of NBNC(CH_2Cl_2) Extract From Fuel 83-65

Compound Class	No. Isomers	Area %
A. Hydrocarbons	(294)	(91.3)
Alkanes	33	44.8
Cycloalkanes	35	2.1
Benzenes	80	10.7
Naphthalenes	22	8.5
Tetralins	53	11.1
Indanes	15	2.8
Fluorenes	15	4.2
Phenanthrenes	9	3.8
Biphenyls	11	2.1
Other Hydrocarbons	21	1.2
B. Nitrogen Compounds	(37)	(8.7)
Indoles	27	6.0
Other Nitrogen Compounds	10	2.8

Results of Doping Experiments

The polar components of each of the three extracts were added as dopants to a stable shale diesel fuel (fuel D-11). Stress conditions employed termperatures of 80°C and 43°C for periods of time ranging up to 14 and 154 days respectively [8,10]. The results of the doping experiments are given in Table VI. In the table, the amount of total insoluble material is reported as the mean of three experimental trials.

Table VI

Total Insolubles for D-11 with Added Polar Extracts

Extract	Storage Conditions	N Added (ppm-w/v)	Total Insolubles(mg/100 ml) Mean	Std. Dev.
BNC	80°C-7d	337	1.6	±0.2
	80°C-14d	337	1.3	±0.6
	43°C-77d	337	0.5	±0.0
	43°C-154d	337	0.7	±0.1
NBNC(CH_2Cl_2)	80°C-7d	264	4.3	±0.6
	80°C-14d	264	4.7	±0.6
	43°C-70d	264	4.1	±0.2
NBNC(CH_3OH)	80°C-14d	163	63.7	±22.5
undoped D-11	80°C-14d	0	0.0	±0.1
	43°C-52d	0	0.1	±0.2
	43°C-154d	0	0.4	±0.0

The results of the dopant experiments indicated that the methanolic NBNC extract was by far the most active sediment promoter in the D-11 fuel, about as active as 2,5-dimethylpyrrole on a ppm N (w/v) basis [4]. This is the most active fuel extract we have yet isolated; it is considerably more reactive than the NBNC(CH_3OH) extracts obtained from other shale fuels in earlier work [10]. Notable constituents of the methanolic NBNC extract were branched alkylpyridines as well as alkylcarbazoles, which have yet to be studied as model dopants in well-defined systems [4]. We speculate that these species may be involved in the oxidation reactions of storage instability. It was surprising to isolate such a reactive extract from fuel 83-65, since the fuel is actually quite a bit more stable than other shale fuels which we have studied (cf. Table I and ref. 10). This clearly indicates the importance of complex "interactive effects" present in a given fuel in controlling and allowing the expression of oxidative lability of sensitive molecules [7]. Thus, it is possible that natural antioxidants present in fuel 83-65 normally suppress the tendency of the components of extract NBNC(CH_3OH) to oxidize or initiate oxidation processes.

The NBNC(CH_2Cl_2) extract was found to be a mild promoter of instability, while the BNC extract had little effect despite the fact that some 337 ppm N (w/v) had been added to the D-11 base fuel. The inertness of the BNC extract may be a result of reduced oxidizability of straight-chain alkylpyridines (relative to branched) or may be due to inhibition as a result of the high tetrahydroquinoline content [10]. Instability promoted by the NBNC(CH_2Cl_2) extract may be a consequence of the presence of modest amounts of olefins and alkylindoles in this extract.

CONCLUSIONS

Polar fractions have been isolated and characterized from a recently refined shale-derived liquid. When the extracts were added as dopants to a stable shale diesel fuel and stored at elevated temperatures, the formation of insoluble material was observed. The most active extract in promoting instability consisted primarily of branched alkylpyridines (not acid-extractable) together with modest amounts of tetrahydroquinolines and alkylcarbazoles.

ACKNOWLEDGEMENT

This work was funded by the Department of Energy under an interagency agreement, contract no. DE-AI-19-81-BC10525. References to brand names were made for identification only and do not imply endorsement by DOE or NRL.

LITERATURE CITED

(1) Frankenfeld, J.W., Taylor, W.F. and Brinkman, D.W., U.S. Department of Energy Report No. DOE/BC/10045-12 (1981).

(2) Frankenfeld, J.W., Taylor, W.F. and Brinkman, D.W., Ind. Eng. Chem. Prod. Res. Dev., 22, 608, 615, 622 (1983).

(3) Goetzinger, J.W., Thompson, C.J. and Brinkman, D.W., U.S. Department of Energy Report No. DOE/BETC/IC-83/3 (1983).

(4) Cooney, J.V., Beal, E.J. and Hazlett, R.N., Liq. Fuels Tech., 2, 395 (1984).

(5) Dahlin, K.E., Daniel, S.R. and Worstell, J.H., Fuel, 60, 477 (1981); Worstell, J.H. and Daniel, S.R., Fuel, 60, 481 (1981); Worstell, J.H., Daniel, S.R. and Frauenhoff, G., Fuel, 60, 485 (1981).

(6) Frankenfeld, J.W., Taylor, W.F. and Brinkman, D.W., U.S. Department of Energy Report No. DOE/BC/10045-23 (1982).

(7) Cooney, J.V., Beal, E.J. and Beaver, B.D., Preprints, Div. of Fuel Chem., ACS, 30, in press (1985).

(8) Cooney, J.V., Beal, E.J. and Hazlett, R.N., Preprints, Div. of Petro. Chem., ACS, 28, 1139 (1983).

(9) Cooney, J.V., Beal, E.J., Wechter, M.A., Mushrush, G.W. and Hazlett, R.N., Preprints, Div. of Petro. Chem., ACS, 29, 1003 (1984).

(10) Cooney, J.V., Beal, E.J. and Hazlett, R.N., Preprints, Div. of Petro. Chem., ACS, 29, 247 (1984).

(11) Cooney, J.V., Beal, E.J. and Hazlett, R.N., Ind. Eng. Chem. Prod. Res. Dev., in press (1985).

(12) Thompson, L.F. and Holmes, S.A., Fuel, 64, 9 (1985).

CALORIMETRIC DETERMINATION OF THE HEATS OF RETORTING GREEN RIVER AND RUNDLE OIL SHALES TO 500°C AND OF THE HEAT OF COMBUSTION OF SPENT GREEN RIVER SHALE AT 705°C

Stephen C. Mraw and Charles F. Keweshan

Exxon Research and Engineering Co.
Clinton Township, Annandale, New Jersey 08801

INTRODUCTION

Two important considerations for the future production of oil from shale are solids handling and heat management. For a resource yielding about 90 ℓ/tonne†, two tonnes of rock must be handled for each barrel of oil produced, and large quantities of heat must be supplied or removed for the high-temperature processes involved. Proper reactor design and efficient process operations require accurate enthalpy data for retorting raw shale and combusting spent shale. It is part of our program in high-temperature calorimetry to develop novel techniques for oil-shale measurements and to provide accurate enthalpy data for shales of commercial interest. In previous papers, we have described a new method for determining the enthalpy of vaporization of organic materials at high temperatures (1), demonstrated the application of this method to oil-shale systems (2), and given a complete set of results for the heat of retorting raw Colorado Green River and Australian Rundle oil shales to 500°C (3). In the present paper we present new results for the heat of combustion of spent Green River shales at 705°C.

EXPERIMENTAL METHOD

Our apparatus is the high-temperature Calvet-type calorimeter described previously (4). Briefly, it consists of a central inconel block surrounded by a furnace designed for operation from room temperature to 1000°C. Within the block are two symmetrically mounted wells which serve as sample chambers. Each well is surrounded by a multi-junction thermopile which monitors the temperature difference between the well and the block. When any process within the sample chamber absorbs or liberates heat, the thermopile signal observed is proportional to the heat flow between the chamber and the block. The twin thermopiles are wired in opposition so that a difference reading is obtained for the left versus right sample chambers. A diagram of the apparatus is shown in Figure 1.

Most of the experiments to be described are "drop" experiments. A quartz or ceramic tube within the sample chamber is continuously swept with gas (nitrogen or oxygen, depending on the experiment), and a sample is dropped from room temperature into the receiving tube at the high temperature of the calorimeter. A peak in the thermopile signal records the total heat necessary to bring the sample from room temperature to its final state at high temperature. The area of the peak is directly proportional to the total heat.

---

† ℓ/tonne = 4.174 U.S. gal/ton

In the case of samples dropped into nitrogen, we have developed a novel method for determining the heat necessary for rapid vaporization processes in the calorimeter (1). When a sample of an organic compound, or of a complex mixture, is dropped into the calorimeter at a temperature where evaporation or boiling is rapid, all processes can be completed within the time constant of the calorimeter (about 2 to 3 minutes). The calorimeter thermopile then responds "ballistically", and the peak height (as well as the more traditional peak area) is directly proportional to the total heat transferred to the sample. In Reference 2 we showed that the method was accurate beyond pure compounds and could be used to determine the heats associated with oil-shale processes. Results on Green River oil shale for the total enthalpy change

$$\text{raw shale (25°C)} \rightarrow \text{spent shale} + \text{volatiles (500°C)} \qquad 1)$$

agreed very well with those from an earlier study using an entirely different technique (5).

In addition, this experiment for a complex material such as oil shale presents an opportunity to study the physical chemistry of the associated processes. When a sample is dropped into high temperature, some processes may be completed within the response time of the calorimeter, and other processes may take longer. The peak-height value will accurately represent the heat for the rapid processes, while the peak-area value will represent the total heat for all of the processes until the calorimeter returns to equilibrium (about 1.5 to 2.5 hours). Although comparison of the peak-height and peak-area values for each run nominally distinguishes rapid vs. slower processes, this can sometimes allow a distinction between organic and inorganic contributions. In Reference 3, we presented results for two complete sink-float series of raw shales, Colorado Green River and Australian Rundle. The enthalpy quantities for equation 1 were accurately determined, and the comparison of peak-height and peak-area values showed the importance of slower inorganic processes occurring in the Rundle shales at 500°C.

Calibration of the calorimetric sensitivity, both for endo- and exothermic events, is interspersed repeatedly among the actual shale experiments. For endothermic drops into nitrogen, the calorimetric sensitivity is determined by dropping samples of α-Al_2O_3 into the calorimeter and recording both the height and area of the resulting peak. From the known enthalpy change (6) of Al_2O_3 between room temperature and the calorimeter temperature, both a peak-height and a peak-area calibration constant are calculated. For exothermic combustion experiments, the calorimetric sensitivity is determined using a calibration heater wound onto the ceramic tube which serves as the gas delivery inlet. A heat pulse is generated using a precision power supply, and the total heat is calculated from the known voltage and the measured resistance.

OIL-SHALE SAMPLES

The raw Green River oil-shale samples are from the sink-float separation procedures developed at Exxon Research and Engineering Company in Baytown, Texas (7). They are the same as those used in our retorting studies (3) and are from the Mahogany Zone (Colony Mine), ranging from 87 to 340 ℓ/tonne (21 to 82 U.S. gal/ton) Fischer Assay. Compositional details, includ-

ing mineral analyses, have been given by Vadovic (7). The powdered shale samples were dried in our laboratory over a P_2O_5 desiccant to remove surface moisture and loosely held water. Occasional checks have indicated that this process removes an amount of water comparable to that removed by drying at 105°C.

COMBUSTION OF SPENT GREEN RIVER SHALE AT 705°C

Combustion of Model Carbonaceous Materials

The electrical calibration procedure outlined earlier determines the calibration constant for the relatively "sterile" procedure of a controlled electrical power input within the thermopile reaction zone. To determine whether this constant is applicable to a vigorously combusting organic sample at high temperature, we performed several chemical checks using model combustions.

At 750°C, we measured the heat of combustion of SP-1 graphite (8). In our first experiments, using dry oxygen, the heat of combustion values were widely scattered and invariably low with respect to the literature value for graphite (9). We suspected incomplete combustion of carbon monoxide, and, when we humidified the oxygen by bubbling it through liquid water at room temperature (10), the combustion values immediately improved to within 3 to 4 percent of the literature value. By adjusting the gas flow rate to change the residence time of gases in the reaction zone, we eventually obtained an accuracy of 1 to 2 percent. Thus, all subsequent combustions of shale samples used humidifed oxygen at a flow rate of 20 cm^3/min. Further tests, both at 705 and 750°C, were made by combusting the highly-porous amorphous carbon, spherocarb (11), to simulate the rapid burning of a spent shale sample, and these tests indicated that the electrical calibration constant, even when applied to a rapid combustion, gives the true enthalpy value within a few percent.

To test whether volatile materials would combust within the thermopile zone under our conditions, we dropped samples of heavy, pure aromatic compounds directly into the oxygen stream in the calorimeter at 705°C. We used 1,2,5,6-dibenzanthracene (t_{bp} = 524°C) and coronene (t_{bp} = 525°C), and sample sizes (about 2 to 3 mg) were chosen to simulate the amount of organic that might volatilize from a spent shale sample. Even though combustion was not complete (60 to 90 percent of the expected enthalpy), we concluded that, if our system was this efficient in combusting these refractory molecules, we could expect volatile materials evolving from a spent shale to be combusted as well.

Preparation of Spent Shales

Pellets of each raw shale were pyrolyzed in a thermogravimetric analyser (TGA) to 500°C at heating rates of 50 to 100°C/min and held for 20 minutes. Most of the pellets could be recovered intact from the TGA and used for subsequent experiments. For pellets of the two richest samples, however, there was considerable swelling and cracking, often causing mechanical loss of some of the material. These pellets had to be held in gold crucibles during the TGA runs and in subsequent calorimetry experiments. To check that the TGA purge gas was reasonably free of oxygen, occasional samples were

held at 500°C for periods of 40 minutes to four hours. There was no detectable mass change during these time periods. When the subsequent heat of combustion was compared to that of samples held for only 20 minutes, no loss of heating value was observed, indicating that no serious sample oxidation had occurred.

For each raw shale in the series, several pellets (approximately 30 to 100 mg each) were pyrolyzed in the TGA. Some were saved for calorimetric experiments, while, in general, two of each member of the series were sent for analysis (12). The resulting analyses are given in Table 1 and were used to calculate the amount of organic and inorganic material in each sample. However, the amount of Ca plus Mg, if assumed to be exclusively due to the minerals calcite, $CaCO_3$, and dolomite, $CaMg(CO_3)_2$, predicts carbonate contents higher than those from the acid CO_2 tests. To arrive at a value for CO_2 content, we eventually took the simple average of the two possiblities for each sample. The inorganic carbon was then calculated and subtracted from the total carbon to yield the organic carbon value.

Spent Shale Experiments and Results

Using the 30 to 100 mg pellets described above, several experiments were performed on each spent shale at 705°C. This temperature was chosen because organic combustion is rapid, while carbonate decomposition is slow (13), giving us an opportunity to partially separate the heat effects.

In one set of experiments, the calorimeter sample chamber was continuously swept with nitrogen at flow rates ranging from 115 to 210 cm^3/min, and samples were dropped from room temperature into 705°C. From the endothermic peak in the thermopile signal, a peak-height and a peak-area enthalpy value were calculated for the process

$$\text{spent shale (25°C)} \rightarrow \text{pyrolyzed shale + products (705°C)} \qquad 2)$$

Because of the slow carbonate decomposition, a long tail is evident on the peak, and there is a considerable difference between the peak-height and peak-area enthalpies (see below, Figure 2). In separate experiments, samples of spent shale were also dropped directly into the humidified oxygen stream (20 cm^2/min) to determine the total enthalpy

$$\text{spent shale (25°C)} + O_2\ \text{(705°C)} \rightarrow \text{burnt shale (705°C)} + CO_2,\ H_2O,\ \text{etc. (705°C)} \qquad 3)$$

A typical thermopile signal showed a number of events. It first moved in the endothermic direction to record sensible heat but then quickly changed to the exothermic direction to record rapid combustion. Finally, it returned endothermic to continue recording slow carbonate decomposition. The character of the signal depends on the balance between organic material and carbonate minerals in the sample. For peaks of this type, the peak-height value is meaningless, and the area from initial to final baselines was used to calculate the enthalpy.

Figure 2 shows all of the experimental results from the nitrogen experiments (height and area) and from the oxygen experiments (area only), plotted vs. the percent organic carbon on the spent shale samples.

Experimental Heat of Combustion and Comparison to Literature

When the peak-area value from the nitrogen drop (Equation 2) is subtracted from that of the oxygen drop (Equation 3) the result is the heat of combustion of spent shale at 705°C, including shale volatiles:

$$\text{(pyrolyzed shale + products)} + O_2 \rightarrow \text{burnt shale} + CO_2,\ H_2O,\ \text{etc.} \qquad 4)$$

We assume that all processes which occur under nitrogen also occur to the same extent under oxygen and that the combustion is then an additive contribution. In particular, both the carbonate decomposition enthalpy and any enthalpy of producing volatiles from the spent shale cancel in the subtraction. The enthalpy of volatiles production is expected to be small, and the carbonate decomposition enthalpy can be added back to give an adjusted form of Equation 4:

$$\text{spent shale (including carbonate)} + O_2 \rightarrow \text{burnt shale} + \text{mineral } CO_2 + CO_2,\ H_2O,\ \text{etc.} \qquad 5)$$

The experimental combustion values for Equation 5 are given in Table 2, where they are compared to literature values derived as follows.

Burnham et al. (14) report a correlation which represents the heats of combustion of spent Green River oil shales as determined by classical bomb combustion calorimetry. Since these heats refer to a set of specified standard states which are not typical of those expected at high temperatures, they adjust their correlation and give the following (their Equation 4) for the heat of combustion expected at high temperatures

$$\Delta H\ (J/g) = -375.3\ (\%\ \text{organic C}) - 512.5\ (\%S) + 20.85\ (\%\ CO_2) \qquad 6)$$

We have adjusted this further to change the final state for water from liquid to gas (by changing the term for % organic C from -375.3 to -368.0 as they recommend) and to change the final state for nitrogen from N_2 to a mixture of NO and NO_2. The resulting equation then assumes that the following processes occur: combustion of organic material, combustion of organic sulfur and inorganic sulfides, capture of SO_2 as sulfates, and decomposition of carbonates. However, one important question concerning the combustions at 705°C in our calorimeter is whether calcium and magnesium oxides have reacted with SiO_2 to form new silicate compounds. Literature indicates that the rates of these reactions are enhanced by steam (13), but we do not know whether the low level of moisture in our oxygen is enough to have a significant effect. Thus, in Table 2 we have calculated "literature" values in two ways, assuming either no silicate formation or complete silicate formation, using the terms given by Burnham et al. (14).

In Table 2, the overall agreement between our new data and the literature values, even toward the richer fractions, shows that to first order the heat of combustion at high temperatures is understood fairly well. However, as Burnham et al. (14) also concluded (concerning their bomb calorimetry

results), there are important questions remaining, particularly on the role of mineral reactions. For example, the experimental scatter does not permit a definitive statement on the occurrence of silicate reactions in our calorimeter, since some of the points in Table 2 support one assumption and some the other.

CONCLUSION

High-temperature Calvet calorimetry is a powerful means of determining accurate enthalpy values for oil shale processes at high temperatures, using very small samples (50 to 200 mg). By using samples from sink-float separation procedures (7), a wide range of organic and inorganic contributions can be studied. In a previous paper (3), values for the heat of retorting Green River oil shales to 500°C have been extended beyond the oil yields previously studied (5,15), and the first accurate values for Rundle shales were determined. To our knowledge, the present study also represents the first attempt to measure heats of combustion of spent shales in a high-temperature calorimeter (i.e. other than by differential scanning calorimetry or differential thermal analysis). Results for spent Green River oil shales at 705°C agree reasonably well with those derived from classical bomb calorimetry, but there are important questions remaining on the contributions of mineral reactions to the enthalpy.

ACKNOWLEDGEMENT

We thank Charles J. Vadovic for providing us with the valuable series of sink-float samples and the many colleagues at Exxon who have offered valuable comments and suggestions during the course of this work.

REFERENCES

1. Mraw, S. C.; Keweshan, C. F. J. Chem. Thermodynamics 1984, 16, 873.
2. Mraw, S. C.; Keweshan, C. F. Ind. Eng. Chem., Fundamentals 1985, in press. (See also, AIChE Spring National Meeting, May 20-23, 1984, Anaheim, California, USA.)
3. Mraw, S. C.; Keweshan, C. F., paper submitted to Fuel.
4. Mraw, S. C.; Kleppa, O. J. J. Chem. Thermodynamics 1984, 16, 865.
5. Wise, R. L.; Miller, R. C.; Sohns, H. W., U.S. Bureau of Mines, 1971, Report of Investigation 7482.
6. JANAF Thermochemical Tables. Stull, D. R.; Prophet, H., directors. 2nd ed. NSRDS-NBS 37: U.S. Government Printing Office, Washinton, DC 1971.
7. Vadovic, C. J. Prepr. Am. Chem. Soc. Div. Fuel. Chem. 1983, 28(3), 148.
8. Union Carbide Corporation, Carbon Products Division, New York, New York.
9. Stull, D. R.; Westrum; E. F., Jr.; Sinke, G. C., The Chemical Thermodynamics of Organic Compounds, Wiley: New York, 1969.
10. We thank James E. Hardy of this laboratory for this valuable suggestion.
11. Analabs, Inc., 80 Republic Dr., North Haven, Connecticut 06473.
12. Galbraith Laboratories, Inc., P. O. Box 4187, Knoxville, TN 37921.
13. Burnham, A. K.; Stubblefield, C. T.; Campbell, J. H. Fuel 1980, 59, 871.
14. Burnham, A. K.; Crawford, P. C.; Carley, J. F. Ind. Eng. Chem. Process Des. Dev. 1982, 21, 485.
15. Carley, J. F., Lawrence Livermore National Laboratory, private communication, to be published.

Table 1

Analyses of Green River Shale Samples Retorted by TGA to 500°C (Galbraith Laboratories (12))

Sample	C (total)	% of dried spent shale H	N	S	Ca	Mg	ash	carbonate C	SO_3 (% on ash)
2.2S	8.74	0.27	0.29	0.81	16.60	3.96	74.75	6.64	2.80
2.2F	9.48	0.28	0.33	0.70	17.74	4.03	74.27	6.53	2.89
2.0F	9.54	0.32	0.42	0.98	14.97	4.06	75.73	5.76	3.20
1.9F	10.24	0.45	0.65	1.36	10.89	3.96	78.03	4.52	4.89
1.8F	11.19	0.56	0.71	1.60	9.63	3.71	77.36	4.13	5.74
1.7F	12.16	0.59	0.80	2.06	8.60	3.36	78.13	3.76	7.04
1.6F	12.10	0.61	0.79	2.34	8.62	2.66	78.82	3.19	6.57

Table 2

Experimental values, derived from the present work, for the heat of combustion of spent Green River oil shale at 705°C, and comparison to values derived from bomb calorimetry (14); see text.

sample	organic C (% spent shale)	$-\Delta H_c$ (kJ/g of spent shale) this work[a]	Reference 14 w/o silicates	Reference 14 w silicates
2.2S	1.96	0.34 ± 0.05	0.22	0.59
2.2F	2.56	0.79 ± 0.14	0.36	0.75
2.0F	3.42	1.15 ± 0.06	0.93	1.26
1.9F	5.37	2.26 ± 0.06	2.01	2.26
1.8F	6.77	2.57 ± 0.11	2.71	2.92
1.7F	8.16	3.37 ± 0.07	3.51	3.69
1.6F	8.56	3.77 ± 0.06	3.86	4.00

[a]Values given for each sample represent the average peak-area enthalpy from the oxygen drops minus that from the nitrogen drops and then adjusted to include carbonate decomposition, according to Equation 5 in the text.

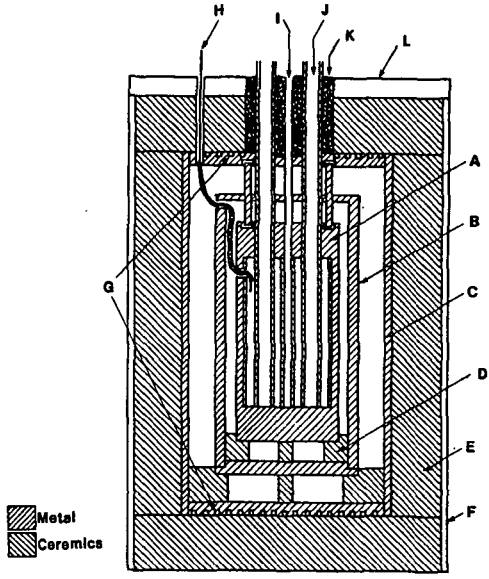

Figure 1

Assembly diagram of the high-temperature calorimeter (overall dimensions: h=80 cm; d = 65 cm). A: Inconel block; B: temperature homogenizing shield; C: furnace shell; D: ceramic support blocks; E: cast refractory insulation; F: side water jacket; G: grooves for top and bottom heater wires; H: typical thermopile lead wire; I: central well for precision thermocouple; J: ceramic tube sample chamber; K: ceramic wool; L: top water jacket.

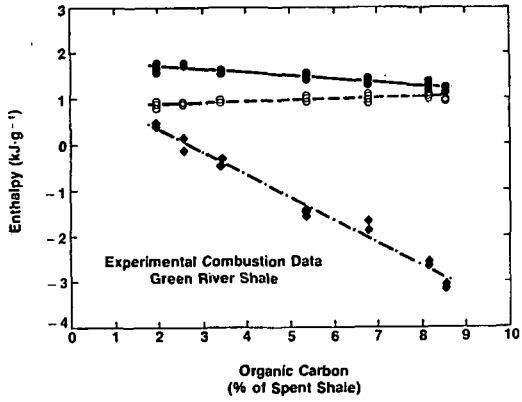

Figure 2

Experimental enthalpy values determined from drops of spent Green River shale into nitrogen or oxygen at 705°C, vs. the percent organic carbon on spent shale.

o, — — — nitrogen peak height
●, ——— nitrogen peak area
◆, — • — oxygen peak area

A NEW MODEL OF KEROGEN STRUCTURE

By

C.J.R. FOOKES and D.A. JOHNSON

CSIRO Division of Energy Chemistry, Lucas Heights Research Laboratories,
Private Mail Bag 7, Sutherland, NSW 2232, Australia.

INTRODUCTION

By far the most prominent components of a typical shale oil are n-alkanes and n-alkenes, which form a homologous series extending to C_{30} or beyond. Since it is now clear that these molecules are readily converted into aromatics and branched aliphatics under retorting conditions(1), it is likely that n-alkanes and n-alkenes are the major primary products of kerogen pyrolysis. Knowledge of how they are generated is thus of crucial importance to oil shale chemistry, particularly with respect to the nature of kerogen.

Although the literature abounds with proposals for the structure of kerogen, most are based on the results of oxidative degradations(2). Although these experiments provide useful information about individual structural fragments, very little can be learned about the way in which they are linked, since virtually all functional groups are converted into carboxylic acids. Nevertheless, it is generally accepted that kerogen is composed of both aliphatic and aromatic structures, with the most convincing evidence for the latter coming from solid-state ^{13}C nuclear magnetic resonance (NMR) and infrared studies of intact kerogens and shales.

We have made the assumption that the aromatic and aliphatic moieties are associated, and that kerogen consists mainly of n-alkyl chains attached to a largely involatile aromatic (or more likely heteroaromatic) nucleus. On pyrolysis, the aliphatic side chains are cleaved to form oil, whereas most of the hydrogen-deficient nucleus forms coke. To test this hypothesis, we have pyrolysed a range of appropriate model compounds, 1 - 5, and compared the products and kinetics of their decomposition with data obtained from oil shales.

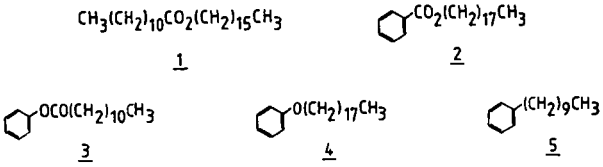

EXPERIMENTAL

Pyrolyses were carried out in a quartz flow tube enclosed in the oven of a gas chromatograph. The compounds were transferred in a stream of helium from an evaporation chamber held at a temperature (usually around 200°C) sufficient to give a partial pressure of reactant of approximately 150 Pa. The products were collected in U-tubes immersed in liquid nitrogen and analysed by ^{1}H NMR using a JEOL GX400 spectrometer. For each compound, the residence time was constant but the reactor temperature was varied to give between 5 and 50% decomposition.

Activation energies were then calculated from a plot of log x v. 1/T, where x is the fraction decomposed at temperature T (in K). Rate constants (k) were calculated from the formula $kt = \ell n(1-x)$. Solid state ^{13}C spectroscopy was performed on a Bruker CXP300 instrument, using the Dixon total side-band suppression sequence(3).

RESULTS AND DISCUSSION

Support for the presence of n-alkyl chains is gained from the high field solid-state ^{13}C NMR spectrum of a Condor carbonaceous kerogen (Figure 1, upper trace). The lower trace is the solution spectrum of a carbonaceous shale oil for comparison. Particularly noteworthy is the correspondence of signals A and D between the two spectra, which shows that long n-alkyl chains, free at one (or each) end, are present in the kerogen.

Information about the site of attachment of these chains was provided by ^{13}C NMR examination of the alkene fraction isolated from a Condor oil. Although the occurrence of 1-enes in shale oils is well documented, there is very little information on the distribution of other double-bond isomers. Figure 2 shows that high field ^{13}C NMR is an excellent method for determining this distribution, at least for the first five or six carbons along the chain, giving cis/trans ratios as well.

The quantitative data from this spectrum were best interpreted as indicating that 1-enes are in fact the initially-formed olefins and that the double bond then migrates along the chain.* Thus the terminal carbon is the likely site of their original linkage to the kerogen. This is consistent with the widespread occurrence in the biosphere of long-chain fatty acids and, to a lesser extent, primary alcohols and their isolation from the hydrolysis of kerogens(4). We have therefore based the following models on these two classes of compounds and used the benzene ring as the simplest aromatic nucleus.

Hexadecyl dodecanoate - 1. This wax ester pyrolysed readily between 430 and 460°C to give almost exclusively 1-hexadecene and dodecanoic acid. Significantly, very little n-undecane was formed. The reaction was shown to be first order by varying the partial pressure of substrate between 40 and 600 Pa; except at the lowest concentration, no significant change in the fractional decomposition at 450°C was observed. The calculated activation energy and rate constant at 450°C are given in Table 1, together with the corresponding parameters for the evolution of hydrocarbons by pyrolysis of several oil shales. As can be seen, neither the kinetics nor the products of this reaction correspond well with those from oil shales.

Octadecyl benzoate - 2. This ester decomposed even more readily than the previous compound, giving 1-octadecene and benzoic acid as almost the only products. However, a small amount of benzene was also formed, presumably from decarboxylation of the benzoic acid. Thus, this compound cannot be considered a good kerogen model.

Phenyl dodecanoate - 3. Phenolic esters of fatty acids have been implicated in the structure of humic substances(9) such as those derived from lignins. It was therefore interesting to discover that although phenyl dodecanoate pyrolysed rather slowly, the activation energy for its decomposition is similar to that

---

* dehydrogenation of alkanes is an additional pathway(1), leading to a significant proportion of olefins with a random distribution of double-bond positions.

for Nagoorin carbonaceous shale, which contains large quantities of lignitic materials. Furthermore, the major products derived from the side chain were n-undecane and 1-decene (Figure 3). Pyrolysis of phenolic esters of a natural series of carboxylic acids, where even numbered chains predominate, should therefore generate n-alkanes with odd over even preference and 1-enes with a less pronounced even over odd preference. This is often observed in shale oils.

Phenyl octadecyl ether - 4. The decomposition kinetics of this compound were complicated. Above about 460°C, the reaction appeared to have an activation energy of less than 200 kJ mol^{-1}, whereas at lower temperatures the value was more than 500 kJ mol^{-1}. This probably indicates that the initial bond-cleavage is not the rate-determining step below 460°C, but it may be above this temperature. The products were even more complex; their chromatogram is shown in Figure 4.

Note the homologous series of n-alkanes dominated by heptadecane, and the more abundant series of 1-enes, with 1-octadecene the major compound. Phenol and, unexpectedly, benzaldehyde are the major aromatic products, although styrene and various alkylbenzenes including n-heptadecylbenzene were also identified. In addition, products arising from the random scission of the side chain of 4 are present in significant amounts.

Although the products and rate of decomposition of this compound correspond well to those of oil shales, the complicated activation energy precludes a decision about its validity as a kerogen model.

Decylbenzene - 5. This compound, which represents the simplest linkage of an alkyl chain to an aromatic ring, pyrolysed extremely slowly, although its activation energy was virtually identical to those reported for the decomposition of typical oil shales. The major products were styrene, toluene, ethylbenzene and 1-nonene; only very small amounts of n-alkanes were detected. As with the previous compound, there was also cleavage of carbon-carbon bonds along the side chain.

CONCLUSIONS

Of the five compounds pyrolysed in this study, only phenyl dodecanoate can be considered as a good model of kerogen structure, but only for the carbonaceous shales. None of the other compounds, with the possible exception of phenyl octadecyl ether, adequately mimicked either the high or low activation energy processes of oil shale pyrolyses.

The nature of the higher activation energy process is rather intriguing. The fact that roughly equal quantities of n-alkanes and alkenes are generated by the rapid pyrolysis of shales and kerogens suggests that the two classes of compounds have a common origin; indeed kinetic data(7,8) indicate that a single rate-determining process is involved in the formation of the bulk of the oil. We believe that this process involves the generation of primary n-alkyl radicals which would then disproportionate to give equal quantities of n-alkanes and 1-alkenes. Certainly, other have provided evidence for the involvement of radicals in kerogen pyrolysis(10). However, the reaction which produces these radicals has yet to be elucidated.

ACKNOWLEDGEMENTS

We thank Ms C. Walters and J. Wymer for syntheses of model compounds and NMR measurements, Mr. I. Liepa and Dr. A. Chaffee for GC/MS data, Mr. J. Levy

for the use of a least-squares analysis program, and Dr. J.K. Saunders (University of New South Wales) for assistance in determining the solid-state NMR spectrum. We are also grateful to Dr. A. Ekstrom for helpful discussions and permission to quote unpublished data.

LITERATURE CITED

1. Regtop, R., Ellis, J., Crisp, P.T., Ekstrom, A. and Fookes, C.J.R., Proceedings of the Second Australian Workshop on Oil Shale, Brisbane, December 1984, p. 170.

2. For a review, see D. Vitoric in 'Kerogen', Ed. B. Durand, Editions Technip, Paris, 1980, p. 301.

3. Dixon, W.T., Schaefer, J., Sefcik, M.D., Stejskal, E.O. and McKay, R.A., J. Magn. Resonance, 49, 341 (1982).

4. Regtop, R.A., PhD. Thesis, University of Wollongong, NSW, Australia (1983).

5. Campbell, J.H., Koskinas, G.J. and Stout, N.P., UCRL-50289 (1976).

6. Calculated, assuming first-order kinetics, from the data of Charlesworth, J.M., Proceedings of the First Australian Workshop on Oil Shale, Lucas Heights, May 1983, p. 127.

7. Ekstrom, A., Hurst, H.J. and Randall, C.H. ibid., p. 123.

8. Ekstrom, A., unpublished results.

9. Schnitzer, M. and Negroud, J.A. Fuel, 54, 17, 1975.

10. Solly, R.K., Charlesworth, J.M., Beranek, L.A., Kelso, A.G. Moritz, A.G. and Power, A.J., Proceedings of the First Australian Workshop on Oil Shale, Lucas Heights, May 1983, p. 113.

TABLE 1
ACTIVATION ENERGIES AND RATE CONSTANTS AT 450°C FOR THE DECOMPOSITION OF MODEL COMPOUNDS AND GENERATION OF OIL FROM SHALES

Substance	Activation Energy kJ mol^{-1} ($\pm$ 1 σ)	Rate Constant (450°C) s^{-1}
Hexadecyl dodecanoate	172 ± 2	1.78×10^{-2}
Octadecyl benzoate	163 ± 2	2.21×10^{-2}
Phenyl dodecanoate	147 ± 7	1.60×10^{-3}
Phenyl octadecyl ether	see text	4.26×10^{-3}
Decylbenzene	222 ± 5	4.45×10^{-5}
Green River shale (5)	219	3.95×10^{-3}
Rundle shale		5.8×10^{-3} (6)
Rundle kerogen		7.7×10^{-3} (6)
Condor shale (7)	232	1.73×10^{-3}
Nagoorin carbonaceous shale (8)	152	5.22×10^{-3}

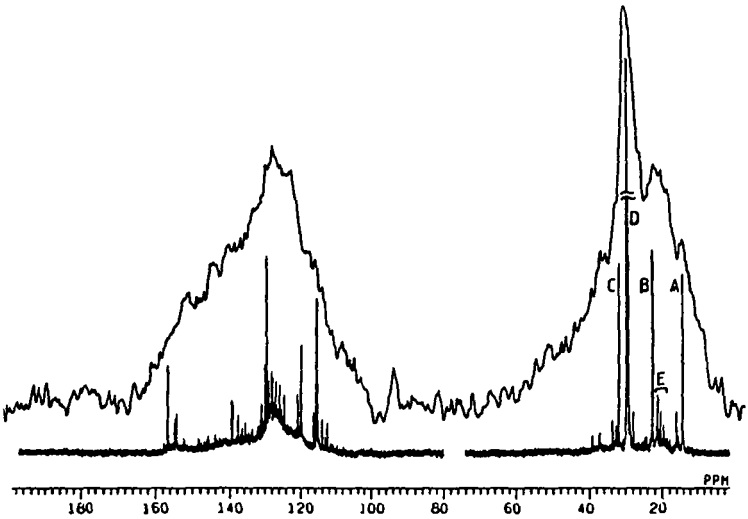

FIGURE 1: (Upper trace) 75 MHz CPMAS ^{13}C NMR spectrum of a Condor carbonaceous kerogen. (Lower trace) solution ^{13}C spectrum of a carbonaceous shale oil showing signals due to A, terminal methyls (C-1); B, C-2; C, C-3; and D, C-4+ of n-alkyl chains, and E, aromatic methyls. Most of the sharp lines in the aromatic region (110-160 ppm) are from phenols.

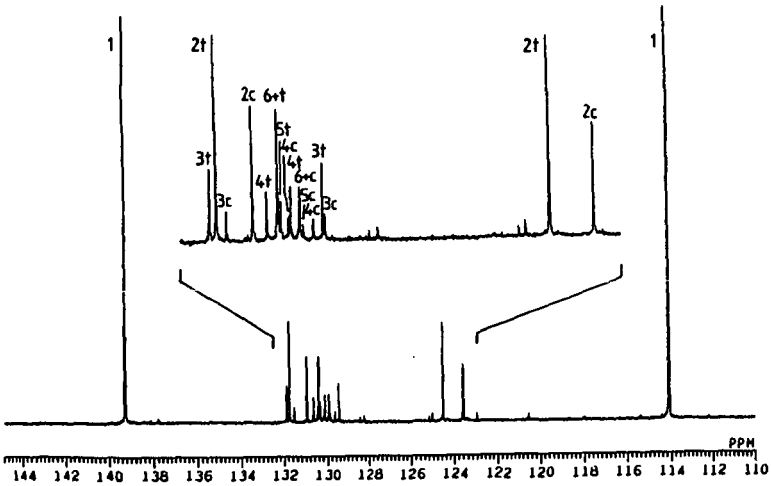

FIGURE 2: Olefinic region of 100 MHz ^{13}C NMR spectrum of the alkene fraction from Condor shale oil. The label 2t (for example) refers to signals from straight chain trans-2-enes.

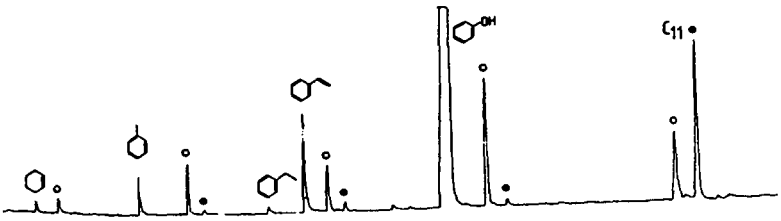

FIGURE 3: Reconstructed ion chromatogram of products from the decomposition of phenyl dodecanoate: ● = n-alkanes, o = 1-alkenes.

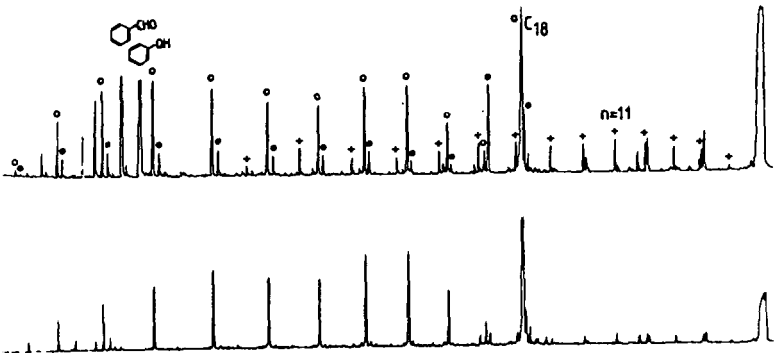

FIGURE 4: Reconstructed ion chromatogram of products from the decomposition of phenyl octadecyl ether; + = $C_6H_5O(CH_2)_nCH{=}CH_2$.

INORGANIC NITROGEN IN GREEN RIVER FORMATION OIL SHALE*

R. W. Taylor
A. K. Burnham
G. S. Smith
R. H. Sanborn
L. S. Gregory

Lawrence Livermore National Laboratory
Livermore, California, 94550

ABSTRACT

Inorganic (mineral) N has been found in both raw and retorted Green River Formation oil shale. Buddingtonite, an ammonium-bearing feldspar, has been identified in some shales by X-ray diffraction, and ammonium ion (NH_4^+) has been found in the same and other shales by infrared adsorption. Measurement of total N content of low-temperature ashed oil shale by a combustion technique is proposed as a method of measuring inorganic-N content. The method is based on the observation that the N content of buddingtonite is not reduced by low temperature ashing. Use of this technique demonstrates that inorganic N content is variable and is the major source of nitrogen in some oil shale samples. The fate of both organic and inorganic N during pyrolysis is also discussed.

INTRODUCTION

Within the United States are large and rich deposits of oil shale. Formost of these is the oil shale of the Green River Formation of Colorado and Utah. This shale contains approximately 0.5 wt% N, but the concentration is variable, ranging from 0.2% to as much as 1%. Pyrolysis of oil shale produces ammonia which needs to be removed from the retort water before recycling or disposal (1). N in shale oil must be reduced to produce stable, non-polluting transportation fuels, and removal of N requires special catalysts and consumes H increasing the cost of refining (2). Nitric oxide (NO) is produced when retorted shale is burned as a fuel (3,4).

The ratio of N to organic C both in samples of Green River oil shale and in kerogen isolated from the same samples has been measured but only a slightly higher ratio in whole shale than in kerogen, was found suggesting that most of the N (90%) is organic (5,6). This is qualitatively consistent with the observation by most workers that N content of oil shale increases with an increase in grade or organic C content (6-9). However, correlation of organic C with N does not prove that N is organic; N may have originated in organic debris, but has been transferred to the inorganic matrix during diagenesis. Finally, some of the published data on N content as a function or organic C content show a non-zero intercept (7-9), suggesting shale contains some N even in the absence of organic C.

Recently, Cooper and Evans (10) utilized HF-HCl digestion in the determination of inorganic N and concluded, in conflict with prevailing opinions, that most N in both raw and retorted shale was inorganic in form. Later, Nadkarni (11) showed that the measured "total" N content for some shales depended on the technique used. For a sample of Colorado shale, the Kjeldahl method measured a N concentration of 0.45±0.05% while combustion (Dumas) methods gave a value of 0.74±0.16%. These two papers cast doubt about the data on which the previous conclusions have been based.

Most of the N in the Condor oil shale deposit of Australia is inorganic. It is found as an ammonium silicate of the feldspar family called buddingtonite, and the concentration of this mineral in the Condor shale is approximately 10 wt% (12).

The purpose of this report is to put proper perspective on the occurrence and abundance of inorganic N in Green River oil shale.

EXPERIMENTAL SECTION

All samples used in this investigation were ground to a talc-like consistency in a rotating concentric disk and ring (Bleuler) mill before analysis. Past experience indicates that essentially all material prepared by this procedure passes a 325 mesh sieve and most was >10μ in diameter. Some samples were treated with 1 M HCl overnight to remove carbonate minerals.

Some samples were low-temperature ashed in an oxygen plasma (LEF Corp. LTA-504) to remove organic matter. The oxygen pressure was maintained a 1 torr, and the total power in each of the four chambers was 250 watts.

Carbon, H and N content were measured at LLNL by either a Perkin-Elmer Model 240 or Leco model CHN-600 elemental analyzer. The samples size for the Perkin-Elmer instrument was 2-4 mg, and the sample size for the Leco instrument was 100 mg. To ensure good precision 3 to 4 replicates were measured for each reported value. Organic C was determined by the difference between total C and that evolved by 1 M HCl and collected on ascarite. Although the reproducibility among determinations of N concentration of a given sample at a given time was generally ±0.02 wt% N, the agreement among groups of N analyses for the same shale over a period of several years was not as good. The reasons for this are not clear. Because of this problem some samples were sent to J&A Associates, Golden, Colorado, for measurement of total N by means of an Antek Chemiluminescence Analyzer Model 707.

A Digilab Model FTS-20c infrared spectrometer was used to measure the infrared spectrum in the transmission mode. Each sample was diluted to approximately 2% in KBr and pressed into a pellet.

A Phillips Diffractometer was used to determine the x-ray powder patterns. Early patterns were recorded on strip-chart recorders, but recent patterns were recorded and processed by computer.

A sample of buddingtonite, identified as California 117751-6, was acquired from the Smithsonian Institution (13). The N content was measured at 1.69% at LLNL and 2.78% at J&A Associates.

A description of the oil shale samples used is given in Table 1. Most of them have been used in other investigations at LLNL or other laboratories. The chemical analyses are values averaged from at least 3 samples from the same batch of shale determined at different times.

RESULTS

Identification of buddingtonite in oil shale by x-ray diffraction

Buddingtonite was first discovered in oil shale (sample L-1 9A/5) by G. Smith at LLNL in 1976 as part of a routine x-ray analysis of raw shale to be used in the L-1 retorting experiment (15). Buddingtonite was also identified in raw and retorted shale (sample RI 8008-76) in an unpublished 1978 investigation on the analysis of dawsonite in oil shale.

Table 2 compares d-spacings for 10 strongest x-ray diffraction peaks of buddingtonite, based on the ASTM standard #17-517, to those from our measurements of the Smithsonian Institution (SI) sample of buddingtonite. Peaks apparently due to buddingtonite in two Colorado oil shale samples and one sample of buddingtonite

Table 1
Green River Oil Shale Samples

#	I.D.	Location	Oil Yield (gpt)	Chemical Composition, Wt%						%Inorg. N[a]
				C	acid CO_2	org. C	H	S	N	
1	Ca37	Tract Ca	34.3	21.90	15.98	17.5	2.38	--	0.61	21
2	Ca25	Tract Ca	24.8	16.57	19.67	11.2	1.68	1.1	0.54	43
3	AP60	Anvil Points	61.0	30.38	12.32	27.0	3.55	0.84	0.95	22
4	AP31	Anvil Points	30.6	19.63	20.55	14.0	1.84	--	0.43	10
5	AP24	Anvil Points	22.4	15.60	17.48	10.8	1.62	0.63	0.41	27
6	AP8	Anvil Points	8.1	9.95	21.44	4.1	0.57	0.23	0.12	13
7	RI8008-76	Co.Core #3[b]	22.0	12.56	12.32	9.2	1.71	1.35	1.16	78
8	USNOSR-638	Naval Reserve-1	1.9	4.65	11.40	1.5	0.46	0.87	0.54	92
9	L-1(9A/5)	Anvil Points	25.0	15.64	17.12	11.0	1.56	0.69	0.47	35
10	GK5	Geokinetics,Ut.	4.7	6.53	15.20	2.4	0.51	--	0.20	67
11	HD25	Horse Draw, Co.[c]	25.0	19.20	29.50	11.1	2.02	0.60	0.45	32

a) Fraction of inorg. N = $\frac{\%N-0.0276(Org.C)}{\%N}$ (see discussion)

b) Northern Piceance Creek Basin at ∿ 230m, dawsonite rich.

c) Multi Mineral Corp., 649m, nahcolite rich.

Table 2
Identification of the 10 strongest diffraction lines of buddingtonite in standards and oil shale samples.

I/Io	hkl	d(Å)				
		ASTM 17-517	SI	RI8008 No76	USNOSR 638'	CONDOR[a]
100	130	3.81	3.82	3.71	3.79	3.82
95	010	6.52	6.52	6.52	6.52	6.52
70	220	3.38	3.35[b]	3.35[b]	3.34[b]	3.386
70	202	3.25	3.24	3.24	3.23	3.2226
65	101	4.33	4.50[b]	4.50[b]	4.48[b]	4.33
60	040	3.26	3.24	3.24	3.29	3.260
40	140	3.01	3.02	3.02	3.00	3.013
35	011	5.91	5.92	5.92	5.90	5.92
35	211	3.98	3.98	3.95	3.96	3.98
35	002	3.31	3.35[b]	3.35[b]	3.34[b]	3.320

[a] Ref. (12).

[b] Spacings probably influenced by contributions from strong quartz peaks at d=3.47 and 4.25Å.

separated from Australian (Condor) shale are also compared in Table 2. The SI sample contains a large percentage of quartz, and the Green River Oil Shale samples contain large fraction of quartz, dolomite, and some dawsonite.

Our first evidence that buddingtonite is thermally stable came from its identification sample RI 8008-76 that had been heated to about 500°C in a covered crucible for one hour. Little of the carbon residue had been oxidized, so that this treatment roughly approximated Fischer Assay heating. Figure 1 compares the diffraction patterns of the raw and heated oil shale. The buddingtonite peaks are the same. In contrast, the dawsonite peaks are missing, confirming that the sample was heated above 350°C. We have also found that buddingtonite releases nitric oxide (NO) during oxidation after being heated to 500°C in an inert gas (4). The amount of NO was not effected by duration of preheating within the range 3 to 10 min. which indicates that the rate of ammonium release at 500°C is slow. These observations are consistent with (12) who found the x-ray diffraction patterns of buddingtonite does not change below 500°C. They found, in addition, that ammonium is lost by heating to 650°C, that remnants of the feldspar structure remains even upon heating to 750°C and that buddingtonite was not reformed by heating in a NH_4OH solution at 180°C.

Ammonium ion identification in oil shale by infrared spectroscopy

Buddingtonite has a characteristic band at 1430 cm^{-1} which distinguishes it from other silicates. The IR spectrum of our SI reference sample of Buddingtonite (13) is shown in Figure 2. The large adsorption in the 900-1300 cm^{-1} region is characteristic of the Si-O stretch. Bands in the 600-800 cm^{-1} region can be due to hydrocarbons as well as silicates. The ammonium ion has another adsorption band in the 3000-3500 cm^{-1} region, but it is strongly overlapped by water bands, making it less characteristic.

In Green River oil shale, the 1430 cm^{-1} band is overlapped by CH bending modes and also from a bending mode in the carbonate ion. Thus, to identify the ammonium ion definitively, it is necessary to remove organic material and carbonate minerals. Figure 3 shows an IR spectrum of sample AP24 that has had carbonate minerals removed by acid leaching. One would not ordinarily suspect the presence of ammonium ion because of the CH bending mode at 1350 to 1410 cm^{-1}. However, when organic material is removed by low-temperature ashing (using procedures described in detail in the next section), the ammonium-ion band emerges clearly, although not to the same relative intensity as in the spectrum of the SI buddingtonite or in the spectrum of buddingtonite reported by Loughnan and Roberts (12).

Figure 4 shows IR spectra of samples AP8 and AP60 after HCl leaching and low-temperature ashing. Sample AP8 shows little adsorption and sample AP60 shows none, which agrees with data on nitrogen content discussed in the next section.

Isolation of inorganic N by low-temperature ashing

The occurrence of inorganic N in Green River oil shale is clear based on x-ray and infrared evidence presented thus far, but a quantitative method of analysis for inorganic N is needed. While both x-ray diffraction and infrared spectroscopy have been used for quantitative mineral analysis, all of the inorganic forms of N have not necessarily been identified. In this section, a low-temperature ashing technique is developed for determination of inorganic N.

The most important variables in low-temperature ashing of oil shale are time, particle size, sample-stirring frequency and plasma activity. We have found that using 1 torr of O_2 and a power of 250 watts removed oil shale organic matter.

The role of particle size on the effectiveness of low-temperature ashing is shown in Figure 5. Both samples came to constant weight within 35 hours of ashing. The weight loss of the finer sample was 13.2%, which is about equal to the weight loss upon Fischer assay (12.84%) but the coarser sample lost only 9.3%. The time necessary to come to constant weight was cut in half if carbonates were removed with HCl before ashing.

The relative loss of organic C, H, and N during low-temperature ashing of Anvil Points shale, sample L-1 (9A/5), is shown in Figure 6. It is unlikely that organic C could be oxidized without also oxidizing organic H and N, so residual content of H and N is probably due to mineral forms.

Since buddingtonite is the only specific N-bearing mineral that has been identified in oil shale, we used it to test whether or not low-temperature ashing affects mineral N content. Table 3 gives total N content for a fine-ground sample of SI buddingtonite before and after being ashed for 35 hours (sample #12). The measured value of N content depended on the type of analysis being used, but the fraction of N remaining was over 90% by either analytical technique. This agrees with the qualitative observation in the previous section that ammonium-ion, as detected in the infrared spectrum, is not affected by ashing.

Table 3 also lists N content for a variety of raw and retorted oil shales before and after low-temperature ashing. The retorted samples were prepared by a modified Fischer Assay technique (16). The fraction of N removed by ashing ranges from nearly none to all. As discussed in more detail in the next section, this implies that the relative organic and inorganic N contents of Colorado oil shale are highly variable. Acid leaching of raw or retorted shale does not seem to make a systematic change in the fraction of N remaining after ashing, and the variation is probably a reflection of uncertainty in N concentration measurements.

DISCUSSION

One would think that a determination of the relative amounts of organic and inorganic N could be made by comparing N in whole shale to that in organic concentrates. Three workers have reported composition of raw shale and also the composition of the organic concentrates from the same shales from which the fractional recovery of N can be calculated (5-7). This is summarized in Table 4 along with a shale sample analyzed at LLNL. Approximately all of the N in raw shale is recovered in organic concentrate. This evidence has caused most workers to assume that the inorganic N content of oil shale is minor. In addition, elemental analysis of the organic material isolated from sample AP60 by Kirkman Bey and Campbell at LLNL indicated that all of the nitrogen in that sample is organic.

However, the results of (11) suggest that is not safe to use these results to conclude that there is little inorganic N in Green River oil shale. Using replicate results from several independent laboratories, (11) found that the Kjeldahl technique (digestion of the sample in hot concentrated sulfuric acid) gives systematically lower N values for Colorado oil shale than the Dumas (combustion) method. This is consistent with the need for HF digestion for the determination of fixed or "nonexchangeable" ammonium in soil and rock samples (17). If only organic N is detected by normal Kjeldahl analysis, it would be logical for most of it to be recovered in the organic concentrates even if greater quantities of inorganic N were present. Moreover, the rich oil shale used at LLNL is uniquely low in organic N.

A second way to estimate the relative abundance of inorganic N in either raw or retorted shale is to plot total N content verses organic C content. If the concentration of inorganic N is independent of organic C content and organic

Table 3
Wt%N in Raw, Retorted, and Low Temperature
Ashed Samples On a Raw Shale Basis

Sample #	Material	Wt% N			% of Raw Shale N Remaining After LTA (±10%)
		Raw	Retorted	LTA[a]	
1	Ca37	0.72	--	0.17	24
1	Ca37	0.72	0.35	0.15	21
2	Ca25	0.58	--	0.25[b]	43[c]
2	Ca25	0.47	--	0.31	66
2	Ca25	0.58	0.43	0.33[b]	57[c]
2	Ca25	0.47	0.49	0.20[b]	42
3	AP60	0.87	--	0.01[b]	1[c]
3	AP60	0.98	--	0.09[b]	9
3	AP60	0.87	0.28	0.02[b]	2[b]
3	AP60	0.98	0.45	0.06[b]	6
4	AP31	0.47	--	0.11	23
4	AP31	0.47	0.27	0.11	23
5	AP24	0.39	--	0.14	36
6	AP8	0.09	--	0.02	22
7	RI8008-76	1.13	--	0.72[b]	64
8	USNOSR-638	0.55	--	0.56[b]	102[c]
8	USNOSR-638	0.49	--	0.43[b]	88
9	L-19A/5	0.47	--	0.28[b]	59
10	GK5	0.32	--	0.28	56
10	GK5	0.32	0.22	0.19[b]	59
11	HD25	0.52	--	0.21	56
11	HD25	0.52	0.26	0.25	48
12	Buddingtonite	1.69	--	1.80[b]	107
12	Buddingtonite	2.78	--	2.58[b]	93[c]

(a) LTA of retorted shale if preceeded in table by retorted shale data, otherwise the LTA was done on raw shale.
(b) Acid leached (HCℓ) to accelerate ashing
(c) Chemical Analysis by J and A Associates, Inc. Golden, CO

Table 4
Comparison of N/org.C mole ratios for raw shale and organic concentrates from the same shales

N/Org.C Mole Ratio		Recovered	Reference
Raw Shale	Org. Concentrate	%N	
0.029 (a)	0.032	110%	(7)
0.027 (b)	0.025	93%	(6)
0.033 (c)	0.029	88%	(5)
0.029 (d)	0.016	89%	(5)
0.032 (e)	0.033	103%	LLNL

(a) Average of 9 samples, mineable beds, mahogany ledge (Anvil Points).
(b) Ten samples from the mahogany zone, 25 gpt.
(c) One sample, mahogany zone.
(d) One sample "papery" shale.
(e) One sample AP60, work done at LLNL.

Table 5
Nitrogen-organic carbon correlation

Data fit to expression: Wt%N=a+b(Wt% org. carbon)
Wt% N=total nitrogen content of sample
a=Wt% inorg. nitrogen
b=Wt ratio org. nitrogen/org. carbon

a	b	Samples	Sample Type and Location	Reference
			Raw Shale	
0.225	0.0275	260	2 core holes, USNOSR	(8)
0.096	0.0286	66	Colorado and Utah	(9)
-0.020	0.0320	40	1 core Utah, Geokinetics	LLNL Analyses
0.10	0.0249	6	1 sample split, Colony (Ca)	(18)
0.036	0.0307	9	Mineable beds, Anvil Points	(17)
0.252	0.015	6	Selected samples, Anvil Points	(7)
0.046	0.0318	58	Core KEP No 5, Kentucky	(18)
0.012	0.031	34	T16 Core, Kentucky	(19)
			Retorted Shale	
0.042	0.0665	66	Colorado and Utah	(9)
-0.009	0.069	9	"mineable" beds, AP	(7)
0.045	0.035	18	from NTU Retort[a]	(20)

[a] Some samples only partly retorted, some samples oxidized.

material has a constant N/C ratio, the slope of the plot gives the ratio of organic N to organic C, and the intercept gives the concentration of inorganic N. The observation that N content of oil is independent of grade (9) supports our assumption of constant kerogen composition. The results of linear regression analysis of several sets of data in the literature are given in Table 5, including data from two Kentucky oil shale cores, and some data for retorted shales.

A positive intercept is found for each set of samples except for those from the Geokinetics core from Utah which has a negative intercept of -0.020. The organic N to organic C wt ratio for Green River oil shales is 0.0276 which is a value calculated from the slopes in Table 4 weighted in proportion to the number of samples. The value of this ratio for retorted shale is 0.064.

A comparison of the fraction of inorganic N determined by the two methods for 11 shale samples is given in Fig. 7. Although a trend is clear considerable differences stand out for some samples.

The correlation coefficient for the linear regression analysis of N/org. C for the data of Giauque et al. (8) is 0.79. We feel that the observed random variation in N content (above a minimum value) for a given organic C content is due mostly to a variation in the inorganic N content.

With respect to the fates of organic and inorganic N during pyrolysis, we have shown that buddingtonite is relatively stable in the absence of air at temperatures up to 500°C and that inorganic N is not generally lost during retorting of shales, but the uncertainty is large due in part to the lack of accuracy in measuring N content in samples with low N concentrations.

CONCLUSIONS

On the average, approximately half of the N in the Green River Formation is inorganic, but the distribution is not uniform. Inorganic N in raw shale tends to remain in the shale after retorting. Buddingtonite, an ammonium feldspar, has been identified by means of x-ray diffraction in some oil shale samples. Ammonium ions have been identified in the same and other samples by means of infrared adsorption. Low-temperature ashing of oil shale by means of an oxygen plasma has been found to remove organic N, but not inorganic N in buddingtonite. Measurement of total N after low-temperature ashing is proposed as a way of determining inorganic N content. Due in part to the difficulty of measuring N concentration is samples with little N the method is qualitative. A second method for the estimation of the inorganic N content of shale is based on the assumption that the org. N/org.C ratio is constant. At present it is not clear if one estimate is better that the other.

In view of the present results, the stoichiometry of retorting must be revised. Organic material in raw shale and in the char in retorted shale contains less N than previously thought. The CH&N composition of organic material in raw shale should be represented by the formula $CH_{1.50}N_{0.024}$. The chemical composition of organic material in retorted shale should be represented by the formula $CH_{0.42}N_{0.06}$.

Acknowledgment

We thank J. S. White, Associate Curator-in-Charge, Division of Mineralogy, U.S. National Museum of Natural History, Smithsonian Institute, for providing us with a reference sample of buddingtonite. We also acknowledge the C-N correlations by D. Fujimoto and T. Coburn of LLNL.

References

(1) Gibbons, J. H., Director,"An Assessment of Oil Shale Technologies," Office of Technology Assessment, U.S. Congress, U.S. Government Printing Office, Washington, D.C. 20402, Stock No.052-003-00759-2, 1980.

(2) Wasilk, N. J. and E. T. Robinson, in Oil Shale, pp. 224-235 in Tar Sands, and Related Materials, H. C. Stauffer Ed., ACS Symposium Series 163, 1981.

(3) Lyon, R. K. and J. E. Hardy, Combustion and Flame, V. 51, pp. 105-107, 1983.

(4) Taylor, R. W., C. J. Morris and A. K. Burnham, Lawrence Livermore National Laboratory, Report UCRL-90155,1985, to be presented at the 18th Oil Shale Symposium.

(5) Forsman, J. P. and J. M. Hunt, Geochem. et Cosmochim. Acta, V. 15, pp. 170-182, 1958.

(6) Smith, J. W., U.S. Bureau of Mines, Report of Investigations 5725, 1961.

(7) Stanfield, K. E., I. C. Frost, W. S. McAuley and N. H. Smith, U.S. Bureau of Mines Rept. of Investigations, 4825, 1951.

(8) Giauque, R. D., J. P. Fox, and J. W. Smith, Lawrence Berkeley National Laboratory Report LBL-10809 UC-91, 1980.

(9) Singleton, M. F., G. J. Koskinas, A. K. Burnham, and J. H. Raley, Lawrence Livermore National Laboratory Report UCRL-53273, 1982.

(10) Copper, J. E. and W. S. Evans, Science, V. 219, pp. 492-493, 1983.

(11) Nadkarni, R. A., ACS, Symposium on Chemistry and Geochemistry of Oil Shales, Seattle, Wash., March 20-25, Preprints, V. 28, No. 3, pp. 200-208, 1983.

(12) Loughnan, F. C. and F. Ivor Roberts, Min. Mag. V. 47, pp. 327-334, 1983.

(13) White, J. S., Associate Curator-in-Charge, Division of Mineralogy, U.S. National Museum of Natural History, Smithsonian Institution, provided us with a sample of buddingtonite. The sample is identified as "California 117751-6. Received 1983.

(14) Young, N. B., J. W. Smith and W. A. Robb, Report of Investigations 8008, Laramie Energy Research Center, Laramie, Wyo., 1975.

(15) Sandholtz, W. A., Raley, J. H., Galloway, T. R., Rothman, A. J., Biermann, A. H., and G. S. Smith. Lawrence Livermore National Laboratory, Report UCID-19261, 1981.

(16) Stout, N. D., G. J. Koskinas and S. Santor, Lawrence Livermore National Laboratory, Report UCRL-52158, November 1976.

(17) Bremner, J. M., in Methods of Soil Analysis, Part 2, edited by C. A., Black, American Society of Agronomy, Inc., Publisher, Madison, Wisconsin, 1965.

(18) Vadovic, C. J., ACS, Symposium on Chemistry and Geochemistry of Oil Shale, Seattle, Wash., March 20-25, V. 28, No. 3, pp. 148-157 (1983).

(19) Robl, T. L., Project Coordinator, Resource Assessment of Oil-Bearing Shales in Lewis and Fleming Counties, Kentucky, V.II Supporting Data, IMMR 80/D-19/2b, 1980.

(19) Rubel, A. M., D. W. Koppenaal, D.N. Taulbee and T. L. Robl, 16th Oil Shale Symposium, Proceedings, p132, Colorado School of Mines Press, Golden Colorado, 1983.

(20) Baughman, G. L., Compiler, Synthetic Fuels, Data Handbook, Second Edition, p. 134, Cameron Engineers, Inc., 1315 South Clarkson Street, Denver, Colorado, 80210, 1978.

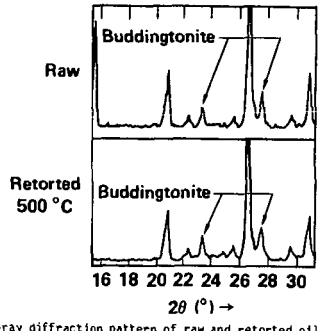

Figure 1. X-ray diffraction pattern of raw and retorted oil shale sample RI 8008-76 in which buddingtonite is found. Retorting does not eliminate the lines due to buddingtonite. The large peak on the left side of the raw-shale pattern is due to dawsonite. This mineral is decomposed during retorting.

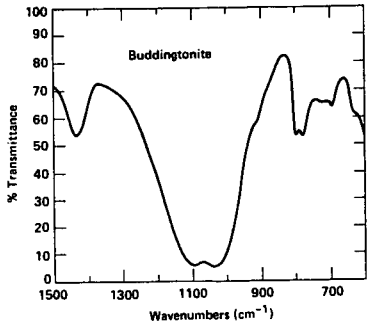

Figure 2. Infrared adsorption of buddingtonite showing the 1430 cm^{-1} peak due to ammonium ions. Sample from the Smithsonian Institute (SI), White (13).

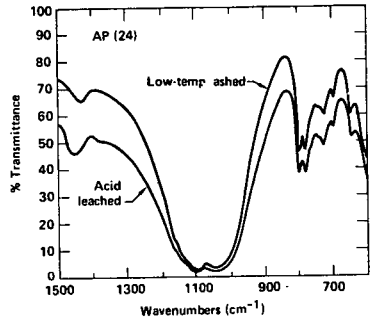

Figure 3. Change of infrared adsorption AP(24) shale. Lower curve acid leached shale and upper curve acid leached and low-temp ashed.

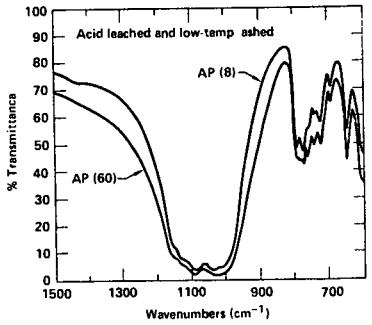

Figure 4. Infrared absorption of shales AP(60) and AP(8) which have been acid leached and low-temperature ashed. Shale AP(8) shows some ammonium-ion absorption and shale AP(60) does not.

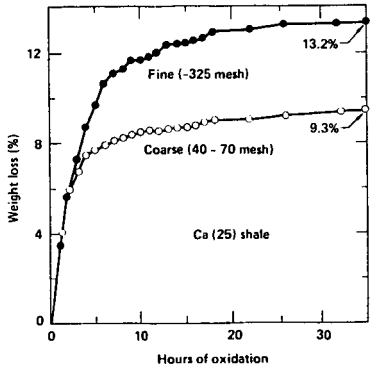

Figure 5. Weight loss during low-temperature ashing of raw shale Ca(25). The samples were stirred at the time of each data point.

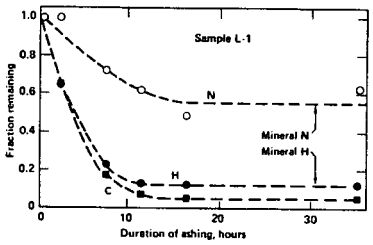

Figure 6. Fractional loss of N, H, and C during low-temperature ashing of sample L-1(9A/5). Residual N and H is due to the presence of these elements in minerals.

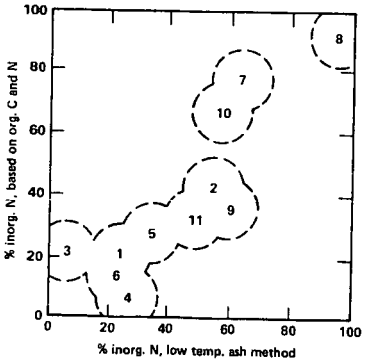

Figure 7. Comparison of inorg. N content of 11 shale samples as determined by two methods.

Naturally Occurring Arsenic Compounds in a Green River Oil Shale

James Jaganathan, Mysore S. Mohan and Ralph A. Zingaro

Department of Chemistry and the Coal and
Lignite Research Laboratory
Texas A&M University
College Station, Texas 77843 U.S.A.

The distribution of arsenic among the various components of a sample of Green River oil shale has been investigated. A number of arsenic species, some of which have not been previously reported, have been identified. The greatest fraction of arsenic, 65 percent of the total, was found to be present as skutterudite, (Co, Fe, Ni)As_3 and safflorite, (Fe, Co)As_2. About 16 percent was present in an HCl-soluble fraction, very probably in the form of arsenate. Almost nine percent was extracted by HF with the quartz and silicates. The bitumens and kerogens accounted for three and four percent of the total As, respectively, and this was found to exist in the form of methylarsenic and dimethylarsenic compounds. No evidence was found for the residence of arsenic in the pyrite.

Among the fossil fuels, oil shales are known to have the highest concentrations of arsenic, averaging 44 ppm. During recent years, and at the present time, there has existed a great deal of public concern about the contamination of the environment. Also, the refining of shale oils will utilize catalysts which are widely used in petroleum technology, viz., platinum and palladium. Arsenic is well-known to act as a poison toward such catalysts. Primarily for these two reasons information about the modes of occurrence of arsenic in oil shales is of importance.

Fish and co-workers (1) using a high performance liquid chromatograph coupled to a graphite furnace atomic absorption detector were able to confirm the presence of methylarsonic acid, benzenearsonic acid and arsenate in oil shale retort and process waters. Fish and Brinckman (2) studied the methanol extracts obtained from Green River oil shales. They reported the presence of the same three arsenic species in such extracts and the presence of other unidentified organoarsenic compounds. Jeong and Montagna (3) performed a gravitational separation followed by an isodynamic magnetic separation of pulverized Green River oil shale. Based on the enrichment of arsenic in fractions with higher magnetic susceptibility, they concluded that there exists an association between the arsenic content and iron-containing sulfide minerals such as $Fe_{1-x}S$ and $Fe(AsS)_2$.

In this report we describe the results of a systematic study of the distribution of arsenic among the various components which constitute a sample of Green River oil shale. Of the total arsenic, 97 percent was accounted for. The most significant result was the discovery of the presence of two arsenic minerals which account for two thirds of the total arsenic. These had not been previously found in oil shales.

EXPERIMENTAL

The oil shale sample used in this study was from the Hell's Hole Canyon of northeast Utah which forms part of the Uinta basin (Mahogany Zone). The sample, after it was disaggregated with a "Shatterbox" and screened through a U.S. standard -100 mesh sieve, had the following proximate analysis:

% moisture, 0.26±0.02; % volatiles, 41.89±0.14; % ash, 57.92±0.24; fixed carbon (by difference), 0.18±0.12.

Metal Analyses. Arsenic and iron in aqueous solutions were determined using a Perkin-Elmer Model 272 graphite furnace atomic absorption spectrometer. Nickel, at a concentration of 400 ppm was added as a matrix modifier in the arsenic analyses. Corroboration of the As and Fe values and the determinations of the other metal ion concentrations were performed with an ARL Model 34000, simultaneous, vacuum inductively coupled argon plasma emission spectrometer (ICPAES).

Ashing. A Branson/IPC, Model 4005-448 AN Automated Radio Frequency Plasma Asher was used to prepare the low temperature ash from the raw shale and the residue obtained following each acid demineralization step (Figure 1).

Arsenic Speciation. Arsenate, arsenite, methylarsonic and dimethylarsinic species were converted to the hydrides which separated and analyzed for separately. Details of the method are described elsewhere (4, 5). The technique, in addition to being very sensitive, makes possible a differentiation between inorganic As(III) (reduction by BH_4^- at pH 6.5) and inorganic As(V)(both As(III) and As(V) are reduced at pH 2). Methylarsenic and dimethylarsenic compounds are reduced to $MeAsH_2$ and Me_2AsH, resp. These are trapped at liquid nitrogen temperatures and easily separated by fractional distillation. Control experiments using $MeAs(O)(OH)_2$ and $Me_2As(O)OH$ showed that the conditions used for digestion of the kerogens and bitumens, viz., concentrated nitric acid at temperatures not exceeding 100°C for 2 h in a capped flask followed by the addition of 1 ml. of $HClO_4$ (70 percent) at the same temperature for 30 min., does not cause any rupture of H_3C-As or H_3C-As-CH_3 bonds. Known compounds were converted quantitatively to the arsines following this treatment.

X-Ray Diffraction and SEM-EDS Measurements. Diffractograms of the minerals in the low temperature ash samples, of the raw oil shale and of the residues remaining after successive demineralization treatments were obtained with the use of a Seifert-Scintag PAD II powder diffractometer automated by a DGC Nova 3 computer.

Scanning electron microscopy with energy-dispersive X-ray spectrometric measurements were carried out at the Electron Microscopy Center, Texas A&M University. The instrument used was a JEOL 35CF electron microscope equipped with energy-dispersive and wavelength dispersive spectrometric capabilities, digital beam control and dual wavelength capability.

RESULTS AND DISCUSSION

Figure 1 outlines a flow diagram which describes the chemical separation sequences used in this study. Powder X-ray diffraction studies revealed the presence of minerals typical of Green River oil shales with albite ($NaAlSi_3O_8$), dolomite ($CaCO_3 \cdot MgCO_3$) and quartz comprising the major mineral phases. Other minerals which were identified and found to be present in significant concentrations were pyrite (FeS_2), orthoclase ($KAlSi_3O_8$) and calcite.

Studies of the X-ray powder patterns at various stages of demineralization showed that treatment with 5M HCl was accompanied by the removal of dolomite and calcite. In the HCl-HF treated shale only pyrites appear to remain. The intensities of their characteristic spacings appear to be enhanced, probably due to the removal of other minerals. As expected, following treatment with HNO_3, the pyrite peaks disappear. The matter remaining at the end of the successive acid treatments was characterized by the absence of diffraction peaks. This is attributed to the amorphous and micro-crystalline nature of the material.

In Table 1 are listed the concentrations of arsenic and iron in various oil shale components separated according to the Scheme in Fig. 1. The results show that the bulk of the arsenic, ∿65 percent of the total, can be extracted by 2M nitric acid. Sixty percent of the iron is also extracted by this reagent.

Identification of Skutterudite and Safflorite. Fragments of the shale were fractured from a large 10 kg sample. Based on visual observation, the fragments collected represented both darker (presumably oil-rich) and lighter layers. The fragments collected were examined as follows: 1. The fragments were embedded in thermoplastic cement (Buehler Sci. Co., Cat. No. 40-8100); 2. the mounted samples were polished with alumina to a grit of 0.3μ. 3. in the case of some fragments originating from the more lightly colored layers of the shale sample, lustrous, silver grey mineral particles became visible. 4. the prepared samples were coated with 25Å thick layer of carbon and examined by SEM-EDS. 5. based on the x-ray microanalysis, large (1∿2 mm) mineral particles of interest were extracted from the SEM speciments after dissolving the cement with acetone; 6. x-ray powder diffractograms were obtained of these particles and, following their dissolution in HNO_3, metal ion concentrations were determined by ICPAES.

Figure 2 shows the electron micrograph of an arsenic-containing mineral particle and the energy-dispersive x-ray spectrum of the same particle. Several spot analyses on the silver-grey mineral grain indicated, based on a standardless semi-quantitative procedure (SSQ), the following uniform composition: %As, 76.7; %Fe, 8.90; %Co, 10.2, %Ni, 4.1. There was no evidence of the presence of sulfur in these particles. Evidence that these particles were composed of skutterudite and safflorite was obtained from measurements of the d-spacings in their x-ray powder diffractograms as is illustrated in Fig. 3. Further corroboration was obtained from the results of analytical measurements (ICPAES) of the metal ion content of these particles: %As, 71.4; %Fe, 10.4; %Co, 3.9; %Ni, 5.1; %Ca, 4.2. The composition of the arsenide minerals excluding calcium was as follows: %As, 74.6; %Fe, 10.8; %Co, 9.3; %Ni, 5.3 giving a stoichiometry of $Fe_{1.0}Co_{0.82}Ni_{0.46}As_{5.1}$.

Examination of about seventy pyrite particles, by SEM-EDS, with x-ray photons being accumulated, in some cases, for periods as long as 5000 seconds, showed no evidence of the presence of arsenic. These results indicated quite conclusively that in this oil shale sample the arsenic is present as skutterudite, $(Co,Fe,Ni)As_3$ and safflorite, $(Fe,Co)As_2$, but not with pyrite.

Methylated Arsenic Compounds in Bitumen and Kerogen. Samples of bitumen and kerogen were analyzed for total arsenic by digestion with con HNO_3 followed by con $HClO_4$ and taken to fuming. They were also analyzed by hydride reduction techniques following digestion methods which keep the H_3CAs and $(H_3C)_2As$ bonds in tact (see exptl. part). The results of these studies show very clearly that only a minor fraction of the total arsenic in these organic components is present in the form inorganic arsenic(V). This is possibly due to the distribution of small quantities inorganic arsenic minerals with these components. The bulk of the arsenic in both the bitumens and kerogens is present as H_3C-As and$(H_3C)_2As$ species. These results have not yet been quantitated.

CONCLUSION

The bulk of the arsenic in a sample of Green River oil shale, almost 65 percent of the total, is present as skutterudite and safflorite.

None was found to be associated with the pyrites. About 16 percent of the arsenic is extracted by HCl, and this may be in the form of arsenates. The HF-solubles, primarily quartz and silicates, have about nine percent of the total arsenic. The bitumens and kerogens accounted for three and four percent of the

total original arsenic and this was found to contain significant amounts of methyl and dimethylarsenic compounds.

ACKNOWLEDGEMENTS

We wish to thank the Center for Energy and Mineral Resources of Texas A&M University and the Robert A. Welch Foundation of Houston, Texas, for financial assistance in support of this work. Mr. James Ehrman, the Electron Microscopy Laboratory of Texas A&M University furnished invaluable advice and assistance in acquiring and interpreting the SEM-EDS data.

REFERENCES

1. Fish, R.G., Brinckman, F.E. and Jewett, K.L., Environ. Sci. Technol., 16, 174 (1982).

2. Fish, R.H., Brinckman, F.E., Preprints ACS Div. of Fuel Chem., 28, No.3, 177 (1983).

3. Jeong, K.M. and Montagna, J.C., Preprints ACS Div. of Fuel Chem., 29, No.3, 307 (1984).

4. Mohan, M.S., Zingaro, R.A., Micks, P. and Clark, P.J., Intern. J. Environ. Anal. Chem., 11, 175 (1982).

5. Clark, P.J., Zingaro, R.A. Irgolic, K.J. and McGinley, A.N., Intern. J. Environ. Anal. Chem., 7, 295 (1980).

Table 1. Distribution of Arsenic and Iron among Oil Shale Components*

Sample description	As μg/g oil shale		Iron g/100 g oil shale	
	GF-AAS	ICPAES	GF-AAS	ICPAES
Raw shale	72.3±0.68	68±1.2	2.23±0.02	2.24±0.01
HCl-soluble	13±0.1	10±0.1	0.49±0.003	0.47±0.004
HF-soluble	6.34±0.06	------	0.35±0.004	------
HNO_3-soluble	46±0.6	47±0.4	1.34±0.03	1.31±0.03
THF-soluble	1.88±0.11	2.12	------	------
R**	3.28±0.02	3.23±0.01	------	------

*Each value represents an average of the results of at least three experiments.
** R: HCl-HF-THF-HNO_3-treated oil shale.

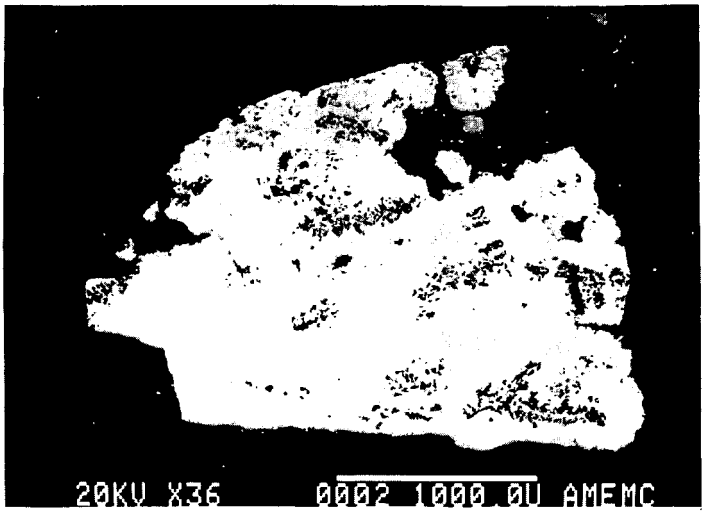

Fig. 2a. Electron micrograph of arsenic-rich mineral, magnification x36.

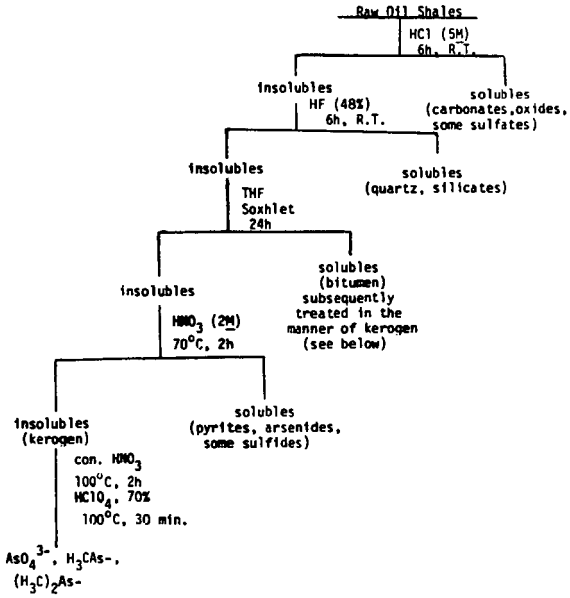

Fig. 1. Flow Diagram of the Sequence of Chemical Separation of Oil Shale Components.

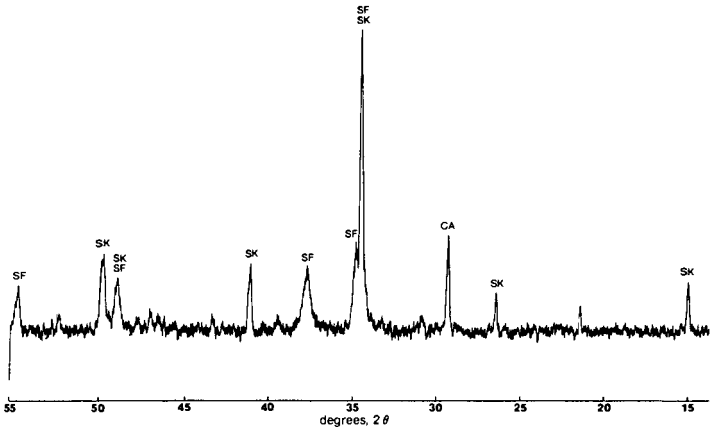

Fig. 3. Powder x-ray diffractogram of the particle in Fig. 2a. Key to symbols: SK, skutterudite; SA, Safflorite; CA, calcite.

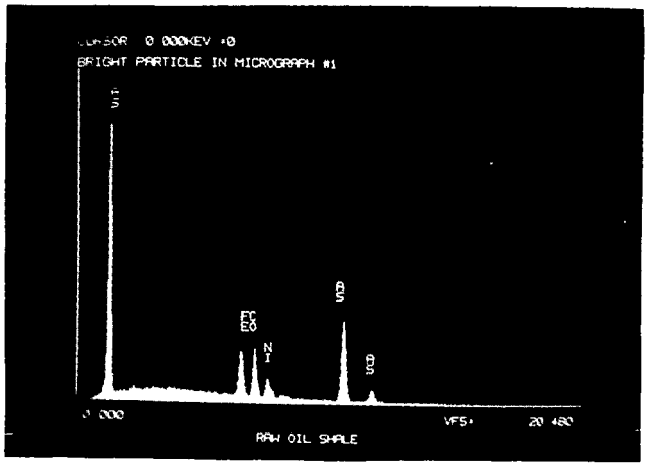

Fig. 2b. Energy-dispersive x-ray spectrum of the particle in Fig. 2a.

Effect of Acid-Clay Treatment on Nitrogen Compound Distribution in Fuels from Shale Oil

Steven A. Holmes and William E. Blanton

Western Research Institute
P. O. Box 3395, University Station
Laramie, Wyoming 82071

INTRODUCTION

The properties of fuels have been studied extensively in relation to the effects of processing on them and their effect on thermal and/or storage instability. Studies indicate nitrogen species in hydrotreated fuels derived from shale oil have deleterious effects on fuel stability (1). The speciation of nitrogen compounds at ppm levels in fuel provides information regarding fuel stability and allows possible selection of antioxidant additives. However, little information is available regarding speciation of nitrogen compounds at trace levels in fuels.

Comparing physicochemical properties of an oil before and after processing has provided insight to processing effects. Nitrogen compound-type distributions in crude shale oil and in fuels produced by catalytic hydrotreatment have been studied (2,3). Catalyst selectivity toward hydrodenitrogenation of different nitrogen types has been determined. Other oil-upgrading schemes have incorporated acid treatment of shale oils (4). In 1979, Standard Oil of Ohio (Sohio) hydrotreated shale oil to remove 80 percent of its nitrogen; however, about 3350 ppm nitrogen remained in the hydrotreated products (5). These products were subsequently treated with acid and clay to remove residual fuel-bound nitrogen and color bodies, making the finished products storage stable. Finished jet fuel contained less than one ppm nitrogen, and finished diesel fuel contained 23 ppm nitrogen. Sohio reported that acid-clay treatment also removed non-nitrogen containing compounds.

With the development of high resolution gas chromatographic capillary columns and computer data base reduction systems, analytical techniques have allowed efficient speciation of nitrogen compounds in fuels (6). The following work presents the speciation of nitrogen compounds in hydrotreated and finished fuels derived from shale. A comparison of these compound types is used to discuss effects of acid-clay treatment of the fuels. An analysis of the nitrogen types in the finished fuel is discussed in terms of their reactivity toward fuel instability.

EXPERIMENTAL

Hydroprocessing of Shale Oil

Shale oil from the Paraho direct heat retort was hydroprocessed by Sohio under a contract with the U.S. Departments of Energy and Defense (5). Whole crude oil was catalytically hydrotreated over a nickel-molydenum catalyst and then fractionated by distillation to maximize yields of military transportation fuels, jet fuels (JP-5 and JP-8) and diesel fuel marine (DFM). Each hydrotreated fuel was treated with acid and clay. About 10.8 kg of 93 weight percent sulfuric acid was used to contact each bbl of fuel; the acid-treated fuel was separated from the acid sludge and passed through clay filters, a clay contactor, and final filter to product storage. An antioxidant was added to the acid-clay treated fuel. The effect of acid-clay treatment on nitrogen compound-type distribution was investigated by analyzing the compositions of the hydrotreated DFM and the finished DFM.

Fractionation by Adsorption Chromatography

Preparative alumina adsorption chromatography was used to fractionate the hydrotreated DFM and finished DFM into hydrocarbon and nitrogen fractions. An accurately weighed amount of hydrotreated DFM (about 10 grams) was diluted with 100 ml of hexane and pumped onto basic alumina in a 0.9 cm i.d. x 50 cm glass column. An additional 100 ml of hexane eluted the hydrocarbon fraction from basic alumina. The nitrogen fraction was backflushed from the column with 40 volume percent ethanol in toluene. Because some nitrogen compounds remained in the hydrocarbon fraction, this fraction was chromatographed again on neutral alumina into hydrocarbon and pyridine fractions. An accurately weighed amount of the finished DFM (about 174 grams) was diluted with 1800 ml hexane and pumped onto neutral alumina. An additional 100 ml of hexane eluted the hydrocarbon fraction from the column and the nitrogen fraction was backflushed from the neutral alumina with 40 volume percent methanol in benzene. Rates for sample charging and fraction elution were 6 ml/min. Solvents were carefully removed from fractions under reduced pressure. Solvent-free fractions were weighed and stored under nitrogen in refrigerated amber glass containers until compound-type analyses.

Analytical Methods

Elemental nitrogen in the fuels and their fractions was determined by chemiluminescence detection. Standard solutions ranging from 3×10^{-2} M to 5×10^{-5} M 9-methylcarbazole in toluene were used as calibrants. Amounts of basic nitrogen were determined by potentiometric titration analysis using acetonitrile-toluene and acetic anhydride-toluene with perchloric acid in dioxane as titrant (3). These reported values are accurate within ±3 relative percent. Infrared spectra were obtained with a Perkin-Elmer model 621 grating spectrophotometer. The nitrogen-containing fractions were diluted in methylene chloride, and spectra recorded in the absorbance mode using solvent compensation with a matched pair of potassium chloride infrared cells of path length 0.5 mm.

High resolution gas chromatographic analysis (HRGC) of the nitrogen-containing fractions was done with an HP model 5730A equipped with a capillary column inlet system. A 60-meter DB-1 fused silica capillary column was used with a glass effluent splitter (1:1) for simultaneous flame ionization (FID) and nitrogen-phosphorous detection (NPD). Helium was used as carrier gas. Column linear flow velocity was 20 cm/sec. Samples were diluted with methylene chloride, and splitless injections having a 45-second delay time were used with a 30°C initial oven temperature for the nitrogen-containing fractions from the hydrotreated DFM. A 140°C initial oven temperature was used for the nitrogen fraction from the finished DFM. Oven temperature was programmed to 300°C at 2°C/min.

Similar gas chromatographic conditions described above were employed for compound-type analysis by high resolution gas chromatography/mass spectrometry (HRGC/-MS). An upgraded HP model 5985 was used with an interface temperature of 300°C. Source temperature was 200°C, and ionization voltage was 70V. A mass range from 45 to 500 amu was scanned.

RESULTS AND DISCUSSION

Concentration of Nitrogen Compounds by Chromatography

The nitrogen compounds in the fuels were concentrated to facilitate detailed compound-type characterization. Two nitrogen-containing fractions from the hydrotreated DFM and one nitrogen fraction from the finished DFM were generated by alumina adsorption chromatography. A pyridine fraction from the hydrotreated DFM was identified by its distinct infrared absorbances at 1598 cm^{-1} (C=C stretch) and 1557 cm^{-1} (C=N stretch), suggesting the presence of pyridinic compounds. The absence of these absorbances in the finished DFM confirmed the lack of a pyridine fraction

as well as pyridinic compounds. The nitrogen fractions from both fuels displayed N-H stretching at 3460 cm^{-1}, suggesting the presence of pyrrolic compounds.

Nitrogen compounds comprised 6 weight percent and 0.13 weight percent of the hydrotreated DFM and finished DFM (Table 1), respectively. The low nitrogen contents in the pyridine fraction (2.92 weight percent) and in the nitrogen fraction from the finished DFM (1.62 weight percent) suggest the presence of non-nitrogen containing compounds. However, excellent nitrogen recovery was obtained. About 99 percent and 91 percent of the nitrogen from the hydrotreated DFM and finished DFM, respectively, was concentrated in the pyridine and nitrogen fractions.

Amounts of basic nitrogen were determined in each of the nitrogen-containing fractions and are presented in Table 2. All the nitrogen in the pyridine fraction was weak base (pka 7 to 9), suggesting the presence of pyridine derivatives. The potentiometric titration analysis of the nitrogen fraction from the hydrotreated DFM indicates not only pyridinic compounds but also the presence of arylamines and hydrogenated indoles and/or quinolines (pka 2 to 7), and indoles and carbazoles (nonbasic nitrogen). The nitrogen fraction from the finished DFM contains predominately nonbasic nitrogen which does not undergo extensive acetylation (27 percent) in acetic anhydride; this suggests the presence of nonactive hydrogens in indole- and/or carbazole-type compounds.

HRGC/FID/NPD and HRGC/MS Analysis

HRGC with simultaneous detection by FID and NPD was used to establish optimal gas chromatographic conditions for the HRGC/MS analysis presented below. Acceptable peak resolution without tailing was achieved on the apolar chromatographic column. In Figure 1, the one-to-one peak correspondence of each detector response to the components in the nitrogen fraction from the hydrotreated DFM suggests that this fraction contains compounds with at least one nitrogen atom. Phosphorous is not expected to be present in these fractions. However, in Figure 2 the FID/NPD responses of the species from the finished DFM indicate few nitrogen compounds which have long column retention times (initial oven temperature, 140°C). FID/NPD responses for species in the pyridine fraction indicate the presence of non-nitrogen-containing compounds. The nitrogen species in the pyridine fraction are distributed about intermediate column retention times compared with the longer times for species in the nitrogen fractions.

Nitrogen in the pyridine fraction is primarily found in the isomers of alkyl-substituted dihydropyridines, pyridines, quinolines, and tetrahydroquinolines shown in Table 3. It is noteworthy that many different isomers of alkyltetrahydroquinolines are indicated relative to fewer alkylquinolines. The buildup of tetrahydroquinolines is indicative of the rate determining step in the hydrogenation of quinoline. The large number of isomers of alkylpyridines has been observed previously (7). Not listed for the pyridine fraction are non-nitrogen-containing compounds which include alkyl-substituted benzenes, naphthenes, biphenyls, and 9-H fluorenes. Because compound-type sensitivity factors were not available at the time of analysis, quantitative data were not obtained.

Large numbers of isomers of alkyltetrahydroquinolines and alkylpyridines are indicated by HRGC/MS analysis of the nitrogen fraction from hydrotreated DFM. These results are listed in Table 3. Infrared absorbances at 3375 cm^{-1} (N-H stretch) and 1612 cm^{-1} and potentiometric titration analysis (pka 2 to 7) suggest that arylamines are also in this fraction. Because chemical ionization was not done, analysis by electron impact ionization cannot differentiate arylamines from pyridines. Previous work (8) showed about 15 percent of the pyridines may be comprised of arylamines. In addition, alkyl-substituted pyrroles, indoles, and carbazoles are present.

The retention time of carbazole in the total ion current chromatogram (TICC) of the nitrogen fraction from the hydrotreated DFM is indicated in Figure 3. The ex-

tracted ion current profiles (EICP) of methylcarbazoles and dimethylcarbazoles are shown in Figure 4. These compound types have long column retention times, and they comprise minor amounts of nitrogen in the fuel as indicated by their ion intensities.

The HRGC/MS analysis of the nitrogen fraction from the finished DFM was facilitated by matching its FID/NPD chromatograms (Figure 2) with that of its TICC. Mass spectral fragmentation patterns of the few nitrogen-containing compounds in this fraction are tentatively identified as carbazole, methylcarbazoles, and dimethylcarbazoles. Except for the ion intensity of carbazole in the finished DFM, relative intensities of the alkylcarbazoles in the finished DFM agree very well with those in the hydrotreated DFM. No other nitrogen types were identified; however, this does not preclude minor amounts undetected at baseline levels. The non-nitrogen-containing compounds were alkyl-substituted naphthalenes and 9-H fluorenes.

Effect of Acid-Clay Treatment on Nitrogen Compound Distribution

A comparison of the nitrogen compound distributions in fuels before and after acid-clay treatment demonstrates which nitrogen types are susceptible to removal. Acid-clay effectively removed 99.3% of the nitrogen from the hydrotreated DFM. As expected, basic nitrogen compounds such as arylamines form salts in reaction with acid; pyridine derivatives adsorb into acidic medium and/or participate in electrophilic substitution reactions, and both compound types are removed as acid sludge. A pyridine fraction was present only in the hydrotreated fuel and was completely removed by the acid-clay treatment. Very weak base and nonbasic nitrogen compounds such as indoles, which experience adsorption and/or acid catalysis and polymerization reactions, are effectively removed by acid-clay treatment. Interestingly, some carbazole derivatives survive acid-clay treatment. Earlier work (8) showed carbazole derivatives constituted about 66 ppm nitrogen in the hydrotreated DFM. Therefore, acid-clay removed almost two-thirds of the carbazole derivatives from the hydrotreated DFM. Nonbasic carbazoles are soluble in mineral acids; their relative unreactivity allows some to remain in the finished fuel.

In the acid-clay treatment of jet fuel (JP-8), nitrogen was not detected in the finished fuel. High resolution mass spectrometric analysis of the hydrotreated JP-8, which contained 3000 ppm nitrogen, indicated similar nitrogen-type distribution to that in the hydrotreated DFM, except carbazole derivatives were not detected. Acid and clay effectively removed all nitrogen types from the JP-8 fuel. Carbazole derivatives in transportation fuels are the nitrogen compounds least affected by acid-clay treatment.

The importance of determining residual nitrogen types in finished fuels relates to fuel stability. Aromatic nitrogen compounds have measurable sediment under low temperature storage conditions. Work reported (9) on model compounds has indicated that symmetrical, highly condensed aromatic nitrogen compounds appear less reactive than the partially hydrogenated counterparts or highly alkylated heterocyclics. These model compound studies suggest carbazole derivatives do not participate as significantly in sediment formation as do pyrrole and indole derivatives. Synergestic effects also play an important role in sediment formation particularly as the hydrocarbon matrix becomes more complex: n-decane<jet fuel<diesel fuel. The nitrogen distributions in the finished DFM and JP-8 fuels indicate these fuels may be storage stable. However, non-nitrogen compound types in these fuels may very well affect fuel stability.

In summary, the analytical techniques presented have been applied successfully to the analysis of moderate and trace quantities of nitrogen in fuels. The determination of nitrogen compound distributions aid in understanding the effects of fuel processing and in discussing fuel stability.

ACKNOWLEDGMENTS

The authors are indebted to E. T. Robinson of Sohio for discussions of this work. The authors thank the following personnel at WRI for their technical contributions: L. F. Thompson, F. A. Barbour, S-L Chong, and M. Harnsberger. They also thank R.E. Robertson for reviewing the manuscript and M. E. Marron for editorial suggestions.

LITERATURE CITED

1. Frankenfeld, J. W., W. F. Taylor, and D. W. Brinkman. Exxon R and E Co., U.S. Department of Energy Contract Report No. DOE/BC/10045-12 (1981).

2. Bett, A., T. G. Harney, T. W. Matheson, and K. C. Pratt. Fuel, 62, 1445 (1983).

3. Holmes, S. A. and L. F. Thompson. Preprints, Div. of Petrol. Chem., ACS, 29 (1), 269 (1984).

4. Reif, H. E., J. P. Schwedock, and A. Schneider. "An Exploratory Research and Development Program Leading to Specifications for Aviation Turbine Fuel From Whole Crude Shale Oil, Part V," Final Report AFWAL-TR-81-2087, March 1982. Available from NTIS.

5. Evin, C. G. and E. T. Robinson. "The Commercial-Scale Refining of Paraho Crude Shale Oil Into Military Fuels," Office of Naval Research, Navy Contract N0014-79-C-0061, Sept. 1979.

6. Ellis, L. C., and P. T. Crisp. J. Chrom., 292, 355 (1984).

7. Cooney, J. V., E. J. Beal, and R. N. Hazlett. Preprints, Div. of Petrol. Chem., ACS, 29 (1), 247 (1984).

8. Holmes, S. A., and L. F. Thompson. Fuel, 62, 709 (1983).

9. Frankenfeld, J. W., W. F. Taylor, and D. W. Brinkman. Exxon R and E Co., U.S. Department of Energy Contract Report No. DOE/BC/10045-23 (1982).

DISCLAIMER

Mention of specific brand names or models of equipment is for information only and does not imply endorsement.

Table 1. Nitrogen Content in Fractions from Fuels Derived from Shale

Fractions	Weight Percent Sample	Weight Percent Nitrogen	Nitrogen (Weight Percent of Sample)
Hydrotreated DFM			
Pyridine Fraction	1.46	2.92	0.043
Nitrogen Fraction	4.58	6.31	0.289
Hydrocarbon Fraction	91.5	11 ppm	10 ppm
Recovery (%)	98	NA	99
Finished DFM			
Nitrogen Fraction	0.13	1.62	21 ppm
Hydrocarbon Fraction	94.2	2 ppm	2 ppm
Recovery (%)	94	NA	100

Table 2. Distribution of Basic Nitrogen Contents in Fractions from Fuels Derived from Shale

Fractions	Weight Percent of Nitrogen		
	Weak Base pka 7 to 9	Very Weak Base pka 2 to 7	Nonbasic Nitrogen
Hydrotreated DFM			
Pyridine Fraction	2.92	--	--
Nitrogen Fraction	4.78	0.76	0.77
Finished DFM			
Nitrogen Fraction	0.04	0.06	1.52

Table 3. Compound Classes in Fractions from Hydrotreated DFM

Compound Class[a]	No. of Isomers in Fraction		Compound Class	No. of Isomers in Fraction	
	Pyridine	Nitrogen		Pyridine	Nitrogen
Dihydropyridines			Quinolines		
C_7	6	--	C_0	--	1
C_8	4	--	C_1	--	1
C_9	4	--	C_2	1	2
Pyridines[b]			C_3	4	6
C_2	--	3	C_4	7	4
C_3	--	21	C_5	4	2
C_4	4	28	Indoles		
C_5	10	44	C_1	--	4
C_6	15	42	C_2	--	5
C_7	29	33	C_3	--	8
C_8	24	21	C_4	--	16
C_9	30	26	C_5	--	18
C_{10}	19	39	C_6	--	24
C_{11}	21	33	C_7	--	18
C_{12}	17	11	C_8	--	2
C_{13}	9	2	Pyrrole		
C_{14}	2	--	C_{10}	--	1
Tetrahydroquinolines			Carbazoles		
C_1	--	11	C_0	--	1
C_2	--	19	C_1	--	3
C_3	3	30	C_2	--	1
C_4	11	22	Acridines/		
C_5	13	37	Phenanthridines/		
C_6	9	28	Benzoquinolines	2	--
C_7	2	13			
C_8	1	--			

[a] Listing of C_x refers to the number of carbons in substituents on the heteroaromatic compound.

[b] Alkylarylamines are included with pyridines in the nitrogen fraction.

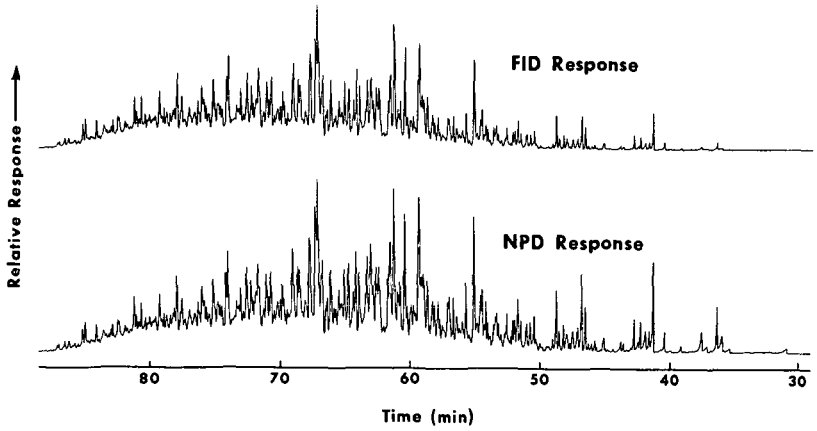

Figure 1. HRGC Chromatograms of Nitrogen Fraction from Hydrotreated DFM (Initial Oven Temperature, 30°C)

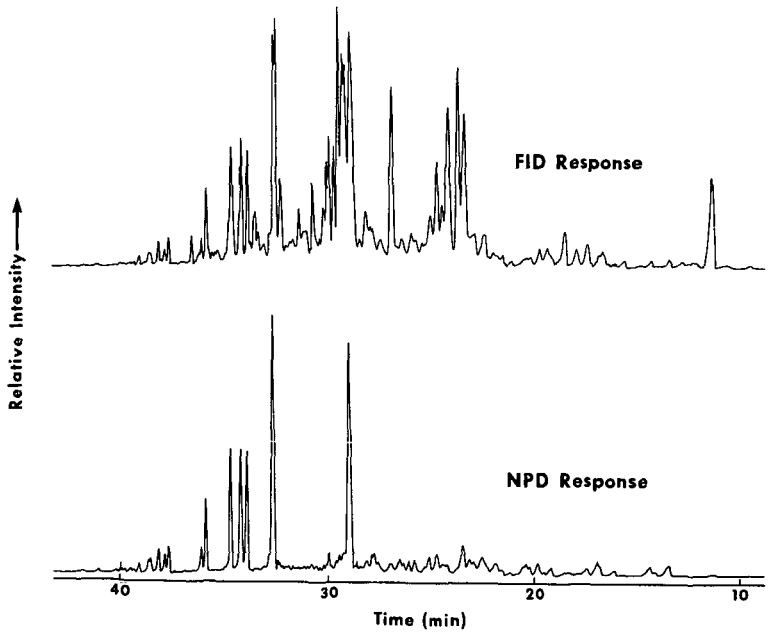

Figure 2. HRGC Chromatograms of Nitrogen Fraction from Finished DFM (Initial Oven Temperature, 140°C)

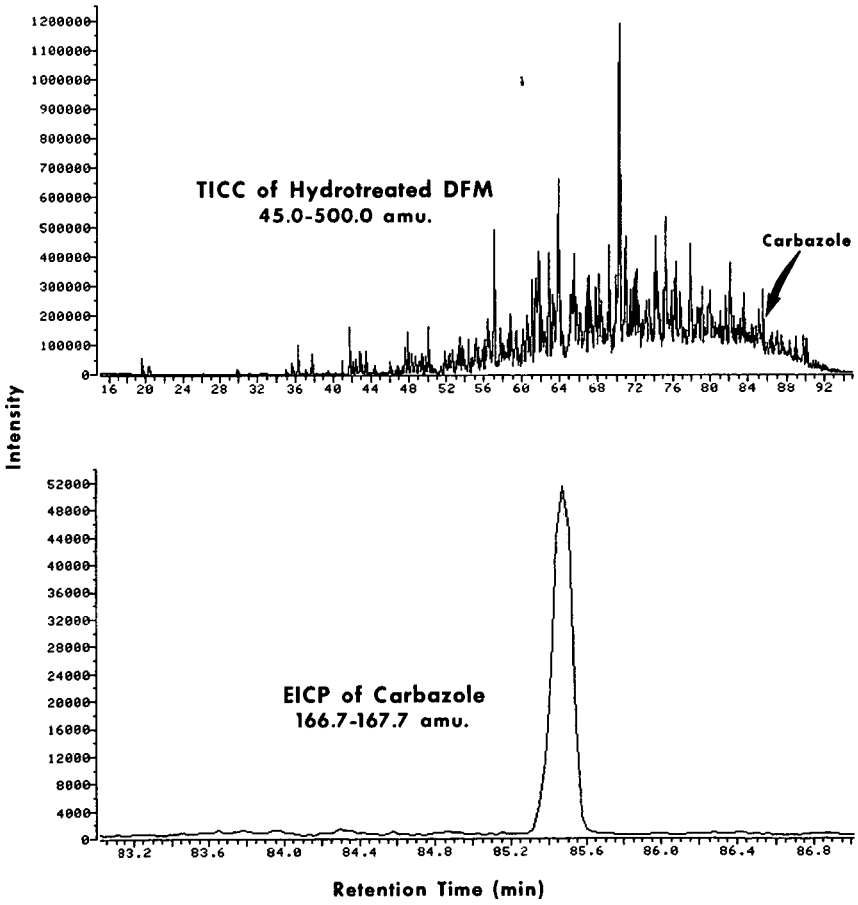

Figure 3. HRMS/GC Analysis of Hydrotreated DFM

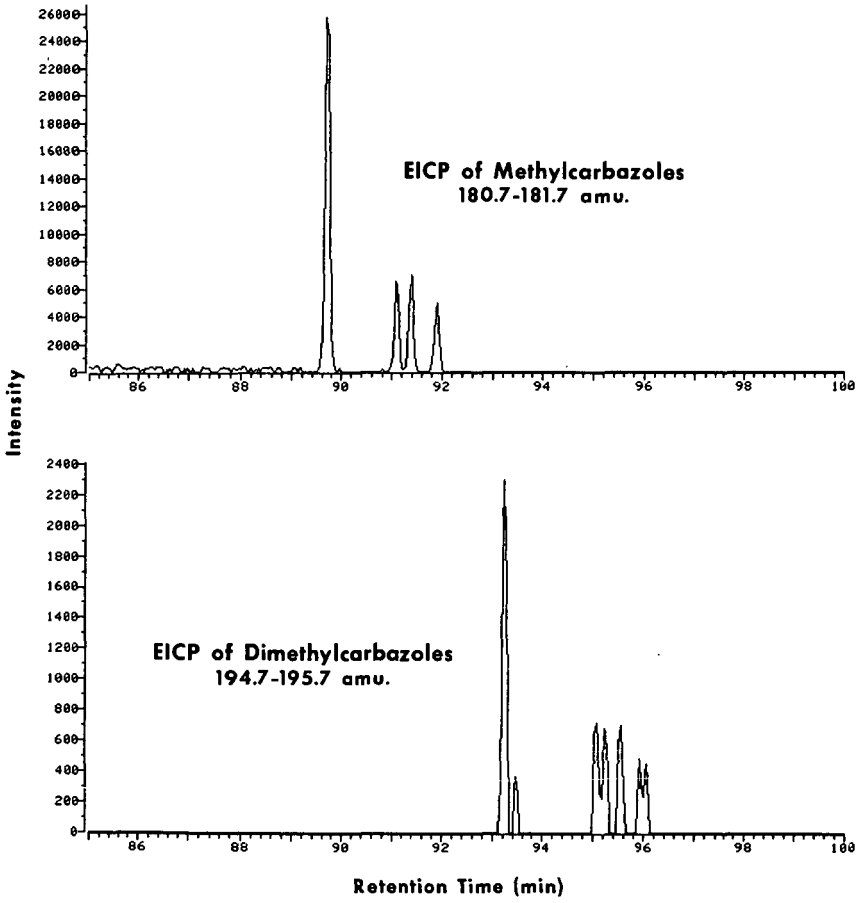

Figure 4. Extracted Ion Current Profile of Alkylcarbazoles

CHARACTERIZATION OF "HEAVY" CRUDE COMPONENTS

M. M. Boduszynski

Chevron Research Company, P.O. Box 1627,
Richmond, California 94802-0627

The current trend toward processing petroleum residua or whole "heavy" crudes requires adequate compositional information to understand the chemistry of reactions that are involved. Monitoring compositional changes by a mere comparison of operationally defined fractions or by a determination of "average structures" for feedstock and product components provides inadequate and frequently misleading information. (1) Much more detailed compositional data are needed to unravel the structural transformations which occur during processing or to explain product properties.

This paper discusses recent results of characterization work on "heavy" crudes and petroleum residua. The emphasis of this paper is on distribution of homologous series of compounds, their molar mass and structure, all as a function of boiling point. The detailed discussion of the experimental procedures used in this study is beyond the scope of this paper. It is important to note, however, that the unique combination of short-path distillation, high performance liquid chromatography (HPLC), and field ionization mass spectrometry (FIMS) was essential for obtaining the detailed compositional information which was not available before. The nitrogen-rich, 13.6°API gravity, Kern River crude oil (a blend of crudes from San Joaquin Valley, California) is used as an example.

EXPERIMENTAL

Kern River crude oil was first distilled using a Penn State column to produce two distillates, Cut 1 and Cut 2, and atmospheric residuum (~650°F+). The residuum was then fractionated into eight distillates, Cut 3 through Cut 10, and the nondistillable residuum (~1300°F+) using the short-path distillation. The detailed description of the short-path distillation apparatus, DISTACT, can be found elsewhere. (2, 3) The true boiling point (TBP) distributions of the distillation cuts were determined using a vacuum thermal gravimetric analysis (VTGA) method developed at Chevron Research. (4) The molar mass distributions of all cuts were determined using FIMS and field desorption mass spectrometry (FDMS). (5) The FIMS data were obtained at SRI International,

Encl. - Table I
Figures 1-8

Menlo Park, California. Average molecular weights were determined by vapor pressure osmometry (VPO) using toluene as a solvent. Carbon (C), hydrogen (H), sulfur (S), total nitrogen (N_t), basic nitrogen (N_b), and oxygen (O) were determined using standard procedures. Nickel (Ni), vanadium (V), and iron (Fe) were determined by inductively coupled plasma (ICP) emission spectroscopy method.

Chromatographic separations of all distillation cuts involved a two-step procedure. First, a fraction of polar components (mainly N-, O-, and metal-containing compounds) was isolated from each distillation cut before further HPLC separation to prevent possible damage of high efficiency columns. "Polars" were separated using liquid chromatography on basic alumina. In the second step, the "polars-free" fraction was further separated into saturates, monoaromatics, diaromatics, triaromatics, tetraaromatics, pentaaromatics, and a fraction designated "hexaaromatics and/or azarenes."

The HPLC system consisted of two preparative columns, ZORBAX-NH_2 and ZORBAX-SIL, connected through a switching valve. The system was calibrated using model compounds. The actual cut points between the aromatic ring-type fractions were determined using ultraviolet (UV) spectra collected from 200-400 nm by the UV photodiode array detector at 20-sec. intervals. Weight percent yields of the fractions were determined gravimetrically. The HPLC fractions were analyzed by FIMS. The principles of the HPLC/FIMS approach and its application to characterization of coal-derived liquids were reported previously. (6-8) However, a different HPLC system was used in this study. Elemental analysis, infrared spectrometry, ^1H and ^{13}C nuclear magnetic resonance (NMR) spectrometry, and EIMS were used occasionally to aid interpretation of the HPLC/FIMS data.

RESULTS AND DISCUSSION

How Heavy is the "Heavy" Crude Oil?

The adjectives "heavy," "high boiling," and "high molecular weight" are commonly but inappropriately used as equivalent terms to describe crude oils or their fractions. The term "heavy" refers to crude oil density. Heavy crudes, of which Boscan (10.1°API gravity in Figure 1) is a classic example, have high densities (low °API gravities) because they are rich in high density naphthene-aromatics and heteroatom-containing compounds and poor in low density alkanes. They are commonly either immature or degraded. (9) Light crudes, which have low densities (high °API

gravities) are rich in alkanes. Altamont crude oil (42.2°API gravity in Figure 1), an extreme example, has an exceptionally high alkane content as a result of its predominant source being lacustrine algae, which also happens to have been the source of the nearby Green River shale. (9)

For each of the crudes considered in Figure 1, the °API gravity decreases with increasing depth of distillation. Hence the term "heavy ends" tends to correlate with "high boiling" within a given crude. However, the correlation between "heavy" and "high boiling" does not necessarily hold if different crudes are being compared. For example, the nondistillable residuum (~1300°F+) from Altamont crude has a lower density (higher °API gravity) than whole Boscan, Kern River, or Maya crude.

The terms "heavy" and "high boiling" are frequently but incorrectly used as if they were synonymous with "high molecular weight." The boiling point of a compound at a given pressure is a rough measure of the attractive forces between the molecules. These forces vary with the structure of molecules, leading to the great differences in boiling point for compounds of a given molar mass but a different chemical structure. This is illustrated in Figure 2. Compounds having similar molar masses cover a broad boiling point range and, conversely, a narrow boiling point cut contains a wide molar mass range. The molar mass range increases rapidly with increasing boiling point, as illustrated by the extended curves "A" and "C" at the right side of Figure 2. For a given class of compounds, the boiling point increases with molar mass. This is due to the increase of the weak, van der Waals attractive intermolecular forces as molecules of a given type become larger. However, compounds having fused aromatic rings and functional groups capable of hydrogen bonding or other types of polar interactions have additional attractive intermolecular forces and may have a relatively low molar mass but a high boiling point and thus are expected to concentrate in the "heavy ends."

Figure 3 shows boiling point, molar mass, and heteroatom distributions in Kern River petroleum. The apparent molar mass distributions of all distillation cuts, including the nondistillable residuum, were measured by FIMS and FDMS. The results obtained by both techniques were in very good agreement. The molar mass distributions are illustrated in Figure 3 by using the molar mass scale as a radius of each "slice." The radius of the inner circle corresponds to the lowest molar mass of that cut while the radius of the outer circle extends to the highest molar mass value. A significant trend can be observed. The molar mass range of the successive distillation cuts widens with increasing boiling

point in a fashion that is consistent with the trend indicated by the curves in Figure 2. The low molar mass end of each cut (radius of the "hole" in each slice) shows only a moderate increase with increasing boiling point while the high molar mass end soars. The resulting significant molar mass overlapping between the cuts is mainly due to the increasing concentration of polynuclear aromatic and heteroatom-containing compounds which have high boiling points but relatively low molar masses.

Interestingly, most of these heavy crude components do not exceed a molar mass of about 1500 and only a few have molar masses extending up to about 1900. The molar mass data for Kern River crude oil are in agreement with the previously reported results for other crudes (10-12) and provide further support for the early speculations by Dean and Whitehead (13) who suggested a molecular weight maximum of 2000 for all compounds in petroleum.

Data in Table I give distributions of elements (C, H, N, S, O, Ni, and V) on a molecular basis. The decreasing Z value in the general formula $C_nH_{2n+Z}X$ for each successive cut indirectly indicates the increasing "aromaticity." The C number range and the concentration of heteroatom-containing molecules also increase with increasing boiling point. For example, the low boiling Cut 1 (385-499°F) consists of molecules having about 10-14 C atoms, with only two molecules in 100 containing S and one in 1000 containing a N atom. The high boiling Cut 5 (795-943°F) involves molecules having about 18-48 C atoms and on the average every other molecule may contain a heteroatom. The nondistillable residuum has the highest concentration of heteroatoms and shows the greatest H deficiency (lowest Z value) among all distillation cuts. One must bear in mind, however, that the above are only average estimates which cannot reveal the actual distribution of heteroatoms in the diverse molecules present in each cut.

What are the Components of a "Heavy" Crude Oil?

The complexity of petroleum increases rapidly with increasing boiling point as the result of the increasing number of atoms in a molecule and the immense number of their possible structural arrangements. It has long been recognized that compositional analysis of high boiling petroleum fractions by the isolation of individual compounds is a practical impossibility. (14) Instead, many attempts have been made to separate those complex mixtures into groups or classes of compounds. Numerous separation methods and schemes have been developed over the years. (15) One of the most recent systematic studies on composition of petroleum high

boiling distillates and residua was the American Petroleum Institute Research Project 60 and the later work based on the characterization scheme developed under this project. (10-12, 16-22)

Petroleum components can be viewed as two major groups of compounds, namely, hydrocarbons and nonhydrocarbons. Hydrocarbons include acyclic alkanes (paraffins) and cycloalkanes (naphthenes), both commonly referred to as saturates, and the third group known as aromatics. Most of the aromatics bear normal or branched chains and naphthenic cycles. A molecule containing one aromatic ring is regarded as monoaromatic, a molecule with two aromatic rings--diaromatic, etc., even if several naphthenic rings and side chains are attached to the aromatic ring. In the same manner, naphthenes containing both saturated rings and chains are defined by the number of rings, i.e., monocyclic, dicyclic, etc. Nonhydrocarbons include compounds which in addition to C and H atoms also involve one or several heteroatoms such as S, N, O, Ni, V, and Fe.

A complete separation of hydrocarbons from nonhydrocarbons in high boiling petroleum fractions is not possible. S-containing compounds which during chromatographic separations behave similarly to hydrocarbons of the equivalent molar structure (i.e., dibenzothiophene and fluorene) are commonly found in hydrocarbon fractions. Some N heterocycles (azarenes), particularly those with the N atom sterically hindered or N-substituted, also frequently interfere with hydrocarbons. Nonhydrocarbons having "polar" functional groups such as -COOH, -OH, -NH, C=O or those containing several heteroatoms in a molecule (i.e., metalloporphyrins) are less difficult to separate from hydrocarbons.

The separation method used in this study produced up to eight "compound-class" fractions from each distillation cut depending on the cut composition. The fraction of "polars" which is regarded as a concentrate of mainly N-, O-, and metal-containing species was separated from each cut prior to further separations of the remaining "polars-free" portion into saturates, monoaromatics, diaromatics, triaromatics, tetraaromatics, pentaaromatics, and a fraction designated "hexaaromatics and/or azarenes." The last fraction reflects the difficulty in separating polycyclic aromatic hydrocarbons having six or more rings from azarenes.

It is important to note, however, that even the most sophisticated HPLC system cannot provide a complete separation and the adjacent fractions therefore show some overlapping. This, however, is detected by the following FIMS analysis of the fractions. The FIMS provides further "separation" into various homologous series according to the Z value in the general formula C_nH_{2n+Z} and reveals the molar mass (C number) distribution of the components.

The structural assignments are based on the HPLC retention data, UV spectra (for aromatics), and if necessary are aided by such analytical techniques as ^{1}H and ^{13}C NMR, and EIMS.

Figures 4, 5, and 6 show examples of the HPLC/FIMS analyses for distillate Cuts 2, 6, and 10, respectively. Only a few most prominent homologous series are presented. Most likely structures are shown although various isomers are possible. The extensive compositional information provided by this analytical approach is evident. Of particular importance are series of polycyclic molecules many of which are related to steroid and terpenoid structures ranging from the saturated form to various stages of aromatization.

The earlier discussed effect of chemical structure on molar mass distribution for components of a given distillation cut is illustrated in Figure 5. The molar mass profile of acyclic alkanes shows the maximum at C_{39} while that of the pentaaromatic C_nH_{2n-30} series has the maximum at C_{30}. Molar mass profiles of "polars" (not shown) were "shifted" even further toward lower molar mass values than those of the corresponding hydrocarbons but showed similar patterns in terms of wide C number distributions. The interpretation of the FIMS data for "polars" is much more difficult than in the case of hydrocarbons, particularly if more than one heteroatom per molecule is involved. Infrared and NMR data, together with elemental analysis results, provided important additional information. Compounds having pyrrolic NH groups (i.e., carbazoles) and amide types were found to be particularly abundant. Although various homologous series were identified, the results indicate the need for further separation of "polars" to facilitate the interpretation of data.

Figure 7 shows distributions of various "compound-class" fractions in the heavy Kern River crude oil. The concentration of "polars" increases steadily with increasing boiling point from zero in Cut 1 to about 82 wt % in the nondistillable residuum. Notably, "polars" in the distillable portion (Cut 1 through Cut 10) account for over 42% of total "polars" present in this heavy crude oil. The mono- through pentaaromatics and the fraction designated "hexaaromatics and/or azarenes," together show a peculiar distribution pattern with two minima, one at the top and the other at the bottom of the barrel. The concentrations of individual fractions vary in each successive distillation cut. The mono- and diaromatics predominate in the low boiling cuts. It is worthwhile noting, however, that the composition of the individual fractions within these classes changes considerably with increasing boiling point. For example, the monoaromatics in Cut 2 are rich in di- and

tricyclomonoaromatics (homologous series C_nH_{2n-8} and C_nH_{2n-10}) while the monoaromatics in Cut 4 involve mainly tri-, tetra-, and pentacyclomonoaromatics (homologous series C_nH_{2n-10}, C_nH_{2n-12}, and C_nH_{2n-14}).

The data in Figure 7 show a dramatic decrease in saturates with increasing boiling point from about 88 wt % in Cut 1 to only about 1 wt % in the nondistillable residuum. Similarly, as with other compound-class fractions, the composition of saturates changes with increasing boiling point. This is illustrated in Figure 8 which shows distributions of the alkane homologous series in the entire Kern River crude oil. Acyclic alkanes (paraffins) are almost completely absent in this degraded heavy crude oil. The concentrations of tetra-, penta-, and hexacyclics increase with increasing boiling point at the expense of mono-, di-, and tricyclic alkanes. Steranes and hopanes were found to be particularly abundant in Cuts 3 through 6.

CONCLUSIONS

Data derived from this study dispel many misconceptions about the composition of high boiling components in petroleum. The results presented show that the molecular structure more than molecular weight of petroleum components predominantly determines the boiling point distribution and density (°API gravity) of the crude oil. The majority of compounds found in the "heavy" Kern River crude oil have molar masses not exceeding about 1500 with only a few extending up to about 1900. They involve mainly polycyclic structures with varying degree of aromatization, and many of them contain N and O atoms with pyrrolic and amide types prevailing.

The results of this study also demonstrate the necessity of a high degree of sample fractionation in order to obtain meaningful compositional information.

ACKNOWLEDGMENTS

The author expresses his appreciation to Messrs. T. H. Attoe, R. M. Bly, R. J. Brown, M. Karigaca, C. E. Rechsteiner, F. Su, X. Urrutia, and D. M. Wilson of Chevron Research Company; R. Malhotra and G. St. John of SRI International; S. Hughes of UIC Inc.; and W. Fischer of Leybold-Heraceus GmbH for their contributions to this study.

Appreciation is also expressed to Messrs. K. H. Altgelt, T. R. Hughes, A. L. McClellan, and J. H. Shinn of Chevron Research Company for helpful suggestions and review of this manuscript.

REFERENCES

1. Boduszynski, M. M., "Liquid Fuels Technology," 2 (3), 211-232 (1984).

2. Vercier, P., and Mouton, M., "Analusis," 101 (2), 57-70 (1982).

3. Fischer, W., "Decomposition-Free Distillation of Crude Oil Fractions with Boiling Ranges of 350-700°C," Leybold-Heraeus GmbH, Hanau, Germany.

4. Su, F., unpublished results.

5. Rechsteiner, C. E., unpublished results.

6. Boduszynski, M. M.; Hurtubise, R. J.; Allen, T. W.; and Silver, H. F., "Anal. Chem.," 55, 225-231 (1983).

7. Boduszynski, M. M.; Hurtubise, R. J.; Allen, T. W.; and Silver, H. F., "Anal. Chem.," 55, 232-241 (1983).

8. Boduszynski, M. M.; Hurtubise, R. J.; Allen, T. W.; and Silver, H. F., Fuel, in Press.

9. Tissot, B. P., and Welte, D. H., "Petroleum Formation and Occurrence," Springer-Verlag, Berlin, Heidelberg, New York (1978).

10. McKay, J. F., and Latham, D. R., Preprints, ACS, Div. Petrol. Chem., 26 (4), 831-838 (1981).

11. Boduszynski, M. M.; McKay, J. F.; and Latham, D. R., Preprints, ACS, Div. Petrol. Chem., 26 (4), 865-881 (1981).

12. Boduszynski, M. M.; McKay, J. F.; and Latham, D. R., Proc. Assn. Asph. Pav. Technol., 49, 123-142 (1980).

13. Dean, R. A, and Whitehead, E. V., Proc. Sixth World Petroleum Congress, Sec. V, Paper 9, 261-276 (1963).

14. Van Nes, K., and Van Westen, H. A., "Aspects of the Constitution of Mineral Oils," Elsevier Publishing Co., Inc., New York, Amsterdam, London, Brussels (1951).

15. Altgelt, K. H.; Jewell, D. M.; Latham, D. R.; and Selucky, M. L., "Chromatography in Petroleum Analysis," Chapter 9, 195-214, Altgelt, K. H., and Gouw, T. H., editors, Marcel Dekker, Inc., New York, Basel (1979).

16. Haines, W. E., and Thompson, C. J., "Separating and Characterizing High Boiling Petroleum Distillates: the USBM-API Procedure," Rept. of Inv. LERC/RI-75/5, BERC/RI-75/2, (1975).

17. Thompson, C. J.; Ward, C. C.; and Ball, J. S., "Characteristics of World's Crude Oils and Results of API Research Project 60," Rept. of Inv. BERC/RI-76/8 (1976).

18. McKay, J. F.; Amend, P. J.; Harnsberger, P. M.; Cogswell, T. E.; and Latham, D. R., Fuel, 60, 14-16 (1981).

19. McKay, J. F.; Harnsberger, P. M.; Erickson, R. B.; Cogswell, T. E.; and Latham, D. R., Fuel, 60, 17-26 (1981).

20. McKay, J. F.; Latham, D. R.; and Haines, W. E., Fuel, 60, 27-32 (1981).

21. Grizzle, P. L.; Green, J. B.; Sanchez, V.; Murgia, E.; and Lubkowitz, L., Preprints, ACS, Div. Petrol. Chem., 26 (4) 839-850 (1981).

22. Sturm, Jr., G. P.; Grindstaff, Q. G.; Hirsch, D. E.; Scheppele, S. E.; and Hazos, M., Preprints, ACS, Div. Petrol Chem., 26 (4) 851-856 (1981).

TABLE I

DISTRIBUTIONS OF C, H, N, S, O, Ni, AND V ATOMS IN KERN RIVER PETROLEUM

Cut No.[1]	Cumulative Wt % from Crude Oil	Approximate C Atom Range[2]	Average Number of Atoms in Molecule[3]								Z in $C_nH_{2n+Z}X$[4]
			C	H	N	S	O	Ni	V	Total Heteroatoms	
1	6.4	10-14	13.2	24.1	0.001	0.02	-	-	-	0.02	-2.3
2	18.0	12-24	17.8	29.9	0.015	0.06	0.05	-	-	0.12	-5.7
3	35.8	14-36	22.6	36.9	0.07	0.10	0.08	-	-	0.25	-8.3
4	45.0	16-42	27.3	43.5	0.12	0.12	0.11	-	-	0.35	-11.1
5	53.2	18-48	30.6	47.8	0.20	0.15	0.16	-	-	0.51	-13.4
6	60.3	20-53	35.7	55.3	0.28	0.18	0.19	2×10^{-5}	3×10^{-6}	0.65	-16.1
7	66.0	22-62	41.7	63.8	0.35	0.24	0.26	3×10^{-4}	8×10^{-5}	0.85	-19.6
8	70.9	25-71	47.0	71.1	0.47	0.29	0.39	1.3×10^{-3}	5×10^{-4}	1.15	-22.9
9	74.7	27-81	52.1	77.9	0.59	0.31	0.43	2×10^{-3}	9×10^{-4}	1.34	-26.3
10	79.1	29-93	58.5	87.4	0.70	0.33	0.48	1.4×10^{-3}	7×10^{-4}	1.51	-29.6
Nondistillable Residuum	100.0	32-134	84.8	116.4	1.49	0.54	0.82	5×10^{-3}	3×10^{-3}	2.86	-53.2

[1]See Figure 3.

[2]From FIMS and wt % C data.

[3]Calculated using average molecular weight value by FIMS and elemental analysis results.

[4]X = heteratom(s).

FIGURE 1

THE EFFECT OF DISTILLATION ON API GRAVITY FOR VARIOUS CRUDE OILS

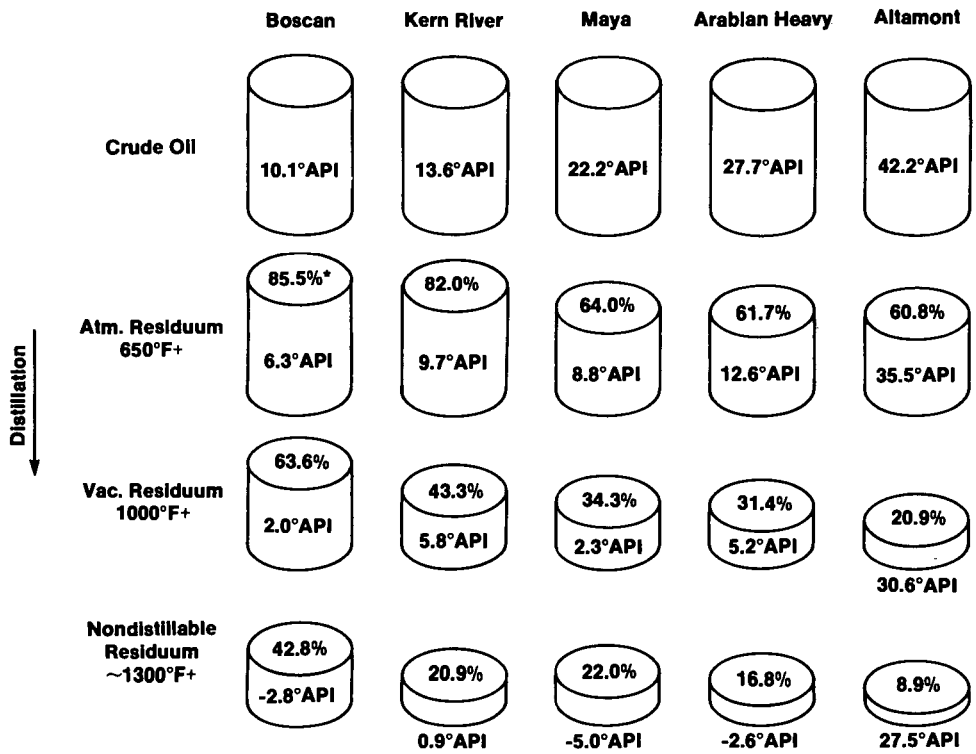

FIGURE 2
THE EFFECT OF MOLECULAR STRUCTURE ON BOILING POINT

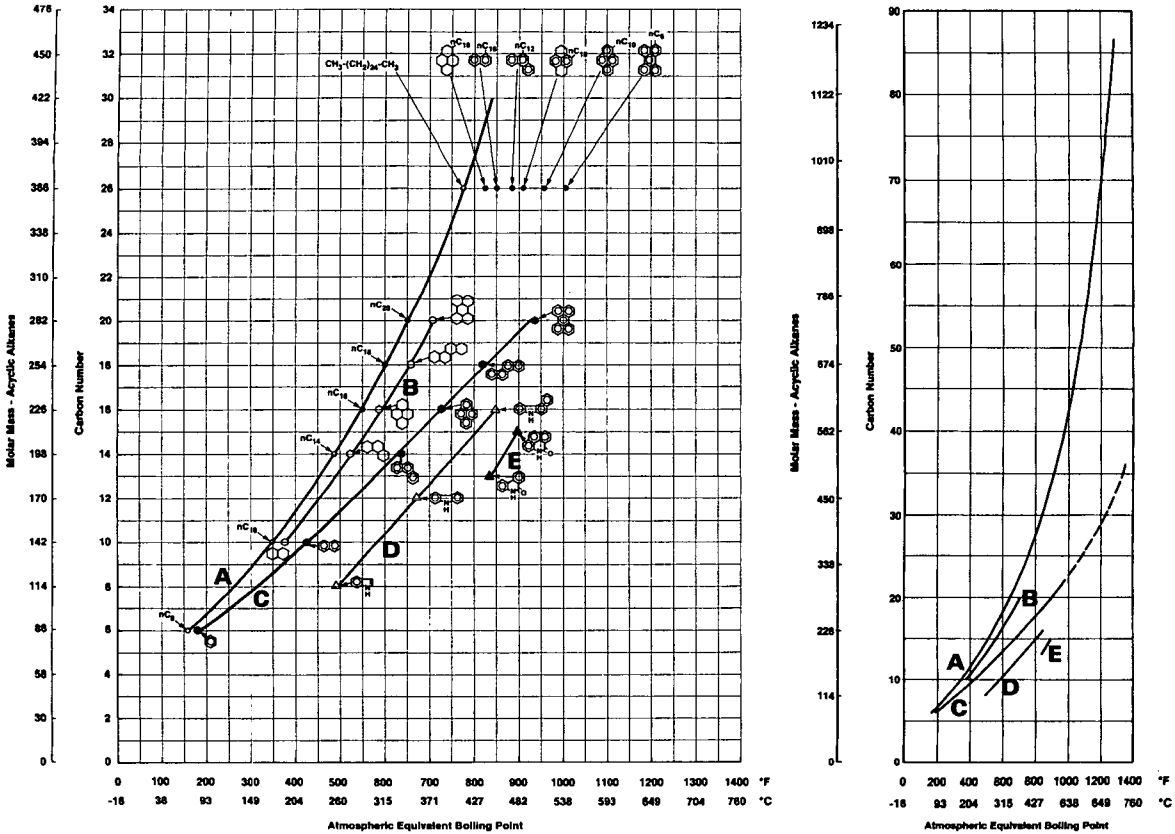

FIGURE 3

BOILING POINT, MOLAR MASS, AND HETEROATOM DISTRIBUTIONS IN KERN RIVER PETROLEUM (13.6°API)

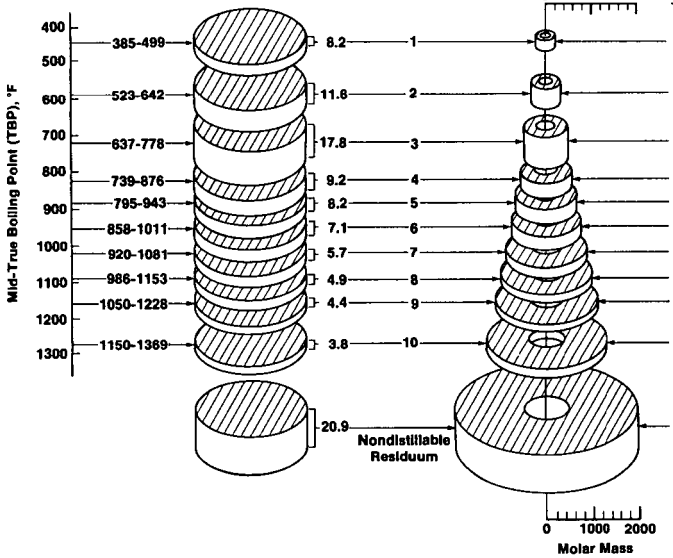

10-90% TBP, °F	Yield from Crude, Wt %	Cut No.	Average Molecular Weight FIMS	Average Molecular Weight VPO	Atomic Ratio H/C	Heteroatoms: Nonmetals, Wt % S	O	N_t	N_b	Ratio N_b/N_t	Metals, ppm Ni	V	Fe
385-499	8.2	1	184	190	1.628	0.33	-	0.008	-	-	-	-	-
523-642	11.6	2	246	260	1.686	0.79	0.31	0.088	0.058	0.66	-	-	-
637-778	17.8	3	318	337	1.631	0.99	0.42	0.31	0.11	0.35	-	-	-
739-876	9.2	4	381	420	1.598	1.02	0.45	0.46	0.15	0.33	-	-	-
795-943	8.2	5	428	471	1.563	1.11	0.60	0.65	0.17	0.26	-	-	-
858-1011	7.1	6	498	527	1.553	1.19	0.60	0.78	0.21	0.27	2	0.3	0
920-1081	5.7	7	584	594	1.532	1.34	0.71	0.84	0.23	0.27	29	7	0.9
986-1153	4.9	8	859	662	1.514	1.34	0.94	1.01	0.27	0.27	117	40	1.4
1050-1228	4.4	9	730	755	1.496	1.34	0.94	1.14	0.28	0.25	160	65	7
1150-1369	3.8	10	620	678	1.494	1.39	0.95	1.19	0.30	0.25	102	45	8
Nondistillable Residuum	20.9		1200	1916	1.374	1.43	1.10	1.74	0.41	0.24	249	122	183

FIGURE 4

SCHEMATIC DIAGRAM OF HPLC-FIMS ANALYSIS OF CUT 2 (523-642°F) FROM KERN RIVER PETROLEUM

Note: Only Selected Homologous Series Are Shown as Examples

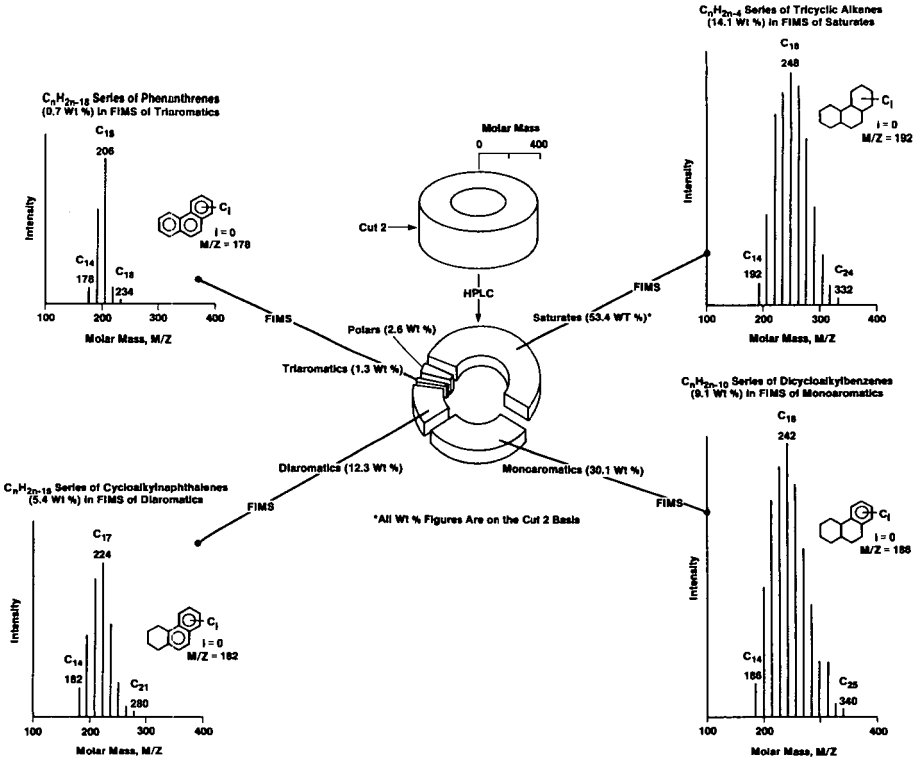

FIGURE 5

SCHEMATIC DIAGRAM OF HPLC-FIMS ANALYSIS OF CUT 6 (858-1011°F) FROM KERN RIVER PETROLEUM

Note: Only Selected Homologous Series Are Shown as Examples

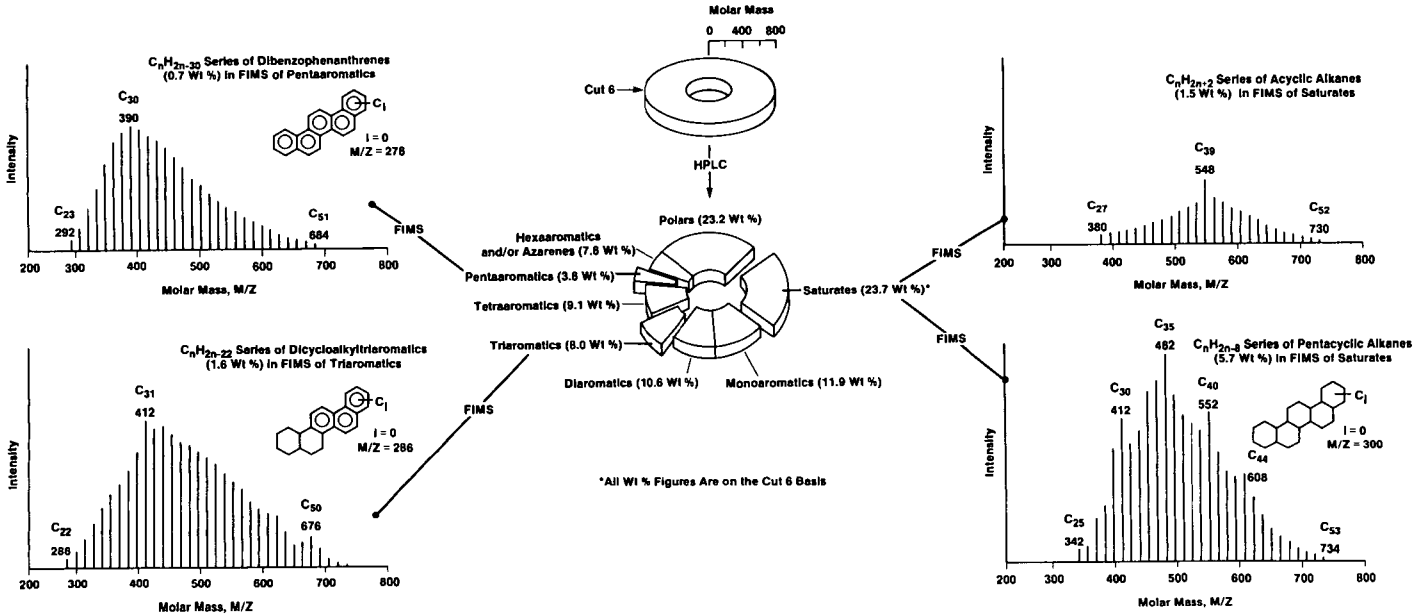

FIGURE 6

SCHEMATIC DIAGRAM OF HPLC-FIMS ANALYSIS OF CUT 10 (1150-1369°F) FROM KERN RIVER PETROLEUM

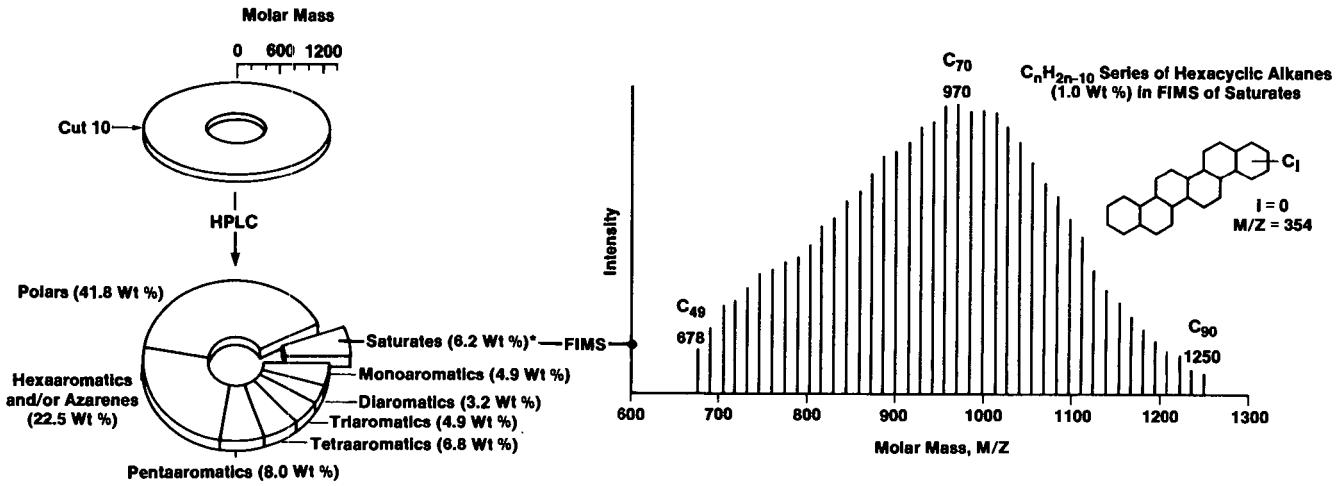

*All Wt % Figures Are on the Cut 10 Basis

FIGURE 7

COMPOUND-CLASS DISTRIBUTIONS IN KERN RIVER PETROLEUM

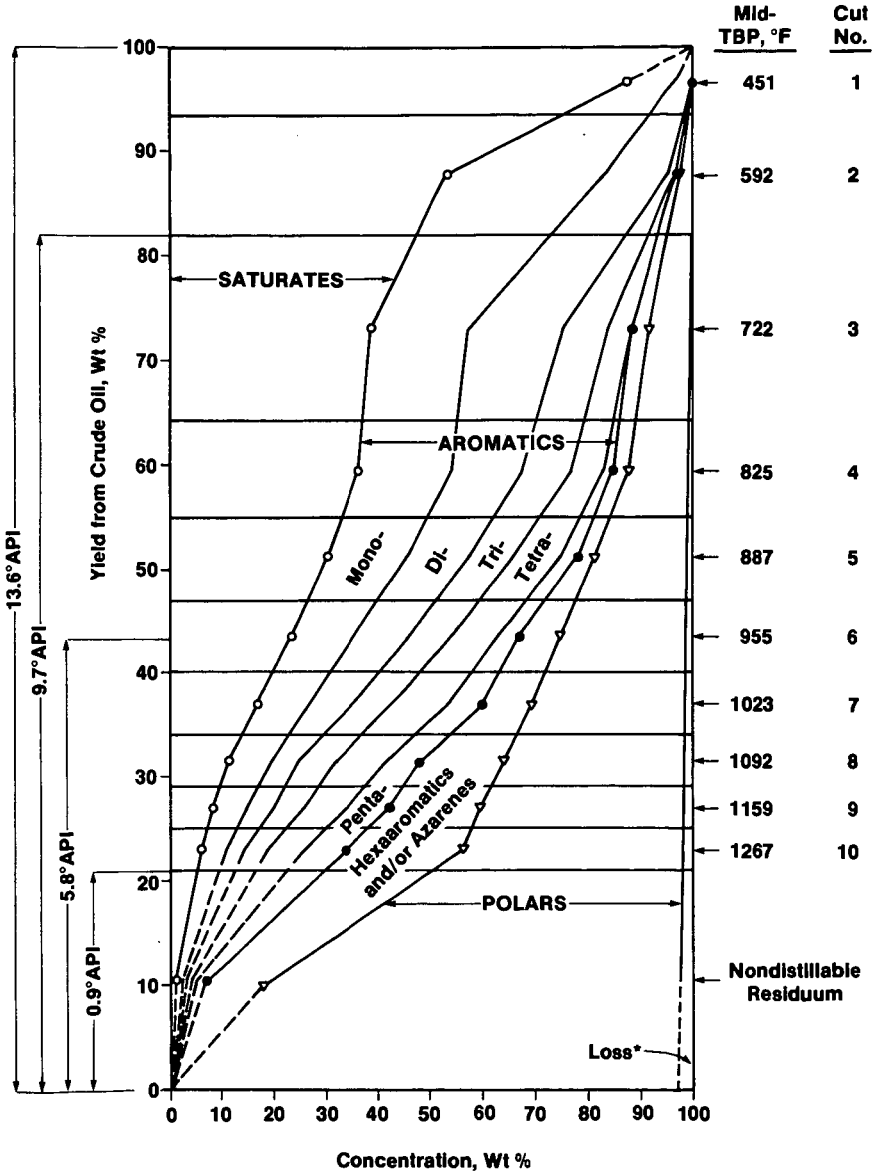

*Unrecovered material during chromatographic separations.

FIGURE 8

DISTRIBUTIONS OF ALKANE HOMOLOGOUS SERIES IN KERN RIVER PETROLEUM

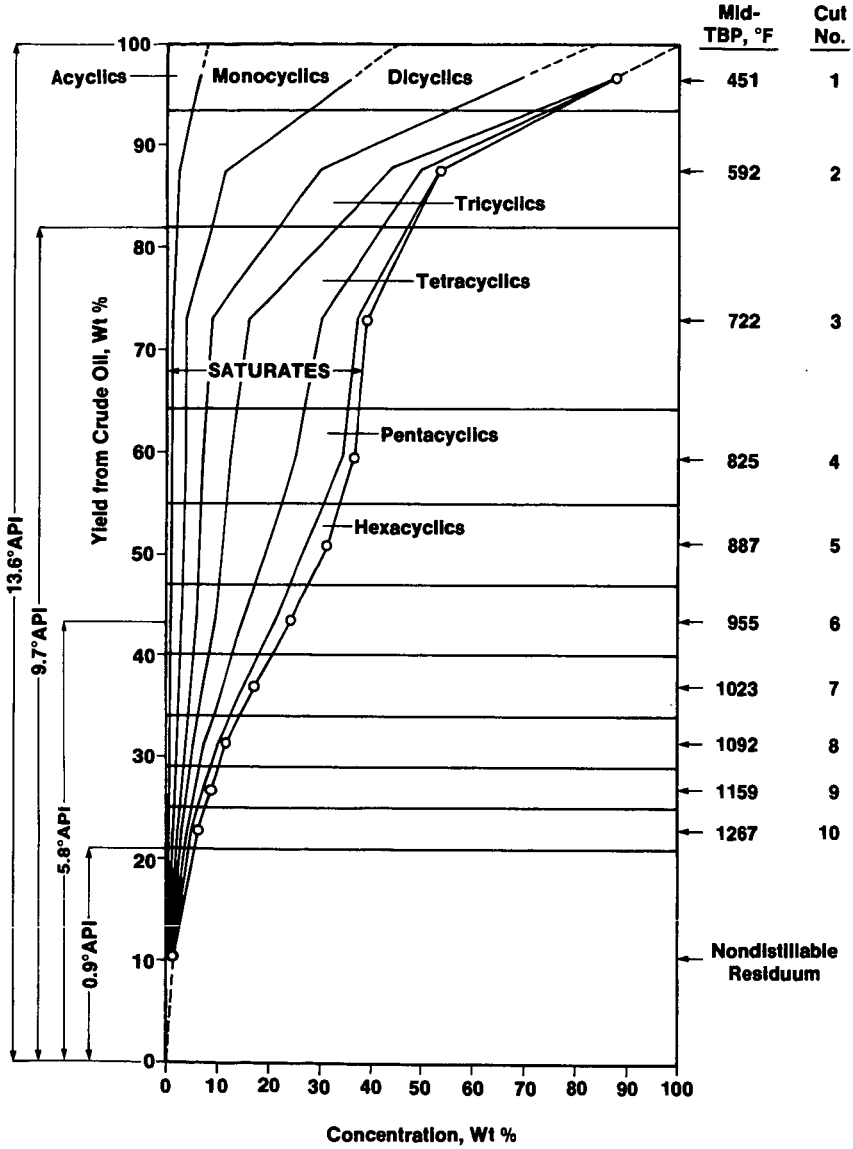

STRUCTURES OF LIQUID-LIKE SYSTEMS: X-RAY DIFFRACTION OF MODEL ORGANIC HYDROCARBONS.

Lawrence B. Ebert, Joseph C. Scanlon, and Daniel R. Mills
Exxon Corporate Research Labs
Route 22 East
Annandale, New Jersey 08801

Introduction

Since the work of T. F. Yen in 1961 (1), there has been much effort in the determination of the structure of petroleum heavy ends. Although x-ray diffraction shows broad lines, indicative of correlation lengths of ~ 10-30 A, the d values of the peaks have been associated with specific organic functionality: 4.5-4.8 A (aliphatic), 3.4-3.8 (aromatic stacking), and 2.1 A (aromatic diameter).

In two previous papers (2,3), we have performed x-ray diffraction on the liquid phases of model organic hydrocarbons to obtain additional insights into these assignments. In contrast to earlier work (1), we found that the "γ-band" at 4.6 A was related to intermolecular interference among paraffins, but not to interference among naphthenes, which we found to appear at 5.3 to 5.4 A (2,3). Although the "(002) band" at 3.4 to 3.6 A presumably does arise from the approximately parallel stacking of planar aromatic molecules, we found evidence for (00L) peaks at lower values of 2θ, arising from the small stack height of the aromatic clusters. The true identity period became the stack height itself, thereby giving rise to lines at "d value" greater than that of the "(002) band." The above inferences indicated that the x-ray diffraction-based method of determining fractional aromaticity, by comparing areas of the γ-band and (002) band, fails for a number of reasons.

In the present paper, we extend our work on the x-ray diffraction of liquid-phase organic hydrocarbons. Analysis of the patterns of the methyl-branched paraffins pristane and phytol shows an intermolecular interference maximum at 4.7 to 4.8 A, slightly higher than that found for n-paraffins, but significantly lower than that found for naphthenes. Diffraction of quinoline shows two (00L) peaks, exactly the behavior exhibited by 1-methyl naphthalene (2,3). When a given molecule contains both sp^2 and sp^3 hybridized carbon, as in tetralin or tetrahydroquinoline, broadening of the lines results, although when one carbon type predominates (as in n-heptadecyl benzene), that carbon type will dominate the diffraction pattern.

Experimental details

Diffraction experiments on liquids were carried out as described previously (2,3). A cell with Be windows was mounted on a Siemens Type F diffractometer, equipped with a divergent 1° slit and a receiving 0.1° slit. Copper radiation was used.

Quinoline (99%) was obtained from Aldrich. The methyl branched paraffins pristane (2,6,10,14 tetramethyl pentadecane, 99%) and phytol (3,7,11,15 tetramethyl-2-hexadecen-1-ol, 70%) were obtained respectively from Wiley Organics and Aldrich. The purity of the quinoline and pristane was verified by GC/MS; the MS pattern of the major component of the phytol showed peaks at m/e of 71 (I=100), 55 (I=56), 57 (I=52), and 81 (I=33), with the highest detected m/e=278, reflecting a loss of water from the pure phytol (molecular weight = 296.5). A high resolution C-13 NMR pattern of the pristane showed resonances at 19.8 δ (the methyl groups on the 6 and 10 carbons), 22.7 δ (the four equivalent "terminal" methyl groups), 24.6 δ (the central, 8, methylene carbon), 24.9 δ (the 4 and 12 methylene carbons), 28.1δ (the 2 and 14 methylene carbons), 32.9 δ (the 6 and 10 methylene carbons), 37.5 δ (the 7 and 9 methylene carbons), and 39.5 δ (the 3 and 13 methylene carbons). The reader should note that the spectrum of this isoprenoid carbon skeleton is quite distinct from that of an n-paraffin (e.g., internal methylenes at 29.8 δ, terminal methyl groups at 14.2 δ). The remarkable finding reported here is that branched paraffins and normal paraffins show different patterns in liquid-phase x-ray diffraction, because of differences in **intermolecular** packing.

Results and Discussion

The diffraction patterns of the liquids pristane, phytol, and quinoline are given in Figure 1. The "d value" of the single observed interference maximum is 4.8 A for pristane and 4.7 A for phytol, measureably higher than the 4.6 A that we have found for n-paraffins. This increase is presumably related to the presence of the methyl groups, and confirms the identification of the "γ-band" as an intermolecular interference peak of paraffins (2,3).

In contrast to the paraffins, the diffraction pattern of liquid quinoline contains two peaks in the region 10 - 45° 2θ. The larger peak is at 3.9 A, with a shoulder at 5.1 to 5.4 A. This behavior is analogous to that previously reported for 1-methyl naphthalene, and confirms our suggestion of the presence of high d value (00L) lines in aromatic clusters of stack height 15 - 25 A (2,3).

To see the origin of these lines, one may make an analogy between aromatic clusters and the intramolecular order of n-paraffins. In the infinite n-paraffin, polyethylene, the fundamental intramolecular repeat distance is that between the first and third carbons, a distance of about 2.5 A. As one goes to finite-sized n-paraffins, as n-C_{20} or n-C_{28}, the fundamental intramolecular repeat distance is the length of the paraffin, and one observes a family of high d value lines obeying the relation d(L)= constant/(L), in which the constant is either the length of the paraffin or twice the length of the paraffin (2,3). Exactly the same situation exists for our aromatic clusters. For the infinite aromatic stack, graphite, the fundamental stacking repeat distance in an ABAB... arrangement is the AB distance, which is 6.7 A in graphite, and the most intense observed line is the (002) at 3.35 A. As one goes to clusters of small stack height, one can observe lines obeying the relation d(L) = constant/(L), just as in the case of intramolecular order of paraffins. If one insists on indexing the line near 3.4 to 3.6 A as a "(002)" line, one finds that the values of L for the other lines can be either integers or rational numbers (2,3).

In the diffraction of liquids, the major peaks observed are those arising from intermolecular interference. In the case of paraffins, the single peak observed is the γ-band, arising from interference between approximately parallel paraffin groupings. Ironically, although most discussions of the γ-band occur in the context of petroleum materials, the γ-band obtained its name from a study of coal materials (4). Of course, most coals show a dominant (002) band, arising from the intermolecular interference between aromatic molecules (5).

X-ray diffraction can, of course, be used for liquids more complex than simple paraffins or aromatics. The narrowest diffraction lines, representing the longest correlation lengths, seem to occur with spherically symmetric molecules, such as 1, 3 di-methyl adamantane (2,3) or (+)-longifolene (Aldrich 23,517-2), whose pattern is given in Figure 2. The one dimensional order of aromatic stacking can be seen even for the single ring compound, hexafluoro benzene, as seen in Figure 2. Here, the scattered intensity is increased relative to that of benzene by virtue of the fluorine atoms which are co-planar with the carbon atoms. This "assistance" does not extend to perfluoro decalin, in which case the scattering arising from carbon-carbon, carbon-fluorine, and fluorine-fluorine intermolecular distances is more complex.

What happens when one has molecules containing both sp^2 and sp^3-hybridized carbon? In tetralin, with six aromatic

and four aliphatic carbons, one observes only a broad diffraction envelope, but in n-heptadecyl benzene (six aromatic, seventeen aliphatic) one sees a γ-band much as in liquid n-paraffins (3).

To more systematically study these mixed systems, we have performed reductive alkylation on model aromatic hydrocarbons (6). In the case of perylene, for which we found a potassium consumption of two moles K per mole perylene (7), we quenched with methyl iodide (CD_3I) and actually obtained a crystalline product of di-methyl di-hydro perylene, as illustrated in Figure 3. GC/MS analysis of this product showed 72% to be a single isomer of di-methyl di-hydro perylene (parent peak m/e = 288.2), with perylene itself, a second isomer of di-methyl di-hydro perylene, and a small amount of tri-methyl di-hydro perylene also present. It is likely that the crystallinity of our product is correlated with the dominance of one isomer of di-methyl di-hydro perylene.

References

(1). T. F. Yen, J. G. Erdman, and S. S. Pollack, Anal. Chem., 33, 1587 (1961).

(2). L. B. Ebert, J. C. Scanlon, and D. R. Mills, Preprints, Petroleum Division of the American Chemical Society, 28, 1353 (1983).

(3). L. B. Ebert, J. C. Scanlon, and D. R. Mills, Liq. Fuels Tech., 2, 257 (1984).

(4). H. E. Blayden, J. Gibson, and H. L. Riley, Proceedings of the Conference on the Ultra-fine Structure of Coals and Carbons, p. 176 (1944).

(5). P. B. Hirsch, Proc. Roy. Soc. A, 226, 143 (1954).

(6). L. B. Ebert, "Reductive Chemistry of Aromatic Hydrocarbons," in Chemistry of Engine Combustion Deposits, pp. 303-376, Plenum, 1985.

(7). L. B. Ebert, submitted to Fuel, April, 1985.

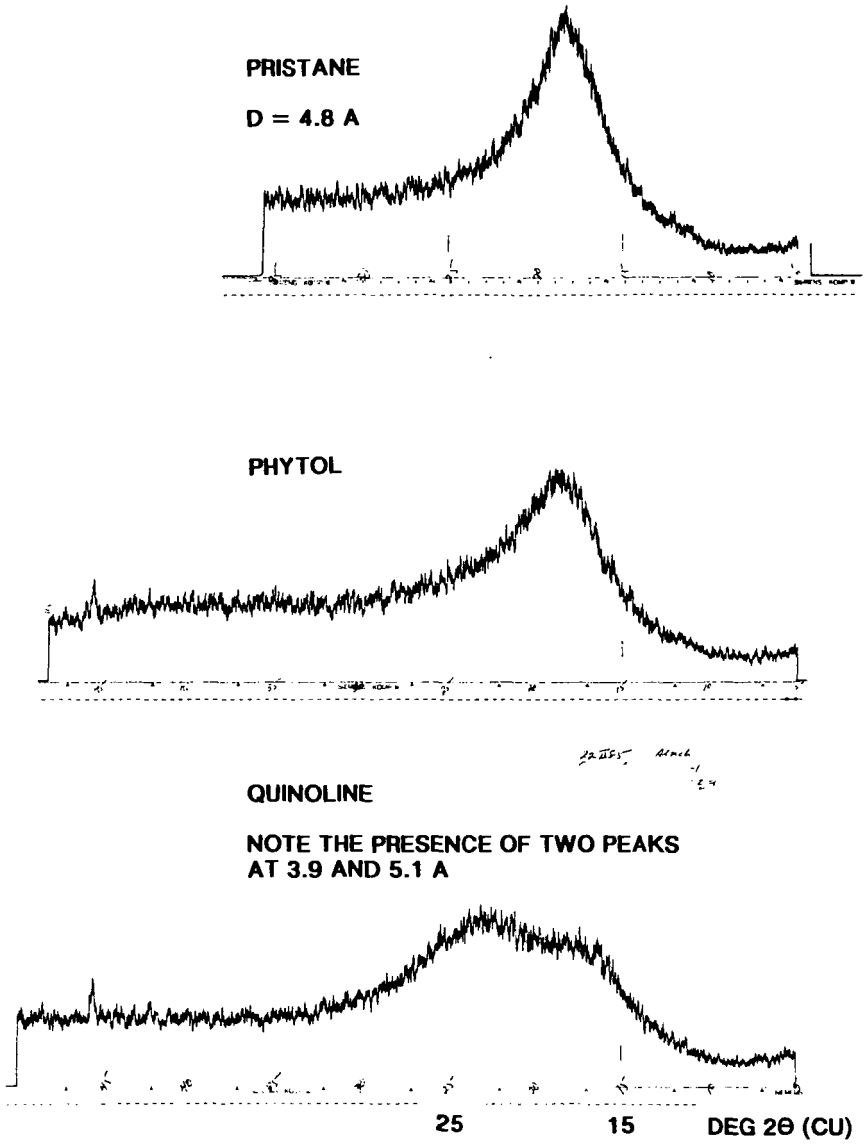

FIGURE 1. XRD OF LIQUIDS.

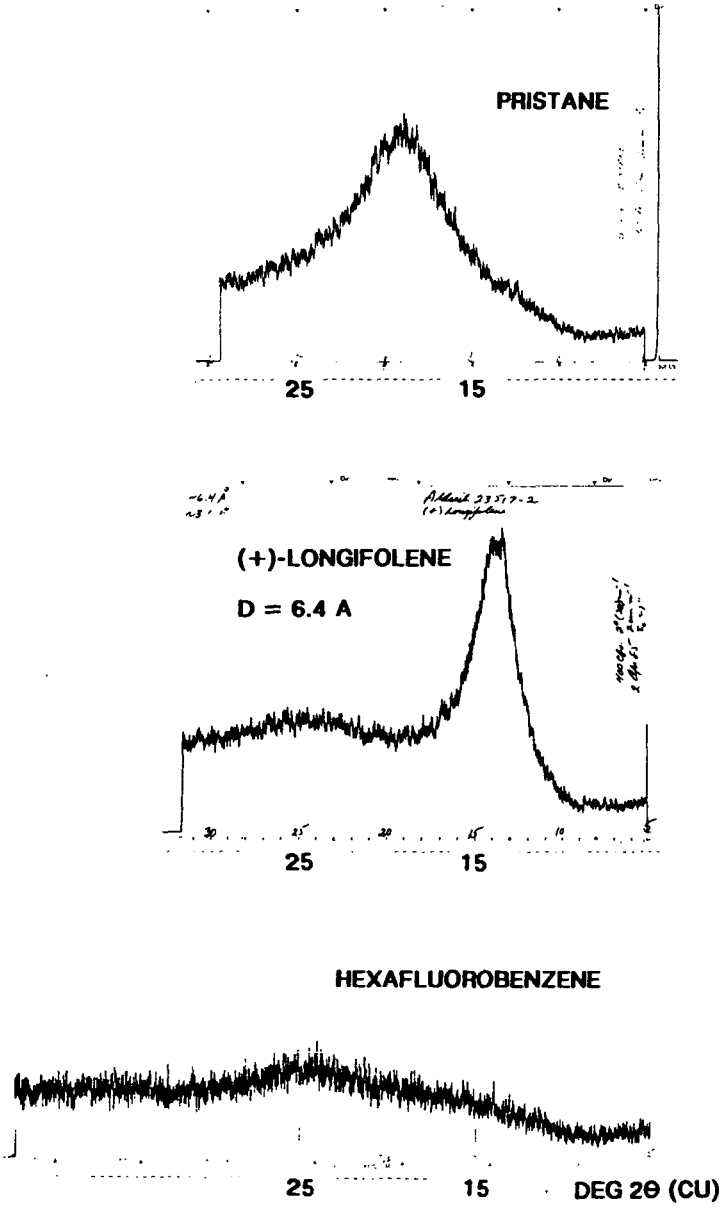

FIGURE 2. XRD OF LIQUIDS.

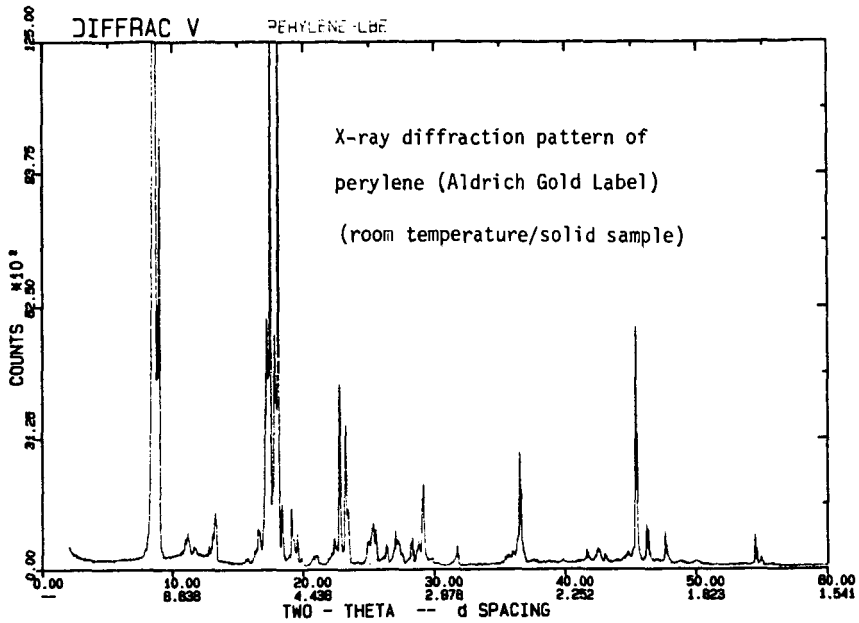

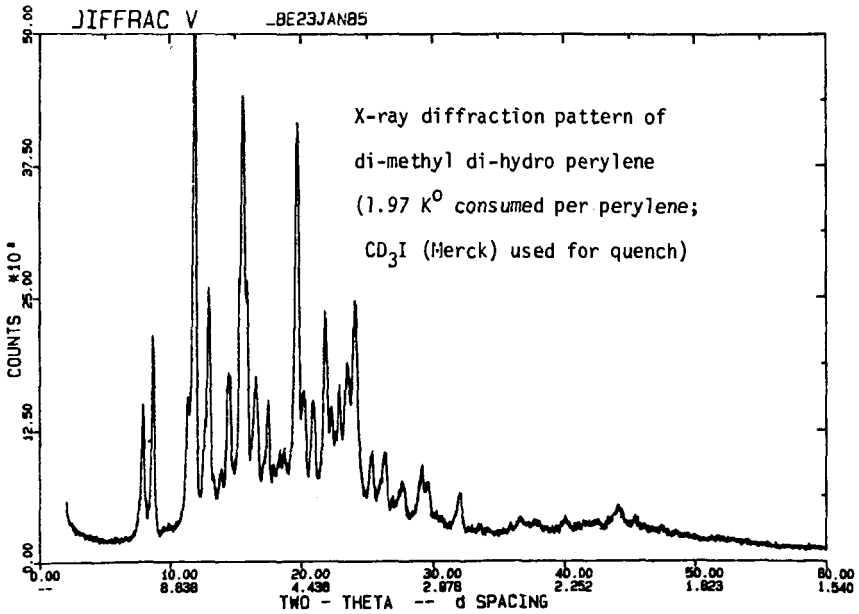

FIGURE 3. XRD OF PERYLENE PRODUCT.

REACTIONS OF HYDROGEN DURING HYDROPROLYSIS PROCESSING OF HEAVY ENDS

by

James W. Bunger
Department of Fuels Engineering
University of Utah
Salt Lake City, Utah 84112-1183

INTRODUCTION

When heavy oils are subjected to pyrolysis in the presence of hydrogen, cracking to lower molecular weight compounds is accelerated and production of coke is inhibited compared to the case in which an inert atmosphere is present.[1-3] It has previously been reported that at very high hydrogen concentrations (>10^3 vol/vol) production of coke is virtually eliminated.[4] Others have reported that the presence of hydrogen improves liquid hydrogen yield when cracking residual oils.[5]

In the course of our investigations considerable attention has been given to changes in molecular structure and product characteristics. By comparing results with those obtained in the absence of hydrogen an understanding of the reactions of hydrogen is beginning to emerge. In this paper, an attempt is made to categorize the major reactions of hydrogen and to justify these reactions in terms of the observations made.

Chemical Effects Observed in Hydropyrolysis

Reduction of Coke Formation

The most obvious and perhaps most important effect of hydrogen is the inhibition of coke forming reactions. In hydropyrolysis of tar sand bitumen, which yields 16-20% coke in delayed coking processes, conditions exist in which virtually no coke is produced.[2-4] Representative results are shown in Table 1.

Table 1

Product Yields from Coking and Hydropyrolysis of Tar Sand Bitumen

	SUNNYSIDE BITUMEN		ATHABASCA BITUMEN	
	Coking	Hydropyrolysis (Coiled Tube)	Coking	Hydropyrolysis (Verticle Tube)
	WEIGHT PERCENT YIELDS			
Gas	8.9	27.0	7.5	1.7
Liquid	71.0	73.0	76.5	93.7
Coke	20.1	NIL	16.0	4.6

When model compounds are subjected to hydropyrolysis there is no evidence for products of higher molecular weight than the starting material.[2-6] Thus, addition and condensation reactions are completely inhibited. The chemistry of coke forming reactions and the inhibition of these reactions during hydropyrolysis are discussed in greater detail in a companion paper.[7]

Reduction of Dehydrogenation of Naphthenes

It has also been observed that during hydropyrolysis little change in total aromatic carbon occurs (C_a = .22 for products and .19 for feedstock) while coking dramatically increases the aromatic carbon (C_a = .30).[8] It has also been observed that hydropyrolysis products possess a higher fraction aromatics and lower content of diaromatics than do coker products[3] (see Table 2).

Table 2

Compound Type Analysis of Total Products*
From Asphalt Ridge Bitumen

	Coking	Hydropyrolysis
Saturates	52.4	59.4
Monoaromatics	8.4	12.0
Diaromatics	6.1	4.4
Poly-Polar Aromatics	33.0	24.1
Gas/Liquid/Coke (weight percent)	4/81/15	17/83/0
Avg. M.W. Liquids	321	336

*Values given are on a feed basis; gas production is lumped into the saturates portion and coke production is lumped into the poly-polar aromatics fraction.

From the data above it is not possible to tell whether the principal effect of hydropyrolysis is to inhibit the denydrogenation of naphthenes to form aromatics or that hydrogenation of condensed aromatics to form monoaromatics is occuring. As will be shown below both appear to be happening. NMR data taken on an Athabasca bitumen and the liquid products from hydropyrolysis (93% yields) suggests that the fraction of monoaromatic carbon increases with hydropyrolysis processing. For the Athabasca case the fraction aromatic carbon (fa) declines from 0.35 t 0.28 while the fraction aromatic hydrogen (H_a) increases from .04 to .05, clearly showing lower levels condensation and/or a lower degree of alkyl substitution.

Hydrogenation of Aromatics and Olefins

The observation that total aromatic carbon remaines virtually constant (or in some cases declines) while the distribution shifts from polycondensed aromatics toward monaromatics strongly suggests that polycondensed aromatics are being hydrogenated. In hydropyrolysis where coke formation is small the amount of polyaromatics in the feed that can be accounted for by loss to coke is limited.

In an attempt to ascertain whether or not aromatics are in fact being hydrogenated during hydropyrolysis, a mixture of 5% naphthalene in n-hexadecane was hydropyrolyzed at 540°C and 2000 psig H_2 and 30 sec residence time. Approximately 6% of the naphthalene was converted to tetralin. The identity of tetralin was confirmed by mass spectroscopy. Calculations of the thermodynamic equilibrium between saturates and aromatics reveal that only the mono-aromatics are strongly favored at these conditions. In the tetralin-naphthalene system and at the reaction conditions given the equilibrium concentration for tetralin is 0.3 mole fraction (in the absence of cracking of tetralin).

As with aromatics there is also a strong tendency to hydrogenate olefins. It has previously been reported[1,2] that olefins content is reduced in hydropyrolysis by as much as 50-80% compared to thermal cracking in an inert atmosphere. At higher pressure Z 2000 psig H_2 terminal olefins are virtually absent from the products of hydropyrolysis of n-hexadecane. It is noteworthy that in the experiment in which naphthalene was added to n-hexadecane the C_5-C_{15} paraffins to olefin ration declined to 3.0 compared to 5.7 for the case when n-hexadecane was hydropyrolyzed in the absence of naphthalene. This data suggests that aromatics compete with olefins for available hydrogen during saturation.

An interesting effect of the presence of naphthalene was to reduce the conversion of n-hexadecane at constant reaction conditions. When other unsaturated bonds such as olefin, carbonyl, or sulfoxide are added to the system a similar reduction in the level of cracking of n-hexadecane is observed[11]. Also, the greater the concentration of unsaturated bonds added, the greater is the production of olefins from n-hexadecane. This inverse relationship between concentration of unsaturated species and cracking rates of saturated species clearly suggests the existence of competitive reactions.

Promotion of Dealkylation

Hydropyrolysis appears to promote dealkylation reactions. Evidence for dealkylation at the ring can be seen from NMR data for the Athabasca case in which the fraction of aliphatic hydrogen alpha to an aromatic ring is reduced from 0.27 to 0.21. In coking, by contrast, dealkylation at the benzylic position is generally favored and the fraction of aliphatic hydrogen alpha to the ring tends to increase. Further, when pentane soluble maltenes from tar sand bitumen are subjected to hydropyrolysis the products are shown to contain 11% pentane-insoluble material.[8] This material is characterized as highly dealkylated material (H/C Z 0.9).

In an attempt to examine the chemistry of dealkylation, a mixture of 20% n-propyl benzene in n-hexadecane was subjected to hydropyrolysis at 2000 psig, 540° and 30 sec residence time. In order to separate the hydrogen pressure effects from the total pressure effects a second run was made with a partial pressure of 500 psi H_2 and 1500 psi He. Reaction conditions were otherwise identical. Results are shown in Table 3. As the concentration of aromatics is increased or the partial pressure of hydrogen is decreased, the level of conversion of both reactants is decreased. These results are consistent with those stated above, which shows that hydrogen accelerates the cracking reactions.

The results show that dealkylation at the ring position is promoted by the presence of hydrogen. The ratio of benzene to toluene varies directly with the partial pressure of hydrogen. These results are consistent with hydrodealkylation chemistry in which attack by a hydrogen atom at an ipso position results in cleavage of the alkyl-aromatic bond.

The pressure of aromatic to the system reduces the level of olefin saturation but not as much as a reduction in the partial pressure of hydrogen. These results are consistent with those obtained when naphthalene was added to the system. Thus, the aromatic ring appears to act as a sink to deplete the population of $H^{\bullet}$ in the reaction zone.

Hydropyrolysis Promotes a Broader Distribution of Products

The reduction in the C_4/C_1 ratio seen in Table 3 is consistent with an increasing thermal effect and decreasing hydropyrolytic effect. It is noteworthy that in hydropyrolysis C_3-C_4 gas production is enhanced while methane production is greatly reduced in relationship to coking[3] (at constant conversion). Further, the boiling point distribution of hydropyrolyzate is broader than with coker distillate from the same feed.[4] This is illustrated in Figure-1 which also compares the boiling point distribution of hydropyrolysis products with virgin crude oil. These results suggest that hydrogen plays on important role in free radical transfer (propogation) reactions resulting in a wider variety of cracking events than is the case with coking.

Table 3

Hydropyrolysis of n-Propylbenzene in n-Hexadecane

	Feedstock (Atmosphere)		
	n-hexadecane (H_2)	20% n-propyl benzene in n-C_{16} (H_2)	20% n-propyl benzene in n-C_{16} ($.25H_2$, $.75H_e$)
Conversion			
n-hexadecane	88.5	83.6	79.4
n-propyl benzene	---	31.0	26.6
	Product Yield (percent of n-propyl benzene converted)		
Product			
benzene	0	13.7	8.9
toluene	0	14.7	16.6
styrene	0	12.7	6.4
ethylbenzene	0	52.8	52.4
(unidentified	100	6.1	15.7
or not listed)	100	100.0	100.0
	Other Indicators		
C_8 Paraffin/Olefin	4.3	3.2	0.9
C_4/C_1	2.1	1.9	1.5

Reactions of Hydrogen

Molecular Hydrogen - The principal reaction of molecular hydrogen is as a reactant in the general metathesis reaction [1] (activation energies given are for the alkyl radical):

$$R\cdot\ (\text{or } Ar\cdot) + H_2 \underset{E_a \approx 9\ \text{K cal/mol}}{\overset{E_a \approx 14\text{-}15\ \text{K cal/mol}}{\rightleftharpoons}} RH\ (\text{or } ArH) + H\cdot \qquad \text{Reaction 1}$$

The significance of this reaction to hydropyrolysis cannot be overstated. It is through this reaction that free radicals are saturated. Equally important is the fact that hydrogen atoms are produced. Production of hydrogen atoms is critical to hydropyrolysis chemistry and the mechanism shown in the above reaction provides a means for production of hydrogen atoms at modest temperatures. Good contact between hydrogen and the free radicals, is important and homogeneous, vapor-phase reaction conditions favor this reaction. Hydrogen abstraction reactions are thought to occur at appreciable rates for alkyl hydrogen at 410° and for aromatics at about 425°C during coking.[7] On this basis and considering relative bond dissociation energies, it may be predictd that the forward metathesis reaction accurs at significant rates at temperatures above about 435°C. Indeed many hydrovisbreaking processes operate at temperture regimes just above this temperature [9] and the metathesis reaction is probably important to these processes as well.

The effect of the metathesis reaction can be seen in the observations listed above. First, dehydrogenation of naphthenes is reduced because molecular hydrogen serves the function of providing hydrogen to satuarate free radicals. Second, aryl free radicals are saturated before they can add to arenes forming thermodynamically stable aryl-aryl bonds. The reaction of aryl radicals with arenes is thought to be an elementary step in coke formation[7] and suppression of coke is due in part to reaction-1. Third, alkyl radicals are saturated before they can undergo β-scission and overcrack. There is actually a reverse arguement to this latter point in which the reverse of reaction-1 results in accelerated cracking. The net effect is that molecular and atomic hydrogen act, in effect, as vehicles for the transfer of free radical resulting in a more random point of cracking than is experienced with thermal cracking. Thermal cracking is more energetically controlled and as a result the products tend to be more selectively distributed between very light gases or heavy gas oils. In hydropyrolysis, significant amounts of LPG and middle distillate are generated as discussed above.

Atomic Hydrogen

Evidence for the presence of atomic hydrogen in hydropyrolysis is clear from the observations presented. Based on reaction-1, the population of hydrogen atoms would tend to increase as the overall population of free radicals increases and as the concentration of hydrogen (gas/oil ratio) increases. Reactions of atomic hydrogen can be grouped into two general types: (i) free radical hydrogen addition and (ii) free radical hydrogen abstraction reactions.

The hydrogen addition reactions are characterized by attack on unsaturated bonds, olefins and aromatics, to form alkyl or cyclohexadienyl-type radicals, respectively. These radicals subsequently undergo metathesis

reactions with hydrogen to saturate the radical and regenerate the hydrogen atom. The presence of unsaturated bonds tends to decrease the overall population of H• as evidenced by the reduced cracking rates for n-hexadecane when unsaturated bonds are present.

If hydrogen adds to a substituted aromatic carbon it is probable that ring dealkylation will occur due to the relative strength of the C-H bond vs. the C-C bond. The same effect is not true for aryl-aryl bonds however, which are thought to be stronger than the corresponding C-H bond.[10] If hydrogen adds to an unsubstituted aromatic carbon and a hydrogen is eliminated before the free radical can be hydrogenated an unproductive event occurs which cannot be observed in the products. This reaction may, however, account for the sink for H• observed when aromatics are present.

Hydrogen abstraction reactions are also important to hydropyrolysis results. Hydrogen abstraction, or the reverse of reaction-1, results in a free radical which can subsequently undergo β-scission to crack the molecule in two. The fact that the rate of cracking of n-hexadecane depends upon the H• concentration testifies to the importance of this reaction. The broad distribution of the products as well as the relatively high concentration of LPG range gases indicates that a less selective and more random cracking is occurring. This is probably due to the less discriminating nature of H• abstraction vs. free radical abstraction in the absence of hydrogen.

SUMMARY

In summary, both molecular hydrogen and atomic hydrogen are reactants in hydropyrolysis of residual oil. The reactions of hydrogen postulated can account for the major differences between pyrolysis in an inert atmosphere and hydropyrolysis. Coke is inhibited through saturation of aryl radicals by molecular hydrogen and through hydrogenation of vinyl aromatics (and olefins) by addition of H•. Cracking rates are enhanced through hydrogen abstraction reactions. Product distribution is broadened through less energetically discriminating free radical formation. Hydrogen also seems to act as an effective heat transfer fluid and as a diluant to inhibit bimolecular addition or condensation reactions relative to unimolecular cracking reactions. In time, as the relative kinetics of these reactions become better understood specific process development routes may become apparent. The appliciblity of hydropyrolysis to upgrading feedstocks from a variety of sources and compositions should likewise become more apparent.

References

1. J. S. Shabtai, R. Ramakrishnan, A. G. Oblad, "Thermal Hydrocarbon Chemistry," Adv. Chem. Ser., 183, 297-328, (1979).

2. R. Ramakrishnan, "Hydropyrolysis of Coal Derived liquid and Related Model Compounds," Ph.D. dissertation, University of Utah, 1978.

3. J. W. Bunger, "Processing Utah Tar Sand Bitumen," Ph.D. dissertation, University of Utah, 1978.

4. J. W. Bunger, D. E. Cogswell, R. E. Wood and A. G. Oblad, "Hydropyrolysis: The Potential for Primary Upgrading of Tar Sand Bitumen," Chpt. 25, Oil Shale, Tar Sands and Related Materials, H. C. Stauffer, Ed., Adv. in Chem. Ser. 163, Amer. Chem Soc., (1981) 369-380.

5. B. Schuetze and H. Hofmann, "How to Upgrade Heavy Feeds, Hydrocarbon Processing 63, (2), 75-82, (1984).

6. U.S. Patent # 4,298,457, Nov 3, 1981.

7. J. W. Bunger, "Inhibition of Coke Forming Reactions in Hydropyrolysis of Residual Oils," submitted to Preprints, Div. of Petro. Chem. and Preprints Div. of Fuel Chem. for publication in the procedings of the National Meeting of the Amer. Chem. Soc., Chicago, Sept. 8-13, 1985.

8. J. W. Bunger and D. E. Cogswell, "Characteristics of Tar Sand Bitumen Asphaltenes as Studied by Conversion of Bitumen by Hydropyrolysis," Chpt. 13, Chemistry of Asphaltenes Adv. in Chem., Series 195, Amer. Chem. Soc., 219-236 (1981), J. W. Bunger, N. C. Li, Eds.

9. J. W. Bunger and G. Neff, unpublished data, University of Utah, 1984.

10. M. Szwarc, "Energy Value for the Central C-C Bond in Diphenyl," Nature 161, 890 (1948).

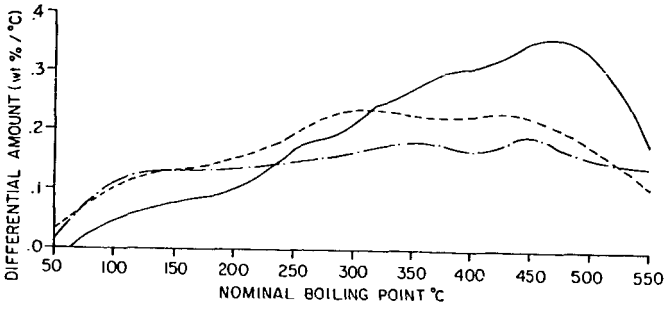

Figure 1. Distillation curves for selected tar sand products and Wilmington crude oil: Asphalt Ridge coker distillate (97% distillable, 27° API) (——); Asphalt Ridge hydropyrolysis condensables (85% distillable, 25° API) (– – –); Wilmington, CA crude oil (65% distillable, 20° API) (– · –).

HYDROGEN INCORPORATION IN RESIDUUM CONVERSION

Samil Beret and John G. Reynolds

Chevron Research Company, Richmond, California 94802-0627

Introduction

In the last ten years there has been a large increase in residuum hydroconversion capacity in the United States and overseas. This expansion was derived from the expectation that the spread in market values between the high sulfur fuel oil and the light transportation fuels would increase to support the large investments required for these conversion facilities.

The reason for residuum conversion is simple--increasing the hydrogen-to-carbon ratio (H/C) and lowering the molecular weight generates marketable distillate products. Figure 1 illustrates this qualitatively. It shows a Stangeland (1) chart for pure paraffins, aromatics, and a number of petroleum fractions. The residuum is located to the right at higher carbon numbers. From a knowledge of the boiling points of pure paraffins and polycyclic aromatics, extra guidelines are drawn to represent approximate boiling points. This chart is very useful because it shows the extent to which carbon number must be reduced or hydrogen added to generate the desired light stocks. To correct this hydrogen imbalance, various residuum conversion processes either add hydrogen or reject carbon. A partial list of conventional residuum conversion options is shown in Table I. Thermal and extractive processes generally reject carbon while hydroconversion schemes add hydrogen.

Residuum Hydroconversion

The choice of residuum conversion process depends on the unique set of circumstances for each refinery, for example, feedstocks, existing equipment, and capital constraints. If the objective is to produce a distillate product slate, then hydroconversion can serve as an efficient process for conversion of lower value hydrocarbon feedstocks and heavy residuum to high quality distillate products.

Figure 2 shows a residuum hydroconversion refinery in its basic form is shown in Figure 2. The residuum feedstock is partially converted to C_4-1000°F distillate liquids and C_1-C_3 gas. The hydrogen necessary for the operation is supplied from an outside source. The hydroconversion reaction system may be thermal, catalytic, or may consist of a series of thermal and/or catalytic steps. Operating conditions, nature of the catalysts, and various processing schemes

Encl. - Tables I-IV
Figure 1 (RE 832399)
Figures 2-6

(for example, "recycle") all affect and define the process severity. The process severity in turn affects conversion, product slate, volumetric expansion, and hydrogen consumption.

It should be noted that the operating conditions, catalysts, and processing techniques vary considerably among the commercial hydroconversion processes; but as shown in Figure 3, both the total hydrogen consumed and the residuum conversion increase invariably with increasing process severity. Figure 3 represents hydrogen consumption and conversion data for Arabian Light residuum processing at different sulfur levels (2). This representation is based on Chevron-designed catalysts operating at conditions capable of giving run lengths of at least six months. For maximum conversion, operation at high severities is required.

In this paper, we use total conversion to distillates and the hydrogen consumed by the process as relative measures of process severity. Admittedly, these are relative definitions, but they allow evaluation of hydroconversion processes in general without regard to the details unique to each process (e.g., catalyst, reactor type, temperature, etc.). For a given example, referring to Figure 3, the relative hydrogen consumed at hydrocracking conversion depends upon the desired S specification of the product. Because we are only interested in the relative hydrogen consumed, knowledge of the specific process details are not necessary.

Under the usual hydroconversion conditions (elevated temperatures and pressure, high hydrogen-to-feed ratios, and high activity catalysts), many reactions with hydrogen proceed simultaneously. These include: hydrocracking, aromatization, hydrogenation, condensation, hydrodesulfurization, hydrodenitrification, deoxygenation, demetalation, and isomerization. However, these reactions do not all occur at equal ratios. Judicious selection of catalysts and processing conditions favor one or more of these reactions over others. One can learn more about the relative impact of these reactions by studying the stoichiometry of hydrogen incorporation.

Stoichiometry of Hydrogen Reactions

We used the same analytical approach as Finseth et al. (3) in formulating the hydrogen/residuum reactions. Finseth and his colleagues were interested in coal conversion chemistry and the role of hydrogen during coal liquefaction. However, the same approach with some modifications can be used to study the role of hydrogen during residuum conversion. The fact that it is difficult to understand the molecular level mechanisms of hydrogen incorporation should not preclude understanding the overall chemistry.

As Finseth, hydrogen/residuum reactions are classified into six categories:

1. Hydrogenation and dehydrogenation.
2. Hydrocracking and (its reverse) condensation.

3. Isomerization and hydrogen exchange.
4. Desulfurization.
5. Denitrification and deoxygenation.
6. C_1-C_3 gas production.

This grouping is done basically to generalize the stoichiometries of very high number of reactions. Once the stoichiometry is established then it is possible to devise a technique which discriminates among these six hydrogen reaction routes.

We used ^1H and ^{13}C NMR to determine the hydrogen distribution during hydrogenation/dehydrogenation reactions. We have seen only aromatization as the dehydrogenation reactions. Hydrogenation consumes one hydrogen atom for every carbon reduced. For example, if a residuum sample containing 25 aromatic, 75 aliphatic carbons is hydrogenated to 20 aromatic, 80 aliphatic carbons, ^{13}C NMR should detect the change in aromaticity from 25% to 20%.

The second category of reactions, cracking/condensation, is more difficult to determine. No satisfactory method is available to count the number of cracking reactions occurring during residuum conversion. However, if all of hydrogen involved in the other five categories of reactions are accounted for, then we can calculate the hydrogen consumed due to cracking by difference.

The total change in hydrogen content can be determined by classical elemental analysis.

The third class of reactions, isomerization/exchange, does not affect net hydrogen incorporation. Therefore it is not considered here.

The remaining three categories are basically bond scission reactions eliminating heteroatoms and forming C_1-C_3 gases. Gas production is easily measured and analyzed with commonly available analytical instruments. Since two hydrogens are incorporated for every molecule of C_1-C_3 formed (mostly due to alkyl chain cracking reactions), these gas analyses provide a good estimate of hydrogen consumed in gas formation.

It is difficult to quantify accurately hydrogen consumed due to heteroatom (S, N, O) removal due to the multiplicity of reactions. For simplicity, we assume sulfur in the residuum occurs as thiophenic. Therefore, two hydrogen atoms are incorporated into the residuum for each sulfur removed.

We also assume nitrogen as pyrrolic and oxygen as a mixture of carboxylic and phenolic. Therefore, one hydrogen atom is incorporated into the residuum for each N or O removed.

Even though carboxylic acid amides and other compounds have been detected in residua (4), the above assumptions should not affect the calculations significantly because no residua studied contained more than 2% N, O. Furthermore, probably any deviations in

stoichiometry due to very large number of reactions involving heteroatoms tend to cancel each other and are therefore self-correcting.

Coking reactions produce insoluble organic material which is not accounted for in the above analysis, primarily reducing the amount of measurable aromaticity of the processed products. In hydroconversion, these levels were all under 1%, and generally less than 0.5%. These levels should have little affect on the calculations.

Therefore, using ^{1}H and ^{13}C NMR, as well as elemental analysis and quantitative gas analysis, one can determine the net hydrogen incorporated due to each of the six categories of reactions. Furthermore, if these determinations are coupled to process parameters, they greatly enhance the understanding of residuum conversion chemistry and hydrogen utilization. With these goals in mind, we conducted residuum hydroconversion experiments at different process severities and analyzed both the liquid and gas products as well as the feed extensively using the technique described here.

Experimental

Three California residua (designated A, B, and C) were obtained by single-plate distillation of the corresponding crude.

The ^{13}C NMR and ^{1}H NMR spectra were recorded on either a Bruker CXP 300 or WH-90 spectrometers. The samples were prepared as dilute solutions in deuterated chloroform with tetramethylsilane as reference. Integrations were performed by the spectrometers, and the ratios were calculated by hand. The NMR spectra were interpreted by the method of Young and Gayla (5). No olefins were observed in spectra. Gadolinium tris(1,1,2,2,3,3-heptafluoro-7,7-dimethyl-4,6-octanedione) was added as a relaxation agent to ensure accurate integration of the aromatic region. The aromatic region was integrated between 110-180 ppm. The aliphatic region was integrated between 0-60 ppm. Each were calculated as percentage of the total integrated area (minus the solvent peaks).

Total aromatic content of liquid is adjusted for the composition of the gas.

Elemental analyses were performed by Chevron Research Company Analytical Department. C,H were done by Carlo Erba, N by either Mettler (Dumas) or Dohrmann (ASTM D 3431), S by Dohrmann (ASTM D 3120), and metals by either X-ray fluorescence or inductively coupled plasma emissions. Boiling point distribution was determined by thermogravimetric analysis (TGA). Gas composition was determined by gas chromatography.

Hydroconversion Experiments

Hydroconversion experiments were conducted in a flow reaction system using the heavy residua from California crudes. Inspections of these residua are given in Table II. These residua are very rich in nitrogen, sulfur, and metals. Arabian Heavy 730°F+ oil

is included for comparison. They represent a big challenge for the refining industry in the coming decades.

These feedstocks were processed at different severities using different sets of operating variables such as temperature, pressure, residence time, hydrogen circulation rate, and catalyst. Total hydrogen consumption varied from 600-2100 SCF/bbl of feed. Residuum conversion (1000°F+/1000°F-) ranged from 50-95%. Hydrogen consumption, 1000°F+ conversions, and the percent aromatic carbon are summarized in Table III.

Hydrogenation, Cracking, and Process Severity

The number of hydrogen atoms incorporated per 100 carbon atoms is compared in Figure 4 for Residuum A, 850°F+ cut point at three different conversion levels (Table III: Runs 2A, 2B, and 2C). With increasing process severity, the number of hydrogen atoms consumed due to cracking and gas formation reactions appears to increase linearly. The bulk of the hydrogen is used to cap the ends of cracked fragments. Since two hydrogens are incorporated for every molecule of C_1-C_3 gas formed, it is natural that hydrogen consumed in gas formation reactions also increases with increasing conversion. On the other hand, the net number of hydrogens involved in aromatic saturation remains constant in all three experiments. This may be due to all three experiments were at high levels of 1000°F+ conversion. At these high conversion levels, incremental conversion probably comes from cracking off alkyl branches from already hydrogenated species.

In Figure 5, hydrogen incorporation into Residuum A 850°F+ is compared to that of Residuum A 650°F+. As shown in Tables II and III, 850°F+ is more aromatic and contains more heteroatoms. Due to its hydrogen deficient nature relative to the 650°F+, the 850°F+ consumes more hydrogen at roughly equal process severities. Comparing Experiments 1A to 2C in Figure 5, we see that cracking reactions consume more hydrogen with 650°F+ compared to the 850°F+. With regard to hydrogenation, this order is reversed, probably because some of the hydrogen deficient species in the 850°F+ have to be hydrogenated before they crack. Due to the high conversion, the number of hydrogens involved in capping the cracked fragments far exceeds the hydrogens involved in net aromatic saturation.

In Figure 6, we compare two hydroconversion experiments conducted with Residuum B 650°F+. Experiment 3A was a thermal treatment of the feedstock, while the Experiment 3B included a catalytic treatment. The effect of these process differences is very apparent in Figure 6. The number of hydrogens incorporated due to net hydrogenation reactions is negative (-1.8/100 carbons) during Experiment 3A. This suggests that at this particular processing condition, aromatization of the residuum is occurring, and it is providing some of the hydrogen consumed for cracking and other hydrogen consuming reactions. During Experiment 3B, under different processing conditions, there is no net aromatization (indicated by the number of

hydrogens incorporated in hydrogenation). In fact, aromatic saturation is the dominant reaction in this case, consuming more hydrogen than cracking. Figure 6 is a good example of how this technique can be used as a sensitive test of the effect of processing conditions on different reaction pathways.

This technique also reveals the sensitivity of hydroconversion to characteristics of the feedstock. In Table IV, comparing 1B to 4A, total number of hydrogens incorporated is roughly the same, 24 per 100 carbons. The gross hydrogen consumption is about the same, about 1600 SCF/bbl. However, the starting feedstocks are very different. In Experiment 4A, the feedstock was Residuum C 950°F+, which is very rich in aromatic carbon and hydrogen, but low in sulfur. (See Tables II and III.) On the other hand, the feed in Experiment 1B was Residuum A 650°F+, which is less aromatic but much higher in sulfur (relative to Residuum C 950°F+). Due to the hydrogen deficient nature of the Residuum C 950°F+, more of the hydrogen is consumed in hydrogenating the aromatic species than for Residuum A 650°F+. Since overall conversion is the same in both experiments, there was not that much difference in the number of hydrogens involved in cracking and gas make. However, substantially more hydrogen was used to remove sulfur from Residuum A 650°F+ compared to Residuum C 950°F+. Therefore, although the same number of hydrogens were involved in both experiments, the distribution of these hydrogen atoms were radically different.

Conclusions

This approach yields a detailed description of hydrogen incorporation during residuum hydroconversion. Character of the feedstock, processing conditions, and the catalyst all affect how hydrogen is incorporated into residuum matrix. The two dominant reaction routes are hydrocracking and hydrogenation.

Our data analysis suggests hydrogenation and hydrocracking reactions incorporate hydrogen equally at moderate process severities. At high severities, the bulk of the hydrogen is consumed by capping reactions of cracking fragments. Judicious selection of processing conditions favor one or the other.

The feedstock characteristics also influence hydrogen incorporation. With aromatic feedstocks, hydrogenation reactions compete equally with hydrocracking for hydrogen. With less aromatic feedstocks, hydrocracking dominates over hydrogenation reactions.

The technique we presented here is useful in relating these processing conditions to understanding of the overall chemistry and exploiting these processing conditions to tailor the process and the products to the desired product slate.

Acknowledgments

We thank Don Wilson and Mike Kang of Chevron Research Analytical Department for recording the NMR spectra, Thomas F. Finger for sample workup.

References

(1) O'Rear, D. J.; Frumkin, H. A.; Sullivan, R. F.; "Refining of Syncrudes from H-Coal Liquefaction Process," 47th Meeting of American Petroleum Institute, New York, May 1982.

(2) Bridge, A. G.; Scott, J. W.; Reed, E. M.; Oil and Gas Journal, May 19, 1975.

(3) Finseth, D. H.; Bockrath, B. C.; Cillo, D. L.; Illig, E. G.; Sprecher, R. F.; Retcofsky, H. C.; and Lett, R. G.; ACS, Div of Fuel Chem., Preprints, 28 (5), 17-25, 1983.

(4) McKay, J. F.; Harnsberger, P. M.; Erickson, R. B.; Cogswell, T. E.; and Latham, D. R.; Fuel, 60, 17-26, 1981.

(5) Young, D. C.; and Galya, L. G.; Liq. Fuels Tech.; 2 (3), 307-326, 1984.

:pgb

FIGURE 1
THE STANGELAND CHART FOR FUELS

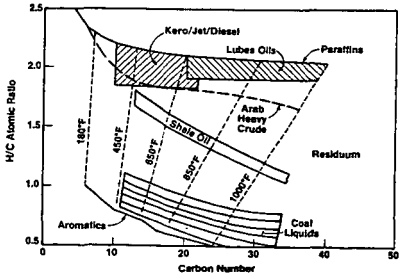

TABLE I

RESIDUUM
PROCESSING OPTIONS

Thermal Processes

- Visbreaking
- Delayed Coking
- Fluid Coking
- Steam Cracking
- Partial Oxidation

Extractive Processes

- Solvent Deasphalting

Catalytic Processes

- Residuum FCC
- Residuum Hydroconversion

TABLE II

INSPECTIONS OF FEEDSTOCKS

	Arabian Heavy	Residuum A	Residuum A	Residuum B	Residuum C
Cut Point, °F+	730	650	650	850	950
Gravity, °API	11	9.8	5	9	4.2
N, %	0.3	0.8	1.1	1.1	1.0
S, %	4.6	5.7	5.7	4.2	1.2
H, %	10.7	10.6	10.1	10.6	10.2
C, %	84.1	82.0	81.5	83.7	85.3
H/C	1.53	1.55	1.49	1.52	1.44
Ni, ppm	24	109	139	115	165
V, ppm	88	274	359	197	75
Fe, ppm	4	0	14	3	75
C_7 Asphaltenes, %	8.4	12	15	10.1	7.6
Ramscarbon, %	14	13	16.8	13.7	20.2
1000°F+ Content, %	60	48	75	46	95

4-8-85

Chevron Research Company
Richmond, California
JGR/10

TABLE III

HYDROCONVERSION EXPERIMENTS

Exp. No.	Identification	Total Hydrogen, % Wt	Aromatic Carbon, %	1000°F+ Conversion, %	H_2 Consumed, SCF/Bbl of Feed
	Residuum A 650°F+				
1	(Feed)	10.6	22.5	-	-
1A	(Product)	12.7	20	95	2000
1B	(Product)	12.4	20.3	84	1530
	Residuum A 850°F+				
2	(Feed)	10.1	26.7	-	-
2A	(Product)	12.3	20.1	79	1660
2B	(Product)	12.3	20.4	82	1750
2C	(Product)	12.4	20.3	87	2050
	Residuum B 650°F+				
3	(Feed)	10.5	29.5	-	-
3A	(Product)	11.2	32	60	600
3B	(Product)	11.79	22.5	73	1100
	Residuum C 950°F+				
4	(Feed)	10.2	33	-	-
4A	(Product)	11.9	26	77	1600

TABLE IV

HYDROCONVERSION OF
RESIDUUM C 950°F+ VERSUS RESIDUUM A 650°F+

	Residuum C 950°F+	Residuum A 650°F+
Feed		
Aromatic C, %*	33.0	22.5
Aromatic H, %**	6.7	3.2
Experiment No.	4A	1B
H Atoms Incorporated/100 C		
Due to Cracking	9.9	11.9
Due to Hydrogenation	8.3	3.0
Due to C_1-C_3	3.5	3.8
Due to Heteroatom Removal	2.4	6.0
Total	24.1	24.7

*From ^{13}C NMR.
**From ^{1}H NMR.

Chevron Research Company
Richmond, California
JGR/10

4-8-85

FIGURE 2

GENERALIZED DIAGRAM
RESIDUUM CONVERSION REFINERY

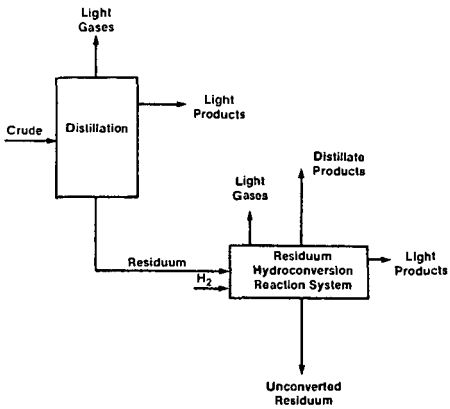

FIGURE 3

H_2 USAGE IN RESIDUUM PROCESSING*

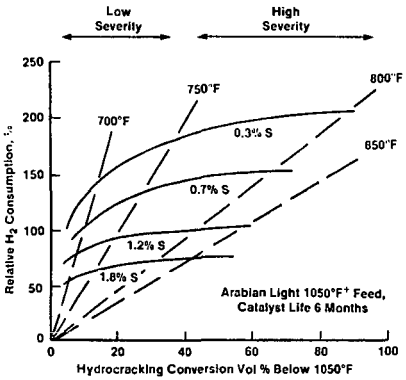

*From A. G. Bridge, J. W. Scott, E. M. Reed, The Oil and Gas J, May 19, 1975

FIGURE 4

HYDROCONVERSION OF RESIDUUM A 850°F+

Hydrogen Incorporation

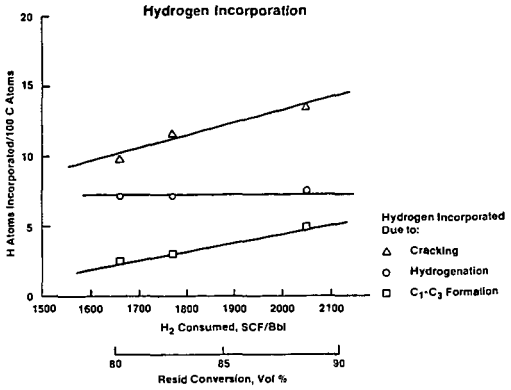

FIGURE 5

HYDROCONVERSION OF RESIDUUM A

Hydrogen Incorporation

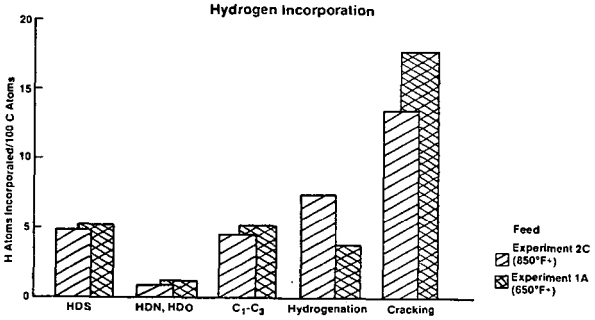

FIGURE 6

HYDROCONVERSION OF RESIDUUM B 650°F+

Thermal Treatment Versus Catalytic Treatment

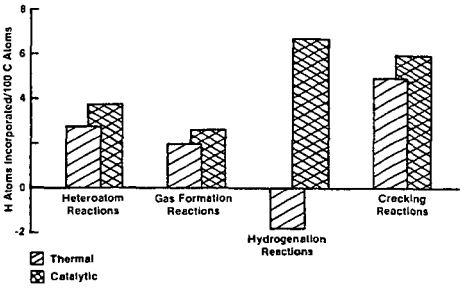

PETROLEUM ASPHALTENE THERMAL REACTION PATHWAYS

P.E. Savage, M.T. Klein, and S.G. Kukes*

Department of Chemical Engineering
and
Center for Catalytic Science and Technology
University of Delaware
Newark, DE 19716

*Research and Development Center
Phillips Petroleum Company
Bartlesville, OK 74004

INTRODUCTION

The industrial trend toward processing comparatively refractory heavy crudes and residua that can contain appreciable portions (10%-30%) of asphaltenes assures interest in their thermolysis. Most previous pyrolyses of asphaltenes have been oriented toward either elucidation of their structure (1,2) or the identification of fragmentation products and the dependence of their yields on pyrolysis temperature (3-6). Pyrolysis kinetics related to global product fractions (e.g. asphaltene, maltene, coke) have also been reported (2,7). Little information exists, however, about the variation of the yields of the individual constituents of the product fractions with both time and temperature. Further, operative thermolysis mechanisms, e.g. pericyclic or free-radical, are obscured in the complexities of the reactions of actual asphaltenes. The foregoing motivated the present investigation of the pyrolysis of both precipitated asphaltenes and an asphaltene model compound, pentadecylbenzene.

EXPERIMENTAL

The asphaltenes were isolated from an off-shore California crude oil via a standard procedure of precipitation with 40 volumes of n-heptane. Pentadecylbenzene (PDB), 99.4% by GC analysis, was obtained from Alfa Products and used as received.

Reactors

The isothermal, batch pyrolyses were at temperatures between 350°C and 450°C for times ranging from 5 to 180 minutes. Two reactors were used. The first, used in asphaltenes' thermolyses, consisted of nominal 3/8 in stainless steel capped Swagelok port connectors attached to the two ends of a union tee. A reducer connected the center port of the tee to a 12 in length of 1/4 in o.d. stainless steel tubing. A 1/4 in Whitey severe service union bonnet valve interposed in the tubing served as a shut-off valve and also allowed attachment of a gauge for measurement of pressure. The second reactor, used in model compound pyrolyses, was assembled from a nominal 1/4 in port connector and two 1/4 in caps.

Procedure

For the asphaltene thermolyses the reactors were typically loaded with 1 g of asphaltene and purged with argon. The shut-off valve was then closed, and the reactor plunged into a Tecam fluidized sandbath that had been preheated to the pyrolysis temperature. After the desired reaction time had elapsed the reactor was removed from the sandbath and immediately immersed in ice water to quench the reaction. After the reactor assembly had cooled and equilibrated at room temperature, the number of moles of gas produced during pyrolysis was estimated by measuring the reactor pressure. The gaseous products were subsequently analyzed by

gas chromatography. After removing the tubing and the shut-off valve, a small amount of phenylether was added to the reactor contents to serve as an external standard in the ensuing chromatographic analysis of the heptane-soluble products. The reaction products were next subjected to a series of solvent extractions (8) to separate and collect the pyrolysis product fractions which were subsequently analyzed gravimetrically and by GC and GC-MS.

During a typical model compound experiment, reactors were loaded with about 50 mg of PDB and then 3 mg of diphenylmethane was added to serve as an internal standard in the chromatographic analysis. After purging with argon, the reactors were sealed, immersed in the preheated sandbath, and after the desired reaction time had elapsed, removed from the sandbath and quenched in cold water. Once cool, the reaction products were collected in acetone and analyzed by GC.

RESULTS AND DISCUSSION

Asphaltene Thermolysis

Asphaltene pyrolysis products and global kinetics are summarized in Table 1, which lists, for reactions at 350, 400 and 450°C, respectively, holding time, product identification, product yields, and the apparent first order rate constant for asphaltene decomposition.

Pyrolyses at 350°C yielded gas, maltene (heptane-soluble), and unreacted asphaltene (heptane-insoluble, benzene soluble) product fractions. Coke (heptane-insoluble, benzene-insoluble) did not form, and mass balance closure averaged 97%. The ultimate asphaltene conversion was less than 10%. Within the product fractions listed above, the most abundant of the individual products were the light nonhydrocarbon and hydrocarbon gases H_2S, CO_2, CH_4, C_2H_6, C_3H_8, n-C_4H_{10}, and n-C_5H_{12}. The maximum total gas yield observed was about 1.0% after 150 min. The maltene fraction yield was about 10% by weight of the original asphaltene after 150 min at this temperature. No individual product constituted a major portion of the maltene fraction but a series of n-paraffins was identified with each present in trace amounts.

Asphaltene thermolysis at 400°C produced coke in addition to gas, maltene, and asphaltene fractions. Mass balance closure varied from 79% to 98%. Major gaseous products at 400°C were H_2S, CH_4, C_2H_6, C_3H_8, nC_4H_{10}, and nC_5H_{12} along with lesser amounts of CO_2 and C_2H_4. The n-alkanes up to C_{26} and various cycloalkanes were the most abundant products in the maltene fraction at this temperature. The single-ring aromatics toluene and the xylenes were also detected in smaller proportions.

Figure 1a summarizes the temporal variation of the yields of pyrolysis product fractions at 400°C. Maltenes were more abundant than gases at all times, and the nearly discontinuous rate of generation of coke at 30 min coincided with rapid asphaltene conversion. Note that during this period of apparently rapid asphaltene reaction the yields of gas and maltene did not increase dramatically.

Figure 1b shows the effect of reaction time on the yield of the major gaseous products. H_2S was once again the major product and its yield reached an asymptotic value of about 18 mg/g asphaltene after 120 min. This represents about 23% of the sulfur content of the original asphaltene.

Figure 1c depicts the temporal variations of selected n-paraffins at 400°C. The yields of each alkane were nearly equal initially, hut at longer times yield decreased as carbon number increased. Note that eicosane and tetracosane exhibit maximum yields. This behavior indicates that these alkanes underwent secondary decomposition.

Asphaltene pyrolysis at 450°C produced gas, maltenes, coke, and unconverted asphaltene. Mass balances ranged from 60% to 74%. Asphaltene conversion, to predominantly coke, was rapid, and was complete after

30 min. The major constituents of the gaseous fraction were saturated hydrocarbons along with H_2S, and the identified maltenes included cyclopentane, methylcyclopentane, methylcyclohexane, toluene, cyclohexane, xylenes, naphthalene, and C_5 to C_{26} n-paraffins.

For pyrolysis at 450°C, the proportions of the product fractions at 90 min aligned in the descending order of coke, gas, and maltene. Within the gas fraction H_2S was a major product, and its nearly constant yield of $\approx$16 mg/g was of the same magnitude as the yields of methane and ethane. The yields of saturated hydrocarbon gases increased steadily with time even after 30 min where asphaltene conversion was complete. Thus in addition to primary routes from the asphaltene, light hydrocarbon gases were also produced hy secondary reactions of the maltenes and/or coke.

Pyrolysis Pathways

Petroleum asphaltenes are generally considered to comprise peri-condensed aromatic units linked by aliphatic, naphthenic, or heteroatomic functionalities. The peripheries of these aromatic sheets are highly substituted by similar moieties (9-12). The present results combine with the foregoing interpretation of asphaltene structure to permit resolution of asphaltene pyrolysis pathways as well as the secondary reactions of primary products. The heteroatomic gases H_2S and CO_2 were the major primary products observed from low temperature thermolyses and likely evolved from scission of low-energy thioether and carboxylic acid moieties respectively. Higher temperature primary products that arose from fragmentation of carbon-carbon bonds were hydrocarbon gases, cycloalkanes and paraffins. It would thus be consistent that the coke observed is actually the aromatic asphaltenic core stripped of its peripheral substituents. This strictly primary product evidently transforms from benzene-soluble to benzene-insoluble over a very small "window" of degradation (see Figure 1a).

The products in the maltene fraction clearly undergo secondary reactions. This is substantiated by the maximum maltene and total paraffin yields observed at 400 and 450°C (see Table 1) which are consistent with the notion of consecutive reactions.

Figure 2 is a summary of the reaction pathways suggested above. Primary asphaltene reactions produce asphaltenic core (coke), maltenes, and gas. Secondary reactions include fission of maltenes to lower molecular weight maltenes and gases, as well as reaction of the core to gas. Note that severe overreaction of primary products is not required to predict the formation of large quantities of benzene-insoluble solid materials. This network is similar to that proposed by Schucker and Keweshan (2) and supported by Speight and Pancirov (1).

Pentadecylbenzene Thermolysis

A summary of PDB pyrolyses at 375, 400, 425, and 450°C is given in Table 2, which lists typical data concerning holding times, major products yields, product groups (i.e. homologous series) yields, and observed first-order rate constants.

Pyrolysis of pentadecylbenzene (PDB) at 400°C yielded toluene, 1-tetradecene, n-tridecane, styrene, and ethylbenzene as major products. Also appearing at the longer reaction times in lower yields were a series of n-alkanes and α-olefins containing 6 to 14 carbon atoms as well as 1-phenylalkanes and phenylolefins (α-phenylalk-ω-enes) with alkyl chains containing 2 to 12 carbon atoms. Phenylbutene was not detected. The ultimate PDB conversion was 73% at 180 minutes. The Identified Products Index (IPI), herein defined as the total weight of all identified GC-elutable products divided by the weight of PDB initially loaded in the reactor, averaged 87%. The molar balance on aromatic rings averaged 86%. Charring occurred at this temperature.

Figure 3 illustrates the temporal variations of the yields of the major products at 400°C. Toluene was the most abundant product throughout the course of the reaction. The 1-tetradecene yield followed toluene

initially, but its yield decreased after reaching a maximum value at 60 minutes. The n-tridecane yield increased steadily at this temperature. During the initial 45 minutes of reaction, the styrene yield exceeded that of ethylbenzene, but after that time its yield decreased while the ethylbenzene yield continued to increase.

PDB thermolysis at 425°C resulted in products identical to those observed at the lower temperatures. The ultimate PDB conversion was 98% after 180 minutes. The IPI averaged 70% but ranged from 98% at short times to 43% at 180 minutes. Char was observed in the reactor, so this product, along with a few unidentified products, may account for the balance of the material. The aromatic ring molar balance averaged 86%.

Table 2 shows that toluene was once more the major product. For short times of less than 15 minutes, 1-tetradecene followed toluene in abundance. The other major products aligned in the order n-tridecane, styrene, and ethylbenzene. As the reaction progressed however, the tetradecene and styrene yields decreased rapidly, and the n-tridecane yield decreased less rapidly. At 150 minutes the product alignment was toluene (50.4%), ethylbenzene (17.1%), tridecane (5.0%), styrene (0.4%), and tetradecene (0.4%).

PDB Thermolysis Pathway

A previous pyrolysis of PDB at 450°C and 600kPa by Mushrush and Hazlett (13) revealed that the major products were toluene, styrene, n-tridecane, 1-tetradecene, and ethylbenzene. They reported no kinetic constants but did explain the observed product distribution on the basis of two-step Fabuss-Smith-Satterfield theory.

The present results, in agreement with Mushrush and Hazlett, show that the major products from PDB thermolysis at low conversion were toluene, 1-tetradecene, n-tridecane, styrene, and ethylbenzene. At higher conversions, a complete series of n-alkanes, α-olefins, phenylalkanes, and phenylolefins were produced. Based on the criterion of a positive initial slope on the molar yield vs. time curve, toluene, 1-tetradecene, styrene, and n-tridecane were all primary products. Ethylbenzene was also a primary product but was produced mainly via secondary reactions. Figure 4, which shows the selectivity of PDB to to each of the major products, confirms the above assignments and also suggests that toluene and 1-tetradecene were produced through the same reaction pathway since their selectivities at zero conversion were similar. Due to the rapid secondary reactions of styrene it is difficult to determine its selectivity at zero conversion. However, it does appear to be nearly that of n-tridecane. Thus styrene and n-tridecane are likely products of the same reaction path.

These experimental observations are summarized in the thermolysis pathway of Figure 5.

Kinetic Analysis

The overall order of the reaction of PDB was determined through a series of pyrolyses at 400°C wherein the initial reactant concentration ranged from 0.0044M to 2.27M. Overall "first order" rate constants corresponding to the initial concentrations studied are presented in Table 2. The concentration dependence of these rate constants indicate that PDB thermolysis was 1.07 order.

Having determined the thermolysis of PDB to be essentially first order, overall PDB decomposition Arrhenius parameters of E°=55,455 cal/mole, A=1.10 X 10^{14} sec^{-1} were determined.

PDB Thermolysis Mechanisms

Two possible operative PDB thermolysis mechanisms are illustrated in Figure 6 and include an intramolecular retro-ene mechanism and a free-radical chain reaction. These were both considered by Mushrush and Hazlett. The retro-ene reaction involves intramolecular hydrogen transfer to produce toluene and 1-tetradecene, whereas the free-radical reaction involves a sequence of elementary steps including initiation, hydrogen abstraction, β-scission, and termination.

Both mechanisms are consistent with the observed first order kinetics as well as the observation that toluene and 1-tetradecene initially formed in equal yields. However, the concerted mechanism alone fails to account for the formation of all observed products. In contrast, the free-radical formed from PDB via hydrogen abstraction at the α-carbon can undergo β-scission to produce styrene and n-tridecane, whereas the radical formed via hydrogen abstraction at the γ-carbon can similarly produce toluene and 1-tetradecene. Hydrogen abstraction at other positions can account for the formation of the minor products.

Rationalization of the selectivity to toluene exceeding that to styrene requires closer scrutiny. Whereas hydrogen abstraction is likely more rapid at the α-carbon (C-H bond energy $\approx$ 85 kcal/mole) (14) than the γ-carbon (ca. 95 kcal/mole) , thus suggesting formation of styrene preferably over toluene, the subsequent β-scission reaction step is more rapid for the γ-radical (C-C bond energy $\approx$ 67 kcal/mole) than the α-radical (ca. 80 kcal/mole). Clearly both of these competing effects influence the relative proportions of toluene and styrene in the products. The higher toluene selectivity observed experimentally thus indicates that the favorable energtics of the β-scission reaction outweigh the unfavorable γ-hydrogen abstraction. Note, however, that the high toluene selectivity can also be accounted for by an efficacious retro-ene mechanism occurring in parallel with a free-radical mechanism.

Implications to Asphaltene Reactivity

Plausible extension of these model compound results to asphaltene reactivity follows. The aromatic portions of petroleum asphaltenes, in contrast to PDB, contain more than a single ring. A hypothetical average structure based on 12 condensed aromatic rings has been proposed for Athabasca asphaltene (15). Furthermore, several of these large aromatic sheets are joined together in polymeric fashion by aliphatic, naphthenic, or heteroatomic linkages (9,10,12) to form an even larger asphaltene particle. Recall that to account for the high toluene selectivity of PDB, the proposed radical mechanism required that the alkylaromatic benzylic radical be an important intermediate and serve as a chain carrier. The analogous asphaltenic alkylaromatic radicals would be markedly larger and considerably less mobile than the benzylic radical. This diminished mobility will trap the radicals near their point of origin and thus constrain them to react with nearby atoms. Furthermore, at reaction conditions, asphaltene is considerably more viscous than PDB, thus further frustrating radical diffusion and transport. These likely diffusional limitations (size and viscosity), most significant at low asphaltene conversion, may increase the initial importance of intramolecular concerted reactions (e.g. retro-ene) and free-radical reactions with neighboring moieties in asphaltene relative to the model compound reactions.

CONCLUSIONS

1. Asphaltene pyrolysis includes primary reactions to its aromatic core, maltene, and gas product fractions. Components in each of these product fractions undergo secondary degradation to lighter products, gas, and presumably, char.

2. The present results indicate that the Schucker and Keweshan asphaltene structural model is a reasonable one, and that the observed yields of pyrolysis products and product fractions can be interpreted using their hypothetical average structure.

3. PDB thermolysis to toluene, styrene, n-tridecane, and 1-tetradecene as major products likely occurs by a β-scission-dominated set of radical steps, but may include a concerted component.

REFERENCES

1. Speight, J.G.; Pancirov, R.J. *Am. Chem. Soc. Div. Pet. Chem. Prepr.* **1983**, 28, 1319.

2. Schucker, R.C.; Keweshan, C.F. *Am. Chem. Soc. Div. Fuel Chem. Prepr.* **1980**, 25, 155.

3. Cotte, E.A.; Calderon, J.L. *Am. Chem. Soc. Div. Pet. Chem. Prepr.* **1981**, 26, 538.

4. Ritchie, R.G.S.; Roche, R.S.; Steedman, W. *Fuel* **1979**, 58, 523.

5. Moschopedis, S.E.; Parkash, S.; Speight, J.G. *Fuel* **1978**, 57, 431.

6. Strausz, O.P.; Jha, K.N.; Montgomery, D.S. *Fuel* **1977**, 56, 114.

7. Schucker, R.C. *Am. Chem. Soc. Div. Pet. Chem. Prepr.* **1983**, 28, 683.

8. Savage, P.E.; Klein, M.T.; Kukes, S.G. *Ind. Eng. Chem. Proc. Des. Dev.* accepted.

9. Speight, J.G.; Moschopedis, S.E. in "Chemistry of Asphaltenes" ; Bunger, J.W. and Li, N.C. Eds.; Am. Chem. Soc. Adv. Chem. Ser. **1981**, 195, 1.

10. Yen, T.F. in "Chemistry of Asphaltenes" ; Bunger, J.W. and Li, N.C., Eds.; Am. Chem. Soc. Adv. Chem. Ser. **1981**, 195, 39.

11. Yen, T.F.; Wu, W.H.; Chilingar, G.V. *Energy Sources* **1984**, 7, 275.

12. Yen. T.F. *Energy Sources* **1974**, 1, 447.

13. Mushrush, G.W.; Hazlett, R.N. *Ind. Eng. Chem. Fundam.* **1984**, 23, 288.

14. "CRC Handbook of Chemistry and Physics", 59th ed.; Weast, R.C., Ed.; CRC Press: Boca Raton, FL, 1978.

15. Speight, J.G. *Fuel* **1970**, 49, 134.

FIGURE 1: ASPHALTENE THERMOLYSIS 400°C

TEMPORAL VARIATIONS OF PRODUCTS

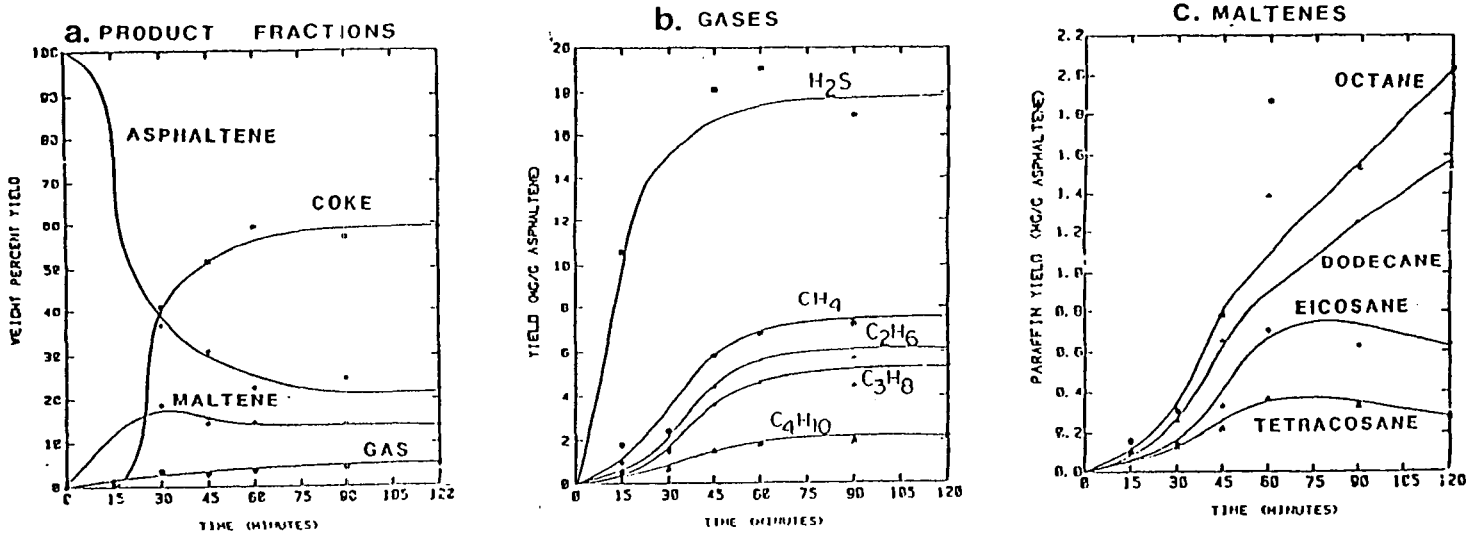

FIGURE 2: ASPHALTENE REACTION PATHWAYS

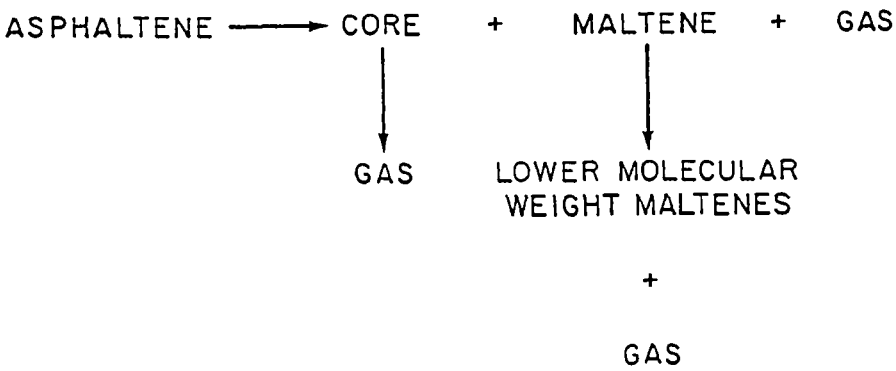

FIGURE 3

PENTADECYLBENZENE THERMOLYSIS 400 C

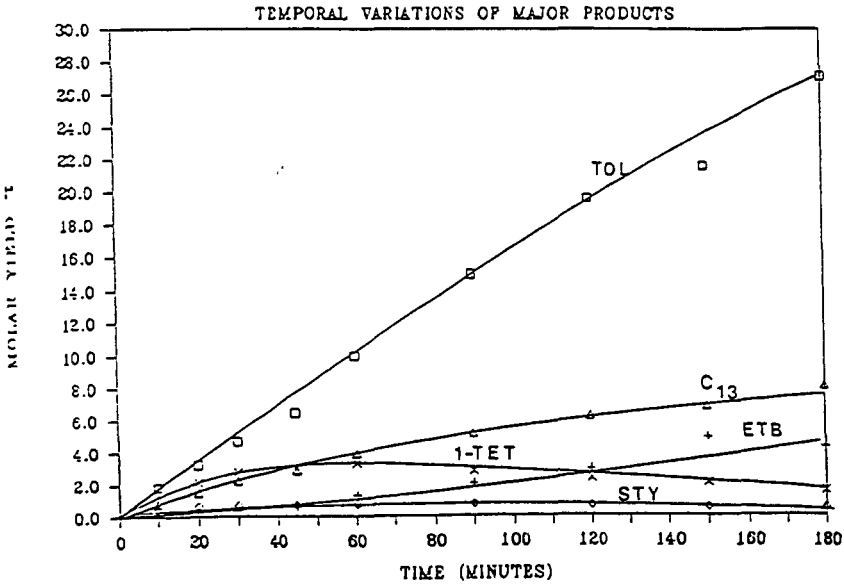

FIGURE 4: PDB SELECTIVITY TO PRODUCTS

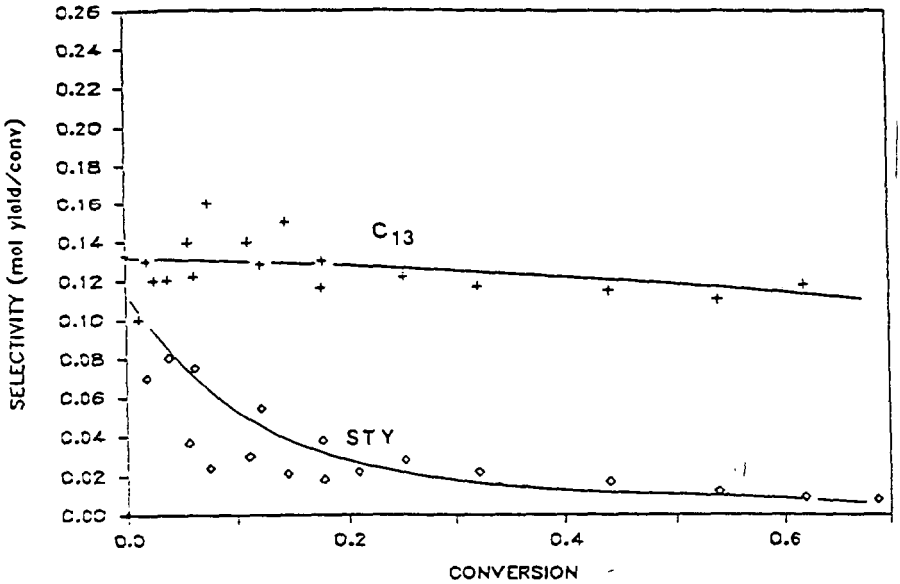

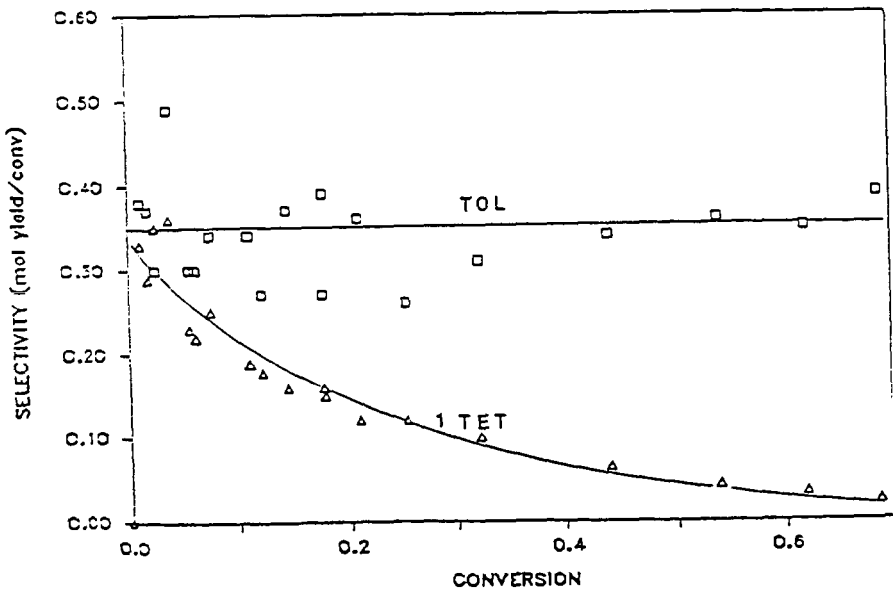

FIGURE 5

PDB THERMOLYSIS PATHWAY

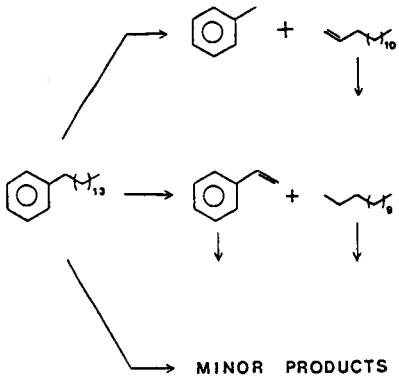

FIGURE 6 PDB THERMOLYSIS MECHANISMS

CONCERTED

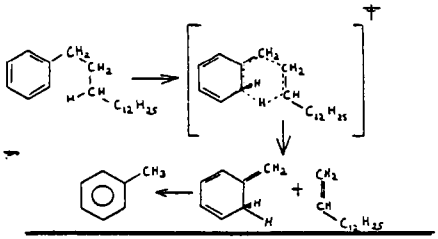

RADICAL

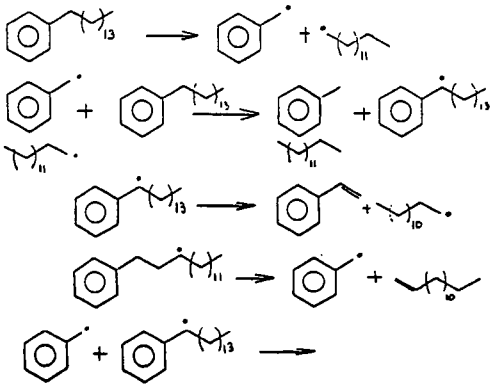

Table I
Asphaltene Master Table

Holding Time (min)	30	60	90	30	60	90	10	60	90
Temperature	350°C			400°C			450°C		
Product Fractions (wt%)									
Asphaltene	95.9	92.6	87.0	36.6	22.6	24.6	8.7	0	0
Maltene	4.9	6.4	8.1	18.6	14.6	14.3	12.2	9.5	10.0
Gas	0.3	0.6	0.7	3.8	3.7	4.5	6.8	12.6	14.0
Coke*	0	0	0	41.0	59.1	56.6	72.3	77.9	76.0
Mass Balance	101.1	99.3	95.8	96.3	79.0	91.8	74.0	66.2	67.2
Gas Yields (mg/g)									
H_2S	0.08	0.61	2.31	10.4	19.0	16.9	14.2	14.7	17.3
CO_2	0.06	0.61	0.69	0.93	1.29	1.18	0.97	0.90	1.23
CH_4	0.07	0.13	0.50	2.41	6.82	7.21	8.24	15.2	19.7
C_2H_6	-	0.05	0.26	1.63	5.59	5.70	6.52	13.2	16.8
C_3H_8	-	0.06	0.22	1.47	4.63	4.45	4.56	9.49	11.7
$n\text{-}C_4H_{10}$	-	0.03	0.09	0.64	1.77	1.92	2.12	3.50	4.24
C_5H_{12}	-	0.09	0.14	0.56	1.79	1.74	2.18	2.65	2.62
C_2H_4	-	0.02	0.03	0.12	0.20	0.19	0.34	0.53	0.58
n-alkane Yields (mg/g)									
$n\text{-}C_8H_{18}$	-	-	0.06	0.31	1.87	1.53	2.33	3.70	1.35
$n\text{-}C_{12}H_{26}$	-	-	0.05	0.26	1.39	1.25	1.83	2.12	0.95
$n\text{-}C_{16}H_{34}$	-	-	0.06	0.46	1.05	1.00	1.32	0.85	0.22
$n\text{-}C_{20}H_{42}$	-	-	0.07	0.15	0.71	0.63	0.74	0.23	0.07
$n\text{-}C_{24}H_{50}$	-	-	-	0.13	0.36	0.33	0.30	-	0.03
Total (C_8-C_{25})	-	-	0.8	4.4	18.4	16.8	20.9	19.5	7.0
Pseudo-First Order k(min^{-1})	0.000597			0.01227			0.24418		

*Coke yields are calculated by difference.

Table 2
PDB Master Table

Holding Time (min)	30	90	150	30	90	150	30	90	150	10	30	60
Temperature	375°C			400°C			425°C			450°C		
Product Yield (mol %)												
PDB	93.1	91.0	78.0	73.6	54.1	35.5	47.0	7.06	4.62	24.4	2.93	0.43
Toluene	1.88	3.84	6.98	4.68	15.0	21.6	18.1	47.4	50.4	20.9	47.9	64.5
1-tetradecane	1.38	2.14	2.62	2.80	2.84	2.09	3.30	0.73	0.40	3.80	0.29	0.10
n-tridecane	0.45	1.28	2.72	2.26	5.17	6.84	5.68	5.17	4.99	6.33	3.42	1.32
Styrene	0.32	0.33	0.32	0.67	0.75	0.54	1.44	0.49	0.40	2.96	0.64	0.39
Ethylbenzene	0.20	0.38	1.07	0.40	2.05	4.88	3.35	18.7	17.1	3.65	18.00	27.24
Product Group Yields (mol %)												
Phenyl-alkanes	3.01	5.44	15.2	7.96	24.8	37.4	31.3	79.8	81.3	35.7	77.0	101.5
Phenyl olefins	0.91	1.09	1.65	1.81	2.47	2.30	4.19	1.62	1.24	6.84	1.53	0.60
Alkanes	1.59	2.58	6.92	4.04	11.2	17.3	14.0	32.3	33.3	18.2	26.9	27.1
α-olefins	2.35	3.04	5.17	4.36	6.46	5.60	10.1	8.15	7.09	10.9	7.38	4.42

Pseudo-First-Order Kinetics

C_0(mol/ℓ)	k(min^{-1})	C_0(mol/ℓ)	k(min^{-1})	C_0(mol/ℓ)	k(min^{-1})	C_0(mol/ℓ)	k(min^{-1})
2.2	.00129	0.0043	.00400	2.0	.0265	1.7	0.1178
		0.0075	.00503				
		0.0150	.00535				
		0.0249	.00521				
		0.0913	.00347				
		0.482	.00452				
		1.12	.00690				
		1.80	.00783				
		2.07	.00732				
		2.29	.00690				

FREE RADICAL CRACKING OF HIGH MOLECULAR WEIGHT BRANCHED ALKANES

Y.V.Kissin

Gulf Research and Development Co.
P.O.Drawer 2038, Pittsburgh, PA 15230

Studies of thermocracking of branched alkanes play an important role in several areas, including high temperature catalytic cracking, delayed coking, manufacture of olefins, degradation of polymers, and geochemistry. Although principal chemical reactions involved in thermocracking under relatively mild conditions are well known (1-4), detailed information about cracking of large branched molecules is lacking from the literature, mostly because of analytical problems - identification of reaction products, various branched alkanes and olefins, in the carbon atom number range $C_8 - C_{20+}$.

This paper discusses principal reaction stages of thermocracking of pristane, phytane, and squalane in the liquid state under mild conditions (250°C, 24 h) and presents analysis of reactivities of various C-H bonds in the hydrogen abstraction reactions as well as reactivities of various C-C bonds in the β-scission reactions.

EXPERIMENTAL PART

Thermocracking of pristane, phytane, and squalane at 250-300°C for 24 h in the liquid state was carried out in small glass ampoules sealed under vacuum. Under these conditions the reaction yields equimolar mixtures of isoalkanes and olefins with branched chains. Addition of a mineral clay (bentonite) to the ampoules results in conversion of the olefins into a complex mixture of various secondary products while keeping the alkanes formed in the cracking reaction intact. Comparison of the gas chromatograms of the cracking products obtained with and without the clay assists in identification of branched alkanes.

A Hewlett-Packard 5880A gas chromatograph equipped with the flame ionization detector, operated in the split injection mode with a split ratio 100:1, was used to obtain chromatographic data. The column used was a 50 m, 0.02 mm i.d., fused silica capillary coated with 0.50 micron film of cross-linked methyl silicone. Helium carrier gas was used at a flow of 1 ml/min. The column oven temperature was programmed from 40°C to 300°C at 5°C/min and held at 300°C until complete elution of a sample. Sample size was 1.0 microliter. Detector and injector temperatures were held at 325°C. Samples were diluted with CS_2 before injection.

The techniques used for assignment of alkane and olefin peaks in gas chromatograms of the thermocracked products are discussed elsewhere (5, 6). They were based on the application of a modified additivity principle (7) which allows quantitative estimation of peak positions of complex molecules (multibranched alkanes and olefins) from the data on peak positions of more simply built molecules (monobranched alkanes, linear olefins).

A generally used procedure of presentation of retention times for peaks of hydrocarbons in gas chromatograms is calculation of their Kovats factors (KF) from their retention times RT (8).

$$KF(\text{iso-alkane } C_nH_{2n+2}) = 100(n-1) + 100[RT(\text{iso-alkane})-RT(n-C_{n-1}H_{2n})]/[RT(n-C_nH_{2n+2})-RT(n-C_{n-1}H_{2n})] \quad 1)$$

For example, the peak of an iso-alkane situtated in the middle between peaks of $n-C_{12}H_{26}$ and $n-C_{13}H_{28}$ has KF 1250. We found it more convenient to use a different parameter for the purpose - a relative retention factor, RRF (5, 6):

$$RRF = [KF(\text{iso-alkane } C_nH_{2n+2}) - KF(\text{n-alkane } C_nH_{2n+2})]/100 \quad 2)$$

This factor is a negative number representing a normalized relative precedence of the peak of a hydrocarbon with respect to the peak of the normal alkane with the same carbon atom number.

RESULTS AND DISCUSSION

Numbering of carbon atoms in the skeletons of the three isoprenoid molecules follows:

Pristane (2,6,10,14-tetramethylpentadecane)

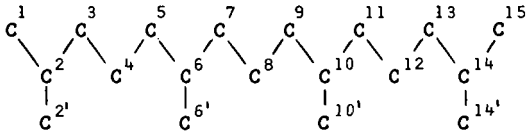

Phytane (2,6,10,14-tetramethylhexadecane)

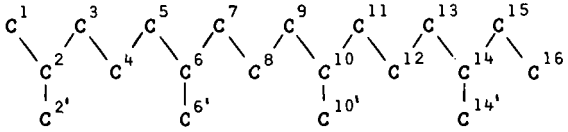

Squalane (2,6,10,15,19,23-hexamethyltetracosane)

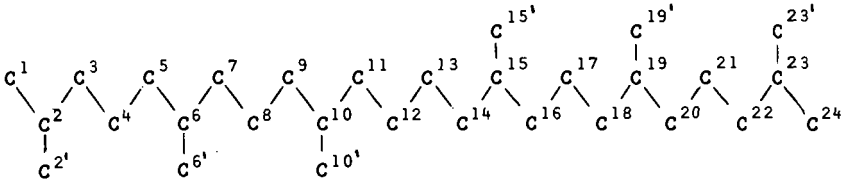

Conversions in the thermocracking reactions (250°C, 24 h) were: for pristane - 6.0%, for phytane - 2.7%, for squalane - 6.4%. Under these mild conditions only three stages of the radical chain reactions should be considered: formation of a parent radical, fission of the radical with the formation of an olefin and a smaller alkyl radical, and the chain transfer reaction yielding a low molecular weight alkane. One example of these three reactions involving a radical attack on the sixth position of the pristane molecule and the β-scission of the C_7-C_8 bond is:

Formation of a parent radical (hydrogen abstraction reaction):

$$R^{\bullet} + \text{2,6,10,14-tetramethylpentadecane} \longrightarrow$$

$$RH + CH_3-\underset{CH_3}{CH}-CH_2-CH_2-CH_2-\overset{\bullet}{\underset{CH_3}{C}}-CH_2-CH_2-CH_2-\underset{CH_3}{CH}-CH_2-CH_2-CH_2-\underset{CH_3}{CH}-CH_3 \qquad 3)$$

β-scission reaction:

$$CH_3-\underset{CH_3}{CH}-CH_2-CH_2-CH_2-\overset{\bullet}{\underset{CH_3}{C}}-CH_2-CH_2-CH_2-\underset{CH_3}{CH}-CH_2-CH_2-CH_2-\underset{CH_3}{CH}-CH_3 \longrightarrow$$

$$CH_3-\underset{CH_3}{CH}-CH_2-CH_2-CH_2-\underset{CH_3}{C}=CH_2 \quad + \quad {}^{\bullet}CH_2-CH_2-\underset{CH_3}{CH}-CH_2-CH_2-CH_2-\underset{CH_3}{CH}-CH_3 \qquad 4)$$

(2,6-dimethyl-1-heptene)

Chain transfer reaction:

$${}^{\bullet}CH_2-CH_2-\underset{CH_3}{CH}-CH_2-CH_2-CH_2-\underset{CH_3}{CH}-CH_3 + \text{2,6,10,14-tetramethylpentadecane}$$

$$\longrightarrow \quad CH_3-CH_2-\underset{CH_3}{CH}-CH_2-CH_2-CH_2-\underset{CH_3}{CH}-CH_3 \quad + \quad R^{\bullet} \qquad 5)$$

(2,6-dimethyloctane)

Reactions 3 and 5 are, in a general sense, the same reaction of hydrogen abstraction and they are separated here to emphasize chemistry of the reaction product formation. It is generally accepted (2, 4) that radical reactions of alkanes at low temperatures in the liquid state are accompanied by intramolecular radical isomerization (hydrogen atom shifts via five- and six-atom cyclic transition states) and by intermolecular hydrogen exchange reactions (reverse of reaction 3 with RH being the substrate molecule). The joint result of these two processes is the equilibrium distribution of primary radicals in terms of radical site positions, with the equilibrium being governed by relative radical stabilities.

Tables 1 and 2 list all possible alkanes and olefins which are formed in the principal thermocracking reactions of pristane, phytane, and squalane, experimental and calculated RRF values for the alkanes and olefins, and positions of radical attacks resulting in the formation of corresponding hydrocarbons. Peak areas for the products were used as the basis for the evaluation of reactivities of various bonds in two reactions - hydrogen abstraction (Reaction 3) and β-scission (Reaction 4).

β-scission reactions

In the majority of cases several β-scission reactions are possible for a radical formed in Reaction 3 (except for radicals in positions 2 in all isoprenoids and in position 16 for phytane). Analysis of reaction products allows estimation of probabilities of the scission reactions.

Tertiary radicals. Tertiary radicals in positions 6 and 10 are situated in very symmetrical environments. As a consequence,

probabilities of β-scissions for the adjacent bonds are virtually equal. The ratios of products formed in the C_4-C_5 and C_7-C_8 bond scissions (radicals in position 6) are in the range 1.06-0.98 for all isoprenoids. The same ratios (1.08-0.99) were found for C_8-C_9 and C_{11}-C_{12} bond scissions in phytane and squalane (radicals in position 10). On the other hand, the probability of the CH_2-CH_2 bond (C_{12}-C_{13}) scission in the phytane radical (in position 14) is 10.6 times higher than that for the CH_2-CH_3 bond (C_{15}-C_{16}) which corresponds to the ΔE_{act} difference, ca. 2.5 kcal/mol.

Secondary radicals. Similarly to the previous case, if a secondary radical is situated in a symmetrical environment (positions 8 in all molecules, position 12 in phytane) the probability of the two β-scissions are identical (with precision ca. 4%) according to expectations. However even a slight deviation from the symmetry, in positions 4, results in a deviation from the equality. The ratio between the probabilities for the scisson of C_2-C_3 and C_5-C_6 bonds is ca. 0.63. When secondary radicals are in positions 7 (or positions 9 in phytane and squalane) the scission involves different chemical bonds. In these cases the ratios of the scission rates for the CH_2-CH_2 bonds (C_8-C_9 for radicals in positions 7) and for the CH_2-CH bonds (C_5-C_6) are ca. 0.71 (+7%). The same ratio (scission of C_{12}-C_{13} vs. C_9-C_{10}) for the phytane radical in position 11 is 0.58. However, the C_{12}-C_{13} bond in squalane is ca. 10% more reactive in β-scission than the C_9-C_{10} bond. Data for the pristane radical (in position 5) provide the most complete information of the relative probabilities of β-scission reactions. The ratios of the reactions for the CH_2-CH_2 bond (C_8-C_9), the CH_2-CH bond (C_5-C_6), and the CH_3-CH bond (C_6-$C_{6'}$) are 4.72 : 6.70 : 1.

Reactivities of C-H bonds in hydrogen abstraction reactions

Tertiary C-H bonds

Tertiary C-H bonds are the most active in radical hydrogen abstraction reactions as emphasized by their low bond energies, ca. 90 kcal/mol (2, 4). Our data show that reactivities of the C-H bonds in 6 and 10 positions are equal for all three isoprenoids (corresponding product yields are in the range 1.00-1.03). The ratios of products formed from the end- and internal tertiary radicals are:

Internal C•	:	$R-\dot{C}(CH_3)-CH_2-CH_3$	: $R-\dot{C}(CH_3)-CH_3$	= 1 : 0.45 : 0.31
(positions 6 and 10)		(position 14 in phytane)	(positions 2)	

If one takes into account different scission patterns for these radicals (discussed earlier) and the exsitence of only one β-scission route for the end-tertiary radicals these ratios translate into the ratios of formation rates for corresponding radicals ca. 1 : 0.7 : 0.8.

Secondary radicals

The isoprenoids studied can form several structurally different secondary radicals.

Radicals $-CH_2-\dot{C}H-CH_2-$. As expected, the radicals in positions 4 and 12 in the phytane molecule have the same reactivity (the corresponding

product ratio is 1.05). However, these radicals positioned in the center of the molecules (positions 8) are slightly more reactive than similar radicals in positions 4: the reactivity ratios are 1.3 for pristane, 1.2 for phytane, and 1.7 for squalane. Reactivity of the secondary radical in position 12 of squalane is 2.4 times less than that of a similarly situated radical in position 8.

Radicals $-CH_2-\dot{C}H-CH-$. Reactivities of all radicals in positions 5, 7, 9, and 11 in the molecules are equal within ±10%.

Relative reactivities of various secondary radicals. Significant differences between reactivities of differently flanked secondary radicals were found for all isoprenoids. Radicals $-CH_2-\dot{C}H-CH_2-$ are 4.8 times (±10%) more reactive than $CH_2-\dot{C}H-CH-$ radicals. The only exception was found for squalane: reactivity of the radical in position 12 is only 2.3 times higher than reactivity of the radical in position 11.

Primary radicals

Information on relative reactivity of primary radicals is limited due to difficulties in identification of the products of their β-scission and due to low content of the products. In the case of phytane the radical in position 6' has the same reactivity as the radical in position 14' and it is ca. 20% less reactive than the radical in position 10'.

The yields of scission products from the primary radicals in positions 1 are ca. 2 times less than those for the radicals in positions 6'. If one takes into account that only one scission route is available for the first radicals, it can be concluded that reactivities of all primary radicals in the isoprenoids are very close.

Comparisons of reactivities of various radicals

Comparisons of the yields of products from β-scissions of radicals of various structures allows approximate evaluation of their relative reactivities.

Primary radicals $\dot{C}H_2-CH-$ vs. secondary radicals $-CH_2-\dot{C}H-CH_2-$. The product ratio for scission of corresponding radicals for all isoprenoids is ca. 0.067. If one takes into account the differences between the numbers of C-H bonds in these groups, the ratios of reactivities of C-H bonds in the methyl group (CH_3-CH-) and the central methylene group in the sequence $CH(CH_3)-CH_2-CH_2-CH_2-\dot{C}H(CH_3)$ is ca. 0.045 which corresponds to ΔE_{act} ca. -3.2 kcal/mol.

Primary radicals $\dot{C}H_2-CH-$ vs. secondary radicals $-CH_2-\dot{C}H-CH-$. The product ratio for scission of corresponding radicals for all isoprenoids is ca. 0.27 which translates into the difference between reactivities of corresponding C-H bonds ca. 0.18 and ΔE_{act} ca. -1.8 kcal/mol.

Secondary radicals vs. tertiary radicals $CH_2-\dot{C}(CH_3)-CH_2-$. The product ratio for scission of secondary radicals (in positions 8) and that for the tertiary radicals in positions 6 or 10 is 0.89. This corresponds to the ratio of ca. 2.25 for C-H bond reactivities in hydrogen abstraction reactions involving the tertiary CH_3-CH- groups and the central methylene groups in the isoprenoids (positions 8). Corresponding ΔE_{act} is ca. 0.8 kcal/mol. As was mentioned before, central CH_2 groups in $-CH_2-CH_2-CH-$ sequences are less reactive than in $-CH_2-CH_2-CH_2-$ sequences. For them the corresponding C-H bond reactivity ratio is 11.6 and ΔE_{act} is ca. 2.6 kcal/mol.

LITERATURE CITED

1. A. Kossiakoff, F. O. Rice, J. Am. Chem. Soc., 65, 590 (1943).
2. Free Radicals (vols. I and II), J. K. Kochi, Ed., J. Wiley, New York, 1973.
3. S. W. Benson, The Foundations of Chemical Kinetics, McGraw-Hill, New York, 1960, p.343.
4. E. Ranzi, M. Dente, S. Pierucci, G. Biardi, Ind. Eng. Chem., Fundam., 22, 132 (1983).
5. Y. V. Kissin, G. P. Feulmer, J. Chromat. Sci., in press.
6. Y. V. Kissin, J. Chromat. Sci., in press.
7. G.I. Spivakovskii, A.I. Tishchenko, I.I. Zaslavskii, N.S. Wulfson, J. Chromatoraphy, 144, 1 (1977).
8. E. Kovats, Z. Anal. Chem., 181, 351 (1961).

Table 1

ALKANES FORMED IN THERMOCRACKING REACTIONS OF PRISTANE, PHYTANE, AND SQUALANE AT 250°C †

Alkane	Formed from (position of radical attack)			RRF (exp.)	RRF (calc.)	ΔRRF %
	Pristane	Phytane	Squalane			
n-C_4		*(12)				
iso-C_4	*(5)	*(5)	*(5)			
2-Me-C_4	*(6)	*(6,11)	*(6)			
2-Me-C_5	*(6',7)	*(6',7)	*(6',7)			
3-Me-C_5		*(10)				
3-Me-C_6		*(9,10')				
2-Me-C_7	*(8)	*(8)	*(8)			
2,6-Me_2-C_7	*(9)	*(9)	*(9)	-0.700	-0.700	0.0%
3-Me-C_8		*(8)				
2,6-Me_2-C_8	*(6)	*(7,10)	*(10)	-0.636	-0.644	1.2%
2,6-Me_2-C_9	*(5,10')	*(10',11)	*(10',11)	-0.747	-0.736	-1.5%
3,7-Me_2-C_9		*(6)		-0.578	-0.568	-1.7%
3,7-Me_2-C_{10}		*(5,6')		-0.695	-0.674	-3.0%
2,6-Me_2-C_{11}	*(4)	*(12)	*(12)	-0.833	-0.812	-2.5%
2,6,10-Me_3-C_{11}	*(3)	*(13)	*(12)	-1.252	-1.175	-6.1%
3,7-Me_2-C_{12}		*(4)		-0.788	-0.753	-4.5%
2,6,10-Me_3-C_{12}	*(2,14)	*(3,14)	*(11)	-1.199	-1.114	-7.1%
2,6,10-Me_3-C_{13}	*(1,2')	*(14',15)	*(10)	-1.353	-1.254	-7.3%
3,7,11-Me_3-C_{13}		*(2)		-1.150	-1.076	-6.4%
2,6,10-Me_3-C_{14}			*(9,10')	-1.430	-1.329	-7.1%
3,7,11-Me_3-C_{14}		*(1)		-1.300	-1.210	-7.0%
2,6,10-Me_3-C_{15}		*(16)		-1.477	-1.386	-6.2%
2,6,10-Me_3-C_{16}			*(8)	-1.531	-1.407	-8.1%
2,6,10,15-Me_4-C_{16}			*(7)	-1.940	-1.788	-7.9%
2,6,10,15-Me_4-C_{17}			*(6)	-1.862	-1.705	-8.5%
2,6,10,15-Me_4-C_{18}			*(5,6')	-2.102	-1.880	-10.6%
2,6,10,15-Me_4-C_{20}			*(4)	-2.115	-2.063	-2.5%
2,6,10,15,19-Me_5-C_{20}			*(3)	-2.345	-2.464	5.1%
2,6,10,15,19-Me_5-C_{21}			*(2)	-2.320	-2.408	3.8%
2,6,10,15,19-Me_5-C_{22}			*(1)	-2.455	-2.608	6.2%

† amounts of methane, ethana, and propane cannot be determined quantitatively and are not reported in the table.

Table 2

OLEFINS FORMED IN THERMOCRACKING REACTIONS OF PRISTANE, PHYTANE, AND SQUALANE AT 250°C †

Olefin	Formed from			RRF	RRF	ΔRRF
	Pristane	Phytane	Squalane	(exp.)	(calc.)	%
	(position of radical attack)					
$C_3=$	*(1)	*(1)	*(1)			
$1-C_4=$		*(14')				
$2-C_4=$		*(14')				
$iso-C_4=$	*(2)	*(2)	*(2)			
$2-Me-1-C_4=$		*(14)				
$3-Me-1-C_4=$	*(3)	*(3)	*(3)			
$3-Me-1-C_5=$		*(13)				
$4-Me-1-C_5=$	*(4)	*(4)	*(4)			
$4-Me-1-C_6=$		*(12)				
$6-Me-1-C_7=$	*(6')	*(6')	*(6')			
$6-Me-2-C_7=$	*(5)	*(5)	*(5)			
$6-Me-1-C_8=$		*(10')				
$6-Me-2-C_8=$		*(11)		-0.228		
$2,6-Me_2-1-C_7=$	*(6)	*(6)	*(6)	-0.520	-0.518	0.4%
$2,6-Me_2-1-C_8=$		*(10)		-0.455	-0.455	0.0%
$3,7-Me_2-1-C_8=$	*(7)	*(7)	*(7)	-0.896	-0.880	1.8%
$3,7-Me_2-1-C_9=$		*(9)			-0.803	
$4,8-Me_2-1-C_9=$	*(8)	*(8)	*(8)	-0.850	-0.846	0.5%
$4,8-Me_2-1-C_{10}=$		*(8)		-0.796	-0.785	1.4%
$6,10-Me_2-1-C_{11}=$	*(6')	*(6',10')	*(10')	-0.915	-0.916	0.1%
$6,10-Me_2-2-C_{11}=$	*(7)	*(9)	*(9)	-0.799	-0.812	1.6%
$6,10-Me_2-2-C_{12}=$		*(7)		-0.751	-0.740	4.1%
$2,6,10-Me_3-1-C_{11}=$	*(6)	*(10)	*(10)	-1.047	-1.008	3.7%
$3,7,11-Me_3-1-C_{12}=$	*(5)	*(11)	*(11)	-1.459	-1.328	9.0%
$2,6,10-Me_3-1-C_{12}=$		*(6)		-0.992	-0.920	7.2%
$4,8,12-Me_3-1-C_{13}=$	*(4)	*(12)	*(12)	-1.436	-1.338	6.8%
$3,7,11-Me_3-1-C_{13}=$		*(5)		-1.398	-1.287	7.9%
$4,8,12-Me_3-1-C_{14}=$		*(4)		-1.379	-1.301	5.6%
$5,9,13-Me_3-1-C_{14}=$			*(12)	-1.505	-1.420	5.6%
$6,10,14-Me_3-1-C_{15}=$	*(1)	*(14')			-1.474	
$6,10,14-Me_3-2-C_{15}=$	*(3)	*(13)				
$2,10,14-Me_3-5-C_{15}=$	*(5)					
$2,10,14-Me_3-6-C_{15}=$	*(7)					
$6,10,14-Me_3-1-C_{16}=$		*(1)			-1.409	
$6,10,14-Me_3-2-C_{16}=$		*(3)			-1.326	
$2,10,14-Me_3-5-C_{16}=$		*(5)			-1.241	
$2,10,14-Me_3-6-C_{16}=$		*(7)			-1.241	
$3,11,15-Me_3-6-C_{16}=$		*(11)			-1.227	
$3,11,15-Me_3-7-C_{16}=$		*(9)			-1.227	
$7,11,15-Me_3-1-C_{16}=$			*(10')	-1.583	-1.494	5.6%
$7,11,15-Me_3-2-C_{16}=$		*(15)	*(11)	-1.530	-1.411	7.7%
$7,11,15-Me_3-3-C_{16}=$		*(13)				
$2,6,10,14-Me_4-1-C_{15}=$			*(14)		-1.525	
$2,7,11,15-Me_4-1-C_{16}=$			*(10)	-1.712	-1.562	8.8%
$3,8,12,16-Me_4-1-C_{17}=$			*(9)	-2.114	-1.909	9.7%
$4,9,13,17-Me_4-1-C_{18}=$			*(8)	-2.00	-1.963	2.0%
$6,11,15,19-Me_4-1-C_{20}=$			*(6')		-2.19	
$6,11,15,19-Me_4-2-C_{20}=$			*(7)		-2.13	
$2,6,11,15,19-Me_5-2-C_{20}=$			*(6)	-2.14	-2.18	1.9%

† olefins C_{26}–C_{29} in the products of squalane thermocracking were not identified quantitatively and are not reported in the table.

USE OF THE STRUCTURE-CHEMICAL REACTIVITY DATA FOR DEVELOPMENT OF NEW METHODS IN PETROLEUM HEAVY ENDS UPGRADING

M. Farcasiu, E. J. Y. Scott and R. B. LaPierre

Mobil Research and Development Corporation
Central Research Laboratory
P. O. Box 1025, Princeton, New Jersey 08540

INTRODUCTION

The chemical structure of the heavy ends of petroleum has been studied extensively (1). However, these studies have had little impact on the processes used commercially to upgrade heavy petroleum fractions. Industrial processes involve thermal (high temperature free radical chemistry) or catalytic routes such as catalytic cracking or hydroprocessing at temperatures greater than 300°C.

Low temperature ionic reactions have not been explored extensively for upgrading petroleum heavy ends. We have examined transalkylation, the transfer of alkyl fragments from high molecular weight components to smaller aromatic acceptor molecules in presence of Friedel Craft catalysts. We present results of transalkylation using catalysts consisting of trifluoromethanesulfonic acid as well as aluminum chloride promoted by water (2). Results are presented for transalkylation to native aromatic compounds present in crude petroleum (whole crude transalkylation) as well as to added aromatic molecules (resid transalkylation).

Most molecules in petroleum heavy ends contain 20 to 40 wt.% aliphatic groups substituted to aromatic (or heteroaromatic) rings (3). These aliphatic substituents are:

- normal and iso alkyl groups (we positively identified C_2 to C_{16} alkyl chains);
- cycloalkyl groups (we identified cyclopentyl and cyclohexyl substituents but the presence of larger saturated polycyclic groups cannot be precluded);
- methylene groups linking two aromatic rings.

In the presence of Friedel Crafts catalysts these aliphatic groups can be transferred to small aromatic molecules (3). The result of transalkylation is then the formation of new distillable products which contain the small aromatic molecules substituted with normal, iso, and cyclo alkyl groups. Obviously, in such complicated mixtures as the petroleum heavy ends are, under the transalkylation reaction conditions, other reactions will also take place; for example, the dialkyl sulfides form mercaptanes and paraffins, and at long reaction times, alkyl substituents with five or more carbons form hydroaromatic rings by cyclization.

The products of the transalkylation and of secondary reactions are mixtures of petroleum like compounds with molecular weights

(and boiling points) ranging from that of the acceptor (the small aromatic molecule) to that of the resid.

If whole crude oils are treated under the conditions of the transalkylation reaction, alkyl groups from heavy ends are transferred to the light aromatic hydrocarbons present in the crude oil. The result is a change of the boiling point distribution of the whole crude toward medium boiling point fractions.

Very early in our work we realized the lack of literature data concerning the transfer of the alkyl substituents between aromatic rings with different degrees of ring condensation. To gain this information we studied the transalkylation reaction with appropriate model compounds (3,4).

The transalkylation reaction can be applied both to materials soluble in aromatics and to solids as kerogens (3) or coals (5,6) and coal liquefaction products (6).

RESULTS AND DISCUSSION

The transalkylation reaction can be formulated:

$$Ar^{I}\text{-}Alkyl^{I} + Ar^{II}H \rightleftharpoons Ar^{I}H + Ar^{II}\text{-}Alkyl^{I}$$

In our discussion Ar^{I}-$Alkyl^{I}$ will denote large aromatic molecules from petroleum heavy ends and $Ar^{II}H$ will be benzene, toluene or o-xylene.

A. Kinetic and thermodynamic constraints of the transalkylation reaction

We have shown previously (3,4) that the rate of the transalkylation reaction between polyaromatic and monoaromatic rings is:

- independent of the chain length (at least for C_2-C_{10} alkyl chains),
- dependent on the nature of the aliphatic substituent (cycloalkyls transfer faster than n-alkyls),
- dependent on the structure of the polyaromatic moiety involved in the transalkylation reaction (the rate of transfer of the aliphatic substituent increases for systems with increased degree of aromatic ring condensation).

Concerning the thermodynamics of transalkylation, we found that the thermodynamic equilibrium is:

- independent of the structure of the polyaromatic moiety (Table I),
- only slightly influenced by temperature in the 27-227°C interval in which we studied the transalkylation reaction (Table II).

Data in Tables I and II show that the equilibrium constant of the

transalkylation reaction is close to unity (i.e. $\Delta G = 0$) for any pair of donor-acceptor. That means that at donor-acceptor molar ratio of 1:1, the maximum conversion to be expected is 50% for any of the starting materials. Thus, the only way to push a transalkylation reaction in a desired direction is to work with excess of acceptor. For example, for a molar ratio of 1:4 at equilibrium, 80% of donor will be converted at 127°C (400°K).

In the case of conversion of petroleum heavy ends by a transalkylation reaction, the big differences between the molecular weight of the donor (average molecular weight 1000) and of the acceptor (molecular weight ~100) insure an advantageous molar ratio even for a weight ratio resid:aromatic hydrocarbon of 1:1.

These thermodynamic constraints are very important for upgrading whole crude (see Section C following).

While the thermodynamic equilibrium is independent of the degree of aromatic ring condensation of the donor, the rates of the transalkylation reaction are faster for transfer of aliphatic groups from more to less condensed aromatic systems. The transfer in the opposite direction necessitates larger acid (catalyst) concentration (4), which in turn favors some secondary reactions.

B. Transalkylation reactions of vacuum resids

Some transalkylation reactions between Arabian Light vacuum resid and toluene or o-xylene are given in Table III. Typical composition of the distillate is shown in Figure 1 for an Alaskan resid. Some properties of the dealkylated resids are given in Table IV. In general, 60-80% of the initial resid remains as dealkylated resid.

If the dealkylated resid is hydrotreated in the presence of Co-Mo catalysts (Table V), the hydrogen consumption is similar to that for the untreated resid, but the degree of desulfurization is somewhat higher (72%) for the dealkylated resid than for the untreated resid (65% desulfurization). It should be observed that the dealkylated resid (76% of the initial resid) was distilled to a lower average molecular weight (620) than that of untreated resid (average molecular weight 1100).

The saturated hydrocarbon fraction in the hydrotreated vacuum resid (for the hydrotreating condition see Table V) represents 20.5% of the product and has an average molecular weight of ~1000. In the hydrotreated dealkylated resid the saturated hydrocarbons represent 24.5% of the product and their average molecular weight is only 386.

C. Transalkylation reactions of whole crude oils

The transfer of aliphatic substituents from the big molecules to lower molecular weight aromatics of a crude oil can be achieved under mild conditions in the presence of a Friedel-Crafts catalyst (Table VI). We used topped (80°C$^+$) crude oils because the lowest boiling point acceptor in crude oils is benzene

(b.p.~80°C). Work with model compounds (4) indicated that the transfer of substituents is easier from polyaromatic to monoaromatic rings. This favors the redistribution of aliphatic substituents in whole crudes in the desired direction.

In the case of aromatic crudes (for example the Alaskan crude in Table VI), there are enough low molecular weight natural acceptors in the crude to achieve a substantial transfer. In the case of a paraffinic crude (North Sea crude), the addition of some small aromatic molecules can be helpful (Table VI).

The net result of the internal transalkylation is a redistribution of boiling points in the crude with an increase in the quantity of medium range products.

D. Chemical composition and mechanistic limitations of upgrading petroleum heavy ends by the transalkylation reaction

The petroleum heavy ends contain large amounts of aliphatic substituents on polyaromatic rings. This makes the use of the transalkylation reaction an attractive alternative for their upgrading.

One element of structure which poses a problem is the presence of basic compounds, especially basic nitrogen compounds in petroleum heavy ends. The basic nitrogen compounds react with the acidic catalysts and form salts.

Another limitation for the use of the transalkylation reaction is the effect of acid concentration on the reaction rate. Our work with model compounds (4) has shown that the concentration of acid must exceed a certain threshold to obtain an acceptable rate of reaction.

Understanding of the quantitative relationship between the chemical structure of the reactants and the concentration of acid is new chemistry and our initial results (4) are only a beginning. Certainly, more research in this area is needed because it is likely to be relevant to other acid catalyzed reactions besides transalkylation.

REFERENCES

1. Speight, J. G., "The Chemistry and Technology of Petroleum", M. Dekker, Inc., New York, 1980, and references therein.

2. Farcasiu, M., U.S. Patent 4,317,712, March 2, 1982.

3. Farcasiu, M, Forbus, T. R., LaPierre, R. B., ACS Petr. Chem. Div. Preprints 28, 279 (1983).

4. Farcasiu, M.,Forbus, T. R., Rubin, B. R., paper submitted to J. Org.Chem.

5. Benjamin, B. M., Douglas, E. C., Canonico, D. M., Fuel 63, 1130 (1984).

6. Farcasiu, M., Proceedings of the Symposium on Chemistry of Coal Liquefaction and Catalysis, March 17-20, 1985, Sapporo, Japan.

7. Stull, D. R., Westrum, Jr., E. F. and Sinke, G. C., "The Chemical Thermodynamics of Organic Compounds", John Wiley (1969).

8. Benson, S. W., "Thermochemical Kinetics", Chapter 2, John Wiley (1968).

9. Stein, S. E., Golden, D. M. and Benson, S. W., J. Phys. Chem 81, 314 (1977).

TABLE I

Equilibrium Constants at 400°K (127°C) for Several Transalkylation Reactions

$$Aryl^{I}\text{-}Alkyl^{I} + Aryl^{II}H \rightleftharpoons Aryl^{I}H + Aryl^{II}\text{-}Alkyl^{I}$$

$Aryl^{I}$-$Alkyl^{I}$ donor	$Aryl^{II}H$ acceptor	$\Delta G°$ 400°K Kcal/mole	$K_{400°K}$
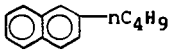		-0.11	1.15
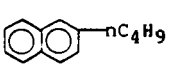		-0.11	1.15
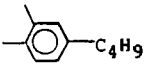		0	~1
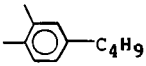		+0.11	0.87
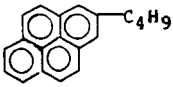		0	~1

$\Delta G°$ values for 2 n-butyl naphthalene, benzene and o-xylene are experimental values (7), those for 1,2-dimethyl 4-n-butyl benzene and 2-n-butyl pyrene are calculated by the method of "group additivity" (8,9).

TABLE II

The Influence of Temperature on Thermodynamical Equilibrium of the Transalkylation Reaction*

Equilibrium Constant at:

300°K (27°C)	400°K (127°C)	500°K (227°C)
1.03	1.15	1.21

*All values are experimental values (7).

TABLE III

Conditions of the Transalkylation Reaction

Vacuum Resid (1050+F) a	Aromatic Hydro-carbon b	Catalyst c	Wt. Ratio a:b:c	Temp. °C	Time Hrs.	Wt.% Distil-late[a] (based on resid)
1. Arabian Light	toluene	$AlCl_3$	1:6.5:0.5	20	18	10
2. Arabian Light	o-xylene	$AlCl_3$	1:0.86:0.5	144	3	15.3
3. Dealky-lated Resid Exp.2	o-xylene	$AlCl_3$	1:1.7:0.5	144	6	25
4. Arabian Light	o-xylene	CF_3SO_3H	1:2.6:0.4	144	6	34

[a]This % includes the light aromatics incorporated by transalkylation.

TABLE IV

Properties of Dealkylated Resids

	Wt.% C	Wt.% H	Wt.% S	MW VPO/Toluene	% ar H
Arabian Light	85.1	10.4	4.0	1100	5.6
Dealkylated Resid exp. 2 Table IvII	86.5	9.6	4.1	620	~11[a]
Dealkylated Resid exp. 3 Table III	87.3	8.7	3.7	503	--

[a]The value of % ar H (^{1}HNMR) is from a similar transalkylation run.

TABLE V

Chemical and Structural Properties of Hydrotreated Arabian Light Vacuum Resid and Hydrotreated Dealkylated Arabian Light Resid

Hydrotreating Conditions: wt.ratio resid:o-xylene:CoMo (HDS1441) catalyst 1:344:0.5; t = 340°C; 1000 psi H_2, 1 h

Material	%arH	Elem. Analysis Wt.% C	H	S	Av. M_W (VPO Toluene)
1. Arabian Light Vac. Resid	5.6	85.1	10.4	4.0	1110
2. Hydrotreated 1 (yield 90% of 1)	1.6	86.5	11.7	1.4	1000
3. Dealkylated ($AlCl_3$ catalyst) Arabian Light Vacuum Resid (76% of initial material)	9.8	84.9	9.1	3.6	620
4. Hydrotreated 3 (yield 90% of 3)	6.8	88.2	10.5	1.0	477

TABLE VI

Boiling Point Distribution of Topped Whole Crude Oils Before and After Transalkylation in the Presence of Trifluromethanesolfonic Acid*

	Boiling Points, °C			
	80-215	215-344	349-426	426+
Topped Alaskan Crude				
Initial	7.9	26.9	17.0	48.2
After transalkylation	9.3	32.0	19.7	39.0
	+1.4	+5.1	+2.7	-9.2
Topped North Sea Crude				
Initial	10.5	35.1	22.0	32.4
After transalkylation	11.7	37.1	24.1	27.1
Δ	+1.2	+2.0	+2.1	-5.3
Topped North Sea Crude 5% o-Xylene				
Initial	15.5	33.4	21.0	30.8
After transalkylation	12.6	40.2	26.3	20.9
Δ	-2.9	+6.8	+5.3	-9.9

*Typical transalkylation conditions: wt. ratio oil : CF_3SO_3H 10:1, reaction temperature ~100°C, reaction time ~4 h. After reaction, the mixture was quenched with aqueous NaOH, the organic layer was separated and dried over $MgSO_4$. The boiling point distribution in the initial material and products was determined by flash distillation over chromosorb followed by simulated distillation by gas chromatography.

FIGURE 1.

GAS CHROMATOGRAM OF THE TRANSALKYLATED PRODUCTS FROM THE REACTION BETWEEN AN ALASKAN VACUUM RESID AND o-XYLENE

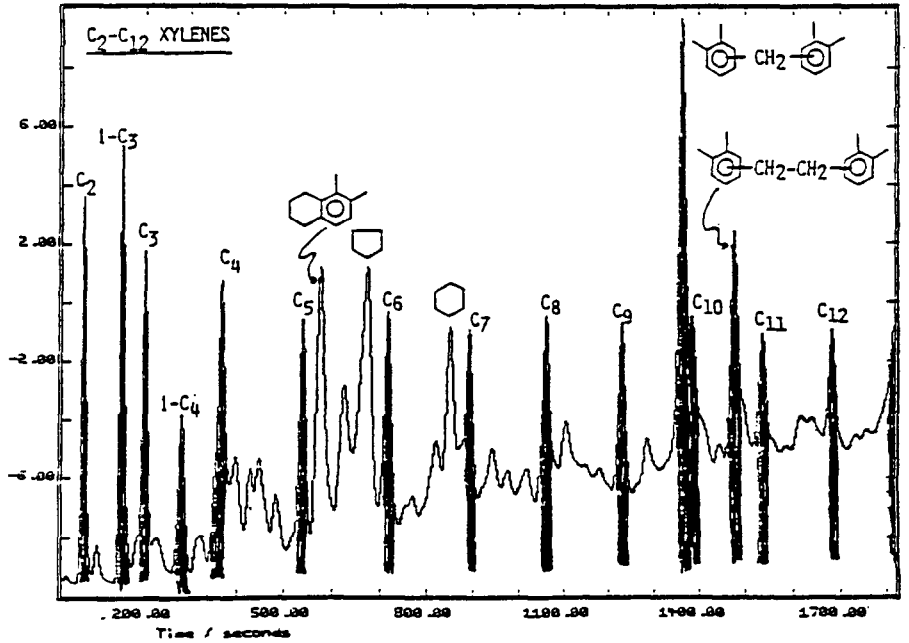

ANALYSIS OF RESIDUUM DEMETALATION BY SIZE EXCLUSION CHROMATOGRAPHY WITH ELEMENT SPECIFIC DETECTION

John G. Reynolds and Wilton R. Biggs

Chevron Research Company
Richmond, CA 94802

ABSTRACT

We analyzed thermally treated heavy residua by element specific size exclusion chromatography (SEC-HPLC-ICP) to elucidate the fate of the V and Ni compounds. Thermal treatment, in addition to removing metals, significantly reduces the size of the remaining metal-containing compounds.

We thermally treated the distillable and nondistillable metals separately. The distilled metals, primarily porphyrins, were completely processed out. The nonvolatile metals, which constituted most of the Ni and V, were either removed, or reduced in size.

When treating heavy residua over commercial fixed-bed hydroprocessing catalysts, the metal-containing molecules in the size range of the catalyst pore are preferentially removed. Those larger than the pore size appear to demetalate more slowly.

The results argue demetalation is a function of the ligand structure and size of the metal-containing species and not the coordination sphere around the metal center.

INTRODUCTION

High metals content is one of the inhibiting factors in the processing of heavy crudes and residua. These metals, particularly V and Ni, are deleterious to fixed bed catalysts, causing deactivation (1).

New technology has recently been developed to process feeds with high metals contents. This technology centers around metals removal by using high metals loading catalyst or guard beds (2), or separation and rejection of poor quality high metals materials (3).

Understanding the mechanism, or mechanisms, by which these metals are removed can ultimately lead to better processing methods. But we are limited by the methods of examination for metals. The inorganic compounds are at ppm levels, which lead to particularly difficult analytical problems. To circumvent this, we have developed and applied size exclusion chromatography, with inductively coupled plasma emission spectroscopy (SEC-HPLC-ICP) to examine V and Ni as a function of process conditions. This technique allows monitoring the size environment of a selected element, without the complications of other components.

EXPERIMENTAL

We obtained California atmospheric residua (AR) No. 1 and No. 2 by single plate distillation of the corresponding crude to a 343°C cut-point. Both AR are high in metals having over 400 ppm Ni + V.

The thermal processing was performed in a tubular flow reactor, under high hydrogen partial pressure. The fixed-bed catalytic processing was performed over commercially available metals loaded alumina catalysts at typical hydroprocessing conditions. The samples were collected from the reactors and stored cold, under nitrogen, until use. Care was taken to protect the samples from oxygen, and to analyze them as soon after processing as possible.

The processing conditions were selected based on the apparent thermal reaction threshold temperature of 410°C (see discussion below). Treatment at and above this temperature is referred to thermal processing. Three standard severities were chosen -- low, moderate, and high. Fixed-bed catalytic treatment was done below this temperature.

The fractionation of the California AR No. 1 into a porphyrin-containing distillate cut (454°C to 677°C) and a nonporphyrin-containing residuum (677°C+) was performed using a short-path distillation apparatus (DISTACT). The cut point between the two fractions was based on the earlier results on metals distribution as a function of boiling point [M. M. Boduszynski unpublished results].

We analyzed both feeds and products by SEC-HPLC-ICP. The technique and the equipment have been described in detail previously (4). The feeds and products were prepared and analyzed by the following procedure:

1) dilute the feed or product to a concentration of 1 to 5% by wt mobile phase of o-xylene, o-cresol, and pyridine.

2) elute the solution by HPLC on Ultragel 50 and 1000 nm analytical columns.

3) detect emission profiles of V (292.40 nm) and Ni (231.60 nm) using an ICP source.

The output, or response profile so obtained, measures the selected elemental content as a function of the elution time. Calibration with polystyrene (PS) standards (4) and model compounds (5,6), changes the response profile from a time domain to a logarithmic size domain. Because we are interested in the relative distribution, and not absolute changes, the profiles shown here are not normalized to absolute metals content.

The porphyrin/nonporphyrin separation methods are also reported elsewhere (4). UV-vis determinations were performed on alumina and capped-silica column separated fractions by techniques discussed elsewhere (4,7).

METAL STRUCTURES IN THE FEEDS

Figure 1 shows the V and Ni SEC-HPLC-ICP response profiles for California AR No. 1. The V profile exhibits the typical bimodal distribution seen for many other crudes and residua (4-6,8,9). The profiles are generally bimodal in distribution, with maxima at MW around 800 and 9000 (PS standards). The maximum at 800 has been assigned by extraction techniques to be metallopetroporphyrins (4). For the crudes examined, the metallopetroporphyrins are most of the small metal compounds, but account for only a minor amount of the

metals in the crude. 26% and 34% of the V is bound as petroporphyrin for California AR No. 1 and No. 2 respectively.

We believe the remaining metal-containing compounds are nonporphyrins. We have examined, the average first coordination sphere around the V in the nonporphyrin fraction using electron paramagnetic resonance (EPR) spectroscopy, and have found various combinations of N, S and O. For California AR No. 2, the nonporphyrin coordination sphere is N O 2S (9).

The Ni SEC-HPLC-ICP profile in Figure 1 exhibits more noise due to the lower response factor of Ni in the ICP determination in comparison with V, and the lower concentration of Ni in the feed. It also shows that there are far fewer Ni porphyrins than V porphyrins, as observed for other crudes and residua (5,6). We discuss the following results using only the V profiles. Ni profiles behaved similarly in all cases.

These results and extraction data (6) have lead to a formulation of models for metals in crude oils. We believe the metals to be of two types: 1) the porphyrins which have a narrow, but well defined molecular weight range due to homologous series substitutions (10), and 2) the nonporphyrins, which span a much broader molecular weight and size range. The nonporphyrin molecular size range could be due to small molecular weight compounds which are convoluted in a tertiary-agglomerated structure. The nonporphyrins could also have homologous series type structure.

THERMAL PROCESSING: TEMPERATURE BEHAVIOR

Figure 2 exhibits the V response profiles for California AR No. 1 thermal products. These products were generated from processing in a tubular reactor at moderate thermal severity and low thermal severity. The profiles correspond to 78% and 38% V removal, respectively.

At moderate thermal severity, the remaining metal compounds exhibit a dramatic shift to smaller molecular sizes. The larger prominent maximum is shifted from its position in the feed and appears to be vanadyl petroporphyrins. This will be discussed in a subsequent section.

At low thermal severity, the remaining metal-containing compounds exhibit similar trends, but shift much less than in the moderate thermal severity case.

These results combined with high thermal severity product profiles (not shown), indicate the extent of size reduction appears to be a function of the thermal reactor temperature.

THERMAL PROCESSING: REACTION TIME EFFECT

Figure 3 shows California AR No. 2 processed at moderate thermal severity in the tubular reactor for different reaction times. V removal was 70% in the long residence time, and 50% in the short residence time. There is little difference in the profile distribution of these products. Liquid residence time appears to have little effect on the amount of size reduction.

CATALYTIC PROCESSING

California AR No. 1 was processed downflow in a fixed-bed reactor over commercially available hydroprocessing catalysts. The V SEC-HPLC-ICP profiles of products from short residence times and long residence times are shown in Figure 4. The short residence time profile corresponds to 50% V removal. The remaining metal-containing compounds exhibit a conspicuous lack of smaller components. The porphyrin and similar size compounds are absent, while some of the larger, nonporphyrin compounds are still evident.

Fixed-bed processing at long residence time also removes the smaller metal-containing compounds. The long residence time profile corresponds to 70% V removal. The profile is very similar to that of the short residence time profile showing the longer reaction time does not appear to affect the size profile of the remaining metal-containing compounds. This is also seen in the thermal treatment results above.

Under fixed-bed processing conditions, the catalyst pore size appears important. The compounds that are in the size range of the catalyst pore are removed. This behavior has been seen in the studies on the processing of Safaniya asphaltenes (11), Arabian Light vacuum residuum (VR) asphaltenes and maltenes (12), in gel permeation chromatography (GPC) studies of Venezuelan crudes (13), and in demetalation kinetic studies of Boscan and Arabian Light residua (14).

The metal-containing compounds which do not fit in the catalyst pores require more severe processing. Longer residence times were required to remove these metals. The kinetics of metals removal over typical hydrodesulfurization catalysts have been determined in some cases to be second order (15). This has been explained as demetalation by two different first-order rate constants (16). These could be the respective demetalation rates for the metals which can fit into the catalyst pores and those which cannot.

THERMAL PROCESSING: PORPHYRINS AND NONPORPHYRINS

To determine the individual fates of the porphyrins and nonporphyrins during processing, California AR No. 1 was separated into distillable and nondistillable metal fractions by distillation, and each fraction was thermally processed. Figure 5 shows the separation by distillation. The 454°C to 677°C fraction shows only small size metal-containing compounds. The V in this fraction was determined by UV-vis spectroscopy to be 98% porphyrin, and by methanol extraction to be 90% porphyrin. The 677°C+ fraction is primarily the nonporphyrin metal compounds. Methanol extraction indicates only 2% of the V bound as porphyrin, and UV-vis spectroscopy indicates only 2% of the V bound as porphyrin in this fraction.

For thermal treatment at moderate thermal severity both fractions were diluted with appropriate vacuum gas oil components to their original metals concentration in the AR. Figure 6 shows the V SEC-HPLC-ICP profiles of the 454°C to 677°C fraction before and after processing. It is clear from the profiles that the porphyrins are completely removed (as well as the rest of the V).

Figure 7 shows the V SEC-HPLC-ICP profiles for the 677°C+ fraction before and after moderate thermal severity treatment. The remaining metal-containing compounds are shifted to the smaller

molecular size, similar to those of the moderate thermal severity processing of California AR No. 1.

Nonporphyrins have been thought of as porphyrins which have been encapsulated in an agglomerative network (17). They would not necessarily be detected as porphyrins because their spectroscopic and physical properties could be changed by this agglomeration. The size reduction seen in the thermal treatment of the 677°C+ cut produces compounds which are smaller than either the feed petroporphyrins, or porphyrin model compounds, as evidenced in Figure 7. Porphyrin extraction and UV-vis determination show less than 3% of the V is bound as petroporphyrin in this product. We feel this verifies the existence of the nonporphyrins which are not encapsulated porphyrins.

This argument would be nullified if the structure of the metal-containing compounds were sufficiently changed during processing. For example, the porphyrins could be demetalated, but instead of falling out completely, the metals could combine with other polar organic molecules and could rebind having a nonporphyrin ligand environment.

DISCUSSION

The results shown here are important in the overall picture of processing residua and heavy oils. Although little data exists on the behavior of the metal-containing compounds monitored by element specific detection, some studies have been done by other techniques.

GPC studies on the organic portion of Arabian Light VR maltenes and asphaltenes thermally processed under vis-breaking conditions showed a dramatic decrease in the average molecular size (12) upon increase of process temperature. The same results were found in the heat treatment of Safaniya VR asphaltenes (11). This agrees well with our thermal processing results for the Ni and V, where we also see size reduction which is dependent on thermal temperatures.

The effect of fixed-bed processing under catalytic conditions has been studied more thoroughly. Arabian Light treated under mild hydroprocessing conditions exhibited metals reduction corresponding to catalyst pore size (14). Similar results for the organic portion have been seen with Arabian Light VR asphaltenes (12), Morichal crude (13), and asphaltenes from Safaniya VR (11). This also agrees well with our fixed-bed processing results where the metals are distinctively affected by the pore size of the catalyst.

One of the important consequences of this study is that the porphyrins appear to be removed first in residuum demetalation. This conclusion has been reached previously. Porphyrins have been found to be preferentially removed in thermal treatment with hydrogen and/or hydrogen sulfide (18). In addition, the reaction threshold temperature for porphyrin demetalation was 400°C without, but only 200°C with a fixed-bed hydrogenative catalyst. Oxidative treatment studies of residua have also shown the same effect -- the porphyrins come out first (19,20).

Our studies support these conclusions. The results from separate processing of the porphyrins and the nonporphyrins are evidence that the porphyrins are the most labile. In addition, the removal of the metals is greatly assisted by the fixed-bed hydroprocessing catalyst, which operates at a substantially lower temperature.

However, it is important to note that these results may not be a consequence of the porphyrin or the nonporphyrin coordination sphere, but simply a consequence of the size of the compounds. In the thermal case, the porphyrins were removed because they were most of the smallest metal-containing molecules. In the fixed-bed processing, the porphyrins were removed because of the metal-catalyst pore size relationship.

Studies of feeds and products from the ABC process (21), showed the isotropic EPR parameters of the vanadyl ion exhibited little change in processing, and therefore little or no change in the first coordination sphere about the metal center (22,23). It was concluded from this that the reactivity of the vanadium is determined by the macrostructure of the residuum, and not by the nature of the coordinating metal ligands.

This is also supported by the rates of hydrodemetalation studies of extracted petroporphyrins. The facility by which hydrogenation of porphyrins (24) occurs strongly argues the rate of demetalation is not a function of the intrinsic reaction rate of the first coordination sphere around the metal ion, but diffusion through or denaturing of the polar medium around the metal-centers.

CONCLUSION

We have examined thermal processing and catalytic fixed bed processing by SEC-HPLC-ICP to determine demetalation mechanisms. Thermal processing removes Ni and V and reduces the size of the remaining metal-containing compounds. Fixed-bed processing removes metals as a function of the pore size.

By separating the porphyrins from the nonporphyrins, we have found the porphyrins process the easiest under thermal conditions. This could be a result of their intrinsic reactivity, or merely a function of size or macrostructure. It is our contention, the macrostructure is rate controlling for at least the nonporphyrins.

ACKNOWLEDGEMENTS

The authors would like to thank Sue Bezman for the fixed-bed processed samples, Mietek M. Boduszynski and Tim Attoe for the short-path fractionation of the AR into porphyrin-containing distillate and nonporphyrin-containing residuum, Rick Brown and Jim Gano for assistance with the ICP, Thomas Finger for assistance in sample work-up, and Chris Kuehler for helpful discussions.

REFERENCES

1. Tamm, P. W., Harnsberger, H. F., and Bridge, A. G. 1981. Ind. Eng. Chem. Process Des. Dev., 20:263.

2. Busch, L. E., Hettinger, W. P., Jr., and R. P. Krock. 1984. Oil and Gas J., 82(52):54-56.

3. Bunch, R. A., Kocisicin, J. J., Schroeder, H. F., and G. N. Shaw. 1979. Hydrocarbon Processing, 59(9): 136.

4. Biggs, W. R., Fetzer, J. C., Brown, R. J., and J. G. Reynolds. 1985. Liq. Fuel Tech., 3(3), XXX.

5. Fish, R. H., and Komlenic, J. J. 1984. Anal. Chem., 56:510-517.

6. Fish, R. H., Komlenic, J. J., and Wines, B. K. 1984. Anal. Chem., 56:2452-2460.

7. Sundararaman, P. 1985. Anal Chem., submitted.

8. Reynolds, J. G., Biggs, W. R., Fetzer, J. C., Gallegos, E. J., Fish, R. H., Komlenic, J. J., and Wines, B. K. 1984. Proceedings of the international symposium on crude oils and petroleum residues, Lyon, France, pg 153-157, June.

9. Reynolds, J. G., Biggs, W. R., and Fetzer, J. C. 1985. Liq. Fuel Tech., 3(3), XXX.

10. Baker, E. W. 1967. J. Amer. Chem. Soc., 88(10):2311-2315.

11. Drushel, H. V. 1976. ACS Div. of Petrol. Chem., Preprints, 21(1):146.

12. Hall, G. and Herron, S. P. 1981. ACS Adv. Chem. Ser., 195:137.

13. Sanchez, V., Murgia, E., and Lubkowitz, J. A. 1984. Fuel, 63:612.

14. Bridge, A. G., and Green, D. C. Green. 1979. ACS Div. Pet. Chem., Preprints, 24:791.

15. Oleck, S. M. and Sherry, H. S. 1977. Ind. Eng. Chem. Process Des. Dev., 16:525.

16. Agrawal, R., and Wei, J. 1984. Ind. Eng. Chem. Process Des. Dev., 23:505-514.

17. Yen, T. F. 1975. In The Role of Trace Metals in Petroleum. T. F. Yen Ed., Ann Arbor Science. Ann Arbor, MI. Chapter 1.

18. Rankel, L. A. 1981. ACS Div. of Petrol. Chem., Preprints, 26(3):689-698.

19. Gould, K. A. 1980. Fuel, 59:733-736.

20. Sugihara, J. M., Branthaver, J. F., and Wilcox, W. 1973. ACS Div. of Petrol. Chem., Preprints, 18:645-647.

21. Asaoka, S. Nakata, S., Shiroto, Y., and Takeuchi, C. 1983. Ind. Eng. Chem. Process Des. Dev. 22:242-248.

22. Dickson, F. E., Kunesch, C. J., McGinnis, E. L., and Petrakis, L. 1972. Anal. Chem., 41:576.

23. Dickson, F. E., and Petrakis, L. 1974. Anal. Chem., 44:1129.

24. Rankel, L. A., and Rollmann, L. D. 1983. Fuel, 62:44-46.

FIGURE 1

SEC-HPLC-ICP PROFILES FOR CALIFORNIA AR NO. 1

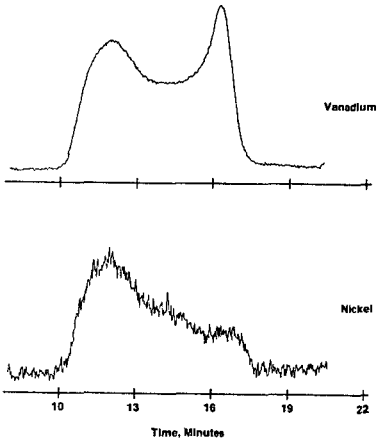

FIGURE 2

CHANGES IN VANADIUM DISTRIBUTION FROM THERMAL TREATMENT OF CALIFORNIA AR NO. 1

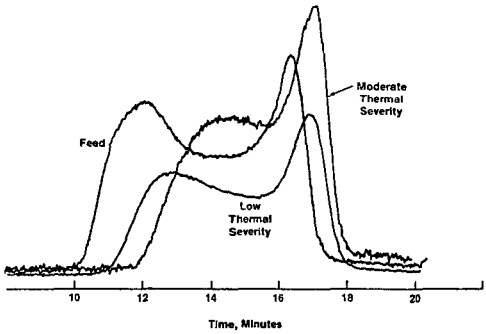

FIGURE 3

CHANGES IN VANADIUM DISTRIBUTION FROM THERMAL PROCESSING OF CALIFORNIA AR NO. 2 AT DIFFERENT REACTION TIMES

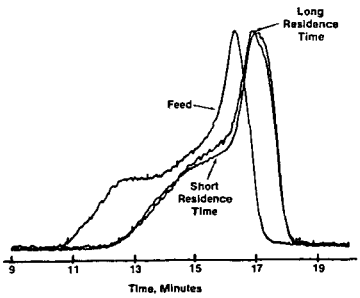

FIGURE 4

CHANGES IN VANADIUM DISTRIBUTION FROM FIXED-BED TREATMENT OF CALIFORNIA AR NO. 1 AT DIFFERENT RESIDENCE TIMES

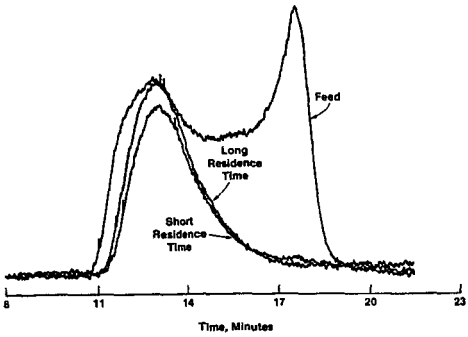

FIGURE 5

VANADIUM SIZE PROFILES OF CALIFORNIA AR NO. 1, 454°C to 677°C DISTILLATION CUT, 677°C+ RESIDUE

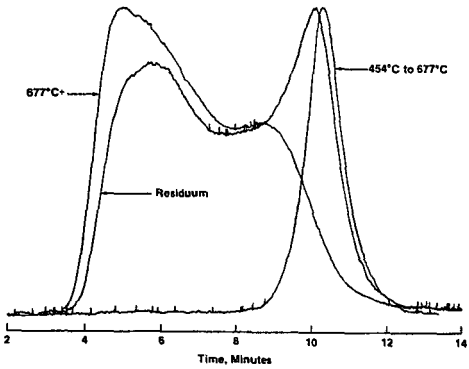

FIGURE 6

CHANGE IN VANADIUM SIZE DISTRIBUTION OF THE 454°C to 677°C DISTILLATION CUT OF CALIFORNIA AR NO. 1 UPON THERMAL TREATMENT

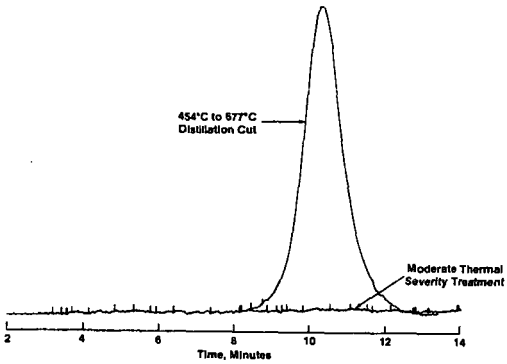

FIGURE 7

CHANGES IN VANADIUM SIZE DISTRIBUTION OF THE 677°C+ RESIDUE OF CALIFORNIA AR NO. 1 UPON THERMAL TREATMENT

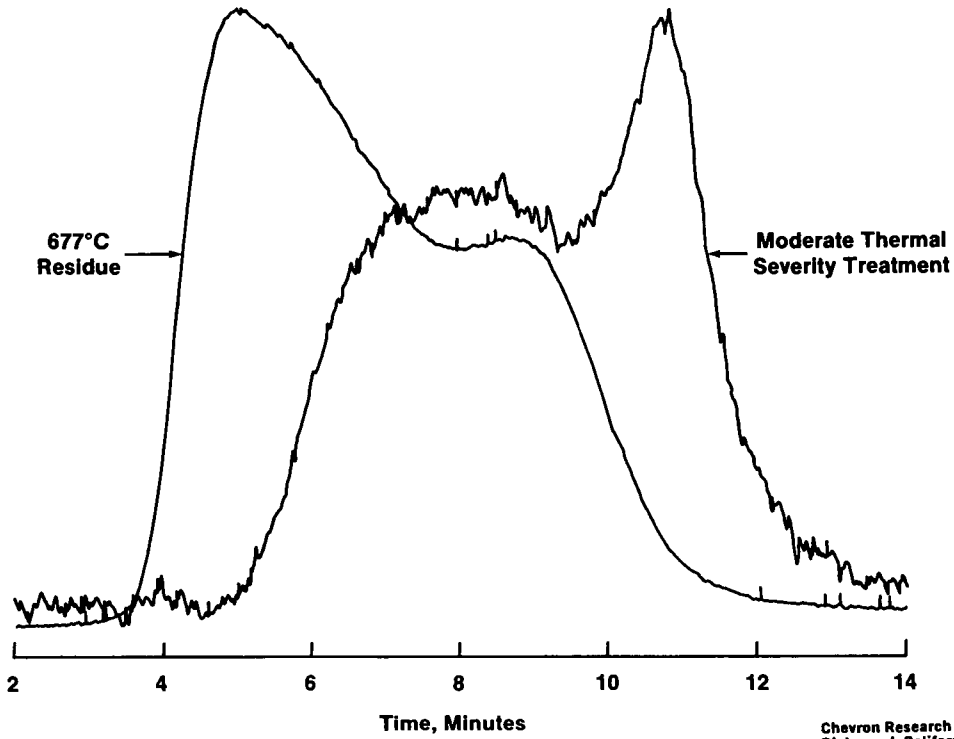

Chevron Research Company
Richmond, California
JGR RA 851575

3-27-85

445

EFFECT OF TRACE METALS ON FCC COKE YIELD

Periaswamy Ramamoorthy
Gulf Research and Development Company
P. O. Drawer 2038
Pittsburgh Pa 15230

An experimental study is underway at the Gulf Research Center in Harmarville, Pennsylvania, aimed at defining the effects of trace metals on the regeneration of fluid cracking catalysts for resid cracking applications. As part of this study a benchscale experimental technique was developed for coking the FCC catalysts under well-mixed conditions. Coke yield was found to correlate well with the type of metal and its concentration.

When contact time was varied the coke yield obeyed the well-known Voorhies-type correlation for each metal:

$$C = AT^n$$

where C is weight percent carbon on the catalyst, T is contact time in minutes, A and n are constants. The experimental technique and results obtained for nickel, antimony, and nickel passivated with antimony are discussed in this paper.

The apparatus used for coking consisted of a shaker bomb with a dipleg as shown in Figure 1. The shaker bomb containing a known weight of catalyst was placed in a fluidised sandbath and heated to a typical temperature of 930 F under nitrogen purge. An oil feed was added at a constant rate to the catalyst over a period of time required 1 minute. The internal catalyst temperature was measured by a thermocouple placed at the center of the dipleg. At the end of run the shaker bomb was transferred to another fluidised sandbath maintained at room temperature. The catalyst was then discharged and its carbon content determined. In addition to carbon, the coke was analysed for hydrogen, sulfur, and nitrogen.

Results obtained for nickel, antimony, and nickel passivated with antimony are discussed here. The metals were added, separately and in combined form, to a batch of an equilibrium catalyst at four concentration levels.

Catalysts containing freshly deposited nickel alone showed a steady increase in coke yield with metal content. When antimony was added to passivate nickel on catalyst a reduction in coke make of approximately 40% was obtained. Typical reduction of 50% is reported for commercial units.

Catalysts containing freshly deposited antimony alone did not affect coke yield, regardless of its concentration.

Coking runs made on aged catalysts of high metal content resulted in coke yield lower than that predicted by the correlation developed

for fresh-metals catalysts.

ACKNOWLEDGEMENT

The author wishes to thank Dr. A. S. Krishna of Gulf Research and Development Company for helpful discussions during the course of this study.

REFERENCE

1. Voorhies, Jr., A., Ind. Eng. Chem., 37(4), 318 (1945)

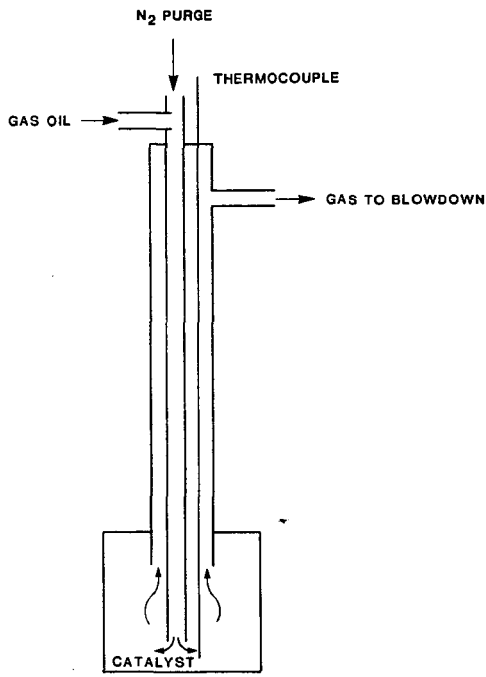

SHAKER REACTOR FOR COKING

THE INFLUENCE OF THE PETROLEUM RESIDUA AND CATALYST TYPE ON COPROCESSING

Christine W. Curtis, Kan-Joe Tsai,
and James A. Guin

Chemical Engineering Department
Auburn University, Alabama 36849

Introduction

The goal of coprocessing heavy petroleum crudes and residua with coal is to simultaneously upgrade both materials into higher quality liquid products. Among the benefits of coprocessing is that it offers a bridge between the present petroleum-based technology and the synthetic fuels coal-based technology of the future. Coal and petroleum residua are both low value hydrocarbon resources, which through coprocessing can be transformed into higher quality and higher value synthetic fuels. The nature of the synthetic fuel produced from coprocessing would be quite different from that of conventional coal liquefaction using a coal-derived recycle stream. The highly aromatic coal-derived synthetic fuel would already be combined with ample quantities of highly paraffinic materials, making the product more similar to fuels used today. In addition, the presence of coal-derived synthetic fuel in the coprocessing product would serve as an octane booster. Another advantage of coprocessing is the elimination or minimization of the coal-derived recycle stream used in conventional coal liquefaction technology.

A number of petroleum materials have been surveyed for their ability to solvate coal and to participate in the upgrading process. (1-4) Both bituminous and subbituminous coals have been successfully used in combined processing (5,6). Using catalytic hydrotreatment with small particle size catalysts, coal conversion of greater than 80% have been achieved for both bituminous and subbituminous coals when using petroleum solvents.(5) The interaction between the petroleum solvent and the coal is complex. Synergistic interactions may exist at different concentration levels of coal and petroleum solvent. In this work the interaction between the petroleum solvent and coal at different solvent to coal ratios is examined in terms of product yield and coal conversion. The chemical composition of the petroleum solvent is substantially different from coal-derived solvents.(1) The effect of improve-ment in the solvent's ability to donate hydrogen through the addition of hydroaromatic compounds on the final product slate has been investigated. Because of the complexity and diversity of the coal-petroleum system, catalyst type may strongly influence one material while not being particularly effective with the other. Examination of the effect of catalyst type on the upgrading of the petroleum residuum and on coprocessing can lead to catalysts that are specifically tailored for enhancement of the coprocessing product slate. In addition, the coprocessing product may be enhanced through a combination of a first stage reaction using a mineral additive and a second stage with a commercial hydrogenation catalyst. This concept is explored in this work.

Experimental

Materials and Feedstocks

The solvents used in this study were heavy petroleum crudes and residua which were supplied by Cities Service Research and Development Company. The specific petroleum materials used were Maya topper long resid (TLR) and West Texas vacuum short resid (VSR). A bituminous Illinois #6 coal, supplied by Wilsonville Advanced

Coal Liquefaction Research and Development Facility, was used as the coal feedstock. The elemental analyses of these feedstocks are given in Table 1. The catalysts used in these reactions were mineralogical pyrite ground to -200 mesh and powdered presulfided Shell 324 $NiMo/Al_2O_3$ that was obtained by grinding 1/16 inch presulfided extrudates. For the hydrogen donor addition experiments, tetralin, 1,2,3,4-tetrahydroquinoline (THQ) and 9,10-dihydrophenanthrene (DHP) were obtained from Aldrich.

Equipment

The combined processing reactions were conducted in stainless steel micro-reactors which have been described in a previous work (7). The reactor has a volume of 50 cc which was charged with a liquid/solid slurry of 9 g and a hydrogen pressure of 1250 psig at ambient temperature at 100% excess hydrogen for the combined processing reactions. A 6g charge was used for the petroleum upgrading experiments. The pressure of 1250 psig at ambient temperature corresponds to approximately 2950 psig at reaction temperature calculated by means of the ideal gas law and ignoring any solubility of the hydrogen. A recovery of greater than 97% of the original charge was obtained from the coprocessing reactions.

Experimental Procedures

A series of experiments were performed using Illinois #6 coal and West Texas VSR in which the solvent to coal ratio was varied from 10:1 to 1:4. The percentage coal present in these reactions ranged from 9.1% to 80%. For comparison, reactions were also performed in which no coal was present and in which no solvent was present. The reaction products were analyzed by a solvent extraction procedure in which the reaction products were sequentially extracted with pentane, benzene, and methylene chloride/methanol. The products obtained were defined as oil, pentane soluble; asphaltenes, pentane insoluble, benzene soluble; preasphaltenes, benzene insoluble, methylene chloride/methanol soluble; and insoluble organic matter (IOM), methylene chloride/methanol insoluble. Analyses performed on the products of the coprocessing reactions were: (1) viscosity at 60°C according to ASTM D-2171 using a Canon-Manning capillary viscometer, (2) specific gravity at 60°F according to ASTM D-70 and ASTM D-287, and (3) Conradson Carbon according to ASTM D-189.

The coprocessing reactions with the addition of hydroaromatic solvents were performed at 425°C, in a N_2 or H_2 atmosphere, for 30 minutes. The charge to the reactor was 3 grams of Illinois #6 coal and 6 grams of total solvent. The solvent was composed of 0.3 g, 1.1 g or 3.0 g of hydroaromatic compound with 5.7 g, 4.9 g or 3.0 g of Maya TLR, respectively. The pressure of N_2 charged to the reactor was 300 psig and of H_2 was 1250 psig.

Mineralogical pyrite and small particle size $NiMo/Al_2O_3$, ground from presulfided 1/16" extrudates were used to determine the effect of catalyst type on the upgrading of West Texas VSR and on coprocessing of Illinois #6 coal with West Texas VSR and Maya TLR. The reactions were preformed at 425°C, 30 minutes, with 6 g of petroleum solvent, 3 g of coal and 1 g of catalyst.

The reaction conditions for single stage processing were 60 minutes, 425°C, 1250 psig H_2 charge, and 2 grams of catalyst. The catalysts used were pyrite, $NiMo/Al_2O_3$ and H_2S which was generated in situ from the reaction of carbon disulfide with hydrogen.

The two stage experiments were performed as two sequential 30 minute reactions at 425°C, 1250 psig H_2 charge, 9 grams of petroleum/coal slurry and 1 gram of catalyst in each stage. The gas weight was determined after the first stage; the reactor was then opened and the second stage catalyst was added. After repressurizing with hydrogen, a second reaction was performed. The total gases were calculated through the addition of the gases produced during each stage. The first stage mineral catalyst was not removed and was present in the second stage reactions. For the calculations of the final amount of reacted FeS_2 remaining, the FeS_2 is assumed to react completely to form FeS.

Results and Discussion

To tailor the coal-resid system for maximal yields of high quality liquid products, the influence of the petroleum solvent on the products obtained from coprocessing must be known. Addition of additives such as hydrogen donors may enhance the desired product yield. With two complex and diverse materials present, catalyst selection becomes more complex, for a particular catalyst may catalyze reactions of one of the materials much more strongly than the other. Combination of catalyst types may prove feasible to achieve the many diverse reactions needed to achieve high coal conversion and high yields of liquid product simultaneously.

The Effect of Solvent to Coal Ratio on Coprocessing

One of the advantages of coprocessing is the elimination or minimization of the coal-derived recycle stream needed in conventional coal liquefaction technology. In conventional liquefaction the solvent to coal ratio usually ranges from 1:1 to 3:1 with the ratio being dependent on the materials used and the operability and range of the mechanical equipment. In coprocessing, a limitation on the solvent to coal ratio will still exist due to physical constraints. In this study, however, we investigated a wide range of solvent to coal ratios to observe the effect of the solvent concentration on the final product distributions obtained. At low solvent to coal ratios, the mass transfer of the hydrogen to the coal may be inhibited. At high solvent to coal ratios, the coal may serve as an extender or enhancer to the petroleum material, by synergistically promoting the upgrading of the petroleum material.

The range of solvent to coal ratios examined was 10:1 to 1:4. The reactions were performed at the coprocessing conditions given in the Experimental section. In these experiments, the reactor liquid plus solid loading was kept constant so that nine (9) grams of petroleum-coal slurry was introduced each time. The amount of catalyst used in each reaction remained constant at one gram. Since both the percentage solvent and coal changed in each reaction, experimental results must be expressed independently of the amounts of petroleum solvent and coal. The hydrogen consumption and coal conversion can be used directly. The amount of material upgraded to oil can also be determined independently of the system by defining it as oil production which is the grams of oil produced (final oil-initial oil) divided by amount of the upgradable material. The upgradable material is composed of maf coal and the nonpentane soluble fraction of the solvent.

As the percentage of coal increased from 9.1% to 50%, coal conversion increased from 42.6% to 87.2% as presented in Figure 1. At increasingly higher levels of coal, the amount of coal conversion steadily decreased. When no solvent was present, a coal conversion of 33% was obtained. Hydrogen consumption, shown in Figure 2, followed the same trend, giving a maximum at 50% coal loading. The percent oil production achieved at coal percentages of 25% to 50% was constant at

~33% as shown in Figure 3. A similar value of 28% oil production was obtained at 9.1% coal loading. At higher coal loading, the percent oil production decreased rapidly, falling to ~15% at 80 and 100% coal loading.

The complexity of the coprocessing reaction system and the many reactions which occur simultaneously make it difficult to ascertain the reasons for the behavior observed as the solvent to coal ratio was varied. The interrelation-ship among coal conversion, oil production and hydrogen consumption is evident. Hydrogen consumption is directly related to the amount of coal conversion achieved and the amount of oil production observed. The behaviors of coal conversion and oil production as a function of the increased weight percentage of coal in the reactions are more difficult to explain.

Numerous factors may be influencing these behaviors and causing interactive effects. Some of the factors involved may be mass transfer effects, concentration of the coal and solvent blends, compositional effect of the blend of liquefied materials, catalyst poisoning and deactivation and solvolysis of the dissolving coal matrix by the liquid phase present. Since in coprocessing, the molecular composition varies rather dramatically from high solvent to coal ratios to low solvent to coal ratios, solvolysis of the dissolving coal matrix by the liquid present in the reactor may be an important factor in the observed behavior of coal conversion and oil production. The 50% blend of coal to petroleum solvent may provide a good coal dissolving solvent. Mass transfer of H_2 to the dissolving coal matrix is most likely better achieved when a higher proportion of solvent is present. Therefore, the higher yields of oil and of coal conversion achieved at higher solvent to coal ratios compared to the lower ratios may be due to the increased availability of hydrogen to the coal. The decline at high coal loadings may be due to mass transfer limitations on H_2. In this system, however, it must be remembered that the coal to catalyst ratio increased as the coal loading increased; or stated in another manner, the catalyst loading remained constant as the percent coal in the reaction increased. The decline in coal conversion and oil production may be due to catalyst deactivation and rapid loss of activity in the concentrated coal matrix. As stated earlier, the exact reasons for the behavior observed can not be pinpointed. One possible rationale is that several different mechanisms are occurring and that different mechanisms are dominant at different coal concentrations.

Analyses of some of the physical properties of coprocessing reaction products have been performed and are compared to the original coprocessing solvent, West Texas VSR, and hydrotreated West Texas VSR in Table 2. Products obtained from reactions using a 10:1 solvent to coal ratio and a 2:1 solvent to coal ratio were examined. The physical properties evaluated were viscosity, degrees API gravity, specific gravity and Conradson Carbon. In the hydrotreatment of West Tesas VSR the viscosity of the resid at 60° C decreased from 324.8 to 1.07 poise; Conradson Carbon decreased by almost half and °API gravity almost doubled. The viscosities of the materials obtained from coprocessing have much lower viscosities than the original residuum. In the coprocessing reaction with a 10 to 1 solvent to coal ratio the viscosity was reduced to 0.363 poise and the Conradson Carbon was lowered to 13.49. The presence of the coal may be producing synergy in that the viscosity was reduced to less than that of West Texas VSR hydrotreated in the presence of $NiMo/Al_2O_3$ but in the absence of coal. Increased coal concentration resulted in an increase in the viscosity to 22.7 poise and an increase in Conradson Carbon to 17.78.

Effect of Hydrogen Donor Addition on Coprocessing

Recent studies have shown the importance of hydrogen donors and transfer agents in the dissolution of coal (8-11). The role and importance of hydrogen transfer in

coprocessing are investigated herein by studying the effect of the addition of hydrogen donor compounds such as tetralin, 1,2,3,4-tetrahydroquinoline (THQ) and 9,10-dihydrophenanthrene (DHP) to the petroleum solvent used in coprocessing. In these coprocessing reactions, the coprocessing solvent was Maya TLR and the coal was Illinois #6. Three levels of donable hydrogen have been studied, 0.15%, 0.55% and 1.5% in N_2 and H_2 atmospheres. The effect of these additions on oil production and coal conversion obtained from coprocessing reactions is presented in Table 3. In the coprocessing reactions in which tetralin was added, both coal conversion and oil production increased when comparing N_2 to H_2 atmospheres for equivalent donable hydrogen addition. However, at the 0.15% tetralin addition level in the H_2 atmosphere, the product slate was very similar to that obtained in H_2 using only Maya TLR. The effect of a H_2 atmosphere on coal conversion was dramatic, increasing coal conversion from 19.6% in N_2 to 58.9% in H_2 at the lowest donor hydrogen addition level. When 1.5% donable hydrogen was present in the tetralin Maya/TLR system, coal conversion in N_2 was 62.1% which was essentially equivalent to the coal conversion obtained with 0.15% donable hydrogen in a H_2 atmosphere. In these reactions, it appears that the form that the hydrogen is in, whether molecular hydrogen or donable hydrogen from hydroaromatic compounds, is not critical. The necessary criterion for coal conversion to be achieved is for the hydrogen to be present in a form which can be utilized by the coal. The use of a H_2 atmosphere to the tetralin/Maya TLR system with 1.5% donable hydrogen further aided in coal conversion, indicating that a hydrogen deficiency existed in the N_2 atmosphere even when a significant amount of tetralin was present.

As in the tetralin system, the effect of the H_2 compared to the N_2 atmosphere on the THQ/Maya TLR system was dramatic. At 0.15% donable hydrogen, coal conversion increased from 23.2% in N_2 to 58.0% in H_2. In contrast, coal conversion in the THQ/Maya TLR system at the highest donable hydrogen level was insensitive to atmosphere. In N_2, 89.0% coal conversion was observed while in H_2, 90.4%, was seen. The amount of pentane soluble materials produced was the same in N_2 regardless of the amount of donable hydrogen. In H_2, only a small increase in pentane solubles was observed by increasing the amount of donable hydrogen from 0.15% to 1.5%.

Oil production increased in the 1.5% donable hydrogen tetralin system compared to the 0.15% tetralin system. A possible reason for the increased oil production is the availability of more hydrogen to the dissolving coal matrix resulting in an increased amount of hydrogenation occurring and the production of hydrogenated products soluble in pentane. The change in solvent composition due to the presence of the hydroaromatic may also be partially responsible for the observed change in percent oil production. Further elucidation of the role of hydrogen donor compounds in coprocessing was sought by comparing the effect of DHP on the product slate to that of tetralin and THQ. The choice of DHP was based upon its comparable ability to convert coal as THQ (12) and upon the fact that it is a hydrocarbon without any of the detrimental characteristics generally associated with nitrogen containing hydroaromatics. When compared at a 0.55% donable hydrogen level, DHP converted more coal to soluble material than THQ and yielded a higher percent oil production than did tetralin.

Comparing the low levels of donable hydrogen using tetralin and THQ showed remarkably similar product distributions in both H_2 and N_2 atmospheres. A contrast is observed, however, when comparing these two at the highest donor level. In THQ, a markedly lower amount of pentane soluble material was produced than in tetralin. The percent oil production in the 1.5% donable hydrogen system in N_2 was -30.7% in THQ and 15.9% in tetralin; likewise, in H_2 the values were 4.0% in THQ and 25.0% in tetralin. The product slate obtained from THQ contained many more asphaltenes than that from tetralin.

These results are in agreement with those observed in coal liquefaction where hydroaromatics having a nitrogen functionality readily dissolve coal. The reasons for their effectiveness resulted from their ability to penetrate and swell coal and their ability to transfer hydrogen. These good features of the nitrogen containing compounds were, however, overridden by their propensity to form adducts with themselves and with coal-derived materials. This adduct formation has been extensively studied by Cronauer (13). The adduct formation is readily apparent in the increased levels of asphaltenes observed during the coprocessing reaction containing THQ.

Effect of Catalyst Type on Coprocessing

The effect of catalyst type on the coprocessing of heavy crudes and residua with coal has been investigated using a mineralogical pyrite and a small particle size NiMo on γ-Al_2O_3. Both of these catalysts were used to study their effect on upgrading residua and on the product slate from coprocessing. In the resid upgrading experiments, West Texas VSR was used; in the coprocessing reactions both West Texas VSR and Maya TLR were used. In Table 4, upgrading reactions of West Texas VSR are compared among the thermal reaction, the reaction containing pyrite and the reaction with small particle size NiMo/Al_2O_3 catalyst. The original solubility distribution obtained prior to reaction is given as a reference. Compared to the original West Texas VSR, the thermal reaction produced gases and IOM, lost oil, and increased slightly the amount of asphaltenes present. When pyrite was added as a catalyst, the asphaltenes were virtually eliminated from the residuum, producing primarily pentane soluble oil. Small amounts of gases, preasphaltenes and IOM were also produced. In contrast, the presence of a small particle size NiMo/Al_2O_3 catalyst did not change the oil fraction but did reduce the asphaltene fraction by ~80% producing gas, preasphaltenes and IOM in almost equal amounts.

The effect of pyrite and NiMo/Al_2O_3 addition on the products obtained from coprocessing are presented in Table 5. Four different reactions are compared with West Texas VSR: (1) thermal reaction (2) two reactions with pyrite and (3) reaction using small particle size NiMo/Al_2O_3. The conditions for all the reactions were the same; both pyrite and NiMo/Al_2O_3 were introduced at the same gram level. The pyrite reaction produced the most coal conversion, 87.6%, compared to 79.3% for the NiMo/Al_2O_3 and 55.0% for the thermal reaction. In terms of pentane soluble oils, the amount produced by the pyrite reaction fell between that obtained by the thermal reaction and by the commercial catalyst. Due to the effect observed on the residuum alone, pretreatment of the solvent with pyrite and hydrogen prior to using as a coprocessing solvent was thought to be possibly beneficial in improving the entire product slate. However, comparison of the product slate using the hydrotreated West Texas VSR to that obtained using the original showed little improvement that could be attributed to hydrotreatment. One possible explanation for this behavior is that the primary effect of the pyrite is in the upgrading of the residuum asphaltenes to pentane solubles and that the reaction producing pentane solubles from coal is not substantially affected by the presence of pyrite. Thus, the majority of the pentane solubles produced from the coprocessing reaction using the original West Texas VSR was produced most probably from the residuum and not from coal. In the hydrogen pretreatment case, most of the upgrading of the residuum had ccurred prior to the coprocessing reaction leaving little material from the residuum for further upgrading. Consequently, little change in the product slate was observed between the original and hydrotreated material. When pyrite was used in coprocessing experiments using Maya TLR, similar results were obtained.

Single Stage and Two Stage Coprocessing Reactions

Two stage processing using sequential and possibly different catalysts in the first and second stages may produce a more favorable product slate from coprocessing as well as a more efficient use of hydrogen. Two sets of experiments were performed to investigate the effects of two stage processing and sequential catalytic treatment on coprocessing. One was a series of one hour reactions in which pyrite, $NiMo/Al_2O_3$ and H_2S were used individually as catalysts and in combination. These results are given in Table 6. In the second set two stage experiments were run for a total of one hour but after the first half hour the gases were vented, a new catalyst was added, and fresh hydrogen was charged. The catalyst charge at the end of both reactions was 2 grams.

The single stage one hour reactions showed similar results to that observed previously. The coprocessing reaction using pyrite catalyst again produced the highest coal conversion; however, the conversions observed from Shell 324 $NiMo/Al_2O_3$ were also both above 80%. The percent oil production observed is given below for the reactions containing the different catalyst

$$NiMo/Al_2O_3 > \text{Pyrite} + NiMo/Al_2O_3 > \text{Pyrite} > H_2S > \text{Thermal} \qquad 1)$$

The small particle size $NiMo/Al_2O_3$ is by far the most effective catalyst in producing pentane soluble oil.

To test the hypothesis that H_2S was the catalytic agent rather FeS_2 in the reactions using the pyrite catalyst, CS_2 which readily reacts with H_2 to form H_2S was added to the reaction. The amount of CS_2 added was equivalent to that needed to produce the same amount of H_2S as would be generated from FeS_2. Under these conditions, the product slate obtained did not vary significantly from the thermal reaction. This result suggests then that the important catalyst in the reactions using pyrite is the pyrite itself or its reduced form, not the evolved H_2S.

In two stage processing, four sets of experiments were performed: thermal for the first stage and thermal for the second stage; pyrite in both stages; then pyrite in the first stage with $NiMo/Al_2O_3$ in the second stage and $NiMo/Al_2O_3$ in both stages. The highest amount of coal conversion achieved, 92.2%, occurred in the experiments using pyrite in both stages. The pyrite/$NiMo/Al_2O_3$ and $NiMo/Al_2O_3$/ $NiMo/Al_2O_3$ reactions also produced high coal conversions, 85.9% and 84.1%, respectively. The oil production from the two stage coprocessing showed the same order as did the single stage experiments. The reaction with $NiMo/Al_2O_3$ in both stages produced the most oil while the combination of pyrite/$NiMo/Al_2O_3$ was second.

Summary and Conclusions

In coprocessing, the solvent to coal ratio has a definite influence on the product distribution, oil production and coal conversion. The highest coal conversion occurred at a 50% coal concentration level and maximal oil production was achieved at 30 to 50% coal concentration. When reacted in a hydrogen atmosphere, the addition of hydrogen donor compounds to the coprocessing solvent definitely influenced the products from coprocessing. At equivalent donable hydrogen levels, DHP produced the highest coal conversion and oil production. At and above the 0.55% donable hydrogen level, THQ was very effective in converting coal but was detrimental to oil production. In general, the hydrogen donor compounds without heteroatoms appear to be more effective in producing oil than the nitrogen containing hydroaromatics.

The catalyst type is important in coprocessing since different catalysts influence different reactions in the two materials. Pyrite affected the upgrading of the residium by promoting the conversion of petroleum asphaltenes into oil. In coprocessing, the notable effect of pyrite was the reduction of the IOM levels and consequent increase in coal conversion. Compared to the thermal reaction, pyrite was effective in increasing the oil production in coprocessing. The small particle size $NiMo/Al_2O_3$ catalyst, however, was still more effective in hydrogenating the dissolving coal matrix and producing pentane soluble oil. In two stage processing, the combination of pyrite in the first stage and $NiMo/Al_2O_3$ in the second produced a much improved product slate compared to thermal processing. The highest oil production and coal conversion were, however, still achieved by using $NiMo/Al_2O_3$ in both stages.

References

1. Curtis, C. W., Pass, M. C. and Guin, J. A., submitted to I & EC Process Design and Development, 1984.
2. Yan, T. Y. and Espenschied, W. F., Fuel Processing Technology, 7, 121, 1983.
3. Shinn, J. H., Dahlberg, A. J., Kuehler, C. W., and Rosenthal, J. W., "The Chevron Co-Refining Process", presented at the EPRI Coal Liquefaction Contractor's Meeting, May 1984.
4. Moschopedis, S. E., Hawkins, R. W., Fryer, J. F. and Speight, J. G., Fuel, 59, 647, 1980.
5. Curtis, C. W., Tsai, K. J. and Guin, J. A., I & EC Process Design and Development, in press, 1985.
6. Miller, Ronald L., "Exploratory Studies in Co-Processing", EPRI Coal Liquefaction Contractor's Conference, May 1984.
7. Curtis, C. W., Guin, James A., Tarrer, Ray and Huang, Wan-Jiao, Fuel Process. Technology, 1983, 7, 277-291.
8. Neavel, R. C. Phil. Trans. R. Soc. Lond., 1981, A300, 141.
9. Brooks, D. G., Guin, J. A., Curtis, C. W. and Placek, T. D., Ind. Eng. Chem. Proc. Des. Dev. 1983, 22, 343.
10. Curran, G. P., Struck, R. T. and Gorin, E. Ind. Eng. Chem. Proc. Des. Dev., 1967, 6, 166.
11. Neavel, R. C., Fuel, 1976, 55, 234.
12. Curtis, C. W., Guin, J. A., Kwon, K. C., Fuel, 1984, 63, 1404.
13. Cronauer, D. D. Heterofunctionality Interaction with Donor Solvent Coal Liquefaction," Fossil Energy Final Report for DOE|PC|50782-T1(DE840132-83).

Table 1
Analysis of Petroleum Solvents

Starting Materials	Oil	Asphaltenes	C	H	N	S	O by difference	Ash
Illinois #6 Coal			68.4	4.4	1.4	3.2	12.0	10.6
Maya TLR	79.5	20.5	85.3	10.8	0.51	4.19		0.082
West Texas VSR	86.2	13.8	86.1	10.4	0.44	3.33		0.012

Table 2
Physical Properties Comparison

Material Tested	Viscosity 60°C, poise	°API	Specific Gravity, 60°C	Conradson Carbon
West Texas VSR	324.8	7.9	1.015	16.4
Product from 10:1 West Texas VSR to Coal Coprocessing Reaction	0.363	13.39	0.9766	13.49
Product from 2:1 West Texas VSR to Coal Coprocessing Reaction	22.7	7.1	1.021	17.78
Hydrotreated West Texas VSR	1.07	15.9	0.96	9.34

Table 3
Effect of Hydrogen Donor Addition on Coprocessing

	Oil Production, %		Coal Conversion, %	
	H_2	N_2	H_2	N_2
Maya TLR	11.8	-11.6	60.0	24.1
0.15% Donable Hydrogen Added				
Tetralin	11.2	- 9.2	58.9	19.6
THQ	6.7	-12.3	58.0	23.2
0.55% Donable Hydrogen Added				
Tetralin	10.5	0.7	58.8	39.3
THQ	2.5	-11.4	75.4	52.7
9,10-DHP	17.5	4.6	81.0	58.8
1.5% Donable Hydrogen Added				
Tetralin	25.0	15.9	81.0	62.1
THQ	4.0	-30.7	90.4	89.0

Table 4
Effect of Catalyst on Upgrading of West Texas VSR

	West Texas VSR Original	West Texas VSR	West Texas VSR	West Texas VSR
Catalyst	NA	None	Pyrite	$NiMo/Al_2O_3$
Coal	NA	None	None	None
Gas	0.0	3.5	1.9	3.9
Oil	86.2	79.1	95.3	86.6
Asphaltenes	13.8	15.0	0.6	3.1
Preasphaltenes	0.0	0.1	1.2	2.8
IOM	0.0	2.3	1.0	3.6
H_2 Consumption, %	NA*	4.9	15.4	31.9

*NA: not applicable

Reaction Time: 30 minutes

Table 5
Effect of Catalyst on the Coprocessing Reactions

	West Texas VSR Original	West Texas VSR	Hydrotreated* West Texas VSR	West Texas VSR
Catalyst	None	Pyrite	Pyrite	$NiMo/Al_2O_3$
Gas	4.2	3.3	3.0	4.3
Oil	58.6	67.1	68.3	72.9
Asphaltenes	15.2	19.6	16.6	13.4
Preasphaltenes	8.2	6.2	6.6	3.0
IOM	13.8	3.8	5.5	6.4
Coal Conversion, %	55.5	87.6	82.3	79.3
H_2 Consumption, %	24.2	37.9	30.0	52.9
Oil Production, %	-2.1	18.8	2.25	33.1

*The solvent was hydrotreated in the presence of pyrite.

	Maya TLR	Maya TLR	Maya TLR $NiMo/Al_2O_3$
Catalyst	None	Pyrite	$NiMo/Al_2O_3$
Gas	4.3	3.3	4.7
Oil	60.1	64.6	69.7
Asphaltenes	14.7	19.1	16.4
Preasphaltenes	8.5	7.1	2.2
IOM	12.4	5.9	7.1
Coal Conversion, %	60.0	81.0	77.0
H_2 Consumption, %	18.9	40.1	55.6
Oil Production, %	11.7	21.5	32.9

Table 6
Single Stage Coprocessing Using West Texas VSR

Catalyst	Thermal	~0.32g CS_2	Pyrite	$NiMo/Al_2O_3$	Pyrite & $NiMo/Al_2O_3$
Coal Conversion, %	58.2	57.4	89.2	85.0	83.7
Hydrogen Consumption, %	30.4	33.3	57.1	72.5	66.5
Oil Production, %	-8.3	-6.9	23.9	54.3	39.3

Two Stage Coprocessing Using West Texas VSR

First Stage Catalyst	None	Pyrite	Pyrite	$NiMo/Al_2O_3$
Second Stage	None	Pyrite	$NiMo/Al_2O_3$	$NiMo/Al_2O_3$
Coal Conversion, %	64.3	92.2	85.9	84.1
Hydrogen Consumption, %	14.5	27.5	35.6	41.1
Oil Production, %	-0.4	26.8	43.0	58.5

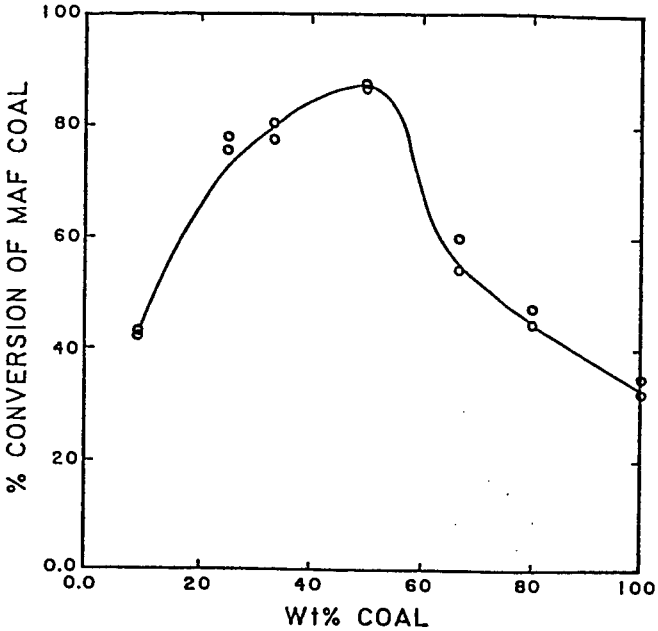

Figure 1. Coal Conversion as a Function of Coal Concentration

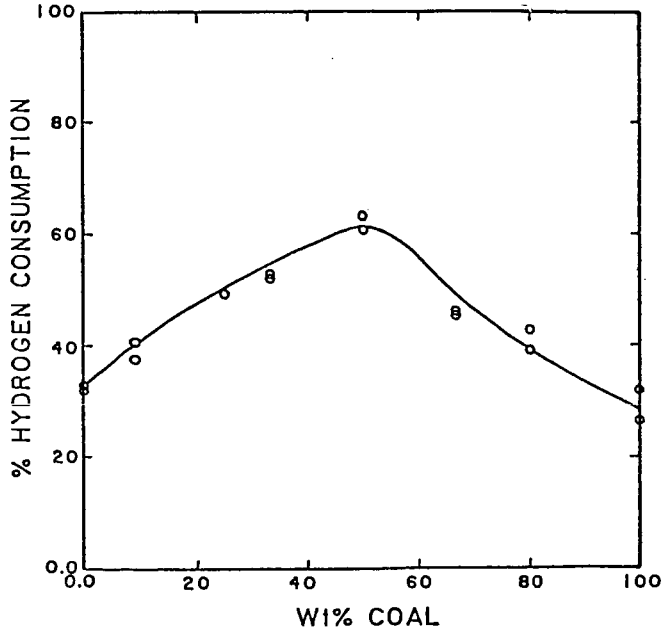

Figure 2. Hydrogen Consumption as a Function of Coal Concentration

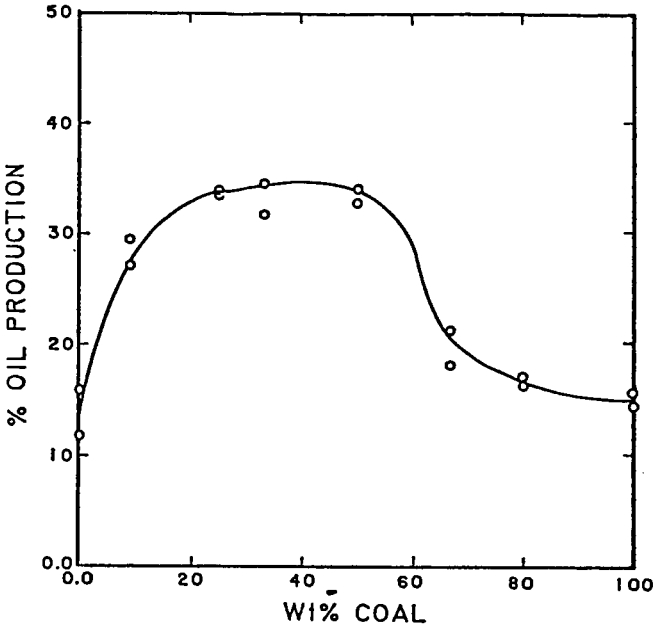

Figure 3. Oil Production as a Function of Coal Concentration

HIGH-PRESSURE CATALYTIC HYDROPROCESSING OF A SIMULATED COAL LIQUID

By

M. J. Girgis, B. C. Gates
Center for Catalytic Science and Technology, Department of Chemical Engineering
University of Delaware, Newark, Delaware 19716
and
L. Petrakis
Gulf Research and Development Company, Pittsburgh, Pennsylvania 15320

INTRODUCTION

The catalytic hydroprocessing of coal-derived liquids is poorly understood because of the complexity of the liquids and the large number of competing reactions. The goal of this research was to characterize quantitatively the hydroprocessing of a liquid mixture modelling a coal liquid derived from Powhatan No. 5 coal in the SRC-II process. A specific goal was to determine relstive reactivities of representative reactants and determine the competitive inhibition effects of the various reactants. The experiments were carried out with a mixture of at most nine compounds representing the major functional groups in the coal liquid. The reactants included polynuclear aromatic hydrocarbons, sulfur- and oxygen-containing heterocyclics. 1-naphthol, and basic as well as nonbasic organonitrogen compounds.

There is no one typical coal liquid because the compounds and their relative amounts vary with the source of the coal and with the type and operating severity of the coal liquefaction process. In this study, the choice of model compounds and their relative amounts were based on a detailed analysis of the SRC-II heavy distillate (1,2). The concentrations of compounds containing heteroatoms were chosen to give the same concentrations of functional groups present in the SRC II heavy distillate; the concentrations of aromatic hydrocarbons were chosen to give a molar ratio of 3:2:1 of fused 2-ring, 3-ring, and 4-ring aromatic compounds.

EXPERIMENTAL

Apparatus and Procedure

The experiments were carried out with a fixed-bed flow microreactor (3). The feed was prepared by dissolving the reactant compounds in cyclohexane to give a solution with a total solute mass fraction of 0.0025. Approximately 800 ml of solution was added to either of two 1000-ml high-pressure autoclaves equipped with stirrers. The feed and the vapor space above it were purged with hydrogen for two hours at room temperature with a hydrogen flow rate of 50 ml/min. Carbon disulfide dissolved in another 10 ml of feed was then quickly added to give 0.001 mass fraction of carbon disulfide in the feed. [The carbon disulfide served as a source of hydrogen sulfide via the reaction $CS_2 + 4H_2 \longrightarrow 2H_2S + CH_4$, which occurs rapidly under the reaction conditions (4); the CS_2 maintained the catalyst in the sulfided state.] The autoclave was pressured up to 137.1 atm with hydrogen at room temperature, and the feed was saturated with hydrogen. This resulted in a hydrogen mole fraction of approximately 0.05 in the feed (5) or a 50:1 hydrogen to reactant mole ratio, which prevented the hydrogen mole fraction from varying significantly over the length of the reactor.

The saturation of the feed with hydrogen prior to its introduction into the reactor ensured that only two phases were present in the reactor, which allowed

determination of reaction kinetics in the absence of mixing effects or significant radial gradients in concentration or temperature. Because the reactor was held at a higher temperature and pressure than the autoclave, no degassing of the feed occurred, as confirmed by thermodynamic calculations.

The reactor consisted of a vertical 316 stainless steel tube 25.4 cm long with an internal diameter of 0.95 cm. The bottom 11 cm of the reactor were packed with 90-mesh alundum, the next 3 cm were packed with 0.050 g of catalyst mixed with alundum, and the remainder of the tube was packed with alundum. A detailed description of the reactor is given elsewhere (3).

The catalyst was sulfided by passing a mixture of 10% H_2S in H_2 through the catalyst bed at 30 cm^3/min for two hours at 400°C. The reactor was then cooled to the reaction temperature (usually 350°C) under H_2S/H_2 and then brought to the reaction pressure of 171 atm. The feed was pumped through the reactor by a Waters M-6000A liquid chromatography pump. Liquid samples could be taken from either a sampling valve or a dead volume cylinder, both of which were located downstream of the reactor. For each run, the reactor was operated until steady-state was reached (usually 24-30 h); only data from steady-state samples are reported.

The analyses of the liquid samples were performed with a Tracor 560 gas chromatograph (GC) equipped with a 30-m DB-5 bonded phase capillary column. The GC contained an outlet splitter which permitted the column effluent to be divided into two streams, one going to a flame ionization detector (FID) and the other to a Hall electrolytic conductivity detector. The latter was used to identify nitrogen-containing compounds and the former was used for quantitative product analysis using n-decane as an internal standard. FID response factors relative to n-decane were determined for all the reactants. Some of the samples were also analyzed by gas chromatography-mass spectrometry.

Materials

The catalyst used in this work was American Cyanamid HDS-9A, a $NiO-MoO_3/\gamma-Al_2O_3$ catalyst, the properties of which are listed in Table II. Prior to use, the catalyst was ground from 1/16" extrudates to 80-100 mesh particles. The alundum used to pack the reactor was Alundum RR (Fisher Scientific, Blue Label). All chemicals listed in Table I as well as the cyclohexane solvent were obtained from Aldrich Chemical Company and used as received. n-Decane was obtained from Eastman Chemical Co. High-pressure hydrogen (3500 psig) and the 10% H_2S in H_2 were obtained from Linde and Matheson, respectively.

RESULTS AND DISCUSSION

The first series of experiments was conducted with the simulated coal liquid designated in Table I. These experiments had the following objectives:

a) To determine the reactivities of the various reactants in a mixture at different temperatures and weight hourly space velocities (WHSV).
b) To identify as many reaction products as possible.
c) To establish the limitations of the chromatographic analyses of the products (e.g., determine which peaks could not be resolved). Product chromatograms were expected to be complex, with overlapping peaks.

Experiments were carried out at each of the conditions shown in Table III. In Table IV. the reaction products identified are listed with the methods used to identify them (mass spectrometry and co-injection with a pure compound into the chromatograph). Some problems were encountered in resolving important peaks in the product chromatograms. The major resolution difficulty occurred with dibenzothiophene; a peak of comparable size was merged with it on its down slope, and a small peak from a nitrogen-containing compound appeared on its up slope. The small peak on the up slope was not resolvable from the dibenzothiophene peak on the FID trace (we detected it with the Hall detector); as a result, the calculated dibenzothiophene mass fraction was greater in product samples than in

the feed. Therefore, the only way to determine dibenzothiophene hydrodesulfurization (HDS) was to sum the mass fractions of biphenyl and cyclohexylbenzene in the product and divide by the feed dibenzothiophene mass fraction. A similar difficulty occurred with phenanthrene, as the Hall detector indicated a nitrogen-containing peak at approximately the retention time of phenanthrene, whereas the FID trace showed only one large peak. Since the Hall detector was used only for qualitative analysis. it was not possible to subtract the contributions of the nitrogen-containing compounds. Hence, we expect that the actual phenanthrene conversion was somewhat higher than the calculated results. The additional analytical problem occurred with acridine. Of the approximately six organonitrogen compound peaks expected as acridine products, only one, that for 1,2,3,4,5,6,7,8-octahydroacridine, was identified; no hydrocarbon hydrodenitrogenation (HDN) products were identified.

Table V is a summary of the results for runs at constant temperature (350°C) and varying WHSV with the simulated coal liquid designated in Table I. The conversions of the basic nitrogen compounds, quinoline and acridine, were higher than that of indole, the non-basic nitrogen compound. However, the fraction HDN of quinoline (defined as the moles of the quinoline and nitrogen-containing quinoline derivatives in the product divided by the moles of quinoline in the feed) was considerably less than the quinoline conversion. It was not possible to obtain a reliable value for acridine HDN.

Figure 1 is a pseudo first order kinetics plot for quinoline and indole HDN (i.e., a plot of the fraction of non-dehydronitrogenated compounds vs. inverse space velocity). Quinoline HDN followed pseudo first order kinetics, whereas indole HDN did not.

The conversion of dibenzofuran was too low to be measured reliably; this was the least reactive of the reactants. In contrast, the conversion of 5,6,7,8-tetrahydro-1-naphthol was always greater than 80%. No oxygen-containing products of 5,6,7,8-tetrahydro-1-naphthol were found; it is inferred that the 5,6,7,8-tetrahydro-1-naphthol conversion is identical to is hydrodeoxygenation (HDO).

Dibenzothiophene was converted appreciably only at the lowest space velocity; biphenyl and cyclohexylbenzene were detected as HDS products.

The conversions of phenanthrene, fluoranthene, and pyrene were, in order of decreasing reactivity: fluoranthene > pyrene > phenanthrene. As a consequence of the nitrogen compound peak that was merged with that of phenanthrene, the actual phenanthrene conversion is inferred to have been higher than that shown in Table V. The pseudo first order kinetics plots for these three hydrocarbons suggest that the hydrogenation reactions were reversible, as expected.

Table VI is a summary of runs made at constant space velocity but with the temperature varied from 300 to 400°C with the simulated coal liquid designated in Table I. A sharp increase in quinoline HDN was observed from 300 to 350°C. However, the quinoline HDN hardly changed from 350 to 400°C; the product quinoline mass fraction observed in the run at 400°C was approximately five times that observed at 350°C, which is consistent with earlier observations that quinoline hydrogenations are reversible (6).

The HDN trend with indole was rather different: the large change in HDN occurred from 350 to 400°C, whereas the HDN was practically unchanged from 300 to 350°C; inspection of the indole mass fraction in these runs (Table VI) reveals that the indole conversion paralleled that of the HDN, suggesting that nitrogen-containing intermediates of indole were more reactive than indole itself.

The reactivities of the two oxygen compounds were at extremes: dibenzofuran conversion was low, even at the highest temperature, while the HDO of 5,6,7,8-tetrahydro-naphthol was complete at 350°C. As for dibenzothiophene, the HDS increased with temperature, with the largest change occurring from 350 to 400°C.

Phenanthrene conversion also increased with temperature. However, fluoranthene and pyrene gave a different result: in each case conversion

increased from 300 to 350°C but decreased significantly from 350 to 400°C. The decrease in conversion suggests that pyrene and fluoranthene hydrogenations are rapid but limited strongly by equilibrium at the highest temperature.

From the data presented in Tables V and VI it is evident that the conversions of dibenzothiophene, dibenzofuran, and the aromatic hydrocarbons were all low compared with those of the other compounds. In addition, organonitrogen compounds and water (one of the products of 5,6,7,8-tetrahydro-1-naphthol HDO) are known inhibitors (7, 8). These findings motivated the next set of experiments using another simulated coal liquid, Table VII. This simulated coal liquid contains the same mass fractions of dibenzofuran, dibenzothiophene, and the three aromatics as the one designated in Table I, with the nitrogen compounds and 5,6,7,8-tetrahydro-1-naphthol removed.

Experiments were carried out at 350°C and at WHSV with the simulated coal liquid designated in Table VII, and the results are summarized in Table VIII. The results of Figure 2 suggest that the hydrogenations of fluoranthene and pyrene were reversible; phenanthrene appeared to follow pseudo first order kinetics. Dibenzofuran conversion was again very low, suggesting that its low reactivity — referred to above—was not the result of inhibition by organonitrogen compounds and/or water. On the other hand, dibenzothiophene HDS was markedly greater in this coal liquid compared with the one designated in Table I. It is especially instructive to compare the results from Run 6 (Table VIII) with those from Run 1 (Table VI) as both runs were made with the same catalyst loading, feed flow rate, and the same mass fractions of dibenzofuran, dibenzothiophene, phenanthrene, fluoranthene, and pyrene. The inhibition effect of the organonitrogen inhibitors and/or the 5,6,7,8-tetrahydro-1-naphthol was strong for all the reactants except dibenzofuran.

Additional experiments are planned where 5,6,7,8-tetrahydro-1-naphthol, indole, and quinoline will be subsequently added to the simulated coal liquid specified in Table VII; these should give additional information concerning the cause of the inhibition in the runs with the simulated coal liquid given in Table I.

ACKNOWLEDGMENTS

The experimental assistance of S. K. Starry and S. A. Wikoff is gratefully acknowledged. This work was supported by DOE.

REFERENCES

1. Petrakis, L., D. C. Young, R. G. Ruberto, and B. C. Gates, Ind. Eng. Chem. Process Des. Dev. 1983, 22, 298.
2. Gates, B. C., J. H. Olson, G. C. A. Schuit, A. B. Stiles, and L. Petrakis, "Kinetics and Mechanism of Catalytic Hydroprocessing of Components of Coal-derived Liquids," United States Department of Energy Report No. DE-AC22-79ET14880-17, January 17, 1984.
3. Eliezer, K. F. et al., Ind. Eng. Chem. Fundam., 1977, 16, 380.
4. Sapre, A. V., Ph.D. dissertation, University of Delaware, Newark, Delaware, 1981.
5. Berty, T. E., H. H. Reamer, and B. H. Sage, J. Chem. Eng. Data, 1966, 11 (1), 25.
6. Satterfield, C. N. and S. H. Yang, Ind. Eng. Chem. Process Des. Dev., 1984, 23, 11.
7. Bhinde, M. V., Ph.D. dissertation, University of Delaware, Newark, Delaware, 1979.
8. Lipsch, J. M. J. G. and Schuit, G. C. A., J. Catal., 1969, 15, 174.

TABLE I

SIMULATED COAL LIQUID

COMPOUND	STRUCTURE	COMPOUND CLASS	RELATIVE MOLE FRACTION
Quinoline		Basic Nitrogen	0.0265
Acridine	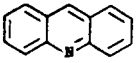	Basic Nitrogen	0.0261
Indole		Nonbasic Nitrogen	0.0384
Dibenzothiophene	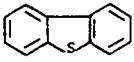	Sulfur Heterocyclic	0.0347
Dibenzofuren	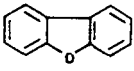	Oxygen Heterocyclic	0.0639
5,6,7,8-tetra-hydro-1-naphthol		Naphthol	0.1133
Fluoranthene	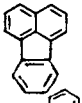	Fused two-ring Aromatic	0.3489
Phenanthrene		Fused three-ring Aromatic	0.2320
Pyrene		Fused four-ring Aromatic	0.1163

TABLE II

PROPERTIES OF AMERICAN CYANAMID[1] HDS-9A CATALYST

Composition, wt.%	
NiO	3.1
MoO_3	18.3
WO_3	0.04
Na_2O	0.05
Surface Area, m^2/g	149
Pore Volume, cm^3/g	0.51

1. The reported values were determined by the catalyst manufacturer.

TABLE III

CONDITIONS OF FIRST SET OF EXPERIMENTS

PRESSURE = 171 ATMOSPHERES

RUN #	*TEMPERATURE, °C*	WHSV, (g of reactants)/(g of catalyst h)
1	350	0.99
2	350	2.17
3	350	4.14
4	400	1.03
5	300	1.10

TABLE IV PRODUCT IDENTIFICATIONS

REACTANT	PRODUCTS	METHODS OF IDENTIFICATION: Co-Injection in GC	Mass Spectrometry
Quinoline	1,2,3,4-tetrahydroquinoline	x	
	5,6,7,8-tetrahydroquinoline	x	
	Decahydroquinoline	x	
	2-propylaniline	x	
	Propylbenzene	x	
	Propylcyclohexane	x	
Indole	Indoline	x	
	2-ethylaniline	x	
	Ethylbenzene	x	
	Ethylcyclohexane	x	
5,6,7,8-Tetrahydro-1-naphthol	Tetralin	x	x
	cis-Decalin	x	*
	trans-Decalin	x	x
	Naphthalene	x	x

*Identified as octahydromethylindan by mass spectrometry.

Dibenzothiophene	Biphenyl	x	x
	Cyclohexylbenzene	x	x
Phenanthrene	Dihydrophenanthrene		x
	Octahydrophenanthrene		x
Acridine	1,2,3,4,5,6,7,8-Octahydroacridine	x	
Fluoranthene	1,2,3,10b-Tetrahydrofluoranthene		x
Pyrene	Dihydropyrene (isomer unidentified)		x
	Hexahydropyrene (isomer unidentified)		x

TABLE V

SUMMARY OF RESULTS OBTAINED AT T=350C AND VARIABLE WHSV

FEED: SIMULATED COAL LIQUID DESIGNATED IN TABLE I

RUN #	1	2	3
WHSV, (g of reactants)/(g of cat h)	0.99	2.17	4.14
PERCENTAGE CONVERSION			
QUINOLINE	97.9	90.7	88.2
INDOLE	46.4	29.9	22.9
5,6,7,8-TETRAHYDRO-1-NAPHTHOL	100	82.4	82.5
DIBENZOFURAN	4.1	7.5	0.0
DIBENZOTHIOPHENE	15.4	0.0	0.0
PHENANTHRENE	9.9	9.3	7.3
ACRIDINE	72.3	91.9	92.2
FLUORANTHENE	41.7	24.9	23.1
PYRENE	20.3	16.6	18.8
QUINOLINE PERCENTAGE HDN	59.6	33.0	15.7
INDOLE PERCENTAGE HDN	27.8	19.7	13.5

TABLE VI

SUMMARY OF RESULTS OBTAINED AT WHSV=1 AND VARIOUS TEMPERATURES

FEED: SIMULATED COAL LIQUID DESIGNATED IN TABLE I

RUN #	5	1	4
TEMPERATURE, C	300	350	400
WHSV, (g of reactants)/(g of cat h)	1.1	0.99	1.03
PERCENTAGE CONVERSION			
QUINOLINE	98.8	97.9	88.4
INDOLE	41.0	46.4	70.5
5,6,7,8-TETRAHYDRO-1-NAPHTHOL	59.8	100	99.9
DIBENZOFURAN	0.9	4.1	5.1
DIBENZOTHIOPHENE	0.0	15.4	75.9
PHENANTHRENE	3.9	9.9	13.8
ACRIDINE	87.7	72.3	75.9
FLUORANTHENE	30.4	41.7	16.2
PYRENE	12.8	20.3	13.6
QUINOLINE PERCENTAGE HDN	4.2	59.6	54.3
INDOLE PERCENTAGE HDN	27.5	27.8	55.0

TABLE VII

COMPOSITION OF SECOND SIMULATED COAL LIQUID

COMPOUND	RELATIVE MOLE FRACTION
Dibenzofuran	0.0807
Dibenzothiophene	0.0437
Fluoranthene	0.4396
Phenanthrene	0.2921
Pyrene	0.1464

TABLE VIII

SUMMARY OF RESULTS OBTAINED WITH THE SIMULATED COAL LIQUID DESIGNATED IN TABLE VII

RUN #	6	7
TEMPERATURE, C	350	350
PRESSURE, ATM	172	173
WHSV, (g of reactants)/(g of cat h)	0.84	1.73
PERCENTAGE CONVERSION		
DIBENZOFURAN	2.8	2.7
DIBENZOTHIOPHENE	30.7	10.3
PHENANTHRENE	33.1	18.0
FLUORANTHENE	65.6	48.6
PYRENE	37.7	27.6

FIGURE 1
QUINOLINE AND INDOLE PERCENT HDN

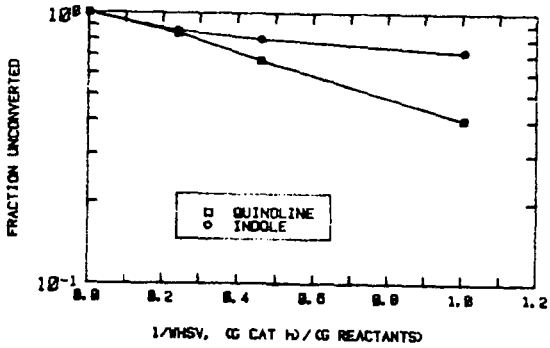

FIGURE 2
REACTIVITIES OF AROMATICS

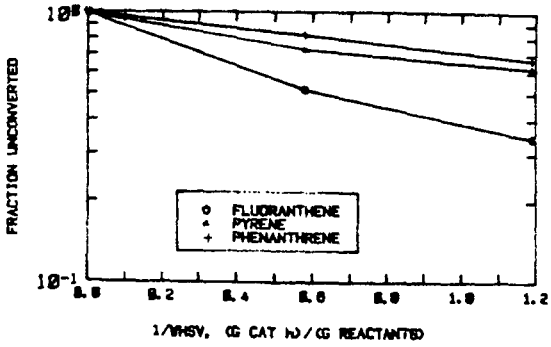

A LABORATORY STUDY OF AGGLOMERATION IN COAL GASIFICATION

C. R. Hsieh and P. T. Roberts

Chevron Research Company, Richmond, California 94802-0627

INTRODUCTION

The agglomerating tendencies of coal during gasification, especially during various stages of reaction, is a complex reaction.

Several investigators have studied the behavior of carbon-free ash. Stallmann and Neavel (1) found that the agglomerates of fused ash appear to form at temperatures below the initial deformation temperature, as defined by the ASTM fusibility test (2). Huffman, et al. (3) observed that significant particle melting of the ashes occurred at temperatures as much as 200-400°C below the ASTM initial deformation temperature. They also noted that melting was greatly accelerated under reducing conditions. Rehmat and Saxena (4) argued that it is not necessary for every reacting particle to attain the ash fusion temperature in order for agglomeration to occur. Only a few particles are required to reach the ash melting temperature. These particles form the nuclei for the formation of the ash agglomerates, and this process will indeed consume the ash produced from other particles.

In a fluidized bed, Langston and Stephens (5) recognized that the defluidizing tendency or the stickiness of the particles is directly proportional to the area of contact, the adhesive property of the particles, and inversely proportional to their momentum. Mason and Patel (6) felt that agglomeration depends on fluidized bed temperature, bed ash concentration, average particle size, superficial velocity, and bed height. Goldberger (7) and Siegell (8) both found that the ash softening temperature had no effect on the defluidization characterization for ash samples in their experiments. Basu (9) concluded that defluidization of a fluid bed is governed by the sintering characteristics of the bed material.

In some gasification processes, however, the carbon is only partially gasified in a reducing atmosphere and the remaining carbon is oxidized in a separate combustion zone (10). In addition, an inert solid is present which serves as a heat carrier and a diluent for the coal. The agglomerating tendencies of coal in such a process are different from the behavior of carbon-free ash.

In this paper, we have evaluated the agglomeration of coal, char, and ash during various stages of reaction. This included a range of temperatures, under reducing and oxidizing conditions, and in a mixture with an inert solid.

EXPERIMENTAL

Sample Preparation - Table I shows the proximate and the ultimate analyses of the three subject coals. Table II summarizes the mineral analyses of the ashes which were generated by heating the

coals in air to 538-649°C and screening all samples to pass between 100-mesh and 200-mesh U.S. standard screen. When sand was used, it was 16-30 mesh.

TABLE I

COAL ANALYSIS

	North Dakota Lignite	Western Subbituminous No. 1	Western Subbituminous No. 2
Proximate Analysis, %			
Moisture	12.3	11.3	8.0
Volatile	34.5	31.3	13.0
Fixed Carbon	44.2	40.2	60.0
Ash	9.1	17.2	19.0
Ultimate Analysis, %			
H_2O	12.3	11.3	8.0
C	60.2	54.8	64.9
H	4.2	4.1	2.0
N	0.9	1.1	0.9
S	1.0	0.8	2.6
O	12.3	10.8	2.5
Ash	9.1	17.2	19.0

TABLE II

MINERAL ANALYSIS OF ASH

% of Ash	North Dakota Lignite	Western Subbituminous No. 1	Western Subbituminous No. 2
SiO_2	39.8	59.3	23.8
Al_2O_3	16.4	25.7	9.2
TiO_2	0.8	0.9	0.5
Fe_2O_3	8.1	5.2	14.3
CaO	13.0	2.7	14.2
MgO	3.9	1.0	4.5
K_2O	0.2	0.8	0.5
Na_2O	0.8	1.9	5.9
SO_3	15.9	2.2	26.6
P_2O_5	0.5	0.2	0.2
SrO	0.4	0.0	0.1
BaO	0.1	0.1	0.3
Mn_3O_4	0.2	0.0	0.1

Equipment and Procedures - Figure 1 shows the experimental setup employed. In a typical experiment, the furnace was purged with nitrogen and preheated to 538°C before a 0.5-g sample of material was placed in a ceramic boat and positioned in the center of the furnace. The sample was heated to the desired temperature in nitrogen before either a reducing or an oxidizing gas was passed over the sample for a predetermined time. The gas flow velocity was approximately 0.8 cm/sec. After each experiment, the sample was allowed to cool outside the furnace and seived to determine the extent of agglomeration. The extent of agglomeration is defined as the weight percent retained on a mechanically vibrated 100-mesh screen.

The oxidizing gas was air. The reducing gas consisted of 51.8 vol % H_2, 25.8 vol % CO, 18.8 vol % H_2O, 1.7 vol % H_2S, 1.1 vol % CO_2, and 0.8 vol % NH_3. In some experiments, water was not used.

The average mass balance varied from a low of 96.9% for the North Dakota Lignite ash to a high of 100.8% for the Western Subbituminous No. 1, assuming complete decomposition of the sulfate and phosphate from the ash under experimental conditions.

In either a reducing or an oxidizing atmosphere at a given temperature, run lengths between 10 min. and 30 min. caused no significant difference in agglomeration, indicating that the agglomeration is complete by 10 min. Varying the sample size from 0.5-1.5 g showed no significant difference in the results, indicating that there is no particle mass transfer limitation in our tests.

RESULTS

Ash Agglomeration - Figure 2 shows the results with carbon-free ashes in the reducing gas. At 927°C, there is no significant agglomeration of any of the samples. The Western Subbituminous No. 1 sample developed substantial agglomeration at 982-1038°C, the No. 2 sample at 1038-1093°C, and the North Dakota Lignite ash at 1093-1149°C. All three samples were completely agglomerated at 1149°C. Figure 3 shows that in a reducing environment, the agglomerates transformed from a loosely packed ash at low temperature to a glassy melt at high temperature.

Figure 4 shows the effects of both reducing and oxidizing environments at 1149°C. Both conditions produce agglomeration, but at this temperature the reducing gas leads to more pronounced agglomeration. There was no agglomeration in a nitrogen environment. Thus, agglomeration is related to reactions between components in the ash and in the surrounding gas environment.

Effect of Carbon Conversion - Western Subbituminous Coal No. 1 was used to prepare samples of varying carbon content. The samples were tested in a variety of environments. Figure 5 shows that the agglomeration tendency correlates well with carbon content. No agglomeration occurs until more than 80% of the carbon is removed. Thus, modest amounts of carbon will retard ash agglomeration, even at quite severe conditions. Figure 6 shows that at 64%

carbon conversion, the sample looks much like the starting coal. At 99% conversion, the sample has agglomerated some, but still not to the extent as a carbon-free ash.

Effect of Inert Solids - Since carbon-free ash samples agglomerated the most, we mixed them with silica sand at a 1/10 ratio. Table III shows that agglomeration decreased in both reducing and oxidizing environments. Figure 7 shows that this decrease in agglomeration is quite dramatic in the reducing atmosphere. The ash samples agglomerated and shrunk; on the other hand, the particles in the ash/sand mixtures are well separated and bulky.

TABLE III

AGGLOMERATION OF
WESTERN SUBBITUMINOUS NO. 1

	% Agglomeration		
	1038°C	1093°C	1149°C
Ash Only			
N_2	0	0	0
Reducing, 10 Min.	74	97	100
Oxidizing, 10 Min.	78	98	100
Oxidizing, 30 Min.	74	99	100
Ash + Sand			
N_2	1	1	2
Reducing, 10 Min.	64	94	91
Reducing, 30 Min.	65	86	91
Oxidizing, 30 Min.	13	60	87

DISCUSSION

Agglomeration Temperature - Stallmann and Neavel (2) defined the agglomeration temperature as the 50% point on a curve like those in Figure 2, which corresponds to the steep part of these curves. Figure 8 compares the agglomeration temperature from both our experiments and those of Stallmann and Neavel (2) with the ASTM initial deformation temperature. This figure confirms the observations made by Stallmann and Neavel that the agglomeration temperature is a few hundred degrees lower than the ASTM temperature and that the ASTM initial deformation temperature cannot be correlated to the agglomeration temperature.

Figure 9 indicates that the agglomeration temperature for these three coal ashes decreases linearly with increasing sodium content of the ash. No other ash component showed a consistent relationship to agglomeration.

Process Implications - The control of agglomeration is important in the design and operation of a coal gasification or combustion process. We found that agglomeration depends on both coal

properties and on process conditions. In particular, the agglomeration of partially converted coal is negligible up to 80 wt % conversion. At higher conversions, agglomeration could be controlled by diluting the reacting material with inert materials such as sand. This study also indicated that agglomeration occurs on a shorter time scale than the nominal residence time in all but the most kinetically rapid gasification systems. These observations suggest that a gasification process which requires only partial gasification in a reducing atmosphere and which employs a diluent inert, such as the one disclosed by Mitchell, et al. (10), can greatly reduce the agglomeration problem which may occur in processing coal.

LITERATURE CITED

(1) Stallmann, J. J. and Neavel, R. C., "Techniques to Measure the Temperature of Agglomeration of Coal Ash," Fuel, Vol. 59, 584 (1980).

(2) Am. Soc. Test Mat., "Fusibility of Coal and Coke Ash," ASTM D 1857-68 (Reapproved 1980).

(3) Huffman, G. P., Huggins, F. E., and Dunmyre, G. R., "Investigation of the High Temperature Behavior of Coal Ash in Reducing and Oxidizing Atmospheres," Fuel, Vol. 60, 585 (1981).

(4) Rehmet, A. and Saxena, S. C., "Agglomeration of Ash in Fluidized Bed Gasification of Coal by Steam-Oxygen (or Air) Mixture," Ind. Eng. Chem., Process Design Develop., 19, 223 (1980).

(5) Langston, B. G. and Stephens, F. M., "Self-Agglomerating Fluidized Bed Reduction," J. Metals, April, 312 (1960).

(6) Mason, D. M. and Patel, J. G., "Chemistry of Ash Agglomeration in the U-Gas Process," Fuel Proc. Tech., 3, 181 (1980).

(7) Goldberger, W. M., "Collection of Fly Ash in a Self-Agglomerating Fluidized Bed Coal Burner," ASME paper, 67 WA/FU-3, November 1967.

(8) Siegell, J. H., "Defluidization Phenomena in Fluidized Beds of Sticky Particles at High Temperature," Ph.D. Dissertation, The City University of New York, 1976.

(9) Basu, P., "A Study of Agglomeration of Coal Ash in Fluidized Beds," Can. J. Ch.E., 60, 791 (1982).

(10) Mitchell, D. S. and Sageman, D. S., "Countercurrent Plug-like Flow of Two Solids," U.S. Patent 4,157,245, June 5, 1979.

FIGURE 1

ASH AGGLOMERATION TEST

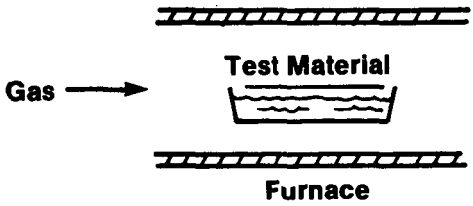

Initial Material
100-200 Mesh

Agglomeration
Material Retained on a 100 Mesh Screen
After Test Expressed as Wt % Ash

FIGURE 2

ASH AGGLOMERATION IN REDUCING GAS

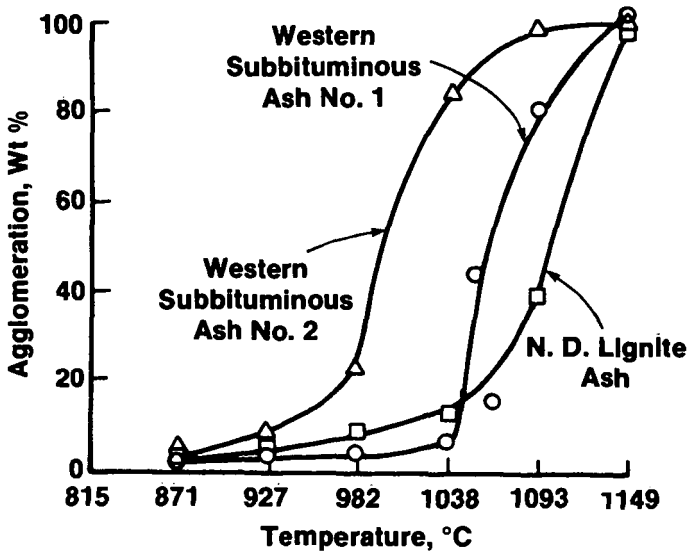

FIGURE 3

EFFECT OF TEMPERATURE ON AGGLOMERATION

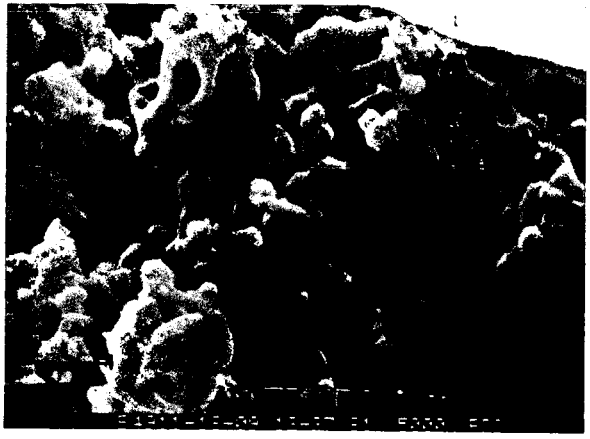

1038°C, Reducing Gas

1149°C, Reducing Gas

FIGURE 4

EFFECT OF GAS ENVIRONMENT ON AGGLOMERATION

Reducing Gas at 1149°C

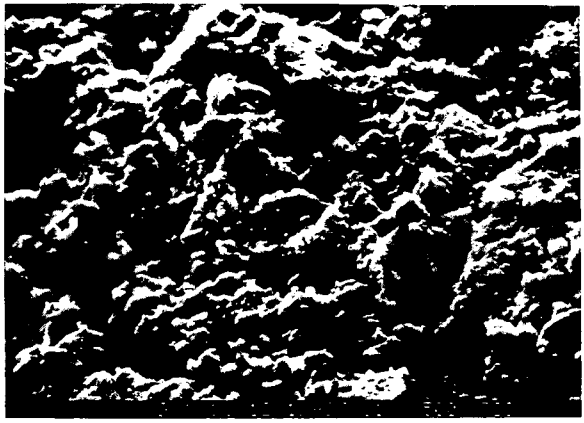

Oxidizing Gas at 1149°C

FIGURE 5

ASH AGGLOMERATION USING A WESTERN SUBBITUMINOUS COAL

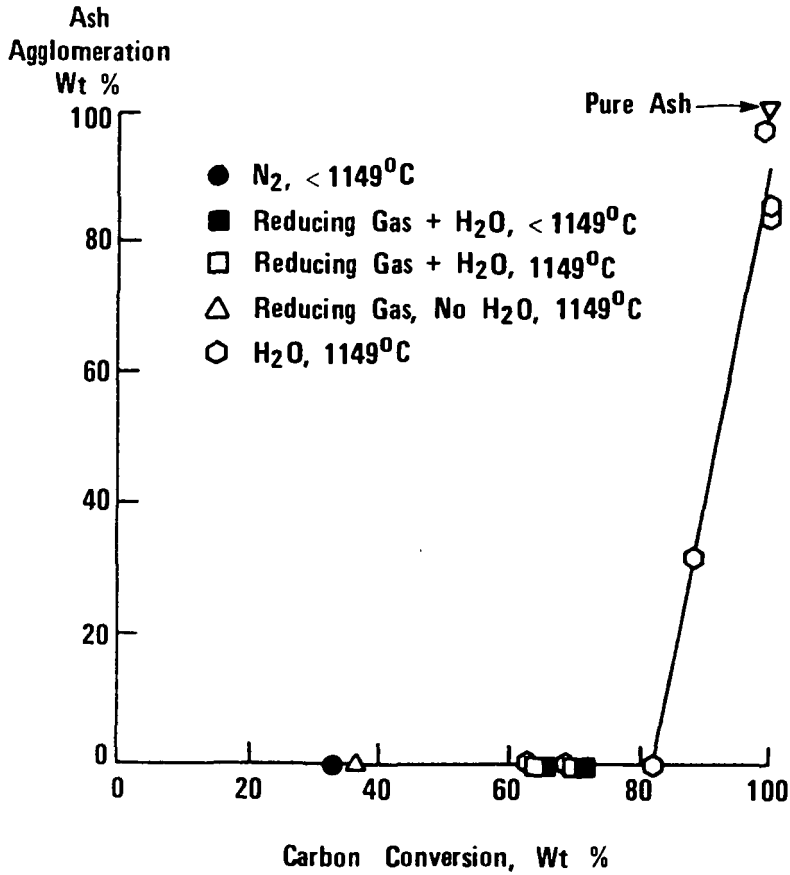

FIGURE 6

AGGLOMERATION OF WESTERN SUBBITUMINOUS COAL NO. 2 AT 1149°C

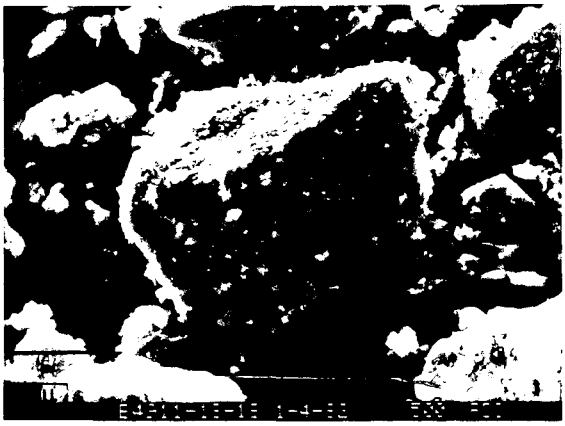

Reducing Gas, 64 Wt % Conversion

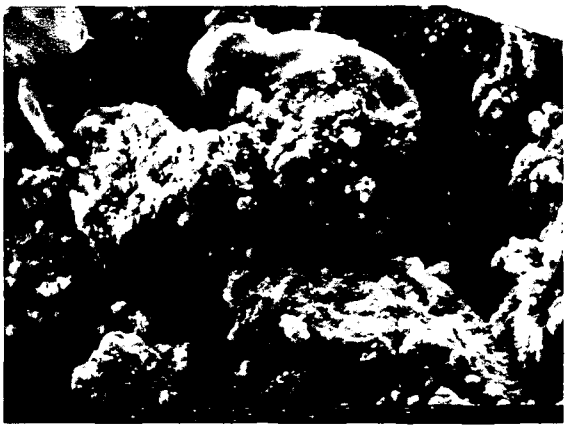

Steam, 99 Wt % Conversion

FIGURE 7

EFFECT OF TEMPERATURE AND INERT MATERIAL ON ASH AGGLOMERATION IN REDUCING GAS

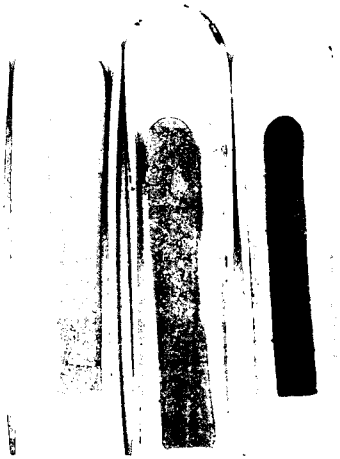

Fresh 1038°C 1093°C 1149°C

Ash Only

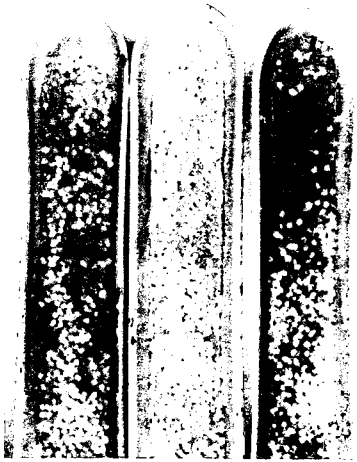

Fresh 1038°C 1093°C 1149°C

Ash + Sand

FIGURE 8

AGGLOMERATION TEMPERATURE VERSUS INITIAL DEFORMATION TEMPERATURE

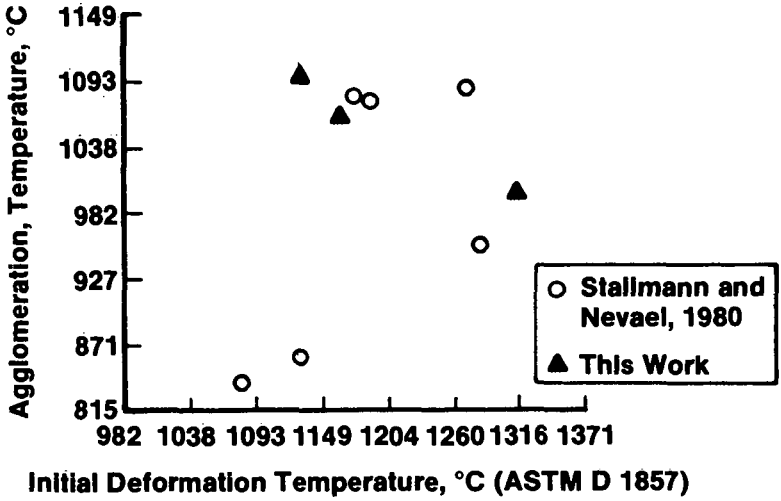

FIGURE 9
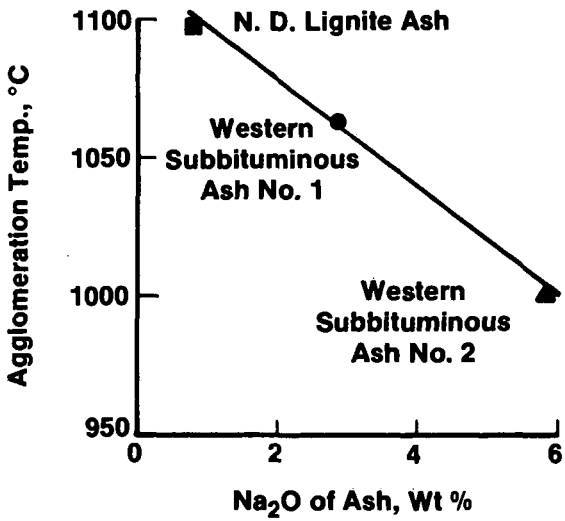
THE EFFECT OF SODIUM CONTENT ON ASH AGGLOMERATION